1997

Geochemistry, geochronology and petrography of feldspathoid-bearing rocks in the Urumiyeh-Dokhtar volcanic belt, Iran

Abbas Moradian Shahrbabaky
University of Wollongong

GEOCHEMISTRY, GEOCHRONOLOGY AND PETROGRAPHY OF FELDSPATHOID-BEARING ROCKS IN THE URUMIYEH-DOKHTAR VOLCANIC BELT, IRAN

A thesis submitted in fulfilment of the

requirements for the award of the degree

DOCTOR OF PHILOSOPHY

from

UNIVERSITY OF WOLLONGONG

by

ABBAS MORADIAN SHAHRBABAKY (BSc and MSc, Tehran University)

SCHOOL OF GEOSCIENCES

1997

DEDICATI0N

I dedicate this thesis to my parents, my wife Masoumeh and my daughters Maryam and Negar.

Except where otherwise acknowledged, this thesis represents the author's original research, which has not previously been submitted to any institution in partial or complete fulfilment of another degree.

A. Moradian Shahrbabaky

March 1997

TABLE OF CONTENTS

ABSTRACT

The Urumiyeh-Dokhtar Volcanic Belt (U-DVB) is the largest volcanic belt in Central Iran and originated as a continental arc in the Tertiary. This dissertation summarises the results of a detailed petrographic, geochemical and isotopic study of potassic rocks from three areas of this belt, comprising the Islamic Peninsula, Aghda and Shahrbabak. The U-DVB is composed mainly of tephrite, tephriphonolite, phonotephrite, phonolite, basalt, trachybasalt, basaltic trachyandesite, trachyandesite, trachyte, dacite and rhyolite. The Islamic Peninsula stratovolcano was active between 8 and 6.5 Ma and produced magmas with between 43.5 and 58.0% SiO_2. All rock types have common mineralogical and textural characteristics. The Aghda region is composed of volcanic rocks which range in age from 23.5 to 15.7 Ma and contain between 49.8 and 71.2% SiO_2. Tephriphonolite being characterised by the occurrence of abundant (commonly 40% by volume), large trapezohedra composed of single crystals of analcime or aggregates of pumpellyite. Volcanic rocks from Shahrbabak have isotopic ages between 37.5 and 2.8 Ma and SiO_2 contents from 47.2 to 67.6%.

Diopside is the only pyroxene present in samples from all three study areas and usually shows decreasing contents of MgO from core to rim, reflecting normal magmatic evolution. Sanidine is the only K-feldspar present in all samples. Plagioclase phenocrysts usually show Ca-rich cores and Na-rich rims, reflecting normal magmatic evolution. Titanomagnetite is the most common Fe-Ti oxide in rocks from the study areas and olivine has a compositional range from $Fo_{85.1}$ to $Fo_{85.6}$. Leucite occurs in rocks from the Islamic Peninsula but this phase has undergone ion-exchange pseudomorphous replacement by analcime in the other two areas. In the Aghda area analcime in the lowest tephriphonolite became unstable and was replaced by pumpellyite which has a wide compositional range, reflecting variable input of Fe, Mg, Ca and Al from the precursor analcime and alteration of inclusions.

Lavas from the Islamic Peninsula are undersaturated in SiO_2 and have high contents of CaO, K_2O and other incompatible elements, and low contents of Al_2O_3, TiO_2, and compatible elements. Rocks from Aghda are characterised by being oversaturated to undersaturated in SiO_2, high in Al_2O_3, CaO and alkalies and incompatible elements but low in TiO_2, MgO and compatible elements. The rocks from Shahrbabak are characterised by being saturated to undersaturated in SiO_2, with low Mg-numbers and contents of TiO_2 and compatible elements, but high contents of Al_2O_3, CaO and the incompatible elements.

The U-DVB developed in the Tertiary in response to northeastward subduction of the Neo-Tethys lithosphere beneath the Central Iran Plate. This tectonic setting together with geochemical and isotopic data provide strong evidence of the involvement of subduction-related processes in the generation of potassic magmas in the U-DVB. The ε_{Nd} values (+1.3 to +4.1) and initial $^{87}Sr/^{86}Sr$ ratios (0.70427-0.70567) for samples from Shahrbabak volcanic rocks are markedly different from those of the Islamic Peninsula and Aghda (ε_{Nd} = -2.2 to -4.7; initial $^{87}Sr/^{86}Sr$ = 0.70651-0.70871) and probably reflect differences in the mantle sources. Geochemical variations in Shahrbabak rocks, particularly in initial $^{87}Sr/^{86}Sr$ ratios and contents of Ba (280-1450 ppm), LREE and incompatible elements reflect heterogeneity in the mantle source. The source mantle for the Islamic Peninsula magmas was heterogeneously enriched in LFSE and LREE, probably during metasomatism by fluids released from the subducted slab. The mafic-intermediate rocks from Aghda with high K, LREE, Th, Zr, $^{87}Sr/^{86}Sr$ and low ε_{Nd} were generated by partial melting of mantle previously metasomatised by fluids derived from dehydration of the subducting oceanic crust and overlying sediment, but felsic rocks with high initial Sr isotopic ratios (0.70871) and low Sr contents were probably derived by anatexis of continental crust.

ACKNOWLEDGMENTS

Many people have provided advice, assistance, support and friendship over different period of this study and although the following list attempts to cite and thank all these, I also extend a general acknowledgment to any others I may have overlooked.

This study was undertaken with the assistance of a scholarship from the Ministry of Culture and Higher Education of the Islamic Republic of Iran.

I would like to express my special thanks and deep appreciation to my supervisor Dr P. F. Carr for his help, guidance, patience and encouragement throughout this project.

Many thanks to Prof. A. R. Chivas Head of the School of Geosciences, and the former heads of the Geology discipline, Assoc. Professors A. T. Wright and B. G. Jones for access to laboratory facilities at the University of Wollongong.

The assistance of the clerical and technical staff of the School of Geosciences, University of Wollongong is acknowledged. I especially thank Max Perkins, David Carrie, Aivars Depers and Barbara McGoldrick.

Numerous PhD students at the School of Geosciences provided friendship and support throughout my PhD project. In particular, Mr A. Soltani for discussions during the progress of this study. I wish to express my appreciation to Dr M. H. Dehghani, Dr S. A. Mazaheri and Mr M. Mohajel. I am also grateful for assistance of Dr Ghezel Ayaq and Mr M. Farahmand. Finally, I deeply appreciate the constant support, patience and encouragement extended by my family.

LIST OF FIGURES

Chapter 5.

Chapter 6.

Chapter 7.

Chapter 8.

LIST OF TABLES

Chapter 6.

Chapter 7.

CHAPTER 1

INTRODUCTION

1.1 INTRODUCTION

The Urumiyeh-Dokhtar Volcanic Belt (U-DVB) is a major Cretaceous to Recent geological structure in Central Iran, extending over a length of approximately 2,000 km and width of about 100 km (Fig. 1.1). The belt contains a wide variety of extrusive and subvolcanic rock units including several well exposed, but poorly understood, areas of Tertiary felspathoid-bearing rocks. Various aspects of this volcanic belt have been studied by many investigators (Schroder, 1944; Forster et al., 1972; Amidi, 1975; Shahabpour, 1982; Moradian, 1991; Hassanzadeh 1993; Atapour, 1994) but few publications deal with the alkaline rocks of the belt.

In the global context, ultrapotassic, potassic alkaline and shoshonitic volcanic rocks are relatively limited in abundance but they are widely distributed, and in many areas have important economic implications. Detailed study of the undersaturated, alkali-rich rocks of the U-DVB should provide not only significant new geological data on the local scale, but also important insights into the tectonic development of the region and the petrogenesis of potassic rocks in general.

1.2 AIMS OF THE STUDY

This thesis presents the results of a study of the petrography, geochronology and geochemistry of Tertiary felspathoid-bearing rocks from the U-DVB of Iran. The major aims of the study have been to:

(a) document the petrography, geochronology and geochemistry of the felspathoid-bearing rocks;

(b) determine the origin of unusual, large (several cm) analcime and pumpellyite crystals in some lavas;

(c) determine the magmatic affinity of, and relationships between, these felspathoid-bearing rocks; and

(d) develop a model for the petrogenesis of, and tectonic setting for, the felspathoid-bearing rocks.

1.3 PREVIOUS WORK

The volcanic rocks of Central Iran have been studied by many investigators but no detailed geochemical and geochronological studies have been carried out in the area. Schroder (1944) studied the tectonics of Iran, particularly in the Central Iran Plate, and recognised the U-DVB. A geological map of Iran at the scale of 1:2,500,000 published by the National Iranian Oil Company (1959) was the first to show the full extent of the U-DVB.

A study of the magmatic rocks in the central-southern part of the U-DVB by Forster et al. (1972) recognised Palaeogene alkaline volcanic units and proposed that they were formed by magmatic differentiation. Subsequent studies by Haynes and McQuillan (1974), Jung et al. (1975) and Berberian et al. (1982) concluded that volcanism in central and southern Iran was related to subduction of the Arabian plate beneath the Eurasian plate. Amidi (1975), however, concluded that the genesis of igneous rocks in the central parts of the U-DVB was not related to subduction and proposed that these rocks were produced by melting or mobilisation of sialic basement during rifting

processes. Contrary to these proposals invoking subduction or rifting in magma genesis, Moine-Vaziri and Aminsobhani (1978) concluded that the available geochemical and geophysical data base was not sufficiently comprehensive to permit definitive interpretation of the structure of the belt and the origin of the volcanism.

Other studies on the U-DVB include two unpublished doctoral theses by Shahabpour (1982) and Hassanzadeh (1993) which proposed a subduction-related origin for metalliferous deposits in the southeastern part of the belt. In the more recent account of the tectonic setting of Iran, Alavi (1994) recognised the Zagros Orogenic Belt which includes the U-DVB as a subduction-related arc.

1.4 THESIS ORGANISATION

This thesis is divided into four major parts. Chapters 1 and 2 are introductory, presenting background information including a discussion of the relevant literature on the geological and tectonic setting of Iran and the U-DVB. Part 2 (Chapters 3, 4, 5 and 6) is essentially descriptive covering topics such as stratigraphic relationships, geochronology, petrography, and geochemistry together with a general discussion about chemical variation within felspathoid-bearing rocks in the U-DVB.

Part 3 (chapters 7, 8 and 9) is largely interpretive and deals with the magmatic affinities and petrogenesis of felspathoid-bearing rocks in the U-DVB. Part 4 consists of tables, figures and Appendices. This part contains details of methods of investigation, analytical techniques, whole-rock major and trace element data, and CIPW norms of the analysed rocks.

1.5 LOCATION

Iran is located in the middle of the Indonesian-Himalayan-Mediterranean mountain belt (Fig. 1.2) which separates the Eurasian Plate in the north from the Gondwanan plates to the south. The U-DVB links the major European and East Asian mountain ranges. Three widely separated areas of felspathoid-bearing rocks occur within this volcanic belt and provide the basis for the present study. These areas comprise the Islamic Peninsula, Aghda and Shahrbabak (Fig. 1.1).

The Islamic Peninsula includes the stratovolcano of Saray which is located in northwestern part of the U-DVB and in the eastern part of Lake Urumiyeh between latitudes $37^{0}44'$ and $37^{0}56'$N and longitudes $45^{0}24'$ and $45^{0}35'$E (Fig. 1.1). The nearest major settlement is Tabriz which is approximately 70 km to the east-northeast. The stratovolcano is exposed over an elliptical area with approximate dimensions of 25 km north-south and 15 km east-west.

The felspathoid-bearing rocks from the Aghda area are developed in the central part of the U-DVB between latitudes $32^{0}9'$ and $32^{0}19'$N and longitudes $53^{0}7'$ and $53^{0}18'$E (Fig. 1.1). The outcrops occur just to the north of the village of Qaleh-e-Khargushi which is approximately 45 km south of the city of Aghda, in the southwestern part of the province of Yazd.

The Shahrbabak area is located in the southeastern part of the U-DVB and in the south-southwestern Kerman province, between latitudes $30^{0}22'$ and $30^{0}34'$N and longitudes $54^{0}59'$ and $55^{0}10'$E (Fig. 1.1).

1.6 CLIMATE AND VEGETATION

The U-DVB extends diagonally from the northwest to southeast of Iran (Fig. 1.1) with climatic changes due mainly to differences in latitude and elevation above sea level. Average data for altitude, rainfall and temperature in each of the three study areas are summarised in Table 1.1. Average temperatures in all three regions are moderate but maxima and minima are extreme and make field work in either summer or winter hazardous. All areas are rugged, sparsely vegetated and have variable rainfall with most precipitation occurring during winter and spring. The arid nature of the study areas coupled with the sparse vegetation provides excellent exposures of the felspathoid-bearing units.

1.7 IGNEOUS ROCK NOMENCLATURE

Recently the International Union of Geological Sciences (IUGS) Subcommission on the Systematics of Igneous rocks published a systematic classification of plutonic and volcanic rocks based on modal mineral contents and chemical parameters (Le Bas and Streckeisen, 1991). The recommended scheme for volcanic rocks where the modal mineral contents cannot be determined accurately because of the microcrystalline, cryptocrystalline or even glassy texture of the groundmass is based on a plot of total alkalis versus silica (TAS) and this is the classification system used throughout this thesis.

In addition, potassium contents in rocks from the Islamic Peninsula, Aghda and Shahrbabak are variable and on the basis of increasing K_2O with increasing SiO_2 (Peccerillo and Taylor, 1976; Wheller et al., 1987), rocks from these areas have been subdivided into four groups comprising the calcalkaline, high-K calcalkaline,

shoshonitic and leucititic series.

1.8 DATA PRESENTATION

All sample numbers refer to material housed in the University of Wollongong. Major element analytical data for whole rocks and minerals are expressed as weight percent (wt%) and for classification purposes have been recalculated to 100% on a volatile free basis. The original total is listed in Appendix D and trace element contents are expressed in parts per million (ppm). Total iron is reported as FeO for both whole rock and mineral analyses.

Data calculation and plotting were achieved by using a variety of computer programs including, in particular, Geochemical Data Analysis (GDA; Sheraton and Simons, 1988). Mg-number and CIPW norms were calculated with analyses normalised to 100.00% on a volatile free basis and with the mole fraction of ferrous iron set at 0.80 (Hughes and Hussey, 1976). Classification and end member calculations for pyroxene analyses were carried out using the computer program of Cebria Gomez (1990).

CHAPTER 2

TECTONIC SETTING

2.1 INTRODUCTION

Iran which is located in a collision zone between the Turan Plate to the north and the Arabian Plate to the southwest (Fig. 1.1) consists of a number of continental segments which are separated by major boundary faults. These continental segments differ in the nature of the sedimentary sequences developed, the timing of magmatic and metamorphic events and also in structural characteristics (Berberian and King, 1981). Throughout the Late Precambrian and Paleozoic, Iran was an extension of the Arabian Continental Platform, and thus a part of Gondwana. During the Late Paleozoic or Early Triassic it separated from the Gondwanan-Arabian Plate and collided with the Eurasian-Turan Plate in the Late Triassic (Stocklin, 1974; Soffel and Forster, 1980; Davoudzadeh and Schmidt, 1982). Today, Iran forms a solid land-bridge between the old continental masses of Afro-Arabia and Eurasia (Stocklin, 1974) and is divided into several major structural zones comprising the Zagros Orogenic Belt, Central Iran Plate, Alborz Belt, Kopeh Dagh Fold Belt and East Iran Belt (Fig. 1.1; Alavi, 1991, 1994).

The continental crust of Iran was metamorphosed, granitised, folded and faulted by the Pan Africa (Katangan) Orogeny of approximately 960-600 Ma. These metamorphosed orogenic rocks, which are poorly exposed, form the basement of the region (Stocklin, 1968; Nabavi, 1976). The consolidation of the Precambrian basement of Iran was followed by a long period of remarkable tectonic calm from Early Cambrian to Middle Triassic. During this time, the whole region lacked major magmatism or folding and

comprised a relatively stable continental platform with epicontinental shelf deposits (Stocklin, 1968).

Late Triassic-Late Jurassic volcanic activity produced tholeiitic basaltic lava flows in the Shemshak Formation of the Central Iran Plate and Alborz Belt. Cretaceous tectonic activity is divided into three phases comprising Late Neocomian-Albian, Late Santonian and Late Maastrichtian events. These phases were associated with episodic imbrication and emplacement of ophiolite-radiolarites along the Main Zagros Thrust Line and within the Central Iran Plate. These Mesozoic ophiolites have been interpreted as remnants of oceanic crust and are unconformably overlain by Paleocene-Eocene shallow water detrital strata (Pilger, 1971; Takin, 1972; Rico, 1974; Stocklin, 1974; 1977; Alavi-Tehrani, 1975, 1976; Nabavi, 1976; Beloussov and Sholpo, 1976; Hushmand-Zadeh, 1977). Volcanism in the Central Iran Plate and Alborz Belt peaked during the Eocene but continued into the Neogene and Quaternary (Berberian and King, 1981).

2.2 ZAGROS OROGENIC BELT

The Zagros Orogenic Belt trends northwest-southeast for about 2000 km from the East Anatolian Fault of eastern Turkey to the Oman Line in southern Iran and forms part of the extensive Alpine-Himalayan mountain range (Bushara, 1995). The Zagros Orogenic Belt formed due to an Early Mesozoic separation of the Iranian continental block from the rest of the Gondwana and subsequent northeast dipping subduction of the Neo-Tethyan oceanic crust beneath the Iranian plate and final collision of the Afro-Arabian and Iranian plates (Takin, 1972; Crawford, 1972; Alavi, 1980; Berberian and King, 1981; Sengor, 1984; Dercourt et al., 1986).

The Zagros Orogenic Belt is subdivided into the Zagros Fold-Thrust Belt, Sanandaj-Sirjan Zone and Urumiyeh-Dokhtar Arc (also known as the Urumiyeh-Dokhtar Volcanic Belt). The Main Zagros Thrust Line separates the Sanandaj-Sirjan Zone from the Zagros Fold-Thrust Belt while the boundary of the Sanandaj-Sirjan Zone with the U-DVB to the northeast is characterised by a series of elongate structural depressions. Rock sequences (including ophiolite complexes) exposed along this boundary which is taken to be the suture between the Afro-Arabian and the Iranian plate are strongly dismembered, sheared and mylonitized (Alavi, 1994). This boundary is discussed in more detail in Section 2.2.2.

2.2.1 Zagros Fold-Thrust Belt

The Zagros Fold-Thrust Belt was defined by Falcon (1969) and consists of several sedimentary sequences which cover Precambrian metamorphic basement. This basement is an extension of the Proterozoic Arabian Shield which extends in a northeastward trending belt below the Persian Gulf-Mesopotamian basin, the Zagros Fold-Thrust Belt, and the Sanandaj-Sirjan Zone (Giesse et al., 1983). Davoudzadeh and Weber-Diefenbach (1987) subdivided the 6-10 km thick sedimentary succession into three main units comprising:

(a) a latest Precambrian to Late Palaeozoic succession of evaporate-dolomite units together with shallow, epicontinental shelf siliciclastic and carbonate rocks;

(b) a succession of Carboniferous-Permian to Late Cretaceous continental shelf/platform carbonates; and

(c) a sequence of latest Cretaceous to Recent synorogenic marine and nonmarine carbonates.

Structurally, the Zagros Fold-Thrust Belt is characterised by well developed northwest-southeast trending, doubly plunging, simple parallel anticlines and synclines which were formed predominantly by flexural slip mechanisms (Colman-Sadd, 1978).

2.2.2 Sanandaj-Sirjan Zone

The Sanandaj-Sirjan Zone of Stocklin (1968), which equates to the Rezayeh-Esfandagheh Belt of Takin (1972), lies to the southwest of the U-DVB. The zone has a width of 150-250 km, and has structural trends which are parallel to the rest of the Zagros orogenic elements. The northeastern part of the zone contains a series of well developed, elongated depressions that are parallel to the southwestern boundary of the U-DVB.

Stocklin (1968) interpreted the Sanandaj-Sirjan Zone as a part of the Central Iran Plate, separated from the Zagros Fold-Trust Belt by the Main Zagros Thrust Line. The Main Zagros Thrust Line has been widely accepted as being the suture between the Afro-Arabian and Iranian plates (e.g. Takin, 1972; Crawford, 1972; Berberian and King, 1981; Sengor, 1990; Darvichzade, 1992), but according to Alavi (1980, 1994), the suture occurs along the boundary between the Sanandaj-Sirjan Zone and U-DVB rather than along the Main Zagros Thrust Line.

The Sanandaj-Sirjan Zone consists of intricately folded and strongly faulted rock assemblages ranging in age from Precambrian to Holocene. Parts of these assemblages have been affected by at least three phases of regional metamorphism including one during the Precambrian and the other two during the Late Mesozoic (Alavi, 1980).

2.3 CENTRAL IRAN PLATE

The Central Iran Plate is a roughly triangular area surrounded by the East Iran belt to the east, the Alborz Belt to the north, and the Sanandaj-Sirjan Zone to the southwest (Fig. 1.1; Stocklin, 1968). During the Precambrian and Paleozoic the Central Iran Plate was a part of the Arabian Plate and was separated from Eurasia by the Hercynian Ocean (Berberian and King, 1981). Central Iran was a stable platform during the Palaeozoic but tectonic activity in the Late Triassic produced a series of horsts and grabens between major faults (Stocklin, 1968).

Late Palaeozoic rifting in the Arabia-Iran platform along the present line of the Main Zagros Thrust Line initiated separation and northward movement of Central Iran, and opened the Neo-Tethys Ocean in the south. During the Middle Triassic narrow troughs formed between the Tabas and Lut Blocks and the remainder of the Central Iran Plate (Fig. 1.1). The Neo-Tethys Ocean in this region started to close in the southwest towards the end of Cretaceous while the northern parts of this ocean largely closed up by the Eocene.

Subduction of the Neo-Tethys Oceanic crust beneath the southern active margin of Central Iran (Sanandaj-Sirjan Zone) produced an Andean-type magmatic-arc during Mesozoic and possibly Tertiary times (Berberian F, 1981). Syntectonic regional greenschist facies metamorphism occurred along the southern margin of the Central Iran Plate during the Late Triassic and was accompanied by a strong compressional deformation of Triassic rocks in the region (Haghipour, 1974; Berberian, 1977). Late Triassic-Early Jurassic granitic intrusions are exposed along the Central Iranian active continental margins (Dimitrijevic, 1973; Berberian and Nogol, 1974; Sabzehei, 1974).

The Jurassic diorites and Cretaceous granites-diorites of the Alvand Batholith in the Hamedan area of the Sanandaj-Sirjan Zone are interpreted as subduction-related magmatism along the Sanandaj-Sirgan Zone (Berberian and Berberian, 1981).

The northward movement of the Arabian Plate and northward subduction of the Neo-Tethys Oceanic Crust led to the closure of the Neo-Tethys Ocean and collision of Arabia with Central Iran in the Late Cretaceous (Stocklin, 1974; Berberian and King, 1981).

2.4 VOLCANISM IN THE CENTRAL IRAN PLATE

The Central Iran Plate has undergone several major orogenic episodes and is characterised by a series of syntectonic metamorphic and magmatic events which affected the southwestern margin, particularly during the Late Palaeozoic, Middle Triassic, Late Jurassic and Late Cretaceous (Berberian, 1983).

Precambrian volcanic units are dominated by post-orogenic alkali rhyolite, rhyolitic tuff, and quartz porphyry of the Taknar Formation in the Kashmar region, northeastern Central Iran Plate, and the Rizu-Desu Series in the southeastern part of the plate (Forster et al., 1973). After a Middle Triassic compressional phase, the plate underwent tensional movements with initiation of this extensional phase being characterised by the emplacement of Late Triassic continental alkali basaltic lavas (Assereto, 1966). Belts of ophiolite-melange composed mainly of ultramafic rocks, pillow lavas, pelagic strata, and metamorphic rocks (Fig. 2.1) were developed during the Late Cretaceous, with the process of ophiolite emplacement continuing until the Late Maastrichtian (Sabzehei and Berberian, 1972; Stocklin, 1974, 1977; Stoneley, 1974, 1975).

The main mountain belts which formed during the Late Cretaceous orogenic movements controlled the development and evolution of volcanogenic sedimentary basins throughout the Eocene. Therefore, most of the main physiographic features of the Central Iran Plate were established by the Eocene.

Tertiary volcanic activity in the Central Iran Plate has been reviewed by Crawford (1972), Dewey et al. (1973), Forster (1976), Alavi-Tehrani (1976) and Farhoudi (1978). The Tertiary volcanism in the Central Iran Plate was followed by Late Eocene tectonic events. Lava flows and tuffs with different compositions developed during the Neogene in the eastern Central Iran Plate, Azarbaijan (northwestern Central Iran Plate), and south of Quchan (northeastern Central Iran Plate). Neogene continental volcanism produced a thick sequence of both lava flows and pyroclastic rocks and volcanism culminated in the Pliocene-Pleistocene with the formation of large stratovolcanoes composed mainly of andesite, dacite and basalt, and with the intrusion of subvolcanic intermediate and felsic rocks.

Volcanic activity in the Central Iran Plate is considered to be related to either subduction of the Arabian Plate under the Iranian Plate along the Main Zagros Thrust Line (Berberian and King, 1981) or melting and mobilisation of sialic crustal material during a rifting process (Takin, 1972; Amidi, 1975, 1977; Conrad et al., 1977).

2.5 URUMIYEH-DOKHTAR VOLCANIC BELT (U-DVB)

The U-DVB is the largest volcanic belt in Iran and runs parallel to the Sanandaj-Sirjan Zone and Zagros Fold-Thrust Belt, approximately 150 km northeast of the Zagros Main Thrust Line which marks the boundary between the Arabian and Central Iranian

continental plates (Berberian and King, 1981). Geomorphologically, the U-DVB comprises a mountain range with elevations up to 4420 m (Kuh-e-Hazard) separated from the Sanandaj-Sirjan Ranges by a continuous zone of depressions, including the Urumiyeh Lake, Tuzlu-Gol, Gavkhuni and Jazmurian depression of Iranian Baluchestan. Outcrops within the U-DVB comprise a wide variety of lithologies including granites, granodiorites, diorites and gabbros as well as widely distributed basaltic lava flows, trachybasalts (locally shoshonitic), andesites, dacites, trachytes and pyroclastic units. The Bouguer gravity map of Iran (Dehghani and Makris, 1983) shows negative anomalies of about -150 m Gal along the U-DVB and the calculated crustal thickness of 45-50 km, which is 5-10 km thicker than the average thickness, is probably related to the magmatic activity and northeastward thrust faulting (Alavi, 1994).

2.5.1 Tectonic Setting of the Urumiyeh-Dokhtar Volcanic Belt

The U-DVB comprises a distinctive, thick sequence of volcanic and subvolcanic units. Genesis of the belt has been controversial with several major tectono-magmatic models being proposed. One model favours continental rifting (Emami, 1981; Amidi et al., 1984; Amidi and Michel, 1985) while another model relates genesis of the belt to Late Cretaceous continent-continent collision between Arabia and Central Iran (Stocklin, 1974; Berberian and King, 1981). The most popular model, however, involves Andean-type subduction of the Tethyan oceanic crust beneath the Central Iran Plate during the Tertiary to generate the volcanism (Berberian et al., 1982; Alavi, 1994). Evidence cited in support of this subduction-based model includes the presence of post-Paleogene calcalkaline plutons (Berberian F. 1981) and porphyry copper mineralisation in the U-DVB (Shahabpour, 1982; Giesse et al., 1984, Hassanzadeh, 1993).

The youngest pelagic fossils incorporated in the Zagros ophiolites are Late Cretaceous in age which Berberian and King (1981) interpret as being indicative of the timing of ophiolite emplacement and thus the age of continent-continent collision. As suggested by Bird (1978) this age may merely record obduction of the offshore intraoceanic arc of the Zagros-Oman passive margin, while the rest of the oceanic crust still existed to be subducted beneath the Central Iran Plate during the Tertiary. A major problem with the model for Late Cretaceous closure of Tethys is that if no Tertiary Tethys Ocean was available for subsequent subduction, then post-Cretaceous opening of the Indian and Red Seas could not have been compensated by plate destruction, and would require an expanding Earth (Stocklin, 1983).

Alavi (1994) noted that the peak magmatic activity in the U-DVB occurred during the Eocene. Geochemical data for Eocene-Oligocene alkaline volcanic rocks of the U-DVB presented in this thesis (section 8.3) are indicative of a subducted-related origin for these volcanic rocks. In addition, isotopic and geochemical data in the three study areas (Chapter 3, 6, 8) are not compatible with closure of the Tethyan Ocean during the Late Miocene which suggested by Berberian F. (1981) and Hassanzadeh (1993).

A dextral strike-slip fault system has been proposed along the Main Zagros Thrust Line and the U-DVB. The cause of this faulting has been assumed to be the counter-clockwise rotation of the Arabian Plate during the opening of the Red Sea and is therefore thought to have begun in the Miocene, not in the Late Cretaceous or Early Tertiary (Berberian, 1976). Several well exposed north-northwest dextral shears (e.g. Zephreh fault) have been mapped within the U-DVB (Stocklin and Nabavi, 1973). The en-echelon nature of these north-northwest faults indicates the presence of a major

northwest-striking, dextral shear between the crustal blocks on the northeast (Central Iran) and the southwest (Sanandaj-Sirjan).

CHAPTER 3

GEOLOGICAL SETTING AND GEOCHRONOLOGY

3.1 INTRODUCTION

The three study areas consist mainly of Tertiary (post Late Eocene) volcanic rocks (Moine-Vaziri, 1985; Bina et al., 1986; Hassanzadeh, 1993) and field observations show that the mafic rocks are older than the felsic ones. Due to the relatively young age of the rocks and occurrence of sanidine, biotite and hornblende, the K-Ar method of isotopic dating was selected for age determination. This method is applicable to a wide range of minerals and rock types and is particularly useful for rocks of the age and composition encountered in the study areas (McDougall and Harrison, 1988). The K-Ar data are summarised in Table 3.1 and are integrated with other isotopic age data for the study areas. Results presented in this thesis are the first radiometric ages for the subvolcanic intrusions in the study areas.

The stratigraphic relationships within each area are summarised in geological maps and stratigraphic tables and only units for which age-data are available are discussed in the text.

3.2 ISLAMIC PENINSULA

The Islamic Peninsula covers an area of approximately 360 km^2 and is bounded by the Tabriz Fault in the north and Zarineh Fault in the south. Included in the area is the Late Miocene stratovolcano of Saray which is located in the eastern part of Urumiyeh Lake. This stratovolcano was formed during two major eruptive episodes which

produced deposits ranging from tephrite to trachyte in composition (Moine-Vaziri et al., 1991). Products of the earlier cycle mainly comprise leucite-bearing tephrite lavas and pyroclastic units whereas the later cycle mainly produced phonotephrite lava together with leucite-bearing tephrite and phonolitic pyroclastic units. These eruptive cycles were followed by intrusion of leucite tephrite, leucitite-phonolite, trachyandesite and trachyte mainly as plugs and dykes.

A major vertical fault trending almost east-west divides the stratovolcano into a northern and southern section (Fig. 3.1). The northern block has been upthrown an unknown amount and the fault truncates several units including the large trachyandesite plug at the centre of the volcano. Precise correlation between blocks on either side of the fault is not possible due to the lack of appropriate marker beds, but in general, the units exposed in the northern block are older than those exposed south of the fault.

Nine stratigraphic units are recognised in the volcanic deposits and their distribution and stratigraphic relationships are summarised in Figures 3.1 and 3.2 respectively. The basal exposures of the volcanic pile consist of intercalations of leucite tephritic lava and pyroclastic breccia which crop out mainly in the northern exposures of the volcano (Fig. 3.1). Moine-Vaziri (1985) reported a whole-rock, K-Ar age of 7.8±0.29 Ma for this unit but on the basis of new K-Ar data for a trachyte dyke and trachyandesite plug (discussed below) this isotopic age appears to be too young.

A trachyandesite plug is exposed in the centre of the stratovolcano and marks the position of the major eruptive vent, with all extensive extrusive units dipping essentially radially away from this area (Fig. 3.1). Similarly, many dykes trend radially

away from this plug. With the exception of several trachyte plugs and dykes, the trachyandesite is the youngest exposed unit of the stratovolcano. Analytical data for both sanidine and biotite from this unit are reported in Table 3.1. The biotite is very fresh as confirmed by the high content of K_2O and, although the sanidine crystals are also very fresh, some phenocrysts have slightly corroded rims which reflects disequilibrium with the trachyandesite magma. The K-Ar dates for the coexisting sanidine and biotite differ by more than the analytical uncertainty and this discrepancy is presumed to reflect the incorporation of xenocrystic sanidine which gives a slightly older age than the biotite. Accordingly, the date for the biotite (8.0±2 Ma) is taken to represent the time of crystallisation of the unit.

Trachyte dykes and plugs are widespread throughout the study area and intrude all other units of the Islamic Peninsula volcano. Leucitite-phonolite dykes are most common in the northern part of the volcano while trachytic dykes crop out mostly in the southern part of the stratovolcano. Many of these small intrusions show at least slight hydrothermal alteration but a dyke which crops out approximately 3 km southeast of the village of Agh-Gonbad (Fig. 3.1) has fresh, groundmass sanidine suitable for K-Ar dating. The age of 6.5±1 Ma is taken to represent the time of crystallisation of the trachyte because of its concordance with field relationships and the K-Ar age of 8.0±2 Ma for the older trachyandesite plug.

The whole-rock, K-Ar age of 7.8±0.29 Ma obtained by Moine-Vaziri (1985) for the basal tephrite unit of the older eruptive cycle in the stratovolcano is discordant with the new K-Ar dates reported in Table 3.1 and the dated sample is presumed to have lost Ar to give an apparently young age. The new K-Ar dates show that the most recent

activity of the younger volcanic cycle continued until at least approximately 6.5 Ma. The major fault across the Islamic Peninsula volcano post-dates this activity.

3.3 AGHDA

The Aghda study area is composed of Eocene-Miocene volcanic rocks and occurs within the large Nain region which Amidi (1975) subdivided into four major zones comprising:

1. a western zone composed of Paleozoic and Mesozoic sedimentary rocks;
2. an eastern zone of Tertiary and Quaternary volcanic and intrusive rocks;
3. a Palaeozoic metamorphic complex, together with Cretaceous volcanic and sedimentary rocks, (the latter are overlain by Palaeocene calcareous strata); and
4. the Surk Zone which is characterised by the occurrence of melange and ophiolites.

Aghda occurs in the eastern zone which is characterised by extensive magmatism, both in space and in time. Amidi (1975) and Bina et al. (1986) have subdivided the magmatic and metamorphic activity into several phases listed below.

(a) Eocene and Miocene volcanic eruptions which produced lavas forming part of the present study and extensive pyroclastic deposits;

(b) an Oligocene rhyolitic phase, involving production of rhyolitic lavas and pyroclastic units;

(c) an Oligocene-Miocene volcanic and sedimentary phase, containing andesitic volcanic lavas and pyroclastic units;

(d) Early Miocene greenschist facies metamorphic rocks;

(e) Middle Miocene plutonic masses; and

(f) Neogene continental and lagoonal deposits unconformably overlain by Pliocene and Pleistocene conglomerates.

The Miocene volcanic sequence is subdivided into several units (Fig. 3.3) which generally have an east-west strike and a dip of between 30 and 40° towards the south (Fig. 3.3). A tephriphonolite lava approximately 150 m above the base of the measured section (Fig. 3.4) has a whole-rock, K-Ar age of 23.5±1.2 Ma (Table 3.1; Bina et al., 1986). The unit contains large trapezohedra of analcime and pumpellyite which are interpreted to reflect ion-exchange pseudomorphous replacement of primary leucite, followed by zeolite facies metamorphism (Section 5.4). Formation of the pseudomorphous analcime and pumpellyite indicates extensive elemental migration in the unit and makes interpretation of the significance of the K-Ar difficult. Bina et al. (1986) recognised that the sequence had been metamorphosed and concluded that the K-Ar date recorded the timing of this metamorphic event rather than the age of crystallisation. A major potential problem with this interpretation, however, is that alteration produced by metamorphism of the style and grade encountered at Aghda is notoriously heterogeneous even on a small scale (Section 5.4.1) and thus is unlikely to produce re-equilibration of the K-Ar system during the metamorphic event. In this case the date does not necessarily record the age of the metamorphic event but may reflect some intermediate time between crystallisation and the peak of metamorphism. The K-Ar date, however, does appear to indicate a minimum age for the lava and a maximum age for metamorphism.

The only fresh, unequivocally magmatic material in the region suitable for K-Ar dating

is hornblende from a trachyandesite plug at Kuh-e-Mil in the northern part of the study area (Fig. 3.3). This plug intrudes the Eocene sequence recognised by Amidi (1975) but its relationship to the lavas overlying this part of the stratigraphy is unknown. The K-Ar date of 15.7±1 Ma (Table 3.1) is interpreted as the age of emplacement of the plug.

3.4 SHAHRBABAK

The Shahrbabak study area is located in the Kerman region which Dimitrijevic (1973) subdivided into four major geological units comprising the:

1. Rafsanjan Belt;
2. Dehaj-Sarduiyeh Belt;
3. Coloured Melange; and
4. Sirjan Belt.

Feldspathoid-bearing rocks occur in the Dehaj-Sarduiyeh Belt where a sequence of basaltic, andesitic and trachytic lavas and pyroclastic units and associated sedimentary strata are developed. This sequence is divided into three series comprising an Early Eocene volcanic series best developed in the southeastern part of belt, the Razak volcanic series which is developed in the northwestern part of the Shahrbabak area, and the Hezar volcanic series (Djokovic et al., 1973). Both the Razak and Hezar series were originally assigned an Eocene age by Dimitrijevic (1973) but more recent dating has shown that at least the Hezar series formed during the Oligocene (Hassanzadah, 1993). The Hezar series contains several undersaturated, K-rich units which form the basis for the present investigation. Volcanism and accompanying intrusive activity in the general region continued until the Pliocene.

Isotopic dates determined by Hassanzadeh (1993) supplemented by two K-Ar dates

determined as part of the present investigation (Table 3.1; Fig. 3.5) provide a sound basis for understanding the timing of magmatic activity in the Shahrbabak region. The histogram of isotopic ages from the region (Fig. 3.5) omits the two Ar-Ar ages determined by Hassanzadeh (1993) for analcime because these are considered to be too young (Section 3.4.2). The isotopic data show that magmatic activity in the region occurred during four episodes comprising eruption of the Razak series, the Hezar series, Mid-Miocene volcanism and Late Miocene-Pliocene activity.

3.4.1 Razak volcanic series

Outcrops of the Razak series occur in the northern and eastern parts of the study area (Fig. 3.6) and consist of trachyte, trachyandesite and basaltic trachyandesite lava flows, tuff and breccia intercalated with calcareous marine strata containing Late Eocene fossils (Srdic et al., 1972). The sequence has undergone a pervasive albitization and silicification which are presumed to be essentially coeval with emplacement and to be related to hydrothermal alteration in a submarine environment (Hassanzadeh, 1993). An Ar-Ar isotopic age of 37.5±1.4 Ma for albite from a silicified trachyte lava (Table 3.1; sample MD30) is consistent with the Late Eocene stratigraphic age and is interpreted as the age of eruption (Hassanzadeh, 1993).

3.4.2 Hezar volcanic series

The Hezar series forms the upper part of the "Eocene" volcanic sequence of Srdic et al. (1972) and covers a large part of the Shahrbabak study area (Fig. 3.6). The succession comprises a series of mainly tephriphonolite lavas intercalated with less voluminous trachyandesite and andesite lavas, together with a few pyroclastic units (Fig. 3.7). Volcanic units of this series lack biotite and amphibole but are characterised by the

occurrence of large analcime pseudomorphs after leucite set in a groundmass rich in K-feldspar (Section 4.4.1).

Hassanzadeh (1993) reported several Ar-Ar dates and one Rb-Sr isotopic age for units from this series. Ages for two stratigraphically equivalent lavas (Table 3.1; samples JZ1 and JZ3) gave a range of Ar-Ar dates which are generally younger than three more precise and restricted isotopic ages for a stratigraphically younger unit (sample FT3). The variable ages for samples JZ1 and JZ3 presumably reflect variable elemental exchange during pseudomorphous replacement of primary leucite by analcime (see Section 5.4) and do not record the age of crystallisation. In contrast, the isotopic data for the stratigraphically higher lava involving different isotopic systems and materials are concordant and reflect an age of approximately 29 Ma for the time of crystallisation.

3.4.3 Mid-Miocene igneous activity

Miocene igneous activity in the Shahrbabak region is characterised by the development of conspicuous calcalkaline domes, plugs and subvolcanic intrusions (Dimitrijevic, 1973), and subordinate andesite lavas which unconformably overlie the Hezar series (Hassanzadeh, 1993). Hornblende from one of these andesite lavas yielded an Ar-Ar age of 19.3±0.4 Ma (Table 3.1, sample SH9).

Hornblende and K-feldspar separates from a quartz monzonite intrusion yield Ar-Ar ages of 18.3±0.2 and 17.9±0.2 Ma respectively, and hornblende from another part of the intrusion gave an age of 16.9±0.2 Ma (Hassanzadeh, 1993; Table 3.1). The dacite plug of Kuh-e-Tezerej in the northeastern part of the study area (Fig. 3.6) contains

fresh biotite suitable for isotopic dating. Isotopic data yield an age of 16.4±1 Ma (Table 3.1) which is essentially coeval with mid-Miocene Ar-Ar dates for the andesite lava and quartz monzonite intrusion obtained by Hassanzadeh (1993).

The isotopic ages for the plug and other subvolcanic intrusions in this region are indistinguishable from the K-Ar age of 15.7±1 Ma obtained for the trachyandesite plug at Kuh-e-Mil in the Aghda study area (Section 3.3). These dates indicate that felsic, calcalkaline magmatism was widespread in the U-DVB during the mid-Miocene.

3.4.4 Late Miocene-Pliocene igneous activity

Several large Late Miocene-Pliocene stratovolcanoes also occur in the Shahrbabak region. The largest of these, the Kuh-e-Masahim volcano, with a basal diameter of approximately 35 km occurs 30 km east of the study area. Three minerals from two samples from different stratigraphic levels in the volcanic pile have been dated by the Ar-Ar method and give concordant ages of 6.3±0.9, 6.8±0.4, and 6.4±0.8 Ma (Hassanzadeh, 1993; Table 3.1). Dating of fresh biotite from a trachyandesite intrusion northeast of Qotb-Abad (Fig. 3.6) yields an age of 6.5±1 Ma (Table 3.1) which is consistent with the field relationships and thus is interpreted as the age of intrusion. Further support for this interpretation is provided by the contemporaneity between the K-Ar date for the trachyandesite intrusion and the age of the Kuh-e-Masahim volcano. Biotite analyses from deposits of the Kuh-e-Madvar volcano 25 km southeast of the study area provide an Ar-Ar age of 2.8±0.2 Ma which probably marks the most recent episode of felsic calcalkaline magmatism in the region (Hassanzadeh, 1993; Table 3.1).

CHAPTER 4

PETROGRAPHY

4.1 INTRODUCTION

The felspathoid-bearing rocks from the U-DVB are petrographically diverse. Most of the Islamic Peninsula rocks are relatively fresh, porphyritic and holocrystalline. The rocks from the two other areas, however, have undergone slight secondary alteration, although in most cases the secondary minerals are too fine-grained for precise optical identification. Some phases of the extrusions are vesicular or amygdaloidal and many samples of the rocks of these study areas are altered with the development of a wide range of secondary minerals. Samples with minimal alteration have been chosen for the present study. Petrographic data for representative samples of the various intrusions and extrusions were determined by routine petrographic techniques. Modal data were obtained from 118 samples (Appendix B) and compositional data for the principal phases in 22 selected samples are listed in Appendix C. Chemical analyses of the major phases were carried out using a CAMEBAX Cameca electron microprobe.

4.2 ISLAMIC PENINSULA

Miocene rocks from the Islamic Peninsula occur as lavas, plugs, dykes and pyroclastic breccias. Based on the TAS diagram these extrusive and intrusive rocks are subdivided into tephrite, phonotephrite, basalt, trachyandesite and trachyte (Section 6.2).

Texturally, most of the extrusive and intrusive rocks of the Islamic Peninsula are similar. They are holocrystalline and porphyritic with abundant phenocrysts of

pyroxene, leucite and sanidine while the groundmass is fine-grained, and shows an intergranular texture. In thin section most pyroxenes show normal zoning and some of them show oscillatory zoning. All phenocrysts of leucite are euhedral and show complex twinning (plate 1A). The less abundant primary minerals comprise biotite, apatite and titanomagnetite. Secondary chlorite, calcite, serpentine and zeolite also occur, mainly as pseudomorphs after olivine.

4.2.1 Tephrite

Petrographic data for tephrite samples from the Islamic Peninsula are listed in Table 4.1. Tephrite occurs as lavas, dykes, and pyroclastic units which crop out all over the study area, especially in the northern part of the stratovolcano. Tephrite samples are grey or dark brown in hand specimen. Petrographic evidence for alteration is limited, but some samples contain pseudomorphous replacements after olivine. Phenocrysts may be poikilitic and consist of leucite and pyroxene, together with pseudomorphs after olivine. These phenocrysts occur in a holocrystalline or cryptocrystalline groundmass.

Diopside occurs both as phenocrysts and in the groundmass. It is the most abundant phenocrystic phase and occurs as green to pale yellow, euhedral to subhedral grains. The largest grains are 6.6 mm across but phenocrysts normally range between 2.0 and 4.5 mm in size, and the size of diopside in the groundmass is between 0.2 and 0.6 mm. The majority of diopside phenocrysts are fresh and many grains contain inclusions of apatite, titanomagnetite and leucite which produce a sieve-like texture. Pyroxene phenocrysts also display simple and polysynthetic twinning. Diopside phenocrysts from the Islamic Peninsula show strong oscillatory zoning (plate 2). Phenocrysts range from $Wo_{47.0}En_{48.5}Fs_{4.5}$ to $Wo_{49.3}En_{36.0}Fs_{14.7}$ in composition (Fig. 4.1).

Leucite is the other abundant phenocryst. It occurs as white trapezohedra with a maximum dimension of 2.8 mm but most leucite phenocrysts range between 1.0 and 2.3 mm across. Groundmass grains range between 0.02 and 0.8 mm in size. Leucite grains are mostly fresh, but in some samples they have been altered to a mixture of analcime and nepheline.

Sanidine occurs as euhedral to subhedral grains which range between 1.5 and 2.5 mm in size. These crystals are mainly fresh, but some grains show kaolinite alteration. Phenocrysts display simple twinning, whereas groundmass grains are untwined microlites. In some samples (e.g. R14448 and R14449) sanidine occurs as thin rims around leucite phenocrysts and was formed by magmatic reaction.

Olivine occurs as subhedral grains between 0.02 and 0.6 mm across. The cores of most grains are fresh but the margins of many olivine grains are altered. Titanomagnetite is common in all samples as phenocrysts, in the groundmass, as inclusions in mafic minerals, and as reaction products around olivine and biotite.

Brown mica occurs in the groundmass as subhedral to anhedral grains, 0.02 to 0.5 mm long. Some grains are corroded and altered to chlorite and titanomagnetite. Brown mica is strongly pleochroic (X = brown, Y = Z = reddish brown) and in some samples (e.g. R14449, R14456, R14457 and R14458) it surrounds other minerals. Based on the pleochroism and associated minerals it is probably biotite.

Fine-grained crystals of apatite occur as inclusions within pyroxene (e.g. R14450) and sanidine phenocrysts, and also occur as needles in the groundmass in some samples

(e.g. R14458). Secondary minerals comprise chlorite, calcite, serpentine and zeolite. Most of these secondary minerals occur as pseudomorphs after olivine, replace rims on biotite grains, or occur along joint surfaces and in small amygdales.

4.2.2 Phonotephrite

Petrographic data for phonotephrite samples from the Islamic Peninsula are listed in Table 4.2. These rocks are exposed in the form of pyroclastic units (R14453), dykes (R14460, R14445 and R14472) and lavas (R14461, R14467). The phonotephrite rocks of the Islamic Peninsula are grey and black in hand specimen, and have undergone only minor alteration.

Samples of phonotephrite from the Islamic Peninsula are glomeroporphyritic with a fine-grained groundmass. Abundant phenocrysts of leucite, pyroxene and pseudomorphs after olivine are visible in hand specimen. The leucite is euhedral with a white colour; pyroxene phenocrysts are also euhedral but are green to black in colour; and pseudomorphs after olivine are anhedral with a brown colour.

Diopside occurs both as a phenocryst and in the groundmass. Phenocrysts are greenish, pale-yellow and euhedral to subhedral, zoned, commonly contain inclusions of apatite and titanomagnetite, and some have corroded crystal margins (e.g. R14461). The grain size of diopside phenocrysts ranges between 1.5 and 5.9 mm. Diopside phenocrysts are less abundant in phonotephrite than in tephrite and basalt from the Islamic Peninsula. Diopside grains range from $Wo_{47.5}En_{43.4}Fs_{9.1}$ to $Wo_{48.7}En_{38.9}Fs_{12.4}$ in composition (Fig. 4.2).

Leucite phenocrysts are euhedral and some have been altered to nepheline and analcime (e.g. R14453, R14467). Leucite phenocrysts normally range between 1.0 and 2.4 mm in size and commonly contain inclusions of titanomagnetite and pyroxene.

Sanidine crystals are simply twinned and occur as small phenocrysts and, more commonly, as laths in the groundmass. Phenocrysts range between 1.0 and 1.4 mm in size and show slight alteration to kaolinite.

Biotite crystals are subhedral to anhedral in shape, brown in colour and contain titanomagnetite inclusions. The grain size ranges between 0.02 and 0.4 mm and some grains have been partially altered to chlorite. The margins of many biotite grains are dark and rounded, which may indicate some resorption. Other minor components of the groundmass comprise titanomagnetite, apatite, calcite, zeolite and chlorite.

4.2.3 Basalt

Petrographic data for basalt dykes from the Islamic Peninsula are listed in Table 4.3. Samples are porphyritic, holocrystalline and grey to greenish grey in colour. Diopside is the dominant phase followed in decreasing order of abundance by leucite, biotite and olivine. The maximum dimension of diopside phenocrysts is approximately 20 mm. Groundmass grains are less than 0.4 mm across and consist of diopside, leucite, biotite, titanomagnetite, accessory apatite, together with secondary chlorite and calcite.

Diopside occurs as euhedral to subhedral, yellowish green grains. Phenocrysts display simple and multiple twinning, and have a compositional range of $Wo_{47.5}En_{49.5}Fs_{3.0}$ to $Wo_{49.2}En_{41.0}Fs_{9.8}$ (Fig. 4.3).

Leucite is the other abundant phenocrystic phase. It is euhedral in shape and lacks complex twinning because most grains have been altered to sanidine and analcime. Biotite occurs as an anhedral groundmass phase, commonly surrounding other minerals.

4.2.4 Trachyandesite

Petrographic data for trachyandesite samples from the Islamic Peninsula are listed in Table 4.4. Trachyandesite occurs mainly as plugs (e.g. R14698), but also occurs as blocks in some pyroclastic units. Samples are grey in hand specimen, fresh, and glomeroporphyritic with a fine-grained groundmass. Phenocrysts comprise sanidine, pyroxene and biotite.

Diopside phenocrysts occur as yellowish green, euhedral to subhedral grains between 1.3 and 3.6 mm in size and which show both polysynthetic and simple twinning. Phenocrysts range from $Wo_{47.7}En_{45.2}Fs_{7.1}$ to $Wo_{49.5}En_{35.4}Fs_{15.1}$ in composition (Fig. 4.4).

Euhedral to subhedral sanidine grains are the main phenocrystic phase, and also occur as a major constituent of the groundmass where they define a flow foliation. At the summit of the trachyandesite plug located between the Saray and Agh-Gonbad Valleys (Fig. 3.1), abundant large (15 mm in length) sanidine phenocrysts show evidence of resorption and reaction around the grain rims and are probably xenocrystic in origin. These sanidine phenocrysts range between $Or_{62.8}$ and $Or_{72.9}$ in composition (Fig. 4.5).

Biotite occurs as a common euhedral to subhedral, strongly pleochroic (X = pale-brown, Y = Z = brown) phase between 1.2 and 4.4 mm in size. Equant, subhedral titanomagnetite grains occur as phenocrysts and in the groundmass. Other minor

constituents include calcite and sericite.

4.2.5 Trachyte

Petrographic data for trachyte exposed as plugs and dykes (e.g. R14465) are listed in Table 4.5. Trachyte samples are light grey in colour and mostly fresh with a glomeroporphyritic texture and a holocrystalline groundmass. Phenocrysts comprise large crystals of sanidine, clinopyroxene and biotite.

Prismatic phenocrysts of clinopyroxene are greenish or pale yellow in colour, range between 1.0 and 2.5 mm in size and commonly contain inclusions of apatite and titanomagnetite. In some instances phenocrysts show partial alteration to uralite. clinopyroxene also occurs in the groundmass.

Euhedral sanidine crystals are a major phenocrystic phase and are also a common groundmass component where they define a flow foliation. The sanidine crystals are simply twinned and generally fresh but some grains show a slight alteration to kaolinite (e.g. R14445). They range from 1.5 to 8.9 mm in length and commonly contain inclusions of titanomagnetite and pyroxene.

Euhedral to subhedral biotite grains occur as a minor phase in trachyte samples from the Islamic Peninsula. All grains are strongly pleochroic (X = brown, Y = Z = dark brown), and are rimmed by titanomagnetite. The phenocrysts range between 1.0 and 5.3 mm in size. Equant grains of titanomagnetite between 0.01 and 0.9 mm in size occur in the groundmass. Accessory minerals include zircon, sphene and apatite. Calcite and kaolinite occur as secondary minerals in the groundmass.

4.3 AGHDA

On the basis of contents of silica and total alkalis (TAS) the rocks of the Aghda region are subdivided into phonotephrite, tephriphonolite, phonolite, basaltic trachyandesite, trachyandesite, trachyte and rhyolite (Section 6.3). These rocks types were emplaced as lavas, pyroclastic units, plugs and dykes.

4.3.1 Phonotephrite

Petrographic data for phonotephrite are summarised in Table 4.6. The phonotephrite rocks occur as lavas which are slightly altered, holocrystalline, glomeroporphyritic and have a fine-grained groundmass. Samples are black to greenish grey in hand specimen, and contain euhedral to subhedral, black to green phenocrysts of diopside, white plagioclase, pale green to pale brown analcime, and anhedral, black to brown pseudomorphs after olivine.

Diopside phenocrysts occur as pale yellowish, subhedral to anhedral grains between 1.6 and 5.4 mm in size. Most phenocrysts are fresh and show simple twinning, compositional zoning and have inclusions of titanomagnetite and apatite. In some instances the crystal margins are corroded. Diopside phenocrysts range from $Wo_{47.8}En_{40.0}Fs_{12.2}$ to $Wo_{46.7}En_{34.6}Fs_{18.7}$ in composition (Fig. 4.2).

Sanidine occurs both as phenocrysts and in the groundmass and many grains show at least partial alteration to kaolinite and sericite. Sanidine is the dominant felsic mineral in phonotephrite from the Aghda region. Phenocrysts range between 1.0 and 5.9 mm in size, show simple twinning and range from $Or_{74.7}$ to $Or_{77.8}$ in composition (Fig. 4.6).

Plagioclase is mostly euhedral to subhedral in shape with many grains showing partial alteration of the more calcic cores to sericite, calcite and zeolite. Plagioclase crystals range between 2.0 and 5.7 mm in length and commonly show polysynthetic twinning. The composition ranges from cores of $An_{74.1}$ to rims of $An_{68.2}$ (Fig. 4.6). Small inclusions of Fe-Ti oxide and pyroxene occur in many plagioclase phenocrysts.

Analcime occurs as trapezohedra between 3.0 and 8.9 mm across and contains inclusions of plagioclase, pyroxene, Fe-Ti oxide and apatite. Some analcime crystals show a relict complex twinning and their origin by pseudomorphous replacement of primary leucite is discussed in Section 5.4.

Biotite is a minor constituent of the groundmass and occurs as subhedral to anhedral, brown flakes which are partly altered to chlorite. Olivine occurs as greenish, subhedral grains between 0.1 and 0.6 mm in size. The cores are fresh but alteration to serpentine and iddingsite around the margins and along fractures is common. Other minor phases present in samples of phonotephrite include apatite, Fe-Ti oxide and secondary calcite, zeolite, epidote, sericite and chlorite.

4.3.2 Tephriphonolite

Petrographic data for tephriphonolite from Aghda are summarised in Table 4.7. Hand specimens are brown or greenish grey in colour and contain prominent large trapezohedra of analcime and pumpellyite, together with phenocrysts of sanidine, plagioclase and diopside. These rocks are holocrystalline and glomeroporphyritic with a fine-grained groundmass consisting of biotite, nepheline, olivine, titanomagnetite, apatite, and secondary prehnite, zeolite, sericite and kaolinite.

Spectacular large trapezohedra composed of single crystals of analcime or aggregates of pumpellyite occur in the tephriphonolite lavas from Aghda. Both pumpellyite and analcime crystals display a euhedral, cubic trapezohedral form and are up to 3 cm in diameter, and collectively the large crystals may comprise up to approximately 40% of the host unit. Trapezohedra released from the lavas are concentrated on the tops of these units during weathering and erosion. Detailed description and discussion of the origin of these trapezohedra are presented in Section 5.4.

Diopside occurs as euhedral to subhedral, pale-yellowish and purplish grains both as phenocrysts and in the groundmass. The majority of diopside phenocrysts are fresh, range from 1.0 to 2.7 mm in size and display simple twinning. Inclusions of titanomagnetite, sanidine and apatite are common. Phenocrysts range from $Wo_{46.9}En_{38.1}Fs_{15.0}$ to $Wo_{46.9}En_{32.8}Fs_{20.3}$ in composition (Fig. 4.7).

Sanidine occurs as euhedral to subhedral phenocrysts between 1.5 and 3.9 mm in length, and it is also the major constituent of the groundmass. Some grains show slight alteration to kaolinite and the phenocrysts range between $Or_{74.6}$ and $Or_{98.1}$ in composition (Fig. 4.8). Plagioclase also occurs both as phenocrystic grains between 1.0 and 5.9 mm in length and also as small, euhedral to anhedral crystals in the groundmass. Prominent alteration to sericite, kaolinite and carbonate is restricted to the cores but all plagioclase grains have been albitised as shown by the compositional range from $An_{3.9}$ to $An_{8.5}$ (Fig. 4.8). Biotite and Fe-Ti oxide inclusions are common in plagioclase phenocrysts. Albite twinning is the dominant twin type, but a few grains also display pericline twinning. Biotite occurs as subhedral to anhedral grains which are strongly pleochroic (X = pale-brown, Y = Z = brown). The size ranges from 0.1 to

0.9 mm with an average size of 0.5 mm. Some grains are corroded at the crystal margins.

4.3.3 Phonolite

Petrographic data for phonolite lavas and dykes from Aghda are summarised in Table 4.8. Some samples contain vesicles infilled with epidote, calcite and zeolite but the amygdales rarely exceed 10% of the volume of the rock. In general, samples of phonolite from Aghda are red to brown in colour and are holocrystalline with glomeroporphyritic aggregates set in a fine-grained to microcrystalline groundmass.

Sanidine is normally the most abundant phenocrystic and groundmass phase in these rocks, with groundmass laths comprising up to approximately 85% of the sample. Alteration to kaolinite and sericite is common in some grains. Sanidine phenocrysts range between 2.0 and 7.7 mm in length and commonly display simple twinning. Plagioclase occurs as euhedral to subhedral grains between 1.0 and 6.0 mm in length. Polysynthetic twinning is common and some grains show at least partial alteration to sericite and carbonate.

Euhedral phenocrysts of diopside are pale-yellowish to greenish in colour and range between 1.5 and 3.8 mm in size. Inclusion of apatite, titanomagnetite and sanidine are common. Equant, subhedral, beige-coloured analcime grains which range between 1.5 and 3.0 mm in size are also common. These have replaced primary leucite (Section 5.4). Small, equant grains of titanomagnetite are common throughout the groundmass. Other minor constituents comprise biotite and apatite, together with secondary calcite, zeolite, sericite, epidote and chlorite.

4.3.4 Basaltic trachyandesite

Petrographic data for samples of basaltic trachyandesite lavas are summarised in Table 4.9. Some areas of exposure of this lithology show evidence of alteration with the development of abundant epidote, which occurs in masses up to 10 cm across, together with veins containing native copper and zeolites. Fresh samples are holocrystalline and porphyritic with phenocrysts of pyroxene, feldspars and nepheline set in a fine-grained groundmass of feldspars, diopside, biotite olivine and Fe-Ti oxides.

Diopside phenocrysts are yellowish, euhedral to subhedral, between 2.0 and 4.0 mm across and display simple twinning. Most of the phenocrysts exhibit zoning and contain inclusions of apatite and titanomagnetite. The groundmass grains occur as anhedral grains and are untwined. Diopside phenocrysts range from $Wo_{46.1}En_{38.9}Fs_{15.0}$ to $Wo_{46.9}En_{34.0}Fs_{19.1}$ in composition (Fig. 4.4).

Sanidine occurs as euhedral to subhedral phenocrysts between 1.0 and 3.6 mm in length and it also is the major constituent of the groundmass. Some sanidine phenocrysts show slight alteration to kaolinite, and inclusions of titanomagnetite are common. The composition of sanidine ranges from $Or_{76.4}$ to $Or_{87.7}$ (Fig. 4.9).

Plagioclase occurs as euhedral to subhedral grains between 2.0 and 5.0 mm long and have polysynthetic twinning. In some samples plagioclase phenocrysts have been partially altered to sericite with the core region showing the most extensive alteration. Compositions range from $An_{60.8}$ to $An_{62.4}$ (Fig. 4.9). In some samples (e.g. R14488) phenocrysts are rimmed by sanidine.

Nepheline phenocrysts are euhedral grains between 1.0 and 3.2 mm long. The nepheline phenocrysts comprise between 4.0 and 10.2% (by volume) of the rock. Biotite occurs as anhedral grains in the groundmass and have a mean grain size of 0.5 mm. Some grains are corroded (R14481) and have very dark brown rims. Equant, subhedral grains of Fe-Ti oxide between 0.01 and 0.8 mm across occur in the groundmass and comprise between 0.5 and 3.5% of the total rock volume. Secondary minerals comprise about 5.5% of the total volume and consist of calcite, sericite, zeolite and epidote.

4.3.5 Trachyandesite

Trachyandesite samples are exposed both as lavas and plugs. Petrographic data are summarised in Table 4.10. Samples of trachyandesite are fresh, light grey in colour, and porphyritic with phenocrysts of hornblende, sanidine and plagioclase set in a fine-grained, holocrystalline groundmass.

Sanidine phenocrysts occur as laths between 2.0 and 4.8 mm long. Some phenocrysts are slightly altered to kaolinite and most grains exhibit simple twinning. Plagioclase is the main felsic mineral in samples of trachyandesite and occurs as euhedral to subhedral grains both as phenocrysts and in the groundmass. Plagioclase phenocrysts range between 1.5 and 5.0 mm in length and commonly show polysynthetic twinning and oscillatory zoning (plate 1B). Some grains are slightly altered to sericite and titanomagnetite inclusions are common.

The main mafic mineral in trachyandesite samples is hornblende which occurs as green, prismatic crystals which range between 1.0 and 3.4 mm long. Most phenocrysts are fresh and inclusions of titanomagnetite and apatite are common. The only other mafic

minerals are biotite and Fe-Ti oxide which occur as subhedral to anhedral grains in the groundmass. Apatite occurs both as inclusions within phenocrysts and also as needles in the groundmass of some samples.

Secondary minerals comprising calcite, sericite, zeolite and kaolinite constitute 9.9% of the total rock volume. Calcite and zeolite minerals occur mainly in cavities and along joints.

4.3.6 Trachyte

Petrographic data for trachyte which occurs as lavas and dykes all over the study area are summarised in Table 4.11. These rocks are porphyritic with phenocrysts of sanidine, clinopyroxene, nepheline and plagioclase set in a holocrystalline, fine-grained, often microlitic groundmass. In hand specimen trachyte samples are brown and grey in colour, and may be vesicular or amygdaloidal with aggregates of epidote and zeolite (e.g. R14489).

Phenocrystic sanidine grains are euhedral to subhedral in shape, between 1.5 and 6.8 mm long and display simple twinning. Some crystals have been altered to sericite and kaolinite and commonly contain inclusions of Fe-Ti oxide. Small laths of sanidine are by far the most voluminous constituent of the groundmass. Plagioclase also occurs as euhedral to subhedral phenocrysts up to 5.0 mm in size, and commonly displays polysynthetic twinning. These phenocrysts contain small inclusions of titanomagnetite and show partial alteration to epidote and sericite. A few phenocrysts of euhedral to anhedral and zoned grains of clinopyroxene also occur in trachyte samples.

Biotite crystals occur as anhedral, pleochroic (X = pale-yellow, Y = Z = red-brown) grains in the groundmass. Titanomagnetite grains are anhedral, range between 0.01 and 1.0 mm across and comprise between 0.5 and 6.2% of the total rock volume. Other minor constituents comprise secondary calcite, epidote, zeolite and chlorite.

4.3.7 Rhyolite

Petrographic data for rhyolite lavas from Aghda are summarised in Table 4.12. Samples are white or grey in colour and consist of phenocrysts of quartz, K-feldspar and plagioclase set in a holocrystalline, fine-grained groundmass. K-feldspar is the major constituent and occurs as subhedral to anhedral phenocrysts between 1.5 and 4 mm long and as small laths in the groundmass. Phenocrysts contain inclusions of titanomagnetite and some grains have been altered to kaolinite. Plagioclase phenocrysts occur as euhedral to subhedral grains up to 6.3 mm long and have common polysynthetic twinning. Some phenocrysts have been partially altered to sericite. Quartz occurs both as a phenocrystic phase and in the groundmass.

Biotite and titanomagnetite occur as subhedral grains which constitute a minor part of the groundmass. Zircon is the accessory phase while secondary calcite, sericite and zeolite make up about 1.3% of the total rock volume.

4.4 SHAHRBABAK

On the basis of the total alkalis versus silica plot (TAS), the intrusive and extrusive rocks of Shahrbabak are subdivided into tephriphonolite, basalt, trachybasalt, basaltic trachyandesite, trachyandesite, trachyte and dacite (Section 6.4). These lithologies occur as lavas, plugs, dykes and pyroclastic units.

Texturally, most of these rocks are similar with abundant phenocrysts of pyroxene, plagioclase, sanidine and less common biotite, olivine and hornblende. In addition to these minerals, the groundmass also contains apatite and titanomagnetite together with secondary minerals including large trapezohedra of analcime and small grains of calcite, epidote, zeolite, chlorite, kaolinite and sericite.

4.4.1 Tephriphonolite

Petrographic data for tephriphonolite are summarised in Table 4.13. In the Shahrbabak region, the tephriphonolite rocks are interbedded with altered trachyandesite and are greenish grey to black in colour. Samples consist of phenocrysts of diopside, sanidine, plagioclase, nepheline and abundant analcime which originated by pseudomorphs replacement of primary leucite (Section 5.4). The groundmass is holocrystalline and fine-grained.

Phenocrystic and groundmass diopside grains are almost colourless with a greenish tint. The phenocrysts of diopside are euhedral to subhedral grains with a maximum dimension of 2.5 mm. Some grains have ragged edges due to resorption (e.g. R14535 and R14544) and most show minor compositional zoning (e.g. R14531 and R14541) and have inclusions of titanomagnetite and apatite. Clinopyroxene phenocrysts range from $Wo_{47.8}En_{38.8}Fs_{13.4}$ to $Wo_{45.6}En_{35.7}Fs_{18.7}$ in composition (Fig. 4.7).

Sanidine is the most abundant phase in the tephriphonolite rocks and occurs both as euhedral phenocrysts up to 5 mm long and as abundant, small laths in the groundmass. Most phenocrysts show at least partial alteration to kaolinite and sericite and commonly contain inclusions of titanomagnetite and apatite. Sanidine compositions range from

$Or_{62.7}$ to $Or_{93.8}$ (Fig. 4.10).

Plagioclase occurs as euhedral to subhedral phenocrysts between 1.2 and 5.8 mm long. Twinning according to the albite and albite-Carlsbad laws is common and thin rims of sanidine occur on many phenocrysts. Compositions of fresh plagioclase crystals range from $An_{50.83}$ to $An_{59.2}$ but some samples contain albitised grains (Fig. 4.10).

Analcime occurs as abundant trapezohedra between 5.0 and 30.0 mm in size and are greenish and pinkish in colour. These trapezohedra differ in size and abundance throughout the study area, with those in the south being larger and more numerous than those in the north. In the southernmost part of the study area trapezohedra of analcime have been released from the groundmass during weathering and erosion. Collectively, the large crystals may comprise up to 30% of the host unit and all crystals contain abundant inclusions of plagioclase, pyroxene and titanomagnetite. Some analcime trapezohedra show a relict complex twinning (e.g. R14541 and R14557).

Nepheline phenocrysts are euhedral to subhedral grains with a maximum dimension of 2.5 mm. Crystals are cloudy in thin section and most show evidence of alteration (e.g. R14540, R14544 and R14551).

Anhedral grains of titanomagnetite occur both in the groundmass and as inclusions in other minerals in tephriphonolite samples. Most of the grain edges are rounded which may indicate some resorption. The grains range between 0.01 and 1.0 mm in size. Apatite is the only accessory phase and occurs as needles in the groundmass and as small inclusions in other phases.

Secondary minerals including calcite, sericite, zeolite, kaolin, chlorite and epidote comprise about 4.4% of the total rock volume. Calcite and zeolite minerals occur mainly as amygdales and fillings along joint surfaces.

4.4.2 Basalt

Petrographic data for basalt samples from Shahrbabak area are summarised in Table 4.14. All samples are dark grey in hand specimen and are porphyritic with a holocrystalline groundmass. Phenocrysts comprise about 34.5% of the total rock volume and consist mainly of olivine, diopside, plagioclase and K-feldspar. Plagioclase crystals are the dominant phase, followed in decreasing order of abundance by sanidine, diopside, and olivine.

Diopside occurs both as phenocrysts and in the groundmass. Most phenocrysts are yellowish, euhedral to subhedral in shape and between 1.0 and 5.4 mm in size. Some grains contain inclusions of titanomagnetite and plagioclase, and most grains display simple twinning. Diopside phenocrysts range from $Wo_{46.5}En_{39.9}Fs_{13.6}$ to $Wo_{46.9}En_{37.7}Fs_{15.4}$ in composition (Fig. 4.3).

Plagioclase is the most abundant felsic phenocrystic phase in basalt from Shahrbabak and occurs as euhedral to subhedral phenocrysts between 2.0 and 4.6 mm in length and as small laths in the groundmass. Most phenocrysts contain titanomagnetite inclusions and grains are generally fresh although a few exhibit minor alteration to sericite. Albite and Carlsbad twinning occur in most of the samples as does oscillatory zoning. The composition of plagioclase phenocrysts ranges from $An_{84.1}$ to $An_{38.3}$ (Fig. 4.11). Sanidine phenocrysts are subhedral with simple twinning. The size of sanidine

phenocrysts is between 1.0 and 2.5 mm. The composition of the phenocrysts ranges from $Or_{37.5}$ to $Or_{44.6}$ (Fig. 4.11).

Olivine usually occurs as greenish, subhedral grains with curved fractures and between 1.3 and 2.8 mm across. The margins of olivine phenocrysts have been altered to iddingsite and serpentine whereas the cores are fresh. Olivine ranges from $Fo_{71.9}$ to $Fo_{72.1}$ in composition (Appendix C).

Titanomagnetite occurs as anhedral crystals scattered throughout the groundmass and as inclusions in the other minerals. Secondary minerals comprise chlorite and sericite, and pseudomorphs of iddingsite and serpentine after olivine.

4.4.3 Trachybasalt

Petrographic data for samples of trachybasalt lavas from Shahrbabak region are summarised in Table 4.15. All samples are dark grey to black in hand specimen and are porphyritic with a holocrystalline groundmass. Phenocrysts comprise approximately 30% of the total rock volume and consist of plagioclase, diopside, sanidine and olivine.

Diopside phenocrysts are pale yellow in colour, euhedral to subhedral in shape and range between 1.5 and 3.7 mm in size. They show oscillatory zoning and contain inclusions of titanomagnetite and apatite. The composition of the diopside phenocrysts ranges from $Wo_{46.9}En_{44.8}Fs_{8.3}$ to $Wo_{47.9}En_{32.7}Fs_{19.4}$ (Fig. 4.12).

Plagioclase is the most abundant phenocrystic and groundmass phase and occurs as euhedral to subhedral phenocrysts between 1.0 and 2.0 mm in length and as small laths

in the groundmass. A flow foliation is defined by alignment of both phenocrystic and groundmass grains. Most phenocrystic grains show albite and Carlsbad twinning and also exhibit oscillatory zoning. Some plagioclase phenocrysts have corroded cores and inclusions of apatite. Most grains are fresh but some show alteration to sericite and calcite. Phenocrysts range from $An_{18.7}$ to $An_{57.6}$ in composition (Fig. 4.13).

Sanidine occurs as euhedral to subhedral, mainly fresh, simply twinned grains between 1.5 and 2.2 mm long. Other primary minerals comprise olivine and titanomagnetite. Olivine crystals from the southern part of study area are fresh and green with a maximum dimension of 2.5 mm, but most olivine grains from the northern part of the area have been completely pseudomorphed by iddingsite and serpentine. Titanomagnetite occurs as subhedral, equant grains crystals scattered throughout the groundmass of trachybasalt samples. Secondary minerals comprise calcite, chlorite, iddingsite and serpentine.

4.4.4 Basaltic trachyandesite

Petrographic data for basaltic trachyandesite lavas from Shahrbabak are summarised in Table 4.16. Samples are brown to black in hand specimen and contain abundant phenocrysts of pyroxene and plagioclase. Some of the samples are vesicular or amygdaloidal, with the amygdales composed of calcite and zeolite (e.g. R14538, R14537), but the cavities or amygdales rarely exceed 15% by volume of the rocks. The groundmass is holocrystalline and composed of fine-grained feldspars, olivine and Fe-Ti oxide. A well-developed flow foliation is defined by alignment of groundmass feldspar laths in some samples (e.g. R14549).

Diopside occurs as yellow to greenish, subhedral phenocrysts with a maximum dimension of 4.5 mm. Simple twinning and inclusions of titanomagnetite and apatite are common. Plagioclase is the dominant felsic mineral in samples of basaltic trachyandesite and occurs both as euhedral to subhedral phenocrysts and as laths in the groundmass. Phenocrysts range between 2.0 and 4.2 mm in size and are commonly zoned and twinned according to the albite and Carlsbad laws. Some plagioclase crystals are partially altered to sericite and carbonate. Inclusions of titanomagnetite are present in some plagioclase phenocrysts (e.g. R14553). Sanidine also occurs both as a phenocrystic and groundmass phase but most grains have been altered to kaolinite.

Other primary minerals comprise titanomagnetite and accessory apatite. Secondary minerals include calcite, zeolite, chlorite, sericite, kaolinite and pseudomorphs of serpentine and iddingsite after olivine.

4.4.5 Trachyandesite

Petrographic data for trachyandesite lavas and small, subvolcanic intrusions from Shahrbabak are summarised in Table 4.17. Samples are greenish grey and brown in hand specimen and are glomeroporphyritic with prominent aggregates of feldspar phenocrysts set in a holocrystalline, fine-grained groundmass.

Diopside phenocrysts are relatively rare and occur as yellowish, subhedral grains which range between 1.2 and 1.8 mm in size. Plagioclase is the major constituent of trachyandesite samples from Shahrbabak and occurs as euhedral to subhedral phenocrysts between 1.0 and 1.7 mm long and as small laths in the groundmass. Phenocrysts commonly show albite, Carlsbad and pericline twinning and oscillatory

zoning. In some samples (e.g. R14554), plagioclase phenocrysts are grouped into aggregates producing a glomeroporphyritic texture. The composition of the plagioclase grains ranges from $An_{8.2}$ to $An_{51.5}$ (Fig. 4.14) but the more anorthite-poor compositions probably reflect partial albitisation.

Sanidine is a common constituent in trachyandesite samples and occurs both as euhedral to subhedral phenocrysts up to 3.4 mm long, and as small laths in the groundmass. Sanidine also occurs as thin rims around plagioclase phenocrysts in some samples (e.g. R14517, R14554). Many grains show simple twinning and are fresh but some grains show partial alteration to kaolinite. The composition of the sanidine grains ranges from $Or_{56.3}$ to $Or_{92.9}$ (Fig. 4.14).

Hornblende is the dominant mafic mineral in most samples of trachyandesite (e.g. R15757) and occurs as green prisms up to 2.5 mm long which have altered rims. Titanomagnetite grains are equant and subhedral with a maximum dimension of 0.8 mm. Primary accessory phases comprise apatite and zircon which usually occur as inclusions in the phenocrystic phases. Secondary minerals include calcite, sericite, epidote, zeolite and chlorite.

4.4.6 Trachyte

Trachytic rocks from Shahrbabak are fresh and form plugs and other subvolcanic intrusions. Petrographic data are summarised in Table 4.18. Samples are light grey in colour and porphyritic with common phenocrysts of hornblende, biotite, plagioclase and sanidine set in a fine-grained, holocrystalline groundmass.

Hornblende is the dominant mafic mineral and occurs as subhedral to euhedral grains up to 2.8 mm long. Most grains are strongly pleochroic (X = pale-green; Y = Z = green) but some of the hornblende in sample R14536 has been converted to opaque minerals.

Plagioclase occurs as euhedral to subhedral phenocrysts between 1.4 and 4.0 mm long. Most phenocrysts have oscillatory zoning, and twinning according to the albite, Carlsbad and pericline laws is common. Inclusions of biotite, hornblende and titanomagnetite are also common. Grains are generally fresh, but some phenocrysts show alteration to sericite (e.g. R14536). Phenocrysts range from $An_{24.2}$ to $An_{31.5}$ in composition (Fig. 4.15).

Sanidine is the dominant groundmass phase and also occurs as subhedral phenocrysts ranging in size from 1.8 to 4.9 mm. The other phenocrystic phase is biotite which occurs as euhedral to subhedral, pleochroic (X = pale-brown, Y = Z = brown) grains between 1.0 and 2.3 mm long. Many biotite grains are fresh, but some are corroded and altered to chlorite and Fe-Ti oxides (e.g. R14536).

Accessory apatite and zircon occur as inclusions in the other minerals and in the groundmass. Minor secondary calcite and sericite occur in the groundmass.

4.4.7 Dacite

Petrographic data for dacite plugs from the Shahrbabak area are summarised in Table 4.19. Most samples of dacite are fresh, grey in colour and have abundant phenocrysts of plagioclase, sanidine, hornblende, biotite and quartz set in fine-grained,

holocrystalline groundmass.

Plagioclase is the major felsic mineral in dacite samples from Shahrbabak and occurs both as phenocrysts and in the groundmass. Phenocrysts are euhedral to subhedral in shape and are generally fresh but in some samples they show slight alteration to sericite. The size of the plagioclase phenocrysts ranges between 1.5 and 4.6 mm and most grains show oscillatory zoning with albite, pericline and Carlsbad twins (Fig. B). Plagioclase phenocrysts range from $An_{21.8}$ to $An_{31.5}$ in composition (Fig. 4.15). Sanidine also occurs both as phenocrysts and in the groundmass. Phenocrysts are euhedral to subhedral grains up to 3.2 mm long. Most phenocrysts show simple twinning and are fresh but some show alteration to kaolinite. Groundmass grains are mainly fresh, fine-grained, simply twinned laths.

Hornblende, biotite and Fe-Ti oxides are the only mafic minerals in samples of dacite from Shahrbabak. Hornblende phenocrysts are euhedral to subhedral, pleochroic (X = brown, Y= Z = dark brown) prisms up to 3.2 mm long. In some samples (e.g. R15811, R14526) most of the hornblende crystals have been replaced by calcite. Inclusions of titanomagnetite and apatite are common in some phenocrysts. Biotite grains are euhedral to anhedral in shape and occur as brownish phenocrysts and in the groundmass. Some grains are corroded and many show alteration to chlorite and opaques. Biotite phenocrysts range between 1.2 and 1.8 mm in size.

Quartz occurs both as phenocrysts (4.5%) and in the groundmass (16%). Most quartz grains are subhedral to anhedral in shape and resorption embayments are common (e.g. R15811). The maximum dimension of the crystals is 1.5 mm. Other primary phases

comprise titanomagnetite, apatite and zircon whereas minor amounts of secondary calcite, sericite and kaolinite are also present.

4.5 MINERAL CHEMISTRY

Chemical data for pyroxene, sanidine, plagioclase, olivine, biotite, Fe-Ti oxides, amphibole and leucite from different rock types are summarised and discussed in the following sections.

4.5.1 Pyroxene

Diopside is the only pyroxene present in samples from all three study areas (Fig. 4.16). In most diopside crystals the average MgO content is higher in the core than the rim whereas the average FeO content is lower in the core than the rim (e.g. Tables 4.20 to 4.23; Fig. 4.17). This enrichment of FeO from core to rim is consistent with normal fractionation during magmatic evolution.

In tephrite from the Islamic Peninsula the mean MgO and CaO contents decrease from core to rim whereas TiO_2, Al_2O_3, FeO and Na_2O increase (Table 4.20). Rims have a more restricted range of compositions and are relatively enriched in ferrosilite compared to the cores (Fig. 4.1).

Compositions of diopside phenocrysts in phonotephrite from Aghda and the Islamic Peninsula are similar but diopside grains from Aghda have higher average contents of Al_2O_3 and FeO and lower MgO and CaO (Tables 4.21, 4.22; Fig. 4.2). Clinopyroxene crystals in tephriphonolite from Aghda and Shahrbabak are very similar in composition, but the average content of FeO in samples from Aghda is slightly higher than in

samples from Shahrbabak (Tables 4.23, 4.24; Fig. 4.7).

Diopside phenocrysts in basalt samples from the Islamic Peninsula have a narrow range of compositions and have the highest average MgO and CaO, and lowest average FeO contents of all pyroxene samples from the three study areas (Table 4.25). Diopside phenocrysts in basalt samples from Shahrbabak also have a very restricted compositional range but are relatively enriched in the ferrosilite component and depleted in enstatite and wollastonite compared to the same rock type from the Islamic Peninsula (Fig. 4.3).

The mean core and rim compositions for diopside phenocrysts in trachyandesite from the Islamic Peninsula are indistinguishable within the limits of analytical uncertainty (Table 4.26). Similarly, the average core and rim compositions for diopside from basaltic trachyandesite from Aghda are indistinguishable (Table 4.27) but differ from the Islamic Peninsula samples in having lower contents of enstatite and wollastonite and higher contents of ferrosilite (Fig. 4.4). In addition, the Aghda samples have higher average contents of Al_2O_3, TiO_2 and FeO compared with diopside in trachyandesite from the Islamic Peninsula.

Analysed diopside grains from the three study areas are characterised by a decrease in MgO, CaO and SiO_2, and an increase in FeO, TiO_2 and Al_2O_3 from core to rim (e.g. Tables 4.20, 4.21, 4.28; Fig. 4.18). This variation records normal composition zoning. In addition, diopside phenocrysts in tephritic rocks from the Islamic Peninsula show oscillatory zoning in thin section (Fig. C). Both types of zoning indicate that complete chemical equilibrium was not reached during crystallisation, and reflect the conditions

of rapid cooling during volcanic crystallisation (Embey-Isztin et al., 1993; Dobosi and Fodor, 1992). Oscillatory zoning in pyroxene phases is probably related to alternating periods of growth, dissolution, reaction and lack of growth; all of which can reflect changes in bulk liquid composition, temperature and pressure (Pearce and Kolisink, 1990; Reeder et al., 1990).

In most of the diopside phenocrysts from tephrite and phonotephrite, SiO_2 content decreases with increasing Al_2O_3 and TiO_2 (e.g. Tables 4.21, 4.26, 4.28). This behaviour in basaltic rocks may reflect the influence of two concurrent factors: an increase of silica activity and a decrease of pressure during crystallisation (Kushiro, 1969; Thompson, 1974).

4.5.2 K-feldspar

Sanidine is the only K-feldspar present in samples from the Islamic Peninsula, Aghda and Shahrbabak (Fig. 4.19) and it is a major constituent of trachyandesite, trachyte, phonotephrite and tephriphonolite samples from these three areas. The sanidine phenocrysts from the Islamic Peninsula, Aghda and Shahrbabak have compositions of $Or_{62.8\text{-}72.9}$, $Or_{74.6\text{-}98.1}$ and $Or_{31.5\text{-}92.9}$ respectively (Tables 4.30 to 4.35).

Spherulite intergrowth of quartz and sanidine occurs in some samples (e.g. R14504, R14467). It seems that in these rocks the composition closely approximates that of an eutectic mixture of quartz and sanidine (Shelley, 1993), so that the intergrowth can be attributed to simultaneous crystallisation of these two minerals.

The amount of TiO_2 (0.00-0.15) and MgO (0.00-1.77) in the all samples from the three

study areas is very low, while FeO ranges from 0.00 to 1.99 percent. CaO is usually less than 2% but it is greater in the basaltic rocks (Table 4.33). With an increase in SiO_2 in sanidine phenocrysts the amount of K_2O increases except in tephriphonolite (Table 4.32). Sanidine grains in the phonotephrite and basaltic trachyandesite from Aghda have higher contents of Al_2O_3 than sanidine in the other rock types.

The average contents of Al_2O_3, TiO_2, FeO and Na_2O are higher in the sanidine phenocrysts in basaltic trachyandesite and trachyandesite from Aghda and the Islamic Peninsula compared with phenocrysts in trachyandesite from Shahrbabak, while K_2O is lower (Tables 4.30, 4.34, 4.35). The K-feldspar phenocrysts in the trachyandesite and basaltic trachyandesite from the study areas are sanidine in composition, and phenocryst composition range from $Or_{56.3}$ to $Or_{92.9}$ (Tables 4.30, 4.34, 4.35; Fig. 4.5). However trachyandesite and basaltic rocks of the Shahrbabak area contain both the lowest and highest average content of anorthite compared with other samples (Tables 4.33, 4.35).

The compositions of sanidine phenocrysts in tephriphonolite from Aghda and Shahrbabak are similar but the content of K_2O in sanidine phenocrysts from Aghda is higher than in the phenocrysts from Shahrbabak. Furthermore, sanidine phenocrysts in phonotephrite from Aghda have lower contents of alkalis and higher contents of Al_2O_3 than the tephriphonolite (Tables 4.31, 4.32, 4.36). The sanidine phenocrysts have a compositional range of $Or_{62.7}$ to $Or_{98.1}$ in tephriphonolite and phonotephrite (Fig. 4.20). The high-potassic sanidine crystals are associated with the high-calcic plagioclase in the tephriphonolite from Shahrbabak, and the most-sodic sanidine crystals coexist with the most-calcic plagioclase in the basalt from Shahrbabak (Tables 4.33, 4.36, 4.37, 4.38; Figs. 4.10, 4.11). Sanidine in basalt from Shahrbabak has the highest anorthite and

lowest orthoclase contents of the analysed K-feldspars from the study areas (Fig. 4.11).

4.5.3 Plagioclase

Plagioclase is the most and second most abundant phase in rocks from the Shahrbabak and Aghda regions respectively. The mean compositions of plagioclase grains in each rock type are shown in Tables 4.37 to 4.45. Most plagioclase phenocrysts from the Aghda and Shahrbabak regions have Ca-rich cores and more Na-rich rims (Fig. 4.21), which is attributed to normal magmatic fractionation. Most plagioclase crystals show an increase in Na_2O and a decrease in Al_2O_3 with increasing SiO_2 content (e.g. Tables 4.37, 4.39, 4.41; Fig. 4.22). Plagioclase phenocrysts in some samples (e.g. R14488) are commonly rimmed by sanidine. This mantling of plagioclase by sanidine may occur due to a shift in composition and temperature of the magma in either the magma chamber or during ascent from the chamber to the surface.

Some plagioclase phenocrysts in the Aghda region and most phenocrysts in the Shahrbabak region show minor normal compositional zoning with the exception of plagioclase in the trachybasalt (R15809) and dacite (R15811) from Shahrbabak, which show oscillatory zoning in thin section. These oscillatory-zoned grains have a wide compositional range from cores of $An_{36.8}$ to rims of $An_{18.7}$ and cores of $An_{31.5}$ to rims $An_{22.1}$ respectively (Appendix C). Zoning in plagioclase is indicative of failure of the mineral to attain equilibrium with the surrounding liquid and is normally attributed to change in temperature and pressure either within the magma chamber or during ascent from the chamber to the vent (e.g. McBirney, 1979). Oscillatory zoning in plagioclase is hiatal or episodic in nature. It is probably due to pulses of growth alternating with periods of dissolution, reaction or lack of growth (possibly very slow growth). The

growth is therefore periodic but discontinuous (Pearce and Kolisnik, 1990; Singer et al., 1995).

The composition of plagioclase phenocrysts in tephriphonolite and phonotephrite from Shahrbabak and Aghda range from labradorite to bytownite, but some samples of tephriphonolite from Aghda and Shahrbabak contain albitised grains (Tables 4.37, 4.39, 4.41; Fig. 4.23). Plagioclase phenocrysts in tephriphonolite from Aghda are more sodic than the phenocrysts from Shahrbabak, and the average content of albite in phenocryst rims is higher than in the cores. In addition, average compositions of plagioclase in phonotephrite are generally richer in the anorthite and orthoclase components than in tephriphonolite (Tables 4.37, 4.39, 4.41). The compositions of core and rim of plagioclase phenocrysts in tephriphonolite from Aghda are similar but the rims are slightly richer in albite (Table 4.39). Plagioclase phenocrysts in tephriphonolite are less calcic than those in phonotephrite and basaltic trachyandesite from the Aghda region (Tables 4.39, 4.41, 4.42; Figs 4.24, 4.25). Plagioclase phenocrysts in tephriphonolite from all study areas, however, have more sodic rims than plagioclase in all other rock types (Tables 4.37, 4.39).

Compositionally the plagioclase phenocrysts in basaltic trachyandesite from Aghda range from oligoclase to labradorite, and are similar in composition to the phenocrysts in trachyandesite from Shahrbabak (Fig. 4.26). Moreover, the plagioclase phenocrysts in trachyandesite from Shahrbabak are relatively enriched in Al_2O_3, CaO and FeO compared with plagioclase in basaltic trachyandesite from Aghda (Tables 4.42, 4.43). Plagioclase cores in basaltic trachyandesite from Aghda show a wide range in composition (Table 4.42) and a decrease in CaO from the core towards the rim is

accompanied by an increase in K_2O (Table 4.42).

Plagioclase crystals in basalt and trachybasalt from Shahrbabak range from oligoclase to bytownite in composition (Fig. 4.13). Cores of plagioclase phenocrysts in basalt have a small compositional range compared with phenocrysts in trachybasalt but the phenocrysts differ markedly in composition between the two rock types (Tables 4.38, 4.44). The average compositions of plagioclase in trachyte and dacite from Shahrbabak are shown in Tables 4.40 and 4.45 respectively. Compositions of cores and rims of plagioclase phenocrysts in dacite do not show any appreciable variation and have a overall range from oligoclase to andesine (Fig. 4.15). The average contents of TiO_2, Al_2O_3, FeO and Na_2O, however, are slightly higher in trachyte than dacite.

4.5.4 Olivine

In the present study, olivine has not been found in rocks from the Aghda region. In the Islamic Peninsula and Shahrbabak areas, it usually occurs as equant grains with a resorbed rim and irregular curved fractures. Some olivine phenocrysts are fresh, especially those from the Shahrbabak region, but many crystals are partially altered along fractures and around grain margins.

Analysed olivine crystals from the Islamic Peninsula and Shahrbabak are unzoned. Both core and rim compositions for olivine in tephrite from the Islamic Peninsula are $Fo_{84.8}$ and $Fo_{84.0}$ respectively (Table 4.46). In the Shahrbabak area the average core and rim compositions for olivine in trachybasalt are $Fo_{85.6}$ and $Fo_{85.1}$ respectively, and the average core and rim compositions in basalt are $Fo_{72.1}$ and $Fo_{72.0}$ respectively (Tables 4.47, 4.48). All olivine analyses are plotted in Figure 4.27, as $Mg/Mg+Fe^{2+}$

versus the atomic proportion per formula unit of Mn. The olivine crystals show a considerable range of $Mg/Mg+Fe^{2+}$ values between 0.72 and 0.86. The $Mg/Mg+Fe^{2+}$ ratio for trachybasalt (Shahrbabak) and tephrite (Islamic Peninsula) is higher than for basalt from Shahrbabak. The CaO content in olivine crystals from both areas is >0.1% which is typical of the composition of olivine phenocrysts from silica undersaturated lavas (Marcelot and Rancon, 1988). The olivine grains have low contents of TiO_2, Al_2O_3, Cr_2O_3 and NiO, but some substitution of CaO for MgO, and MnO for FeO has occurred. Collectively, all the olivine grains from the studied rocks are similar in composition to olivine from the leucite basanites of West Germany (Duda, 1975) and Kharsareh massif in Iran (Leterrior, 1985).

Roeder and Emsile (1970) determined experimentally that at 1 Kb total pressure for basaltic liquids, the distribution coefficient (Kd) for the Fe/Mg partition between olivine and coexisting liquid is 0.3. Nicholls (1974), however, suggested that under high pressure hydrous conditions the value of Kd may be approximately 0.4. The Mg-number of the liquid in equilibrium with the olivine has been calculated on the basis of the analysed olivine composition and Roeder and Emsile's equation. Similarly, the Mg-number of the host whole-rock sample has been calculated and the two Mg-numbers can be compared to determine whether the olivine phenocrysts in samples from the Islamic Peninsula and Shahrbabak regions are in equilibrium with their host rocks. The Mg-number of the olivine has been calculated assuming that all Fe is present as Fe^{2+} whereas the calculation for whole-rock samples assumes that FeO is either 0.8 or 0.9 times total Fe as FeO. Results of these calculations using Kd values of 0.3 and 0.4 are listed in Tables 4.49 and 4.50. The calculated Mg-numbers for the three whole-rock samples and liquid in equilibrium with the analysed olivine show the closest

correspondence when a Kd value of 0.4 is used (Tables 4.49 and 4.50). This suggests that the olivine phenocrysts crystallised at high pressure.

4.5.5 Biotite

Biotite is the second most common mafic mineral in trachyandesite, trachyte and dacite from the Islamic Peninsula and Shahrbabak. Most of the biotite crystals are fresh. The absence of significant alteration is supported by the relatively high K_2O contents (Tables 4.51 to 4.53). Some grains, however, show slight alteration along grain boundaries and cleavage traces, and some grains are surrounded by a rim of granular Fe-Ti oxide.

Chemical data for biotite from the Islamic Peninsula and Shahrbabak have a restricted range of values of $Mg/Mg+Fe^{2+}$ with all analyses except two plotting as biotite ($Mg/Mg+Fe^{2+}$ <0.67; Deer et al., 1966). The exceptions are mica in trachyandesite (R14698) from the Islamic Peninsula and trachyte from Shahrbabak which plot as phlogopite (Fig. 4.28). All Fe has been assumed to be FeO in the calculation because Fe_2O_3 cannot be determined on the electron microprobe; the amount of Fe present as ferric iron is considered to be negligible.

The average compositions of biotite phenocrysts in trachyte and dacite from Shahrbabak are similar and have an essentially constant content of Al_2O_3 (Tables 4.51, 4.52; Fig. 4.28), but the Al_2O_3 content of biotite in trachyandesite from the Islamic Peninsula increases as FeO increases (Table 4.53; Fig. 4.29).

Biotite is accompanied by hornblende in most samples, except in trachyandesite from

the Islamic Peninsula which contains abundant diopside. The absence of hornblende in trachyandesite probably reflects the relatively dry condition of this magma. Biotite phenocrysts in the trachyandesite from the Islamic Peninsula are compositionally similar to biotites in the calcalkaline magma from Northern Territory, Australia (Sheppard, 1995).

4.5.6 Titanomagnetite

Titanomagnetite is very common as scattered, equant grains in all the studied samples, but it is generally more abundant in the mafic than the felsic rocks. It is clearly an early crystallising phase, commonly being included in phenocrysts, particularly in mafic minerals. In some instances grain edges are rounded, probably indicating resorption. In general, the Fe-Ti oxide crystals are relatively Ti-rich and are classified as titanomagnetite except those in trachyte and trachyandesite from Shahrbabak which have low (<3%) TiO_2 contents (Tables 4.54, 4.55) and which are classified as magnetite.

Titanomagnetite grains in tephrite from the Islamic Peninsula have higher SiO_2, FeO and TiO_2 and lower Al_2O_3 and MgO than grains in the basalt and phonotephrite (Tables 4.56, 4.57, 4.58). Also titanomagnetite grains in phonotephrite appear to be chemically homogenous (Table 4.58). Titanomagnetite in trachyandesite from the Islamic Peninsula contains considerably lower amounts of TiO_2 and MgO, and higher FeO contents compared with titanomagnetite grains in all other rocks from this area (Tables 4.56 to 4.59). Titanomagnetite grains from Aghda and Shahrbabak are richer in TiO_2 than samples from the Islamic Peninsula (Tables 4.54 to 4.66). Also titanomagnetite in basaltic trachyandesite from Aghda contains higher SiO_2 and CaO,

and lower FeO and Al_2O_3 contents compared with the titanomagnetite grains in tephriphonolite and phonotephrite (Tables 4.61, 4.62, 4.63). Titanomagnetite grains in trachybasalt from Shahrbabak and phonotephrite from the Islamic Peninsula have the highest MgO contents compared with all other samples (Tables 4.54 to 4.66). The chemical data which are summarised in Tables 4.57 and 4.65, show that the compositions of the titanomagnetite in the basaltic rocks from the Islamic Peninsula and Shahrbabak are different to each other. In particular, titanomagnetite grains from Shahrbabak which are slightly altered to hematite contain higher SiO_2 and Al_2O_3 than unaltered grains from the Islamic Peninsula.

The average contents of SiO_2, Al_2O_3, MgO and CaO are greater and TiO_2 and MnO are lower in titanomagnetite grains from tephriphonolite from Aghda compared with the crystals in tephriphonolite from Shahrbabak (Tables 4.62, 4.66). Magnetite phenocrysts in trachyte from Shahrbabak tend to be lower in MnO and TiO_2 and higher in Al_2O_3, MgO and FeO compared with grains in dacite from this area (Tables 4.54, 4.60). Titanomagnetite grains in tephrite and tephriphonolite from all study areas are compositionally similar to titanomagnetite crystals in the tephrite and phonotephrite from eastern Paraguay (Chiaramonti et al., 1992) and the Roman province, Italy (Cundari, 1979).

4.5.7 Amphibole

Amphibole occurs only in the high-K calcalkaline rocks (Section 4.4) such as trachyte and dacite from the Shahrbabak region. Green to brown prismatic phenocrysts of amphibole are the dominant mafic mineral in the trachyte and dacite from this region. Iron titanium oxides are the only common inclusions in these amphibole grains.

Chemical data and formulae listed in Tables 4.67 and 4.68 show that the amphibole grains are magnesio-hornblende on the basis of the classification of Leak (1978).

All the amphibole crystals are calcic with (Ca+Na)>1.34 and Na<0.67 (Leak, 1978) and they have characteristically low contents of Al (Al_2O_3 = 7.38 to 10.41 wt%) and relatively high contents of Mg (MgO = 12.70 to 14.67 wt%). The average content of SiO_2 in most of the amphibole phenocrysts is low (<47%), and the average content of Na_2O is higher than K_2O (Tables 4.67, 4.68). Furthermore, the average content of Al_2O_3 in magnesio-hornblende from dacite is slightly higher than in amphibole from trachyte, but the MgO content is lower (Tables 4.67, 4.68). The CaO contents of amphibole crystals do not show significant variation from trachyte to dacite (Tables 4.67 and 4.68). This accords with the observation of Cawthorn (1976) that the CaO content of amphibole appears to be insensitive to the CaO content of the magma.

Fractionation factors for MgO, FeO and TiO_2 in amphibole were determined by dividing each of the oxide concentrations in the mineral by that in the whole rock (Cawthorn, 1976). The MgO fractionation factor for amphibole grains in igneous rocks ranges from approximately 2 for high temperature magmas (1000°C) to 10 at lower temperatures (800°C; Cawthorn, 1976). The calculated fractionation factor for magnesio-hornblende from the Shahrbabak region ranges from 9.7 to 13.4, indicating that crystallisation occurred at a lower temperature. Similarly, Cawthorn (1976) determined a range of 2 to 6 for the FeO fractionation factor at lower temperatures. This fractionation factor for amphibole from the Shahrbabak region ranges from 3.5 to 4.9, again being consistent with lower temperature crystallisation.

The TiO_2 fractionation factor for amphibole is pressure dependant and decreases from a value of 5-10 for extrusive rocks, to 1-5 for rocks crystallised at crustal pressures (Cawthorn, 1976). Because the fractionation factor of TiO_2 in amphibole grains from the Shahrbabak region ranges from 2.6 to 4.1, these grains probably crystallised within a subsurface magma chamber or during ascent from the chamber to the surface.

Some amphibole phenocrysts from the study areas are characterised by reaction rims of Fe-Ti oxides (e.g. R14699), and in a few instances (e.g. R14526), grains have been replaced by a granular aggregate of Fe-Ti oxides. Many investigations have noted that hydroxyl hornblende decomposition occurs under conditions of rapid cooling at low pressure, such as those conditions prevailing during eruption (e.g. Luher and Carmichael, 1980).

4.5.8 Leucite

Leucite is a characteristic mineral of K-rich, SiO_2-poor lavas. At high temperatures it has cubic symmetry, but during cooling it reversibly changes to a tetragonal form and develops complex twinning (Lange et al., 1986). In the U-DVB leucite phenocrysts are only abundant in the rocks of the Islamic Peninsula. Leucite is the second-most abundant phase in the rocks of the Islamic Peninsula, and the most common felsic mineral in tephrite from this region.

The composition of the leucite phenocrysts in tephrite and phonotephrite are shown in Tables 4.69 and 4.70. The Na_2O content in leucite phenocrysts from tephrite and phonotephrite is low and may be attributed to volatilisation of the element during microprobe analysis utilising a finely focused beam and a wavelength dispersive

system. The average content of FeO in leucite from tephrite is slightly more than in phonotephrite (Tables 4.69, 4.70). The contents of MgO, MnO and CaO in leucite phenocrysts from tephrite and phonotephrite are negligible. In the north of the study area the rims of some leucite grains have been changed to nepheline (e.g. R14447, Appendix C). Coexisting nepheline and leucite have been reported from basanitic lavas in Kenya (Brown and Carmichael, 1969). In some samples from the Agh-Gonbad Valley exchange of Na and K atoms and breakdown of the leucite structure occurred by reaction between leucite crystals and sodium-rich liquid to produce analcime pseudomorphs after leucite (e.g. R14464).

Leucite in the Islamic Peninsula is characterised by having structural formulae in which the numbers of Si ions is either 1 or 2. At low temperature, the structure of leucite is based on a three-dimensional interconnected tetrahedral framework with three crystallographically distinct tetrahedral sites (Mazzi et al., 1976), but it becomes metrically cubic near 650°C through a series of structural phase transitions (Lange et al., 1986; Phillips and Kirkpatric, 1994). The role of ordering of Si and Al over these three sites in the structural phase transitions that occur at elevated temperatures has recently been studied by Dove et al. (1993) and Kohn et al. (1995). Most analysed leucites are nearly stoichiometric except two analyses (Nos 38 and 39 from sample R14447), which have a cation deficiency with Si/Al<2. Similar non-stoichiometric analyses of leucite have been reported by Marcelot and Rancon (1988) and Vankooten (1980).

Although most of the leucite compositions are nearly stoichiometric with the total number of ions 4 (Appendix C), the sum of Si plus Al is <3 which allows Fe^{3+} to fill

vacancies in the tetrahedral structural sites. This phenomenon is known to characterise crystallisation of leucite from alkaline magma (Mitchell and Bergman, 1991, cited in Hassanzadeh, 1993). The ratio Si/Al in leucite crystals from the Islamic Peninsula is between 2.03 and 2.06 which is characteristic of leucite from many lavas (e.g. Birch, 1978).

Leucite phenocrysts in tephrite and phonotephrite from the Islamic Peninsula are compositionally similar to the leucite crystals from Viruga Range, Rwanda (Marcelot and Rancon, 1988) and West Kimberly, Australia (Carmichael, 1967). Compared with leucite crystals from Roccamonfina, Italy (Gupta and Fyfe, 1975), the Islamic Peninsula leucites have higher K_2O and lower Na_2O and total Fe as FeO.

4.6 SUMMARY

In general, Miocene rocks of the Islamic Peninsula are similar in mineralogy and texture. In hand specimen they are dark to grey, and are porphyritic with either a holocrystalline or cryptocrystalline groundmass. Primary minerals in all samples comprise diopside, sanidine, leucite, biotite, titanomagnetite and accessory apatite. Diopside, leucite and sanidine are the dominant phenocrystic phases. In holocrystalline samples, the phenocrysts are set in a fine-grained groundmass of diopside, sanidine, leucite, biotite and titanomagnetite.

In the Aghda region all rock types except tephriphonolite have a similar texture and mineralogy. Tephriphonolite is distinguished by the occurrence of abundant (commonly 40% by volume), large trapezohedra of analcime and pumpellyite. In hand specimen all rock types are grey, brown or black in colour and are porphyritic with a holocrystalline

groundmass. Major primary minerals comprise sanidine, pyroxene, plagioclase, titanomagnetite and accessory apatite and zircon. Sanidine and plagioclase are the most abundant phenocrystic phases. Diopside is pale-yellowish in colour and occurs as both as phenocrysts and in the groundmass; most phenocrysts show zoning, and some have corroded margins.

Six of the seven different rock types which occur in the Shahrbabak region have common textural and mineralogical characteristics. The exception is the tephriphonolite which contains abundant (up to 30%), large trapezohedra of analcime. All samples are porphyritic with a holocrystalline groundmass. The mineralogy of all samples comprises plagioclase, sanidine, pyroxene, analcime, hornblende, biotite, olivine, and titanomagnetite, together with accessory apatite and zircon. Hornblende phenocrysts in trachyte and trachyandesite are fresh and green to brown in colour. Quartz phenocrysts in samples of dacite are embayed as a result of resorption. Plagioclase is the dominant felsic mineral in most rock types, and in some samples phenocrysts are rimmed by sanidine. Normal and oscillatory zoning are common, as is albite and Carlsbad twinning and alteration to sericite. Pyroxene occurs as phenocrysts and also in the groundmass.

Diopside is the only pyroxene present in samples from all three study areas. In most diopside crystals the average content of MgO is higher in the core than the rim whereas the average FeO content is lower in the core than the rim. This variation is consistent with normal fractionation during magmatic evolution. Most of the diopside phenocrysts from the study areas show normal zoning, except phenocrysts in tephritic rocks from the Islamic Peninsula which show oscillatory zoning.

The K-feldspar phenocrysts from the Islamic Peninsula, Aghda and Shahrbabak have a compositions of $Or_{62.8-72.9}$, $Or_{74.6-98.1}$ and $Or_{31.5-92.9}$ respectively. The amount of TiO_2 and MgO in all sanidine crystals from study areas is very low, while FeO ranges from 0.20 to 0.86 percent.

Most plagioclase phenocrysts from the Aghda and Shahrbabak regions have Ca-rich cores and more Na-rich rims, which is attributed to normal magmatic fractionation. The composition of plagioclase phenocrysts range from labradorite to bytownite (in tephriphonolite and phonotephrite), from oligoclase to labradorite (in basaltic trachyandesite and trachyandesite), from oligoclase to bytownite (in basalt and trachybasalt), and from oligoclase to andesine (in trachyte and dacite).

Analysed olivine crystals from the Islamic Peninsula and Shahrbabak are unzoned. The olivine grains have low contents of TiO_2, Al_2O_3, Cr_2O_3 and NiO, but some substitution of CaO for MgO, and MnO for FeO has occurred. The calculated Mg-numbers for the three whole-rock samples and liquid in equilibrium with the analysed olivine show the closest correspondence when a Kd value of 0.4 is used. This suggests that the olivine phenocrysts crystallised at high pressure.

Most of the biotite crystals from the Islamic Peninsula and Shahrbabak are fresh. The absence of significant alteration is supported by the relatively high K_2O content. Chemical data for biotite from the Islamic Peninsula and Shahrbabak have a restricted range of values of $Mg/Mg+Fe^{2+}$ with all analyses except two plotting as biotite and the exceptions are phlogopite.

In general, the Fe-Ti oxide crystals are relatively Ti-rich and are classified as titanomagnetite except those in trachyte and trachyandesite from Shahrbabak which have low (<3%) TiO_2 contents and which are classified as magnetite.

Amphibole occurs only in the high-K calcalkaline rocks such as trachyte and dacite from the Shahrbabak region. Chemical data show that the amphibole grains are magnesio-hornblende. All the amphiboles are calcic and they have characteristically low contents of Al and relatively high contents of Mg.

In the U-DVB leucite phenocrysts are only abundant in the rocks of the Islamic Peninsula. The rims of some leucite grains have been changed to nepheline and some of phenocrysts have been pseudomorphed by analcime.

CHAPTER 5

ORIGIN OF LARGE TRAPEZOHEDRA OF ANALCIME AND PUMPELLYITE

5.1 INTRODUCTION

Analcime is a cubic, hydrated Na-aluminosilicate which is widespread in nature but most commonly is produced during low grade metamorphism and late stage hydrothermal activity in basaltic and related rocks. It occurs in veins, cavities, as a replacement of other silicate phases and is commonly interstitial in habit. Large crystals are rare but euhedral trapezohedra up to several centimetres in size have been recorded from Alberta (Pearce, 1970, 1993), Mocambique (Woolley and Symes, 1976) and northwest Iran (Comin-Chiaramonti et al., 1979). At these localities the analcime crystals occur in alkali-rich undersaturated igneous rocks variously described as blairmorite, analcimite and phonolite.

Pumpellyite is a monoclinic, hydrated Ca-aluminosilicate which is an index mineral for the recognition of facies in low-grade metamorphism and is also produced during hydrothermal alteration. It commonly occurs as fine-grained aggregates in metamorphosed and altered basaltic and intermediate lavas and volcaniclastic units where it pseudomorphously replaces primary mineral phases and glass, and also forms veins and cavity infillings.

Analcime and pumpellyite co-exist in some mafic igneous and related rocks which have undergone low grade metamorphism or hydrothermal alteration. In the U-DVB analcime crystals are common in tephriphonolite from Aghda and Shahrbabak but are

rare in lavas from the Islamic Peninsula. In addition, pumpellyite is common in the Aghda region but absent from the Islamic Peninsula and Shahrbabak. Due to the common occurrence in the Aghda region of spectacular large euhedral trapezohedra which are now composed of either analcime or pumpellyite, a detailed study was undertaken to describe their occurrence, chemistry and origin. Representative analyses of analcime, pumpellyite and mineral inclusions in the trapezohedra from Aghda are presented in Tables 5.1 to 5.3.

5.2 OCCURRENCE

The trapezohedra occur in an Eocene sequence of lavas and very minor pyroclastic units which occur approximately 45 km southwest of Aghda (Fig. 3.3). The units are mainly phonolite, tephriphonolite, basaltic trachyandesite and trachyte in composition. In addition to variable proportions of the primary igneous phases comprising K-feldspar, plagioclase, clinopyroxene, nepheline, Fe-Ti oxide, biotite, olivine and apatite, the sequence contains a variety of secondary minerals including pumpellyite, prehnite, analcime, zeolites, epidote, calcite, chlorite, sericite, kaolinite and hydrated products after olivine. Low grade metamorphism of the igneous units has been attributed to greenschist facies conditions (Amidi, 1975) but the common occurrence of analcime is indicative of zeolite facies conditions.

Large (up to 3 cm in diameter) euhedral crystals of pumpellyite and analcime occur in three, stratigraphically adjacent tephriphonolite lavas that can be traced for approximately 10 km along strike. The lowermost lava has a maximum thickness of 20 m and is characterised by the presence of large greenish-grey crystals of pumpellyite. The middle unit (1 m thick) and the upper lava (15 m thick) contain large

brownish-grey crystals of analcime. Large pumpellyite crystals are restricted to the lower flow and large analcime crystals are restricted to the middle and upper flows. Both pumpellyite and analcime crystals display a euhedral, cubic trapezohedral form (Fig. 5.1).

Analcime trapezohedra are optically continuous, implying that they are single crystals. The pumpellyite trapezohedra, however, are composed mainly of an aggregate of randomly arranged, colourless, pumpellyite flakes up to 0.25 mm long, but most grains are <0.05 mm in size. A few small patches of colourless prehnite also occur. Both types of trapezohedra contain abundant plagioclase laths up to 2 mm long which are arranged in a well-developed concentric pattern (Fig. 5.2), together with common, randomly distributed pyroxene, Fe-Ti oxide and apatite inclusions. The identity of all phases was confirmed by X-ray diffraction and electron microprobe analysis. X-ray diffraction data from a polished section through the centre of an analcime trapezohedron (Fig. 5.2) confirm that it is a single crystal.

5.3 MINERAL CHEMISTRY

Compositions of the pumpellyite grains from Aghda are typical of pumpellyites from low-grade metamorphic facies (Lucchetti et al., 1990) but, compared to many other occurrences, the variations at Aghda appear to be large for the small areas involved. Within a single trapezohedron MgO and total Fe as FeO range from <0.09 to 3.05% and 2.19 to 12.08% respectively (Table 5.2). The correlation between total Fe as FeO and the sum of Al_2O_3 and MgO (Fig. 5.3) indicates that compositional variations are principally related to Fe-Al and Fe-Mg substitution. Larger grains of pumpellyite appear to have lower contents of total Fe as FeO compared to smaller grains. Plots of

contents of Al_2O_3, total Fe as FeO and MgO versus distance from the rim of a large trapezohedron show no simple correlation between composition and position (Fig. 5.4). Variation in CaO which ranges from 21.44 to 22.86% is minimal and within the limits of analytical uncertainty (Table 5.2).

Prehnite is relatively rare in the trapezohedra and the main chemical variation relates to minor Fe-Al substitution. The compositions are typical of prehnite produced during hydrothermal alteration and low-grade metamorphic facies (Bevins and Merriman, 1988). All plagioclase inclusions in the pumpellyite trapezohedra have been altered to albite (Table 5.2). Precipitation of native-copper in parts of the Aghda volcanic sequence is consistent with hydrothermal activity in this region.

The analcime trapezohedra are remarkably homogeneous (Tables 5.1) with chemical variation being within analytical uncertainty associated with electron microprobe analysis. In contrast to the albitised plagioclase inclusions in the pumpellyite trapezohedra, feldspar inclusions in analcime are fresh with very minor normal zoning and range between $An_{56.0}$ and $An_{69.3}$ in composition. Core compositions of plagioclase inclusions show no correlation with position in the trapezohedra (Fig. 5.5). Pyroxene grains are relatively fresh diopside with low contents of Na_2O and the Fe-Ti oxide phase is titanomagnetite (Table 5.3).

5.4 ORIGIN OF THE TRAPEZOHEDRA

Analogous large trapezohedra composed of analcime have been recorded from Alberta (Pearce, 1970), Mocambique (Woolley and Symes, 1976) and northwest Iran (Comin-Chiaramonti et al., 1979) but similar occurrences of pumpellyite have not been recorded

in the literature. The primary or secondary origin of large analcime crystals in igneous rocks has been the topic of debate for a considerable time and is discussed in more detail below. The secondary origin of the pumpellyite is less equivocal.

Pumpellyite is a metamorphic or alteration mineral which commonly replaces glass, plagioclase, pyroxene, olivine, hornblende and biotite, and also forms veins and cavity infillings. It has monoclinic symmetry and characteristically forms with a fibrous habit (Deer et al., 1986), and in many cases pseudomorphously replaces primary mineral phases. Depending on the whole-rock composition, fluid pressure and oxygen fugacity the upper stability limit for pumpellyite is approximately 375°C (see Deer et al., 1986 for review). In the Aghda area the pumpellyite clearly originated by pseudomorphous replacement of a precursor which had an euhedral cubic trapezohedral crystal form. In addition, the high modal content (up to approximately 40%) of the pseudomorphous pumpellyite trapezohedra requires that the precursor is a common mineral in undersaturated, alkali-rich volcanic rocks. On the basis of the trapezohedral crystal form and occurrence in rocks of this type, potential precursors are garnet, leucite and analcime.

Although garnet is reasonably common in igneous rocks, particularly alkaline types where Ti-rich andradite (melanite) is developed (Deer et al., 1982), it is a very unlikely precursor for the pumpellyite crystals. Melanite garnet is unaltered and shows no evidence of resorption in phonolites from the Crowsnest Formation of Alberta (Pearce, 1970; Dingwell and Brearley, 1985). These rocks are compositionally very similar to the tephriphonolites from Aghda and have been subjected to zeolite facies metamorphism (Ferguson and Edgar, 1978). The stability of garnet at Crowsnest and

other localities where rocks of similar composition occur and have undergone similar styles of metamorphism implies that garnet, if developed, would also be stable at Aghda. In addition, the trapezohedral crystal form of the pseudomorphs at Aghda is not consistent with melanite (or andradite) being the precursor. The melanite at Crowsnest forms dodecahedra (Pearce, 1970; Dingwell and Brearley, 1985) which is the preferred habit for ugrandite series garnets such as andradite rather than members of the pyralspite series which crystallise as trapzohedra (Kostov, 1968). The whole-rock geochemistry of the tephriphonolite from Aghda (Table 6.8) also precludes the former occurrence of appreciable Ti-garnet. Elemental mobility during conditions of low grade metamorphism is a well documented and widespread phenomenon but Ti is generally considered to be relatively immobile during this style of alteration (e.g. Crawford et al., 1992). The low TiO_2 contents (<0.56) in the tephriphonolites from Aghda are inconsistent with the former occurrence of significant amounts of any Ti-bearing phase.

Because many of the data relevant to consideration of leucite as being the precursor mineral also impinge on the origin of the large analcime trapezohedra, these two potential precursors will be considered concurrently. Leucite and its alteration products comprising analcime, nepheline, alkali feldspars, muscovite, biotite and carbonates commonly occur in undersaturated, K-rich volcanic rocks. The most spectacular crystals consist of large (several cm) euhedral trapezohedra now composed of analcime but which are interpreted as having originated by pseudomorphous replacement of leucite (Karlsson and Clayton, 1991). The origin of small analcime trapezohedra which occur in igneous rocks in veins, cavities and as replacement of glass is widely accepted as being due to low grade metamorphism or hydrothermal processes but the large crystals have been interpreted both as primary phases which have crystallised from a silicate

melt and as pseudomorphs after leucite formed by ion-exchange reactions. The major arguments based on petrography, geochemistry and experimental data both for and against the primary origin of these large crystals have been presented and discussed in recent papers by Karlsson and Clayton (1991; 1993), Pearce (1970; 1993) and Line et al. (1995).

A major feature in support of a secondary origin of large analcime crystals in igneous rocks is the very restricted, high range of pressure (5-12 Kbar P_{H2O}) and temperature (600-660°C) for analcime stability in simplified synthetic systems (see Karlsson and Clayton, 1991). In addition, the transformation of leucite to analcime has been demonstrated experimentally and proceeds very rapidly at a subsolidus temperature either during cooling (Taylor and MacKenzie, 1975) or after the host magma solidification (Gupta and Fyfe, 1975). The analcime-rich lavas from the Aghda area contain only minute amounts of an unequivocally primary hydrous phase (biotite), and lack evidence for rapid transport of crystals from the depths indicated by the stability field for analcime. In addition, primary crystallisation of a Na-rich phase such as analcime would necessitate crystallisation of a sodic pyroxene rather than diopside. The homogenous nature of the large, single analcime crystals is also more consistent with a secondary origin rather than formation by magmatic crystallisation.

The large analcime trapezohedra are interpreted as having formed by ion-exchange pseudomorphous replacement of primary leucite either during cooling or shortly afterwards. The ease, rapidity and selectivity of the replacement process are evidenced by the lack of effect on the other phases included in analcime. This replacement of leucite by analcime presumably occurred in all three phonolite lavas, with subsequent

metamorphic replacement of analcime by pumpellyite in the lower unit. Formation of analcime as an intermediate phase rather than direct replacement of primary leucite by pumpellyite is envisaged due to the apparent ease and rapidity of analcime replacement of leucite. The preferential replacement of analcime by pumpellyite in a specific phonolite lava may reflect differences in permeability.

In the lower phonolite lava the sources of Ca, Fe and Mg ions required for the development of pumpellyite were the plagioclase, pyroxene and titanomagnetite which occur as fresh inclusions in the analcime trapezohedra but which are replaced or extensively altered in the pumpellyite trapezohedra. The variable chemistry of the pumpellyite grains within a single trapezohedron reflects the distribution of these inclusions. In particular, the variability in the content of total Fe as FeO in the pumpellyite grains reflects the scattered nature of small granules of Fe-Ti oxide inclusions in analcime. The relatively small variation in Al_2O_3 content may reflect an essentially homogeneous input from the precursor analcime coupled with a variable input from the albitisation of plagioclase.

5.4.1 Metamorphic conditions

The common occurrence of analcime at Aghda is indicative of zeolite facies conditions rather than greenschist facies metamorphism as has been suggested previously (Amidi, 1975). Important variables involved in the development of the alteration assemblages include temperature (T), load pressure (P_{total}), fluid pressure (P_{fluid}), fluid composition, f_{O2}, permeability and host-rock chemistry. In the Aghda area the juxtaposition of the three tephriphonolite lavas and close similarity in bulk-rock compositions, clearly demonstrate that the development of pumpellyite rather than analcime or vice versa was

not determined by temperature, load pressure related to burial nor to the whole-rock composition of the host lavas. The most important variables in determining the composition and identity of the pseudomorphous replacement mineral at Aghda appear to have been fluid chemistry and P_{fluid}. This conclusion is consistent with the findings of several earlier studies of low grade metamorphism and hydrothermal alteration of mafic and intermediate volcanic successions. Differences in the fluid composition can produce marked effects on the compositions of alteration minerals, even on the scale of an individual phenocryst (Evarts and Schiffman, 1983). Compositional variations of a mineral species at the scale of a contiguous flow, or even the scale of a thin section, show that the intensity of alteration was spatially uneven depending on rock permeability (Aguirre and Atherton, 1987). In a study of the hydrothermal alteration effects associated with intrusion of dolerites into a Proterozoic sequence, AlDahan (1986) concluded that the common occurrence of pumpellyite in intruded basalts but very restricted development in intruded clastic units was not controlled by the composition of the host rocks but was related to fluid composition and P_{fluid}. Several recent studies have clearly demonstrated that not only the composition of individual minerals but also the stability relationships in P-T space are strongly dependent on the fluid composition, particularly the content of CO_2 (Starkey and Frost, 1990; Digel and Ghent, 1994).

In the Aghda tephriphonolites the occurrence of prehnite is indicative of f_{CO2} <0.002 (Digel and Ghent, 1994). The presence of pumpellyite and absence of epidote may be related to conditions of low f_{CO2} and activity of H_2O and probably high P_{fluid} (= $P_{lithostatic}$) which favour the formation of pumpellyite relative to epidote (Liou, 1979). The development of pumpellyite in preference to epidote also indicates that the fluid

composition was relatively reducing rather than oxidising (Metcalfe et al., 1992). The replacement of leucite by analcime presumably occurred either during cooling or shortly afterwards and was related to ion-exchange reactions. In the lowermost tephriphonolite, however, the analcime became unstable and was replaced by pumpellyite. The fine grained nature of the pumpellyite is typical of natural pumpellyite grains which usually form microcrystalline aggregates during replacement of primary phases under zeolite facies conditions (Schiffman and Liou, 1983). The variable chemistry of the pumpellyite grains within a single trapezohedron reflects the distribution of these inclusions. In particular, the variability in the content of total Fe as FeO in the pumpellyite grains reflects the scattered nature of small granules of Fe-Ti oxide inclusions in analcime. The relatively small variation in Al_2O_3 content may reflect an essentially homogeneous input from the precursor analcime coupled with a variable input from the albitisation of plagioclase. The chemical variability in the pumpellyite grains from Aghda supports the contention that alteration is heterogeneous even on the scale of an individual phenocryst as has been suggested in earlier studies of low grade metamorphism (Evarts and Schiffman, 1983).

5.5 SUMMARY

Large (up to 3 cm in diameter), euhedral, cubic trapezohedra composed of single crystals of analcime or aggregates of pumpellyite occur in three stratigraphically adjacent tephriphonolite lavas from the Aghda region. Large pumpellyite crystals are restricted to the lower flow and analcime is restricted to the middle and upper flows. The trapezohedra contain concentrically arranged inclusions of plagioclase, pyroxene, titanomagnetite and apatite. In contrast to the albitised plagioclase inclusions in the pumpellyite trapezohedra, feldspar inclusions in analcime are fresh with very minor

normal zoning and range between $An_{56.0}$ and $An_{69.3}$ in composition.

The analcime crystals are remarkably homogeneous in composition, contain only minute amounts of a hydrous phase (biotite), and lack evidence for rapid transport of crystals from the depths indicated by the stability field for analcime. In addition, primary crystallisation of a Na-rich phase such as analcime would necessitate crystallisation of a sodic pyroxene rather than diopside. The analcime is interpreted as having formed by ion-exchange pseudomorphous replacement of primary leucite, either during cooling of the lavas or shortly afterwards.

The pumpellyite trapezohedra are composed mainly of an aggregate of randomly arranged colourless pumpellyite flakes which are compositionally typical of pumpellyite produce during low-grade metamorphism. In the lower tephriphonolite lava, the analcime became unstable and was replaced by pumpellyite which has a wide range in compositions related to Fe-Al and Fe-Mg substitution. The wide range in compositions reflects the variable input of Fe, Mg, Ca and Al from the precursor analcime and alteration of plagioclase, clinopyroxene and Fe-Ti oxide. The occurrence of analcime and pumpellyite at Aghda is indicative of zeolite facies and may be related to conditions of low f_{CO_2} and H_2O activity and probably high P_{fluid}.

CHAPTER 6

TOTAL-ROCK GEOCHEMISTRY

6.1 INTRODUCTION

In the present study, representative samples of different rock types from the Islamic Peninsula, Aghda and Shahrbabak have been analysed for major and trace elements, using X-ray fluorescence spectrometry. Rare Earth Elements (REE), Hf, Sc, Ta, Th and U concentrations in 18 samples were determined by instrumental neutron activation analysis (INAA), and strontium and neodymium isotopic ratios for the same 18 samples were measured by mass spectrometry. The Sr and Nd isotopic and REE data presented in this thesis are the first isotopic and REE data reported for the volcanic and subvolcanic rocks in the study areas. All analytical methods are listed in Appendix A.

Chemical data and CIPW norms for individual samples are listed in Appendices D, E. Mean composition, elemental ratios, the Differentiation Index (DI) and Mg number (Mg#) for each rock type in the three study areas are presented in Tables 6.1 to 6.24. In this thesis geochemical data are used for rock classification, in the construction of variation diagrams, in comparisons with experimentally determined rock compositions where conditions of formation are known, and to identify the tectonic setting during emplacement.

6.2 ISLAMIC PENINSULA

Based on the TAS scheme the analysed samples from the Islamic Peninsula comprise 12 tephrites, three phonotephrites, one basalt, two trachyandesites and one trachyte

(Fig 6.1). Most of the tephrite and phonotephrite samples have high K_2O (>3.60 wt%), MgO (>6 wt%) and K_2O/Na_2O ratios (>2) and can be classified as ultrapotassic (Foley et al., 1987). The relatively low K_2O/Na_2O ratios (<2) in other tephrite and phonotephrite samples (e.g. R14455, R14464) are due to the conversion of leucite to secondary analcime in these samples (section 5.4).

The mean and range of major and trace element contents in each rock type from the Islamic Peninsula are summarised in Tables 6.1 to 6.6. These rocks are **ultrabasic to intermediate in composition and are characterised by being undersaturated in SiO_2, with low average contents of Al_2O_3 (12.18 wt%) and TiO_2 (1.16 wt%), and high contents of CaO (10.61 wt%) and K_2O (5.30 wt%). The rocks are enriched in the incompatible elements K, Rb, Sr, Ba, Th, Nd and Light REE (LREE). The compatible elements Cr and Ni are relatively low in abundance (Table 6.6).

6.2.1 Major elements

Major element results are expressed as weight percent of the ten elements traditionally listed as oxides in a major element chemical analyses. The chemical features of the Islamic Peninsula rocks are illustrated in more detail by compositional histograms (Fig. 6.2) and have been plotted on MgO diagrams (Fig. 6.3). The MgO plot is the most appropriate for rock series which include abundant mafic members (Rollison, 1993).

The content of SiO_2 has a broad range between tephrite (43.54 wt%) and trachyte (58.02 wt%) (Tables 6.1, 6.5). Figure 6.2 shows that the SiO_2 distribution emphasises the abundance of tephrite and phonotephrite samples in the Islamic Peninsula. The

compositional histogram in Figure 6.2 shows that TiO_2 values are commonly between 0.70 and 1.2 wt%, but up to 1.4 wt% over the sample set. The frequency increase at higher TiO_2 contents reflects the abundance of tephrite and phonotephrite samples. Figure 6.3 shows that the TiO_2 content increases from basalt towards tephrite and phonotephrite then at ~5% MgO decreases to trachyandesite and trachyte, reflecting the higher modal abundance of titanomagnetite in tephrite and phonotephrite rocks (Tables 4.1, 4.4). High TiO_2 contents (1.06-1.37) in tephrite and phonotephrite lavas are unusual compared to typical arc magmas (<1% TiO_2). The content of Al_2O_3 in the Islamic Peninsula rocks are relatively low and variable (Table 6.6; Fig. 6.2) and are lower in the mafic than the felsic rocks. The Al_2O_3 content exhibits an increasing frequency until ~12 wt% then decreases at higher Al_2O_3 values (Fig. 6.2). In Figure 6.3 Al_2O_3 shows a positive correlation with MgO, which reflects an increase in modal K-feldspar from mafic to felsic rock types (Tables 4.1 to 4.5). Tephrite and phonotephrite have the highest contents of total iron as Fe_2O_3 of all analysed samples from the Islamic Peninsula (Tables 6.1 to 6.5). In Figure 6.2 total iron as Fe_2O_3 content shows an increasing frequency towards higher total iron as Fe_2O_3 until 9 wt% then decreases. The content of total iron as Fe_2O_3 decreases from mafic to felsic rocks which may be related to crystal fractionation of clinopyroxene and olivine (Tables 4.1 to 4.5; Fig. 6.3; Feely et al., 1993). Basalt has the highest content of MgO compared with all other samples from the Islamic Peninsula (Tables 6.1 to 6.5). The MgO content ranges from 2.30 to 14.33 wt%, with variable distribution (Table 6.6; Fig. 6.2) which are comparable with MgO contents for Vulsini and Roccamonfina lavas, Italy (Rogers et al., 1985). The CaO contents are dominated by values between 10 and 13 wt%, and have a broad range between 3.5 and 15 wt% (Fig. 6.2). Figure 6.3 shows that CaO content has a negative correlation with MgO, which is probably related to crystal

fractionation of clinopyroxene and plagioclase (Cox, 1980). However, tephrites have higher MgO, CaO and Fe_2O_3 but lower SiO_2, Al_2O_3 and K_2O than phonotephrites (Tables 6.1, 6.2). The unusually high CaO/Al_2O_3 value (1.9) in the basaltic dike from the Islamic Peninsula reflect clinopyroxene accumulation by flow differention which is consistent with petrographic evidence (Table 4.3). The average content of Na_2O in trachyandesite is higher than in all the other rocks from the Islamic Peninsula (Tables 6.1 to 6.5). The Na_2O content has an almost symmetrical distribution with a maximum frequency between 2.20 and 2.40 wt% (Fig. 6.2). The increase in K_2O content from trachyandesite to trachyte is probably related to the higher abundance of sanidine in trachyte from the Islamic Peninsula (Table 4.4, 4.5). Figure 6.2 shows that K_2O contents have a large variations from tephrite to trachyte (1.63 to 7.98 wt%; Tables 6.1 to 6.5), probably related to variability of leucite, K-feldspar and biotite in different rock types from the Islamic Peninsula (Tables 4.1 to 4.5). The K_2O enrichment is accompanied by enrichment of other LFSE, including Rb (44-380 ppm), and Ba (2380-4800 ppm). The Na_2O and K_2O contents show an inverse correlation with MgO, but with considerable scatter in data which could be related to the variation in leucite content in different rock types and presence of secondary analcime in some samples (Fig 6.3). The average content of P_2O_5 decreases from basalt (1.14 wt%) to trachyte (0.39 wt%; Tables 6.1, 6.5) and P_2O_5 show a variable distribution, dominated by values between 1.1 and 1.8 wt% (Fig. 6.2). The content of P_2O_5 shows an increases from basalt towards the tephrite and phonotephrite then at 6.5% MgO decreases to trachyandesite and trachyte, these changes may be related to the higher abundance of apatite in tephrite (Tables 4.1 to 4.4).

Mg-numbers decrease from basalt (80.96) to trachyte (47.95), while the DI increases

from basalt (22.85) to trachyte (77.32; Tables 6.3, 6.5). The majority of Mg-numbers range between 55 and 75 (Fig. 6.4). Basaltic dyke (R14457) with a Mg-number of 80.96, MgO = 14.33 wt% and high Ni (153 ppm) and Cr (650 ppm) values can be regarded as being close to a primary magma (Frey et al., 1978; Clague and Frey, 1982). Most of the Islamic Peninsula lavas have a Mg-number less than 74 and must have suffered some differentiation. The Mg-number in tephrite is lower than the basalt from the Islamic Peninsula (Table 6.1, 6.3).

6.2.2 Incompatible elements

Trace elements usually represent concentration of less than 1000 ppm in the analysed rocks from the Islamic Peninsula, with the only exceptions being Ba and Sr.

Incompatible trace elements of Tertiary rocks from the Islamic Peninsula, normalised to Mid-Ocean Ridge Basalt (MORB), using the normalising values of Pearce (1983) are ploted in Figure 6.5. They show most elements, especially Ba, Th, Nb and Ce, are significantly enriched in the Islamic Peninsula rocks compared to MORB (Fig. 6.5). All patterns show an overall relative enrichment with increasing incompatibility from right (Yb) towards left (Ba) on the plot, with negative anomalies for Rb, K, Ta and Ti. Except for Ti and P the anomalies are much stronger for the basalt than the other rock types. Contents of Zr and Hf in the trachyandesite are higher than in the other samples. The patterns for all rock types are almost parallel, implying their cogenetic nature.

6.2.2.1 Low Field Strength Elements (LFSE)

Tephrite samples from the Islamic Peninsula have the widest range of Sr between 835 and 1980 ppm (Table 6.1). The Sr content in the phonotephrites ranges from 1060 to

1410 ppm (Table 6.2), and in the trachyandesites from 1370 to 1570 ppm (Table 6.4). The content of Sr increases from basalt towards thephrite and phonotephrite, then remains the same through the trachyandesite and trachyte (Fig. 6.6) this is probably related to the basalt being relatively primitive (section 6.2.1).

The average content of Rb ranges between 44 and 269 ppm from basalt to trachyte (Tables 6.3, 6.5). The K/Rb ratio has been used by many authors (e.g. Shaw, 1968; Jakes and white, 1970; Bose et al., 1982) as an indicator of fractionation in igneous systems. Rubidium and K have similar chemical properties and similar ionic radii. As a result of this close association, the K/Rb ratio is restricted in most common igneous rock types and is usually constant in each rock type as the fractionation evolves.

The K/Rb ratio for each rock type from the Islamic Peninsula is listed in Tables 6.1 to 6.6. Two samples of tephrites (R14455, R14464) are excluded due to conversion of leucite to secondary analcime in these samples. The content of Rb in biotite is very high resulting in a low K/Rb ratio for this mineral (Ewart and Griffin, 1994). If biotite is removed from the system, the residual liquid will increase in the K/Rb ratio. In contrast, K-feldspar has a high K/Rb ratio and if it is removed from the system, the K/Rb ratio will decrease (Jakes and White, 1970). The average content of the K/Rb ratio in tephrite is lower (K/Rb = 178) than the phonotephrite (K/Rb = 252) in the Islamic Peninsula. This increase are possibly related to fractional crystallisation of biotite (Nelson, 1992) and higher abundance of K-feldspar in phonotephrite (Tables 4.1, 4.2). Rubidium shows no good correlation with MgO possibly depending on the variability of biotite, leucite and K-feldspar in different rock types from the Islamic Peninsula and conversion of leucite to analcime in some samples (Fig. 6.6). For

example, basalt (R14457) with the lowest content of Rb has the lowest modal content of leucite and lacks sanidine, also some of the leucite in this sample changed to analcime. Whereas, the tephrite (R14444) with the highest Rb contains the highest modal content of sanidine (Appendix B).

6.2.2.2 High Field Strength Elements (HFSE)

Yttrium ranges between 25 and 44 ppm for different rock types from the Islamic Peninsula (Table 6.6; Fig. 6.6). The content of Y in tephrite is higher than the values for trachyandesite rocks in the Islamic Peninsula (Tables 6.1, 6.4). High contents of Y in tephrite are probably related to the higher modal abundance of clinopyroxene and apatite in tephrite (Tables 4.1, 4.4). Yttrium plotted against MgO shows an increases from basalt towards the tephrite and phonotephrite rocks, then at ~6.5% MgO decreases to the trachyandesite and trachyte rocks. These changes probably related to the higher abundance of clinopyroxene and apatite in tephrite and phonotephrite (Hack et al., 1994; Fig. 6.6).

The average content of Th is high in the rocks from the Islamic Peninsula (Tables 6.1 to 6.5; Fig. 6.6). Thorium is generally accepted as the most incompatible element in an open system and it is also relatively insensitive to hydrothermal alteration processes (Caroff et al., 1993). Trachyte with the highest Th contents is also higher in SiO_2, Zr and Nb and lower in CaO than all other analysed samples (Tables 6.1 to 6.5). In the Islamic Peninsula the content of Th increases from basalt to trachyte (Tables 6.1 to 6.5; Fig. 6.6). High content of Th reflects the presence of abundant zircon and titanite in trachyte from the Islamic Peninsula (Table 4.5).

Niobium has a range from 22 to 92 ppm and is generally higher in the felsic rocks (Tables 6.3, 6.5). The average contents of Nb in tephrite and phonotephrite is from 34 to 36 ppm in the Islamic Peninsula (Table 6.1, 6.2). Tephrites have the greatest range of Nb (23-48) compared with all other samples from the Islamic Peninsula (Table 6.1 to 6.5). The Zr/Nb ratio decreases from mafic to felsic rocks in the Islamic Peninsula (Tables 6.1 to 6.5). The decreasing Zr/Nb from mafic to felsic indicates Nb is better able to enter into tetrahedral coordination in silicate systems than Zr and is thus preferentially retained in residual liquids (Wyborn, 1983). Figure 6.6 shows that Nb content increases from mafic towards the felsic rocks probably related to the higher modal biotite in felsic rocks (Tables 4.1 to 4.4).

The content of Zr is relatively high in the Islamic Peninsula rocks and it ranges from 236 ppm in the basalt to 845 ppm in the trachyte (Tables 6.3, 6.5). Zirconium shows negative correlation with MgO (Fig. 6.6). The Zr/Hf ratio decreases from 53 in the tephrite to less than 41 in the trachyandesite, which may be related to higher partition coefficient of Zr in clinopyroxene than the Hf, so that the mafic rocks have a higher Zr/Hf ratio than the felsic rocks in the Islamic Peninsula (Tables 6.1, 6.4; Wyborn, 1983).

In trachyandesite samples some trace elements have a relatively restricted range; Nb (51-56 ppm), Y (27-28 ppm), Ce (132-135 ppm) and Th (46-47 ppm) (Table 6.4). With the exception of Yb, Sc, Cr, U and Lu the average content of all analysed trace elements in the tephrite is higher than the average value for the basalt (Tables 6.1, 6.3).

6.2.2.3 Rare Earth Elements

The REE comprise a group of 15 trace elements with atomic numbers from 57 (La) to 71 (Lu). The REE with lower atomic numbers are referred to as the Light REE (LREE), those with higher atomic numbers as the Heavy REE (HREE), and those with intermediate atomic numbers as the Middle REE (MREE). All REE are trivalent except Eu and Ce under most geologic conditions.

The REE patterns for three tephrites, one phonotephrite, one basalt and one trachyandesite from the Islamic Peninsula are similar, although the abundances are variable (Fig. 6.7). All the samples are enriched in LREE and strongly fractionated (La_N/Yb_N values of 14.4 to 21.4) with moderate negative Eu anomalies for most of the samples ($Eu/Eu^* = 0.73$ to 0.80).

6.2.3 Compatible elements

The average contents of Ni in tephrite and phonotephrite are 49 and 36 respectively (Tables 6.1 and 6.2). Low Cr and Ni contents in these rocks indicate that they are not primary melts from mantle peridotite, but may be related to the fractionation of olivine and clinopyroxene (Wittke and Mack, 1993; Embey et al., 1993; Muller et al., 1993). However, despite the high MgO contents in the rocks of the Islamic Peninsula, they have relatively low average contents of Ni (47 ppm) and Cr (167 ppm; Table 6.6). Figure 6.6 shows that the contents of Ni and Cr decrease from basalt towards the trachyandesite and trachyte probably related to the higher modal olivine and clinopyroxene in basalt from the slamic Peninsula (Skulski et al., 1994; Green, 1994).

The contents of Sc and V from the Islamic Peninsula are plotted in Figure 6.6 as a

function of MgO content. Scandium has a positive correlation with MgO, as expected, because Sc is concentrated in pyroxenes (Tables 4.1 to 4.4). Figure 6.6 shows that V increases from basalt towards tephrite and phonotephrite then decreases at ~7.5% MgO to trachyandesite and trachyte. This decreases is probably related to the fractionation of titanomagnetite as V has a high partition coefficient for this mineral in mafic rocks (Tables 4.1 to 4.5; Rollinson, 1993). However, average content of V and Sc decrease from phonotephrite to trachyandesite (Tables 6.2 and 6.4; Fig. 6.6). This may be related to the higher modal clinopyroxene in phonotephrite (Peccerillo and Taylor, 1976). This is consistent with petrographic evidence (Tables 4.2 and 4.4).

6.2.4 Sr and Nd Isotopes

As shown in Table 6.7, the high-K alkaline rocks from the Islamic Peninsula have initial $^{87}Sr/^{86}Sr$ ratios of 0.70774 to 0.70848 and the ε_{Nd} values ranging from -4.7 to -3.3. The range of initial isotopic values for the analysed samples is significantly larger than the estimated 2σ analytical uncertainties which equal to ± 0.00005 and ± 0.5 for initial $^{87}Sr/^{86}Sr$ and ε_{Nd} units respectively. These uncertainties are considered to represent maximum values based on the 2σ uncertainties derived from replicate measurements of standards (Table 6.7) and other, non quantifiable variables (e.g. sample selection). The initial $^{87}Sr/^{86}Sr$ ratio for tephrite samples are from 0.70820 to 0.70848. Tephrite (R14447) has the higher initial $^{87}Sr/^{86}Sr$ ratio and lower ε_{Nd} than all the other rocks from the Islamic Peninsula (Table 6.7). The initial $^{87}Sr/^{86}Sr$ ratio of the trachyandesite (0.70800) is higher than the basalt and phonotephrite (0.70778 and 0.70774, respectively). This difference is not related to a simple fractionation processes.

6.3 AGHDA

The mean and range of compositions for representative samples from Aghda are listed in Tables 6.8 to 6.15. The plot of K_2O+Na_2O versus SiO_2 (TAS) shows that samples from Aghda comprise six tephriphonolites, one phonotephrite, one phonolite, six basaltic trachyandesites, one trachyandesites, two trachytes and two rhyolites (Fig. 6.8). These rocks are characterised by being oversaturated to undersaturated in silica, mafic to felsic in composition, high in Al_2O_3, CaO, alkalies and the incompatible elements Ba, Rb, Sr, Th, Zr, Nd and LREE, but low in TiO_2, MgO and compatible elements (Table 6.15).

6.3.1 Major elements

The chemical features of Aghda samples are illustrated by compositional histograms (Fig. 6.9) and Harker type variation diagrams (Fig. 6.10). The Harker diagrams show two distinct groups of rocks comprising a mafic-intermediate group with <60% SiO_2 and a felsic group with >60% SiO_2. Most of the analysed rocks from Aghda belong to the mafic-intermediate group which, on average, contains higher contents of TiO_2, Al_2O_3, Fe_2O_3, MgO, CaO, P_2O_5 and most of the incompatible elements than the felsic rocks (Tables 6.8 to 6.14).

The content of SiO_2 ranges from 49.81 in phonotephrite to 71.15 wt% in rhyolite (Tables 6.9, 6.14). Although there is a wide range of values for SiO_2, the distribution of SiO_2 contents emphasises the abundance of tephriphonolite, phonolite and basaltic trachyandesite (Fig. 6.9). Also there is probably a gap due to fractional crystallisation in the SiO_2 contents (58-64 wt%) between the two groups. Figure 6.9 shows that the TiO_2 content has an almost symmetrical distribution, is generally low and has a broad

range between 0.2 and 0.95 wt%. The content of TiO_2 decreases from mafic towards the felsic rocks with considerable scattering (Fig. 6.10) and reflects the higher modal content of titanomagnetite in mafic rocks (Tables 4.7 to 4.12; Seymour and Vlassopoulos, 1992). The content of Al_2O_3 ranges between 14.10 and 20.83 wt% (Table 6.15) and is higher in the rocks with lower SiO_2 content (53.08) than the rocks with higher SiO_2 content (71.15%). Tephriphonolite samples from Aghda have the highest contents of Al_2O_3 compared with all other samples, reflecting higher modal content analcime in this rock type (Tables 6.8 to 6.14; 4.7). Figure 6.9 shows that Al_2O_3 exhibits an increasing frequency towards the higher Al_2O_3 contents in samples from Aghda. The content of Al_2O_3 generally decreases from rocks with lower SiO_2 contents (49.81-51.13%) to rocks with higher SiO_2 contents (63.85-71.15%), although there is considerable scatter and a gap in the Al_2O_3 contents between the two groups, reflecting different modal content of analcime, plagioclase and K-feldspar in different rock types (Tables 4.6 to 4.12; Fig. 6.10). The average contents of total Fe as Fe_2O_3 and MgO are higher in basaltic trachyandesite than all other samples from Aghda (Tables 6.8 to 6.14). The compositional histogram in Figure 6.9 show that the Fe_2O_3 content is variable, but has a maximum frequency between 3.5 and 4 wt%. The content of MgO decreases from basaltic trachyandesite towards trachyandesite which may be related to crystal fractionation of clinopyroxene and olivine (Tables 4.9, 4.10). In felsic rocks, the content of MgO is essentially the same in both trachyte and rhyolite (Fig. 6.10). Figure 6.10 shows Fe_2O_3 content in basaltic trachyandesite is higher than the other samples, reflects the higher modal content of clinopyroxene in this rock (Tables 4.6 to 4.12). In felsic rocks, the content of Fe_2O_3 decreases from trachyte to rhyolite reflecting higher modal clinopyroxene and titanomagnetite in trachyte (Tables 4.11, 4.12). Rhyolite from Aghda is enriched in alkalis, and depleted in MgO,

total Fe as Fe_2O_3 and CaO (Table 6.14) relative to the more mafic rock types. The CaO content ranges from 0.54 in rhyolite to 8.02 wt% in basaltic trachyandesite (Tables 6.11, 6.14; Fig. 6.9). The content of CaO decreases from basaltic trachyandesite towards phonolite then increases to trachyandesite which may be related to the different modal content of plagioclase and clinopyroxene in mafic rocks (Tables 4.8 to 4.10). In felsic rocks the content of CaO in trachyte is higher than rhyolite reflecting higher modal clinopyroxene in trachyte (Tables 4.11, 4.12; Fig. 6.10). The K_2O has a greater range (1.80 to 9.82 wt%) than Na_2O (2.47-6.15 wt%) in the rocks from Aghda (Table 6.15). In Figure 6.9, K_2O shows a gradually increasing frequency until 5.5 wt%, then decreases towards the higher K_2O contents, whereas the maximum frequency for Na_2O is between 4 and 4.25 wt%, but most values have similar frequencies. In mafic rocks the content of K_2O in tephriphonolite and phonolite is higher than the other samples reflects the higher modal K-feldspar in these rocks (Figure 6.10; Tables 4.6 to 4.10). In felsic rocks the content of K_2O decreases from trachyte to rhyolite reflecting higher modal K-feldspar in trachyte (Tables 4.11, 4.12). In mafic rocks the content of Na_2O does not show any regular variation with SiO_2 probably depending on the variability of analcime and plagioclase in different rock types (Fig. 6.10). In felsic rocks, the content of Na_2O is essentially the same in both trachyte and rhyolite (Fig 6.10). Among the rocks with SiO_2 contents (<56%), phonolite has the lowest content of Na_2O, reflecting lower modal plagioclase in this rock type (Tables 4.6 to 4.10; Fig. 6.10). Phonotephrite has the highest content of P_2O_5 compared with all other samples from Aghda. The distribution of P_2O_5 is variable, with maximum frequency between 0.2 and 0.3 wt% (Fig. 6.9). The P_2O_5 content decreases from mafic to felsic rocks (Fig. 6.10) and reflects the higher abundance of apatite in the mafic rocks.

The range of Mg-numbers is between 16.2 and 52.6 (Table 6.15). The majority of samples have Mg-numbers less than 50; only three samples have Mg-numbers of more than 50 and the maximum frequency of values falls in the range of 48-50 (Fig. 6.11). The low Mg-numbers for mafic rocks from the Aghda region implies that these rocks do not represent primary, mantle derived melts.

6.3.2 Incompatible elements

Incompatible element contents of rocks from Aghda normalised to MORB are plotted on Figure 6.12. Spidergram patterns show most elements are significantly enriched in Aghda samples compared to MORB, while K, Ta, P and Ti show negative anomalies. These patterns show considerable similarity for the less incompatible elements (Zr, Yb and Ti). The morphology of the P-Ti sector of the spidergram for the felsic rocks shows a continuous increase from P to Zr then decrease towards the Hf and Ti (Fig. 6.12). Aghda spidergram patterns show enrichment from right towards left, except for P, Ti and Ba; depletion of Ba with respect to Rb for the acidic samples and this relationship is reversal for the mafic samples. The LFSE show considerable scatter, with no clear difference between the mafic and felsic group samples, which is probably related to the variability of K-feldspar, plagioclase, clinopyroxene and biotite abundances in different rock types from Aghda (Tables 4.6 to 4.12). The stronger negative P and Ti anomalies could reflect apatite and titanomagnetite removal. Enrichment of Zr and Hf is also stronger for the felsic group compared to the mafic group samples. Differences in the incompatible element patterns implies that rocks with SiO_2 contents (<59%) and rocks with SiO_2 contents (>66%) from the Aghda region are genetically unrelated (Fig. 6.12).

6.3.2.1 LFS Elements

Strontium ranges between 106 and 1340 ppm for rhyolite and phonotephrite respectively (Tables 6.9, 6.14). Trachyandesite has the widest range of Sr with between 448 and 1280 ppm (Table 6.12), and rhyolite has the lowest range of Sr between 106 and 166 ppm (Table 6.14). In tephriphonolite the range of Sr values is between 575 and 818 ppm (Table 6.8). The tephriphonolites have less Sr than the phonotephrites. This is probably due to plagioclase in phonotephrites being more calcic than in the tephriphonolites (Tables 4.39, 4.41). The low Sr in rhyolite from Aghda is related to lack of plagioclase (Table 4.12; Nash and Crecraft, 1985). Figure 6.13 shows Sr content decreases from phonoterphrite towards phonolite and trachyandesite probably related to the crystal fractionation of clinopyroxene (Tables 4.6, 4.10; Green, 1994). In felsic rocks the content of Sr remains constant in both trachyte and rhyolite.

Rubidium ranges between 35 and 385 ppm in basaltic trachyandesite and phonolite respectively (Tables 6.10, 6.11). In general, the content of Rb increases from basaltic trachyandesite towards the tephriphonolite and phonolite then decreases to trachyandesite, these changes possibly indicating different modal of K-feldspar and biotite in mafic rocks (Tables 4.6 to 4.10; Fig. 6.13; Ewart and Griffin, 1994). In felsic rocks the content of Rb decreases from trachyte to rhyolite reflecting higher modal K-feldspar in trachyte (Tables 4.11, 4.12; Fig. 6.13). Comparison of Figure 6.13 with Harker type diagrams for major elements (Fig. 6.10) show that Rb follows the trend of K_2O since K-rich minerals host this element.

6.3.2.2 HFS Elements

The content of Y in samples from Aghda is within the range of 8 to 34 ppm

(Table 6.13), and is higher in the felsic rocks than the mafic rocks (Fig. 6.13). High contents of Y normally reflect the presence of abundant apatite but this is not a plausible explanation for felsic rocks from Aghda, because neither the modal abundance of apatite nor the content of P_2O_5 is high in felsic rocks from this region. The other common minerals which readily accommodate Y are biotite and zircon (Ewart and Griffin, 1994), which are both more common in the Aghda rhyolite than the other rock types of the region (Tables 4.6 to 4.12).

Thorium ranges from 16 ppm in trachyandesite to 51 ppm in trachyte (Tables 6.12, 6.13), and is higher in the felsic rocks than the mafic rocks from Aghda (Tables 6.8 to 6.14). Figure 6.13 shows that Th increases from phonotephrite towards tephriphonolite then decreases to trachyandesite. These changes may be related to the different abundances of clinopyroxene and accessory minerals such as apatite and zircon in mafic rocks (Tables 4.6 to 4.12). In felsic rocks the content of Th in trachyte is higher than the rhyolite probably related to the presence of abundant clinopyroxene and apatite in trachyte (Green, 1994; Fig. 6.13).

Niobium ranges from a minimum of 6 ppm in trachyandesite up to 32 ppm in trachyte (Tables 6.12, 6.13). Figure 6.13 shows that Nb increases from phonotephrite towards the tephriphonolite then decreases to trachyandesite. These changes are probably related to the different abundances of clinopyroxene, titanomagnetite and biotite in mafic rocks (Tables 4.6 to 4.10; Pearce and Norry, 1979; Green, 1994). In felsic rocks the content of Nb decreases from trachyte to rhyolite reflecting higher modal titanomagnetite and clinopyroxene in trachyte (Tables 4.11, 4.12; Fig. 6.13).

Zirconium in Aghda volcanic rocks ranges in value between 118 and 490 ppm (Table 6.15). In Figure 6.13 the Zr content increases from phonotephrite towards the phonolite then decreases to trachyandesite may be related to the different abundances of clinopyroxene and titanomagnetite in mafic rocks (Tables 4.8, 4.10; Nielsen et al., 1994; Forsythe et al., 1994). The content of Zr in felsic rocks is higher than the mafic rocks, which can be regarded as the presence of abundant zircon in felsic rocks (Tables 4.6 to 4.12).

6.3.2.3 Rare Earth Elements

The REE concentrations for samples of trachyte, rhyolite, basaltic trachyandesite, phonotephrite and two samples of tephriphonolite from Aghda are plotted relative to chondrite in Figure 6.14. The ∑REE ranges from 139 to 216 ppm and some REE have a relatively restricted range (Table 6.15). All the analysed rocks are enriched in LREE, and show a high degree of fractionation (La_N/Yb_N values of 9.30 to 15.69) except trachyte and rhyolite. The main difference is that the trachyte and rhyolite have a flat MREE to HREE pattern, with strong negative Eu anomalies ($Eu/Eu^* = 0.37$-0.39), implying that these rocks are genetically unrelated to other rocks from Aghda (Fig. 6.14). Fractionation in mafic rocks (tephriphonolite, phonotephrite and basaltic trachyandesite) can be controlled by separation of clinopyroxene, apatite and plagioclase, because partition coeficient of REE in these minerals is high (Green, 1994).

6.3.3 Compatible elements

The contents of Ni, Cr and V in the basaltic trachyandesite are higher than the all other samples from Aghda (Tables 6.8 to 6.14). The Cr content has a wide range from 1

(rhyolite) to 96 ppm (basaltic trachyandesite; Tables 6.11, 6.14). In mafic rocks the contents of Cr and Ni do not show any regular variation reflecting different modal contents of clinopyroxene and olivine in different rock types from Aghda (Green, 1994; Skulski et al., 1994; Fig 6.13). In felsic rocks, the contents of Cr and Ni are the same in both trachyte and rhyolite (Fig. 6.13). The content of Sc decreases from basaltic trachyandesite and phonotephrite towards tephriphonolite reflecting the higher modal clinopyroxene and biotite in basaltic trachyandesite (Tables 4.6, 4.7, 4.9; Fig. 6.13). Figure 6.13 shows that V decreases from mafic towards felsic rocks, probably related to the higher modal titanomagnetite and clinopyroxene in mafic rocks (Tables 4.6 to 4.12). The mafic rocks from Aghda are very low in Ni (Table 6.15), and cannot represent primitive magmas (Wittk and Mack, 1993).

6.3.4 Sr and Nd Isotopes

The Tertiary rocks from Aghda show a wide range of initial $^{87}Sr/^{86}Sr$ values from 0.70651 to 0.70871 and the ε_{Nd} value ranges from -3.8 to -2.2 (Table 6.7). The range of initial isotopic values for the analysed samples is significantly larger than the estimated 2σ analytical uncertainties which equate to ± 0.00005 and ± 0.5 for initial $^{87}Sr/^{86}Sr$ and ε_{Nd} units respectively. A sample of trachyte (R14480) has the highest initial $^{87}Sr/^{86}Sr$ ratio (0.70871), and the lowest ε_{Nd} value (-3.8) for samples from the Aghda region. The Rocks with SiO_2 contents (63.85-71.15%) have a wide range of initial $^{87}Sr/^{86}Sr$ ratios (0.70718-0.708710). Figure 6.15 shows SiO_2 and Rb/Sr contents increase, conversely Sr decreases from rocks with lower SiO_2 contents (49.81-51.13%) to rocks with higher SiO_2 contents (63.85-71.15%). The overall positive correlation between initial $^{87}Sr/^{86}Sr$ ratio and SiO_2 from Aghda (Fig. 6.15) indicates that the proportion of the isotopically enriched end-member in the magma increased with

magmatic differentiation (Reiner et al., 1996). The initial $^{87}Sr/^{86}Sr$ ratio differences between rocks with different SiO_2 contents (49.81-71.15%) indicate that they are genetically unrelated. However, isotope variability in rocks with SiO_2 contents (49.81-51.13%) is not related to a simple fractionation processes, because the range of initial isotopic values is outside the range of analytical uncertainity.

6.4 SHAHRBABAK

Various features of the total-rock geochemistry of the Tertiary, mafic to felsic volcanic rocks from Shahrbabak are summarised in Tables 6.16 to 6.24. Based on the TAS classification (Fig. 6.16), the rocks analysed from Shahrbabak comprise two basalts, one trachybasalt, three basaltic trachyandesites, one phonotephrite, ten tephriphonolites, two trachyandesites, one trachyte and four dacites. Although there are some significant geochemical differences among the volcanic rocks from Shahrbabak, particularly in the abundances of alkalies and the degree of silica saturation. But there are some similarities including low Mg-numbers, TiO_2 and compatible elements, but high contents of Al_2O_3, CaO, and the incompatible elements, K, Ba, Sr, Rb, Th, Nd and LREE (Table 6.24).

6.4.1 Major elements

The compositional histograms and Harker type variation diagrams show the chemical features of the rocks from Shahrbabak (Figs. 6.17; 6.18). The Harker diagrams show three distinct groups of rocks comprising a group of rocks with <50% SiO_2, second group with 50-60% SiO_2, and third group with >60% SiO_2. Most of the analysed rocks from Shahrbabak belong to the mafic-intermediate group which, on average, contains higher contents of TiO_2, Fe_2O_3, MgO, CaO, Al_2O_3, P_2O_5 and incompatible elements and

lower TiO_2, Fe_2O_3, MgO and CaO than the felsic and mafic groups respectively (Tables 6.16 to 6.24).

In Figure 6.17 the SiO_2 distribution emphasises the abundance of intermediate rocks such as tephriphonolite, phonotephrite, basaltic trachyandesite and trachyandesite. Figure 6.18 shows the large variation in SiO_2 content from 47 wt% in basalt to 68 wt% in dacite. The content of TiO_2 has a broad range between 0.35 and 1.10 wt% and shows variable frequency (Fig 6.17). The TiO_2 content decreases from mafic to felsic rocks reflecting the higher modal titanomagnetite in mafic rocks (Tables 4.14 to 4.19; Fig. 6.18). The content of total Fe as Fe_2O_3 ranges from 1.99 in dacite to 11.22 wt% in basalt (Tables 6.18 to 6.23). Content of total Fe as Fe_2O_3 are dominated by values between 2.5 and 7.5 wt% (Fig. 6.17). Figure 6.18 shows that mafic rocks have the highest content of Fe_2O_3 compared with other rocks, reflecting the higher modal of olivine in these rocks (Tables 6.14 to 6.19). In mafic-intermediate rocks the decrease in Fe_2O_3 content from trachybasalt to trachyandesite is probably related to the crystal fractionation of olivine and titanomagnetite (Fig. 6.18; Tables 4.15, 4.17). In felsic rocks the content of Fe_2O_3 in trachyte is slightly higher than dacite. The content of Al_2O_3 is relatively high and variable (14.44 to 20.33 wt%; Table 6.24). The Al_2O_3 content exhibits an increasing frequency towards the maximum values of 19.4 wt%, then decreases for higher Al_2O_3 contents (Fig. 6.17). The Al_2O_3 content does not show any regular variation with SiO_2, but the content of Al_2O_3 is higher in tephriphonolite and phonotephrite than the other samples, and reflects the higher modal abundance of analcime and K-feldspar in these rocks (Table 4.13 to 4.19). Also, high abundances with scattered data for Al_2O_3 indicate probably feldspar accumulation as phenocrysts commonly observed in subduction related magma (Gill, 1981). The contents of CaO

and MgO are higher in the mafic than the felsic rocks from Shahrbabak (Tables 6.16 to 6.23). The high MgO value for trachybasalt is related to the higher modal olivine in this sample (Embey et al., 1993). Figure 6.17 shows MgO content gradual increases to a mode of 2 wt%, whereas CaO exhibits a variable distribution, with maximum frequency between 4 and 4.5 wt%. The content of MgO decreases from basalt and trachybasalt towards tephriphonolite and trachyandesite, reflecting the higher modal content of olivine and clinopyroxene in basalt and trachybasalt (Tables 4.13 to 4.17; Fig. 6.18). In felsic rocks the content of MgO in trachyte is slightly higher than the dacite. The content of CaO in basalt is higher than the other rocks probably related to the higher modal clinopyroxene in these rocks (Tables 4.13 to 4.17). In Figure 6.18 CaO content decreases from trachybasalt towards trachyandesite may be related to the crystal fractionation of plagioclase and clinopyroxene (Tables 4.14, 4.17) but few samples show higher CaO abundances for their SiO_2 levels and plot away from the general trend, which could be related to secondary processes owing to mobile nature of CaO. In felsic rocks, the content of CaO is the same in both trachyte and dacite except one sample of dacite (Fig. 6.18).

The average content of Na_2O is higher than K_2O in the rocks from Shahrbabak (Tables 6.24). The Na_2O content is dominated by values between 3.60 and 5.80 wt%, whereas K_2O shows a variable distribution (Fig. 6.17). Figure 6.18 shows that the content of K_2O in basalt is lower than the other rocks, reflecting the lower content of K-feldspar in these rocks. The K_2O content increases from trachybasalt towards the tephriphonolite then decreases to trachyandesite reflecting higher modal content of K-feldspar in tephriphonolite (Tables 4.13, 4.17). In felsic rocks the content of K_2O is essentially the same in both trachyte and dacite (Fig. 6.18). In Figure 6.18 Na_2O

content does not show any regular variation with SiO_2 (Tables 4.13 to 4.19). The content of P_2O_5 ranges from 0.14 and 0.56 wt% (Table 6.24) and has an almost symmetrical distribution. The average content of P_2O_5 in basic-intermediate group is higher than the other groups. In mafic-intermediate rocks the content of P_2O_5 decreases from trachybasalt towards tephriphonolite and trachyandesite, reflects the higher abundance of apatite in trachybasalt (Fig. 6.18).

The trachybasalt (R15812) shows the maximum Mg-number (71.90) for analysed samples from Shahrbabak. The majority of samples have Mg-numbers in the range of 34-50, and only two analyses have an Mg-number of more than 70 (Fig. 6.19). The low Mg-number, Cr and Ni contents in these mafic rocks preclude their being primary melts of mantle peridotite (Seymour and Vlassopoulos, 1992).

6.4.2 Incompatible elements

Incompatible element contents of samples from Shahrbabak normalised to MORB are plotted on Figure 6.20. Spidergram patterns show most elements are significantly enriched in the Shahrbabak samples compared to MORB, while K, Ta and Ti show negative anomalies except for basalt which has a negative anomaly for Ta only, and continuous increase in enrichment with increasing incompatibility from Yb to Ba on the plot. The patterns are similar for felsic and mafic rocks, but the negative anomaly for Ta is stronger for the basalt. The Th, Nb, Ce, Zr and Hf contents are high for the trachyandesite (R14528), relative to the other samples. Spidergram patterns show depleted Ti, Y and Yb in the felsic group compared to the mafic and mafic-intermediate groups. The patterns drawn for incompatible elements of three rock groups of Shahrbabak are not well parallel, implying they are not cogenetic.

6.4.2.1 LFS Elements

Shahrbabak rocks have a wide range of Sr contents between 410 and 1330 ppm for trachyandesite and trachybasalt respectively (Tables 6.20, 6.21). The average content of Sr in mafic group is lower than the other groups from Shahrbabak (Tables 6.16 to 6.23). In mafic-intermediate group the content of Sr decreases from trachybasalt towards the tephriphonolite and trachyandesite reflecting higher modal plagioclase in trachybasalt (Tables 4.13 to 4.17; Fig. 6.21). The removal of ferromagnesian minerals such as clinopyroxene resulted in the trachybasalt from Shahrbabak being enriched in the constituent of plagioclase (Hall, 1987). In felsic rocks, the content of Sr does not show any regular variation with SiO_2 (Fig. 6.21).

Rubidium ranges between 19 and 383 ppm for basalt and tephriphonolite respectively (Tables 6.16, 6.18). In mafic-intermediate rocks the Rb content increases from trachybasalt towards the tephriphonolite then decreases to trachyandesite reflecting higher modal K-feldspar in tephriphonolite (Tables 4.13, 4.17; Fig. 6.21). In felsic rocks the content of Rb is very similar in both trachyte and dacite (Fig. 6.21).

6.4.2.2 HFS Elements

Yttrium has a range from 7 to 33 ppm and is generally higher in the mafic than the felsic rocks (Tables 6.16 to 6.24). Dacites have the greatest range of Y (7-28 ppm) and trachyandesites have the highest content of Y compared with all other samples from Shahrbabak (Tables 6.16 to 6.23). The content of Y in basic group is lower than the mafic-intermediate group. In mafic-intermediate rocks the content of Y increases from trachybasalt towards the trachyandesite, and reflects the presence of apatite and zircon in trachyandesite (Lambert and Holland, 1974; Green 1994; Table 4.17). In felsic rocks

the content of Y remains the same from trachyte to dacite except one sample (R14526) of dacite, and reflects the higher abundance of zircon in this sample (Fig. 6.21).

The average content of Th ranges between 4 and 21 ppm from basalt to trachyandesite in Shahrbabak (Tables 6.18, 6.21). Trachyandesite has the highest value of Th compared with all other samples (Tables 6.16 to 6.23; Fig. 6.21). Thorium is significantly incorporated in apatite and zircon (Caroff et al., 1993). The mafic rocks have the lowest content of Th relative to other rocks, reflecting the absent of zircon in these rocks. In mafic-intermediate rocks the increase in Th from trachybasalt towards the trachyandesite is related to the presence of apatite and zircon in trachyandesite (Tables 4.13 to 4.17). In felsic rocks Th content increases from trachyte to dacite may be depending to the higher abundance of zircon in dacite (Fig. 6.21).

Niobium concentration is up to 15 ppm in different rock types of Shahrbabak and is highest in trachyandesite (Tables 6.16 to 6.23). Figure 6.21 shows that mafic rocks have the lowest content of Nb relative to other rocks may be related to absent of biotite and zircon in these rocks (Table 4.14). In mafic-intermediate rocks the increase in Nb content from phonotephrite towards trachyandesite probably related to the presence of zircon in trachyandesite (Pearce and Norry, 1979; Green, 1994). In felsic rocks Nb content does not show any regular variation with SiO_2, but the content of Nb in some samples of dacite is higher than trachyte and reflects the higher modal content of zircon in these samples (Fig. 6.21).

Trachyandesite and basalt from Shahrbabak have the highest (402 ppm) and the lowest (66 ppm) contents of Zr respectively (Tables 6.18, 6.21). The Zr/Hf ratio in

trachyandesite is higher than the dacite, and reflects the presence of abundant clinopyroxene and zircon in trachyandesite (Tables 6.21, 6.23, 4.17, 4.19). Also the increase in Zr content from trachybasalt towards the trachyandesite may be related to the presence of zircon in trachyandesite (Table 4.13 to 4.17; Fig. 6.21). In felsic rocks the content of Zr is very similar in both trachyte and dacite (Fig. 6.21).

6.4.2.3 Rare Earth Elements

The REE concentrations in two tephriphonolites, one basalt, one trachyandesite, one trachyte and one dacite are plotted relative to chondrites in Figure 6.22. The ∑REE content ranges from 75 to 157 ppm in the samples from Shahrbabak (Appendix D). The REE patterns for the tephriphonolites and the trachyandesite of Shahrbabak are similar except that the trachyandesite is more enriched in HREE. These rocks are strongly fractionated in LREE and have a flat MREE to HREE pattern (La_N/Yb_N values of 6.61 to 7.98), with moderate to strong negative Eu anomalies (Eu/Eu^* = 0.60 to 0.79). Negative Eu anomalies are normally interpreted as resulting from removal of plagioclase or may be due to increasing oxygen fugacity (Hanson, 1980). Basalt (R14550) is characterised by a lower enrichment in LREE compared with other samples and unfractionation for HREE (Fig. 6.22), with a La_N/Yb_N ratio of 5.43, implying that it is unrelated to the other rocks. Two samples of dacite and trachyte (R14512, R14699) display similar patterns and have the most fractionated REE pattern compared with other samples with La_N/Yb_N ratios between 21 and 32.51. These samples show a slight to moderate negative Eu anomaly (Eu/Eu^* = 0.78-0.86). However, these two samples appear to be genetically unrelated to other rocks from Shahrbabak. The high La_N/Yb_N ratios, suggest an important role for clinopyroxene in their formation, because partion coefficient of HREE are higher than the LREE in clinopyroxene (Green, 1994).

6.4.3 Compatible elements

The average contents of Cr, Ni, V and Sc decrease from mafic to felsic rocks in Shahrbabak (Tables 6.16 to 6.23). Most of the rocks from Shahrbabak have low Sc, Cr and Ni contents. The low Cr and Ni contents in the mafic and mafic-intermediate rocks of Shahrbabak may be attributed to olivine and clinopyroxene fractionation (Stolz et al., 1990). Trachybasalt has the highest average content of both Cr and Ni compared with other samples, reflecting the higher modal content of olivine in this rock (Table 6.16 to 6.23). The contents of V and Sc in mafic rocks is higher than the other rocks probably related to the high abundant of olivine and clinopyroxene in these rocks. In mafic-intermediate rocks the decrease in V content from trachybasalt towards tephriphonolite and trachyandesite may be related to the crystal fractionation of clinopyroxene, titanomagnetite and olivine (Tables 4.14, 4.17; Fig. 6.21). In felsic rocks the contents of Sc and V remain constant in both trachyte and dacite. The contents of Ni and Cr do not show any regular variation with SiO_2, but the contents of Ni and Cr in basalt, trachybasalt and one of the basaltic trachyandesite samples are higher than the other samples, and reflects the higher modal contents of olivine and clinopyroxene in these rocks (Tables 6.16 to 6.23; Fig. 6.21).

6.4.4 Sr and Nd Isotopes

The Tertiary rocks from Shahrbabak have initial $^{87}Sr/^{86}Sr$ ratios between 0.70427 and 0.70567 and the ε_{Nd} values range from +1.3 to +4.1 (Table 6.7). The range of initial isotopic values for the analysed samples is significantly larger than the estimated 2σ analytical uncertainties which equate to ±0.00005 and ±0.5 for initial $^{87}Sr/^{86}Sr$ and ε_{Nd} units respectively. The sample of tephriphonolite (R14522) has the highest initial $^{87}Sr/^{86}Sr$ ratio (0.70567), and the lowest ε_{Nd} (+1.3) compared for samples from the

Shahrbabak area. The acidic rocks (trachyte and dacite) have a restricted range of initial $^{87}Sr/^{86}Sr$ ratio (0.70427-70451) and trachyte (R14512) has the lowest initial $^{87}Sr/^{86}Sr$ ratio (0.70427) for the group. Figure 6.15 shows the relationship of the Sr isotopic data with SiO_2, Sr and Rb/Sr contents. The Sr isotopic data show a negative correlation from mafic to felsic rocks relative to SiO_2 (Fig. 6.15). Due to negative correlation of Sr isotopic value from mafic to felsic rocks of the Shahrbabak region, these rocks can not be genetically related. However, isotope variability in mafic rocks is not related to a simple fractionation processes, because the range of initial isotopic values is higher than the analytical uncertainty.

6.4.5 SUMMARY

The Islamic Peninsula rocks possess the characteristics of a typical high-K alkaline suite. These rocks are characterised by being undersaturated in SiO_2, with low average contents of Al_2O_3 and TiO_2, and high contents of CaO and K_2O. The rocks are enriched in the incompatible elements, but compatible elements are relatively low in abundance. The behaviour of different major and trace elements relative to MgO content, suggests that fractional crystallisation seems to be the main process involved in development of these rocks. Most of the Islamic Peninsula rocks have Low Mg-number, Cr, Ni and V contents and must have suffered some differentiation. Multi-element patterns for all rock types are almost parallel, implying their cogenetic nature. All the samples from the Islamic Peninsula are enriched in LREE and strongly fractionated with moderate negative Eu anomalies for most of the samples. Decreasing content of the trivalent ferromagnesian elements V and Sc from tephrite to trachyandesite suggests clinopyroxene fractionation. The high-K alkaline rocks from the Islamic Peninsula have initial $^{87}Sr/^{86}Sr$ ratios of 0.70774-0.70848 and the ε_{Nd} value ranging from -4.7 to -3.3.

This difference is not related to a simple fractionation processes, because the range of initial isotopic values is higher than the analytical uncertainty. The Aghda region contains are mostly of alkaline rocks. These rocks are characterised by being oversaturated to undersaturated in SiO_2, mafic to felsic in composition, high in Al_2O_3, CaO and alkalies and incompatible elements but low in TiO_2, MgO and compatible elements. The Harker diagrams show two distinct groups comprising mafic-intermediate and felsic rocks. The low Mg-number, Cr, Ni and V contents for mafic rocks from the Aghda region implies that these rocks do not represent primary mantle derived melts. Spidergram patterns show overall enrichment from Yb to Ba with negative anomalies in K, Ta, P and Ti. The REE patterns for samples of Aghda are all enriched in LREE and show a high degree of fractionation, except trachyte and rhyolite which are genetically unrelated to other rocks from Aghda. The Tertiary rocks of Aghda show a wide range of initial $^{87}Sr/^{86}Sr$ ratios and ε_{Nd} values. The differences in isotopic values between mafic and felsic groups indicate that these two groups are genetically unrelated. In mafic rocks the range of initial isotopic values is outside the range of analytical uncertainty then, they are not related to a simple fractionation processes.

The Tertiary volcanic rocks from Shahrbabak are characterised by being saturated to undersaturated in silica, mafic to felsic in composition and have some common features, such as low Mg-numbers, contents of TiO_2 and compatible elements and high Al_2O_3, CaO and incompatible element. Harker diagrams show three distinct groups comprising mafic, mafic-intermediate and the felsic rocks. The low Mg-number, Cr and Ni contents of the rocks from Shahrbabak preclude their being primary melts of mantle peridotite. Incompatible elements show a continuous increase in enrichment with increasing incompatibility from Yb to Ba. The REE patterns for tephriphonolite and

trachyandesite are similar. Trachyte and dacite display similar patterns and are genetically unrelated to other samples from Shahrbabak. The Tertiary rocks from Shahrbabak have initial $^{87}Sr/^{86}Sr$ ratios between 0.70427 and 0.70567 and the ε_{Nd} values from 1.3 to 4.1. Tephriphonolite has the highest initial ratio of $^{87}Sr/^{86}Sr$ and the lowest ε_{Nd} value of the samples from Shahrbabak. The variability in isotopic values, suggests that these three rock groups are genetically unrelated in the Shahrbabak region.

CHAPTER 7

MAGMATIC AFFINITIES

7.1 INTRODUCTION

The major magma series recognised in island arc systems and active continental margins comprise low-K (tholeiite), calcalkaline, high-K calcalkaline, shoshonitic and leucititic. The volcanic and plutonic rocks of active continental margins range in composition from basalt to rhyolite (Wilson, 1989). In the study areas, alkaline rocks are dominant and are usually associated with calcalkaline rocks particularly in the Aghda and Shahrbabak regions.

The chemical analyses of samples from the study areas have been plotted on the K_2O versus SiO_2 diagram with boundaries between low-K, calcalkaline, high-K calcalkaline and shoshonite suites from Peccerillo and Taylor (1976) and the boundary between shoshonite and leucititic suites from Wheller et al. (1987). Figure 7.1 shows that, for the Islamic Peninsula, all samples of tephrite and basalt except two (R14455, R14457) are leucititic in affinity. These two samples have relatively low K_2O and plot in the shoshonitic field because leucite phenocrysts have been replaced by analcime (section 5.4). Trachyandesite and trachyte samples also plot in the shoshonitic field. Figure 7.1 shows that about half of the samples from Aghda are shoshonitic while trachyandesite samples fall within the high-K calcalkaline field, and most of the tephriphonolite and phonolite plot in leucititic field. The analysed samples from Shahrbabak belong to four series comprising leucititic, shoshonitic, high-K calcalkaline, and calcalkaline rocks (Fig. 7.1).

7.2 TEPHRITE AND TEPHRIPHONOLITE OF LEUCITITIC SERIES

According to Washington (1927) the term leucitite was first proposed for a rock containing leucite and pyroxene (in equal amounts) with a small amount of nepheline. Leucite-bearing rocks, notably leucitite and leucite tephrite, form a rare group of alkaline mafic or ultramafic rocks (Marcelot and Rancon, 1988). As a felspathoid, it is restricted to rocks that are deficient in silica but enriched in K_2O. Leucite is not commonly found in nature and normally occurs either in sodium-poor phonolites or in mafic extrusions quenched from high temperature (Heaney and Veblen, 1990).

The leucititic series from the study areas are undersaturated in silica based on CIPW norm calculations (Fig. 7.2). Typically the U-DVB leucititic series have SiO_2 less than 50 wt%, SiO_2/K_2O lower than 9, and K_2O/Na_2O greater than 1 (Table 7.1). Other notable features of these rocks are high concentrations of some elements including Ba, Rb, Sr, Zr, Nb, La and Y (Table 7.2). These characteristics are similar to the leucite bearing rocks from Vulsini, Central Italy (Varekamp and Kalamarides, 1989). In the AFM diagram all samples plot in the alkaline field and have strong alkali enrichment in the most felsic samples (Fig. 7.3). In the Na_2O-K_2O-CaO ternary diagram (Fig. 7.4) the overall trend reflects the enrichment of K_2O over Na_2O in all samples. In the U-DVB the high alkali and low silica content of leucite-bearing rocks is reflected by the common occurrence of minerals such as leucite and nepheline.

7.3 SHOSHONITIC SERIES

The term shoshonite was originally coined for potassic orthoclase bearing basalt from Yellowstone Park, Wyoming, USA (Iddings, 1895). The geochemical characteristics of the shoshonitic rock association have been identified by various workers. Corrireau and

Gorton (1993) defined shoshonitic rocks as displaying strong enrichment in Al, Ca, K and LFSE relative to the HFSE and low Mg content characteristic of arc related magmas. Morrison (1980) stated that the high-K shoshonite lavas are usually associated with calcalkaline rocks along subduction zones at continent collision margins. Such rocks typically have high K_2O/Na_2O (>0.5), low iron enrichment, high Na_2O+K_2O (>5 wt%), high LFSE (e.g. K, Rb, Sr and Ba), high but variable Al_2O_3 (9-20 wt%) and generally low TiO_2 (Tables 7.3, 7.4). The characteristics identified by Morrison (1980) compared to the relevant data for rocks from the U-DVB are presented in Table 7.3. Most of the shoshonitic samples from studied rocks in the U-DVB are unsaturated in silica although a few samples from Aghda and Shahrbabak are saturated in respect to the CIPW norm (Fig. 7.5). Morrison (1980) noted that shoshonites are characterised by low-iron enrichment. This feature is also demonstrated in the U-DVB by a calcalkaline affinity for the shoshonite association (Fig. 7.6). Similarly, the total alkali content of shoshonitic rocks from the U-DVB is generally high (>5%; Fig. 7.7) and the K_2O/Na_2O ratio is also high (>0.5 at 50% SiO_2, >1 at 60% SiO_2; Fig 7.8). Lavas from the U-DVB contain up to 1.10% TiO_2 (Fig. 7.9) which is lower than maximum value of 1.3% suggested by Morrison (1980). The Al_2O_3 content of shoshonitic rocks from the U-DVB ranges from 14 to 20.50% (Fig. 7.10) and is slightly higher than the maximum value of 19% suggested by Morrison (1980).

7.4 HIGH-K CALCALKALINE ROCKS

The importance of the distinction between the alkaline and calcalkaline groups of igneous rocks was first pointed out by Iddings (1892). The calcalkaline group was assigned various names such as subalkaline, calcalkaline and nonalkaline by different authors. The term subalkaline is somewhat ambiguous because various authors use it

only for transitional rocks between the alkaline and calcalkaline. The term calcalkaline is used by most petrologists today for compositions between low-K (tholeiitic) and alkaline. In this thesis, the term high-K calcalkaline is used to describe the most potassic representatives of the calcalkaline rocks.

In terms of the CIPW normative mineralogy, the high-K calcalkaline rocks from the U-DVB range from Ne-normative to Q-normative (Fig. 7.11). The high-K calcalkaline rocks of the U-DVB are characterised by low-iron enrichment, as exhibited by a typical calc-alkaline trend on an AFM plot (Fig. 7.12). Total alkali content of the U-DVB rocks is generally high (>4 wt%; Fig. 7.7) and the K_2O/Na_2O ratio is >0.5 at 58% SiO_2 (Fig. 7.8). The TiO_2 content of high-K calcalkaline rocks from the U-DVB has a maximum of 1.05 wt%, but most values are between 0.35 and 0.65 wt% (Fig. 7.9). The Al_2O_3 contents range from 15 to 18.50 wt%, with the majority in the range of 15-17 wt% (Fig. 7.10).

7.5 COMPARISON OF LEUCITITIC, SHOSHONITIC AND HIGH-K CALCALKALINE ROCKS FROM THE U-DVB

The studied rocks from the U-DVB are mainly shoshonitic and leucititic in affinity. All tephrite, and the majority of tephriphonolite and phonotephrite samples are leucititic in composition. Other rock types from the three study areas have shoshonitic to high-K calcalcaline affinity. Using age data and field evidence, shoshonitic and leucititic association occurred at the early stage of magmatism in Shahrbabak and Aghda (Table 3.1). In these regions, magmatism was followed by production of high-K calcalkaline rocks. The shoshonitic and leucititic rocks from the Islamic Peninsula are younger than those from Aghda and Shahrbabak (Table 3.1).

In term of major element contents, the average content of TiO_2, Fe_2O_3, MgO, CaO, K_2O and P_2O_5 is higher, but SiO_2, Na_2O and Al_2O_3 contents is lower in the leucitic rocks than the shoshonitic rocks from the U-DVB (Tables 7.2, 7.4) due to higher abundance of leucite, clinopyroxene, titanomagnetite and apatite in leucititic than the shoshonitic rocks (Tables 4.1 to 4.17). The average content of SiO_2 and CaO is lower and the TiO_2, Al_2O_3, Fe_2O_3 and K_2O higher in shoshonitic rocks compared to the high-K calcalkaline rocks from the study areas (Tables 7.4, 7.5) reflecting more abundances of analcime, sanidine and titanomagnetite in shoshonitic rocks (e.g. Tables 4.7, 4.8 4.13). Although there are some significant geochemical differences among the shoshonitic and high-K calcalkaline rocks, particularly in the abundances of alkalies and in degree of silica saturation, all these rocks have some common features. The similarities include a low Mg-number, TiO_2 and high Al_2O_3 and K_2O contents and porphyritic character. These feature are typical of calcalkaline and shoshonitic suites of orogenic zones.

The leucititic rocks contain higher average contents of the trace elements Rb, Nb, Pb, Y, Ba, Zn, Cu, Ta, Cr and V than shoshonitic rocks in the U-DVB (Tables 7.2, 7.4). The shoshonitic rocks contain higher average contents of the incompatible elements Rb, Nb, Pb, Y, Ba, Zn and Ta and lower average contents of compatible elements such as Ni and Cr than the high-K calcalkaline rocks (Tables 7.4, 7.5). The leucititic, shoshonitic and high-K calcalkaline rocks from the U-DVB are enriched in LREE. In general, the leucititic rocks have a higher average content of LREE than the shoshonitic and high-K calcalkaline rocks probably related to the high abundances of clinopyroxene and apatite in leucititic rocks. The amounts of HREE in these three rock associations are variable (Tables 7.2, 7.4, 7.5).

The leucititic rocks have initial $^{87}Sr/^{86}Sr$ ratios between 0.70738 and 0.70848 which are higher than the initial $^{87}Sr/^{86}Sr$ ratios for shoshonitic rocks. The shoshonitic rocks, however have a wide range of initial $^{87}Sr/^{86}Sr$ ratios (0.70475-0.70800) compared with rocks from other series, and are higher than the restricted range for high-K calcalkaline rocks (0.70427-0.70452) from the U-DVB. Conversely the ε_{Nd} values in high-K calcalkaline samples are higher than those of the leucititic and shoshonitic rocks (Tables 7.2, 7.4, 7.5). However, isotope variability in these rocks suggestes that these three series rocks are genetically unrelated in the U-DVB.

In order to facilitate comparison between Tertiary volcanic rocks of the U-DVB and volcanic rocks from other regions the rock series are further subdivided into low (<52%) and high (>52%) SiO_2 groups.

7.6 COMPARISON WITH OTHER LEUCITITIC ROCKS

Leucite-bearing rocks are found in widely scattered localities all over the world. The best known localities include the volcanic fields of East Africa Rift, Kastamonu area (Turkey), east and southeast Ruwenzori (Uganda), West Kimberley, and New South Wales (Australia), Java and Celebes (Indonesia), the Leucite Hills of Wyoming, the Roman province of Italy, Mauricia and Almaria provinces (Spain) and the Laacher See district (Germany). All these localities are confined to continental regions. Occurrence of leucite-bearing rocks in oceanic areas is very limited (e.g. Tristan da Cunha Islands). Analytical data for leucititic rocks from the U-DVB are compared with analytical data for rocks from various of tectonic and geographic regions (Tables 7.6, 7.7, 7.8).

7.6.1 Leucitites (<52% SiO_2)

A compilation of published whole-rock geochemical data for leucititic rocks with less than 52% SiO_2 from various regions show many similarities between regions, but also some significant differences (Table 7.6). Data for the U-DVB leucititic samples fall near the middle range of values for all regions with the exception of P_2O_5 which is much higher in the U-DVB samples than the other areas. Leucititic rocks from the Roman province, Central Italy (Holm et al., 1982; Table 7.6, column C) have lower MgO and higher K_2O compared with similar rocks from elsewhere. Leucititic rocks from Umbria-Latium, Italy (Stoppa and Lavecchia, 1992; Table 7.6, column E), have much higher values for MgO and CaO, but lower contents of Al_2O_3, MnO, and Na_2O compared with all other leucititic rocks from elsewhere (Table 7.6).

Relatively few comparative trace element data are available (Table 7.6) but the trace element data for the U-DVB rocks are within the range of values for all regions. The major exceptions are the contents of Zr and Nb which are higher than the other regions. The HREE and V contents of the U-DVB leucititic samples are similar to those of Vulsini, Central Italy (Rogers et al., 1985; Table 7.6, column B) but the contents of some trace elements (e.g. Cr and Zr) are higher in the U-DVB. The abundances of MREE (Sm and Eu) for the leucititic rocks in Vulsini, Central Italy (Rogers et al., 1985; Table 7.6, columns B) are higher than the Roman province, Italy (Peccerillo, 1992 ; Table 7.6, column D). Leucititic rock from Roman province, Italy (Peccerillo, 1992; Table 7.6, column D) have lower contents of REE and Ba than similar rocks from other regions, but the content of Cr is higher.

The Sr isotopic values of the U-DVB leucititic rocks fall near the middle range of

values for all regions and are close to those for rocks from Roccamonfina (Rogers et al., 1987; Table 7.7. column F). Leucititic rocks from the Alban Hills (Conticelli and Peccerillo, 1992; Table 7.7, column G) have higher Sr isotopic ratios, while rocks from the Western and Central Europe (Wilson and Downs, 1991; Table 7.7, column H) have lower Sr isotopic ratios than similar rocks from elsewhere. The average Nd isotopic ratio for samples from the U-DVB is higher than the average for the Roman province (Holm et al., 1982; Table 7.7, column C).

7.6.2 Leucitites (>52% SiO_2)

There are few publications with analytical data for leucititic rocks with more than 52% SiO_2. Comparison of the mean analyses of the U-DVB with analytical data for rocks from other regions (Table 7.8, column A) indicates close similarities in whole-rock geochemistry between most regions except Leucite Hill. Leucititic rocks from Leucite Hill, Italy (Bergman, 1987; Table 7.8, column F) have much higher values for TiO_2, MgO and K_2O, but lower Al_2O_3, MnO and Na_2O in comparison with other samples. Leucititic rocks from Roccamonfina (Appleto, 1972; Table 7.8, column G) have higher Al_2O_3 compared with similar rocks from elsewhere.

The U-DVB rocks have lower contents of most trace elements compared to leucititic rocks from elsewhere (Table 7.8). The REE contents of the U-DVB samples are lower than the rocks from other regions (Table 7.8). Contents of Ni, Cr, Zr, Ba, Sr, Nb, La, Ce, Sm and Eu in rocks from Leucite Hill (Bergman, 1987; Table 7.8, column F) are much higher compared with all samples from other regions, but Y and Lu are lower.

7.7 COMPARISON WITH OTHER SHOSHONITIC ROCKS

Comparison of the mean analyses of the shoshonitic rocks from the U-DVB with analytical data for rocks from other regions (Tables 7.9, 7.10) indicates close similarities in whole-rock geochemistry.

7.7.1 Shoshonites (<52% SiO_2)

A compilation of published whole-rock geochemical data for shoshonitic rocks with less than 52% SiO_2 from various regions shows many similarities between regions, but also some significant differences (Table 7.9). Data for the U-DVB samples fall in the range of values for all regions with the exception of relatively low SiO_2. Shoshonitic rocks from Northwestern Alps (Venturelli et al., 1984; Table 7.9, Column C) have much lower values for Al_2O_3 and Na_2O than similar rocks from elsewhere. Both TiO_2 and Fe_2O_3 values for shoshonitic rocks from Ascenison Island (Sorensen, 1974; Table 7.9, Column J) are relatively high compared with all other samples.

The U-DVB rocks have higher Pb, Th, U and Tb contents compared with shoshonitic samples from elsewhere. Shoshonitic rocks from Walton Peak, Colorado (Thompson et al., 1993; Table 7.9, Column H) have much higher contents of Ba, Zr, Nb and Hf, whereas rocks from Greece (Pe-Piper, 1983; Table 7.9, Column I) contain low Ba, Sr and Ni compared with similar rocks from elsewhere. The REE (La, Ce, Nd, Yb and Lu) are more abundant in Roman province samples than in the U-DVB rocks (Peccerillo, 1992; Table 7.9, Column B), and the contents of Sm, Eu and Tb are slightly lower. The REE contents of the U-DVB rocks are higher than those of the Abitibi Greenstone Belt (Dostal and Muller, 1992; Table 7.9, Column F). Shoshonitic rocks from the Permian Sydney Basin (Carr, 1984; Table 7.9, Column E) have

consistently lower contents of light REE (La and Ce) than similar rocks from other regions. In contrast, shoshonitic rocks from Walton Peak, Colorado (Thompson et al., 1993; Table 7.9; Column H), contain higher contents of LREE (La and Ce) and medium REE (Sm and Eu) than similar rocks from elsewhere. Both V and Ni are relatively low for the U-DVB rocks and the contents of REE are not identical for the rocks from the U-DVB and Guffey volcanic (Wobus et al., 1990; Table 7.9, column J).

The Sr isotopic values of the U-DVB shoshonitic rocks fall near the upper end of the range of values for all regions documented in Table 7.7 and are close to the values for rocks from Stromboli (Francalanic et al., 1988; Table 7.7, column E). Shoshonitic rocks from the Birunga and Toro-Ankole (Bell and Powell, 1969; Table 7.7, column I) have higher Sr isotopic values, whereas rocks from Taru Volcano (Rogers and Setterfield, 1994; Table 7.7, column D) have relatively low Sr isotopic ratios compared to similar rocks from other regions. The Nd isotopic ratios for samples from the U-DVB lie within the range of values for similar rocks from elsewhere (Table 7.7).

7.7.2 Shoshonites (>52% SiO_2)

Comparison of major element geochemical data for shoshonitic rocks with more than 52% SiO_2 from many regions (Table 7.10) shows these rocks form a coherent group and that data for U-DVB rocks lie within the range of values for all regions. The exceptions being K_2O, which is higher than all other regions (Table 7.10). The contents of SiO_2 for shoshonitic rocks from the Roman province (Peccerillo, 1992; Table 7.10, column J) is higher than other regions. Rocks from Canary Islands (Borely, 1974; Table 7.10, column K) have higher TiO_2, Al_2O_3 and Na_2O and lower P_2O_5, CaO, MgO and Fe_2O_3 than similar rocks from elsewhere.

In general, the trace element data for the U-DVB rocks are within the range of values for all regions. The exceptions are U, Pb, Hf and Ta contents which are higher and V and Sc are lower than the other regions. Shoshonitic rocks from Fiji (Gill and Whelan, 1989; Table 7.10, column C) have higher contents of Sr and V, while rocks from the Northern Mariana Arc (Bloomer et al., 1989; Table 7.10, column E) have lower Ni than similar rocks from elsewhere. The HREE (Yb and Lu) contents of the U-DVB samples show a similar abundance to rocks from the Northwestern Alps (Venturelli et al., 1984; Table 7.10, column H). The rocks from Roman province (Peccerilo, 1992; Table 7.10, column J), contain higher contents of LREE (La and Ce) and MREE (Sm and Eu) than similar rocks, while the HREE (Yb and Lu) contents of samples from the Southern Sydney Basin (Carr, 1984; Table 7.10, column D) are higher than the other regions, except Roman province.

7.8 COMPARISON WITH OTHER HIGH-K CALCALKALINE ROCKS

A compilation of major and trace element data for high-K calcalkaline rocks from various part of the world is presented in Tables 7.11 and 7.12.

7.8.1 High-K calcalkaline (<52% SiO_2)

A compilation of major element data for high-K calcalkaline rocks with less than 52% SiO_2 from many regions (Table 7.11) indicates that these rocks form a coherent group, and the data for rocks of the U-DVB lie in the range of values for all regions. High-K calcalkaline rocks from northwest Colorado (Thompson et al., 1993; Table 7.11, Column I) have higher values for Fe_2O_3 and P_2O_5, whereas high-K calcalkaline rocks from the Abitibi Greenstone Belt (Dostal and Muller, 1992; Table 7.11, Column F) have higher contents of MgO and lower contents of TiO_2 and Al_2O_3 compared with

other regions. Rocks from east Africa rift system (Gurenko et al., 1991; Table 7.11, column D) have higher TiO_2, CaO and lower SiO_2 than similar rocks from elsewhere.

The trace element data for the U-DVB rocks lie in the middle range of values for other regions with the exception of Sr which is much higher in the U-DVB samples than the other areas (Table 7.11). Compared to the other regions the concentration of Ce and Ni in the U-DVB samples is higher, with the exception of rocks from the Guffey Volcano (Wobus et al., 1990; Table 7.11, Column E) and northwest Colorado (Thompson et al., 1993; Table 7.11, Column I), however the content of U is lower. Rocks from north Wales (Kokelaar, 1986; Table 7.11, Column J) have the lowest REE values whereas La, Ce, Nd and Sm abundances for northwest Colorado (Thompson et al., 1993; Table 7.11, Column I) represent the highest values of other regions. Contents of Yb and Hf in rocks from Roman province (Peccerillo, 1985; Table 7.11, Column C) are much lower when compared with similar rocks from elsewhere. Rocks from the Northern Azerbaijan (Riou et al., 1981; Table 7.11, Column G) have lower Tb than other regions.

7.8.2 High-K calcalkalines (>52% SiO_2)

Compilation of major element data for high-K calcalkaline rocks with more than 52% SiO_2 from various regions (Table 7.12) show these rocks also form a coherent group and the data for the U-DVB rocks lie within the range of values for all regions except for the relatively high Na_2O and low TiO_2. High-K calcalkaline rocks (Gill and Whelan, 1989; Table 7.12, Column D) have much higher values for TiO_2, Al_2O_3, Fe_2O_3, MgO and CaO and lower values for SiO_2, Na_2O and K_2O compared with the U-DVB rocks. Rocks from northern Italy (Barth et al., 1993; Table 7.12, Column J) have higher MgO

and lower Na_2O than similar rocks from Costarica.

The U-DVB rocks have lower Y and V contents compared with high-K calcalkaline rocks from elsewhere, but have high Ba contents. High-K calcalkaline andesite from Kastamonu (Peccerillo and Taylor, 1976; Table 7.12, Column C) has much higher contents of Ni, Cr and Sc, whereas rocks from Ungaran (Claproth, 1989; Table 7.12, Column B) contain relatively low Cr compared with similar rocks from other regions. Rocks from the Northwestern Alps (Venturelli et al., 1984; Table 7.12, Column G) have higher LREE and rocks from the Northern Azerbaijan (Riou et al., 1981; Table 7.12, Column E) have lower Sm, Eu, Tb and Yb compared with elsewhere. Also, both Nb and Y contents of samples from Costarica (Cigolini et al., 1991, Tables 7.12, Column K) are higher than the other regions.

The Sr isotopic values for the U-DVB high-K calcalkaline rocks fall near the lower end of the range of values for all regions presented in Table 7.7. High-K calcalkaline rocks from Latir Volcano (Johnson et al., 1990; Table 7.7, column F) have higher Sr isotopic values than those of similar rocks from other regions. The Nd isotope values for high-K calcalkaline rocks from the U-DVB lie within the range of values for all regions (Table 7.7).

7.8.3 Calcalkaline rocks

Comparison of major element geochemical data for calcalkaline rocks from various region is shown in Table 7.13. These rocks form a coherent group and the data for the U-DVB rocks are within the range of values for all regions with exceptions of TiO_2, MnO and MgO which are much lower in the U-DVB samples than the other regions.

Calcalkaline rocks from Sardinia, Italy (Montanini et al., 1994; Table 7.13, Column E), have higher values for TiO_2, Fe_2O_3 and K_2O, but lower Al_2O_3, while rocks from the Kastamonu (Peccerillo and Taylor, 1976; Table 7.13, Column I) have higher Al_2O_3 and CaO than similar rocks from elsewhere. Rocks from northern Italy (Barth et al., 1993; Table 7.13; Column G) have higher MgO and lower CaO than rocks from other regions.

The trace element contents of the U-DVB rocks fall near the lower end of the range of values for all regions documented in Table 7.13. The major exceptions are the content of U, Yb, Lu, Sc and V which are lower than for other regions. Rocks from northwest Colorado (Thompson et al., 1993; Table 7.13, Column C) have higher light REE, U, Nd and Ni, but lower Y, while rocks from the Atesina-Cimad Asta (Barth et al., 1993; Table 7.13, Column G) have relatively high Yb, Sc, but lower Ni than rocks from elsewhere. The calcalkaline rocks from eastern Anatolia, Turkey (Pearce et al., 1990; Table 7.13, Column J) have much higher Zr and V, and Nb and Cr in the rocks from Sardinia, Italy (Montanini et al., 1994; Table 7.13, Column E) are higher than other rocks.

7.9 SUMMARY

Based on the K_2O and SiO_2 contents the volcanic rocks from the U-DVB are typical of the leucititic, shoshonitic and high-K calcalkaline rock associations. Leucititic rocks are dominant in the Islamic Peninsula while shoshonitic rocks are more common in the Aghda and Shahrbabak areas. Although there are significant geochemical differences among the three volcanic series, particularly in the abundance of alkalies and in degree of silica saturation, common features include low TiO_2, high Al_2O_3 and K_2O contents

and porphyritic character. These features are typical of alkaline and calcalkaline suites of orogenic zones.

The average content of TiO_2, Fe_2O_3, MgO, CaO, K_2O and P_2O_5 is higher and SiO_2, Na_2O and Al_2O_3 is lower in the leucitic rocks when compared to the shoshonitic rocks from the U-DVB. Also incompatible elements such as Rb, Nb, Pb, Y, Ba, Ta and compatible element Cr and V are higher in the leucititic rocks than shoshonitic rocks.

The shoshonitic rocks from the U-DVB have higher contents of TiO_2, Al_2O_3, Fe_2O_3, and incompatible trace elements including Rb, Nb, Y, Ba and Ta than the high-K calcalkaline rocks. The leucitic, shoshonitic and high-K calcalkaline rocks from the U-DVB are enriched in LREE; in general, the leucitic rocks have a higher average content of LREE than the shoshonitic and high-K calcalkaline rocks. In the AFM plots the leucititic rocks show a more restricted range of compositions than the shoshonites and high-K calcalkalin rocks. Comparison of geochemical data for leucititic, shoshonititic and high-K calcalkaline rocks from various tectonic and geographic regions shows the rocks of each association from coherent groups, and most of the U-DVB rocks fall in the range of values. The REE contents of leucititic rocks from the U-DVB are lower than the rocks from Roccamonfina Volcano (Luhr and Gianetti, 1987) whereas, the HREE and V contents are similar to those of the Vulsini (Rogers et al., 1985). The REE contents for the U-DVB shoshonitic rocks are higher than those of Abitibi Greenston Belt rocks (Dostal and Muller, 1992), and the HREE contents of the U-DVB shoshonitic rocks have a similar abundance to the rocks from the northwestern Alps (Venturelli et al., 1984). The REE contents for the U-DVB high-K calcalkaline rocks are lower than those of Colorado rocks (Thompson et al., 1993).

The leucititic rocks from the U-DVB have higher initial Sr isotopic ratios than shoshonitic and high-K calcalkaline rocks. The shoshonitic rocks, however, have a wide range of Sr isotopic ratios compared with rocks from other series, and are higher than the restricted range of high-K calcalkaline rocks from the U-DVB. Conversely the ε_{Nd} values in high-K calcalkaline are higher than those of the leucititic and shoshonitic rocks.

CHAPTER 8

PETROGENESIS

8.1 INTRODUCTION

Potassic rocks are defined as those that are characterised by a molar K_2O/Na_2O ratio that is around or slightly higher than unity at MgO>3 wt% and the term ultrapotassic is reserved for the rocks that have MgO>3 wt% and molar K_2O/Na_2O>2.5 (Peccerillo, 1992; Foley et al., 1987). Potassium-rich rocks are limited in abundance but are found in widely scattered localities all over the world. They include volcanic, subvolcanic and plutonic bodies that are found in three distinctive environments (Thompson and Flower, 1986). Potassic and ultrapotassic igneous rocks include a variety of compositions that range from shoshonitic magmas associated with calcalkaline volcanics in many volcanic arcs to ultrapotassic lamproites, lamprophyres, kimberlites, melilitic and leucitic rocks (Foley and Peccerillo, 1992 and Wooley et al., 1996). Potassic volcanic rocks form by low degree of partial melting, under hydrous conditions in a low heat-flow environment, of upper mantle lherzolite that have been metasomatically enriched in LILE and LREE (Meen, 1987). In the U-DVB four groups of potassic igneous rocks occur:

(a) a potassic calcalkaline series ranging from trachytes to dacites,

(b) a high-K calcalkaline series ranging from basalts to trachyandesites,

(c) a high-K shoshonitic series ranging from phonotephrites to tephriphonolites; and

(d) ultrapotassic leucititic series ranging from tephriphonolites to tephrites.

The K-rich igneous rocks from the Islamic Peninsula, Aghda and Shahrbabak in the U-DVB are located in the middle of the extensive Alpine-Himalyan orogenic belt between

the Arabian and Eurasian plates. Potassium-rich igneous rocks of Tertiary age are common along the Alpine-Himalayan orogenic belt. A large number of occurrences of shoshonites and leucitites in Italy (Coltorti et al., 1991), Spain (Venturelli et al., 1984), Turkey (Keller, 1983), Pakistan (Searle, 1991), Tibet (Arnaud et al., 1992; Turner et al, 1996), China (Pognante, 1990), and Indonesia (Wheller et al., 1987) have been investigated and the current study fills the missing link to the database of Tethyan K-rich magmas in Iran. Volcanic rocks from the U-DVB are mainly alkaline and calcalkaline in composition, and were emplaced between the Early Tertiary and the Present. Important features for the petrogenesis of the U-DVB rocks include the occurrence of leucititic, shoshonitic and high-K calcalkaine series (Chapter 6, 7) combined with the tectonic setting involving subduction of the Neo-Tethys oceanic crust beneath the Central Iran Plate (Chapter 2).

There are two major theories for the genesis of the U-DVB rocks. The first ascribes the origen of the volcanic belt to continental rifting (Amidi et al., 1984; Amidi and Michel, 1985) while the second, more widely accepted model involves subduction (e.g. Takin, 1972; Stocklin, 1977; Berberian and King, 1981; Berberian F., 1981; Shahabpour, 1982; Sengor, 1990; Hassanzadeh, 1993; Alavi, 1994).

8.2 ROLE OF CONTINENTAL RIFTING IN PRODUCING POTASSIUM-RICH VOLCANIC ROCKS

The term rift refers to a major normal fault zone caused by wholly extensional stress at right angles to the strike of the fault (e.g. Quennell, 1985). The best examples of continental rifts comprise the East African rift zone, the Baikal rift zone and rifts in Western North America. Such rift zones are characterised by recent volcanism, seismic

activity and normal faulting.

The tectonic setting together with available geochemical and isotopic data from this study do not characterise a rift model for the U-DVB rocks. According to many Iranian geologist, the U-DVB is parallel to the Zagros Main Thrust Line, ophiolite-melange belt and linear metamorphic belt of the Sanandaj-Sirjan could have resulted from subducting Neo-Tethys oceanic crust beneath the Central Iran. Also development of the major Iranian porphyry copper deposits and extensive formation of andesite-dacite stratovolcanoes in the U-DVB may indicate that rifting was not developed in the U-DVB region (Stocklin, 1974; Berberian and King, 1981; Hassanzadeh, 1993; Alavi, 1994).

There are three major chemical end-members recognised for ultrapotassic rocks (Foley et al., 1987). The analyses of the Islamic Peninsula have been plotted on the CaO versus Al_2O_3 and CaO versus SiO_2 diagrams (Fig. 8.2) and all data points except sample R14457 fall in the subduction-related field. Also Zr-Nb diagram (Fig. 8.1) shows that not any samples plot in rifting field.

Geochemically, the LREE contents in the U-DVB tephrite are lower and HREE are higher than those of western branch of the East African Rift (Davies and Lioyd, 1988). The $^{87}Sr/^{86}Sr$ ratios for the tephritic rocks in the U-DVB are significantly higher than the western rift of Africa (Bell and Powell, 1969). Ultrapotassic rocks from the Islamic Peninsula (Table 6.2), have much higher values for Ba, Rb, Sr, Th, U and Zr but lower content of Nb, Cr, Ni, Hf and Ta compared to similar rocks in the western branch of the East Africa Rift System (Thompson et al., 1984). Consequently, none of the

geochemical and other geological data for the volcanic rocks from the U-DVB support a model in which the volcanism is related to rifting.

8.3 ROLE OF SUBDUCTION IN POTASSIUM-RICH VOLCANIC ROCKS FROM THE U-DVB

It is generally accepted that arc basalts are derived from partial melting within the sub-arc mantle wedge either subsequent to, or concomitant with, the addition of an enriched component from the subducted oceanic plate (Gamble et al., 1993; Plank and Langmuir, 1993; Muller et al., 1992;). Various hypotheses for the origen of the added component include partial melts from subducted lithosphere (Marsh, 1982; Myers et al., 1986b), the incorporation of subducted sediments (Tera et al., 1986) and an incompatible element enriched fluid phase derived by dehydration of the uppermost hydrothermally altered portion of the oceanic crust (Kay, 1980; Gill, 1981; Tatsumi et al., 1986; Sun and McDonough, 1989), or some combination of these (Johnson et al., 1996).

The content of trace elements of ultrapotassic rocks from the Islamic Peninsula are relatively comparable with similar rocks from Alban Hill (Peccerillo, 1992). Also HREE and LREE contents of tephritic rocks are similar to those of Roman region (Giannetti and Ellam, 1994). The HREE, Ba, Sr, Rb, Ni, Cr, Th and V contents of the U-DVB shoshonitic rocks are within the range of values for similar rocks from the Tibetan plateau (Turner et al., 1996). The Sr isotopic values of the ultrapotassic rocks from the U-DVB are close to the values for rocks from Roccamonfina (Giannetti and Ellam, 1994). In addition, high-K calcalkaline and shoshonitic rocks from Shahrbabak show similar Sr isotopic ratios with rocks from Stromboli (Francalanci et al., 1988). Generally, the potassic rocks from the Islamic Peninsula, Aghda and Shahrbabak show

high Al_2O_3, K_2O, LFSE and LREE abundances and low abundances of TiO_2 and HFSE (Ta, Nb and Zr) in addition to LREE>Nb and Zr>Y (Tables 6.1 to 6.24). These features provide strong evidence of the involvement of subduction-related processes in the generation of orogenic potassic magmas in the U-DVB (Stolz et al., 1990; Ellam and Harmon, 1990; Nelson, 1992). Also trace-element ratios suggest a subduction zone source for the U-DVB lavas. Values for La/Nb (2.3-3.3), La/Th (2.5-3.0) and Ba/La (27.9-62.2) are all within the range defined by orogenic volcanics (Gill, 1981). In addition, the Ba/Nb values of the U-DVB volcanic rocks range from 60.5 to 139.5 and are all much greater than the value of 28 considered by Fitton et al. (1988) to mark the lower limit for arc magmas (Tables 6.3, 6.11, 6.19).

Figures 8.1 (Zr vs Nb and K_2O vs TiO_2) and 8.3 (La-TiO_2*100-HF*10) show that all samples from the studied areas plot within the subduction field. These diagrams are useful in distinguishing potassic and ultrapotassic rocks related to intra-plate activity from those directly or indirectly related to subduction (Wilson, 1989; Thorpe, 1987).

Development of the U-DVB within a subduction related setting during Tertiary time is supported by the following evidences: (1) The occurrence of Post-Palaeogene calcalkaline plutons and porphyry copper mineralisation along the U-DVB (Shahabpour, 1982; Berberian F. 1981; Hassanzadeh, 1993), (2) The trend of U-DVB is parallel to the Main Zagros Thrust Line indicating a structural relationship exists between the Arabian and Central Iranian plates, and (3) The presence of ophiolitic rocks preserved along tha Main Zagros Thrust Line. Neo-Tethys oceanic crust was being subducted beneath the Central Iran Plate (continental crust) throughout Tertiary, and the U-DVB is interpreted as results from this subduction.

According to Berberian F. (1981) and Hassanzadeh (1993) the Neo-Tethys ocean between Arabian and Central Iran Plates was consumed towards Neogene, and final closure took place during Late Miocene. On the other hand, petrochemical studies and isotopic age dating of the Oligo-Miocene volcanic rocks (this study Chapters 3, 6) disagree with the Late Miocene closure of the Neo-Tethys ocean between Arabian and Central Iran plates. Since all samples from mafic to intermediate composition with Oligo-Miocene age plotted in postcollisional field (Fig. 8.4), consequently the closure could have taken place in the Late Eocene.

Based on the isotopic and geochemical evidence of this study, it is proposed that the U-DVB rocks can not be wholy derived from subduction of Neo-Tethys beneath the Central Iran Plate. The geochemical and isotopic data from the U-DVB imply that the volcanic rocks have been generated from two source materials: one yielding material rich in K-group elements with relatively high $^{87}Sr/^{86}Sr$ (>0.7065) values and low $^{143}Nd/^{144}Nd$ values for the Islamic Peninsula and Aghda; and the other yielding material low in K-group elements compared to the Islamic Peninsula and Aghda with relatively low $^{87}Sr/^{86}Sr$ (<0.7057) values and high $^{143}Nd/^{144}Nd$ values for Shahrbabak (Tables 6.6, 6.7, 6.15, 6.24). The Islamic Peninsula and Aghda rocks are considered to be from Neo-Tethys ocean, but those of Shahrbabak region are related to Nain-Baft Ocean which formed by tearing of the Central Iran Plate (Sengor, 1990). The isotopic and geochemical data from Shahrbabak are similar to those obtained by Hassanzadeh (1993) from Miduk and Sar Cheshmeh copper mines located in Shahrbabak area. He realised that the evolution of the copper mines is related to Nain-Baft Ocean. The plot of Zr versus Zr/Nb (Fig. 8.5) implying distinct overlap of samples from the Islamic Peninsula and Aghda regions, but separated field is remarkably indicated for all samples from

Shahrbabak. However, potential source regions for the U-DVB rocks comprise the subducted oceanic crust and the mantle wedge above the subducted slab, and/or combinations of these two endmember sources.

8.3.1 Subducted lithosphere as the source region

Modern theories in petrogenesis of magmatic arcs discuss two principal groups: those which derive primary magmas directly by melting of a peridotite mantle and those which derive magmas directly from the melting of subducted oceanic crust or from the melting of peridotitic mantle which has been modified by the introduction of water and/or a silicate liquid originating in this crust. Many authors have argued convincingly that much of the LFSE enrichment is a result of addition of a subduction component to the mantle wedge via aqueous fluid derived from dehydration of the subducting oceanic crust and overlying sediment (e.g. Peccerillo, 1990; Beccaluva et al., 1991; Foley and Peccerillo, 1992).

For several reasons, geochemical data obtained from most samples of the studied rocks are not consistent with generation of the U-DVB lavas by melting of the subducted oceanic slab. The exception is only for two samples of dacite and trachte (R14512, R14699) from Shahrbabak, which will be discussed in the next paragraph. The occurrence of abundant mafic lavas (44-59% SiO_2) in the U-DVB necessitates high degrees of partial melting of eclogite which is unlikely to occur. In addition, the high degrees of partial melting required for this model are inconsistent with the observed relatively high contents of K_2O which imply small degrees of partial melting. Also, very low degree partial melts of a MORB-like source mantle cannot yield K_2O contents >0.8% (Allan et al., 1993). Other weaknesses of the eclogite partial melting model have

been found in both major and trace elements studied. The major element chemistry of partial melts of quartz eclogite, estimated from experimental studies are not typically calcalkaline (Stern, 1974). Trace element contents of most samples in the U-DVB, particularly REE data are inconsistent with this model. If the liquids were derived from an eclogitic source, then it must be strongly depleted in HREE (e.g. Gill, 1981), due to high values of HREE partition coefficients for equilibrium between basaltic to andesitic liquids. Most of the samples from the U-DVB do not show strong depletion in HREE (e.g. R14457, R14550) and indicate that garnet is absent from the source material, or at most, it is a minor phase for these samples.

The dacite and trachyte from Shahrbabak show high Na_2O/K_2O, high Sr and low Y (Tables 6.22, 6.23) and strongly HREE depletion (Fig. 6.25). Recent authors (e.g. Peacok et al., 1994; Sen and Dunn, 1994) belive that such composional behaviour of dacite and trachytic rocks is consistent with their generation by melting of subducting oceanic lithosphere. The low radiogenic Sr and high ε_{Nd} value (+4.1 and +3.8) for dacite and trachyte respectively (Table 6.7) indicate that pelagic sediments could not have been involved in the genesis of the dacite and trachyte from Shahrbabak. Partial melting of an amphibole eclogite source would generate melts that have high Sr/Y but low Y (Defant and Drummond, 1990). Figure 8.6 shows that dacite and trachyte samples from Shahrbabak plot at high Sr/Y and low Y compared to other samples from the U-DVB. However, as noted above, they are high in Na_2O/CaO values and Sr content. Also, HREE depletion and low Sc abundances are due to early crystallisation of amphibole or possibly partitioning in garnet at the source, all suggest that the involvement of a slab in the genesis of these two rock types is likely.

8.3.2 MANTLE AS THE SOURCE:

8.3.2.1 Primary and derivative magmas

Primary basaltic magmas are those formed by partial melting of the upper mantle, the compositions of which have not been modified subsequently by fractional crystallisation, crustal contamination, or other processes during movement from the source region to the surface, or following emplacement. The subcontinental upper mantle is mineralogically complex and chemically heterogeneous (e.g. Zindler and Hart, 1986) and although a variety of primary magma compositions are to be expected, several features are available for the recognition of primary mantle-derived magmas. These are include Mg-number, trace element contents and the presence of high pressure inclusions. If the Tertiary rocks of the U-DVB are the products of mantle-derived melts, the primary or derivative nature of the most mafic rocks of the province must be ascertained. Two features are particularly relevant for the recognition of primary mantle-derived rocks. Assuming the primary mantle-derived melts will be in equilibrium with olivine of composition Fo_{86-90}, the primary magmas should have Mg-numbers between 68-75 (Wilson, 1989). The maximum Mg-number for samples from the Islamic Peninsula is 74.2 (Table 6.1), from Aghda is 50.3 (Table 6.8), and from Shahrbabak is 49.4 (Table 6.16). The composition of olivine from the Islamic Peninsula and Shahrbabak are Fo_{84-86} and Fo_{72-86} respectively (Appendix C). Except the high Mg-number of the Islamic Peninsula which is close to the value of primary magma; the low values of Mg-number and olivine for other regions indicate that if magmas were derived from the mantle, they were not primary but must have undergone subsequent fractionation. The behaviour of major and trace elements in respect to the MgO and SiO_2 content or evolution of the rock series (Chapter 6) possibly suggests that fractional crystallisation of olivine, spinel, clinopyroxene and plagioclase were mainly responsible

for the formation of different rock types.

Trace element data have been utilised to prove the primary or derivative signature of basalts from many areas. The elements which have proved to be most useful for this purpose are Ni, Sc and Cr. Wilson (1989) suggested a content of 400-500 ppm Ni for primary magmas in equilibrium with typical upper mantle, whereas, Wass (1980) proposed a wider range of Ni contents between 403 and 890 ppm for primary basalts from the Southern Highlands of New South Wales. Although, the Ni contents of primary mantle-derived magmas vary from one region to another, Ni contents of at least 200-300 ppm are normal (BVSP = Basaltic Volcanic Special Project, 1981). The maximum Ni contents in the rocks of the studied areas are 153, 28 and 158 ppm for the Islamic peninsula, Aghda and Shahrbabak respectively which are below the lower limit of Ni contents for primary mantle-derived magmas. Schilling et al. (1983) introduced range of 40.02-36.47 and 528-278 ppm for Sc and Cr respectively from primary magma. In contrast to the data for Ni, the basalt (sample R14457) from the Islamic Peninsula contains relatively high contents of Sc (38.5 ppm) and Cr (650 ppm) probably related to the abundances of clinopyroxene in basalt (Table 4.3), which are consistent with primary mantle derivation. If the Islamic Peninsula basalt derives from mantle, the low Ni content suggests that considerable fractionation of olivine has been occurred during upward moving to the surface. The tephriphonolite samples from Aghda and Shahrbabak have relatively low contents of Sc (3.67-3.72 ppm) and (7.58-7.76 ppm) respectively, indicating that these rocks did not form from primary magmas.

8.3.2.2 Fractionation model and major element composition of the primary magma

As previously mentioned (Chapter 6), most mafic to intermediate rocks from the U-

DVB developed by fractional crystallisation of olivine and clinopyrexene from a mantle source. Analyses of the most primitive lavas from representative volcanic rocks in the U-DVB are listed in Table 8.1. Assuming that these primitive compositions were once a mixture of liquid in equilibrium with crystal phase, and ultimately derived from the mantle.

A useful model for the derivation of the lavas listed in Table 8.1 is based on the proposal that olivine was the major crystalline phase involved in fractionation (Chapter 6). Modelling was accomplished by the incremental addition of small (0.5 wt%) amounts of olivine to the lava compositions of Table 8.1 until the calculated primary magma was in equilibrium with two distinct olivine compositions ($Mg/Mg+Fe^{+2}$ = 0.84 and 0.88) were obtained. These compositions correspond to the range thought to exist in the mantle (Nicholls and Whitford, 1976). The calculation, was based on a program (GDA) Sheraton and Simons (1988) and a Kd value of 0.3 was utilised.

Tables 8.1 and 8.2 summarise the observed compositions and calculated primary magma compositions together with the amount of olivine fractionated for analysed rocks from the U-DVB. The results show that the amount of olivine removed from primary melt is: 3.9-13.9, 11.7-14.8 and 9.5-17.7 wt% for the Islamic Peninsula, Aghda and Shahrbabak respectively. This olivine composition is in equilibrium with olivine of composition ($Mg/Mg+Fe^{+2}$ = 0.84) to produce the observed lavas. If the primary magma is in equilibrium with olivine of composition ($Mg/Mg+Fe^{+2}$ = 0.88), it requires removal of olivine ranges 6.3-24, 18.1-23.6 and 18.9-25.5% for the Islamic Peninsula, Aghda and Shahrbabak, respectively.

The modelled primary compositions for the studied areas are compared with other primary magmas from different places in Tables 8.2 and 8.3. Compared to the data for Karisimbi (Rogers et al., 1992), the calculated primary compositions for the Islamic Peninsula have low contents of SiO_2, TiO_2 and Al_2O_3 and relatively high contents of CaO and K_2O (Tables 8.2, 8.3). Compared to the major element composition used by Roeder and Emslie (1970; Table 8.3), the calculated compositions for Aghda show low contents of TiO_2, FeO and CaO and relatively high contents of SiO_2, Al_2O_3 and K_2O. Compared to the primary magma compositions of BVSP (1981) and Best (1982) listed in Table 8.3, the calculated compositions for Shahrbabak show high contents of SiO_2, Al_2O_3 and K_2O and low contents of TiO_2 and CaO.

8.3.2.3 RARE EARTH ELEMENTS

Based on the data and discussion presented in section 8.3 the mantle appears to be most likely source region for the most rocks from the U-DVB. The REE are a very powerful tool for petrogenetic studies because they are geochemically similar and are very sensitive indicators of petrogenetic processes and can therefore be used to constrain the composition of the mantle source region. The upper mantle is heterogeneous in REE content, especially in LREE. The LREE concentration in primary liquids depends essentially on the degree of partial melting and the initial concentration of these elements in the source rock. Most of the rocks from study areas are alkaline, and are characterised by a large enrichment of total REE and LREE relative to chondrite.

8.3.2.3.1 Islamic Peninsula

In Figure 6.7 La and Ce exhibit variable behaviour with the LREE varying from 180 to

250 times chondrite and HREE concentrations are between 4 and 8 times the chondrite abundances. The REE Patterns for the rocks from the Islamic Peninsula are linear with a small negative Eu anomaly, except trachyandesite which have greater negative Eu, implying their cogenetic nature.

As shown in Figure 6.7 tephrite, phonotephrite and basalt samples (R14447, R14454, R14455, R14466 and R14457) from the Islamic Peninsula have very similar REE characteristics, although the absolute abundances are variable. The concentration of REE in these rocks is high due to abundance of accessory minerals, such as apatite. Apatite is enriched in REE particularly where associated with alkaline igneous rocks (Henderson, 1984; and Rae et al., 1996), and is common in the rocks from upper mantle (O'Reilly and Griffin, 1988). Also clinopyroxene is a major repository for REE during mantle melting and low-pressure crystallisation (Gaetani and Grove, 1995). Several factor, may contribute to the variability of REE partitioning in clinopyroxene. Partitioning is dependent on temperature, pressure and compositional effects (Eickschen and Harte, 1994). According to Gallahan and Nielson (1992), the most important compositional factors controlling the REE partitioning between clinopyroxene and melt at constant temperature and pressure are the Ca content of the clinopyroxene and the Al content of the melt. Petrographic evidence indicate an abundance of clinopyroxene and apatite within the Tephrite, phonotephrite and basalt samples in the Islamic Peninsula rocks (Tables 4.1, 4.2, 4.3). These rocks may be derived by partial melting of source rich in clinopyroxene and apatite.

The trachyandesite (R14698) shows a fractionated REE pattern (Fig. 6.7) for both LREE and HREE with La_N/Yb_N ratios 17.72 and total REE 277. A negative Eu

anomaly seems to be quite common in trachyandesitic rocks. Negative Eu anomalies are normally interpreted as the result of removal of plagioclase. Petrographic data indicate a lack of plagioclase within the rocks from the Islamic Peninsula. The negative anomaly may be related to the fractional crystallisation of apatite, because the partitioning of the REE between apatite and silicate melts varies systematically with atomic number, the middle REE (e.g. Eu) being more easily accommodated than either the light or the heavy elements (Watson and Green, 1981; Green, 1994). Consequently when apatite starts fractionating the Eu tend to be extracted from the melt at a greater rate than the other elements. The similarity of trachyandesite REE pattern compared to that of the more mafic members of the Islamic Peninsula indicates a common mechanism of genesis for all these rocks.

The REE patterns from the Islamic Peninsula show strongly fractionated patterns for both light and heavy REE. The steep REE patterns with HREE depletion suggest that clinopyroxene was a residual phase during partial melting to produce these magmas, and that they were derived from a LREE-enriched source. Abundances of HREE are rather constant (Yb = 1.90-2.67), but abundances of LREE are variable (La = 49.10-81.10), so that there is a range in La_N/Yb_N = 14.4-21.4. These features are typical of alkaline magmas derived from mantle lherzolite source (Alibert et al., 1983 and Leat et al., 1990).

Experimental petrology indicates small degrees of melting (less than about 10%) of peridotite in the mantle, yield alkali-rich basalt which are characterised by high LREE contents and La/Lu ratios (Henderson, 1984). Also Meen (1987) considered that potassic volcanic rocks produce by low degrees of partial melting, of upper mantle

lherzolite that has been enriched in LFSE and LREE. Therefore according to the results of geochemical and REE analyses, generation of K-rich alkaline magmas from the Islamic Peninsula could be related to the partial melting of a metasomatised mantle-peridotite, such as a phlogopite-bearing wehrlite or a phlogopite and amphibole-bearing clinopyroxenite. However, the overlaps in the data (Fig. 6.8) indicate that they may have been derived from same mantle source. The REE patterns in the Islamic Peninsula lavas are closely similar and overlap those from Vulsini, Central Italy, which Rogers et al. (1985) argued were derived from mantle source.

8.3.2.3.2 Aghda

The total REE content of Aghda are variable (Table 6.15) with an average value of 172 ppm. These values are within the range for shoshonite which is characteristic of continental arc shoshonite (Henderson, 1984). In mafic rocks the MREE decrease in abundance from Sm to Ho, and the HREE are variable in composition from Ho to Lu. The Yb and Lu exhibit highly variable behaviour from tephriphonolite to rhyolite in Aghda rocks, with the HREE varying from 6 times to 20 times chondrite (Fig. 6.14).

As shown in Figure 6.14 sample R14480 (trachyte) and R14493 (rhyolite) from Aghda have very similar REE characteristics. Both patterns show high degree of fractionation for LREE (La-Sm) whereas MREE and HREE are almost unfractionated with strong negative Eu anomalies (Eu/Eu^{*} = 0.37-0.39). The negative Eu anomaly may indicate the removal of plagioclase from the magma, because Eu is preferentially partitioned into plagioclase. Petrographic studies support this with a lack of the plagioclase being observed within these samples (Table 4.11, 4.12). The value of Yb and Lu in two samples (R14480, R14493) are considerably higher than the other samples of Aghda

region (Fig. 6.14). Petrographic and geochemical features indicate that the afore mentioned samples contain a large amount of zircon. Since HREE accumulate in zircon (Sawka, 1985), then abundance of Yb in these samples is attributed to the presence of significant amounts of zircon. Figure 6.14 also shows that, in terms of the total REE content and the presence of a distinct negative Eu anomaly (Eu/Eu^{*} = 0.37-0.39), the Aghda felsic rocks are similar to an average upper continental crust as determined from post-Archean composite shale (Taylor and Mclennan, 1985). However, felsic rocks from Aghda may be derived by melting of continental crust.

Two tephriphonolite samples (R14483, R14508), one phonotephrite (R14500) and basaltic trachyandesite (R14488) from Aghda show similar REE characteristics (Fig. 6.14). These patterns show a high degree of fractionation for LREE and HREE with La/Yb ratios between 9.30 and 15.69. A moderate but significant negative Eu anomaly (Eu/Eu^{*} = 0.72-0.75), is observed in all the patterns. The fractionation of REE is probably related to clinopyroxene and apatite removal because clinopyroxene and apatite have high partition coefficients for the REE (Green, 1994; Hauri et al., 1994; Gaetani and Grove, 1995). However, suggest that these rocks are derived from parental magmas that evolved from primary magmas produced by the partial melting of the mantle lherzolite.

The almost parallel REE patterns of the analysed samples illustrated in Figures 6.7 and 6.14 suggest that mafic-intermediate rocks from the Islamic peninsula and Aghda have close similarities in their chemical characteristics, probably indicate their derivation from the same mantle source.

8.3.2.3.3 Shahrbabak

All the analysed rocks show an enrichment in LREE and fractionated. The La and Ce exhibit highly variable behaviour in Shahrbabak rocks, with the LREE varying from 50 times to 110 times chondrite (Fig. 6.22). The MREE decrease in abundance from Sm to Ho, and the HREE are variable in composition from Ho to Lu. The REE patterns for the three rock groups from Shahrbabak are not well parallel, implying that they are not genetically related.

REE abundances for trachyte and dacite are plotted relative to chondrites in Figure 6.22. Two patterns are similar although the absolute abundances are variable with the more silicic rocks generally more enriched in the REE. None shows a significant Eu anomaly. The two patterns display a strong degree of fractionation for both LREE and HREE and ∑REE range 87-102 which are considerably lower than ∑REE tephriphonolites and trachyandesite. The overall similarity in shape of the REE patterns of the dacite and trachyte (Fig. 6.22) indicates that parental magmas to the dacite and trachyte were derived from source regions that had similar relative concentrations of REE and similar residual mineralogy. The parallel nature of the HREE patterns establishes that the residues had a big partition coefition for these elements, and consequently that they were garnet. Low abundances of HREE in trachyte and dacite magma reflect retention of these elements in residual garnet in the partially melted subducted slab eclogite. The lack of Eu anomalies and very high Sr abundances implies that plagioclase was not likely to have been a residual phase.

The basalt (R14550) shows a REE pattern (Fig. 6.22), with moderate degrees of fractionation for LREE and has a flat MREE to HREE pattern. No Eu anomaly

observed in this pattern. The absence of negative Eu anomaly with Mg-numbers greater than 50 in basalt suggests that such magmas can be produced by partial melting of spinel lherzolites (Jaques and Green, 1980).

Shoshonites are normally characterised by steep LREE patterns and rather flat HREE (Henderson, 1984; Geringer and Ludick, 1990). Two tephriphonolite (R14522, R14557) and one trachyandesite (R14528) shoshonitic samples from Shahrbabak region (Figure 6.22), show very similar REE characteristics, and a high degree of fractionation for LREE and almost unfractionation for middle and heavy REE, with La_N/Yb_N ratios between 6.61 and 7.98. A moderate negative Eu anomaly ($Eu/Eu^* = 0.60$-0.79) is observed in these two patterns. The flat HREE patterns of these rocks exclude the presence of garnet during the melting. However, tephriphonolite and trachyandesite with a strong LREE enrichment but a much flatter HREE patterns from Shahrbabak compared with modelling results of suggestive of a spinel lherzolite source (Manetti et al., 1979; Dostal and Muller, 1992)

8.4 MODEL FOR MAGMA GENESIS

8.4.1 Nd isotopes

Isotopic composition of Sr and Nd provide some of the most useful information for elucidating magmatic processes at convergent plate boundaries, because the various source components involved have contrasting isotopic signatures. Neodymium isotopic ratios measured in rocks from the Islamic Peninsula, Aghda and Shahrbabak regions, along with calculated ε_{Nd} at 9, 20 and 15 Ma are presented respectively in Table 6.7. A significant variation is evident in the ε_{Nd} of the samples from the U-DVB, which ranges from -4.7 to +4.1 and can be interpreted in terms of variable mantle sources (Pin

and Marini, 1993). The ε_{Nd} values of Tertiary volcanic rocks from the U-DVB are vary widely above and below CHUR (Chondritic Uniform Reservoir). A positive epsilon value implies that the magmas were formed from depleted mantle whereas, a negative value indicates that they were derived from enriched mantle sources (Faure, 1986). The ε_{Nd} of Shahrbabak volcanic rocks is markedly different from those of the Islamic Peninsula and Aghda. However, the high ε_{Nd} values of volcanic rocks from Shahrbabak also display lower LREE and incompatible trace element contents in comparison to low ε_{Nd} volcanic rocks from Aghda and the Islamic Peninsula (Tables. 6.6, 6.15, 6.24). The ε_{Nd} isotopic values of the Islamic Peninsula and Aghda are generally low (Table 6.7) suggesting an interaction between fluids released from subducted slab and mantle components (Jones and Cann, 1994). It is proposed that the positive ε_{Nd} values, low TiO_2, Y and HREE abundances characteristic of Shahrbabak rocks are due to derivation of magmas from depleted zone of uppermost mantle compared to the Islamic Peninsula and Aghda (McCulloch, 1993; Dupuy et al., 1995). It follows that these rocks came from two isotopically distinct source regions. The Nd isotope data give an ε_{Nd} of (-2.2 to -4.7) for the Islamic Peninsula and Aghda, which are generally low, suggesting that the fluids responsible for metasomatism of the mantle source regions could have been derived from subducted oceanic crust and overlying sediments (Jones and Cann, 1994) and for Shahrbabak is from +1.3 to +4.1 which are consistent with derivation from the mantle without or with little crustal input.

Figure 8.7 shows rocks from the U-DVB have a low and relatively restricted range of $^{143}Nd/^{144}Nd$ ratios but a wide range of $^{87}Sr/^{86}Sr$ ratios. These ratios clearly distinguish them from MORB which has higher $^{143}Nd/^{144}Nd$ (>0.5130, Saunders et al., 1988) and lower $^{87}Sr/^{86}Sr$ ratios. Then suggest that the mantle beneath the U-DVB is not of the

MORB-type, but is more radiogenic in Sr. Also, Figure 8.7 shows that the rocks of the U-DVB plot along mainly two trends reflecting Nd heterogeneity. One of these trends includes of the Shahrbabak samples, which have plotted parallel and close to mantle array, and the other trends include Islamic Peninsula and Aghda, which have relatively close trend to the Roccamonfina and Batu Tara (Stolz et al., 1988, Nelson, 1992). However, Nd isotopic differences between the Islamic Peninsula, Aghda and Shahrbabak rocks preclude any comagmatic relationships between the lavas of the Islamic Peninsula, Aghda and Shahrbabak.

8.4.2 Sr Isotopes

The regional variation in $^{87}Sr/^{86}Sr$ ratios of volcanic rocks along the U-DVB are 0.704273-0.705668 for the eastern part (Shahrbabak), 0.706508-0.708710 for central part (Aghda) and 0.707735-0.708478 for the western part (Islamic Peninsula). These variations fall within the range of values associated with magmas produced at destructive plate margins such as the Tibetan Plateau (Turner et al., 1996); Lr Antilles (Davidson, 1983; White and Patchett, 1984), Sunda arc (Stolz et al., 1990) and Roman Province (Holm et al., 1982). The observed increase in these values compared to that of MORB (typically 0.7030) is usually ascribed either to a lithospheric mantle with higher Rb/Sr ratios over a geologically long period or by fluid released from dehydration of altered basaltic crust and subducted sediments. Figure 8.8 displays the distribution of $^{87}Sr/^{86}Sr$ ratios from the Islamic Peninsula and Aghda are different from Shahrbabak and histograms from the Islamic Peninsula and Aghda are skewed toward higher values of the $^{87}Sr/^{86}Sr$, which may result from metasomatism of the upper mantle source region by a fluid that had high $^{87}Sr/^{86}Sr$ and low $^{143}Nd/^{144}Nd$ and was enriched in K, Rb and LREE. Despite the age differences between the Islamic Peninsula (8 Ma) and Aghda

(24 Ma) volcanic rocks, both areas have very close and relatively high $^{87}Sr/^{86}Sr$ and low ε_{Nd} values (Table 6.7), which suggests same mantle source for their parental magma.

8.4.2.1 Islamic Peninsula

The K-rich lavas from the Islamic Peninsula have a wide range of Sr and Nd isotopic compositions (Table 6.7). Isotopic ratios of Sr and Nd in the Islamic Peninsula lavas are shown in conventional isotope diagram in Figure 8.7 relative to other mantle derived K-rick rocks. The $^{87}Sr/^{86}Sr$ and ε_{Nd} values show large variation and have relatively overlap with those lavas from Aghda but are different from Shahrbabak. Also they fall close to the high $^{87}Sr/^{86}Sr$ and low ε_{Nd} of the Roccamonfina field (Rogers et al., 1987; Fig. 8.7). The initial $^{87}Sr/^{86}Sr$ ratios for rocks from the Islamic Peninsula are slightly more radiogenic than those for the ultra-potassic rocks from Leucite Hill, Wyoming (range 0.70537 to 0.70779; Vollmer et al., 1984) and are low radiogenic compared to the leucitites for Vulsini, Italy (range 0.70879 to 0.71105; Rogers et al., 1985). The variable $^{87}Sr/^{86}Sr$ values are taken as evidence of large geochemical heterogeneities in the mantle source.

The geochemical variation within the Islamic Peninsula province cannot be explained with different degrees of partial melting and subsequent fractionation from a broadly homogeneous mantle. The source mantle for the Islamic Peninsula magmas was anomalously and heterogeneously enriched in LFSE, LREE, high $^{87}Sr/^{86}Sr$ and low ε_{Nd} which probably related to metasomatised mantle. Because of the tectonic peculiarities of the region, processes of mantle metasomatism can be related to the migration of fluids from Cretaceous-Tertiary subduction of the Neo-Tethys oceanic crust beneath Central Iran. As proposed for high-K rocks from Italy by Dupuy et al. (1981), Civetta

et al. (1981), Rogers et al. (1985), Nelson (1992). Also data from the Islamic Peninsula rocks show negative Ta and Ti anomalies relative to the other elements (Fig. 6.6) which providing some support for this model (Maury et al., 1992).

8.4.2.2 Aghda

The Sr and Nd isotopic compositions of representative Aghda lavas are illustrated on conventional Sr-Nd covariation diagram relative to other mantle derived K-rich rocks (Fig. 8.7). Aghda lavas have a restricted range in Nd isotopic composition (ε_{Nd} = -2.2 to -3.8) and slightly more radiogenic $^{87}Sr/^{86}Sr$ (0.70651-0.70871). They plot close to the high $^{87}Sr/^{86}Sr$ and low ε_{Nd} of the field defined for Roccamonfina and Batu Tara fields (Stolz et al, 1988; Nelson, 1992; Fig. 8.7). Also initial $^{87}Sr/^{86}Sr$ ratios for rocks from Aghda are slightly less radiogenic than those for the rocks from Tibetan plateau (range 0.70792 to 0.71370; Turner et al., 1996), but are considerably more radiogenic than values for rocks from Tavua Volcano, Fiji (range 0.70356 to 0.70410; Rogers and Setterfield, 1994). The broad range of Sr and Nd isotope ratios for mafic and felsic rocks from Aghda indicates that these two groups were derived from isotopically different sources. The Sr isotope ratio of the felsic rocks are high and have low Sr contents (Tables 6.7, 6.14) suggest that probably are derived by anatexis of continental crust (Hawkesworth and Vollmer, 1979).

The mafic-intermediate rocks from Aghda with high K, LREE, Th, Zr, high $^{87}Sr/^{86}Sr$ ratios and low ε_{Nd} were generated by partial melting of metasomatism mantle (Venturelli et al., 1984, Jones and Cann, 1994) and suggest that the fluids responsible for metasomatism of the mantle source region could have been derived from subducted Neo-Tethys oceanic crust beneath Central Iran plate. As proposed for other shoshonitic

rocks in the Alpine-Himalayan orogenic belt such as Tibetan Plateau (Turner et al., 1996), Northern Karakorum (Pognante, 1990), Eastern Anatolia, Turkey (Pearce et al., 1990). It is probably most likely that the isotopic variations of the aghda volcanics reflect heterogeneities of the mantle source.

8.4.2.3 Shahrbabak

The rocks from Shahrbabak have high initial $^{143}Nd/^{144}Nd$ ratios with ε_{Nd} values (at 15 Ma) from +1.3 to +4.1 and low initial $^{87}Sr/^{86}Sr$ ratios in the range 0.70427-0.70567, contrasting with the values for the Islamic Peninsula and Aghda lavas, which show a wider range of higher $^{87}Sr/^{86}Sr$ ratios and lower ε_{Nd} (Table 6.7). The Sr and Nd isotope ratios from Shahrbabak are plotted in standard isotopic covariation diagram relative to other mantle derived rocks in Figure 8.7. The Shahrbabak samples fall far than Aghda and the Islamic Peninsula fields within the lower radiogenic field, slightly outside the mantle array, at a positive ε_{Nd} field, indicating derivation from a depleted mantle compared to the Aghda and the Islamic Peninsula, and ruling out involvement of continental crustal components in their petrogenesis. Initial $^{87}Sr/^{86}Sr$ ratios for felsic rocks from Shahrbabak are slightly low radiogenic than those for dacitic rocks from western Japan (range 0.70436 to 0.70511; Notsu et al., 1990) and $^{87}Sr/^{86}Sr$ ratios of the trachytic and dacitic rocks are relatively simillar, suggesting the same source magmas for felsic rocks (Table 6.7). But shoshonitic rocks from Shahrbabak are high radiogenic compared to shoshonitic rocks from Tavua Volcano, Fiji (range 0.70356 to 0.70410; Rogers and Setterfield, 1994). It is more likely that the isotopic variations of Shahrbabak rocks reflect that they were derived from isotopically heterogeneous mantle sources (Stolz et al., 1990).

It is accepted that comagmatic igneous rocks have been consolidated with the same $^{87}Sr/^{86}Sr$ ratio but they have different $^{87}Rb/^{86}Sr$ ratios. The plot of $^{87}Rb/^{86}Sr$ versus $^{87}Sr/^{86}Sr$ for Tertiary lavas from Shahrbabak should display a horizontal line. On the other hand, The data for Shahrbabak, do not define a horizontal line (Fig. 8.9) but have considerable scatter. The scatter in isotopic ratios may be due to contamination but the lack of correlation between the $^{87}Sr/^{86}Sr$ ratio and contents of SiO_2, Sr and Rb/Sr (Fig. 6.17) makes these possibilities unlikely.

8.4.3 Model for LFSE enrichment and HFSE depletion

Abundances of moderately and strongly incompatible elements from the U-DVB show the enrichment in LFSE and LREE and relative depletion in HFSE compared with MORB that are characteristic of magmatic arcs of convergent plate boundaries (Bacon, 1990; Stolz et al., 1996). This variation probably results from differences in degree of partial melting and amount of LFSE enrichment of the mantle wedge and extent of fractional crystallisation. Many authors have argued convincingly that much of the LFSE enrichment is a result of addition of a subduction component to the mantle wedge via aqueous fluid derived from dehydration of the subducting oceanic crust and overlying sediment (e.g. Tatsumi et al., 1986; Davidson et al., 1987; Ellam and Hawkesworth, 1988; Pearce and Peat, 1995).

In the U-DVB rocks, if crustal contamination of mantle derived liquid was minimal or non-existent, the high concentration of LFSE must be inherited from the source region. In regions where the presence of an active Benioff zone has been established, most authors generally accepted that subducting slabs act more like a catalyst for inducing melting in the overlying mantle wedge by supplying fluids released by dehydration

reactions (e.g. McCulloch, 1993; Tatsumi and Eggins, 1996). The released super critical fluids carry water soluble components such as alkalies and LFSE including Rb, Sr, Ba, Th, U and LREE (McCulloch and Gamble, 1991). There are numerous theories for the origin of HFSE depletions in arc magmas, but no consensus. One hypothesis is that Nb and Ta are relatively insoluble in hydrous fluids evolved by the dehydration of the downgoing slab in a subduction zone, compared to LFSE and LREE (Saunders et al., 1980; Hawkesworth et al., 1993). Metasomatism by these fluids may enrich the mantle source of arc magmas in LFSE and LREE, but not Nb and Ta. Also HFSE depletions may result from reaction between ascending basaltic liquids and depleted peridotite in mantle wedge (Kelemen et al., 1990; Kelemen et al., 1992). The HFSE including Ti, Zr, Nb, Y and HREE are immobile during alteration of mafic or even felsic rocks by hydrous fluids (Saunders et al., 1979). Thus, it is probable that HFSE is refined in the subducting slab which sinks into lower mantle. It has also been suggested that under high PH_2O and fO_2 (normally expected in subduction zone environment) minor mineral phases such as ilmenite, sphene (containing Ti, Nb and Ta) and zircon (containing Zr and Hf) gets stabilised within the subducting slab or mantle wedge (Saunders et al., 1980). Thus, on melting of such enriched mantle wedge will generate magma enriched in alkalies, LFSE, LREE and depleted in HFSE-HREE, erupting as magmatic arc volcanics located about 100 to 150 km above the subducting slab (Crawford et al., 1987; Tatsumi, 1986). The above petrogenetic models suggesting fluid phase mantle metasomatism can explain most of the observed chemical features in the U-DVB. This model has been invoked in many area such as the Tibetan Plateau (Turner et al., 1996), Leucite Hills, Wyoming (Vollmer, 1984), Sunda arc (Stolz et al., 1990), Tavua Volcano, Fiji (Rogers and Setterfield, 1994).

The geochemical features of the mafic to intermediate rocks from the Islamic Peninsula and Aghda, suggest that: alkaline and calcalkaline melts may have been generated by partial melting of metasomatised peridotitic material and subsequent fractional crystallisation. Also, plot of highly incompatible element ratios (Fig. 8.10) shows strong overlap in these ratios for the Islamic Peninsula and Aghda rocks indicate that probably they were derived from same mantle source. But differences in the most mafic rocks from the Islamic Peninsula and Aghda reflect compositional differences or the degree of enrichment of incompatible elements in the source regions. However, many observed geochemical variations in Shahrbabak rock, particularly in $^{87}Sr/^{86}Sr$ ratios, Ba, LREE and scatter incompatible elements in Figure 8.5 reflects heterogeneity in the mantle source for Shahrbabak rocks.

8.5 SUMMARY

There are two major theories for the genesis of the U-DVB rocks. The first ascribes the origin of the volcanic belt to continental rifting while the second, more widely accepted model involves subduction. The tectonic setting together with available geochemical and isotopic data, for the studied rocks do not characterise a rift model for the U-DVB rocks. Most of the potassic rocks from the studied areas show high Al_2O_3, K_2O, LFSE and LREE abundances and low abundances of TiO_2 and HFSE, Ta, Nb and Zr in addition to LREE>Nb and Zr>Y. Those features provide strong evidence of the involvement of subduction-related processes in the generation of orogenic potassic magmas in the U-DVB. Also, trace-element ratios suggest a subduction zone source for the U-DVB. Based on the isotopic and geochemical evidence of this study, the Islamic Peninsula and Aghda rocks are considered to be from Neo-Tethys ocean, but those of Shahrbabak region are related to Nain-Baft ocean. For several reasons, geochemical

data obtained from most samples of the studied areas are not consistent with generation of lavas by melting of the subducted oceanic slab. The exception is only for two samples of dacite and trachyte from Shahrbabak. The maximum Ni contents in the rocks of the studied areas are below the lower limit of Ni contents for primary mantle-derived magmas. According to the results of geochemical and REE analyses, generation of K-rich alkaline magmas from the Islamic Peninsula could be related to a small degree of partial melting of mantle lherzolite source. The REE Patterns for the rocks from the Islamic Peninsula are linear with a small negative Eu anomaly, implying their cogenetic nature. Trachyte and rhyolite from aghda have very similar REE characteristics. Both patterns show high degree of fractionation for LREE whereas MREE and HREE are almost unfractionated with strong negative Eu anomalies. These features indicate that felsic rocks from Aghda may be derived by melting of continental crust. However, suggest that mafic-intermediate rocks from Aghda are derived from parental magmas that evolved from primary magmas produced by the partial melting of the mantle lherzolite. The REE patterns for the three rock groups from Shahrbabak are not well parallel, implying that they are not genetically related. The REE patterns for trachyte and dacite display a strong degree of fractionation for both LREE and HREE. Low abundances of HREE in trachyte and dacite magma reflect retention of these elements in residual garnet in the partially melted subducted slab eclogite. The absence of negative Eu anomaly with Mg-number greater than 50 in basalt suggests that such magmas can be produced by partial melting of spinel lherzolites. However, tephriphonolite and trachyandesite with a strong LREE enrichment but a much flatter HREE patterns from Shahrbabak compared with modelling results of suggestive of a spinel lherzolite source. A significant variation is evident in the ε_{Nd} of the samples from the U-DVB, which ranges from -4.7 to +4.1 and can be interpreted in terms of

variable mantle sources. The ε_{Nd} of Shahrbabak volcanic rocks is markedly different from those of the Islamic Peninsula and Aghda. The ε_{Nd} isotopic values of the Islamic Peninsula and Aghda are generally low (Table 6.7) suggesting an interaction between fluids released from subducted slab and mantle components. It is proposed that the positive ε_{Nd} values, low TiO_2, Y and HREE abundances characteristic of Shahrbabak rocks are due to derivation of magmas from depleted zone of uppermost mantle compared to the Islamic Peninsula and Aghda. The source mantle for the Islamic Peninsula magmas was anomalously and heterogeneously enriched in LFSE, LREE, high $^{87}Sr/^{86}Sr$ and low ε_{Nd} which probably related to metasomatised mantle. The broad range of Sr and Nd isotope ratios for mafic and felsic rocks from Aghda indicates that these two groups were derived from isotopically different sources. The Sr isotope ratio of the felsic rocks are high and have low Sr contents (Tables 6.7, 6.14) suggest that probably are derived by anatexis of continental crust. The mafic-intermediate rocks from Aghda with high K, LREE, Th, Zr, high $^{87}Sr/^{86}Sr$ ratios and low ε_{Nd} were generated by partial melting of metasomatised mantle. However, It is more likely that geochemical variations in Shahrbabak rocks, particularly in $^{87}Sr/^{86}Sr$ ratios, Ba, LREE and scatter incompatible elements reflects heterogeneity in the mantle source for Shahrbabak rocks.

CHAPTER 9

CONCLUSIONS

9.1 CONCLUSIONS

The U-DVB is the largest volcanic belt in Iran and runs parallel to the Zagros Fold-Thrust Belt, approximately 150 km northeast of the Zagros Main Thrust Line which marks the boundary between the Arabian and Central Iranian continental plates.

The three study areas (Islamic Peninsula, Aghda and Shahrbabak) in the U-DVB consist mainly of Tertiary (Oligocene-Miocene) volcanic rocks. Due to the relatively young age of the rocks and occurrence of sanidine, biotite and hornblende, the K-Ar method of isotopic dating was used for age determinations. Stratigraphic relationships within each area are summarised in geological maps and stratigraphic tables and only units for which age-data are available are discussed in the text.

The Islamic Peninsula stratovolcano was formed during two major eruptive episodes which produced deposits ranging from tephrite to trachyte in composition. The K-Ar dates for sanidine and biotite in the trachyandesite and trachyte were determined. The age of 6.5±1 Ma is taken to represent the time of crystallisation of the trachyte because of its concordance with field relationships and the K-Ar age of 8.0±2 Ma for the older trachyandesite plug.

The Aghda area is composed of Eocene-Miocene volcanic rocks. Tephriphonolite rocks from Aghda contain large trapezohedra of analcime and pumpellyite which are interpreted to reflect ion-exchange pseudomorphous replacement of primary leucite,

followed by zeolite facies metamorphism. Whole-rock K-Ar dating from tephriphonolite obtained by Bina et al. (1986) indicates a minimum age for the lava and a maximum age for metamorphism. The K-Ar age of 15.7±1 Ma on hornblende from the trachyandesite (in Kuh-e-Mil located in the northern part of the Aghda), is interpreted as the age of emplacement of the plug.

Isotopic data from this study are combined with those of obtained by Hassanzadeh (1993) (Tble 3.1) indicate that magmatic activity in Shahrbabak region occurred during four episodes: comprising eruption of the Razak series, the Hezar series, Mid-Miocene volcanism and late Miocene-Pliocene activity. An Ar-Ar isotopic age of 37.5±1.4 Ma for albite from a silicified trachyte lava in the Razak volcanic series is consistent with the late Eocene stratigraphic age and is interpreted as the age eruption (Hassanzadeh, 1993). Volcanic units of the Hezar series lack biotite and amphibole but are characterised by the occurrence of large analcime pseudomorphs after leucite set in a groundmass rich in K-feldspar. The variable ages for tephriphonolites presumably reflect variable elemental exchange during pseudomorphous replacement of primary leucite by analcime and do not record the age of crystallisation.

The isotopic age (Ar-Ar) of 29.8±0.6 Ma for tephriphonolite from a stratigraphically higher lava in the Hezar series is considered to represent the time of crystallisation. Isotopic data from the dacite plug of Kuh-e-Tezerj in the northeastern part of the study area yield a K-Ar age of 16.4±1 Ma which is essentially coeval with mid-Miocene Ar-Ar dates (Hassanzadeh, 1993) for andesite lava and quartz monzonite intrusion. Several large Late Miocene-Pliocene stratovolcanoes also occur in the Shahrbabak region. The K-Ar age of the trachyandesite intrusion located northeast of Qotb-Abad is 6.5±1 Ma

which is consistent with the field relationships and thus is interpreted as the age of intrusion.

Miocene rocks of the Islamic Peninsula are similar in mineralogy and texture. Primary minerals comprise diopside, sanidine, leucite, biotite, titanomagnetite and accessory apatite. Diopside, leucite and sanidine are the dominant phenocrystic phases.

In the Aghda region all rock types except tephriphonolite have a similar texture and mineralogy. Tephriphonolite is distinguished by the occurrence of abundant (commonly 40% by volume), large trapezohedra of analcime and pumpellyite. Primary minerals comprise sanidine, diopside, plagioclase, titanomagnetite and accessory apatite and zircon. Secondary analcime and pumpellyite are common.

Six of the seven different rock types which occur in the Shahrbabak region have common textural and mineralogical characteristics. The exception is the tephriphonolite which contains abundant (up to 30% by volume), large trapezohedra of analcime. The mineralogy of all samples comprise plagioclase, sanidine, diopside, analcime, hornblende, biotite, olivine and titanomagnetite, together with accessory apatite and zircon. Plagioclase is the dominant felsic mineral in most rock types, and in some samples phenocrysts are rimmed by sanidine. Normal and oscillatory zoning are common, as is albite and carlsbad twinning and alteration to sericite.

Diopside is the only pyroxene present in samples from all three study areas. In most diopside crystals the average content of MgO is higher in the core than the rim. This variation is consistent with normal fractionation during magmatic evolution. Most of

the diopside phenocrysts from the study areas show normal zoning, except phenocrysts in tephritic rocks from the Islamic Peninsula which show oscillatory zoning.

Anorthoclase is the only K-feldspar present in samples from the Islamic Peninsula, Aghda and Shahrbabak and have a compositions of $Or_{62.8\text{-}72.9}$, $Or_{74.6\text{-}98.1}$ and $Or_{31.5\text{-}92.9}$ respectively. Spherulite intergrowths of quartz and anorthoclase occur in some samples and are attributed to simultaneous crystallisation of these two minerals.

Most plagioclase phenocrysts from the Aghda and Shahrbabak regions have Ca-rich cores and more Na-rich rims, which is attributed to normal magmatic fractionation. Some plagioclase phenocrysts in some samples are commonly rimmed by sanidine. Some Plagioclase phenocrysts from the study areas show minor normal compositional zoning with the exception of plagioclase in the trachybasalt, dacite and trachyandesite from Shahrbabak and Aghda respectively which show oscillatory zoning. The composition of plagioclase phenocrysts ranges from oligoclase to bytownite.

Analysed olivine crystals from the Islamic Peninsula and Shahrbabak are unzoned. The olivine grains have low contents of TiO_2, Al_2O_3, Cr_2O_3 and NiO, but some substitution of CaO for MgO, and MnO for FeO has occurred. The calculated Mg-numbers for the three whole-rock samples and liquid in equilibrium with the analysed olivine show the closest correspondence when a Kd value of 0.4 for Mg in olivine is used. This suggests that the olivine phenocrysts crystallised at high pressure.

Most of the biotite crystals from the study areas are fresh. The absence of significant alteration is supported by the relatively high K_2O content. Chemical data for biotite

from the Islamic Peninsula and Shahrbabak have a restricted range of values of $Mg/Mg+Fe^{2+}$ with all analyses except two plotting as biotite; the exceptions plot in the phlogopite field.

The Fe-Ti oxide crystals from the study areas are relatively Ti-rich and are classified as titanomagnetite except those in trachyte and trachyandesite from Shahrbabak which have low (<3%) TiO_2 contents and which are classified as magnetite.

Amphibole occurs only in the high-K calcalkaline rocks from the Aghda and Shahrbabak regions. Chemical data show that the amphibole grains are magnesio-hornblende. The fractionation factors calculated for MgO and FeO in magnesio-hornblende indicate that crystallisation occurred at a low temperature. The fractionation factor for TiO_2 in the studied samples suggests crystallisation at crustal pressures.

Leucite phenocrysts are abundant in the rocks of the Islamic Peninsula. The rims of some leucite grains have been changed to nepheline and some of phenocrysts have been pseudomorphed by analcime. Leucite from the Islamic Peninsula is characterised by having structural formulae in which the numbers of Si ions is either 1 or 2. All analysed leucites are nearly stoichiometric except for two analyses, which show a cation deficiency with Si/Al<2.

In the tephriphonolite lavas from the Aghda region, analcime crystals are remarkably homogeneous in composition and lack evidence for rapid transport of crystals from the depths indicated by the stability field for analcime. In addition, the rocks contain only minute amounts of a hydrous phase (biotite) and primary crystallisation of a Na-rich

phase such as analcime would necessitate crystallisation of a sodic pyroxene rather than diopside. The analcime is interpreted as having formed by ion-exchange pseudomorphous replacement of primary leucite, either during cooling of the lavas or shortly afterwards. The pumpellyite trapezohedra are composed mainly of an aggregate of randomly arranged colourless pumpellyite flakes which are compositionally typical of pumpellyite produce during low-grade metamorphism. In the tephriphonolite lava, the analcime became unstable and was replaced by pumpellyite which has a wide range in compositions related to Fe-Al and Fe-Mg substitution. The occurrence of analcime and pumpellyite at Aghda is indicative of zeolite facies metamorphism and may be related to conditions of low f_{co2} and H_2O activity and probably high P_{fluid}.

Lavas from the Islamic Peninsula exhibit a continuum of compositions which range from 43.54% to 58.02% SiO_2 and posses the characteristics of a typical high-K alkaline suite and are characterised by being undersaturated to saturated in SiO_2, with low average contents of Al_2O_3 and TiO_2, and high contents of CaO and K_2O. The content of total Fe as FeO decreases from mafic to felsic rocks which may be related to crystal fractionation of clinopyroxene and olivine. The rocks are enriched in incompatible elements, but compatible elements are relatively low in abundance. The behaviour of different major and trace elements relative to MgO content suggests that fractional crystallisation is the main process involved in the development of these rocks. The high-K alkaline rocks from the Islamic Peninsula have initial $^{87}Sr/^{86}Sr$ ratios of 0.70774-0.70848 and the ε_{Nd} value ranging from -4.7 to -3.3. This difference is not related to a simple fractionation processes, because the range of initial isotopic values is higher than the analytical uncertainty. Multi-element patterns for all rock types from the Islamic peninsula are almost parallel, implying their cogenetic nature and most

elements (especially Ba, Th, Nb and Ce) are significantly enriched compared to MORB (Fig. 6.6).

Rocks from Aghda are characterised by being oversaturated to undersaturated in SiO_2, mafic to felsic in composition, high in Al_2O_3, CaO and alkalies and incompatible elements but low in TiO_2, MgO and compatible elements. The average contents of total Fe as FeO and MgO are higher in basaltic trachyandesite than all other samples from Aghda. The content of MgO decreases from basaltic trachyandesite towards trachyandesite which may be related to crystal fractionation of clinopyroxene and olivine. Harker diagrams show two distinct groups comprising mafic-intermediate and felsic rocks. The low Mg-number, Cr, Ni and V contents for mafic rocks from the Aghda region imply that these rocks do not represent primary mantle derived melts. Spidergram patterns show most elements are significantly enriched in Aghda samples compared to MORB, while K, Ta, P and Ti show negative anomalies. Differences in the incompatible element patterns implies that mafic and felsic rocks from the Aghda region are genetically unrelated.

Although there are some significant geochemical differences among the volcanic rocks from Shahrbabak, particularly in the abundances of alkalies and the degree of silica saturation, there are some similarities including low Mg-numbers and contents of TiO_2 and compatible elements, but high contents of Al_2O_3, CaO, and the incompatible elements (K, Ba, Sr, Rb, Th, Nd and LREE). Harker diagrams show three distinct groups comprising mafic, mafic-intermediate and the felsic rocks. Most of the rocks from Shahrbabak have low Sc, Cr and Ni contents. The low Mg-number, Cr and Ni contents of the rocks from Shahrbabak preclude their being primary melts of mantle

peridotite. Spidergram patterns show most elements are significantly enriched in the Shahrbabak samples compared to MORB, while K, Ta and Ti show negative anomalies. The multi- element patterns of three groups from Shahrbabak are not parallel, implying they are not cogenetic.

On the basis of K_2O and SiO_2 contents the volcanic rocks from the U-DVB are typical of the leucititic, shoshonitic and high-K calcalkaline rock associations. The studied rocks from the U-DVB are mainly shoshonitic and leucititic in affinity. Comparison of geochemical data for leucititic, shoshonititic and high K-calcalkaline rocks from various tectonic and geographic regions shows that the rocks of each association form a coherent group, and that most of the U-DVB rocks fall in the range of values from these regions.

The tectonic setting together with geochemical and isotopic data for the studied rocks do not support a rift model for the generation of the U-DVB rocks. Most of the potassic rocks from the studied areas show high contents of Al_2O_3, K_2O, LFSE and LREE abundances and low abundances of TiO_2 and HFSE, Ta, Nb and Zr in addition to LREE>Nb and Zr>Y. Those features, together with trace element ratios, provide strong evidence of the involvement of subduction-related processes in the generation of potassic magmas in the U-DVB. The geochemical and isotopic data from the U-DVB imply that the volcanic rocks have been generated from two source materials; one yielding material rich in K-group elements and high $^{87}Sr/^{86}Sr$ values and low $^{143}Nd/^{144}Nd$ values for the Islamic Peninsula and Aghda; and the other yielding material low in K-group elements and low $^{87}Sr/^{86}Sr$ values and high $^{143}Nd/^{144}Nd$ values for Shahrbabak. Generation of K-rich alkaline magmas from the Islamic Peninsula could be

related to a small degree of partial melting of mantle lherzolite source. The REE patterns for the rocks from the Islamic Peninsula are parallel with a small negative Eu anomaly, implying their cogenetic nature. Trachyte and rhyolite from Aghda have very similar REE characteristics. Both patterns show a high degree of fractionation for LREE whereas MREE and HREE are almost unfractionated with strong negative Eu anomalies. These features indicate that felsic rocks from Aghda may be derived by melting of continental crust. The REE patterns for the three groups from Shahrbabak are not parallel, implying that they are not genetically related. The REE patterns for trachyte and dacite display a strong degree of fractionation for both LREE and HREE. Low abundances of HREE in trachyte and dacite magma reflect retention of these elements in residual garnet in partially melted subducted slab eclogite.

The ε_{Nd} values for samples from Shahrbabak volcanic rocks are markedly different from those of the Islamic Peninsula and Aghda and probably reflect differences in the mantle sources. The ε_{Nd} values for Islamic Peninsula and Aghda are generally low (Table 6.7) suggesting an interaction between fluids released from subducted slab and mantle components. It is proposed that the positive ε_{Nd} values, low TiO_2, Y and HREE abundances characteristic of Shahrbabak rocks are due to derivation of magmas from a depleted zone of uppermost mantle compared to the Islamic Peninsula and Aghda. The source mantle for the Islamic Peninsula magmas was anomalously and heterogeneously enriched in LFSE, LREE, high $^{87}Sr/^{86}Sr$ and low ε_{Nd} which was probably related to metasomatism. The broad range of Sr and Nd isotope ratios for mafic and felsic rocks from Aghda indicates that these two groups were derived from isotopically different sources. The felsic rocks have high initial Sr isotopic ratios and have low Sr contents (Tables 6.7, 6.14), suggesting that they were probably derived by anatexis of

continental crust. The mafic-intermediate rocks from Aghda with high K, LREE, Th, Zr, high $^{87}Sr/^{86}Sr$ ratios and low ε_{Nd} were generated by partial melting of metasomatised mantle. Geochemical variations in Shahrbabak rocks, particularly in $^{87}Sr/^{86}Sr$ ratios and contents of Ba, LREE and incompatible elements reflect heterogeneity in the mantle source.

AGUIRRE L. & ATHERTON M. P. 1987. Low-grade metamorphism and geotectonic setting of the Macuchi Formation, Western Cordillera of Ecuador. *Journal of Metamorphic Geology* **5**, 473-494.

ALAVI M. 1980. Tectonostratigraphic evolution of the Zagros side of Iran. *Geology* **8**, 144-149.

ALAVI M. 1991. Sedimentary and structural characteristics of the Paleo-Tethys remnants in northeastern Iran. *Geological Society of America, Bulletin* **103**, 983-992.

ALAVI M. 1994. Tectonics of the Zagros orogenic belt of Iran: new data and interpretations. *Tectonophysics* **229**, 211-238.

ALAVI-TEHRANI N. 1975. On the metamorphism in the ophiolitic rocks in the Sabzevar region. Proceeding of Tehran Symposium, Geodynamics of SW Asia. *Geological Survey of Iran, Special Publication*, 25-52.

ALAVI-TEHRANI N. 1976. Geology and petrography in the ophiolite range NW of Sabzevar (Khorassan/Iran) with special regard to metamorphism and genetic relations in an ophiolite suite. *dissertation der mathematisch-naturwissenschaftlichen Fakultat der Universitat Saarlande.*

ALDAHAN A. A. 1986. Occurrence of epidote, pumpellyite and prehnite in Proterozoic clastics, dolerites and basalts from central Sweden. *Neues Jahrbuch fur Geologie und Palaontologie Abhandlungen* **155**, 147-164.

ALIBERT C., MICHARD A. & ALBAREDE F. 1983. The transition from alkali basalts to kimberlites: Isotope and trace element evidence from melilitite. *Contributions to Mineralogy and Petrology* **82**, 176-186.

ALLAN J. F., CHASE R. L., COUSENS B., MICHAEL P. J., GORTON M. P. & SCOTT S. D. 1993. The Tuzo Volcanic Field, NE Pacific: Alkaline volcanism at a complex, diffuse, transform-trench-ridge triple junction. *Journal of Geophysical Research* **98**, 22367-22387.

AMIDI S. M. 1975. Contribution a l'etude stratigraphique, petrologique et petrochimique des roches magmatiques de la region Natanz-Nain-Surk (Iran Central). Thesis, Universite Scientifique et Medicale de Grenoble, France (unpubl.).

AMIDI S. M. 1977. Etude geologique de la region de Natanz-Surk (Iran Central), stratigraphie et petrologie, *Geological Survey of Iran* **42**, 316 p.

AMIDI S. M., EMAMI M. H. & GRENOBLE R. M. 1984. Alkaline character of Eocene volcanism in the middle part of Central Iran and it's geodynamic situation. *Geologische Rundschau* **73**, 917-932.

AMIDI S. M. & MICHEL R. 1985. Cainozoic magmatism of the Surk area (Central Iran): stratigraphy, petrography, geochemistry and their geodynamic implications. *Geologie Alpine* **61**, 1-17.

APPLETON J. P. 1972. Petrogenesis of potassium-rich lavas from the Roccamonfina volcano, Roman region, Italy. *Journal of Petrology* **13**, 425-456.

ARNAUD N. O., VIDAL PH., TAPPONNIER P., MATTE PH. & DENG W. M. 1992. The high K_2O volcanism of northwestern Tibet: Geochemistry and tectonic implications. *Earth and Planetary Science Letters* **111**, 351-367.

ASSERETO R. 1966. The Jurassic Shemshak Formation in Central Elburz (Iran). *Review Italian Palaeontology Strata* **72**, 1133-1182.

ATAPOUR H. 1994. Petrological study of shoshonitic rocks, Bardsir (God-e-Biabany), Iran. MSC thesis, University of Shahid Bahonar, Kerman (unpubl.).

BACON C. R. 1990. Calcalkaline, shoshonitic, and primitive tholeiitic lavas from monogenetic volcanoes near Crater Lake, Oregon. *Journal of Petrology* **31**, 135-166.

BARBIERI M., PECCERILLO A., POLI G. & TOLOMEO L. 1988. Major, trace element and Sr isotopic composition of lavas from Vico volcano, Central Italy and their evolution in an open system. *Contributions to Mineralogy and Petrology* **99**, 485-497.

BARTH S., OBERLI F., MEIER M., BLATINER P., BARGOSSI G. M. & BATTISTINI G. D. 1993. The evolution of a calcalkaline basic to silica magma system: Geochemical and Rb-Sr, Sm-Nd, and 180/160 isotopic evidence from the late Hercynian Atesina-Cimad, Asta volcano-plutonic complex, Northern Italy. *Geochemica et Cosmochimica Acta* **57**, 4285-4300.

BASALTIC VOLCANISM STUDY PROJECT (BVSP). 1981. *Basaltic volcanism on the terrestrial planets*. Pergamon press, New York.

BECCALUVA L., DIGIROLAMO P. & SERRI G. 1991. Petrogenesis and tectonic setting of the Roman Province, Italy. *Lithos* **26**, 191-221.

BELL K. & POWELL J. L. 1969. Strontium isotopic studies of alkalic rocks: The potassium-rich lavas of the Birunga and Toro-Ankole regions, East and Central Equatorial Africa. *Journal of Petrology* **10**, 536-572.

BELOUSSOV V. V. & SHOLPO N. V. 1976. Geodynamics of the eastern part of the Mediterranean Alpine Belt. *Tectonophysics* **35**, 27-34.

BERBERIAN F. 1981. Petrogenesis of Iranian plutons: A study of the Natanz and Bazman intrusive complexes. PhD Thesis, University of Cambridge, London (unpubl.).

BERBERIAN F. & BERBERIAN M. 1981. Tectono-plutonic episodes in Iran. *In* Gupta H.K. and Delany F.M. eds. *Zagros, Hindu Kush, Himalaya. Geodynamic Evolution,* pp. 5-32. American Geophysical Union Geodynamics Series **3**.

BERBERIAN F., MUIR I.D., PANKHURST R.J. & BERBERIAN M. 1982. Late Cretaceous and Early Miocene Andean-type plutonic activity in northern Makran and Central Iran. *Journal of the Geological Society of London* **139**, 605-614.

BERBERIAN M. 1976. Contribution to the seismotectonics of Iran (part II). *Geological Survey of Iran, Internal Report* **39**, 518 p.

BERBERIAN M. 1977. Contribution to the seismotectonics of Iran (part III). *Geological Survey of Iran, Internal Report* **40**, 279 p.

BERBERIAN M. 1983. The Southern Caspian: A compressional depression floored by a trapped, modified oceanic crust. *Canadian Journal of Earth Sciences* **20**, 163-183.

BERBERIAN M. & KING G. C. P. 1981. Towards a paleogeography and tectonic evolution of Iran. *Canadian Journal of Earth Sciences* **18**, 210-265.

BERBERIAN M. & NOGOL M. 1974. Preliminary Khalor maps with some remarks on the metamorphic complexes and tectonics of the area (two geological maps 1:100,000 from the Hajiabad quadrangle map). *Geological Survey of Iran, Internal Report,* 60 p.

BERGMAN S. C. 1987. Lamproites and other potassium-rich igneous rocks; a review of their occurrence, mineralogy and geochemistry. *in*: Fitton J. G. and Upton B. G. J. eds. *Alkaline igneous rocks,* pp. 103-190. Geological Society London Special Publicatio

BEST M. G. 1982. *Igneous and Metamorphic Petrology*. Freeman, New York.

BEVINS R. E. & MERRIMAN R. J. 1988. Compositional controls on coexisting prehnite-actinolite and prehnite-pumpellyite facies assemblages in the Taly Fan metabasite intrusion, North Wales; implications for Caledonian metamorphic field gradients. *Journal of Metamorphic Geology* **6**, 17-39.

BINA M. M., BUCUR I., PREVOT M., MEYERFELD Y., DALY L., CANTAGREL J. M. & MERGOIL J. 1986. Palaeomagnetism, petrology and geochronology of Tertiary magmatic and sedimentary units from Iran. *Tectonophysics* **121**, 303-329.

BIRCH W. D. 1978. Mineralogy and geochemistry of the leucitite at Cosgrove, Victoria. *Journal of the Geological society of Australia* **25**, 369-385.

BIRD P. 1978. Finite element modelling of lithosphere deformation: The Zagros collision orogeny. *Tectonophysics* **50**, 307-336.

BLOOMER S. H., STERN R. J., FISK E. & GESCHWIND C. H. 1989. Shoshonitic volcanism in the Northern Mariana Arc. Mineralogic and major and trace element characteristics. *American Geophysical Union* **94**, 4469-4496.

BORIANI A., GIOBBI ORIGONI E. & PINARELLI L. 1995. Paleozoic evolution of southern Alpine crust (northern Italy) as indicated by contrasting granitoid suites. *Lithos* **35**, 47-63.

BORLEY G. D. 1974. Oceanic Islands, *in*: Sorensen H. ed. *The Alkaline Rocks*, pp. 311-330. Johen Wiley and Sons, London.

BOSE M. K., GHOSH A. K. & CZYGAN W. 1982. K-Rb relations in the alkaline suites of the eastern Ghats Precambrian belt, India. *Lithos* **15**, 77-84.

BROPHY J. G. 1990. Andesites from northeastern Kanaga island, Aleutians. *Contributions to mineralogy and petrology* **104**, 568-581.

BROWN F. H. & CARMICHAEL I. S. E. 1969. Quaternary volcanoes of the Lake Rudolf region: Part 1, The basanite tephrite series of the Korath Range. *Lithos* **2**, 239-260.

BUSHARA M. N. 1995. Subsurface structure of the eastern edge of the Zagros Basin as inferred from gravity and satellite data. *American Association of Petroleum Geologists, Bulletin* **79**, 1259-1274.

CARMICHAEL I. S. E. 1967. The iron-titanium oxides of salic volcanic rocks and their associated ferromagnesian silicates. *Contributions to Mineralogy and Petrology* **14**, 36-64.

CAROFF M., MAURY R. C., LETERRIER J., JORON J. L., COTTEN J. & GUILLE G. 1993. Trace element behaviour in the alkali basalt-comenditic trachyte series from Mururoa Atoll, French Polynesia. *Lithos* **30**, 1-22.

CARR P. F. 1984. The Late Permian shoshonitic province of the southern Sydney Basin. PhD thesis, University of Wollongong, Wollongong (unpubl.).

CAWTHORN R. G. 1976. Some chemical controls on igneous amphibole compositions. *Geochimica et Cosmochimica Acta* **40**, 1319-1328.

CEBRIA GOMEZ J. M. 1990. PX: A program for pyroxene classification and calculation of end-members. *American Mineralogists* **75**, 1426-1427.

CHIARAMONTI P. C., CUNDARI A., GOMES C. B., PICCIRILLO E. M., CENSI P., DEMIN A., BELLIENI G., VELAZQUEZ V. F. & ORUE D. 1992. Potassic dyke swarm in the sapucai graben, eastern paraguay: Petrographical, mineralogical and geochemical outlines. *Lithos* **28**, 283-301.

CIGOLINI C., KUDO A. M., BROOKINS D. G. & WARD D. 1991. The petrology of Poas volcano lavas: Basalt-andesite relationship and their petrogenesis within the magmatic arc of Costa Rica. *Journal of Volcanology and Geothermal Research* **48**, 367-384.

CIVETTA L.,INNOCENTI F., MANETTI P., PECCERILLO A. & POLI G. 1981. Geochemical characteristics of potassic volcanics from Mt. Ernici (Southern Latium, Italy). *Contributions to Mineralogy and Petrology* **78**, 37-47.

CLAGUE D. A. & FREY F. A. 1982. Petrology and trace element geochemistry of the Honolulu volcanics, Oahu: Implications for the oceanic mantle beneath Hawaii. *Journal of Petrology* **23**, 447-504.

CLAPROTH R. 1989. Petrography and geochemistry of volcanic rocks from Ungaran, Central Java, Indonesia. PhD Thesis, University of Wollongong, Wollongong (unpubl.).

COLMAN-SADD S. 1978. Fold development in Zagros simply folded belt southwest Iran. *American Association of petroleum Geologists, Bulletin* **62**, 984-1003.

COLTORTI M., BATTISTINI G., NAPPI G., RENZULLI A. & ZEDA O. 1991. Structural setting and magmatic evolution of Montefiascone volcanic complex, Vulsini district, central Italy. *Journal of Volcanology and Geothermal Research* **46**, 99-124.

COMIN-CHIARAMONTI P., MERIANI S., MOSCA R. & SINIGOI S. 1979. On the occurrence of analcime in the northeastern Azerbaijan volcanics (northwestern Iran). *Lithos* **12**, 187-198.

CONRAD G., CONRAD J. & GIROD M. 1977. Les formation continentals tertiaries et quaternaires du block du lout (Iran): Importance du plutonisme et du volcanisme. *Memoire Hors-Serie N° 8 de la Societe Geologique de France* **8**, 53-75.

CONTICELLI S. & PECCERILLO A. 1992. Petrology and geochemistry of potassic and ultrapotassic volcanism in central Italy: Petrogenesis and inferences on the evolution of the mantle source. *Lithos* **28**, 221-240.

CORRIREAU L. & GORTON M. P. 1993. Coexisting K-rich alkaline and shoshonitic magmatism of arc affinities in the Proterozoic: A reassessment of syenitic stocks in the southwestern Grenville province. *Contributions to Mineralogy and Petrology* **113**, 262-279.

COX K. G. 1980. A model for flood basalt volcanism. *Journal of Petrology* **21**, 629-50.

CRAWFORD A. J., CORBETT K. D. & EVERARD J. L. 1992. Geochemistry of the Cambrian volcanic-hosted massive sulfide-rich Mount Read Volcanics, Tasmania, and some tectonic implications. *Economic Geology* **87**, 597-619.

CRAWFORD A. J., FALLOON T. J. & EGGINS S. 1987. The origin of island arc high-alumina basalts. *Contributions to Mineralogy and Petrology* **97**, 417-430.

CRAWFORD A. R. 1972. Iran continental drift and plate tectonic. *International Geological Congress, 24th Montreal* **3**, 106-112.

CUNDARI A. 1979. Petrogenesis of leucite-bearing lavas in the Roman Volcanic Region, Italy. The Sabatini lavas. *Contributions to Mineralogy and Petrology* **70**, 9-21.

CUNDARI A. & MATTIAS P. P. 1974. Evolution of the Vico lavas, Roman volcanic region, Italy. *Bulletin of Volcanology* **38**, 98-114.

DARVICHZADEH A. 1992. *Geology of Iran.* Basic science book collections, Neda Publication, Tehran.

DAVIDSON J. P. 1983. Lesser Antilles isotopic evidence of the role of subducted sediment in island arc magma genesis. *Nature* **306**, 253-256

DAVIDSON J. P., DUNGAN M. A., FERGUSON K. M. & COLUCCI M. T. 1987. Crust-magma interactions and the evolution of arc magmas: The San pedro-pellado volcanic complex, Southern Chilean Andes. *Geology* **15**, 443-446.

DAVIES G. R. & LIOYD F. 1988. Pb-Sr-Nd isotope and trace element data bearing on the origin of the potassic subcontinental lithosphere beneath south west Uganda. *In Proceding 4th. International conferences on the kimberlite.* Perth, Western Australia. Blackwell Scientific, Oxford.

DAVOUDZADEH M. & SCHMIDT K. 1982. Contribution to the Palaeogeography, stratigraphy and tectonics of the Middle and Upper Jurassic of Iran. *Neues Jahrbuch fur Geologie und Palaontologie Abhandlungen* **166**, 327-346.

DAVOUDZADEH M. & WEBER-DIEFENBACH K. 1987. Contribution to the paleogeography, stratigraphy and tectonics of the Upper Palaeozoic of Iran. *Neues Jahrbuch fur Geologie un Palaontologie Abhandlungen* **175**, 121-146.

DEER W. A., HOWIE R. A. & ZUSSMAN J. 1966. *Rock-Forming Minerals*. Volume three , Second Edition, Sheet Silicates, Longman, London.

DEER W. A., HOWIE R. A. & ZUSSMAN J. 1982. *Rock-forming Minerals.* Volume 1A, Second Edition, Orthosilicates, Longman, London.

DEER W. A., HOWIE R. A. & ZUSSMAN J. 1986. *Rock-forming Minerals.* Volume 1B, Second Edition, Disilicates and Ring Silicates. Longman, London.

DEFANT M. J. & DRUMMOND M. S. 1990. Derivation of some modern arc magmas by melting of young subducted lithosphere. *Nature* **347**, 662-665.

DEHGHANI G. & MAKRIS J. 1983. The gravity field and crustal structure of Iran. *Geological Survey of Iran, Internal Report* **51**, 51-68.

DERCOURT J., ZONENSHAIN L. P., RICOU L. E., KAZMIN V. G., PICHON X. LE., KNIPPER A. L., GRANDJACQUET C., SBORTSHIKOV I. M., GEYSSANT J., LEPVRIER C., PECHERSKY D. H., BOULIN J., SIBUET J. C., SAVOSTIN L. A., SOROKHTIN O., WESTPHAL M., BAZHENOV M. L., LAUER J. P. & BIJU-DUVAL B. 1986. Geological evolution of the Tethys Belt from the Atlantic to the Pamirs since the Liassic. *Tectonophysics* **123**, 241-315.

DEWEY J. F., PITMAN W.C., RYAN W. B. & BONNIN J. 1973. Plate tectonics and the evolution of the Alpine system. *Geological Society of America, Bulletin* **84**, 3137-3180.

DIGEL S. & GHENT E. D. 1994. Fluid-mineral equilibria in prehnite-pumpellyite to greenschist facies metabasites near Flin Flon, Manitoba, Canada: Implications for petrogenetic grids. *Journal of Metamorphic Geology* **12**, 467-477.

DIMITRIJEVIC M. D. 1973. Geology of Kerman region. *Geological Survey of Iran,* **Yu/52**, 334 p.

DINGWELL D. B. & BREARLEY M. 1985. Mineral chemistry of igneous melanite garnets from analcite-bearing volcanic rocks, Alberta, Canada. *Contributions to Mineralogy and Petrology* **90**, 29-35.

DJOKOVIC I., CVETIC S. & DIMITRIJEVIC M. D. 1973. *The geological map of Dehaj.* Geological Survey of Iran, Scale 1:100,000.

DOBOSI G. & FODOR R. V. 1992. Magma fractionation, replenishment, and mixing as inferred from green-core clinopyroxenes in Pliocene basanite, southern Slovakia. *Lithos* **28**, 133-150.

DOSTAL J. & MULLER W. 1992. Archean shoshonites from the Abitib Greenstone Belt Chibougamau (Quebec, Canada): Geochemistry and tectonic setting. *Journal of Volcanology and Geothermal Research* **53**, 145-165.

DOVE M. T., COOL T., PALMER D. C., PUTNIS A., SALJE E. K. H. & WINKLER B. 1993. On the role of Al-Si ordering in the cubic-tetragonal phase transition of leucite. *American Mineralogist* **78**, 486-492.

DUDA A. 1975. *Petrologie der Basanit Tephrite Reihe des Laacher Seegebietes.* Diplomarbeit Ruhr Universitat, Bochum.

DUDA A. & SCHMINKE H. U. 1978. Petrology and chemistry of potassic rocks from the Laacher See area. *Neues Jahrbuch fur Geologie und Palaontologie Abhandlungen* **132**, 1-33.

DUPUY C., DOSTAL J., GIROD M. & LIOTARD M. 1981. Origin of volcanic rocks from stromboli, Italy. *Journal of Volcanology and Geothermal Research* **10**, 49-65.

DUPUY C., MICHARD A., DOSTAL J., DAUTEL D. & BARAGAR W. R. A. 1995. Isotope and trace-element geochemistry of Proterozoic Natkusiak flood basalts from the northwestern Canadian Shield. *Chemical Geology* **120**, 15-25.

EICKSCHEN G. W. & HARTE B. 1994. Distribution of trace elements between amphibole and clinopyroxene from mantle peridotites of the Eifel (Western Germany): An ion-microprobe study. *Chemical Geology* **117**, 235-250.

ELLAM R. M. & HARMON R. S. 1990. Oxygen isotope constraints on the crustal contribution to the subduction related magmatism of the Aeolian islands, Southern Italy. *Journal of Volcanology and Geothermal Research* **44**, 105-122.

ELLAM R. M. & HAWKESWORTH C. J. 1988. Elemental and isotopic variations in subduction related basalts: evidence for a three component model. *Contributions to Mineralogy and Petrology* **98**, 72-80.

EMAMI M. H. 1981. Geologie de la region de Qom-Aran (Iran). Contribution a letude dynamique et geochimique du volcanisme tertiaire de l Iran central. These Doctorat Etat, Universite Scientifique et Medicale de Grenobe, (unpubl.).

EMBEY-ISZTIN A., DOWNES H., JAMES D. E., UPTON B. G. J., DOBOSI G., INGRAM G. A., HARMON R. S. & SCHARBERT H. G. 1993. The petrogenesis of Pliocene alkaline volcanic rocks from the Pannonian Basin, eastern Central Europe. *Journal of Petrology* **34**, 317-343.

EVARTS R. C. & SCHIFFMAN P. 1983. Submarine hydrothermal metamorphism of the Del Puerto ophiolite, California. *American Journal of Science* **283**, 289-340.

EWART A. 1979. A review of the mineralogy and chemistry of the Tertiary-Recent dacitic, latitic, rhyolitic and related salic volcanic rocks. *In*: Barker F. ed. *Trondhjemites, dacites and related rocks,* pp 13-21. Elsevier, New York.

EWART A. 1982. The mineralogy and petrology of Tertiary-Recent orogenic volcanic rocks: with special reference to andesite-basaltic compositional range. *In*: Thorpe R. S. ed. *Andesites: orogenic andesites and related rocks,* pp. 25-95. John Wiley and Sons.

EWART A. & GRIFFIN. 1994. Application of proton-microprobe data to trace-element partitioning in volcanic rocks. *Chemical Geology* **117**, 251-284.

FALCON N. 1969. Problems of the relationship between surface structure and deep displacements illustrated by the Zagros Range. *In*: Kent P., Satterthwaite G. and Spencer A. eds. *Time and place in orogeny*, pp. 9-22. Geological Society of London, Special publication.

FARHOUDI G. 1978. A comparison of Zagros geology to island arc. *Journal of Geology* **86**, 323-334.

FAURE G. 1986. *Principples of Isotope Geology*. John Wiley & Sons, New York.

FEELEY T. C., DAVIDSON J. P. & ARMENDIA A. 1993. The volcanic and magmatic evolution of Volcan Ollague, a high-K, late Quaternary stratovolcano in the Andean Central Volcanic Zone. *Journal of Volcanology and Geothermal Research* **54**, 221-245.

FERGUSON L. J. & EDGAR A. D. 1978. The petrogenesis and origin of the analcime in volcanic rocks of the Crowsnest Formation, Alberta. *Canadian Journal of Earth Sciences* **15**, 69-77.

FITTON J. G., JAMES D., KEMPTON P. D., ORMEROD D. S. & LEEMAN W. P. 1988. The role of lithospheric mantle in the generation of late Cenozoic basic magmas in the western United States. *Journal of Petrology, Special Lithosphere Issue*, 331-349.

FOLEY S. F. & PECCERILLO A. 1992. Potassic and ultrapotassic magmas and their origin. *Lithos* **28**, 181-185.

FOLEY S. F., VENTURELLI G., GREEN D. H. & TOSCANI L. 1987. The ultrapotassic rocks: Characteristics, classification, and constraints for petrogenetic models. *Earth Science Reviews* **24**, 81-134.

FORSTER H. 1976. Continental drift in Iran in relation to the Afar structures. *In*: Pilger A. and Rosler A. E. eds. *Afar between continental and oceanic rifting* , pp. 182-190. Schweiserbatche Verlagsbuchhandlung, Stuttgart.

FORSTER H., BACHTIAR I. & BOURUMANDI H. 1973. Petrographische Drtailuntersuchungeh im Bereich der Eisenerzlagerstatten von Bafql zentral Iran. *Zeitschrift der Geologischen Gesellschaft* **124**, 121-134.

FORSTER H., FESELFELDT K. & KURSTEN M. 1972. Magmatic and orogenic evolution of the Central Iranian Volcanic Belt. *24th International Geological Congress, Montreal, Section* **2**, 198-210.

FORSYTHE L. M., NIELSEN R. L. & FISK M. R. 1994. High-field strength element partitioning between pyroxene and basaltic to dacitic magmas. *Chemical Geology* **117**, 107-125.

FRANCALANIC L., BARBIERI M., MANETTI P., PECCERILLO A. & TOLOMEOL. 1988. Sr isotopic systematics in volcanic rocks from the island of Stromboli, Italy (Aeolian Arc). *Chemical Geology* **73**, 109-124.

FREY F. A., GREEN D. H. & ROY S. 1978. Integrated models of basalt petrogenesis: A study of quartz tholeiites to olivine melilitites from southeastern Australia utilising geochemical and experimental petrologic data. *journal of Petrology* **19**, 463-513.

GAETANI G. A. & GROVE T. L. 1995. Partitioning of rare earth elements between clinopyroxene and silicate melt: Crystal-chemical controls. *Geochimica et Cosmochimica Acta* **59**, 1951-1962

GALLAHAN W. E. & NIELSON R. L. 1992. The partitioning of Sc, Y and the rare earth elements between high-Ca pyroxene and natural mafic to intermediate lavas at 1 atmosphere. *Geochimica et Cosmochimica Acta* **56**, 2387-2404.

GAMBLE J. A., SMITH I. E. M., McCULLOCH M. T., GRAHAM I. J. & KOKELAAR B. P. 1993. The geochemistry and petrogenesis of basalts from the Taupo Volcanic Zone and Kermadec island arc, S. W. Pacific. *Journal of Volcanology and Geothermal Research* **54**, 265-290.

GERINGER G. J. & LUDICK D. J. 1990. Middle-Proterozoic calcalkaline, shoshonitic volcanism along the eastern margin of the Namaqua Mobile Belt, South Africa-implications for tectonic evolution in the area. *South Africa Journal of Geology* **93**, 389-399.

GIANNETTI B. & ELLAM R. 1994. The primitive lavas of Roccamonfina volcano, Roman region, Italy: new constraints on melting processes and source mineralogy. *Contributions to Mineralogy and Petrology* **116**, 21-31.

GIESSE P., MAKRIS J., AKASHE B., ROWER P., LETZ H. & MOSTAANPOUR M. 1983. Seismic crustal studies in southern Iran between the Central Iran and the Zagros Belt. *Geological Survey of Iran, Internal Report* **51**, 71-84.

GIESSE P., MAKRIS J., AKASHE B., ROWER P., LETZ H. & MOSTAANPOUR M. 1984. The crustal structure in southern Iran derived from seismic explosion data. *Neues Jahrbuch fur Geologie und Palaontologie Abhandlungen* **168**, 230-243.

GILL J. B. 1981. *Orogenic andesites and plate tectonics*. Springer-Verlag, Berlin.

GILL J. & WHELAN P. 1989. Early rifting of an oceanic island arc (Fiji) produced shoshonitic to tholeiitic basalts. *Journal of Geophysical Research* **94**, 4561-4578.

GREEN T. H. 1994. Experimental studies of trace element partitioning applicable to igneous petrogenesis-Sendona 16 years later. *Chemical Geology* **117**, 1-36.

GUPTA A. K. & FYFE W. S. 1975. Leucite survival: The alteration to analcime. *Canadian Mineralogist* **13**, 361-363.

GUPTA A. K. & YAGI K. 1980. *Petrology and genesis of leucite bearing rocks*. Springer-Verlag, New York.

GURENKO A. A., SOBOLEV A. V. & KONONKOVA N. N. 1991. Magmas that produced the subalkalic basaltic volcanic rocks of the east African Rift system. *Doklady Akademii Nauk SSSR* **319**, 707-712.

HACK P. J., NIELSEN R. L. & JOHNSTON A. D. 1994. Experimentally determined rare-earth element and Y partitioning behavior between clinopyroxene and basaltic liquids at pressures up to 20 Kbar. *Chemical Geology* **117**, 89-105.

HAGHIPOUR A. 1974. Etude geologique de la region de Biabanak-Bafq (Central Iran), petrologie et tectonique du socle Precambrian et de sa couverture. These, Universite Scientifique et Medicale de Grenoble, (unpubl.).

HALL A. 1987. *Igneous Petrology*. Longman, London.

HANSON G. N. 1980. rare earth elements in petrogenetic studies of igneous systems. *Annual Review of Earth and Planetary Sciences* **8**, 371-406.

HASSANZADEH J. 1993. Metallogenic and tectonomagmatic events in the SE sector of the Cainozoic active continental margin of Central Iran (Shahrbabak area, Kerman Province). PhD thesis, University of California, Los Angeles (unpubl.).

HAURI E. H., WAGNER T. P. & GROVE T. L. 1994. Experimental and natural partitioning of Th, U, Pb and other trace elements between garnet, clinopyroxene and basaltic melts. *Chemical Geology* **117**, 149-166.

HAWKESWORTH C. J., GALLAGHER K., HERGT J. M. & McDERMOTT F. 1993. Trace element fractionation processes in the generation of island arc basalts. *Philosophical Transactions of the Royal Society of London* **A342**, 179-191.

HAWKESWORTH C. J. & VOLLMER R. 1979. Crustal contamination versus enriched mantle: $^{143}Nd/^{144}Nd$ and $^{87}Sr/^{86}Sr$ evidence from the Italian volcanics. *Contributions to Mineralogy and Petrology* **69**, 151-165.

HAYNES S. J. & McQUILLAN H. 1974. Evolution of the Zagros suture zone southern Iran. *Geological Society of America Bulletin* **85**, 739-744.

HEANEY P. J. & VEBLEN D. R. 1990. A high-temperature study of the low-high leucite phase transition using the transmission electron microscope. *American Mineralogist* **75**, 464-476.

HENDERSON P. 1984. General geochemical properties and abundances of the rare earth elements. *In*: Henderson P. ed. *Rare Earth Element Geochemistry, Developments in Geochemistry,* Elsevier, New York.

HOLM P. M., LOU S. & NIELSEN A. 1982. The geochemistry and petrogenesis of the lavas of the Vulsinian district, Roman Province, central Italy. *Contributions to Mineralogy and Petrology* **80**, 367-378.

HUGHES C. J. & HUSSEY E. M. 1976. M and Mg values in igneous rocks: Proposed usage and a comment on currently employed Fe_2O_3 corrections. *Geochimica et Cosmochimica Acta* **40**, 485-486.

HUSHMANDZADEH A. 1977. Ophiolites of south Iran and their genetic problems. *Geological Survey of Iran. Internal Report,* 89 p.

IDDINGS J. P. 1892. The origin of igneous rocks. *Philosophical Society, Washington Bulletin* **12**, 89-214.

IDDINGS J. P. 1895. Absarokite-shoshonite-banakite series. *Journal of Geology* **3**, 935-959.

JAKES P. & WHITE A. J. R. 1970. K/Rb ratios of rocks from island arcs. *Geochimica et Cosmochimica Acta* **34**, 849-856.

JAQUES A. L. & GREEN D. H. 1980. Anhydrous melting of peridotite at 0-15 Kb pressure and the genesis of tholeiitic basalts. *Contributions to Mineralogy and Petrology* **73**, 287-310.

JOHNSON C. M., LIPMAN P. W. & CZAMANSKE G. K. 1990. H, O, Sr, Nd and Pb isotope geochemistry of the Latir Volcanic field and cogenetic intrusions, New Mexico, and relations between evolution of a continental magmatic center and modifications of the lithosphere. *Contributions to Mineralogy and Petrology* **104**, 99-124.

JOHNSON K. E., HARMON R. S., RICHARDSON J. M., MOORBATH S. & STRONG D. F. 1996. Isotope and trace element geochemistry of Augustine Volcano, Alaska: Implications for magmatic evolution. *Journal of Petrology* **37**, 95-115.

JONES E. V. & CANN J. R. 1994. Controls on the Sr and Nd isotopic compositions of hydrothermally altered rocks from the pindos ophiolite, Greece. *Earth and Planetary Science Letters* **125**, 39-54.

JUNG D., KURSTEN M. & TARKIAN M. 1975. Post Mesozoic volcanism in Iran and its relation to the subduction of the Afro-Arabian plate under the Eurasian plate. *Afar Monograph, Deutsche Forschungsgemeinschaft.*

KARLSSON H. R. & CLAYTON R. N. 1991. Analcime phenocrysts in igneous rocks: Primary or secondary. *American Mineralogist* **76**, 189-199.

KARLSSON H. R. & CLAYTON R. N. 1993. Analcime phenocrysts in igneous rocks: Primary or secondary reply. *American Mineralogist* **78**, 230-232.

KAY R. W. 1980. Volcanic arc magmas: Implications of a melting-mixing model for element recycling in the crust-upper mantle system. *Journal of Geology* **88**, 497-522.

KELEMEN P. B., DICK H. J. B. & QUICK J. E. 1992. Formation of harzburgite by pervasive melt-rock reaction in the upper mantle. *Nature* **358**, 635-641.

KELEMEN P. B., KINZLER R. J., JOHNSON K. T. M. & IRVING A. J. 1990. High field strength element depletions in arc basalts due to mantle-magma interaction. *Nature* **345**, 521-524.

KOHN S. C., HENDERSON C. M. & DUPREE R. 1995. Si-Al order in leucite revisited: New information from an analcite-derived analogue. *American Mineralogist* **80**, 705-714.

KOKELAAR P. 1986. Petrology and geochemistry of the Rhobell Volcanic Complex: Amphibole-dominated fractionation at an Early Ordovician arc volcano in North Wales. *Journal of Petrology* **27**, 887-914.

KOSTOV I. 1968. *Mineralogy.* Oliver and Boyd, Edinburgh.

KUSHIRO I. & YODER H.S. 1969. Melting of forsterite and enstatite at high pressures under hydrous conditions. *Carnegie Institute of Washington Yearb* **67**, 153-158.

LAMBERT R. St. J. & HOLLAND J. G. 1974. Yttrium geochemistry applied to petrogenesis utilising calcium-yttrium relationships in minerals and rocks. *Geochimica et Cosmochimica Acta* **38**, 1393-1414.

LANGE R. A., CARMICHAEL I. S. E. & STEBBINS J. F. 1986. Phase transitions in leucite ($KAlSi_2O_6$), orthorhombic KAlSiO4, and their iron analogues ($KFeSi_2O_6$, KFeSiO4). *American Mineralogist* **71**, 937-945.

LEAK B. E. 1978. Nomenclature of amphiboles. *American Mineralogist* **63,** 1023-1052.

LEAT P. T., THOMPSON R. N., MORRISON M. A., HENDRY G. L. & DICKIN A. P. 1990. Geochemistry of mafic lavas in the early Rio Grande Rift, Yarmony Mountain, Colorado, USA. *Chemical Geology* **81**, 23-43.

LE BAS M. J. & STRECKEISEN A. L. 1991. The IUGS classification of igneous rocks. *Journal of the Geological Society of London* **148**, 825-833.

LETERRIER J. 1985. Mineralogical, geochemical and isotopic evolution of two Miocene mafic intrusions from the Zagros, Iran. *Lithos* **18**, 311-329.

LINE C. M. B., PUTNIS A., PUTNIS C. & GIAMPAOLO C. 1995. The dehydration kinetics and microtexture of analcime from two parageneses. *American Mineralogist* **80**, 268-279.

LIOU J. G. 1979. Zeolite facies metamorphism of basaltic rocks from the East Taiwan ophiolite. *American Mineralogist* **64**, 1-14.

LUCCHETTI G., CAABELLA R. & CORTESOGNO L. 1990. Pumpellyites and coexisting minerals in different low-grade metamorphic facies of Liguria, Italy. *Journal of Metamorphic Geology* **8**, 539-550.

LUHR J. F. & CARMICHAEL I. S. E. 1980. The Colima Volcanic Complex, Mexico. *Contributions to Mineralogy and Petrology* **70**, 343-372.

LUHR J. F. & GIANNETTI B. 1987. The brown leucitic tuff of Roccamonfina volcano, Roman region, Italy. *Contributions to Mineralogy and Petrology* **95**, 420-436.

MANETTI P., PECCERILLO A. & POLI G. 1979. REE distribution in Upper Cretaceous calcalkaline and shoshonitic volcanic rocks from Eastern Srednorgie, Bulgaria. *Chemical Geology* **26**, 51-63.

MARCELOT G. & RANCON J. P. H. 1988. Mineral chemistry of leucitites from Visoke Volcano, Virunga Range, Rwanda: Petrogenetic implications. *Mineralogical Magazine* **52**, 603-613.

MARSH B. D. 1982. The Aleutians. *In*: Thorpe R.S. ed. *Orogenic andesites and related rocks*, pp. 99-114. John Wiley and Sons, Chichester.

MAURY R. C., CAROFF M., ACHARD S., GUILLE G., JORON J. L., GACHON A., ROCABOY A. & LETERRIER J. 1992. L'atoll de Mururoa (polynesie Francaise). II. La serie magmatique. *Bulletin de la Societe de Geologique France* **163**, 659-679.

MAZZI F., GALLI E. & GOTTARDI G. 1976. The crystal structure of tetragonal leucite. *American Mineralogist* **61**, 108-115.

McBIRNEY A. R. 1979. Effects of assimilation. *In*: Yoder H.S. ed. *The evolution of the igneous rocks*, pp. 307-338. Princeton University press, Princeton, New Jersey.

McCULLOCH M. T. 1993. The role of subducted slabs in an evolving Earth. *Earth and Planetary Science Letters* **115**, 89-100.

McCULLOCH M. T. & GAMBLE J. A. 1991. Geochemical and geodynamical constraints on subduction zone magmatism. *Earth and Planetary Science Letters* **102**, 358-374.

McDERMOTT F., DEFANT M. J., HAWKESWORTH C. J., MAURY R. C. & JORON J. L. 1993. Isotope and trace element evidence for three component mixing in the genesis of the north Luzon arc lavas (Philippines). *Contributions to Mineralogy and Petrology* **113**, 9-23.

McDOUGALL I. & HARRISON T. M. 1988. *Geochronology and thermochronology by the $^{40}Ar/^{39}Ar$ method.* Oxford University Press, New York.

McDOUGALL I. & SCHMINCKE H. U. 1977. Geochronology of Gran Canaria, Canary Islands: Age of shield builiding volcanism and other magmatic phases. *Bulletin of Volcanology* **40**, 57-77.

MEEN J. K. 1987. Formation of shoshonites from calcalkaline basalt magmas: Geochemical and experimental constraints from the type locality. *Contributions to Mineralogy and Petrology* **97**, 333-351.

METCALFE R. BANKS D. & BOTHRELL S. H. 1992. An association between organic matter and localised, prehnite-pumpellyite alteration at Builth Wells, Wales, UK. *Chemical Geology* **102**, 1-21.

MITCHELL R. H. & BERGMAN S. C. 1991. *Petrology of Lamproites*. Plenum, New York.

MOINE-VAZIRI H. 1985. Volcanism Tertiare Et Quaternaire En Iran. These Doctorate Etat, Universite de Orsay, France, (unpubl.).

MOINE-VAZIRI H. & Aminsobhani E. 1978. Volcanology and volcano-sedimentalogy of Sahand area. University of Tarbiat Moalem, Tehran.

MOINE-VAZIRI H., KHALILI MARANDI SH. & BROUSSE R. 1991. Importance d'un volcanism potassique, au miocene superier, en Azerbaijan, Iran. C. R. *Academic Science Paris* **313**, 1603-1610.

MONTANINI A., BARBIERI M. & CASTORINA F. 1994. The role of fractional carystallisation, crustal melting and magma mixing in the petrogenesis of rhyolits and mafic inclusion-bearing dacites from the Monte Aric Volcanic complex, Sardinia, Italy. *Journal of Volcanology and Geothermal Research* **61**, 95-120.

MORADIAN A. 1991. Petrological study of feldspathoid rocks, North Shahrbabak, Javazm, Iran. MSC thesis, University of Tehran, Tehran (unpubl.).

MORRISON G. W. 1980. Characteristic and tectonic setting of the shoshonite rock association. *Lithos* **13**, 97-108.

MULLER D., MORRIS B. J. & FARRAND M. G. 1993. Potassic alkaline lamprophyres with affinities to lamproites from the Karinya syncline, south Australia. *Lithos* **30**, 123-137.

MULLER D., ROCK N. M. S. & GROVES D. I. 1992. Geochemical discrimination between shoshonitic and potassic volcanic rocks in different tectonic settings: A pilot study. *Mineralogy and Petrology* **46**, 259-289.

MYERS J. D., FROST C. D. & ANGEVINE C. L. 1986. A test of a quartz eclogite source for parental Aleutian magmas: A mass balance approach. *Journal of Geology* **94**, 811-828.

NABAVI M. H. 1976. An introduction to Iranian geology. Special Publication (in Persian). *Geological Survey of Iran,* 110 p.

NASH W. P. & CRECRAFT H. R. 1985. Partition coefficients for trace elements in silicic magmas. *Geochimica et Cosmochimica Acta* **49**, 2309-2322.

NATIONAL IRANIAN OIL COMPANY. 1959. *Geological map of Iran.* National Iranian Oil Company, Scale 1:2500,000.

NELSON D. R. 1992. Isotopic characteristics of potassic rocks: Evidence for the involvement of subducted sediments in magma genesis. *Lithos* **28**, 403-420.

NICHOLLS I. A. 1974. liquids in equilibrium with peridotitic mineral assemblages at high water pressures. *Contributions to Mineralogy and Petrology* **45**, 289-316.

NICHOLLS I. A. & WHITFORD D. J. 1976. Primary magma associated with Quaternary volcanism in the western Sunda Arc, Indonesia. *In*: Johnson R. W. ed., *Volcanism in Australasia*, pp. 77-90. Amsterdam, Elsevier.

NIELSEN R. L., FORSYTHE L. M., GALLAHAN W. E. & FISK M. R. 1994. Major and trace-element magnetite melt equilibria. *Chemical Geology* **117**, 167-191.

NORRISH K. & CHAPPELL B. W. 1977. *X-ray fluorescence spectrometry. In*: Zussman J. ed. Physical methods in determinative mineralogy 2nd edition, pp. 201-272. Academic Press, London.

NORRISH K. & HUTTON J. T. 1969. An accurate spectrographic method for the analysis of a wide range of geologic samples. *Geochimica et Cosmochimca Acta*, **33**, 431-453.

NOTSU K., ARAKAWA Y. & KOBAYASHI T. 1990. Strontium isotopic characteristics of arc volcanic rocks at the initial stage of subduction in western, Japan. *Journal of Volcanology and Geothermal Research* **40**, 181-196.

O'REILLY S. Y. & GRIFFIN W. L. 1988. Mantle metasomatism beneath western Victoria, Australia: Metasomatic processes in Cr-diopside lherzolites. *Geochimica et Cosmochimica Acta* **52**, 433-447.

PAPIKE J. J., KEITH T. E. C., SPILDE M. N., GALBRATH K. C., SHEARER C. K. & LAUL J. C. 1991. Geochemistry and mineralogy of fumarolic deposits, Valley of ten thousand smokes, Alaska: Bulk chemical and mineralogical evolution of dacite-rich protolith. *American mineralogist* **76**, 1673-1991.

PARKER R. J. 1989. Geochemical and petrographic characteristics of potassium-rich pyroclastic and lava samples from Vulsini volcano, Roman magmatic region, Italy. *Journal of Volcanology and Geothermal Research* **39**, 297-314.

PEACOCK S. M., RUSHMER T. & THOMPSON A. B. 1994. Partial melting of subducting oceanic crust. *Earth and Planetary Science Letters* **121**, 227-244.

PEARCE J. A. 1983. The role of sub-continental lithosphere in magma genesis at destructive plate margins. *In*: Hawkesworth C. J. and Norry M. J eds. *Continental Basalts and Mantle Xenoliths* pp. 230-349. Shiva Publications, Nantwich.

PEARCE J. A., BENDER J. F., DE LONG S. E., KIDD W. S. F., LOW P. J., GUNER Y., SAROGLU F., YILMAZ Y., MOORBATH S. & MITCHELL J. G. 1990. Genesis of collision volcanism in eastern Anatolia, Turkey. *Journal of Volcanology and Geothermal Research* **44**, 189-229.

PEARCE J. A & NORRY M. J. 1979. Petrogenetic implication of Ti, Zr, Y and Nb variations in volcanic rocks. *Contributions to Mineralogy and Petrology* **69**, 33-47.

PEARCE J. A. & PEATE D. W. 1995. Tectonic implications of the composition of volcanic arc magmas. *Annual Reviews of Earth and Planetary Sciences* **24**, 251-285.

PEARCE T. H. 1970. The analcime-bearing volcanic rocks of the Crowsnest Formation, Alberta. *Canadian Journal of Earth Sciences* 7,46-66.

PEARCE T. H. 1993. Analcime phenocrysts in igneous rocks: Primary or secondary, discussion. *American Mineralogist* **78**, 225-229.

PEARCE T. H. & KOLISNIK A. M. 1990. Observations of plagioclase zoning using interference imaging. *Earth Science Reviews* **29**, 9-26.

PECCERILLO A. 1985. Roman comagmatic province, central Italy: Evidence for subduction-related magma genesis. *Geology* **13**, 103-106.

PECCERILLO A. 1990. On the origin of the Italian potassic magmas comments. *Chemical Geology* **85**, 183-196.

PECCERILLO A. 1992. Potassic and ultrapotassic rocks: Compositional characteristics, petrogenesis, and geologic significance. *Episodes* **15**, 243-251.

PECCERILLO A. & TAYLOR S. R. 1976. Geochemistry of Eocene calcalkaline volcanic rocks from the Kastamonu area, northern Turkey. *Contributions to Mineralogy and Petrology* **58**, 63-81.

PE-PIPER G. 1983. Triassic shoshonites and andesites, Lakmon Mountains, Western Continental Greece: Differences primary geochemistry and sheet silicate alteration products. *Lithos* **16**, 23-33.

PE-PIPER G. & PIPER D. J. W. 1994. Miocene magnesian andesites and dacite, Evia, Greece: adakites associated with subducting slap detachment and extension. *Lithos* **31**, 125-140.

PHILLIPS B. L. & KIRKPATRICK R. J. 1994. Short-range Si-Al order in leucite and analcime: Determination of the configurational entropy from ^{27}Al and variable-temperature ^{29}Si NMR spectroscopy of leucite, its Cs and Rb-exchanged derivatives, and analcime. *American Mineralogist* **79**, 1025-1031.

PILGER A. 1971. die zietlich-tektonische entwicklung der Iranischen gebirge. *Clausthaler Geologische Abhandlungen* **8**, 27-40.

PIN C. & MARINI F. 1993. Early Ordovician continental break-up in Variscan Europe: Nd-Sr isotope and trace element evidence from bimodal igneous associations of the Southern Massif Central, France. *Lithos* **29**, 177-196.

PLANK T. & LANGMUIR C. H. 1993. Tracing trace elements from sediment input to volcanic output at subduction zones. *Nature* **362**, 739-743.

POGNANTE U. 1990. Shoshonitic and ultrapotassic post-collisional dykes from Northern Karakorum, Sinliang, China. *Lithos* **26**, 305-316.

QUENNELL A. M. 1985. *Continental rifts*. Van Nostr and Reinhold Company, New York.

RAE D. A., COULSON I. M. & CHAMBERS A. D. 1996. Metasomatism in the North Qoroq centre, South Greenland: Apatite chemistry and rare-earth element transport. *Mineralogical Magazine* **60**, 207-220.

RAHNEMAEE M. T. 1991. *Special potentials of Iran*: Geographical aspects of national physical plan (in Persian). Roudaki Publication, Tehran, Iran.

REEDER R. J., FAGIOLI R. O. & MEYERS W. J. 1990. Oscillatory zoning of Mn in solution-grown calcite crystals. *Earth Science Reviews* **29**, 39-46.

REINER P. W., NELSON B. K. & NELSON S. W. 1996. Evidence for multiple mechanisms of crustal contamination of magma from compositionally zoned plutons and associated ultramafic intrusions of the Alaska Range. *Journal of Petrology* **37**, 261-292.

RICO L. E. 1974. L'evolution geologique de la region de Neyriz, Zagros Iranien et l'evolution structurale des Zagrides. These Doctorate Etate, Universite de Orsav, France (unpubl.).

RIOU R. 1979. Petrography and geochemistry of the Eocene alkaline lavas of the northern Azerbaijan (Iran). *Neues Jahrbuch fur Geologie und Palaontologie Monatshefte* **9**, 532-559.

RIOU R., DUPUY C. & DOSTAL J. 1981. Geochemistry of coexisting alkaline and calcalkaline volcanic rocks from northern Azerbaijan, NW Iran. *Journal of volcanology and geothermal research* **11**, 253-275.

ROEDER P. L. & and EMSLIE R. F. 1970. Olivine-liquid equilibrium. *Contributions to Mineralogy and Petrology* **29**, 275-289.

ROGERS N. W., HAWKESWORTH C. J., PARKER R. J. & MARSH J. S. 1985. The geochemistry of potassic lava from Vulsini, central Italy and implications for mantle enrichment processes beneath the Roman region. *Contributions to Mineralogy and Petrology* **90**, 244-257.

ROGERS N. W., MULDER M. D. & HAWKESWORTH C. J. 1992. An enriched mantle source for potassic basanites: Evidence from Karisimbi volcano, Virunga volcanic province, Rwanda. *Contributions to Mineralogy and Petrology* **111**, 543-556.

ROGERS N. W. & SETTERFIELD T. N. 1994. Potassium and incompatible-element enrichment in shoshonitic lavas from the Tavua volcano, Fiji. *Chemical Geology* **118**, 43-62.

ROLLINSON H. 1993. *Using Geochemical Data*: Evaluation, presentation, interpretation. Longman, New York.

RUTTNER A. & STOCKLIN J. 1967. *Geological map of Iran.* Geological Survey of Iran, Scale 1:1000,000.

SABZEHEI M. 1974. Les melanges ophiolitiques de la region d'Esfandageh, Iran meridional. These de Docteur es Sciences Naturelles, Universite' scientifique et Medicale de grenoble France, (unpubl.).

SABZEHEI M. & BERBERIAN M. 1972. Preliminary note on the structural and metamorphic history of the area between Dowlatabad and Esfandagheh, south-east Central Iran. *Geological Survey of Iran. Internal Report*, 30 p.

SAUNDERS A. D., NORRY M. J. & TARNEY J. 1988. Origin of MORB and chemically-depleted mantle reservoirs: Trace element constraints. *Journal of Petrology Special Lithosphere Issue* 415- 445.

SAUNDERS A. D., TARNEY J., STERN C. & DALZIEL I. W. D. 1979. Geochemistry of Mesozoic marginal basin floor igneous rocks from southern Chil. *Geological Society of America Bulletin* **90**, 237-258.

SAUNDERS A. D., TARNEY J. & WEAVER S. D. 1980. Transverse geochemical variations across the antarctic Peninsula: Implications for the genesis of calcalkaline magmas. *Earth and Planetary Science Letters* **46**, 344-360.

SAWKA W. N. 1985. The geochemistry of differentiation processes in granite magma chambers. PhD Thesis, Australian National University, Canberra (unpubl.).

SCHIFFMAN P. & LIOU J. G. 1983. Crystallisation of coarse-grained prehnite and pumpellyite in hydrothermal experiments and its petrologic implications. *Neues Jahrbuch fur Mineralogie und Abhandlungen.* **146**, 242-257.

SCHILLING J. G., ZAJAC M., EVANS R., JOHNSTON T., WHITE W., DEVINE J. D. & KINGSLEY R. 1983. Petrologic and geochemical variations along the Mid-Atlantic Ridge from 27°N to 73°N. *American Journal of science* **283**, 510-586.

SCHRODER J. W. 1944. Essai sur la structure de la Iran. *Eclogae Geologicae Helvetiae* **37**. 37-81.

SEARLE M. P. 1991. *Geology and Tectonics of the Karakoram Mountains*. John Wiley and Sons, New York.

SEN C. & DUNN T. 1994. Dehydration melting of a basaltic composition amphibolite at 1.5 and 2 GPa: Implications for the origin of adakites. *Contributions to Mineralogy and Petrology* **117**, 394-409.

SENGOR A. M. C. 1984. The Cimmeride orogenic system and the tectonics of Eurasia. *Geological Society of America, Special Publication* **195**.

SENGOR A. M. C. 1990. A new model for the Late Paleozoic-Mesozoic tectonic evolution of Iran and implications for Oman. *Geological Society of London, Special Publication* **49**, 797-831.

SEYMOUR K. St. & VLASSOPOULOS D. 1992. Magma mixing at Nisyros volcano, as inferred from incompatible trace-element systematics. *Journal of Volcanology and Geothermal Research* **50**, 273-299.

SHAHABPOUR J. 1982. Aspects of alteration and mineralisation at the Sar-Cheshmeh copper-molybdenum deposit, Kerman, Iran. PhD Thesis, University of Leeds, England (unpubl.).

SHARMA M., BASU A. R., COLE R. B. & DECELLES P. G. 1991. Basalt-rhyolite volcanism by MORB-continental crust interaction: Nd, Sr-isotopic and geochemical evidence from southern san joaquin basin, california. *Contributions to Mineralogy and petrology* **109**, 159-172.

SHAW D. M. 1968. A review of K-Rb fractionation trends by covariance analysis. *Geochimica et Cosmochimica Acta* **32**, 573-601.

SHELLEY D. 1993. *Igneous and Metamorphic Rocks Under the Microscope*. Chapman and Hall.

SHEPPARD S. 1995. Hybridisation of shoshonitic lamprophyre and calc-alkaline granite magma in the Early Proterozoic Mt Bundey igneous suite, Northern Territory. *Australian Journal of Earth Sciences* **42**, 173-185.

SHERATON J. W. & SIMON L. 1988. Geochemical data analysis system (GDA) reference manual. *Bureau of Mineral Resources Geology and Geophysics*, **Record 1988/45**.

SIGURDSSON H., CAREY S., PALAIS J. M. & DEVINE J. 1990. Pre-eruption compositional gradients and mixing of andesite and dacite magma erupted from Nevado del Ruiz Volcano, Colombia. 1985. *Journal of Volcanology and Geothermal Research* **41**, 127-151.

SINGER B. S., DUNGAN M. A., & LAYNE G. D. 1995. Textures and Sr, Ba, Mg, Fe, K, and Ti compositional profiles in volcanic plagioclase: Clues to the dynamics of calcalkaline magma chambers. *American Mineralogist* **80**, 776-798.

SKULSKI T., MINARIK W. & WATSON E. B. 1994. High-pressure experimental trace-element partitioning between clinopyroxene and basaltic melts. *Chemical Geology* **117**, 127-147.

SOFFEL H. & FORSTER H. G. 1980. Apparent polar wander path of central Iran and its geotectonic interpretation. *Journal of Geomagnetism and Geoelectricity* **32**, 117-135.

SORENSEN H. (EDITOR) 1974. *The Alkaline Rocks*. Johen Wiley and Sons, London.

SRDIC A., DIMITRIJEVIC M. N., OMALJER V. & RADOVANOVIC Z. 1972. *The geological map of Anar*. Geological Survey of Iran, Scale 1:100,000.

STARKEY R. J. & FROST B. R. 1990. Low-grade metamorphism of the Karmutsen Volcanics, Vancouver Island, British Columbia. *Journal of Petrology* **31**, 167-195.

STERN C. R. 1974. Melting products of olivine tholeiite basalt in subduction zones. *Geology* **2**, 227-230.

STOCKLIN J. 1968. Structural history and tectonics of Iran: A review. *American Association of Petroleum Geologists, Bulletin* **52**, 1229-1258.

STOCKLIN J. 1974. Possible ancient continental margins in Iran. *In*: Burk C.A. and Drake C.D. eds. *The Geology of Continental Margins*, pp. 873-888. Springer-Verlag, New York.

STOCKLIN J. 1977. Structural correlation of the Alpine ranges between Iran and Central Asia. Memoire Hors-Serie N° 8 de la *Societe Geologique de France* **8**, 333-353.

STOCKLIN J. 1983. Himalayan orogeny and earth expansion. *In*: Carey S. W. ed. *Expanding Earth Symposium*, pp. 119-130. University of Tasmania.

STOCKLIN J. & NABAVI M. H. 1973. *Tectonic Map of Iran.* Geological Survey of Iran, Scale 1:100,000.

STOLZ A. J., JOCHUM K. P., SPETTEL B. & HOFMANN A. W. 1996. Fluid and melt-related enrichment in the sub-arc mantle: Evidence from Nb/Ta variations in island-arc basalts. *Geology* **24**, 587-590.

STOLZ A. J., VARNE R., DAVIES G. R., WHELLER G. E. & FODEN J. D. 1990. Magma source components in an arc-continent collision zone: The Flores-Lembata sector, Sunda arc, Indonesia. *Contributions to Mineralogy and petrology* **105**, 585-601.

STOLZ A. J., VARNE R., WHELLER G. E., FODEN J. D., ABBOTT M. J. 1988. The geochemistry and petrogenesis of K-rich alkaline volcanics from the Batu Tara volcano, eastern sunda arc. *Contributions to Mineralogy and Petrology* **98**, 374-389.

STONELEY R. 1974. The evolution of the continental bounding a former southern Tethys. *In*: Burk C.A. ed. *Continental Margins*. pp. 889-903. Springer-Verlag, New York.

STONELEY R. 1975. On the origin of ophiolite complexes in the southern Tethys region. *Tectonophysics* **25**, 303-322.

STOPPA F. & LAVECCHIA G. 1992. Late Pleistocene ultra-alkaline magmatic activity in the Umbria-Latium region, Italy: An overview. *Journal of Volcanology and Geothermal Research* **52**, 277-293.

SUN S. S. & McDONOUGH W. F. 1989. Chemical and isotopic systematics of oceanic basalts: implications for mantle composition and processes. In: Saunders A. D. and Norry M. j. eds, Magmatism in ocean basins. *Geological Society of London, Special Publication* **42**, 313-345.

TAKIN M. 1972. Iranian geology and continental drift in the Middle East. *Nature* **235**, 147-150.

TATSUMI Y. & EGGINS S. M. 1996. *Subduction zone magmatism.* Blackwell Science, Australia, pp 211.

TATSUMI Y., HAMILTON D. L. & NESBITT R. W. 1986. Chemical characteristics of fluid phase released from a subducted lithosphere and the origin of arc magmas: Evidence from high pressure experiments and natural rocks. *Journal of Volcanology and Geothermal Research* **29**, 293-309.

TAYLOR D. & MACKENZIE W. S. 1975. A contribution to the pseudoleucite problem. *Contributions to Mineralogy and Petrology* **49**, 321-333.

TAYLOR S. R. & MCLENNAN S. M. 1985. *The Continental Crust, its Composition and Evolution.* Blackwell, Oxford.

TERA F., BROWN L., MORRIS J., SACKS I. S., KLEIN J. & MIDDLETON R. 1986. Sediment incorporation in island arc magmas: Inferences from 10_{Be}. *Geochimica et Cosmochimica Acta* **50**, 535-550.

THOMPSON R. N. 1974. Some high-pressure pyroxenes. *Mineralogical Magazine* **39**, 768-787.

THOMPSON R. N., HENDRY G. L. & PARRY S. J. 1984. An assesment of the relative roles of crust and mantle in magma genesis: An element approach. *Philosophical Transaction of Royal Society of Edinburph, London* **A310**, 549-590.

THOMPSON R. N. & FLOWER M. B. 1986. Subduction-related shoshonitic and ultrapotassic magmatism: A study of Siluro-Ordovician syenites from the Scottish Caledonides. *Contributions to Mineralogy and Petrology* **94**, 507-522.

THOMPSON R. N., GIBSON S. A., LEAT P. T., MITCHELL J. G., MORRISON M. A., HENDRY G. L & DICKIN A. P. 1993. Early Miocene continental extension-related basaltic magmatism at Walton Peak, northwest Colorado: Further evidence on continental basalt genesis. *Journal of the geological society of London* **150**, 277-292.

THORPE R. S. 1987. Permian k-rich volcanic rocks of Devon: Petrogenesis, tectonic setting and geological significance. *Transactions of the Royal Society of Edinburgh, Earth Sciences* **77**, 361-364.

THORPE R. S. & TINDLE A. G. 1992. Petrology and petrogenesis of a Tertiary bimodal dolerite-peralkaline/subalkaline trachyte/rhyolite dyke association from Lundy, Bristol Channel, UK. *Journal of Geology* **27**, 101-117.

TURNER S., ARNAUD N., LIU J., ROGERS N., HAWKESWORTH C., HARRIS N., KELLEY S., VAN CALSTEREN P. & DENG W. 1996. Post-collision, shoshonitic volcanism on the Tibetan Plateau: Implications for convective thinning of the lithosphere and the source of ocean island basalt. *Journal of Petrology* **37**, 45-71.

Van BERGEN M. J., VROON P. Z., VAREKAMP J. C. & POORTER R. P. E. 1992. The origin of the potassic rock suite from Batu Tara volcano, East Sunda Arc, Indonesia. *Lithos* **28**, 261-282.

Van KOOTEN G. 1980. Mineralogy, petrology and geochemistry of an ultrapotassic basalt suite, Central Sierra Nevada, California, USA. *Journal of Petrology* **21**, 651-684.

VAREKAMP J. C. & KALAMARIDES R.I. 1989. Hybridisation processes in leucite tephrites from Vulsini, Italy and the evolution of the Italian potassic suite. *Journal of Geophysical Research* **94**, 4603-4618.

VENTURELLI G., THORPE R. S., DALPIAZ G. V., DELMORO A. & POTTS P. J. 1984. Petrogenesis of calcalkaline, shoshonitic and associated ultrapotassic oligocene volcanic rocks from the northwestern Alps, Italy. *Contributions to mineralogy and petrology* **86**, 209-220.

VOLLMER R., OGDEN P., SCHILLING J. G., KINGSLEY R. H. & WAGGONER D. G. 1984. Nd and Sr isotopes in ultrapotassic volcanic rocks from the Leucite Hills, Wyoming. *Contributions to Mineralogy and Petrology* **87**, 359-368.

WASHINGTON H. S. 1927. Italite locality of Vila Senni. *American Journal of Science* **14**, 173-182.

WASS S. Y. 1980. Geochemistry and origin of xenolith-bearing and related alkali basaltic rocks from the Southern Highland, New South Wales, Australia. *American Journal of Science* 280A, 639-666.

WATSON E. B. & GREEN T. H. 1981. Apatite/liquid partition coefficients for the rare earth elements and strontium. *Earth and Planetary Science Letters* **56**, 405-421.

WHELLER G. E., VARNE R., FODEN J. D. & ABBOTT M. J. 1987. Geochemistry of Quaternary volcanism in the Sunda-Banda Arc, Indonesia, and three-component genesis of island arc basaltic magmas. *Journal of Volcanology and Geothermal Research* **32**, 137-159.

WHITE W. M. & PATCHETT J. 1984. Hf-Nd-Sr isotopes and incompatible element abundances in island arcs: Implications for magma origins and crust-mantle evolution. *Earth and Planetary Science Letters* **67**, 167-185.

WHITFORD D. J. & JEZEK P. 1982. Isotopic constraints on the role of subducted sialic material in Indonesian island arc magmatism. *Geological Society of America Bulletin* **93**, 504-513.

WILSON M. 1989. *Igneous Petrogenesis*. A Global Tectonic Approach, Unwin Hyman, London.

WILSON M. 1993. Geochemical signatures of oceanic and continental basalts: A key to mantle dynamics. *Journal of the Geological society* **150**, 977-990.

WILSON M. & DOWNES H. 1991. Tertiary-Quaternary extension-related alkaline magmatism in Western and Central Europe. *Journal of Petrology* **32**, 811-849.

WITTKE J. H. & MACK L. E. 1993. OIB-Like Mantle Source for Continental Alkaline Rocks of the Balcones Province, Texas: Trace-Element and Isotopic Evidence. *Journal of Geology* **101**, 333-344.

WOBUS R. A., MOCHEL D. W., MERTZMAN S. A., EIDE. E. A., ROTHWARF M. T., LOEFFLER B. M., JOHNSON D. A., KEATING G. N., SULTZE K., BENJAMIN A. E., VENZKE E. A. & FILSON T. 1990. Geochemistry of high-potassium rocks from the mid-Tertiary Guffey volcanic center, Thirtynine Mile volcanic field, central Colorado. *Geology* **18**, 642-645.

WOOLLEY A. R., BERGMAN S. C., EDGAR A. D., LE BAS M. J., MITCHELL R. H., ROCK N. M. S. & SCOTT SMITH B. H. 1996. Classification of Lamprophyres, Lamproites, Kimberlites and the Kalsilitic, Melilitic and Leucitic rocks. *Canadian Mineralogist* **34**, 175-186.

WOOLLEY A. R. & SYMES R. F. 1976. The analcime-phyric phonolites (blairmorites) and associated analcime kenytes of the Lupate gorge, Mozambique. *Lithos* **9**, 9-15.

WYBORN D. 1983. Fractionation processes in the Boggy plain zoned pluton. PhD thesis, the Australian National University, Canberra (unpubl.).

ZHANG M., SUDDABY P., THOMPSON R. N., THIRLWALL M. F. & MENZIES M. A. 1995. Potassic volcanic rocks in NE China: Geochemical constraints on mantle source and magma genesis. *Journal of Petrology* **36**, 1275-1303.

ZINDLER A. & HART S. 1986. Chemical geodynamics. *Annual Review of Earth and Planetary Sciences* **14**, 493-571.

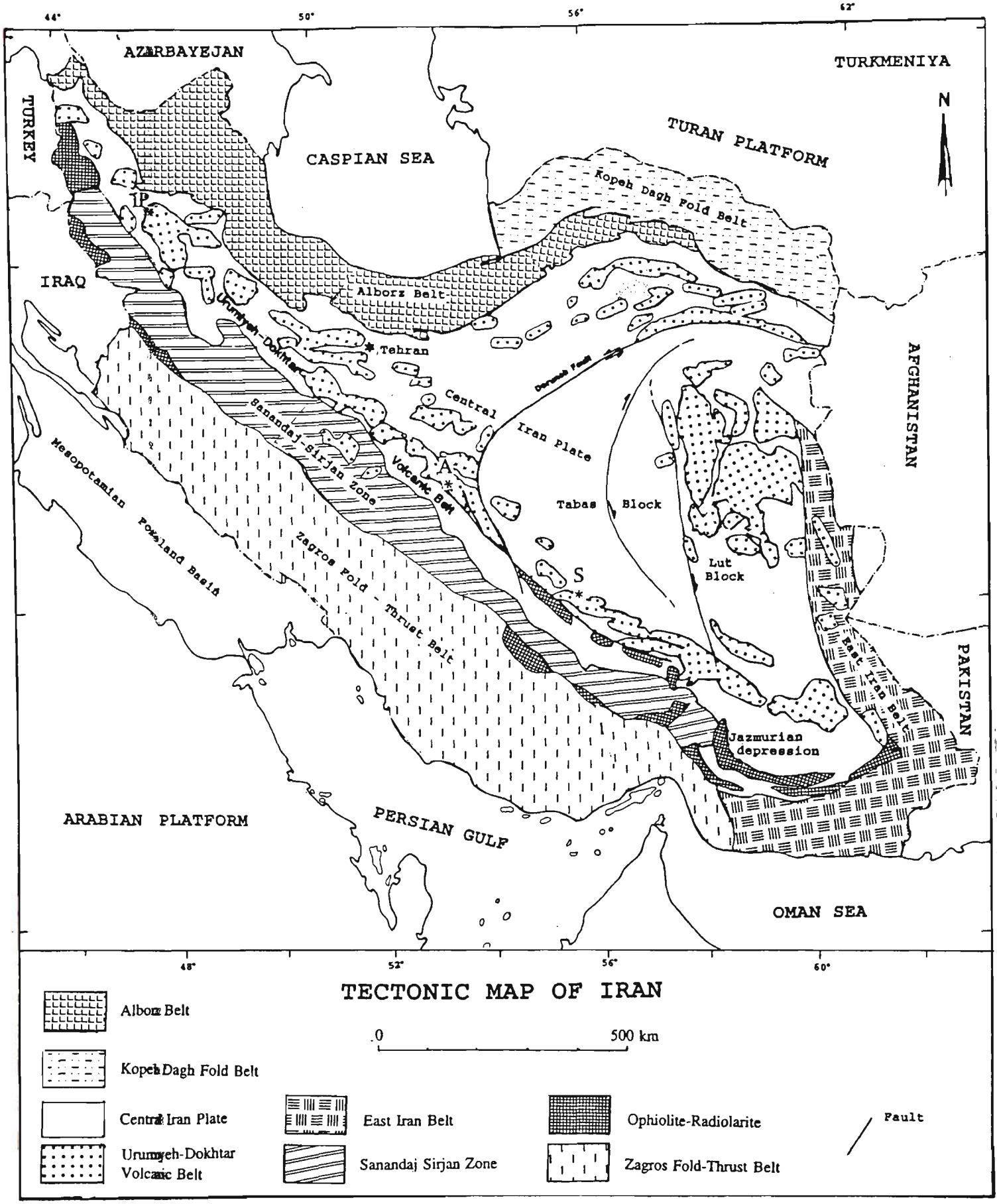

Fig. 1-1. Simplified tectonic map of Iran (after Ruttner and Stocklin, 1967; Alavi, 1991).
IP = Islamic Peninsula, A = Aghda, S = Shahrbabak

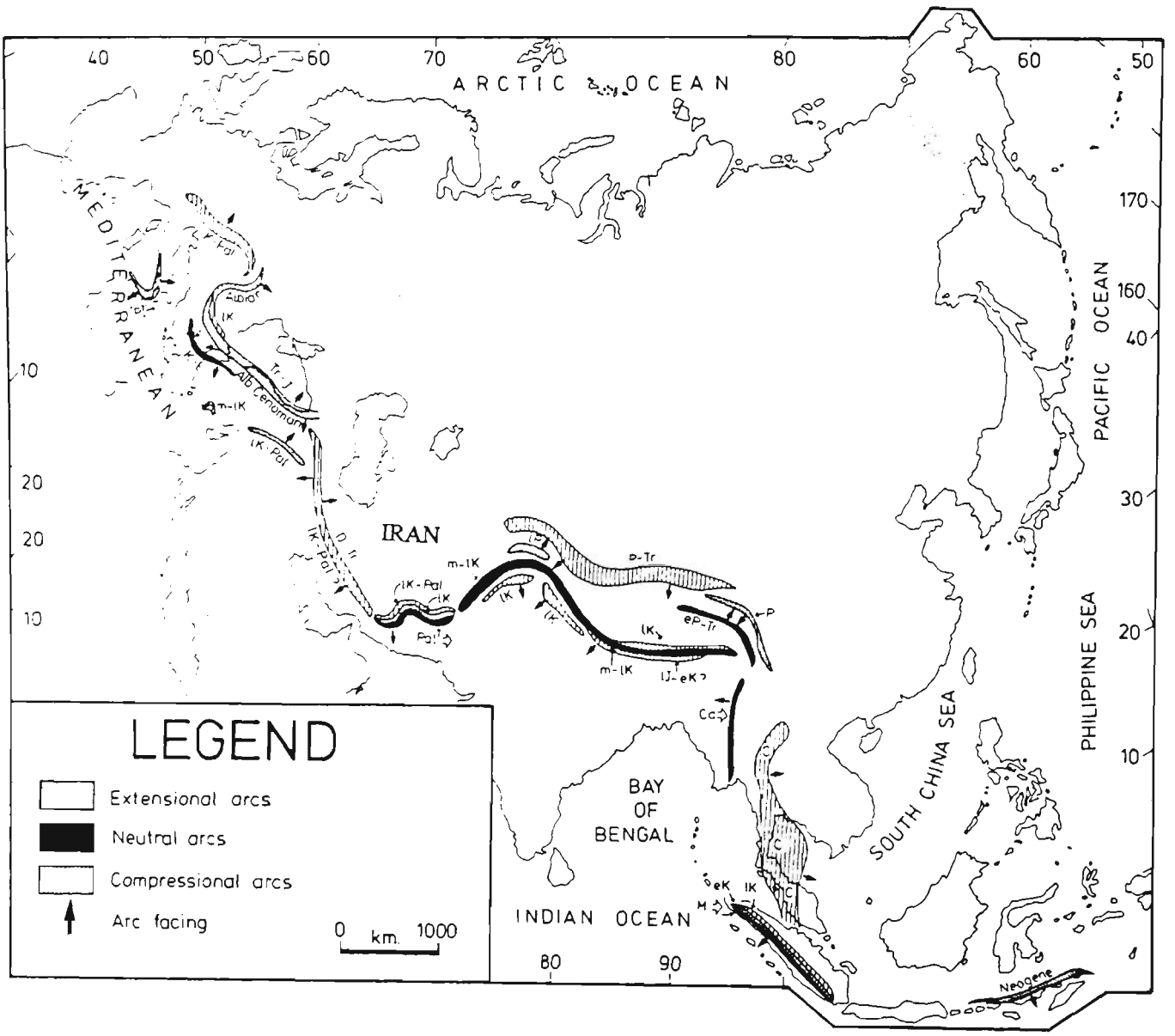

Fig. 1-2. Indonesia Himalaya Mediterranean Belt (from Sengor, 1990). Key to lettering: D = Devonian, C = Carboniferous, P = Permian, Tr = Triassic, J = Jurassic, K = Cretaceous, Ca = Cainozoic, Pal = Palaeocene, E = Eocene, M = Miocene, Pl = Pliocene, e = early, m = middle, l = late.

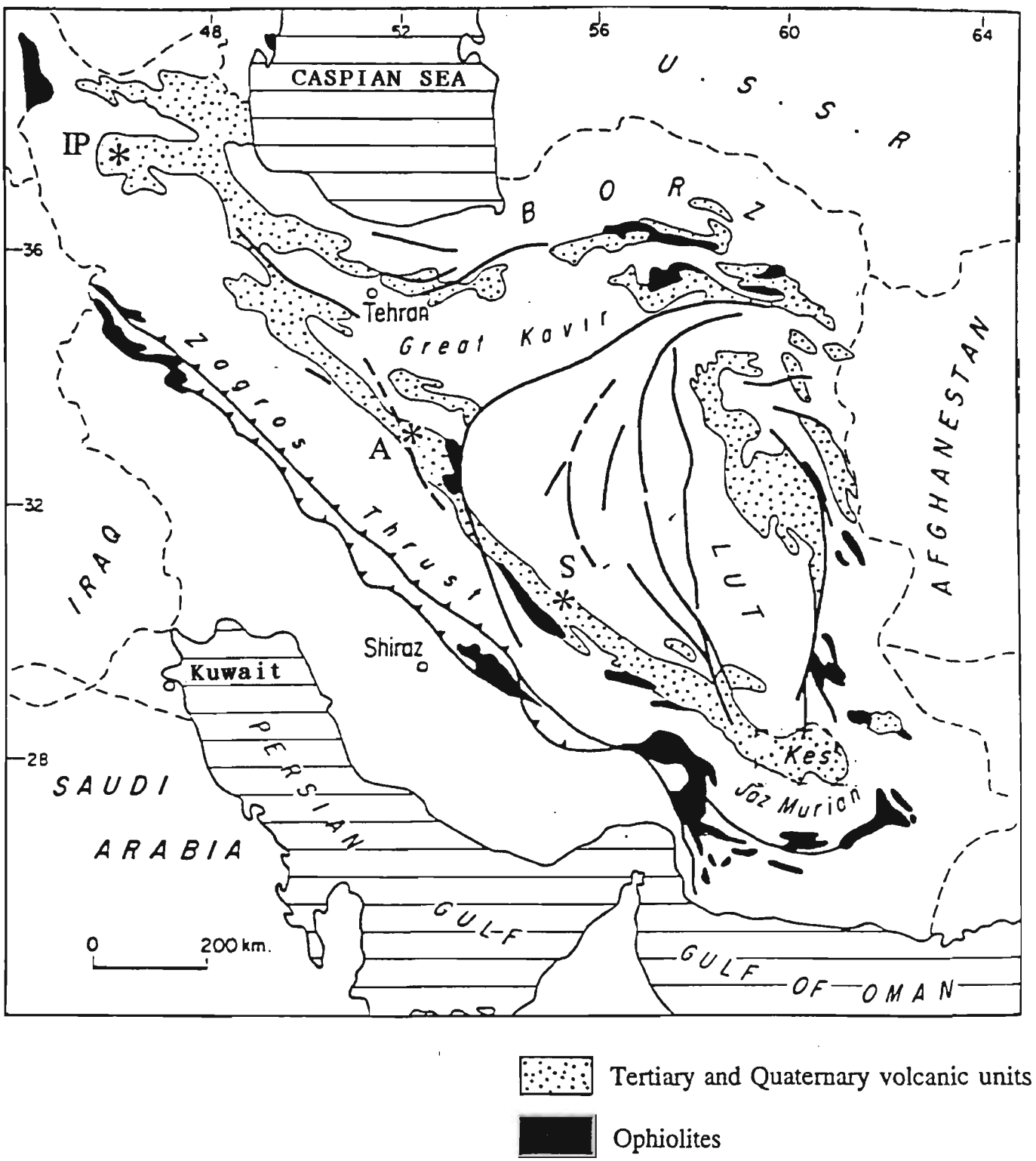

Fig. 2-1. Generalized geological map showing distribution of volcanic rocks and ophiolites in Irán (from Stocklin, 1968). IP = Islamic Peninsula, A = Aghda, S = Shahrbabak

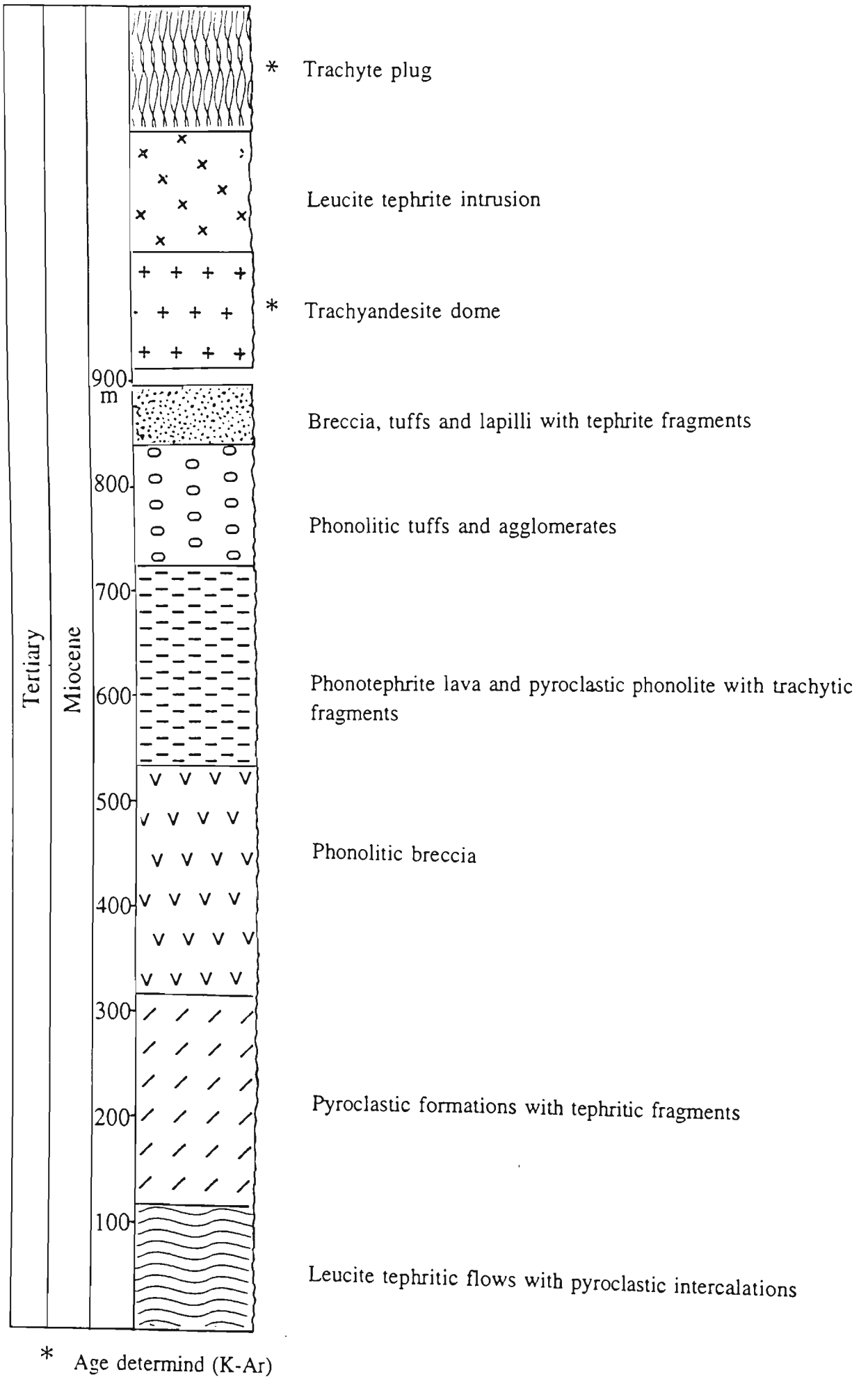

Fig. 3-2. Simplified stratigraphic section for deposits of the Islamic Peninsula volcano.

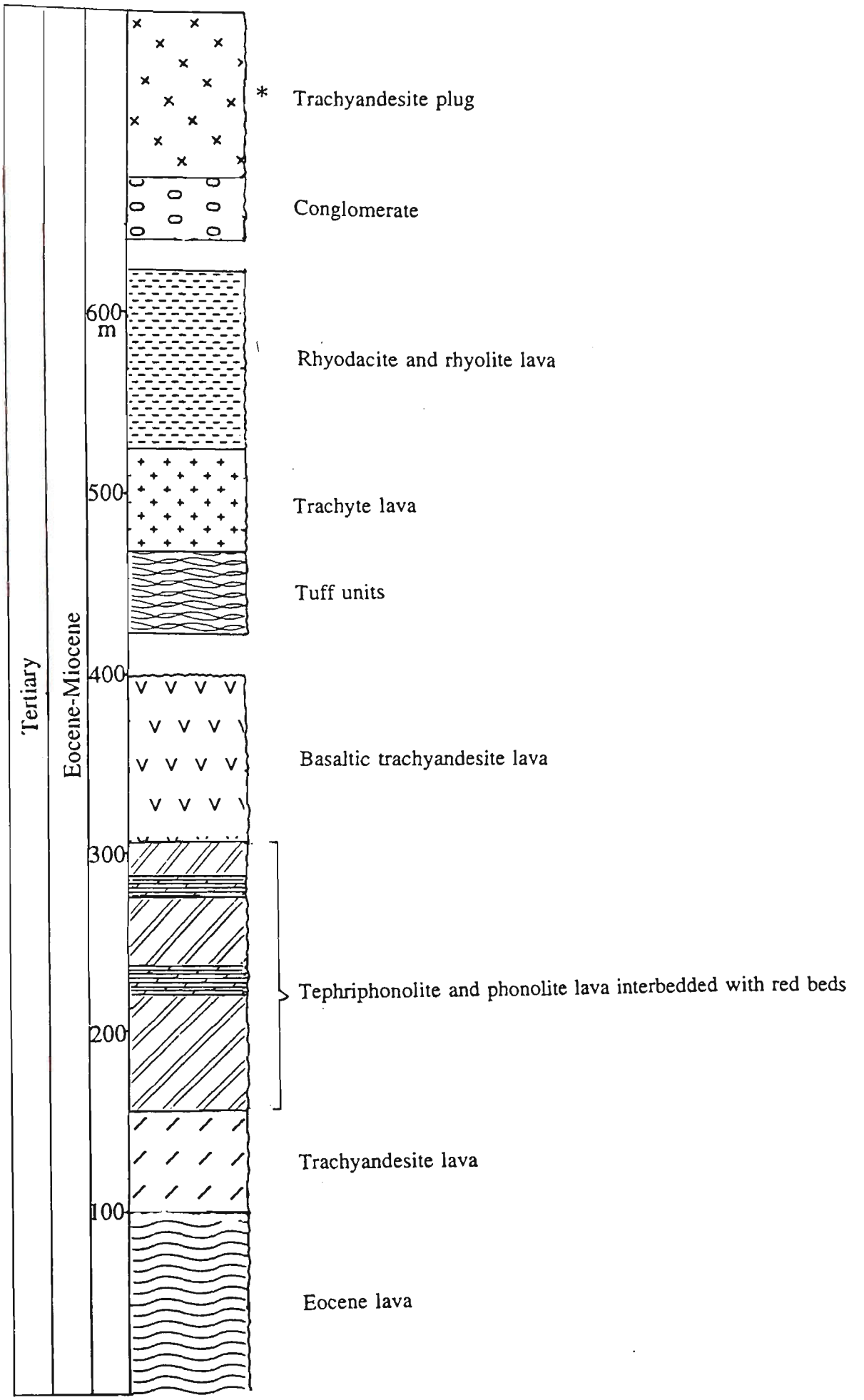

* Age determind (K-Ar)

Fig. 3-4. Simplified stratigraphic section for deposits of the Aghda area.

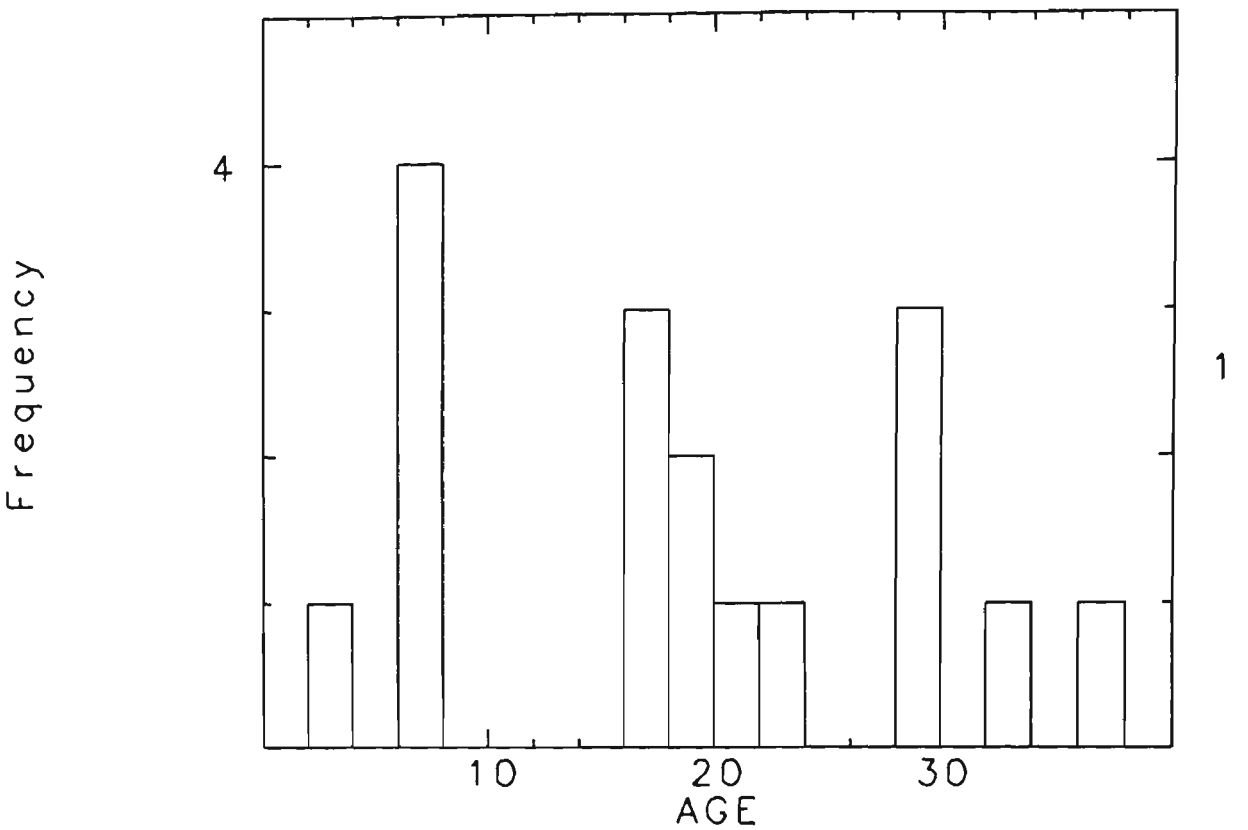

Fig. 3.5. Histogram of isotopic dates for deposits from the Shahrbabak area. Data from Table 3.1.

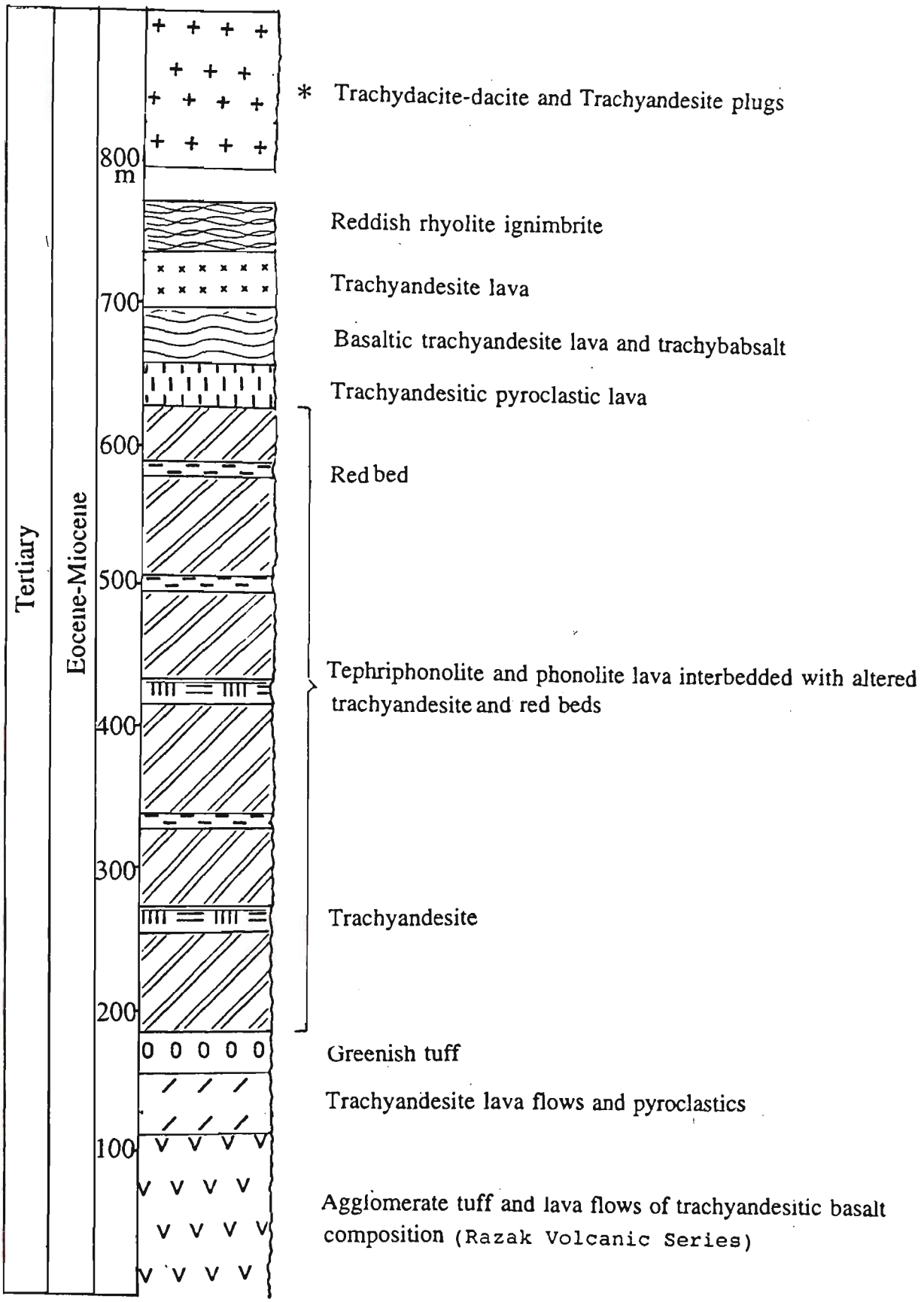

Fig. 3-7. Simplified stratigraphic section for deposits of the Shahrbabak area.

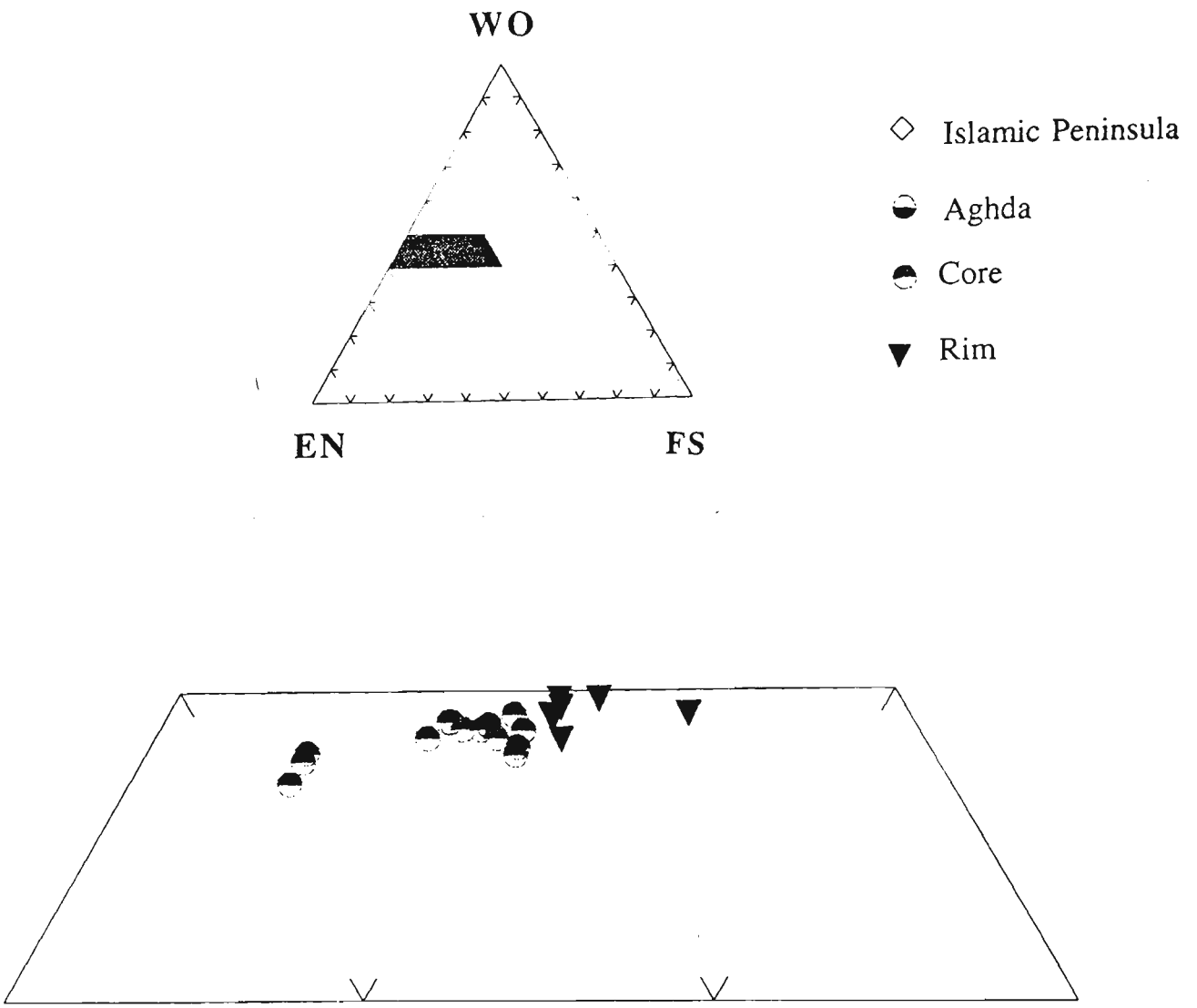

Fig. 4-1. Compositions of diopside phenocrysts for tephrite from the Islamic Peninsula

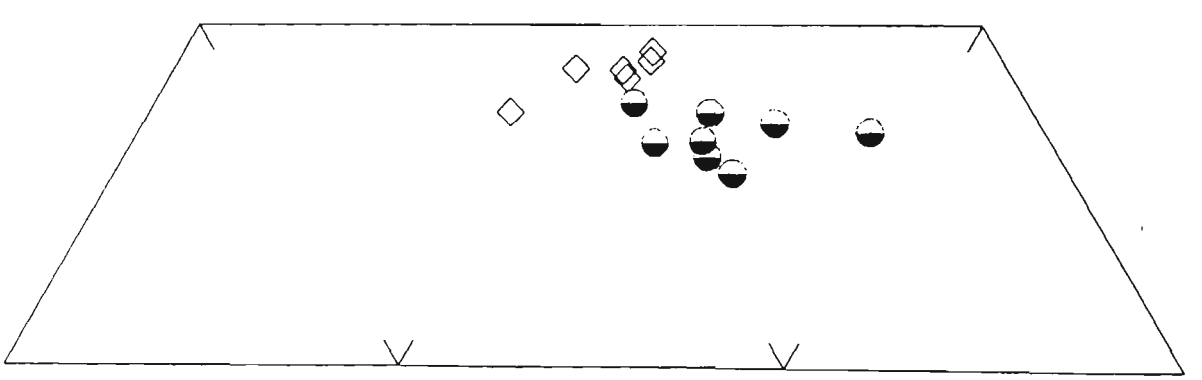

Fig. 4-2. Compositions of diopside phenocrysts for phonotephrite from the Islamic Peninsula and Aghda.

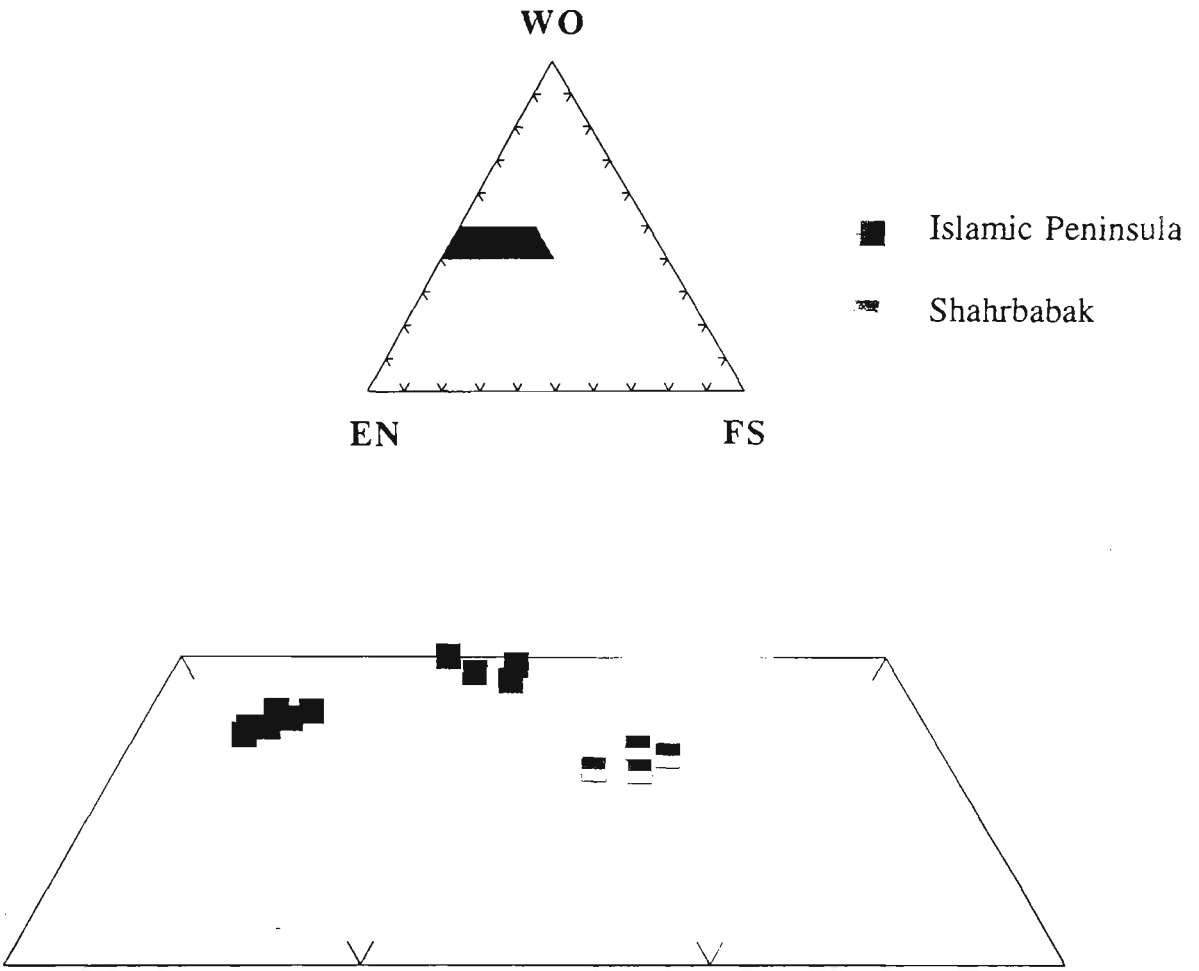

Fig. 4-3. Compositions of diopside phenocrysts for basalt from the Islamic Peninsula and Shahrbabak.

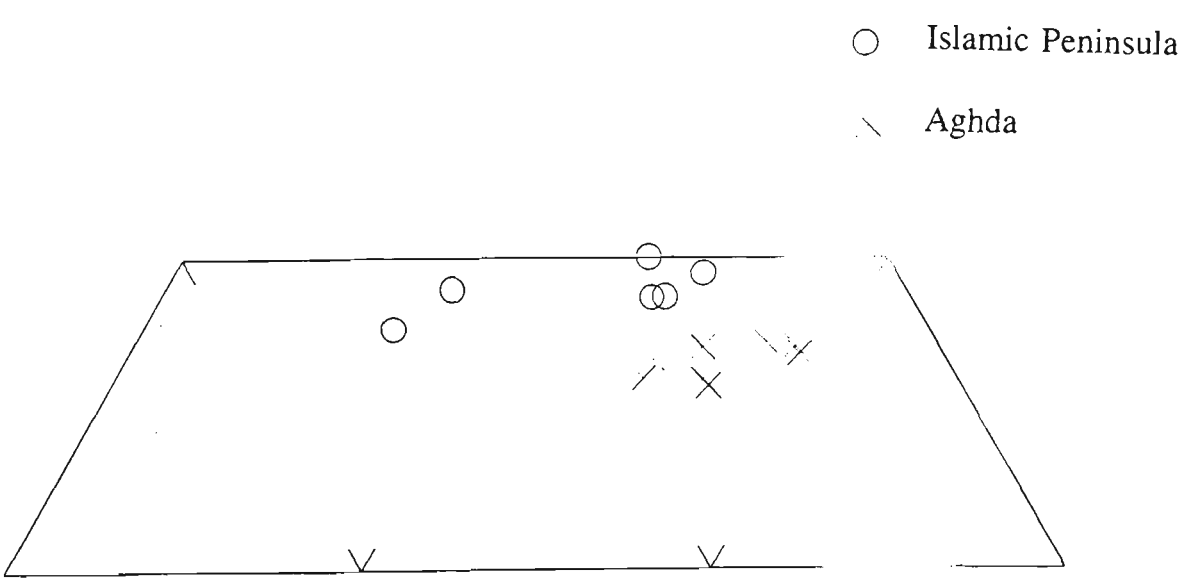

Fig. 4-4. Compositions of diopside phenocrysts for basaltic trachyandesite and trachyandesite from the Islamic Peninsula and Aghda.

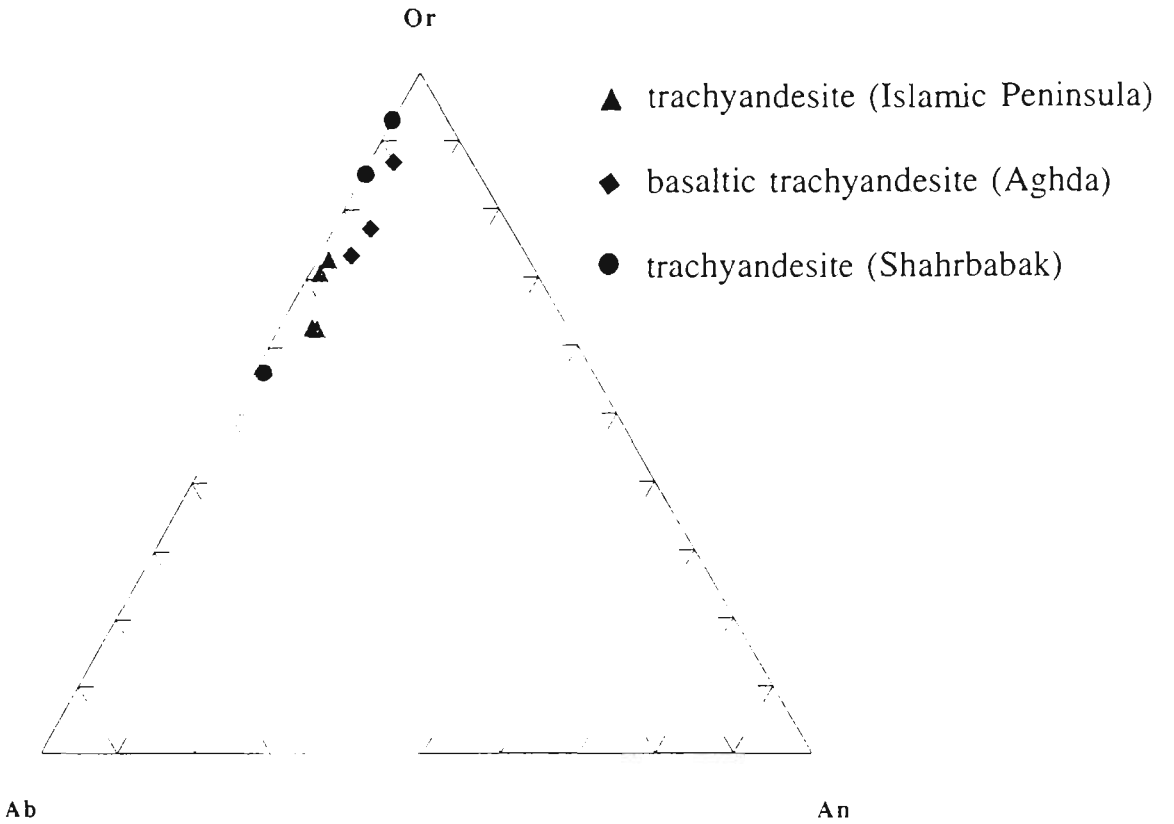

Fig. 4.5. Sanidine compositions for trachyandesite and basaltic trachyandesite from the Islamic Peninsula, Aghda and Shahrbabak.

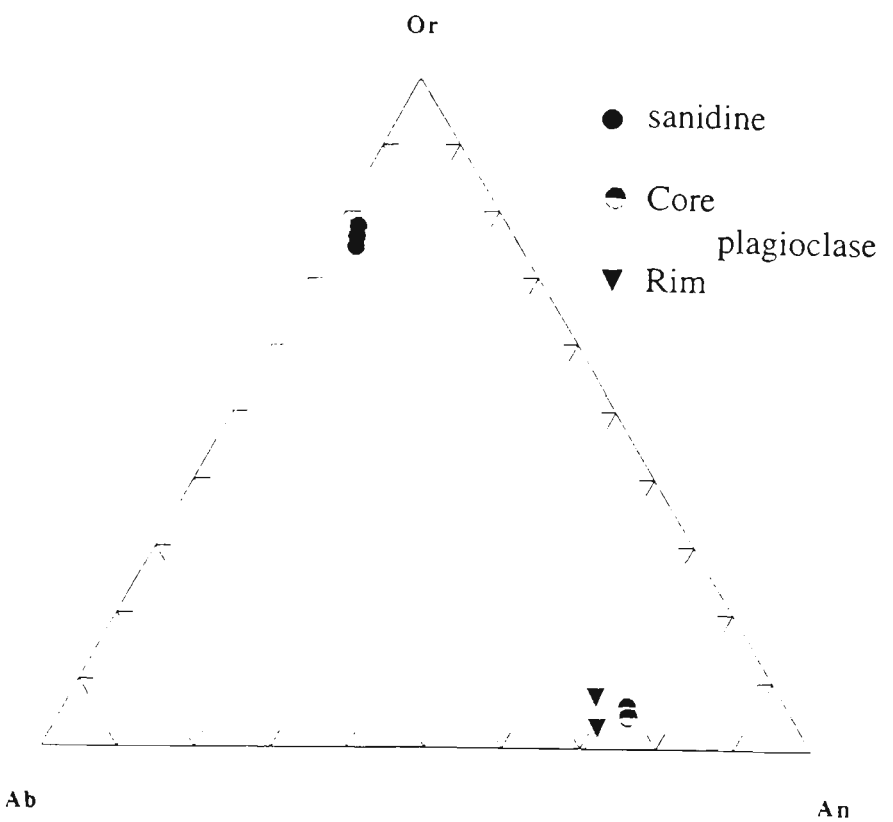

Fig. 4-6. Feldspar compositions for phonotephrite from Aghda.

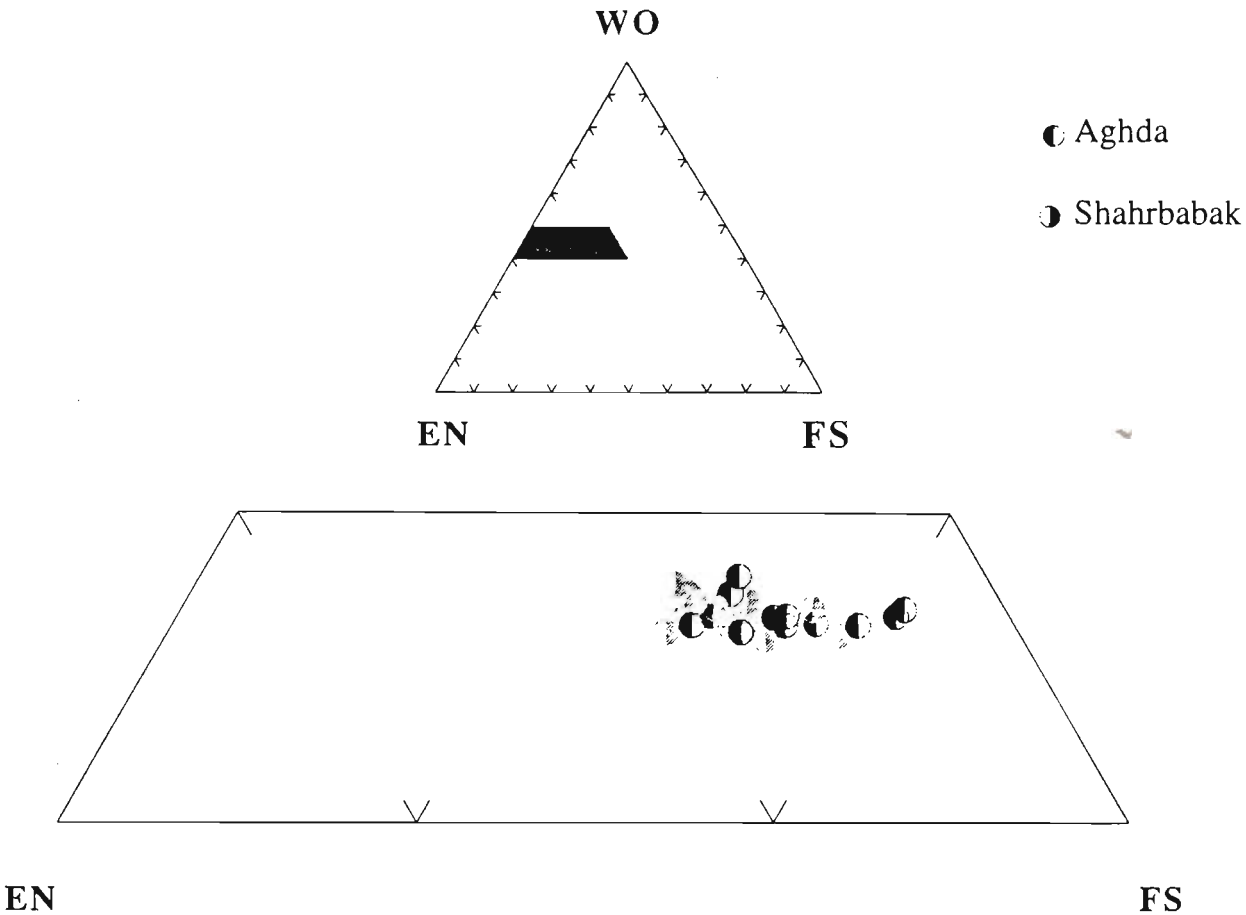

Fig. 4-7. Compositions of diopside phenocrysts for tephriphonolite from Aghda and Shahrbabak.

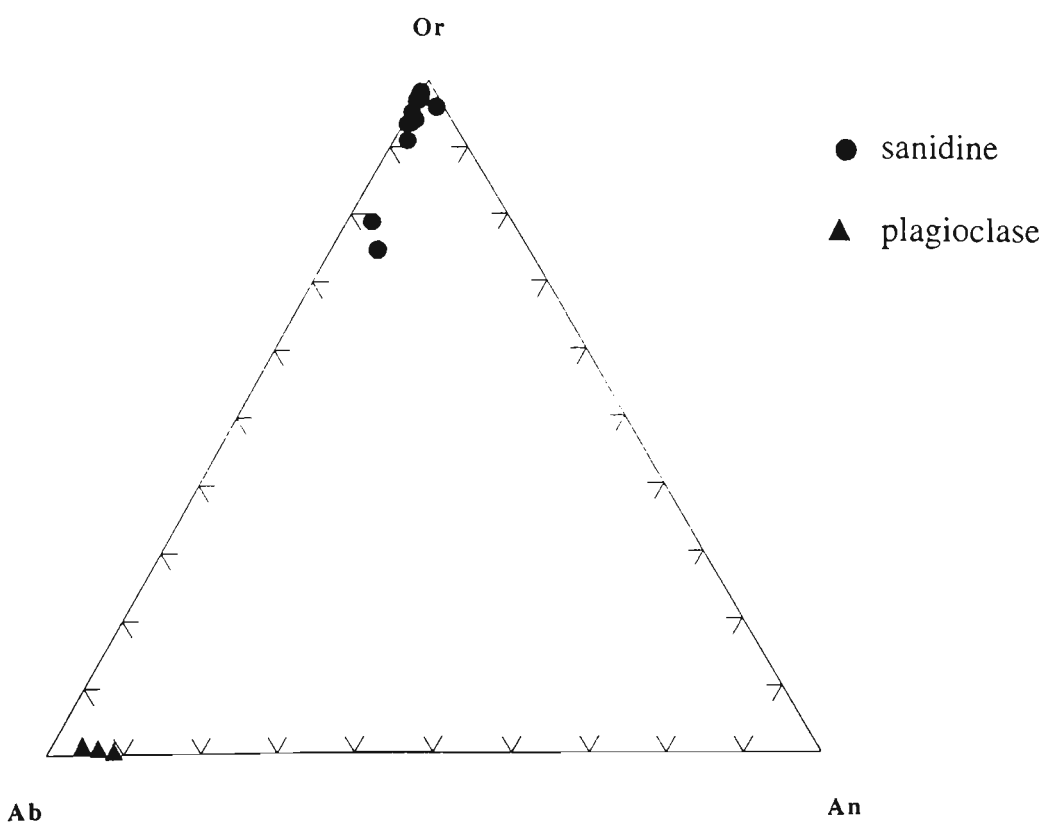

Fig. 4-8. Feldspar compositions for tephriphonolite from Aghda.

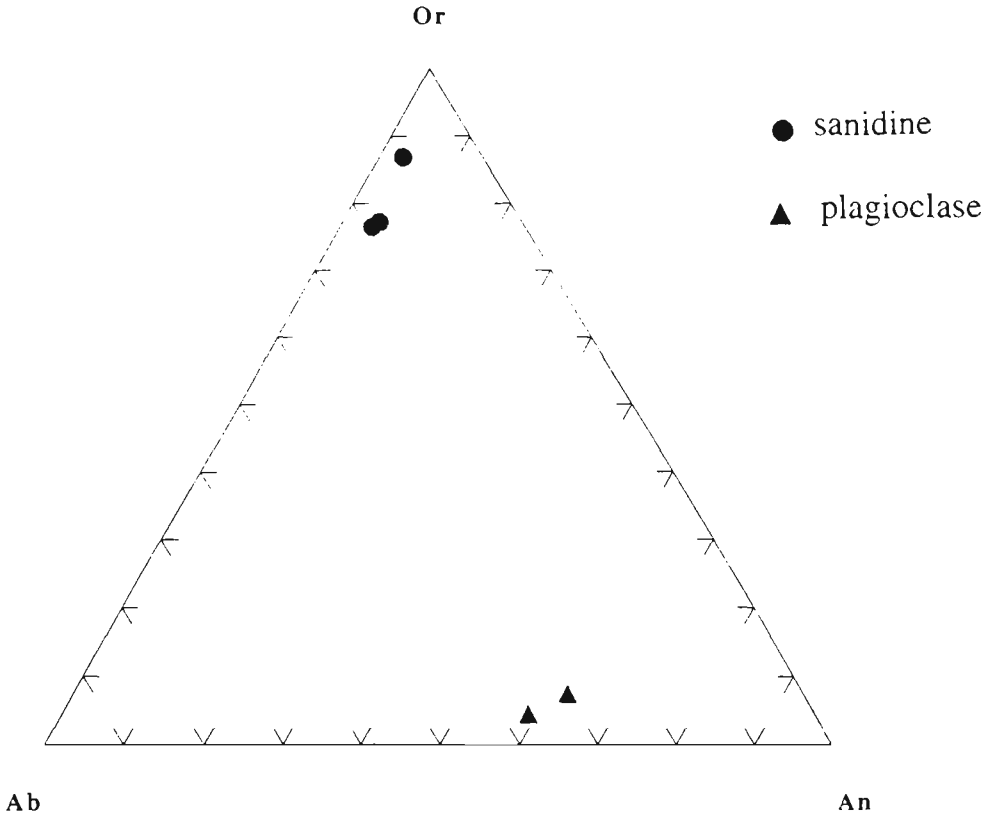

Fig. 4-9. Feldspar compositions for basaltic trachyandesite from Aghda.

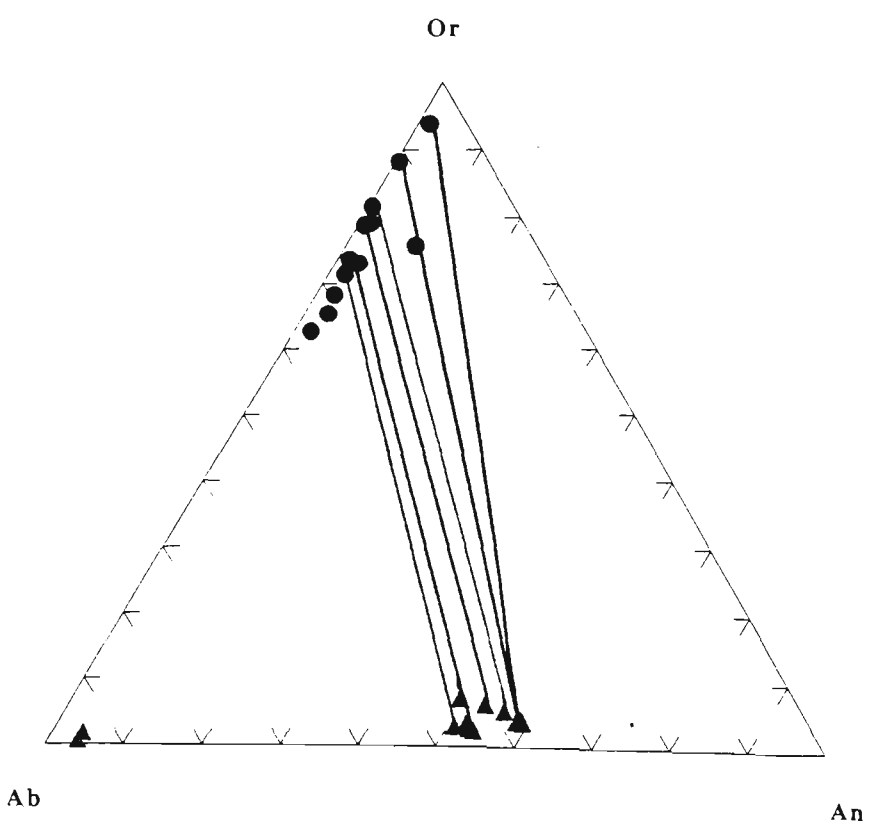

Fig. 4-10. Feldspar compositions for tephriphonolite from Shahrbabak.

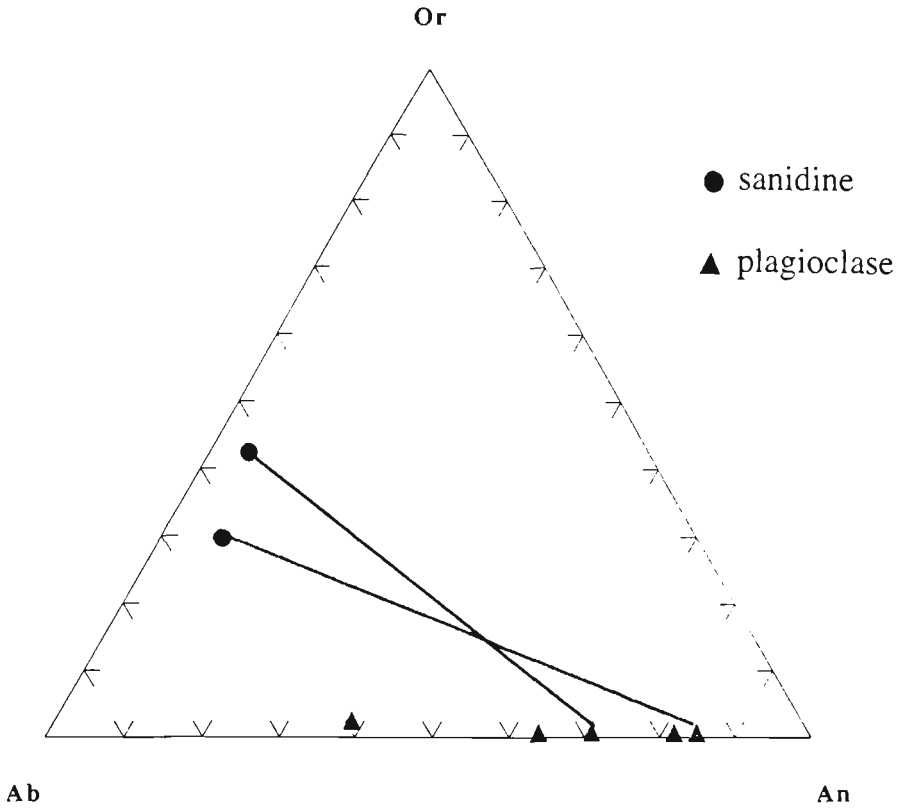

Fig. 4-11. Feldspar compositions for basalt from Shahrbabak.

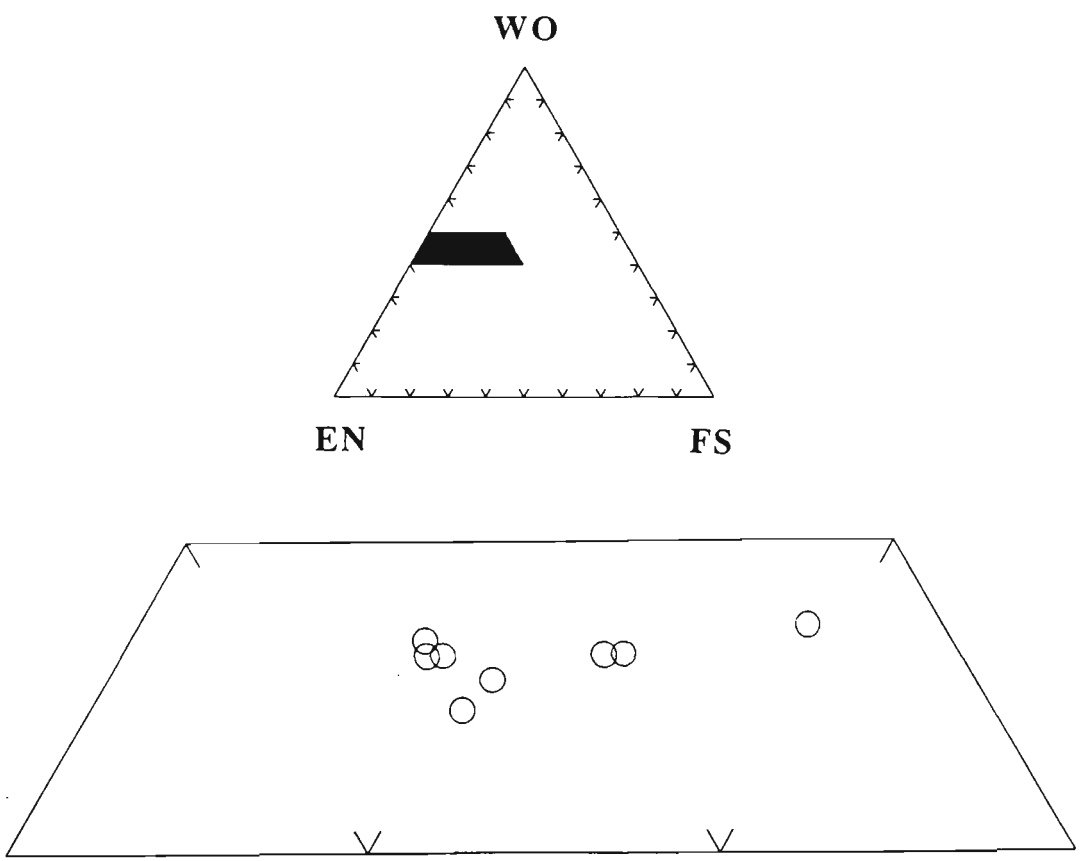

Fig. 4-12. Compositions of diopside phenocrysts for trachybasalt from Shahrbabak.

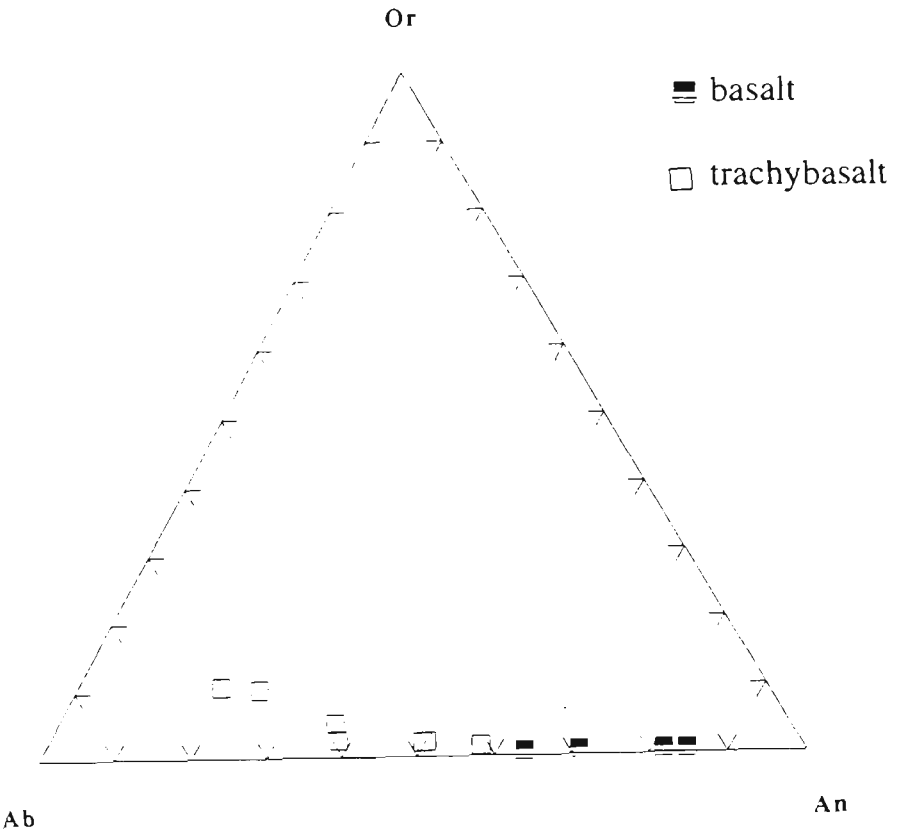

Fig. 4-13. Plagioclase compositions for basalt and trachybasalt from Shahrbabak.

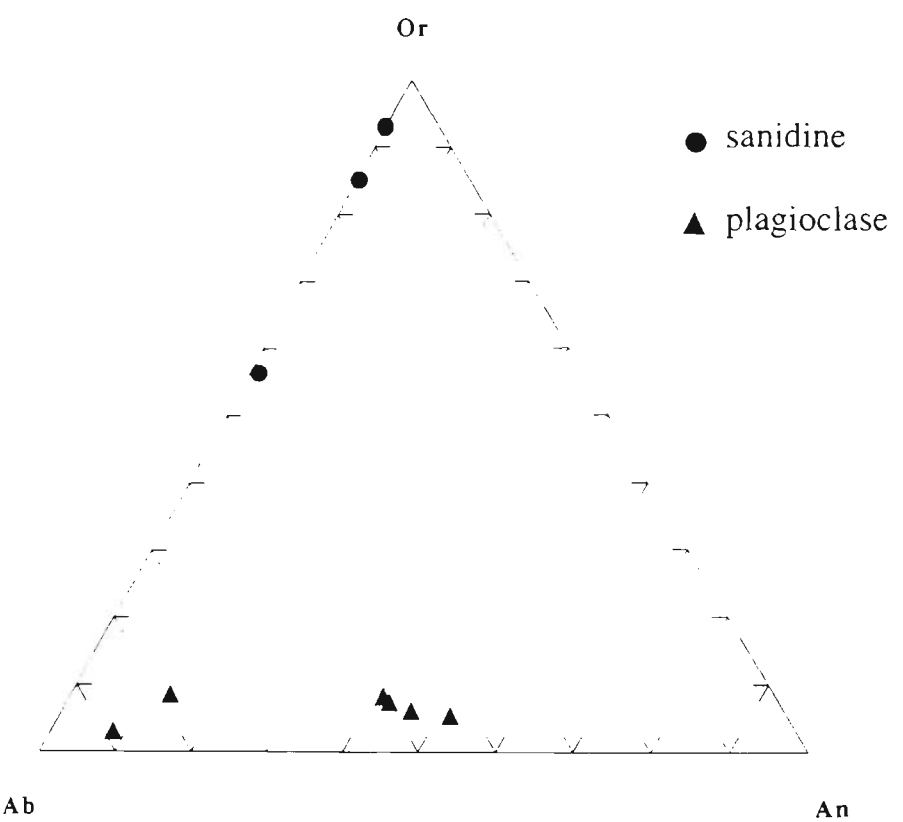

Fig. 4-14. Feldspar compositions for trachyandesite from Shahrbabak.

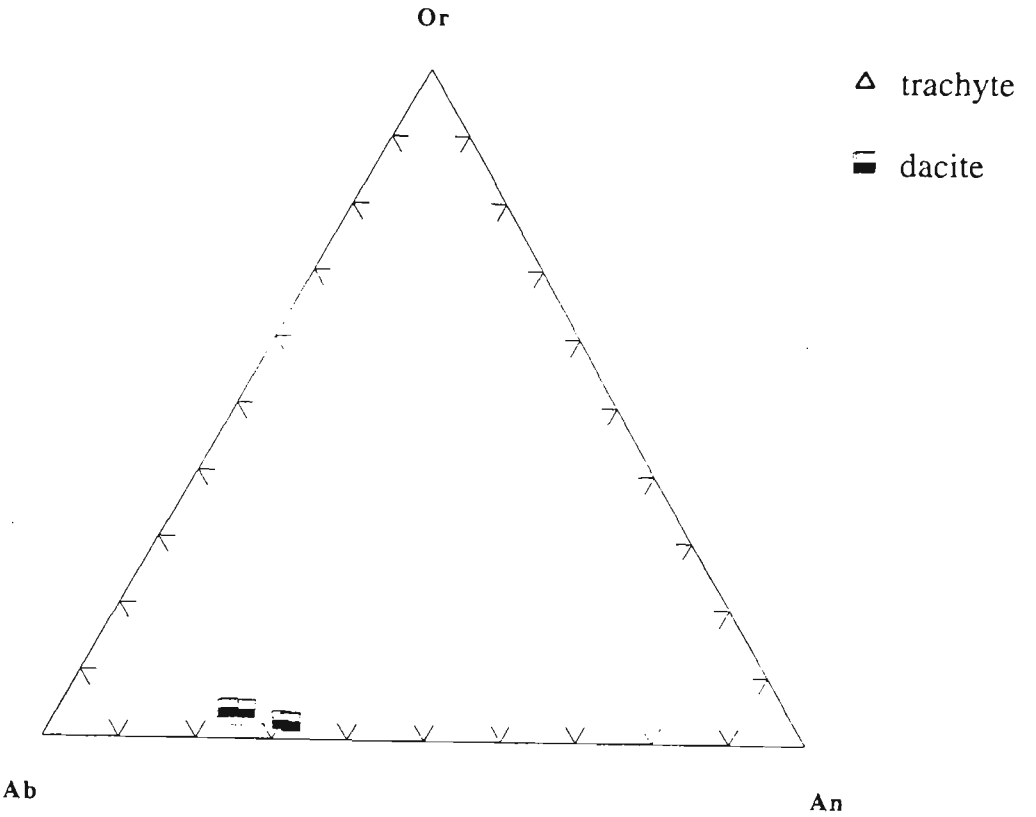

Fig. 4-15. Plagioclase compositions for trachyte and dacite from Shahrbabak.

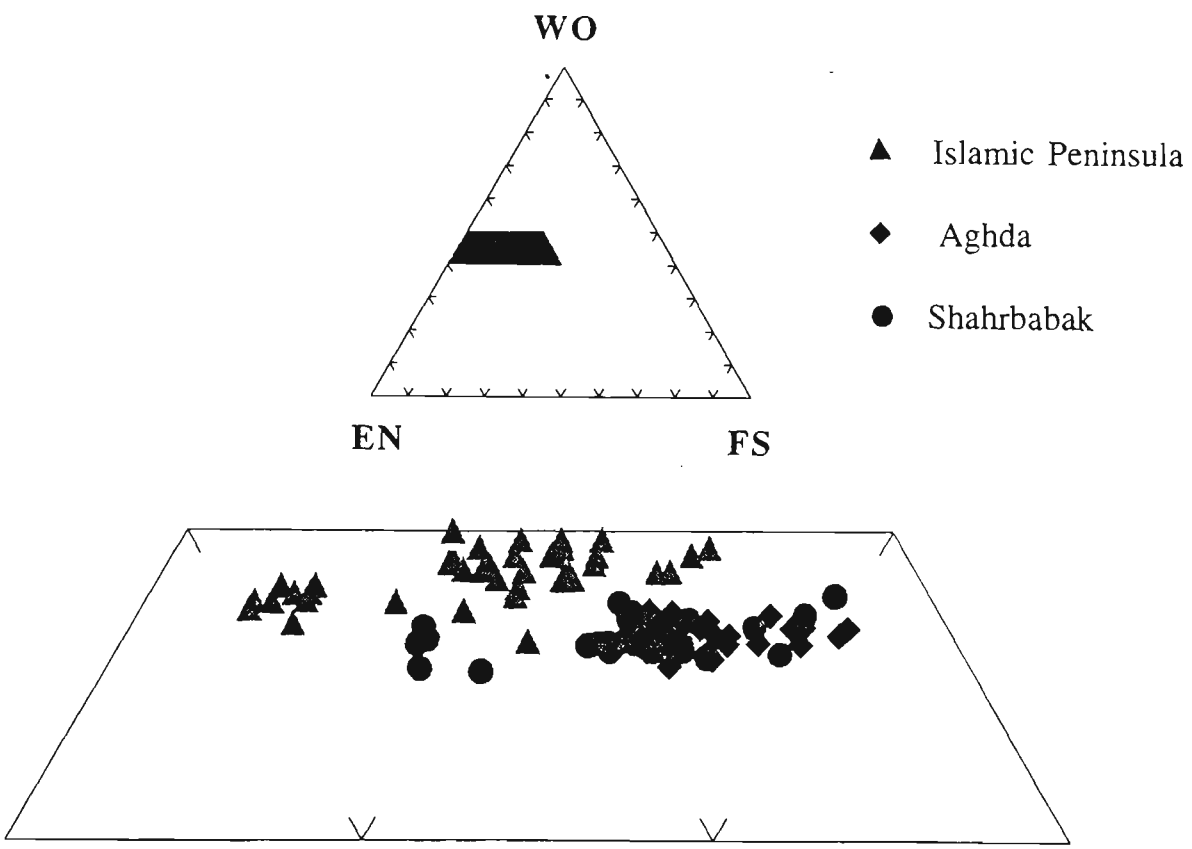

Fig. 4-16. Compositions of diopside phenocrysts for rocks from the Islamic Peninsula, Aghda and Shahrbabak.

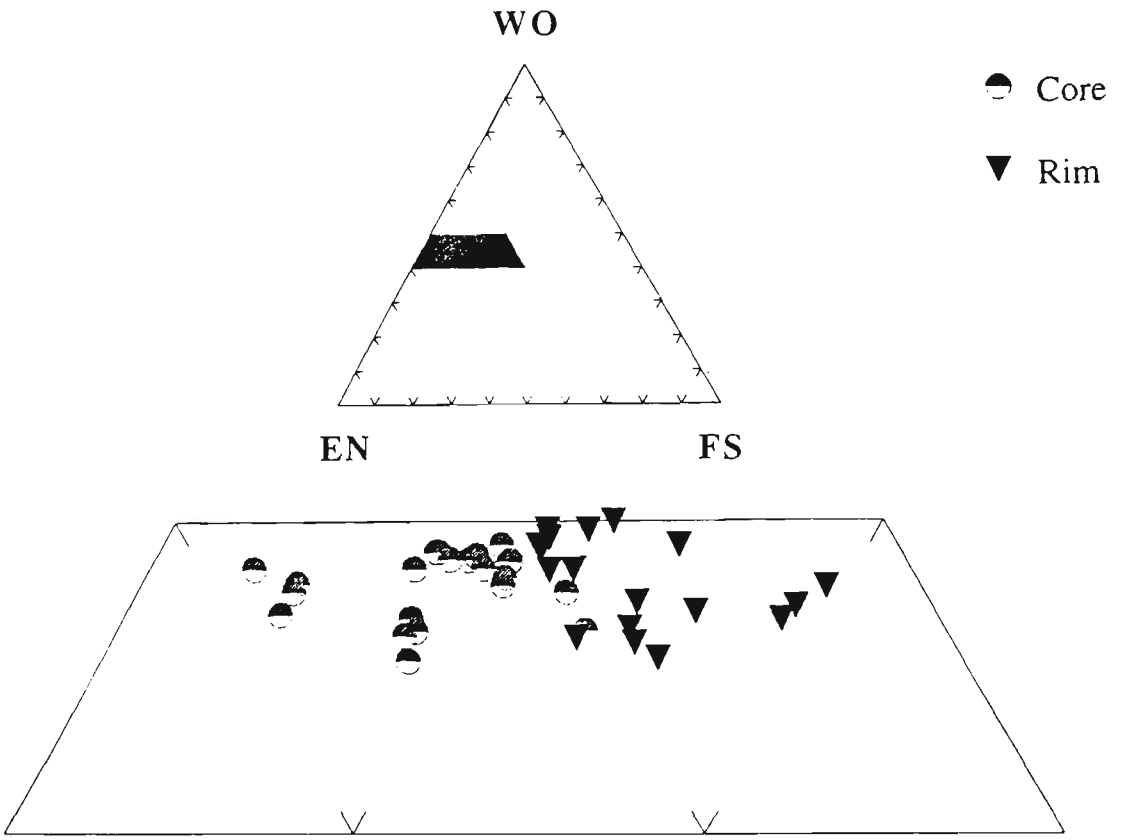

Fig. 4-17. Compositions of diopside phenocrysts for tephrite, phonotephrite and trachybasalt from the Islamic Peninsula, Aghda and Shahrbabak.

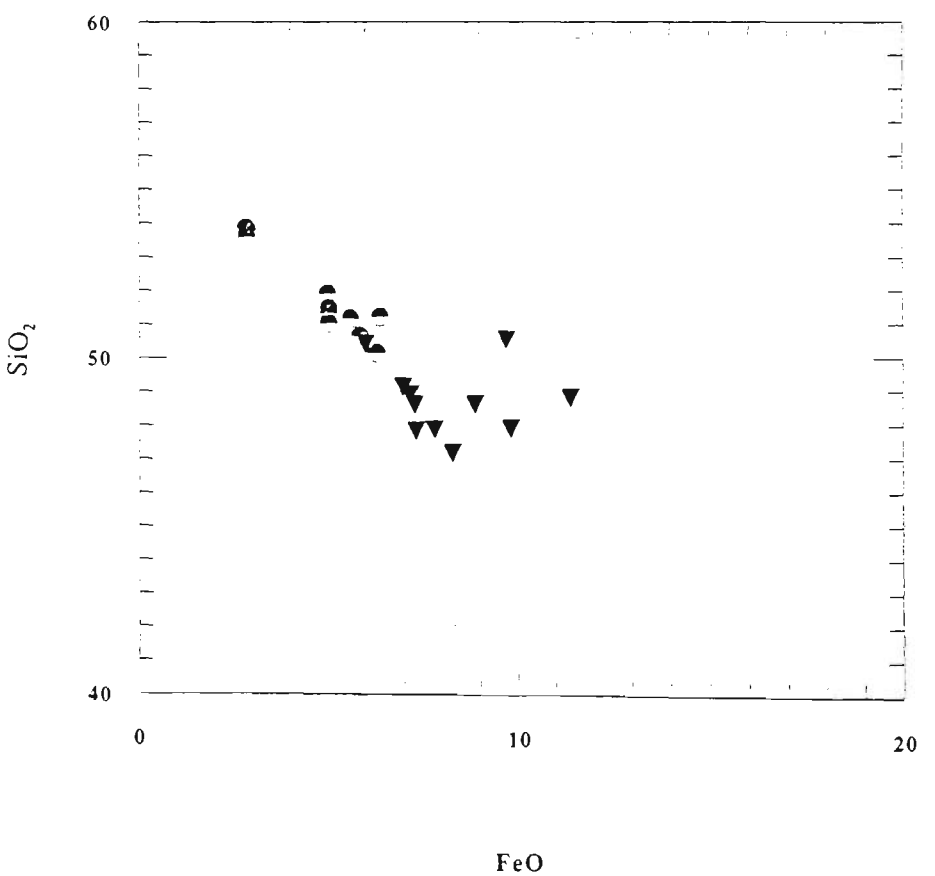

Fig. 4-18. Plot of total Fe as FeO versus SiO_2 in diopsidic clinopyroxene from the Islamic Peninsula, Aghda and Shahrbabak (oxides, wt%).

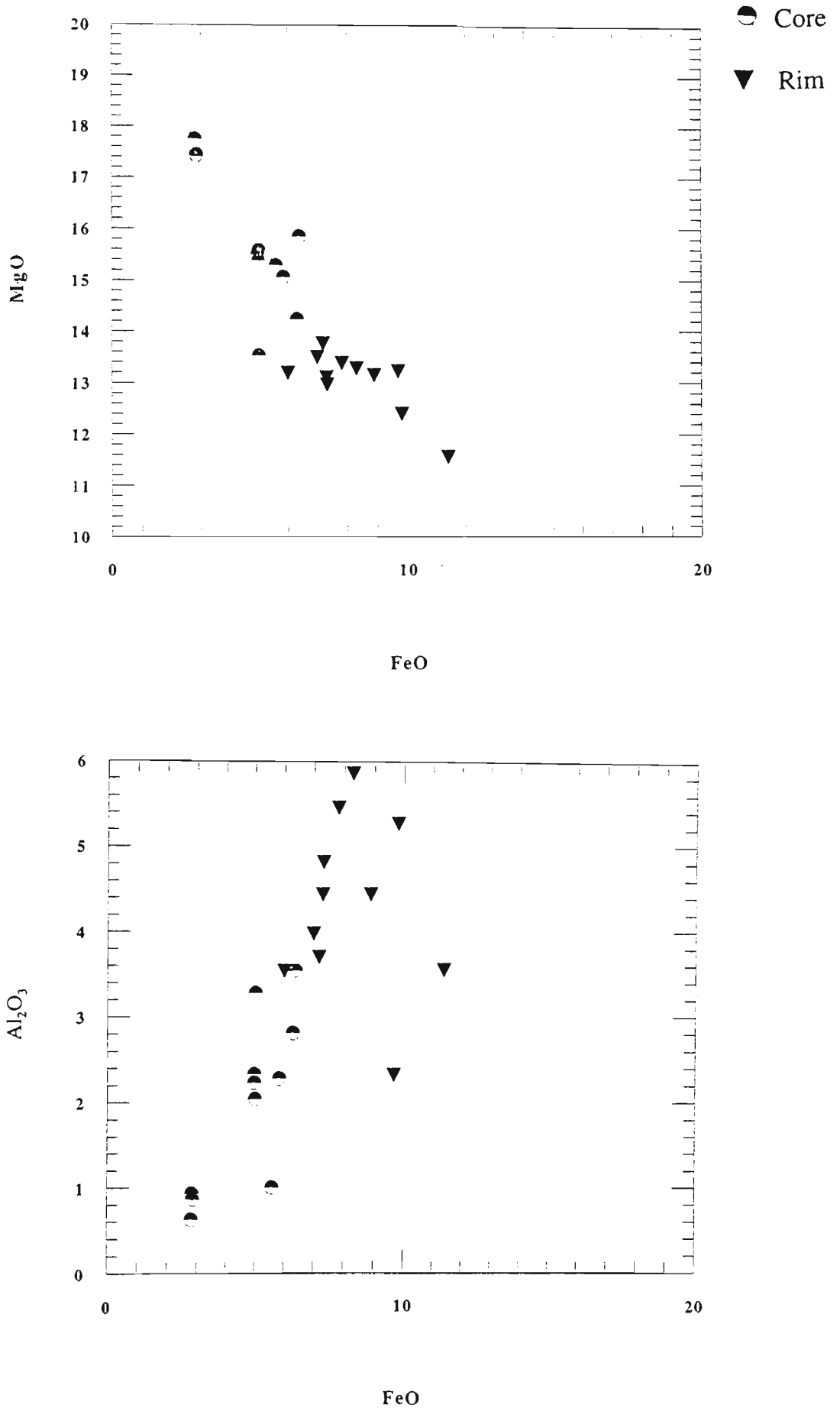

Fig. 4-18. (continued). Plot of total Fe as FeO versus MgO and Al_2O_3 in diopsidic clinopyroxene from the Islamic Peninsula, Aghda and Shahrbabak (oxides, wt%).

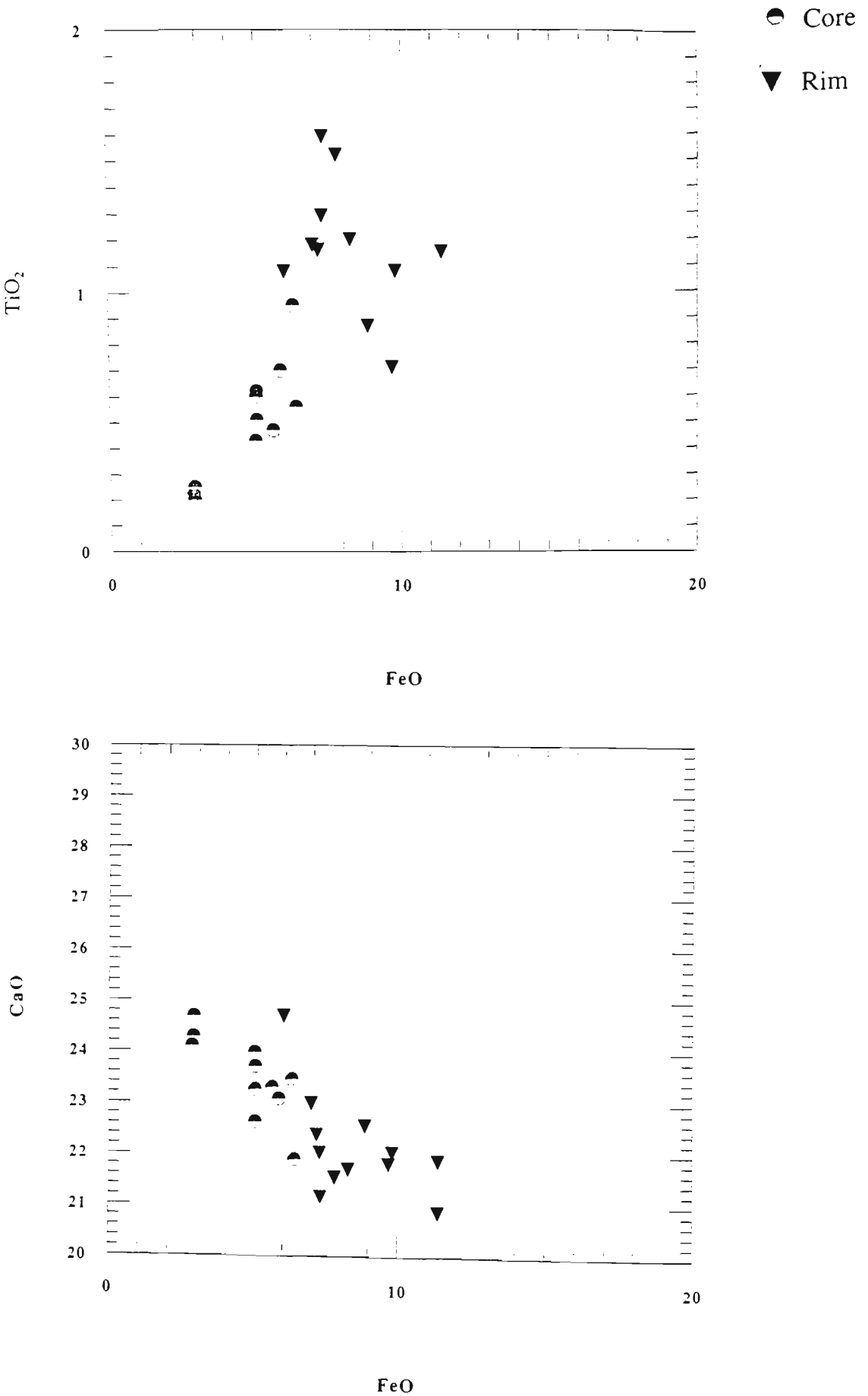

Fig. 4-18. (continued). Plot of total Fe as FeO versus TiO_2. and CaO in diopsidic clinopyroxene from the Islamic Peninsula, Aghda and Shahrbabak (oxides, wt%).

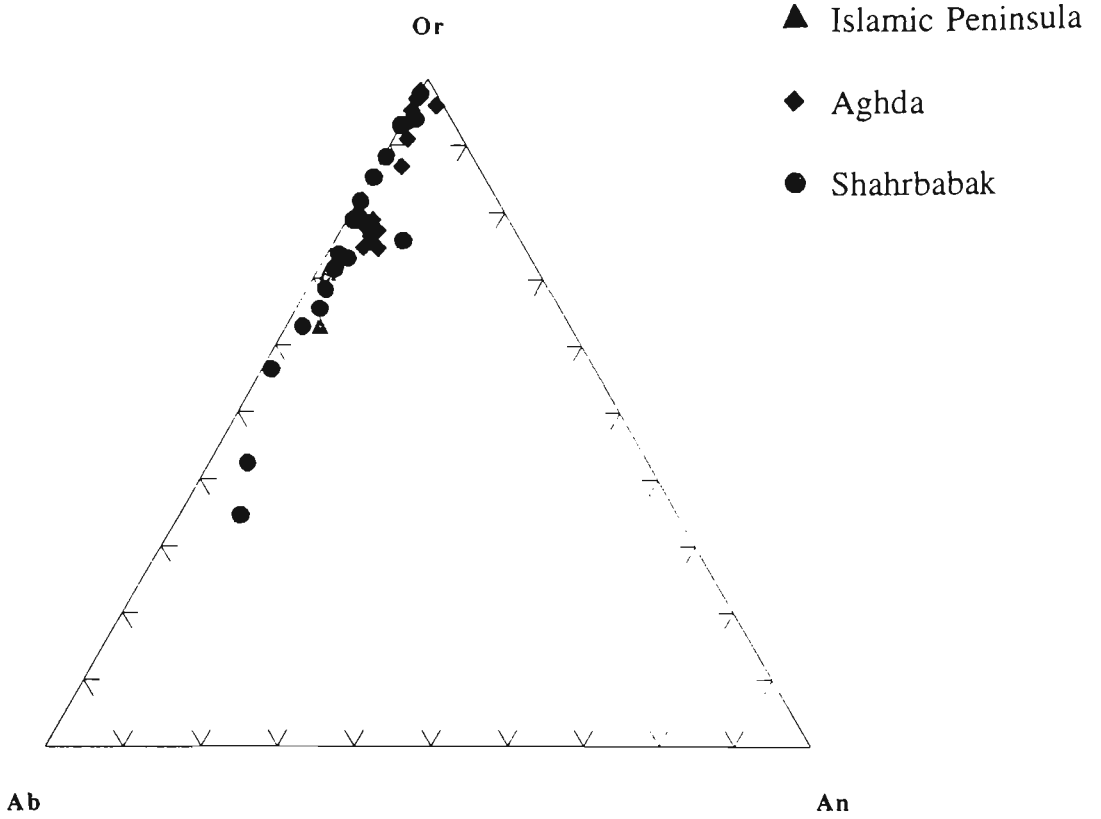

Fig. 4-19. Sanidine compositions for rocks from the Islamic Peninsula, Aghda and Shahrbabak.

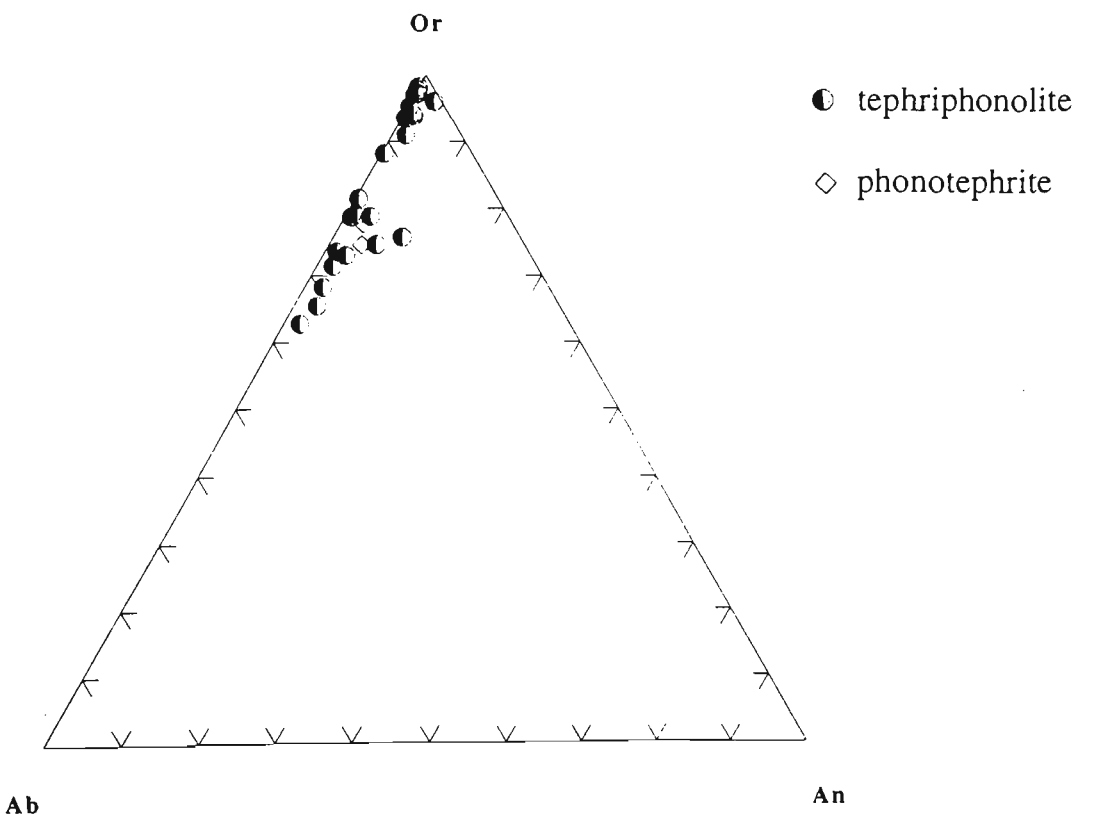

Fig. 4-20. Sanidine compositions for tephriphonolite and phonotephrite from Aghda and Shahrbabak.

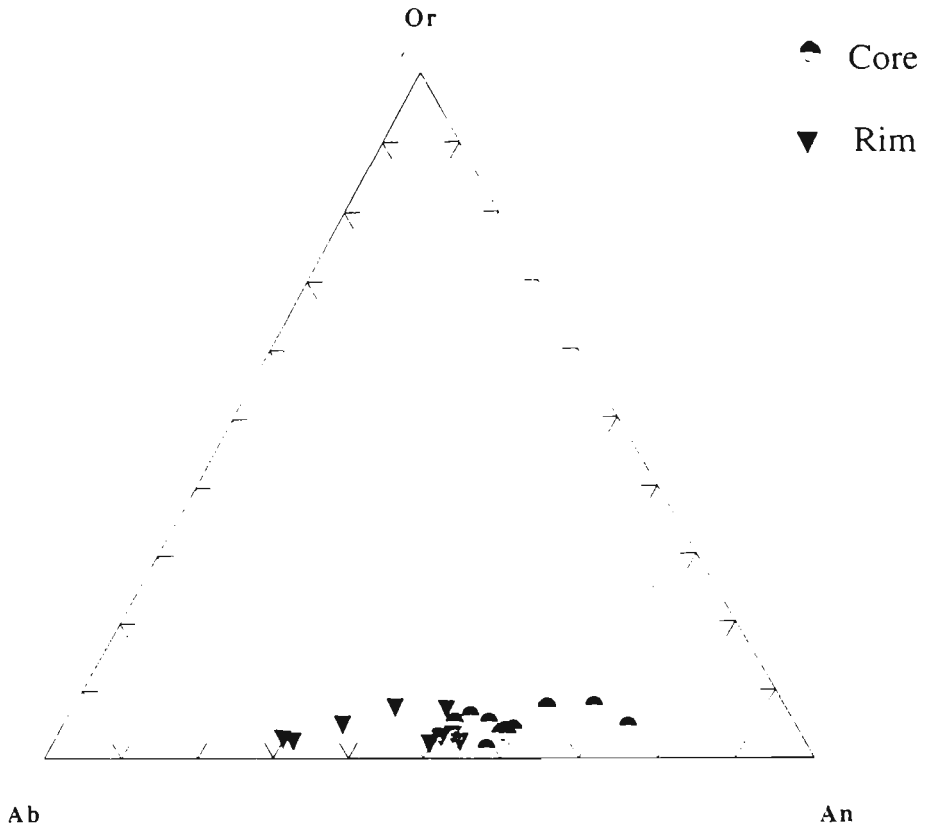

Fig. 4-21. Plagioclase compositions for rocks from Aghda and Shahrbabak.

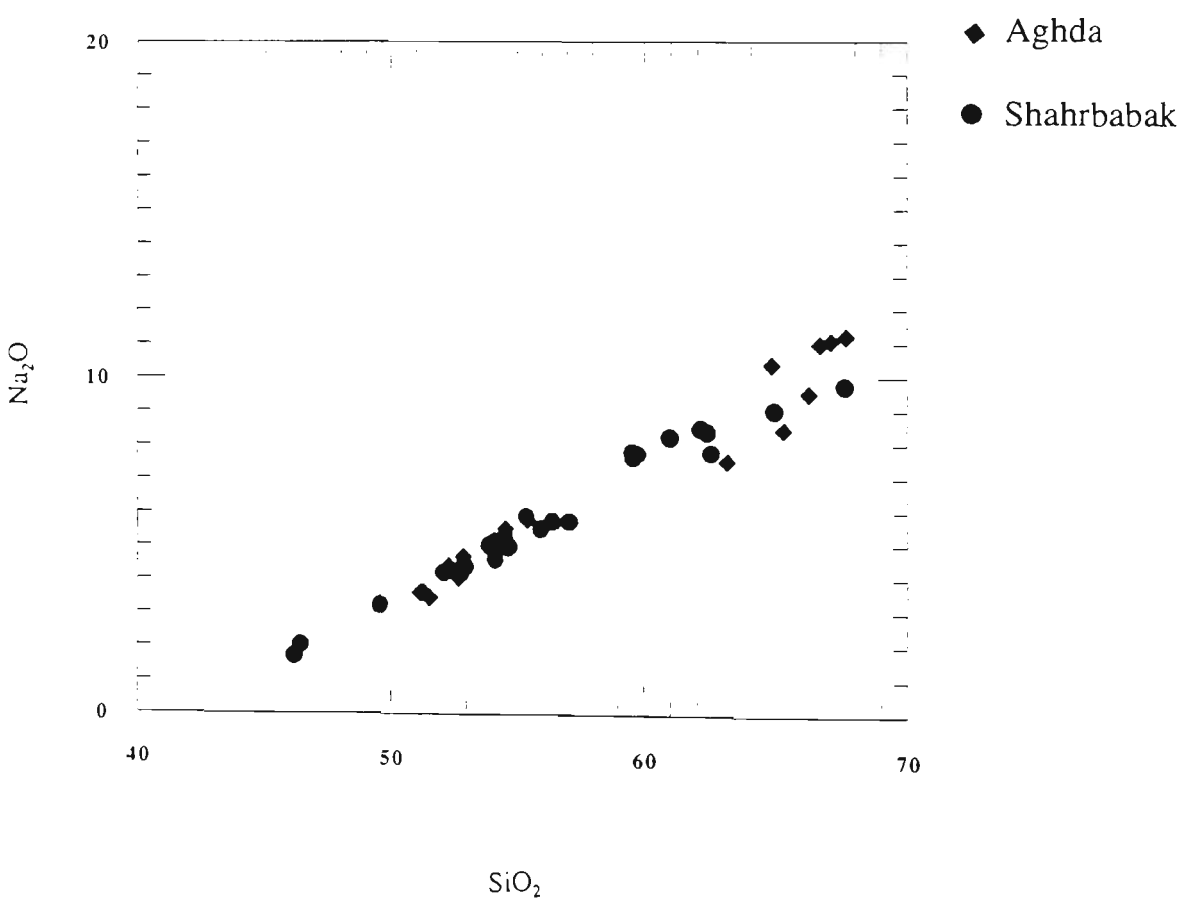

Fig. 4-22. Variation of SiO_2 with Na_2O in plagioclase from Aghda and Shahrbabak(oxides, w

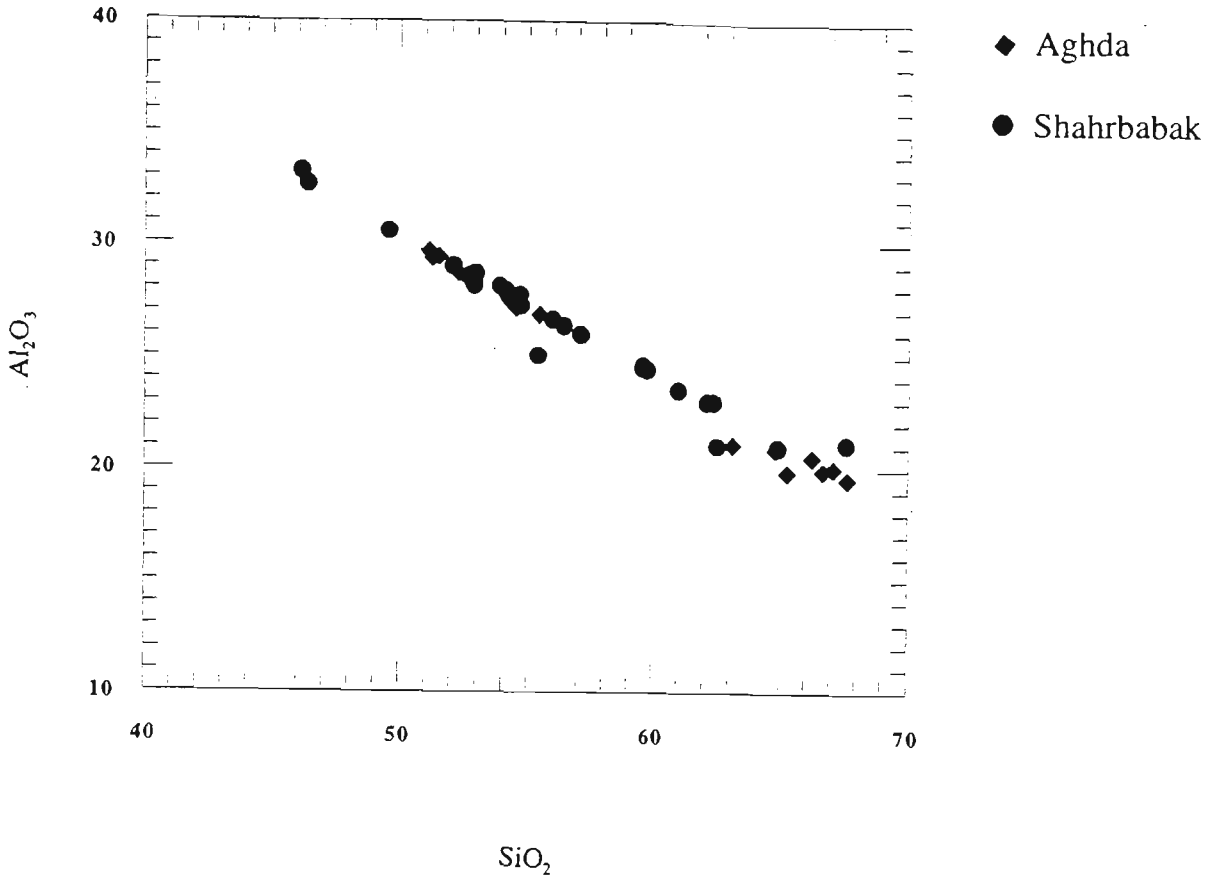

Fig. 4-22. (continued). Variation of SiO_2 with Al_2O_3 in plagioclase from Aghda and Shahrbabak (oxides, wt%).

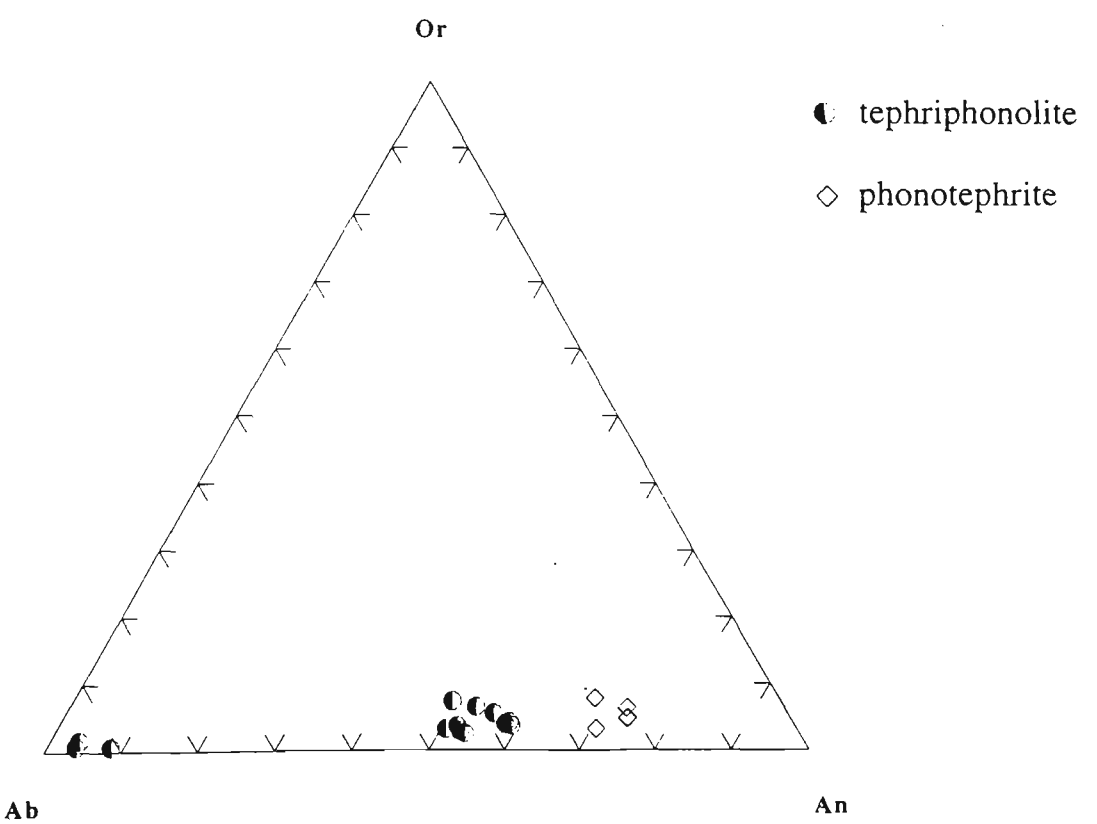

Fig. 4-23. Plagioclase compositions for tephriphonolite and phonotephrite from Aghda and Shahrbabak.

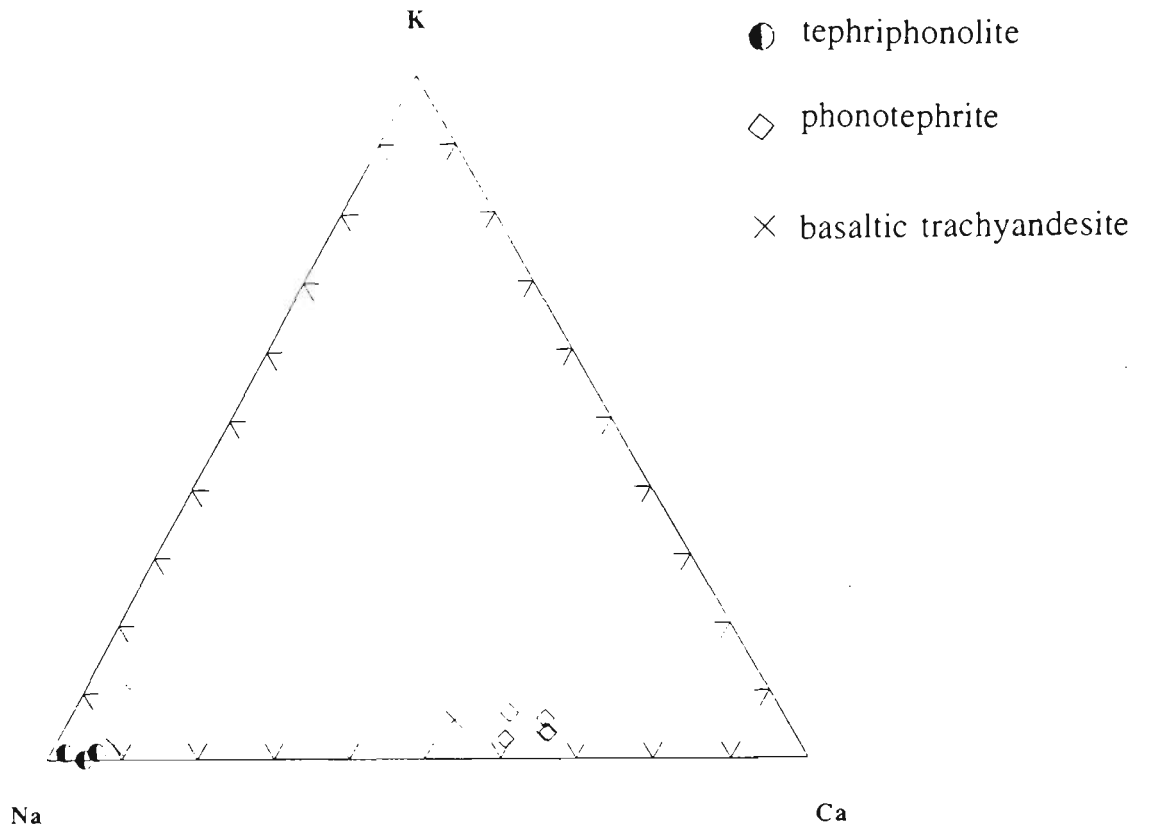

Fig. 4-24. Compositional variation of plagioclase for tephriphonolite, phonotephrite and basaltic trachyandesite from Aghda, in terms of the atomic proportions of Na, K and Ca.

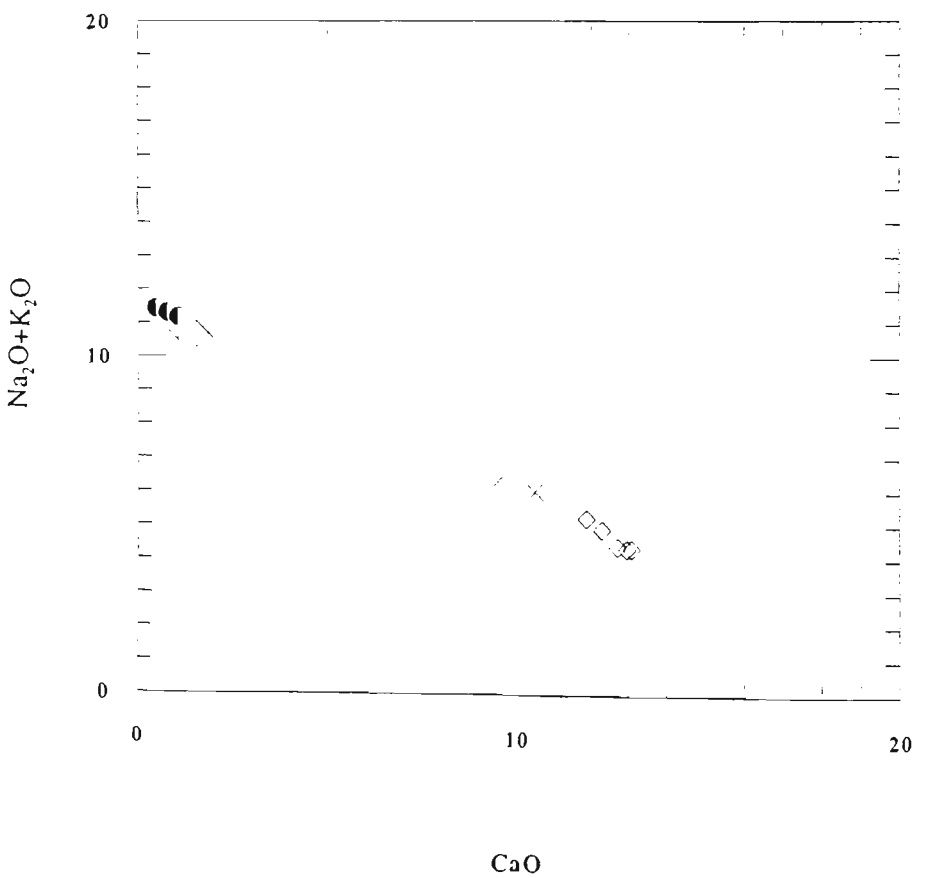

Fig. 4.25. Variation of total alkalis with CaO of plagioclase in tephriphonolite, phonotephrite and basaltic trachyandesite from Aghda.(oxides, wt%).

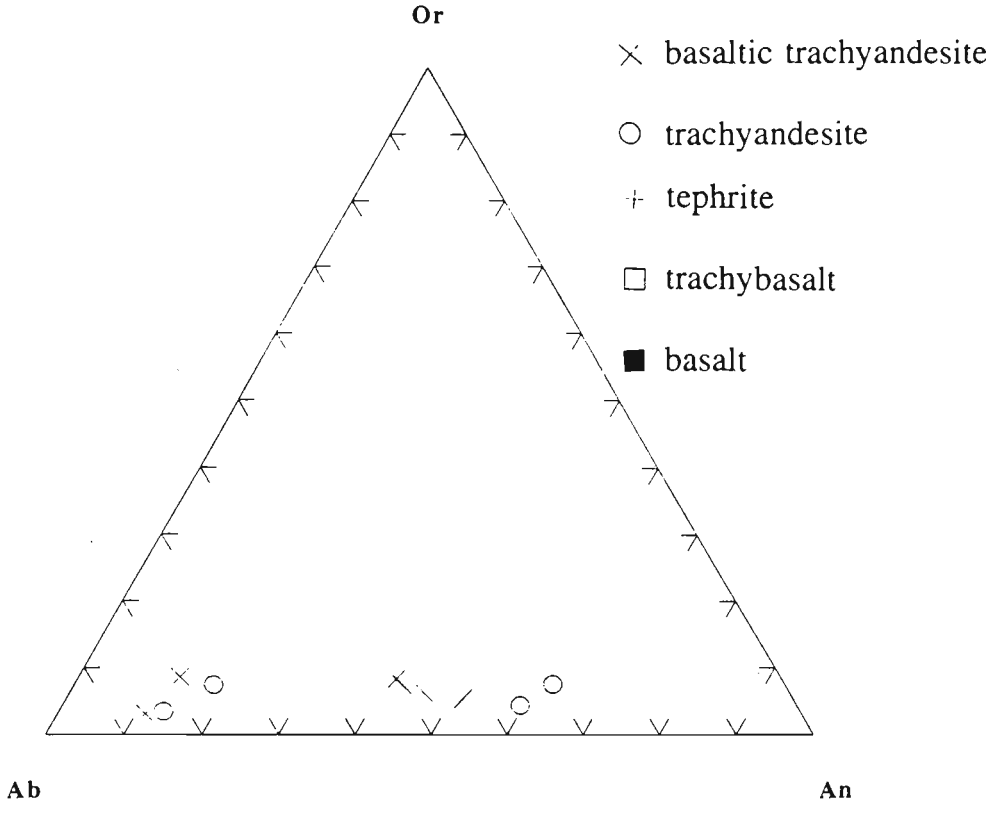

Fig. 4-26. Plagioclase compositions for basaltic trachyandesite from Aghda and trachyandesite from Shahrbabak.

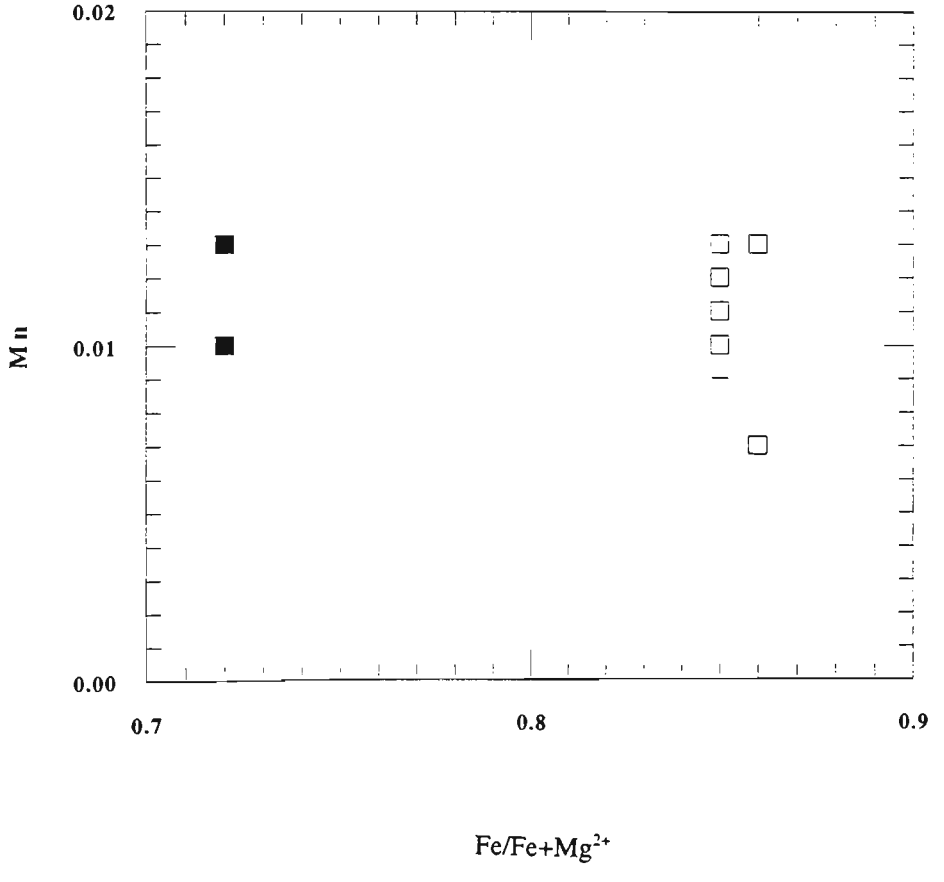

Fig. 4-27. Olivine compositions for tephrite, basalt and trachybasalt from the Islamic Peninsula and Shahrbabak. Mn is in atomic proportion and all Fe is calculated as Fe^{2+}.

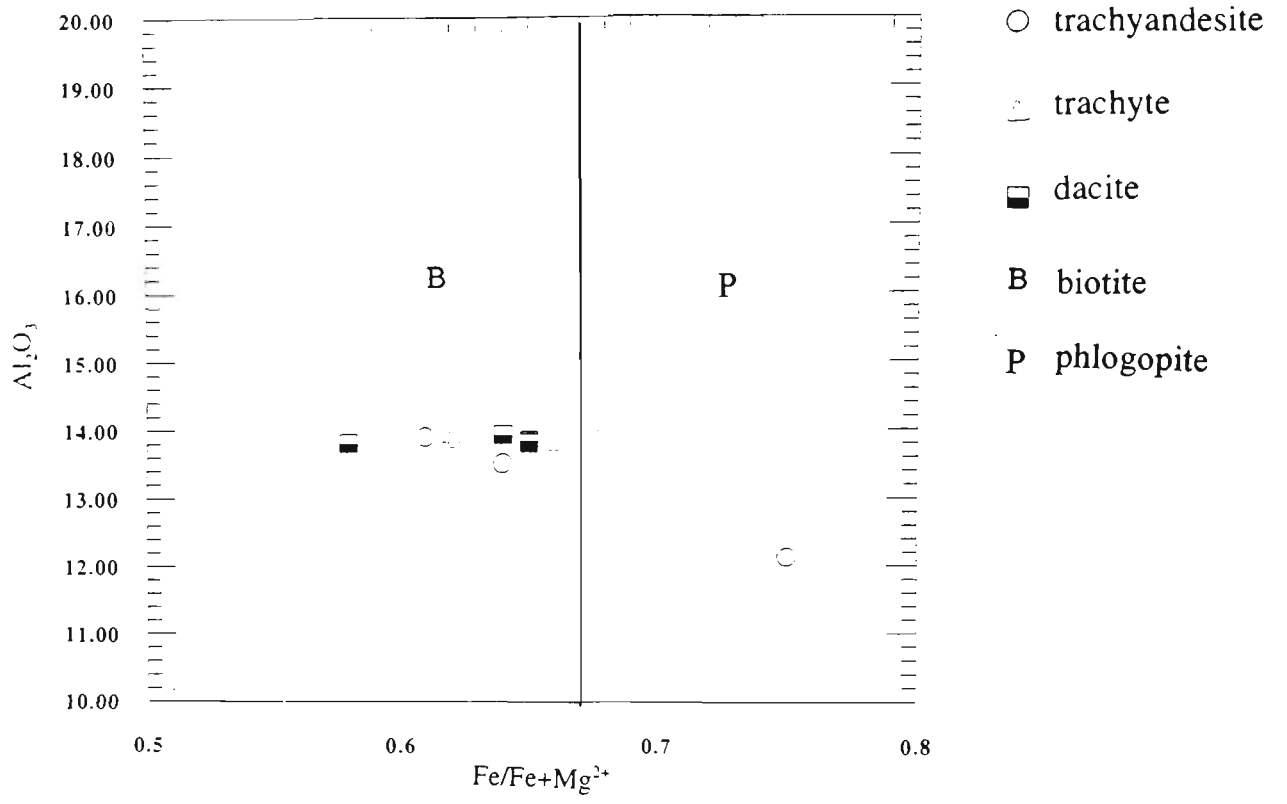

Fig. 4.28. Composition of biotite phenocrysts for trachyandesite, trachyte and dacite from the Islamic Peninsula and Shahrbabak. All Fe is calculated as Fe^{2+}(oxides, wt%).

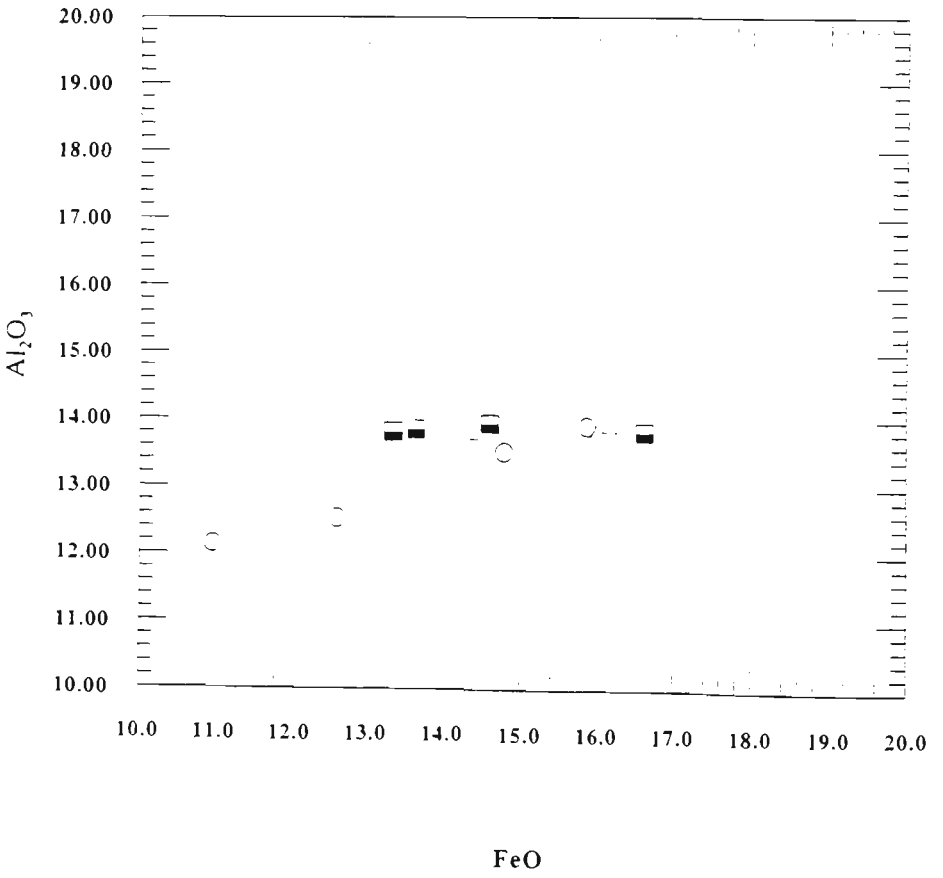

Fig. 4.29. Plot of total Fe as FeO with Al_2O_3 in mica from the Islamic Peninsula and Shahrbabak(oxides, wt%).

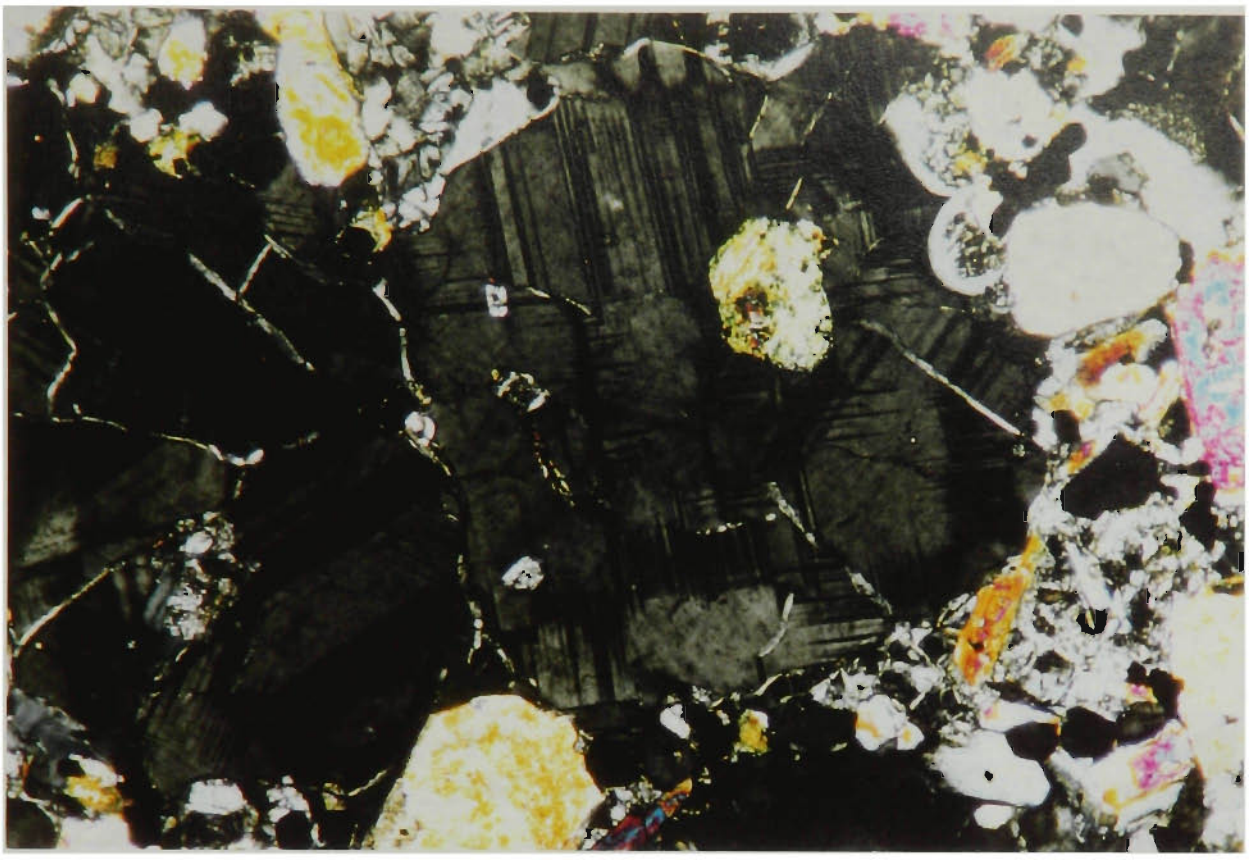

Plate 1A. Multiple twinning in leucite in tephrite from the Islamic Peninsula (R14447; crossed polars; field of view 1.6 mm wide).

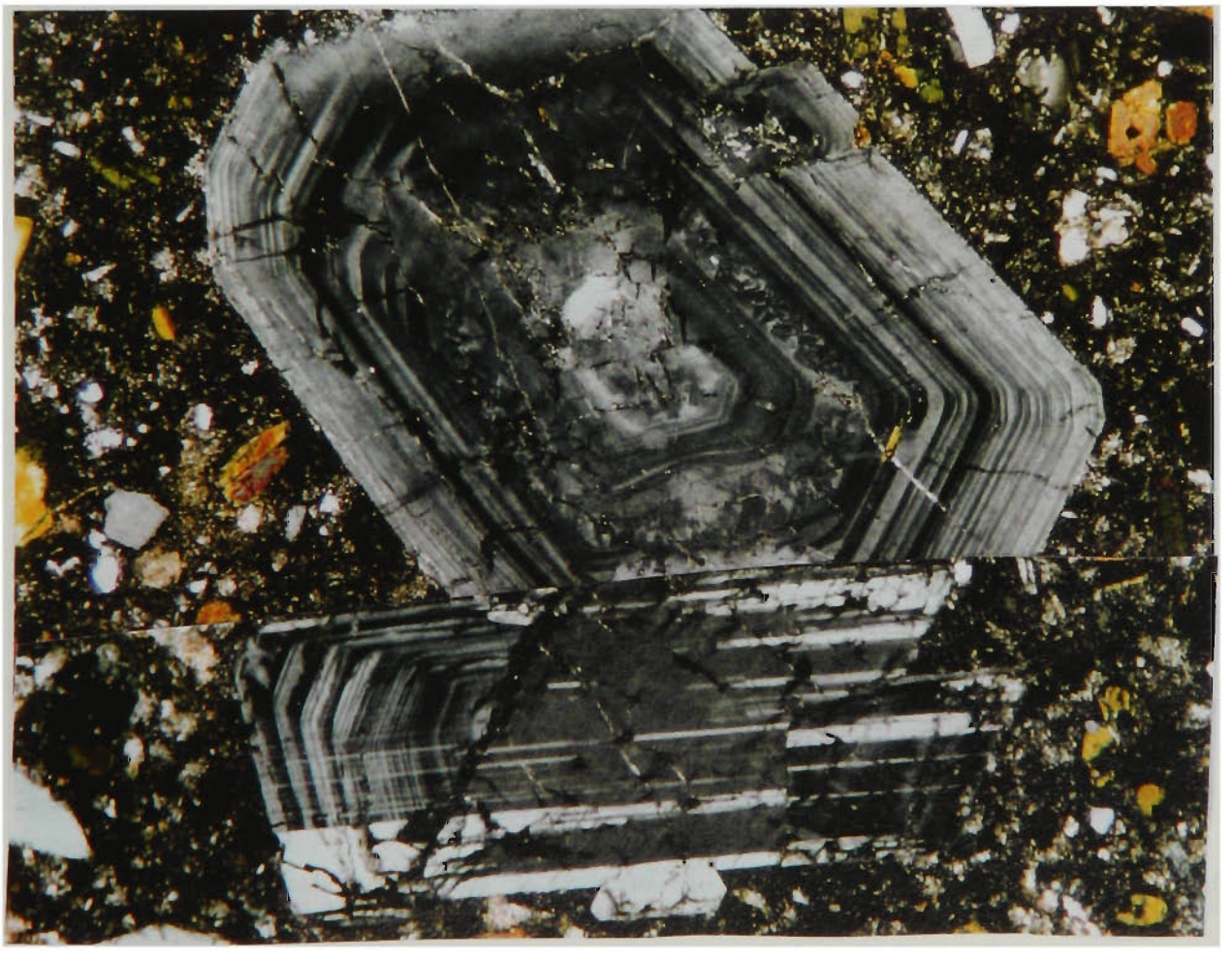

Plate 1B. Oscillatory zoning in plagioclase in trachyandesite from Aghda (R15811; crossed polars; field of view 1.6 mm wide).

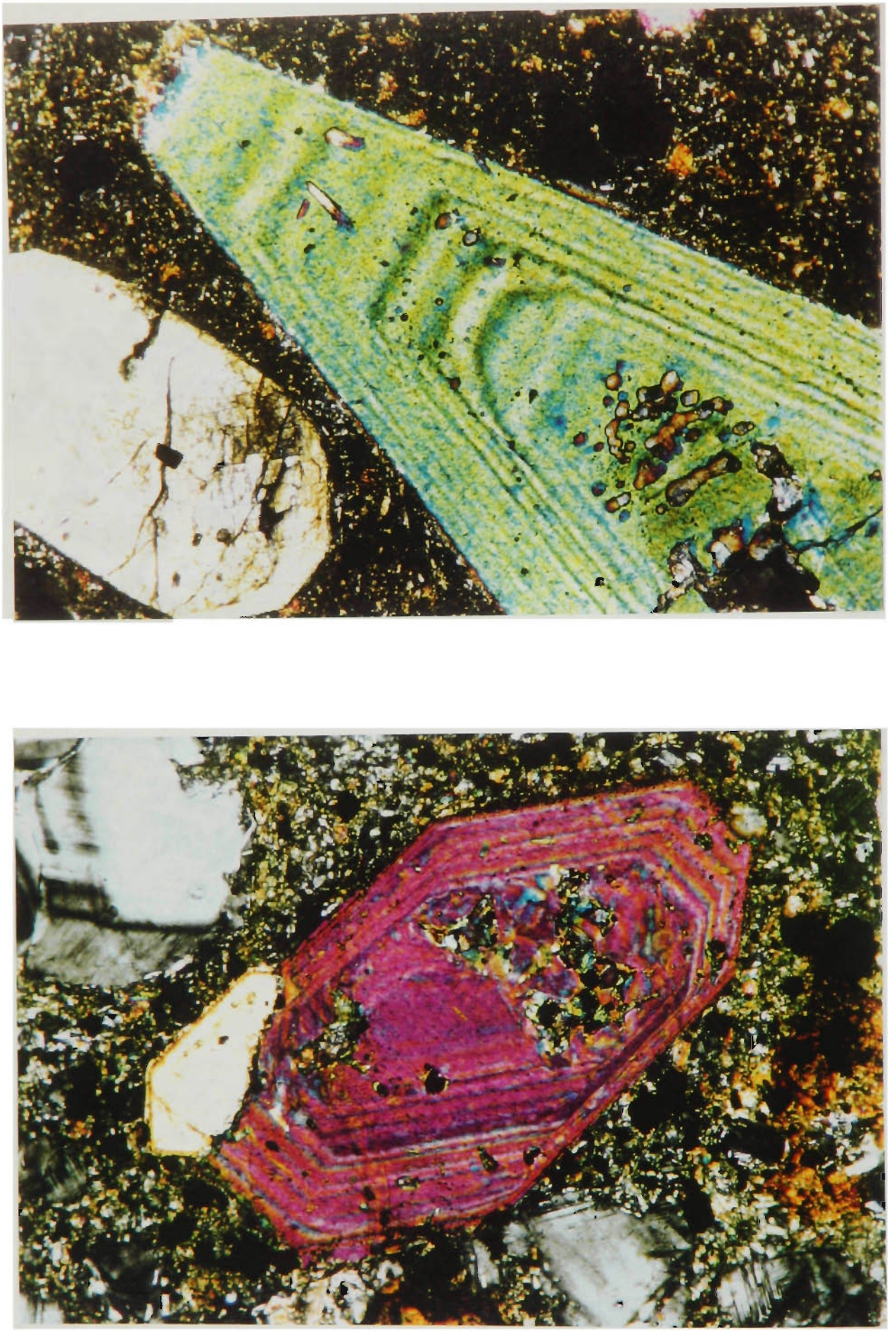

Plate 2. Oscillatory zoning in diopside in tephrite from the Islamic Peninsula (R14447; crossed polars; field of view 1.6 mm wide).

Fig. 5-1. Euhedral trapezohedra of analcime (L or R) and pumpellyite (R or L).

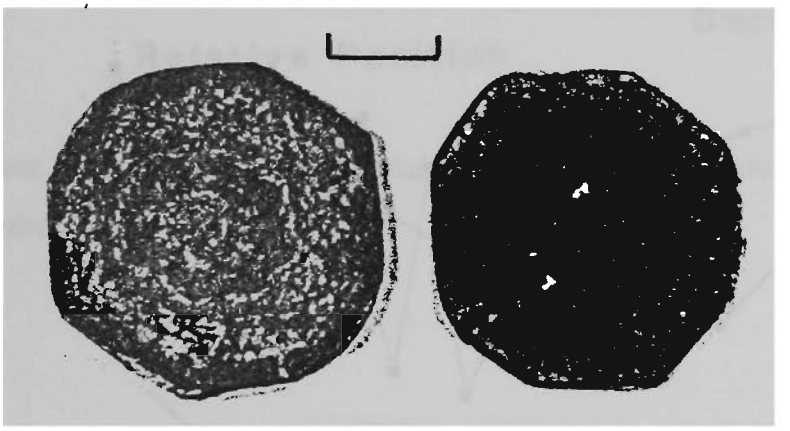

Fig. 5-2. Photograph of polished sections through centres of pumpellyite (left) and analcime (right) showing inclusions arranged in a well-developed concentric pattern. Bar scale is 1 cm long.

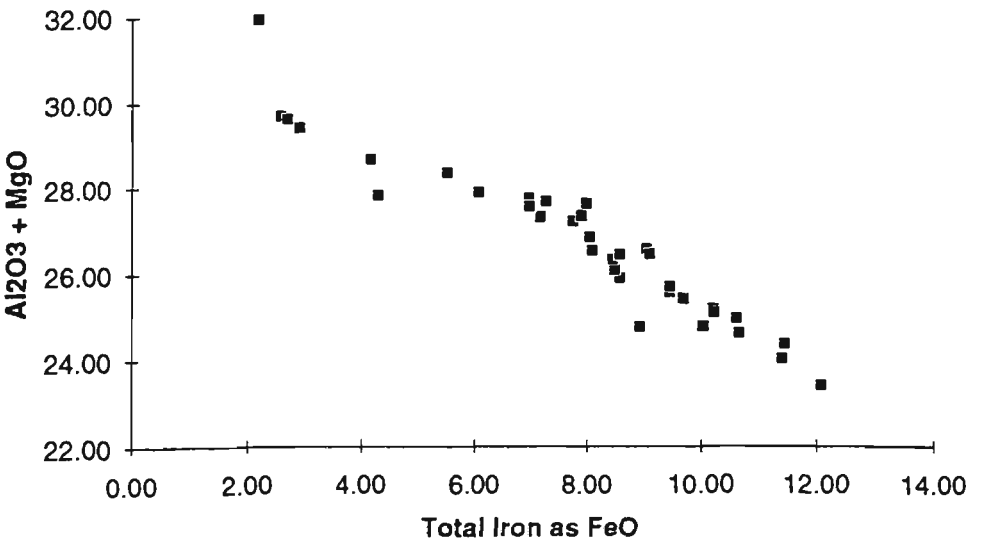

Fig. 5-3. Plot of total Fe as FeO versus the sum of Al_2O_3 and MgO for pumpellyite analyses (oxides, wt%).

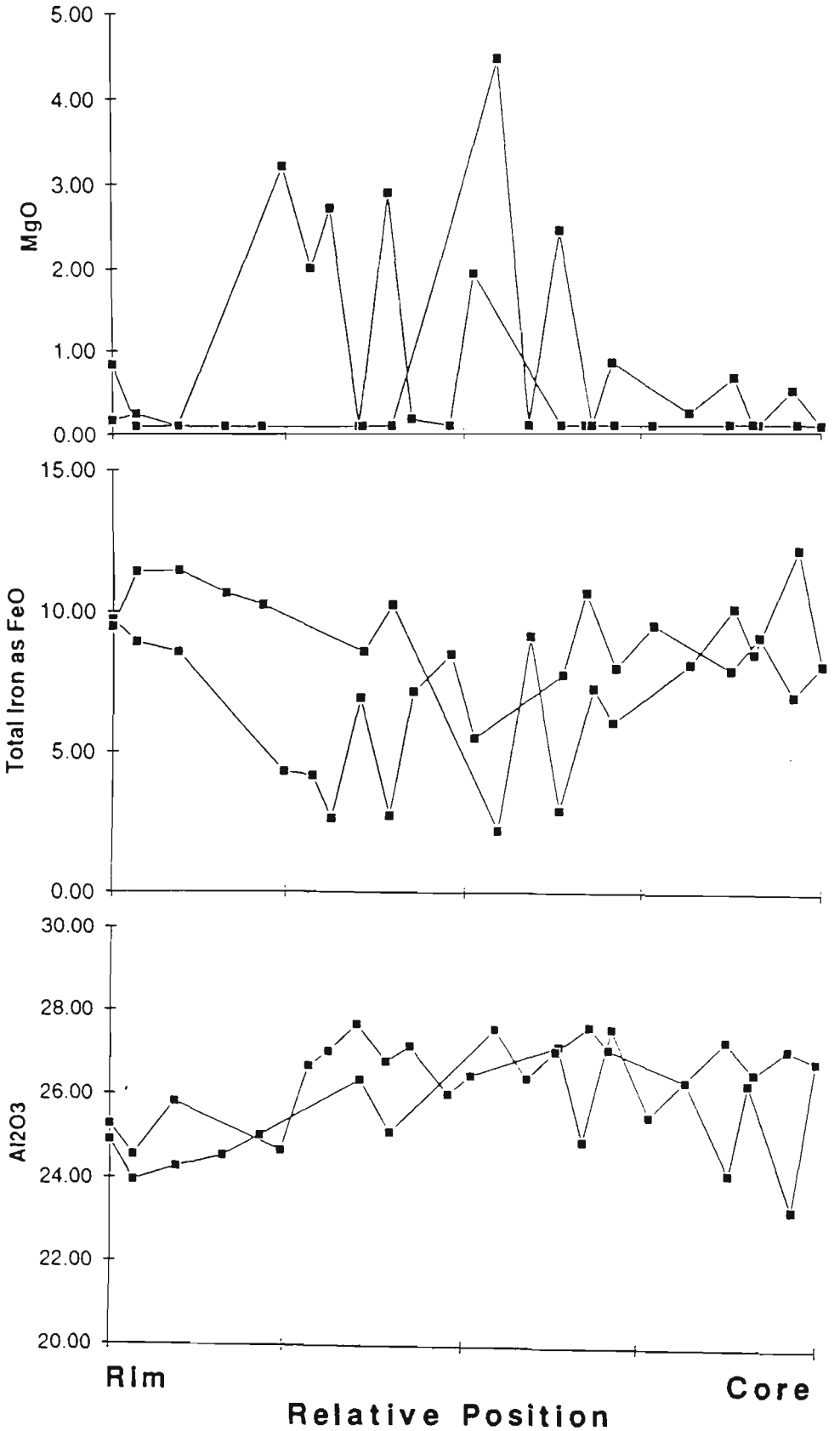

Fig. 5-4. Plots of Al_2O_3, total Fe as FeO and MgO versus relative position in a large pumpellyite trapezohedron. MgO contents below limit of detection (0.09%) plotted as 0.09%

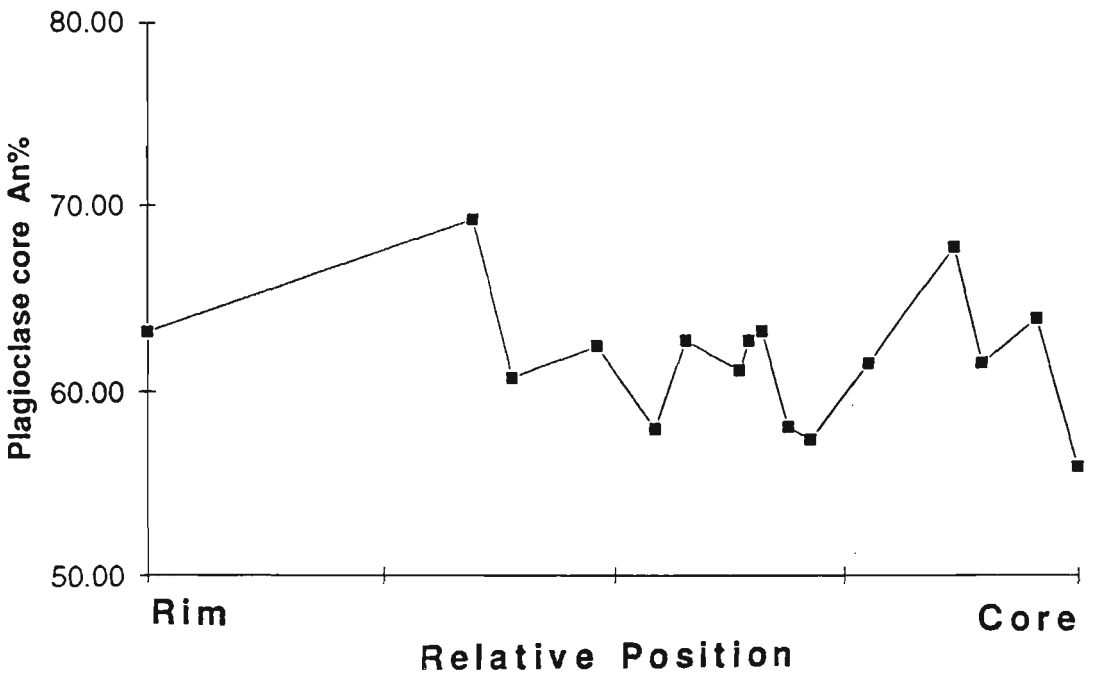

Fig. 5-5. Plot of core composition of plagioclase inclusions versus relative position in an analcime trapezohedron.

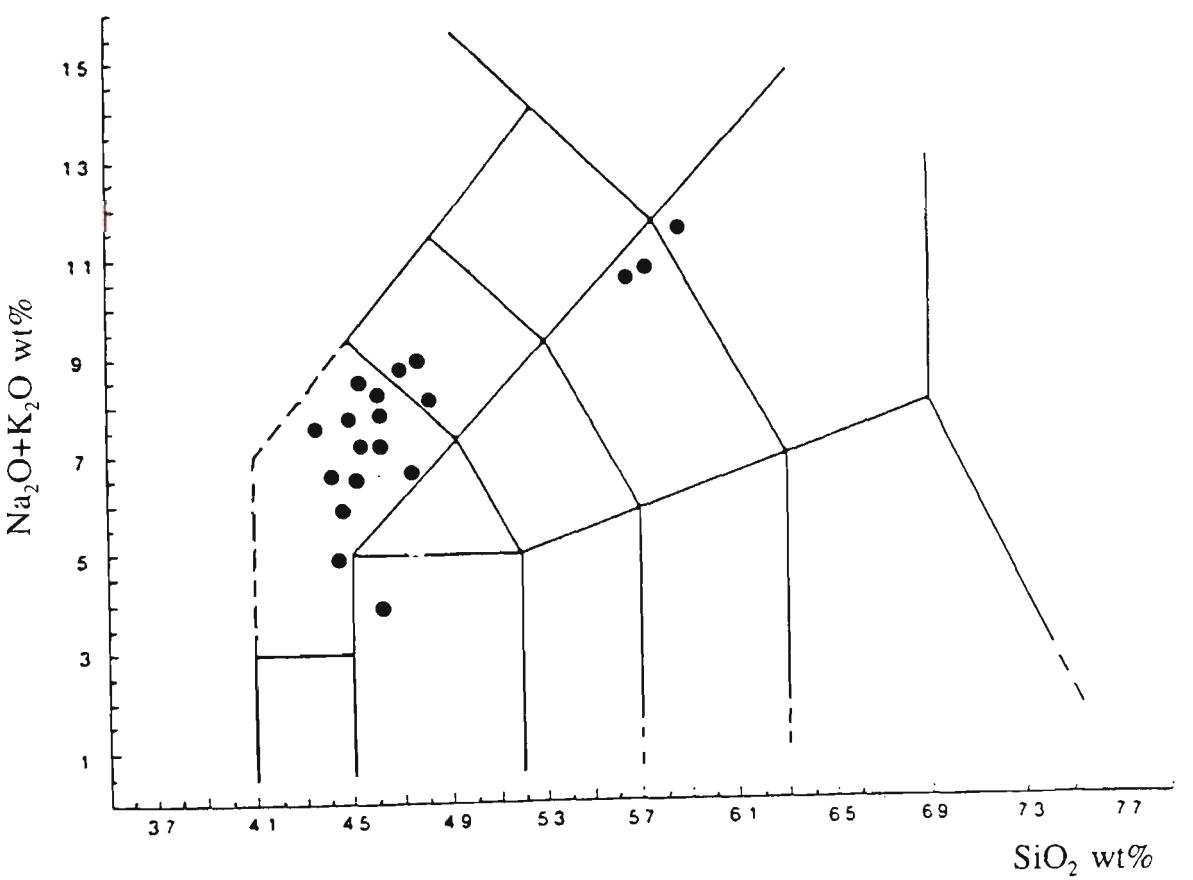

Fig. 6-1. Total alkalis versus SiO_2 (wt%) classification (TAS) for Miocene volcanic rocks from the Islamic Peninsula.

SYMBOL USED (CHAPTER 6)

 RHYOLITE

 DACITE

 TRACHYTE

 TRACHYANDESITE

 BASALTIC TRACHYANDESITE

 TRACHYBASALT

 PHONOLITE

 PHONOTEPHRITE

 TEPHRIPHONOLITE

 TEPHRITE

 BASALT

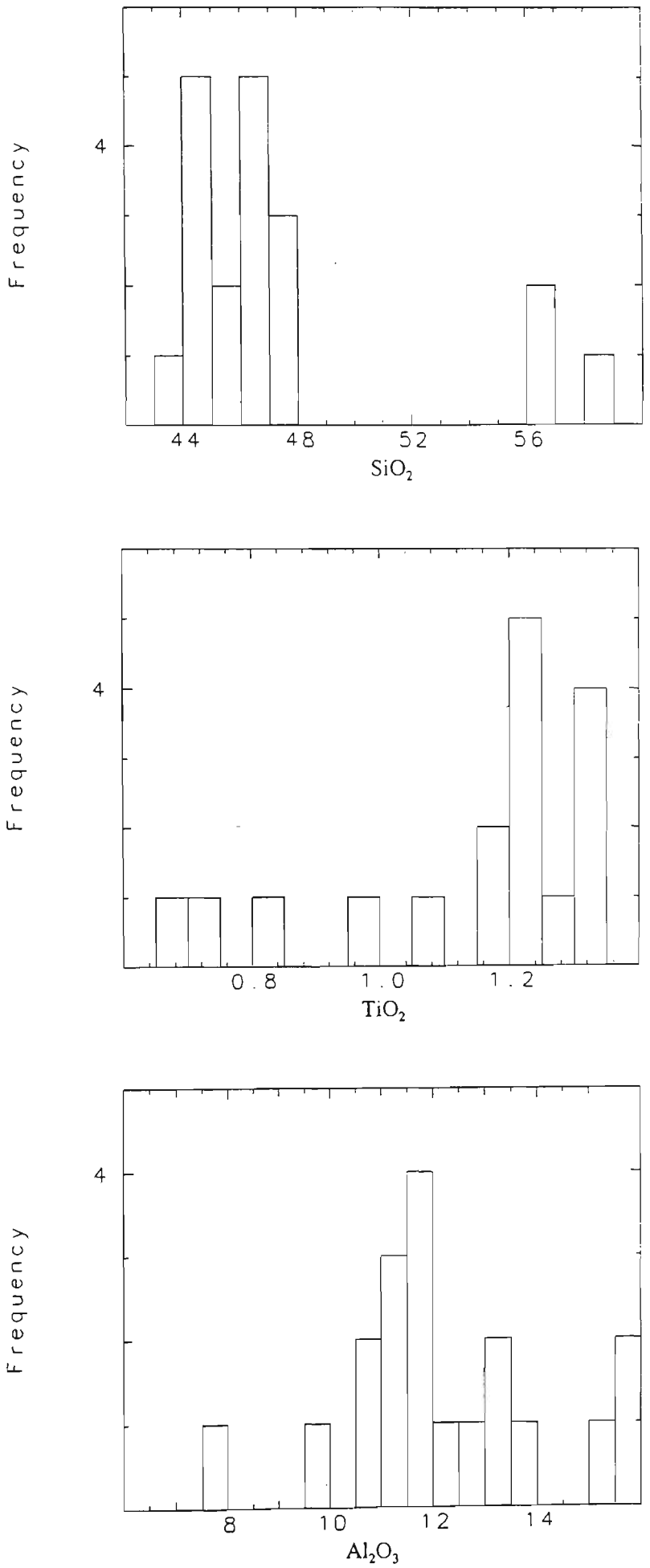

Fig. 6-2. Histograms of compositional frequency for major element oxides for rocks from the Islamic Peninsula (oxides, wt%).

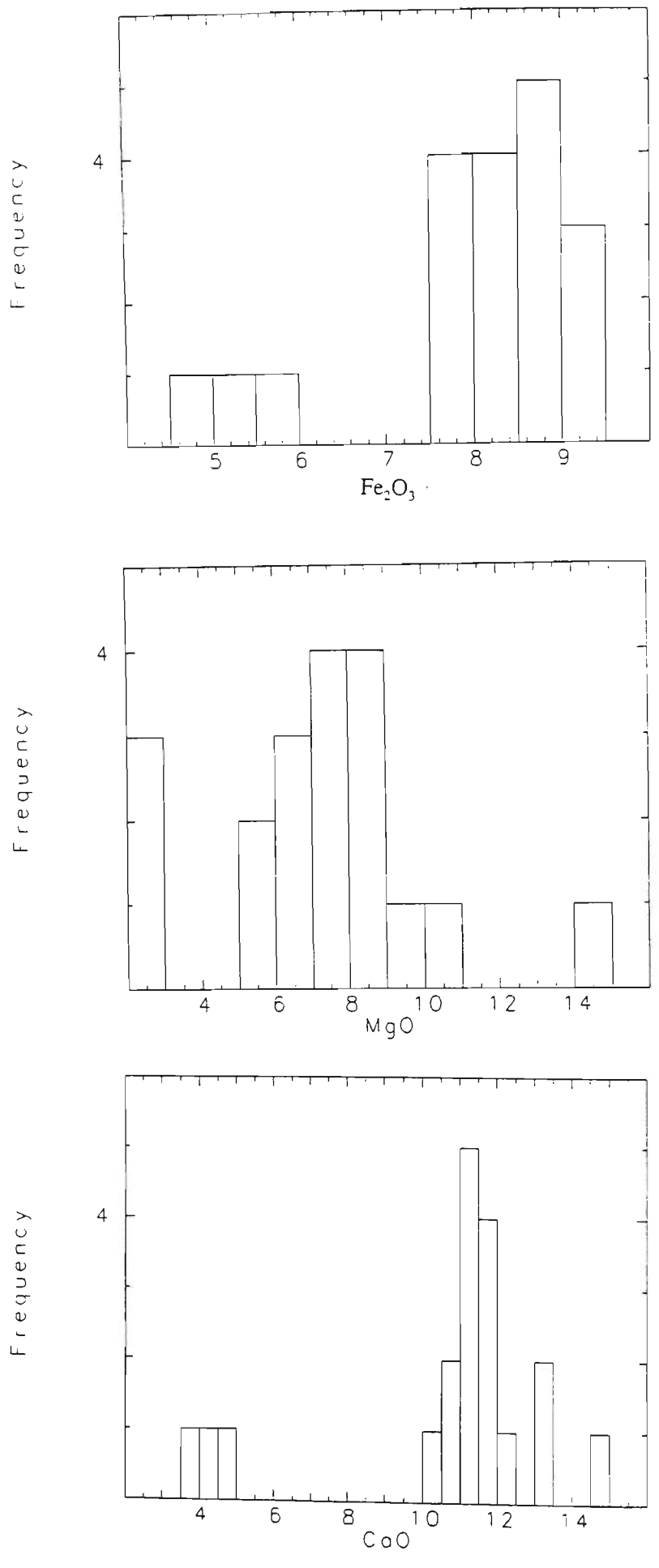

Fig. 6-2. (continued) Histograms of compositional frequency for major element oxides for rocks from the Islamic Peninsula (oxides, wt%).

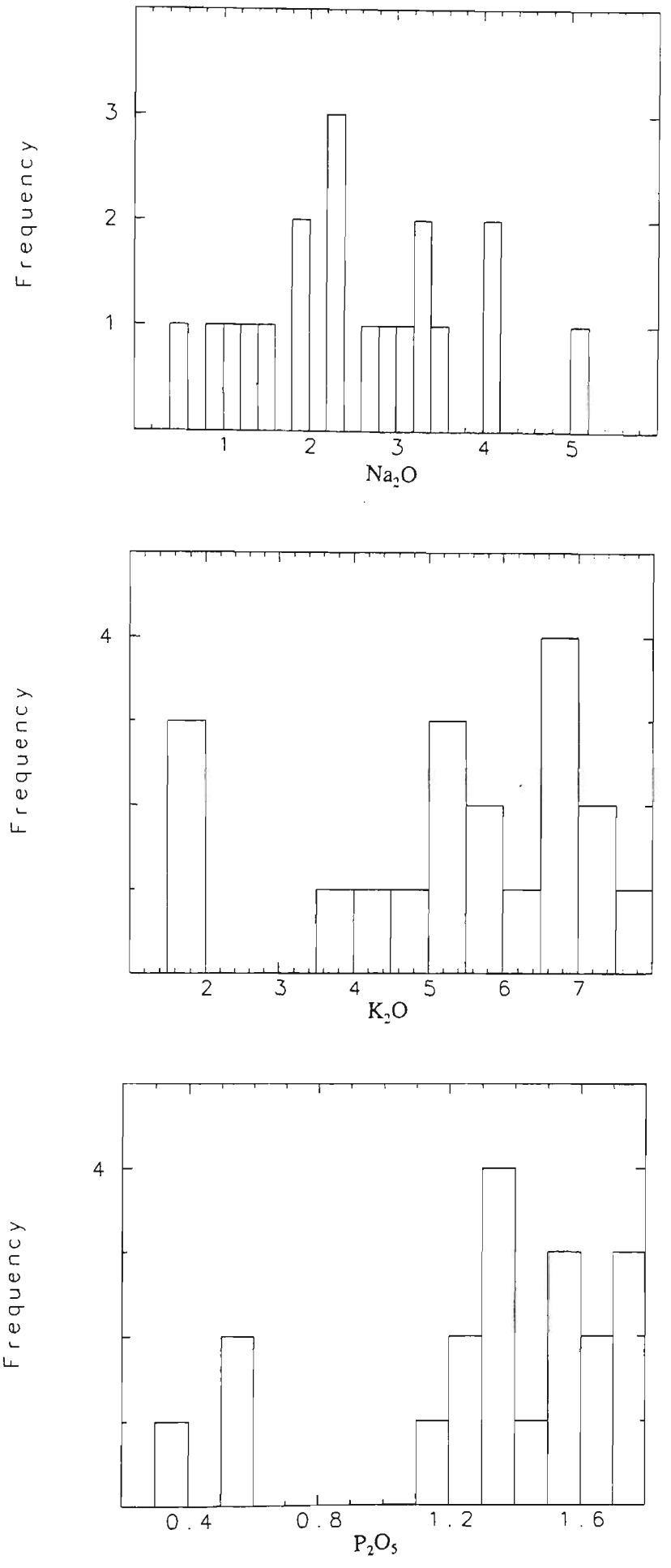

Fig. 6-2. (continued) Histograms of compositional frequency for major element oxides for rocks from the Islamic Peninsula (oxides, wt%).

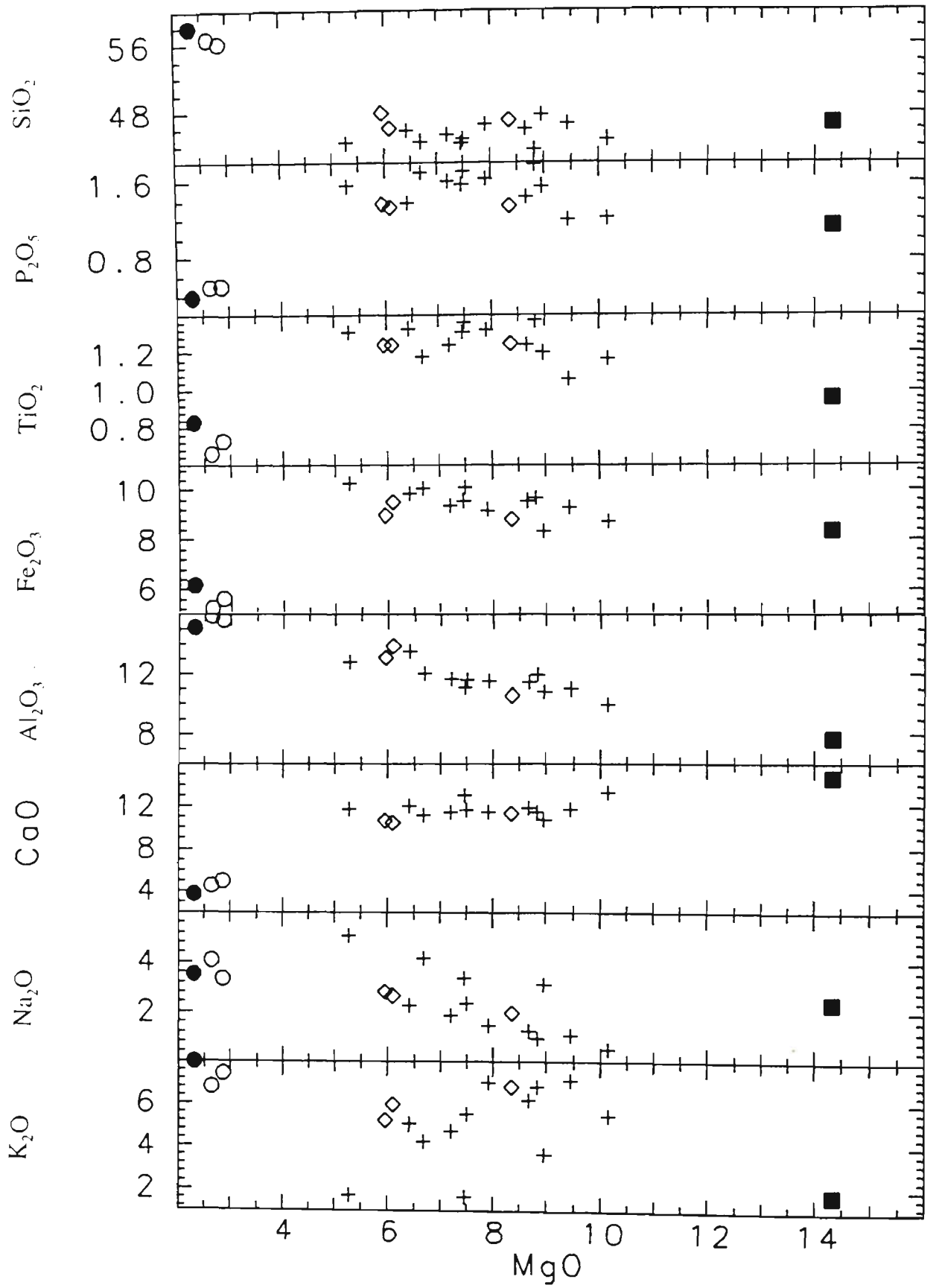

Fig. 6-3. Plot of major element compositions versus MgO for rocks from the Islamic Peninsula (oxides, wt%).

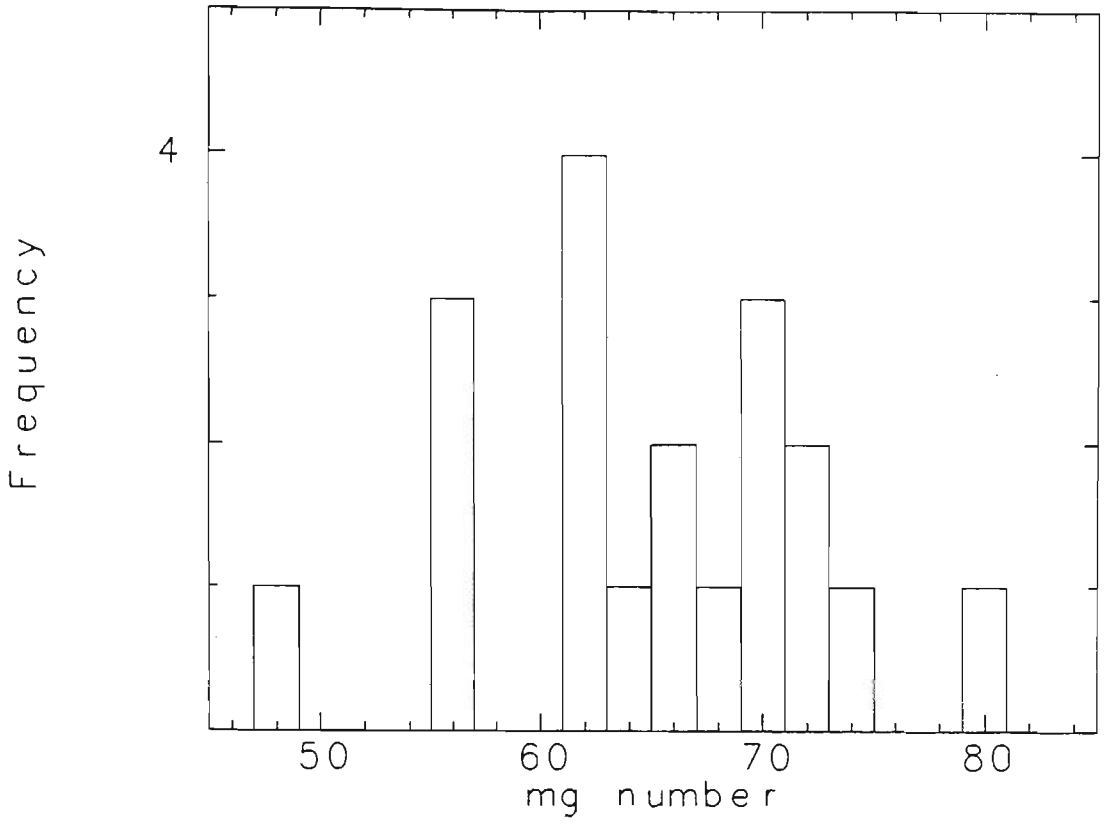

Fig. 6-4. Histogram of Mg-number for rocks from the Islamic Peninsula.

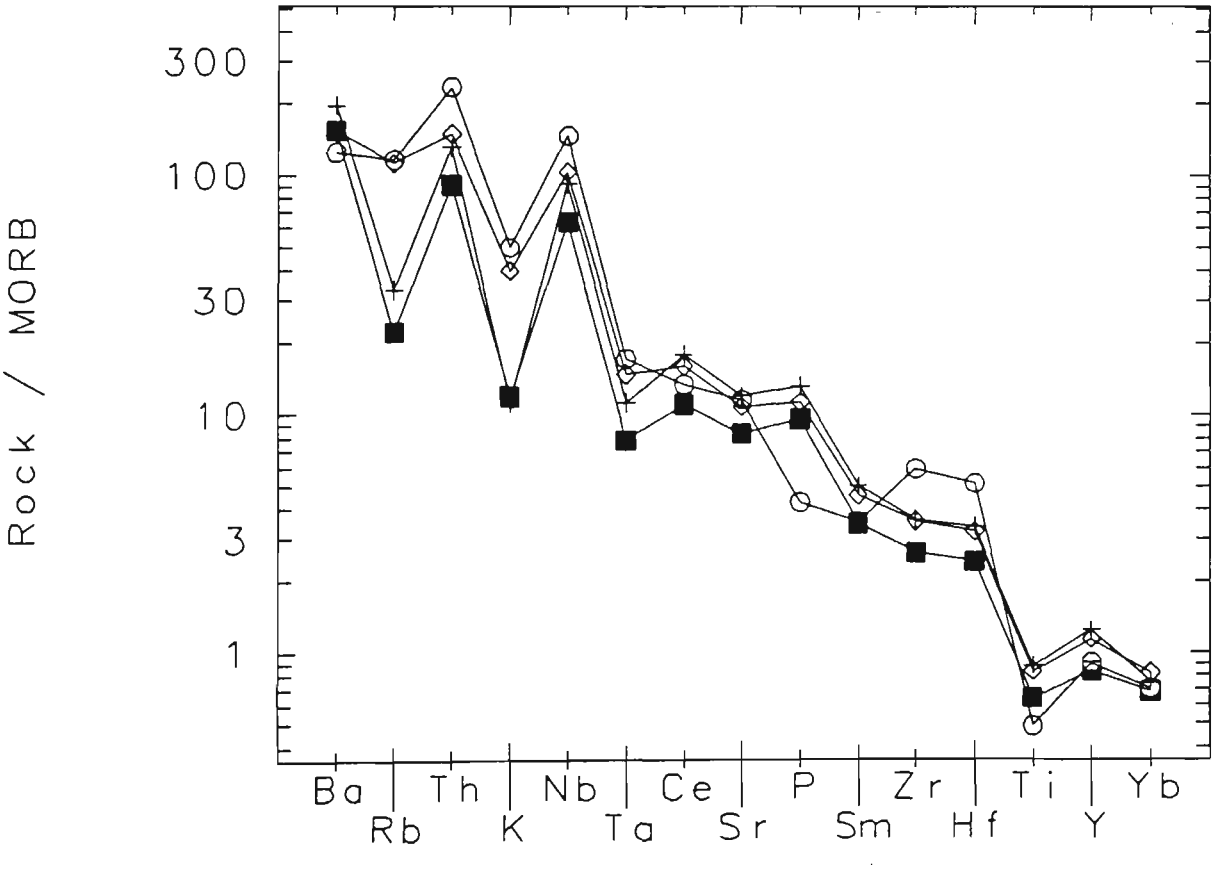

Fig. 6-5. Multi-element patterns (spider diagrams) for the Miocene volcanic rocks from the Islamic Peninsula.

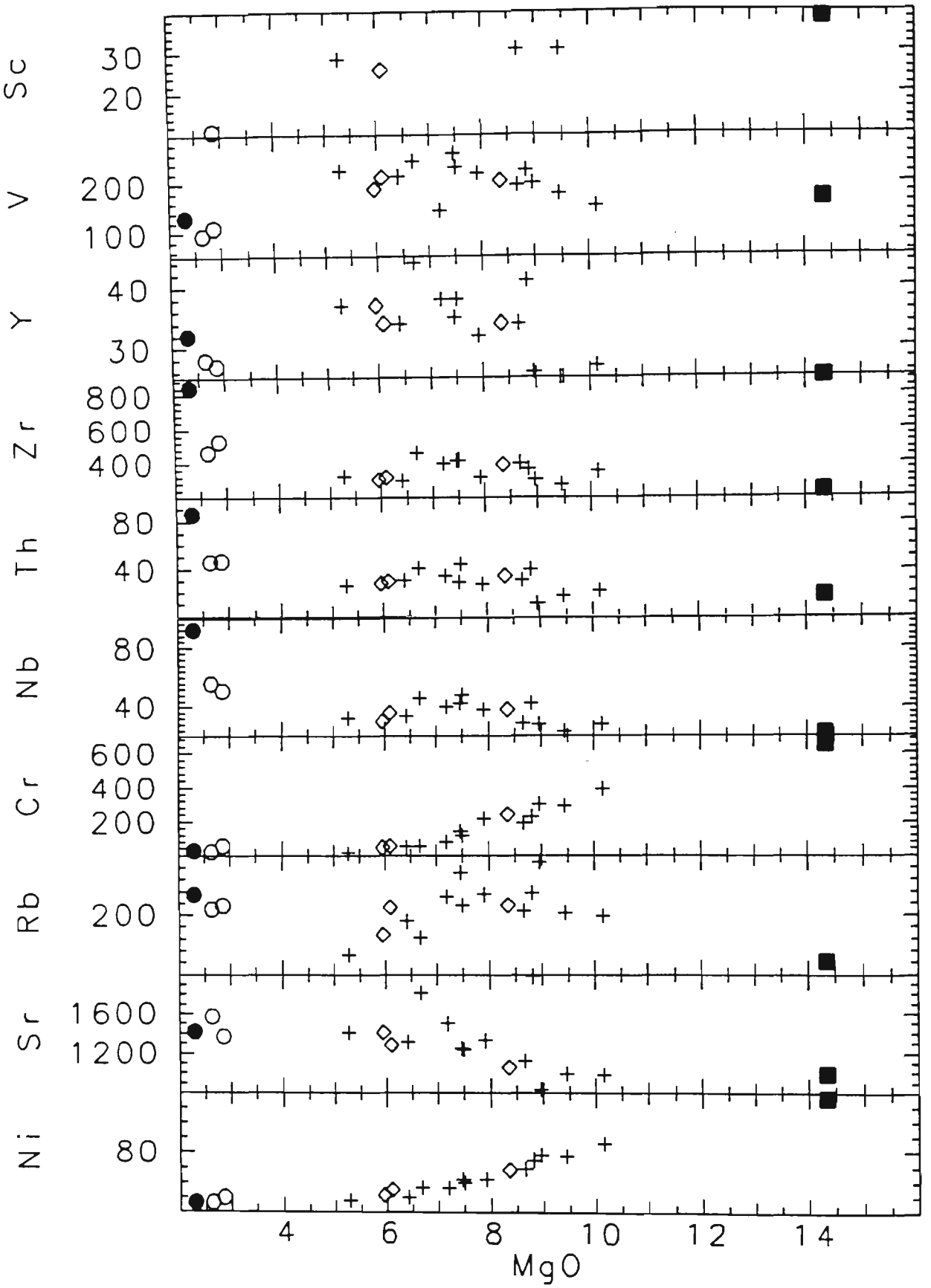

Fig. 6-6. Plot of trace element contents versus MgO for rocks from the Islamic Peninsula (oxides, wt%).

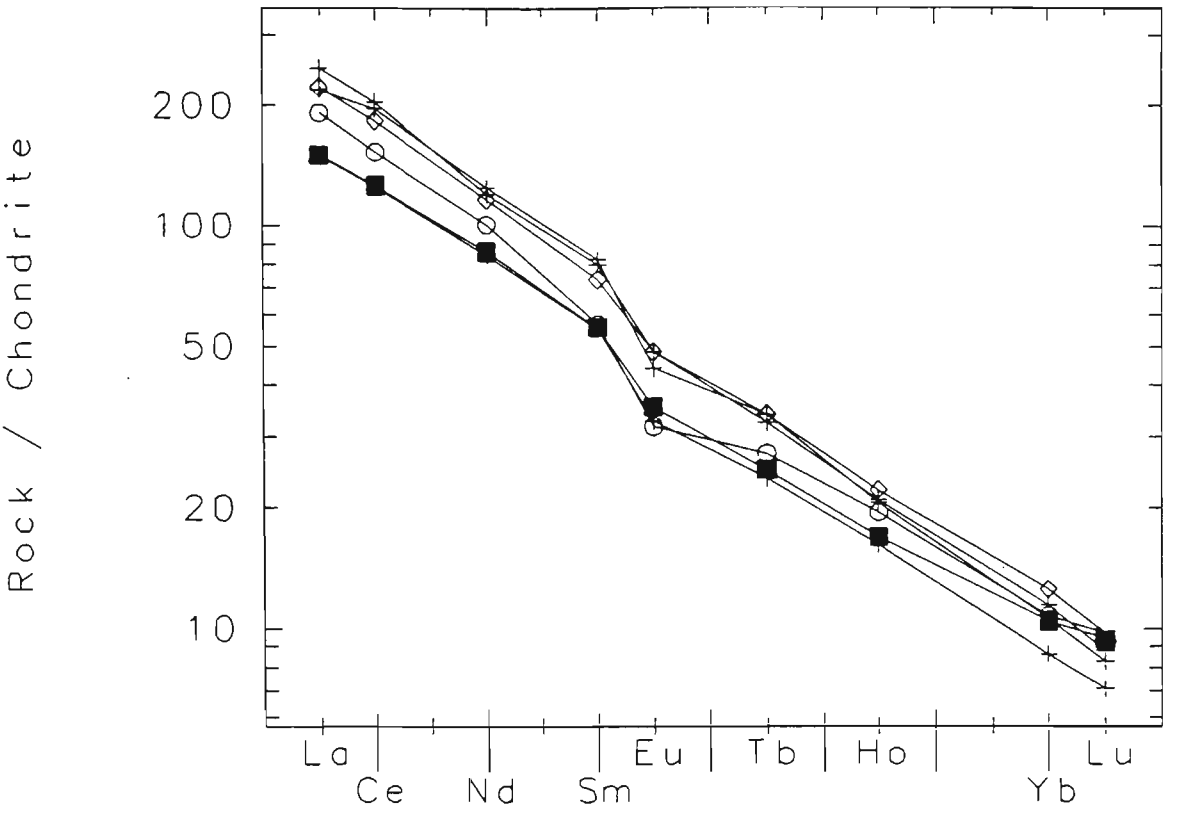

Fig. 6-7. Rare earth element patterns for rocks from the Islamic Peninsula.

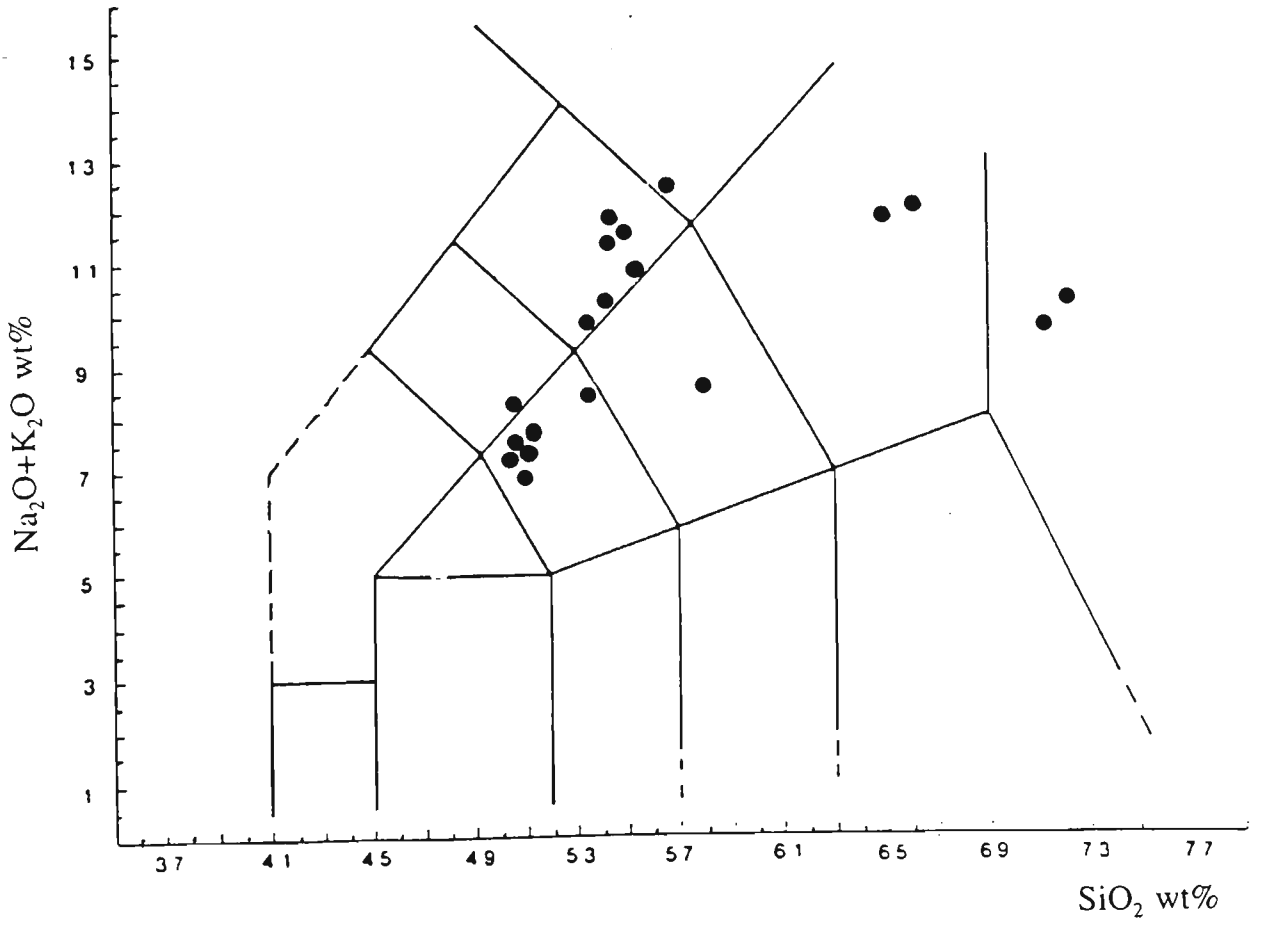

Fig. 6-8. Total alkalis versus SiO_2 (wt%) classification (TAS) for Tertiary volcanic rocks from Aghda.

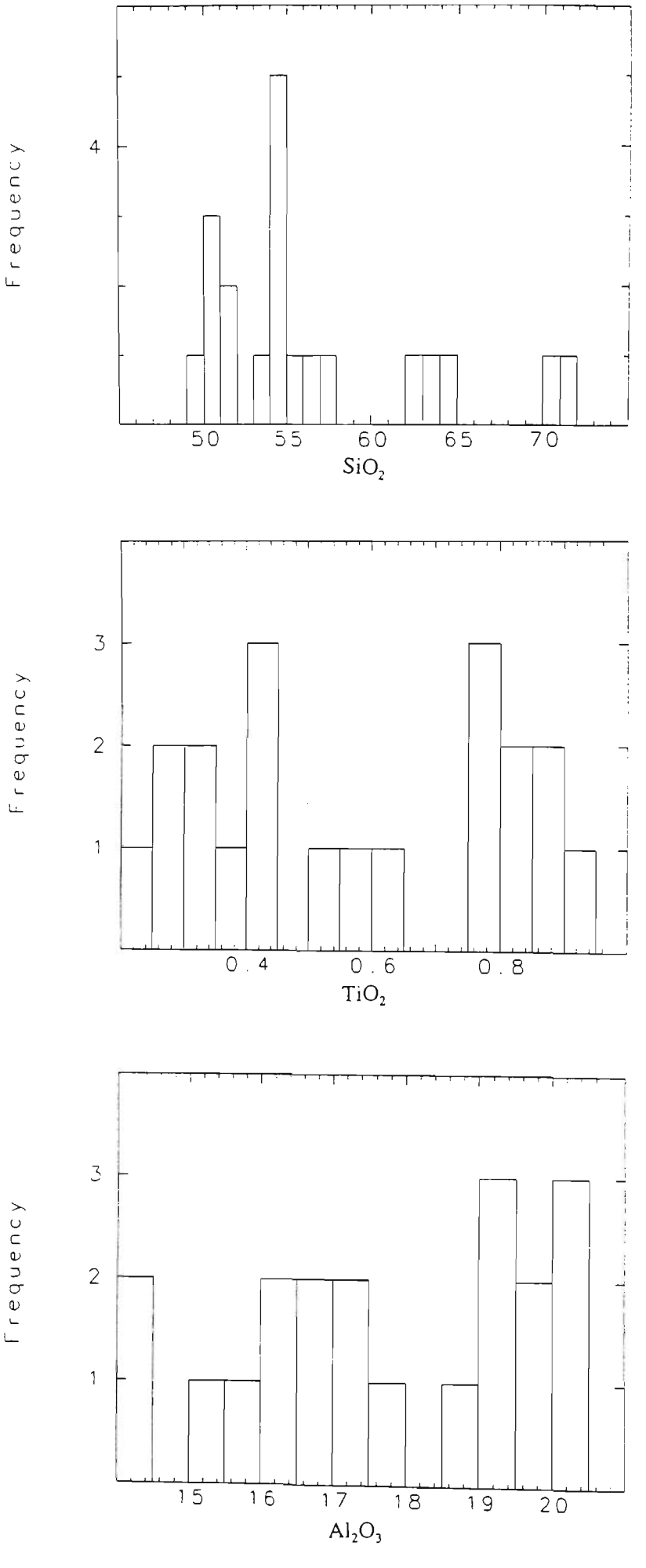

Fig. 6-9. Histogram of compositional frequency for major element oxides for rocks from Aghda (oxides, wt%).

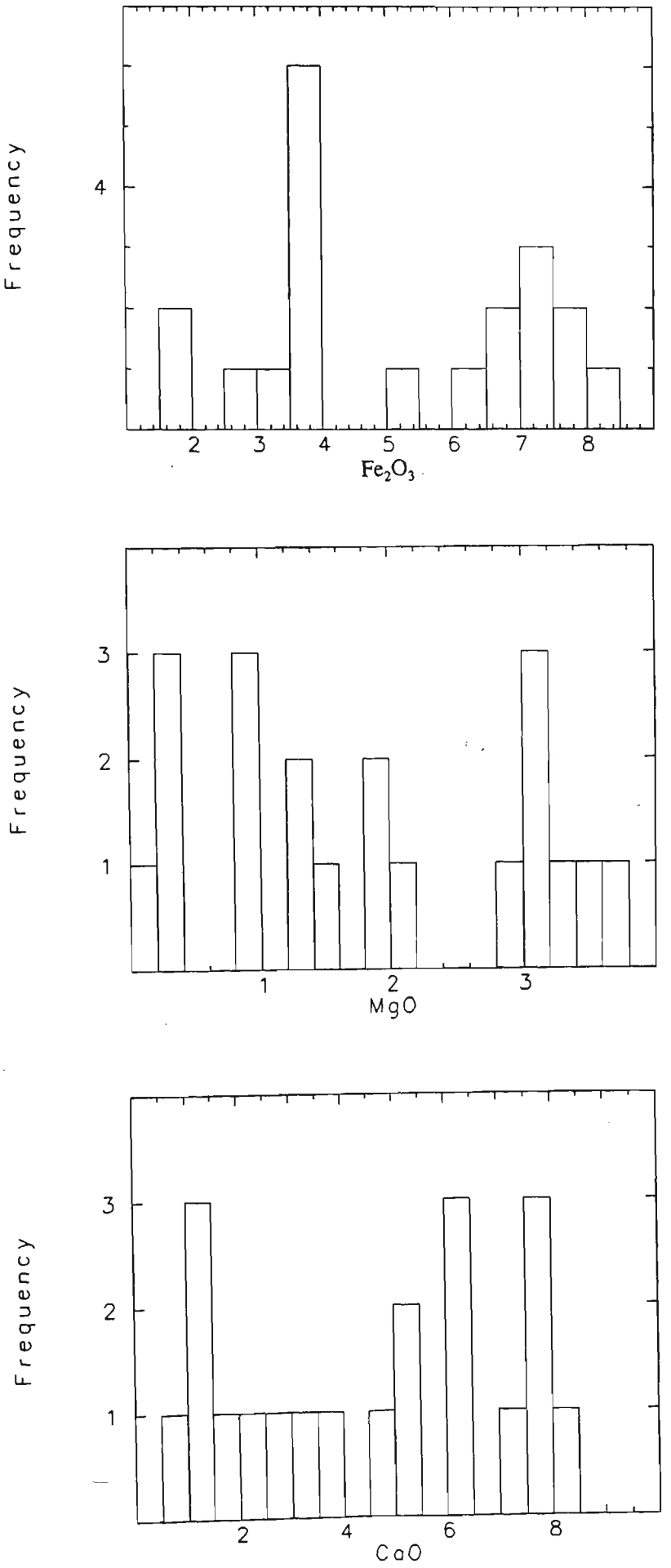

Fig. 6-9. (continued) Histogram of compositional frequency for
oxides for rocks from Aghda (oxides, wt%)

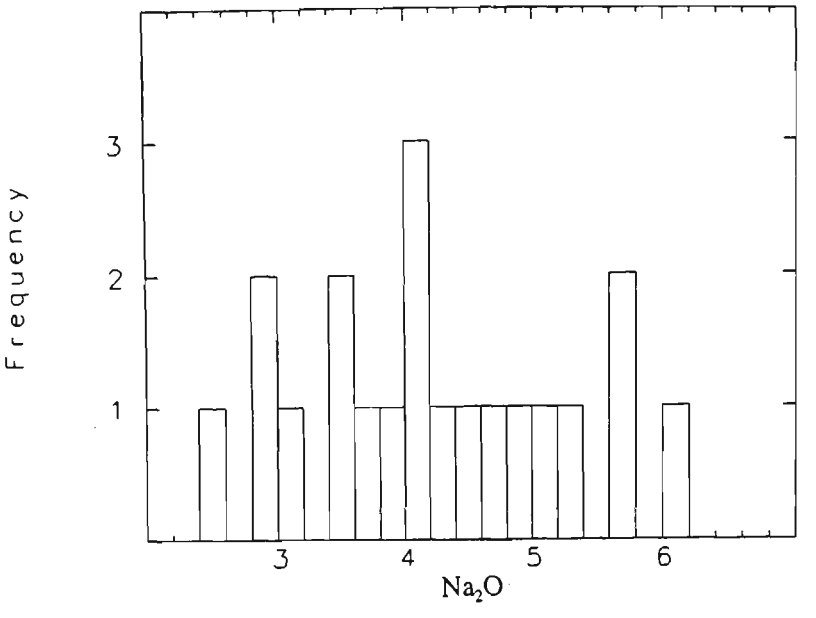

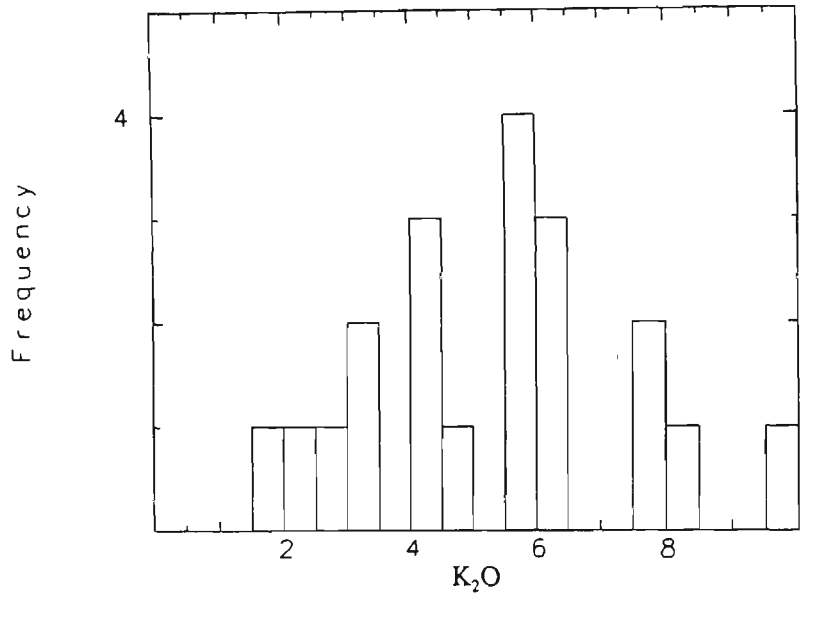

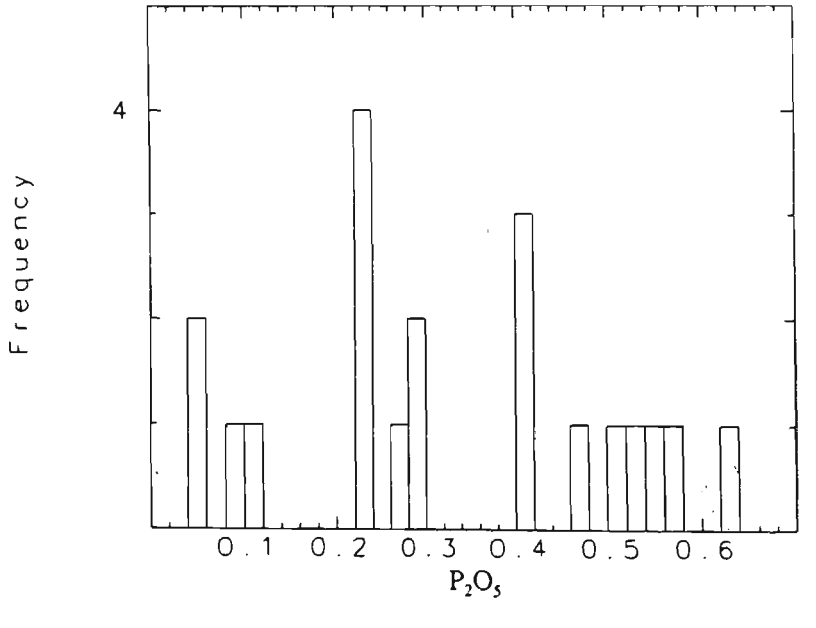

Fig. 6-9. (continued) Histogram of compositional frequency for major element oxides for rocks from Aghda (oxides, wt%).

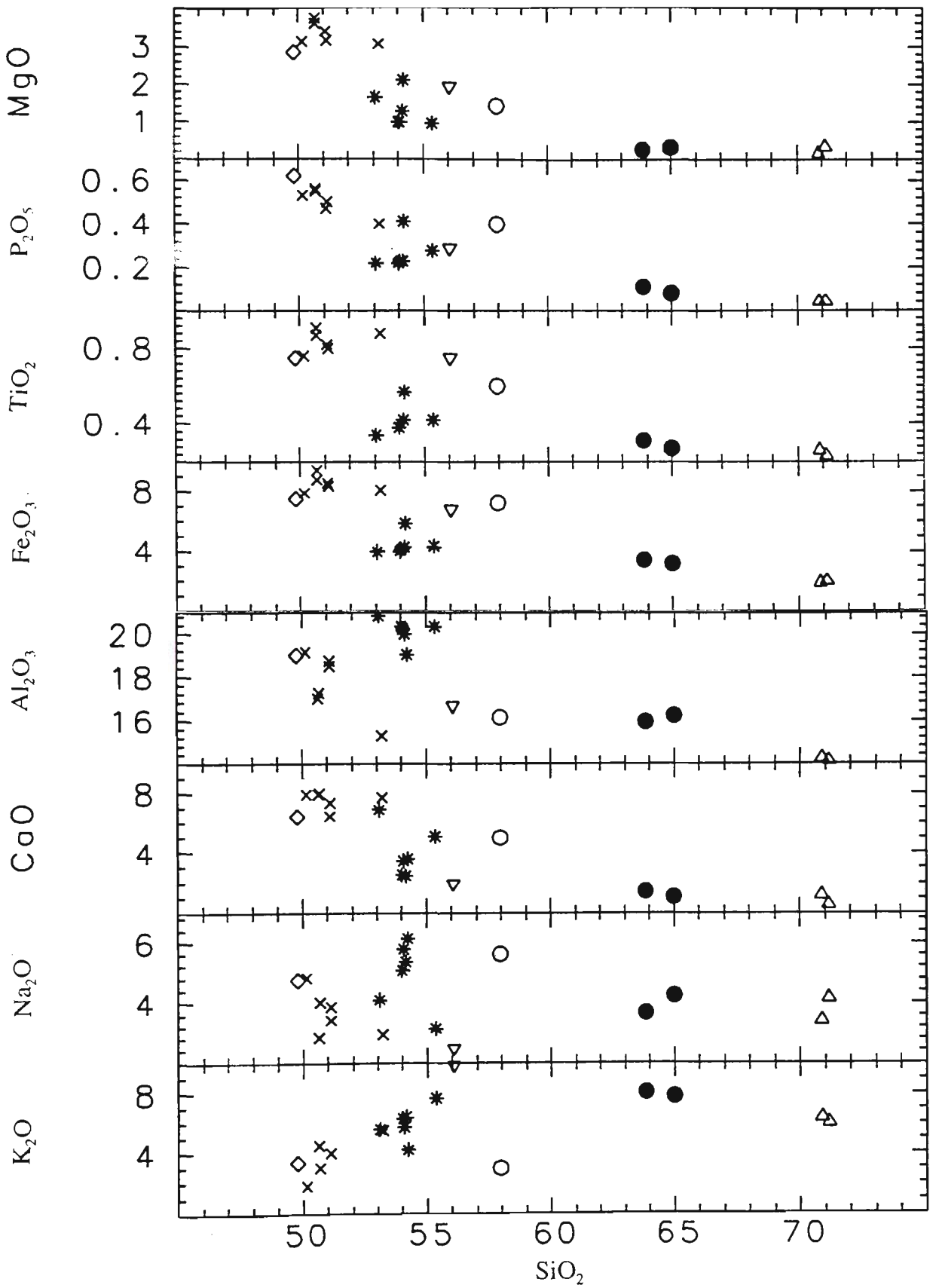

Fig. 6-10. Harker diagrams for Aghda volcanic rocks (oxides, wt%).

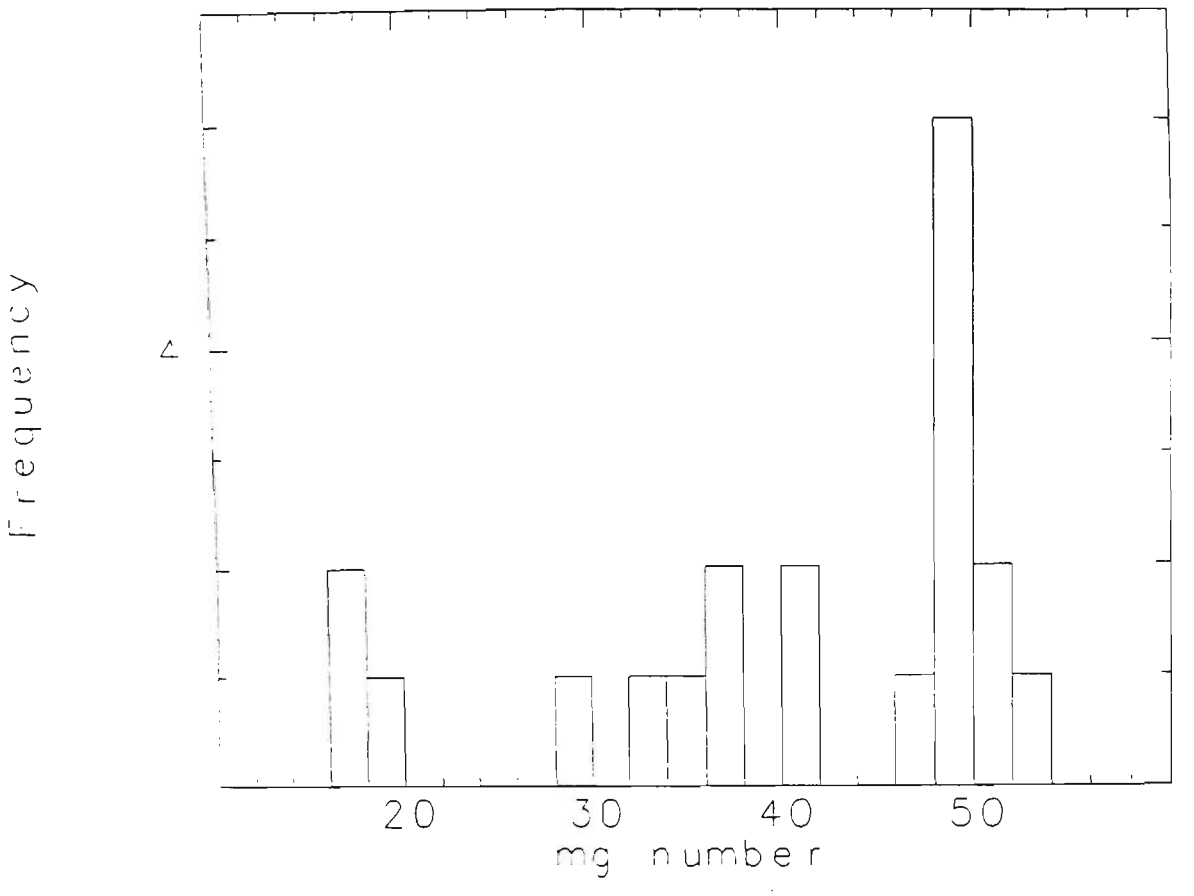

Fig. 6-11. Histogram of Mg-number for rocks from Aghda.

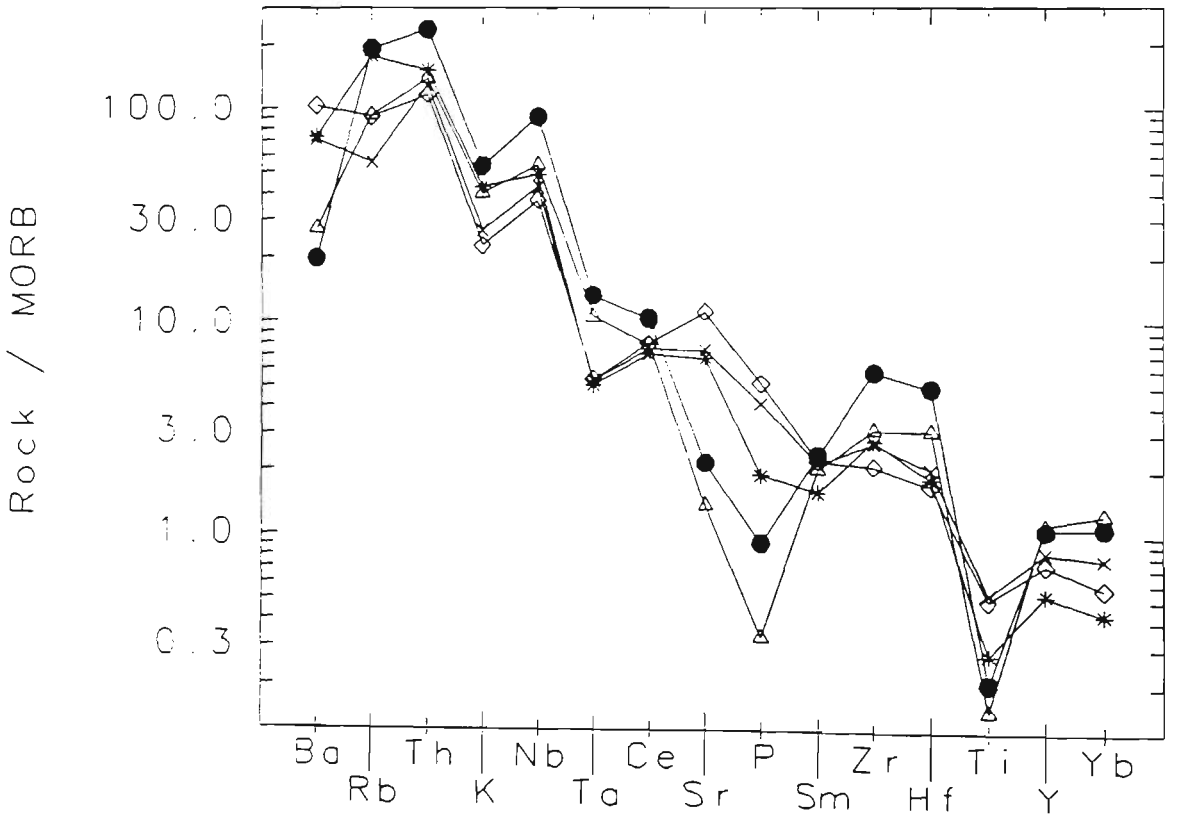

Fig. 6-12. Multi-element patterns (spider diagrams) for the Tertiary volcanic rocks from Aghda.

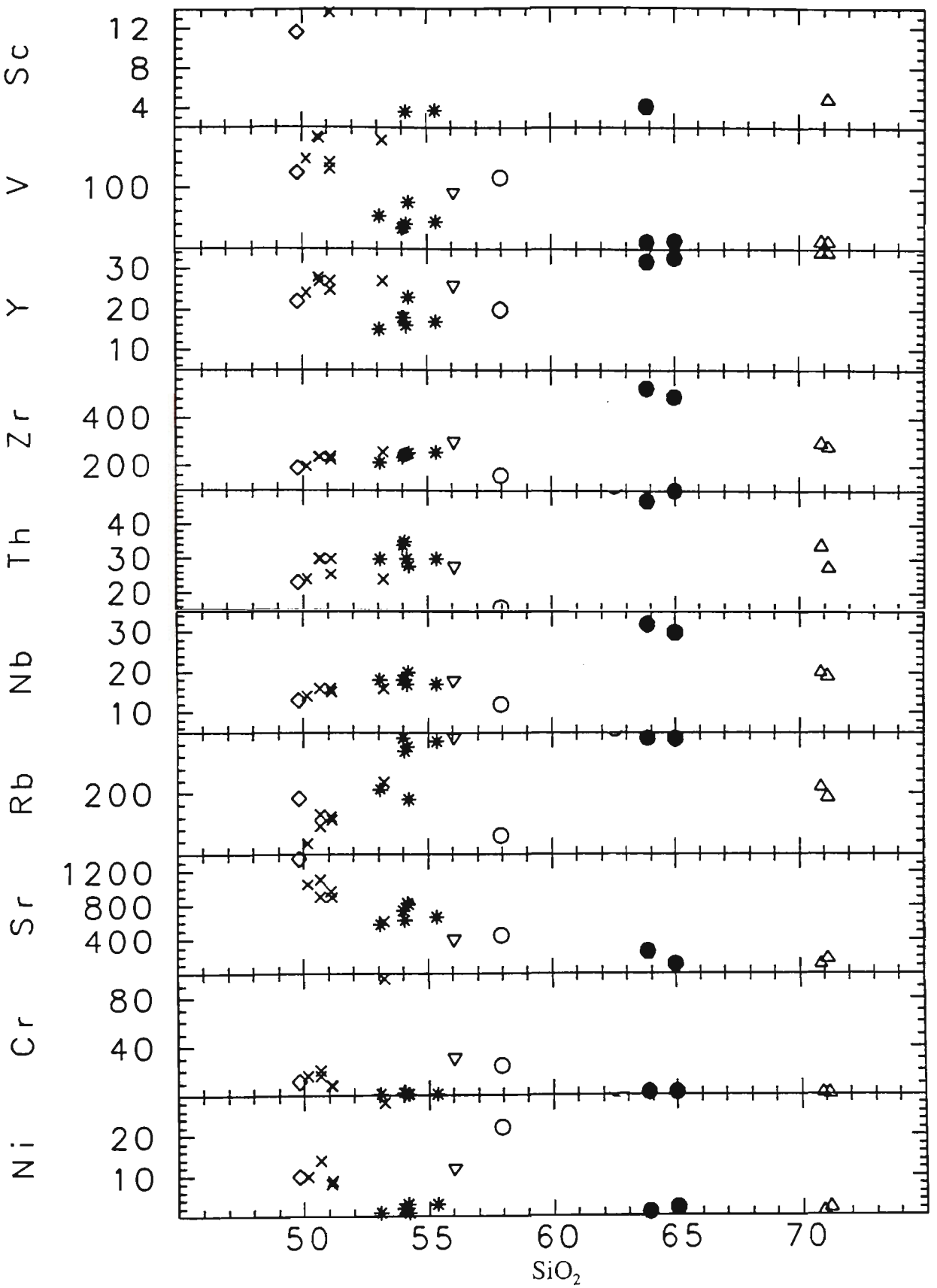

Fig. 6-13. Plot of trace element contents versus SiO_2 for rocks from Aghda (oxides, wt%).

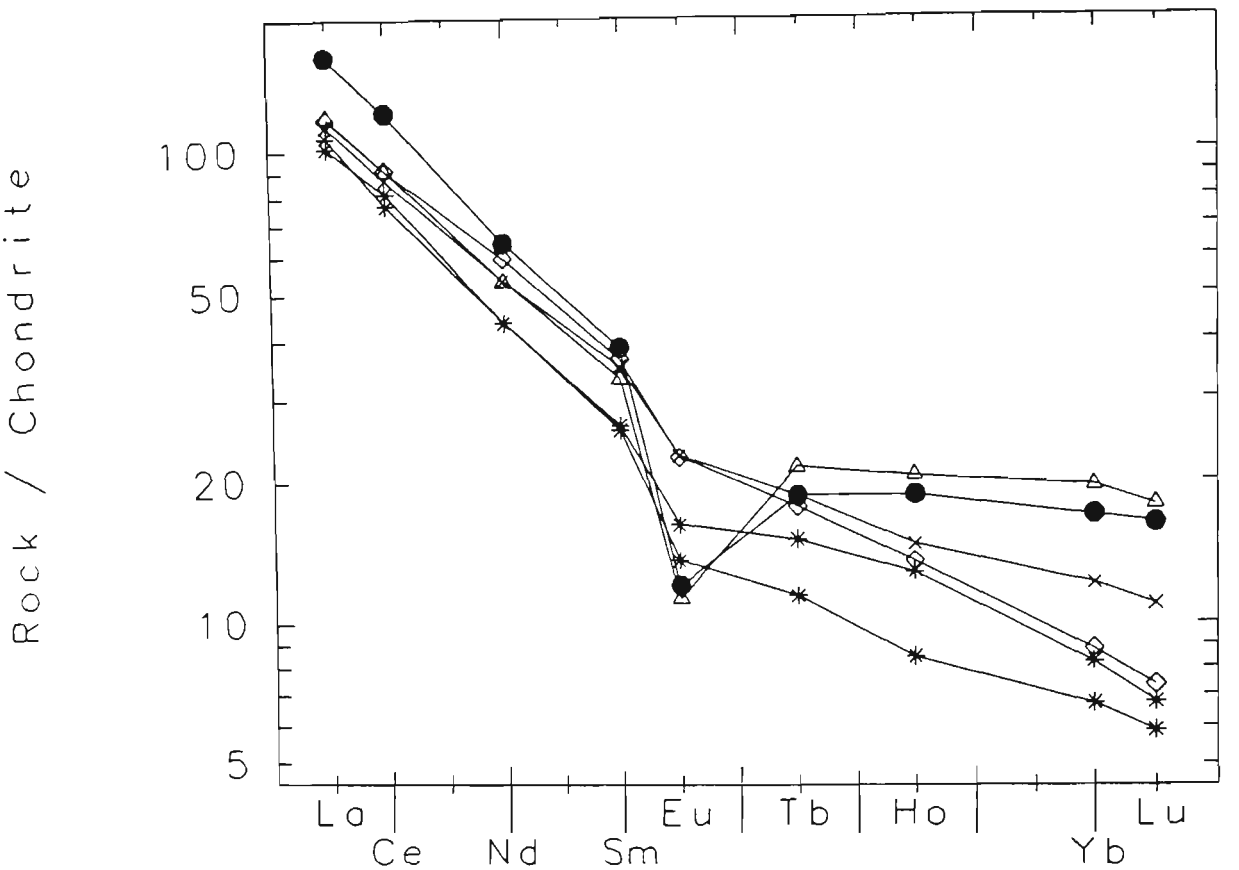

Fig. 6-14. Rare earth element patterns for rocks from Aghda.

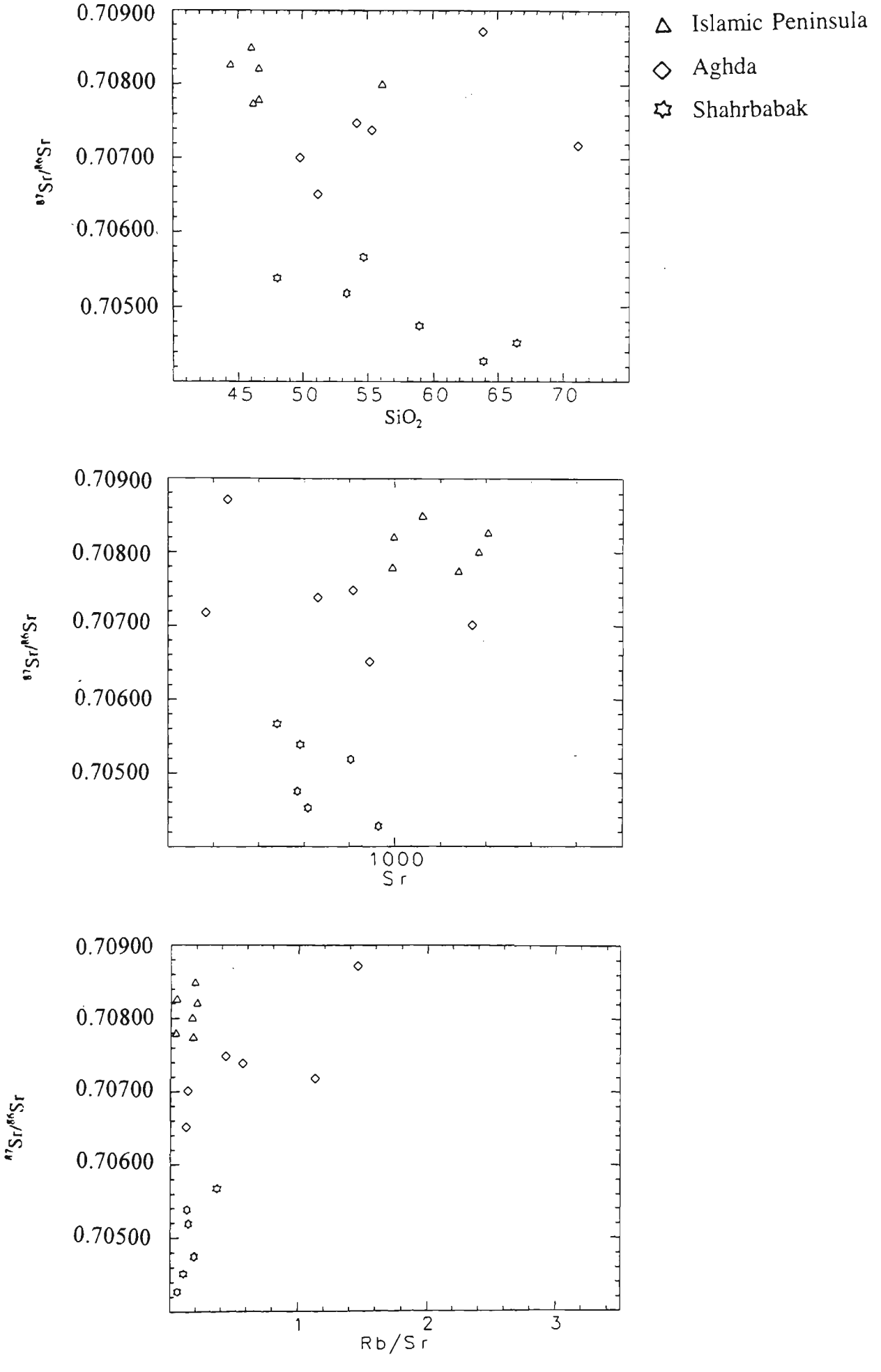

Fig. 6-15. Plot of $^{87}Sr/^{86}Sr$ versus SiO_2, Sr and Rb/Sr for samples from the Islamic Peninsula, Aghda and Shahrbabak

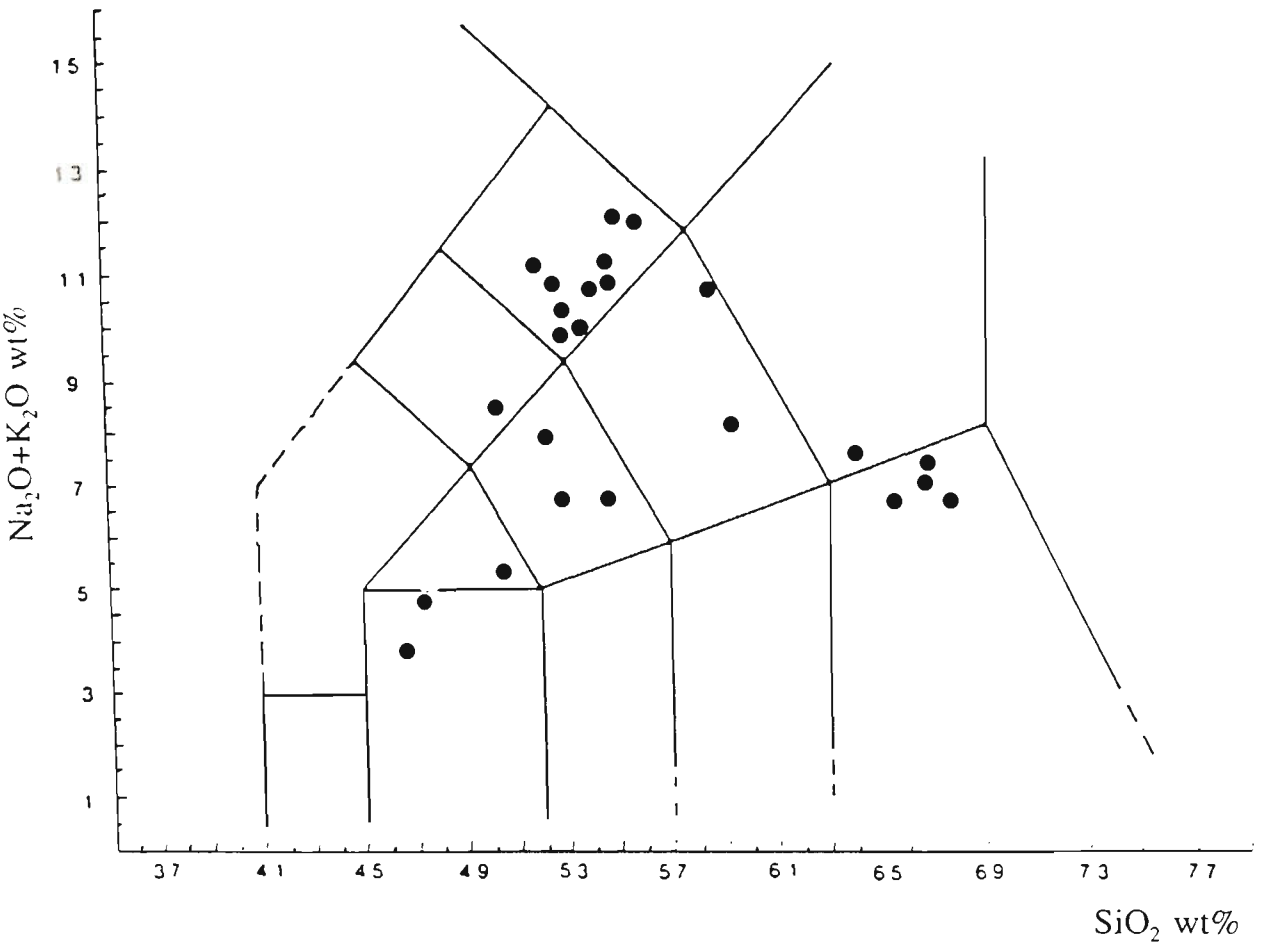

Fig. 6-16. Total alkalis versus SiO_2 (wt%) classification (TAS) for Tertiary volcanic rocks from Shahrbabak.

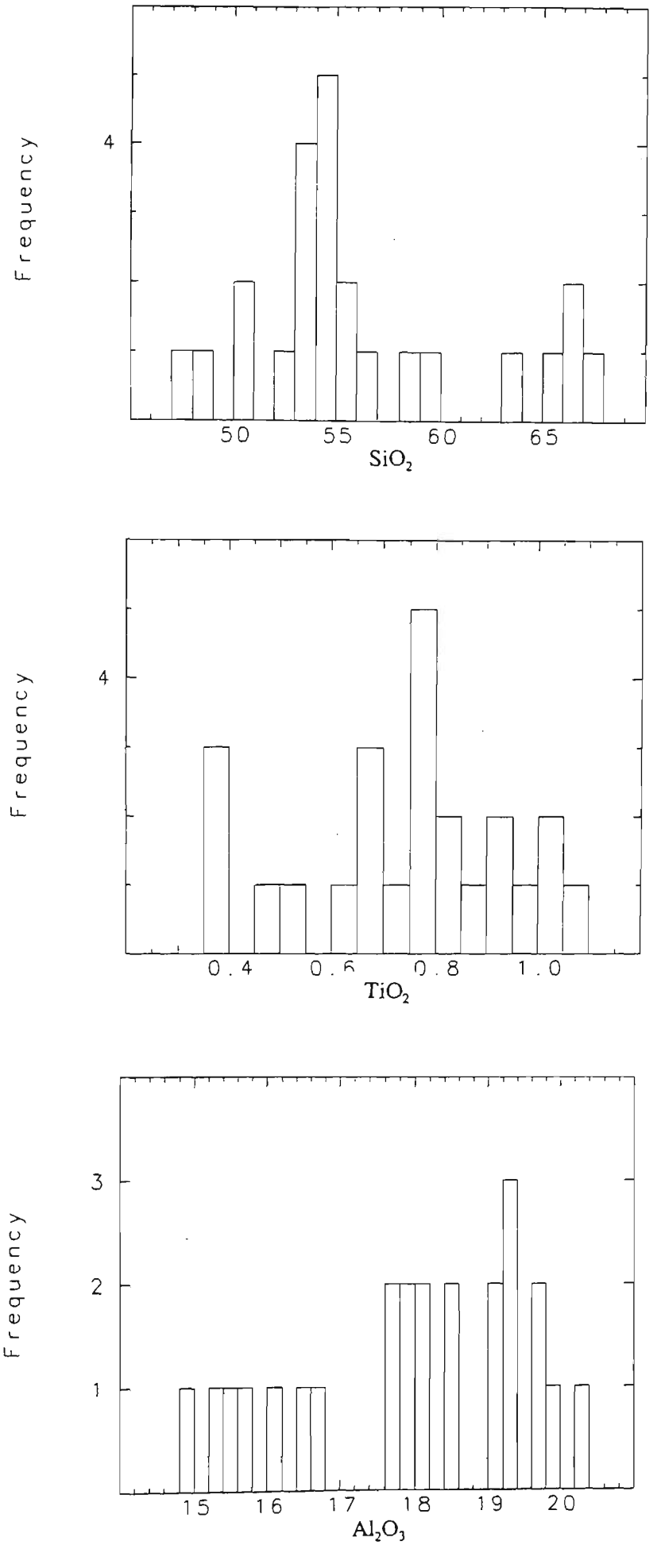

Fig. 6-17. Histogram of compositional frequency for major element oxides for rocks from Shahrbabak(oxides, wt%).

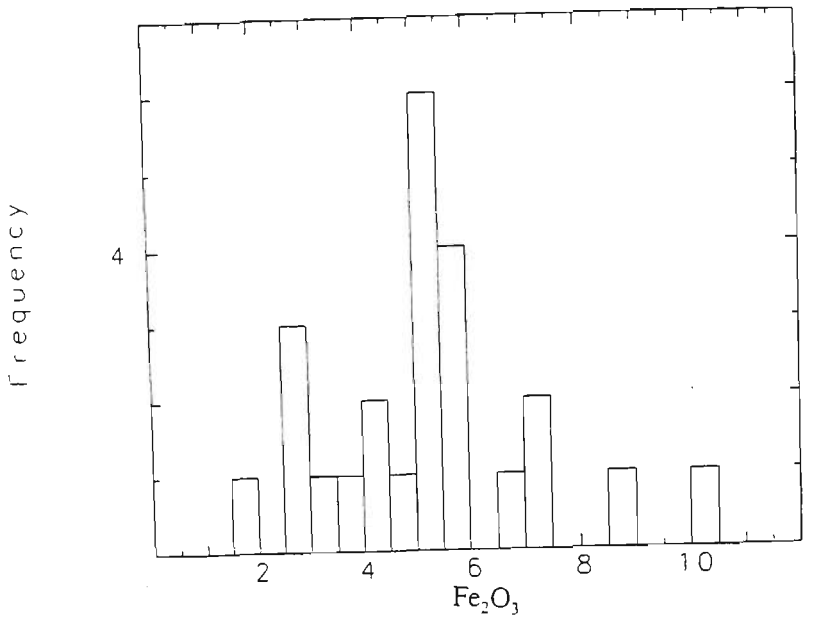

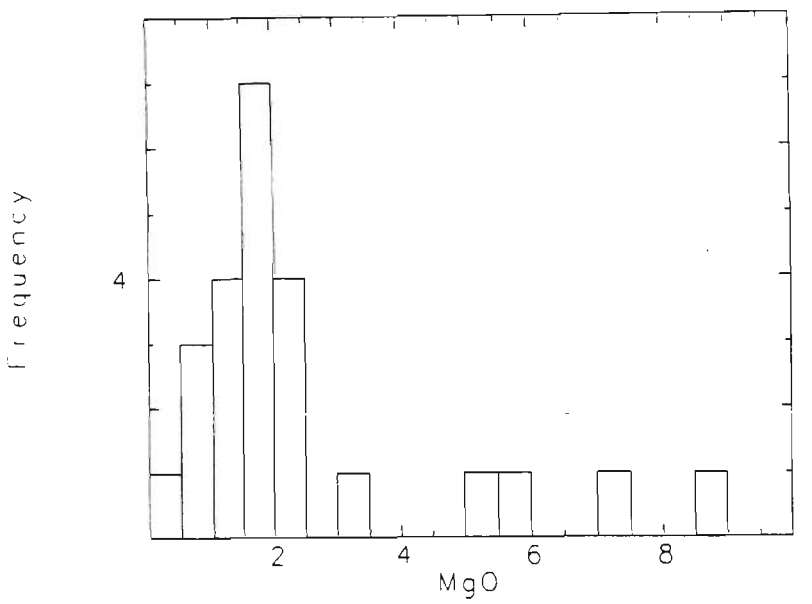

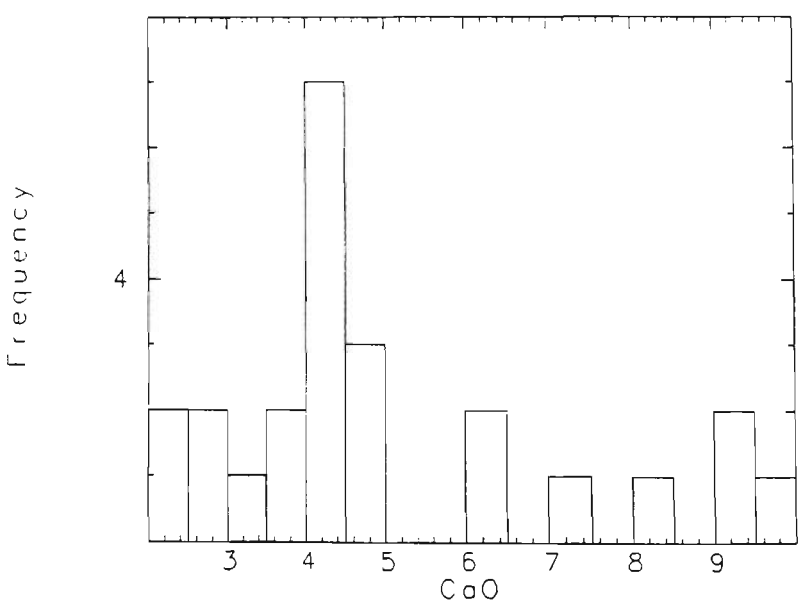

Fig. 6-17. (continued) Histogram of compositional frequency for major element oxides for rocks from Shahrbabak(oxides, wt%).

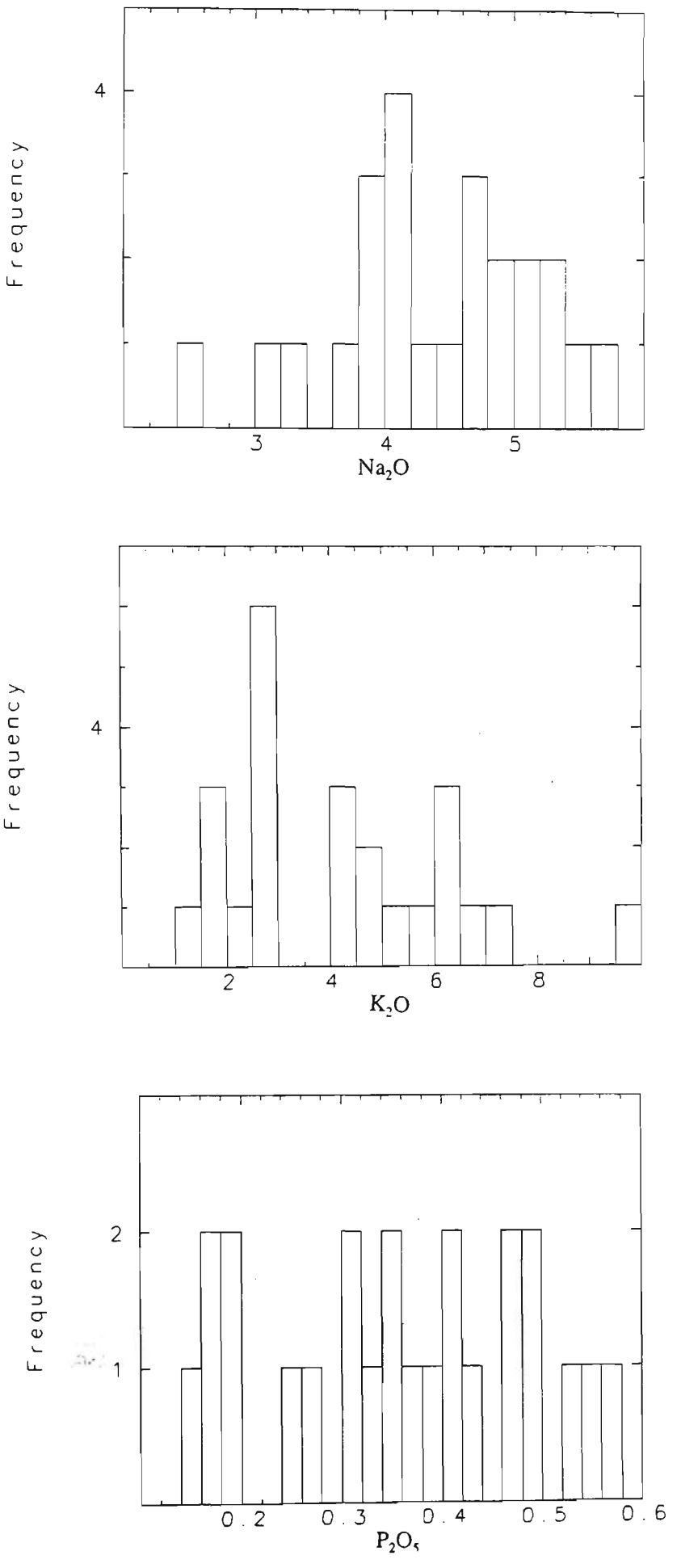

Fig. 6-17. (continued) Histogram of compositional frequency for major element oxides for rocks from Shahrbabak (oxides, wt%).

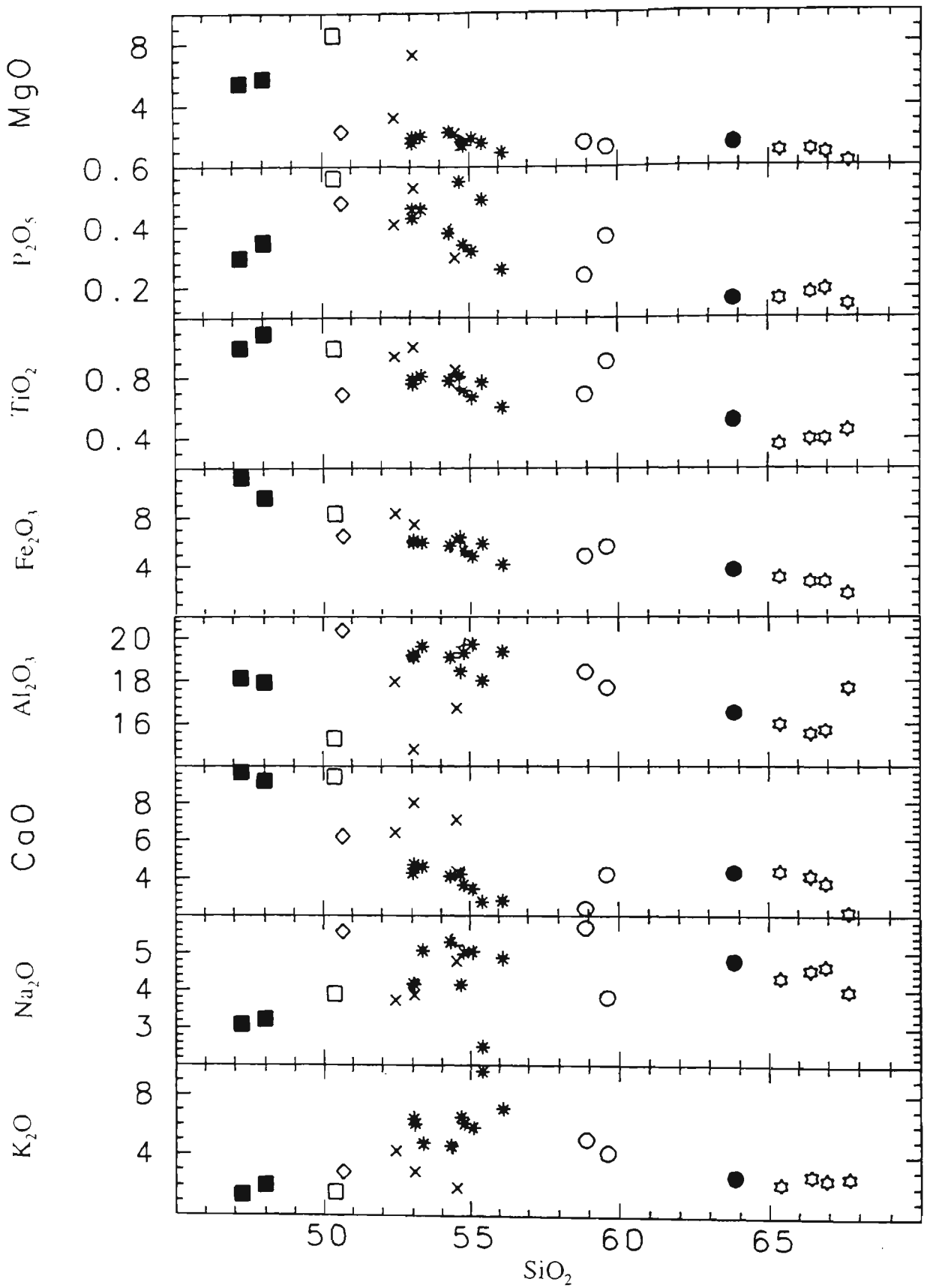

Fig. 6-18. Harker diagrams for Shahrbabak volcanic rocks(oxides, wt%

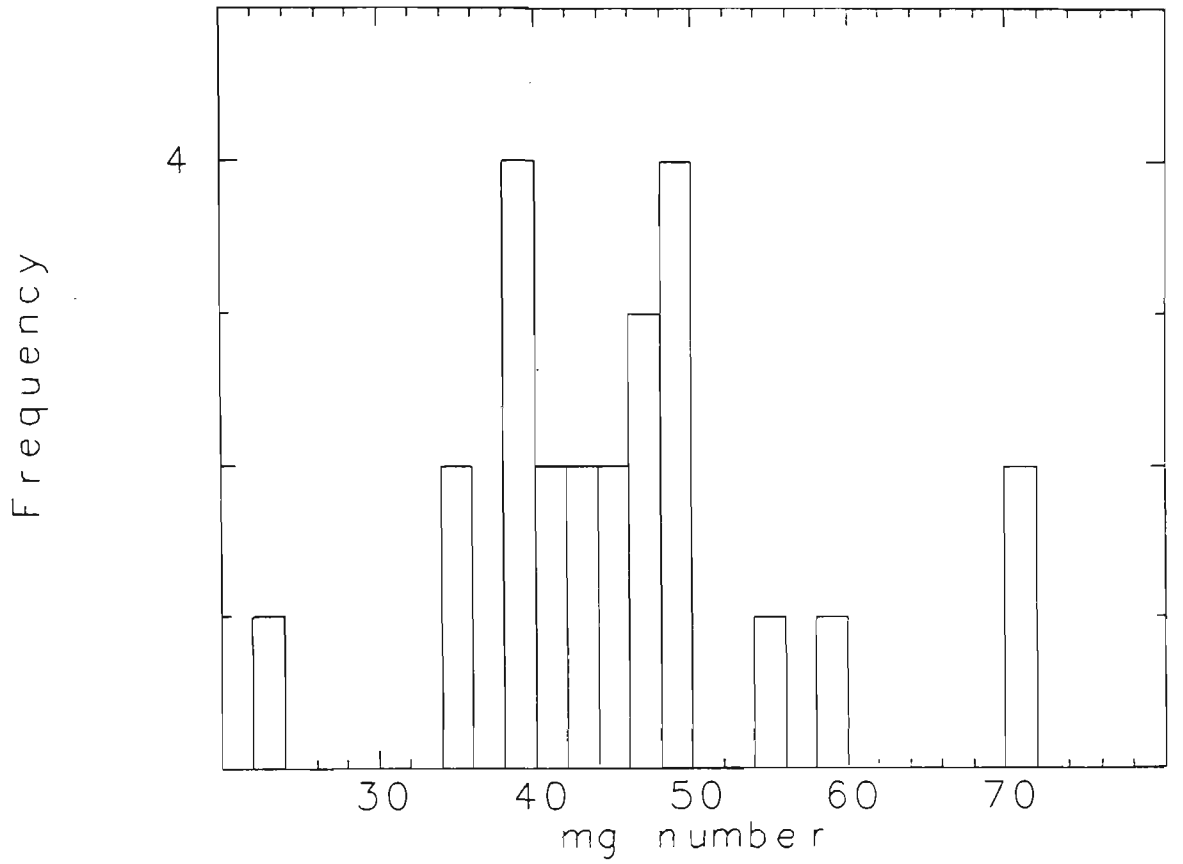

Fig. 6-19. Histogram of Mg-number for rocks from Shahrbabak.

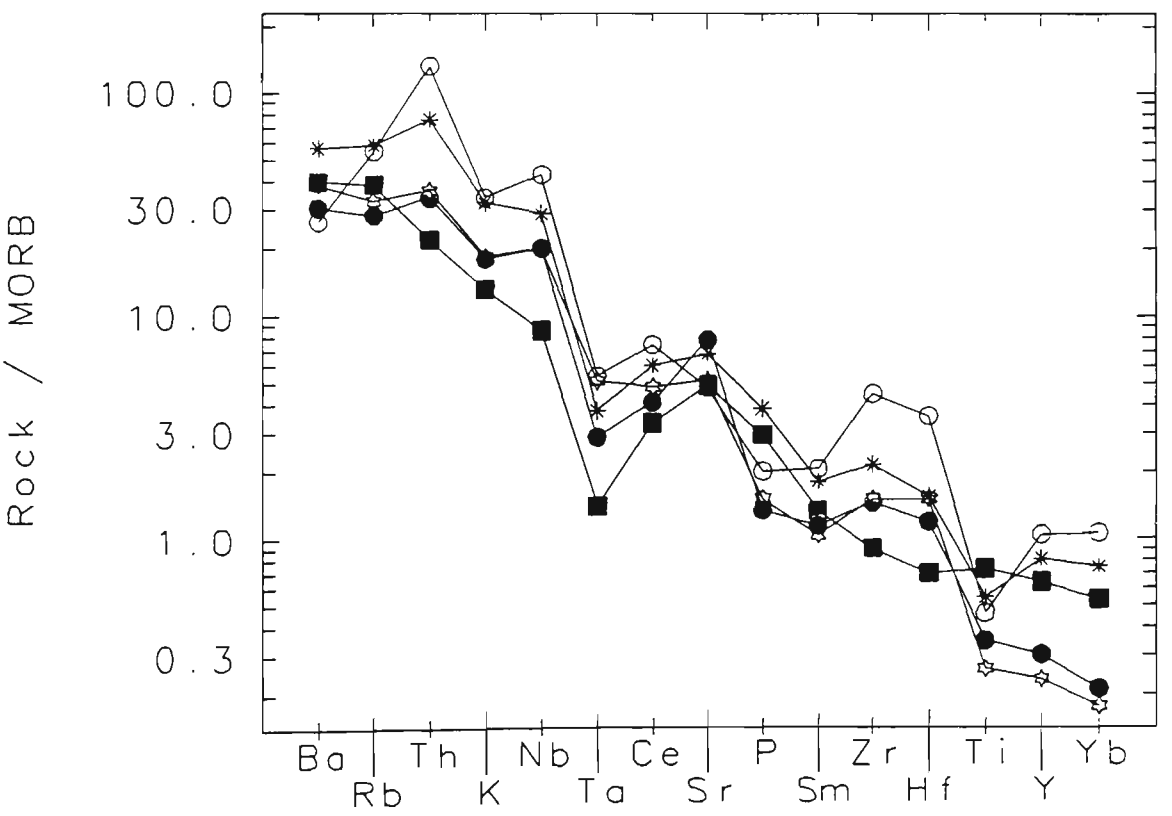

Fig. 6-20. Multi-element patterns (spider diagrams) for the Tertiary volcanic rocks from Shahrbabak.

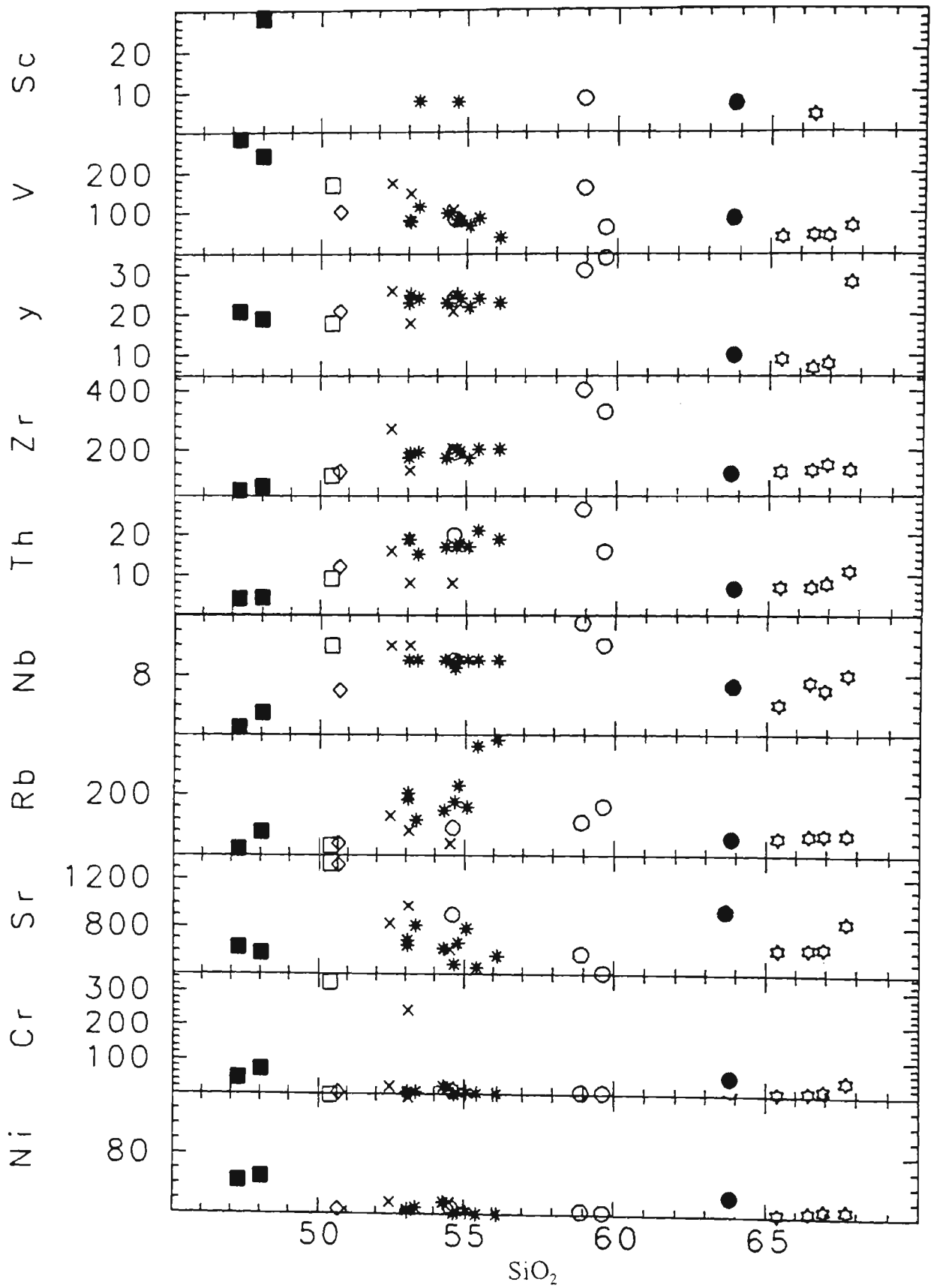

Fig. 6-21. Plot of Trace element against SiO_2 for rocks from Shahrbabak. (overall they have no significant correlation) (oxides, wt%).

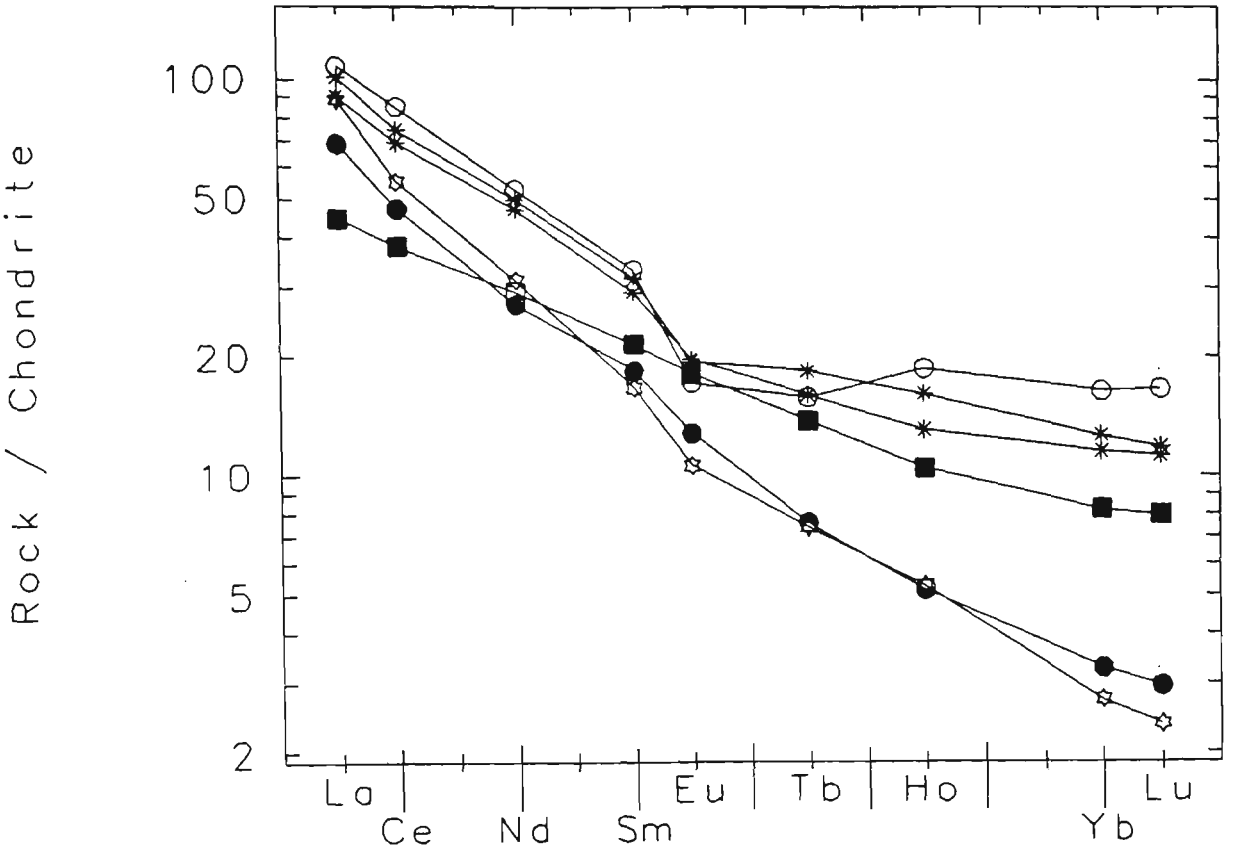

Fig. 6-22. Rare earth element patterns for rocks from Shahrbabak.

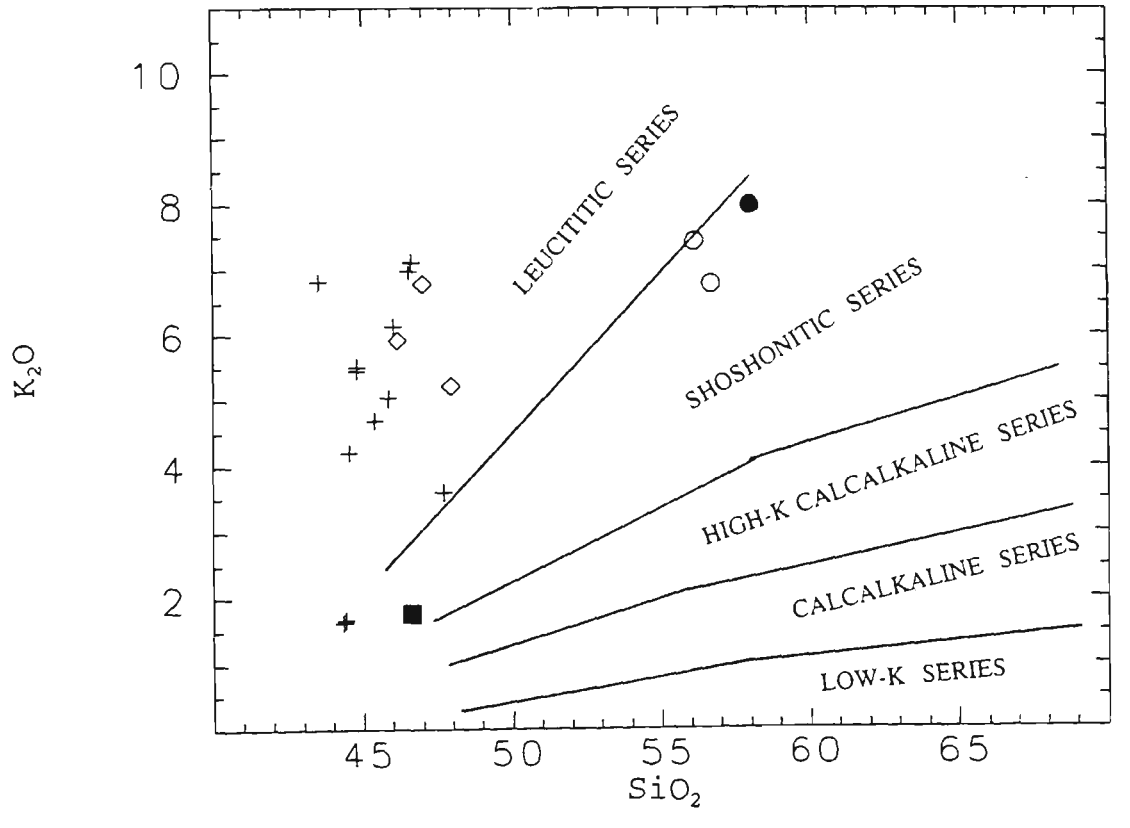

Fig. 7-1. K_2O versus SiO_2 diagram for volcanic rocks from the Islamic Peninsula. Boundaries between calcalkaline, high-K calcalkaline and shoshonite suites are from Peccerillo and Taylor (1976). The boundary between shoshonite and leucititic suites from Wheller et al. (1987).

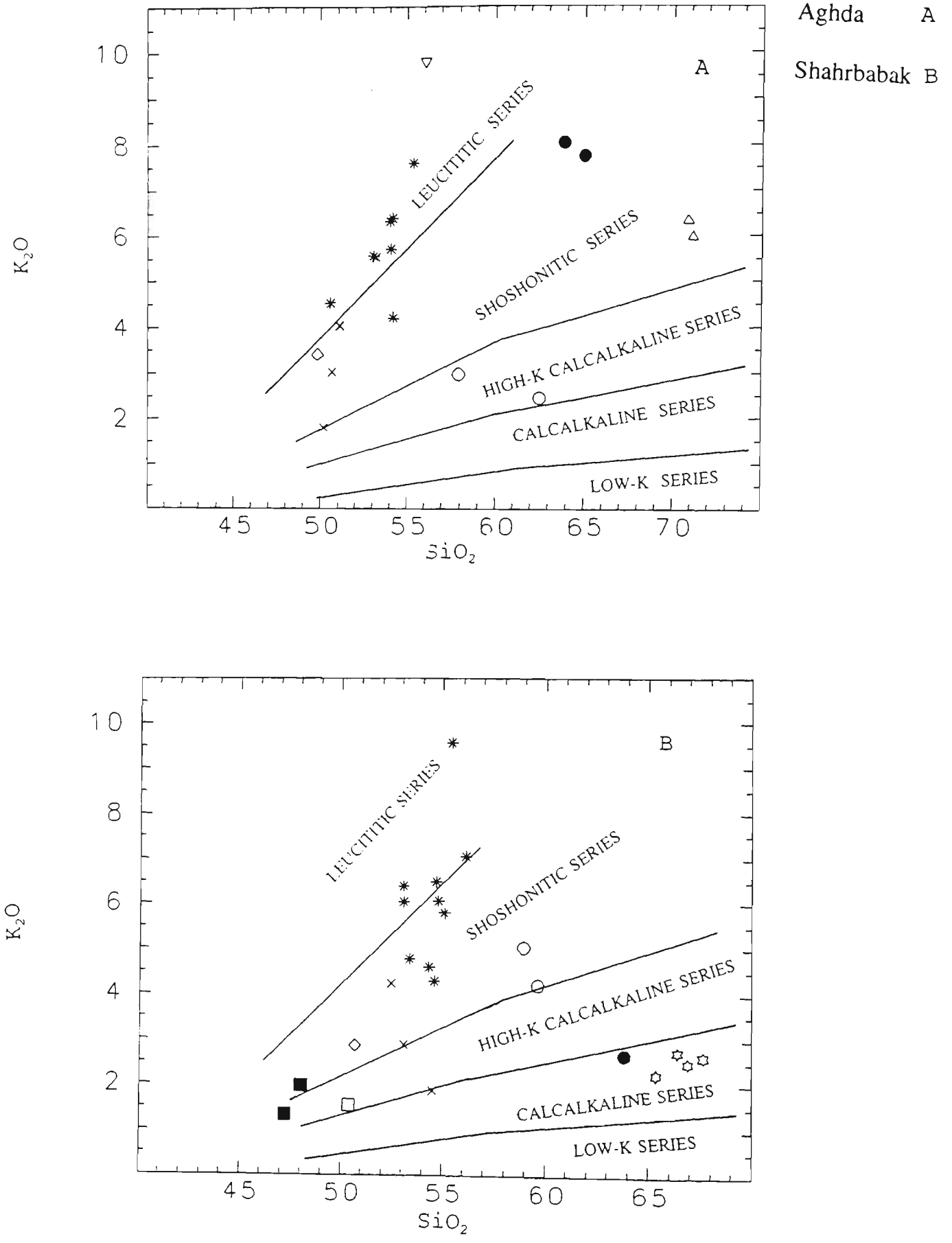

Fig. 7-1. (continued) K_2O versus SiO_2 diagram for volcanic rocks from Aghda and Shahrbabak.

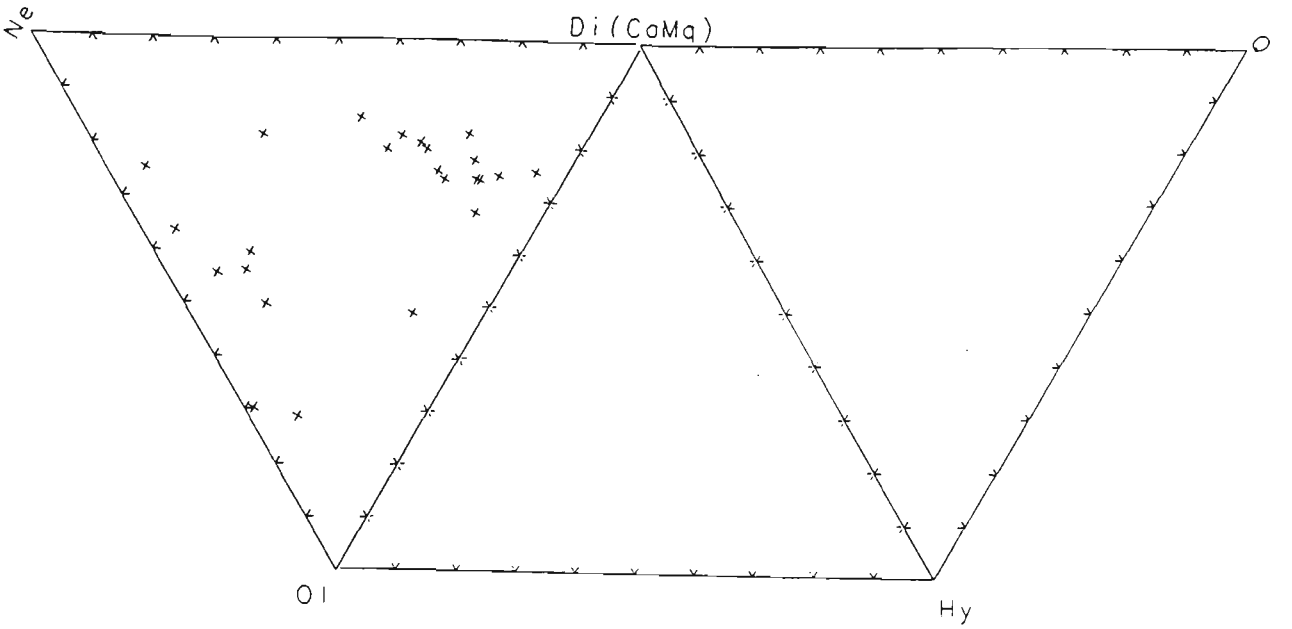

Fig. 7-2. CIPW normative mineralogy for leucititic rocks from the U-DVB.

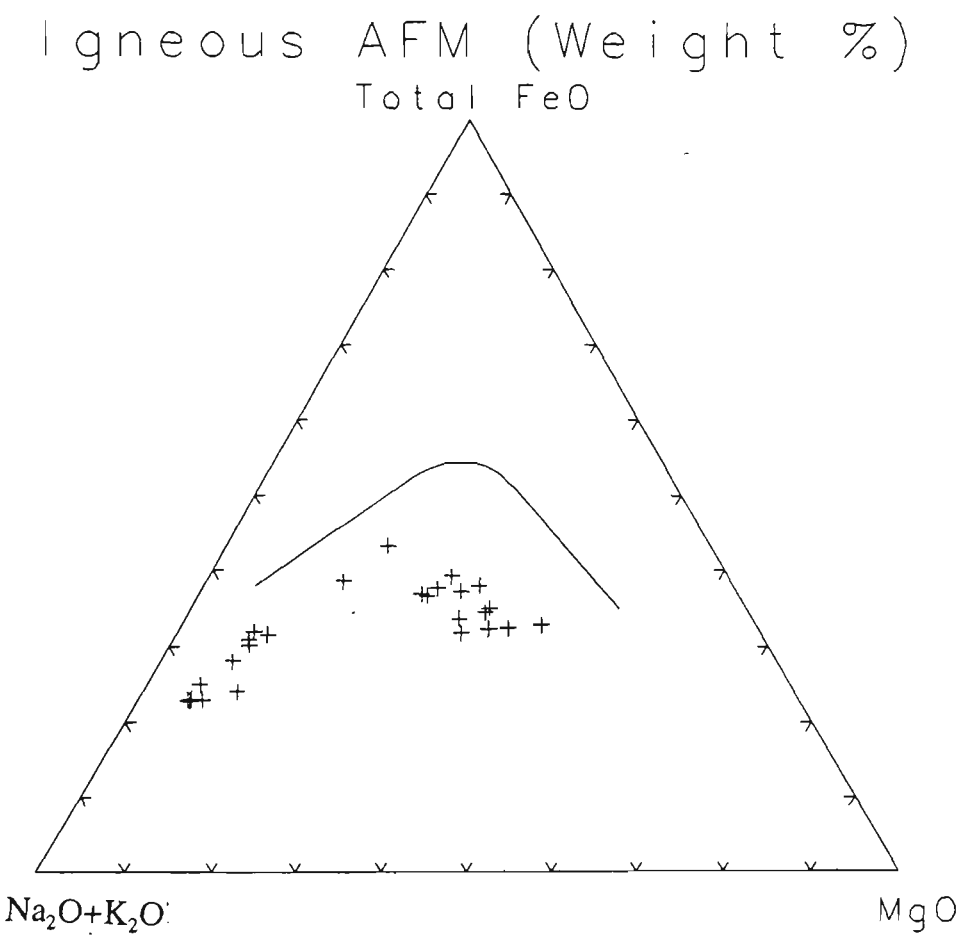

Fig. 7-3. AFM diagram for leucititic rocks from the U-DVB.

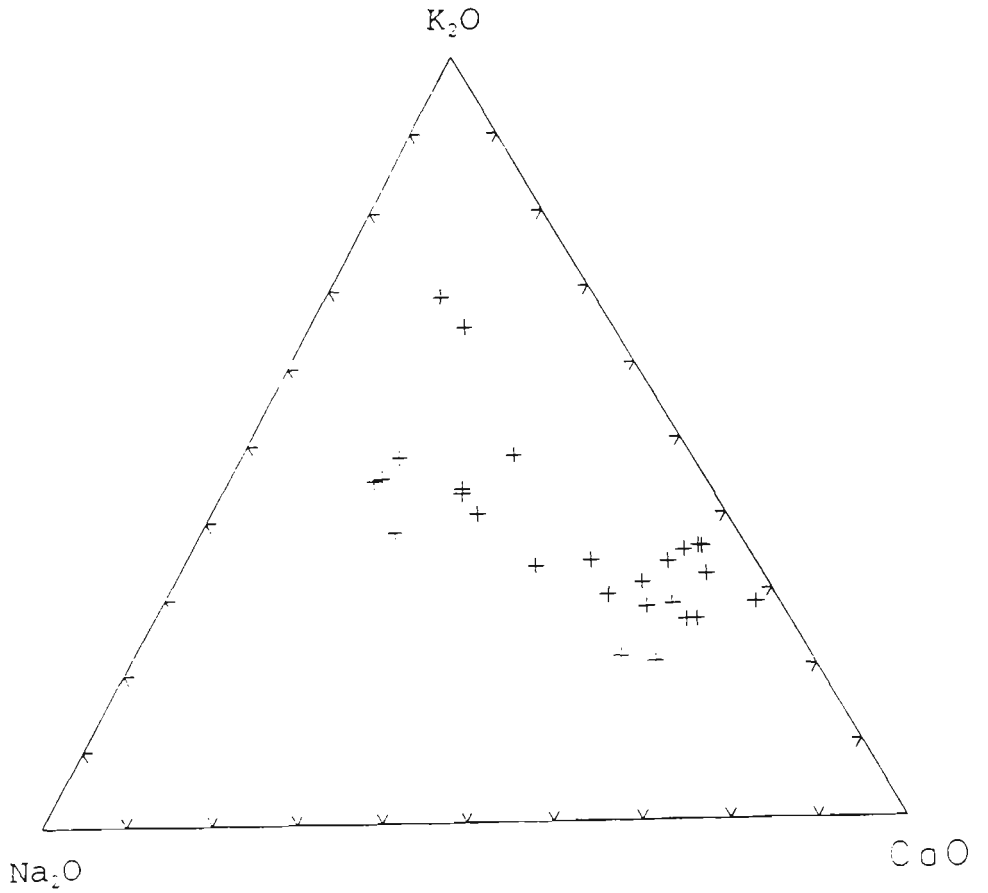

Fig. 7-4. Na_2O-K_2O-CaO diagram for leucititic rocks from the U-DVB.

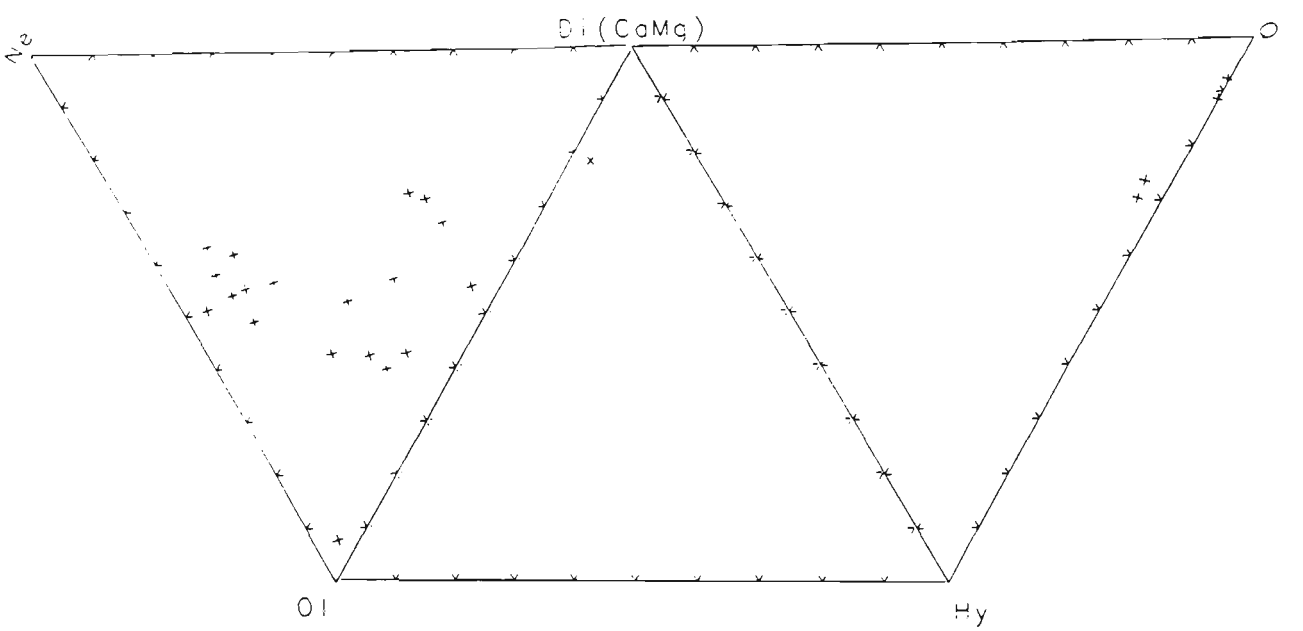

Fig. 7-5. CIPW normative mineralogy for shoshonitic rocks from the U-DVB.

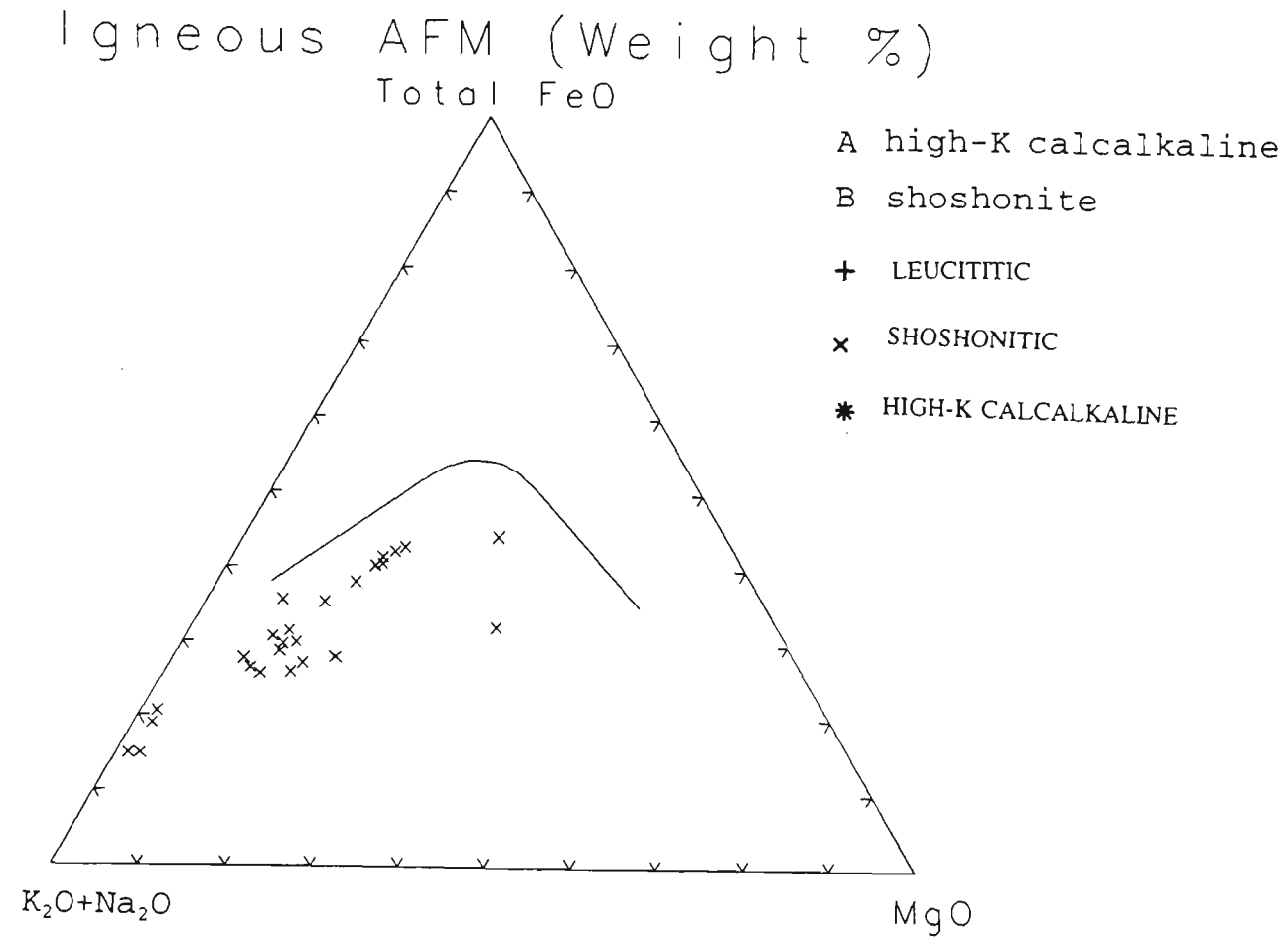

Fig. 7-6. AFM diagram for shoshonitic rocks from the U-DVB.

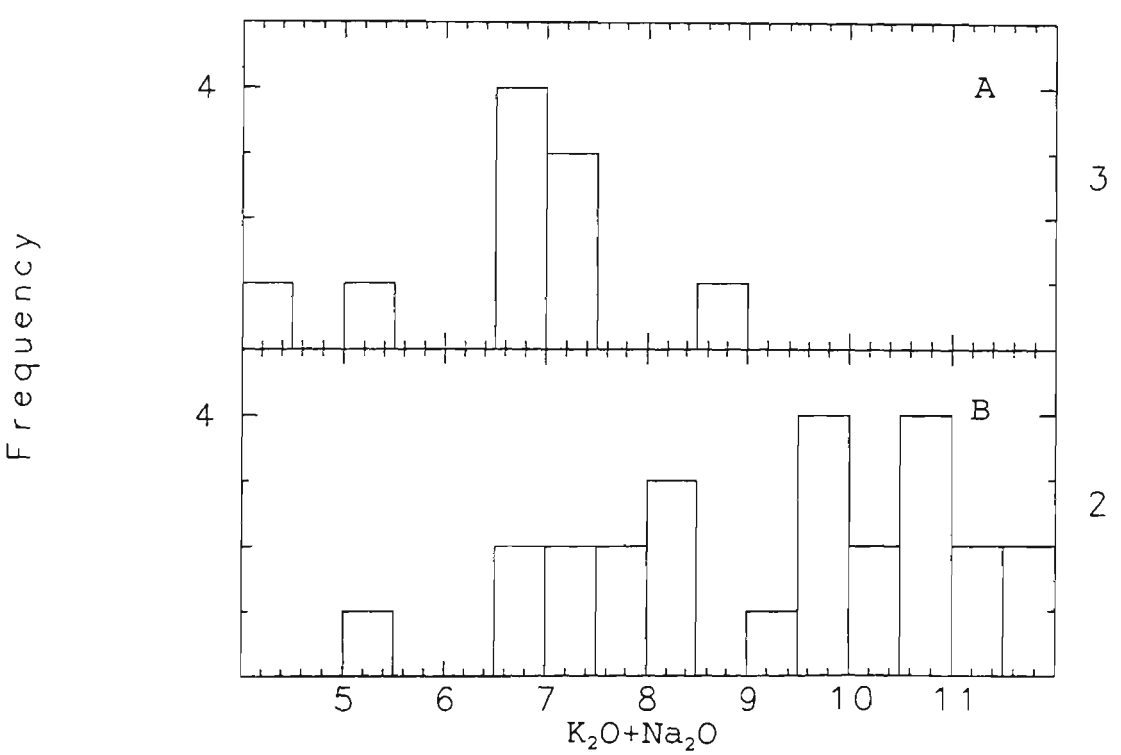

Fig. 7-7. Histogram of the total alkali content of shoshonite and high-K calcalkaline rocks from the U-DVB (oxides, wt%).

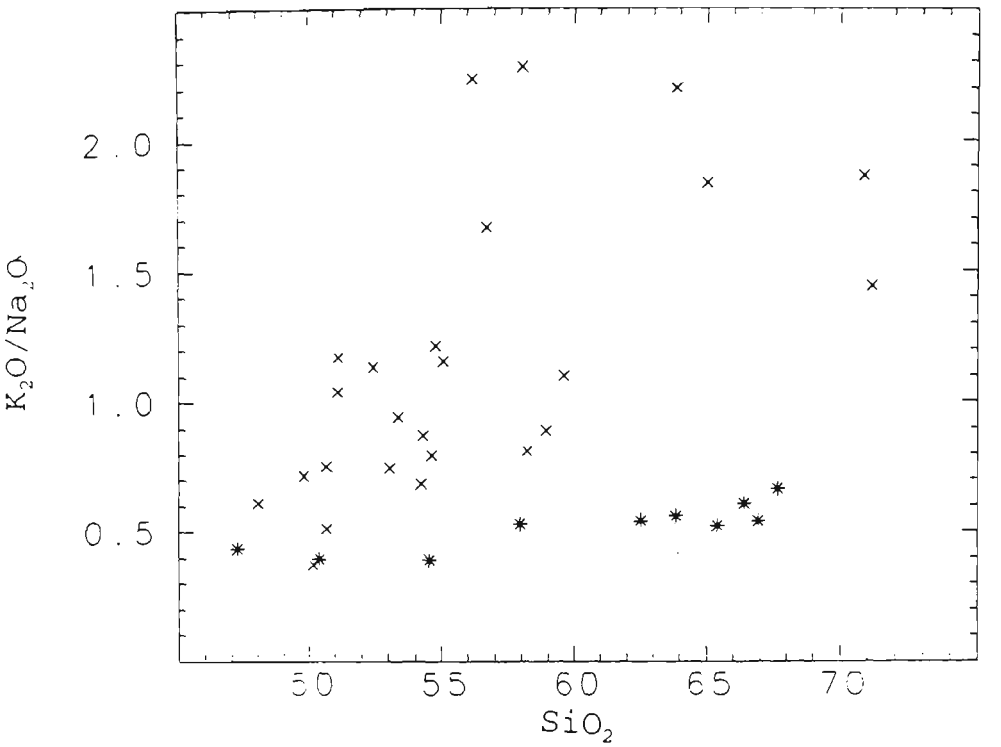

Fig. 7-8. Plot of K_2O/Na_2O versus SiO_2 for shoshonite and high-K calcalkaline rocks from the U-DVB (oxides, wt%).

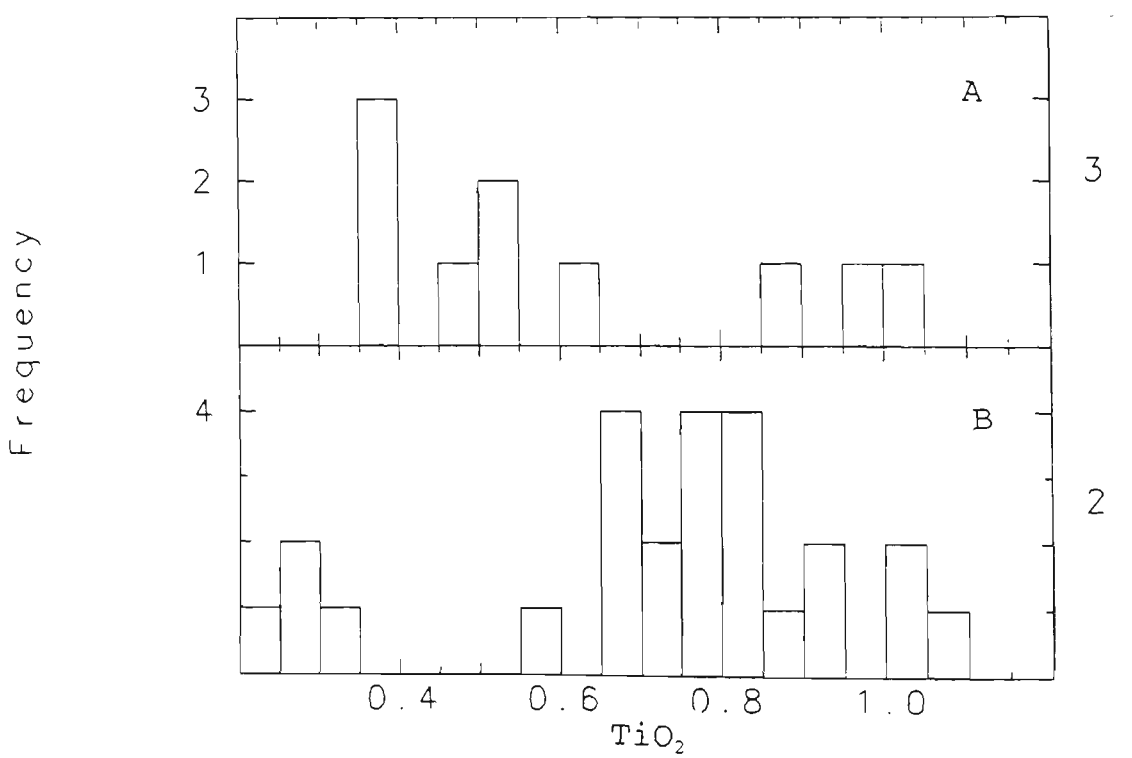

Fig. 7-9. Histogram of TiO_2 contents of shoshonite and high-K calcalkaline rocks from the U-DVB (oxides, wt%).

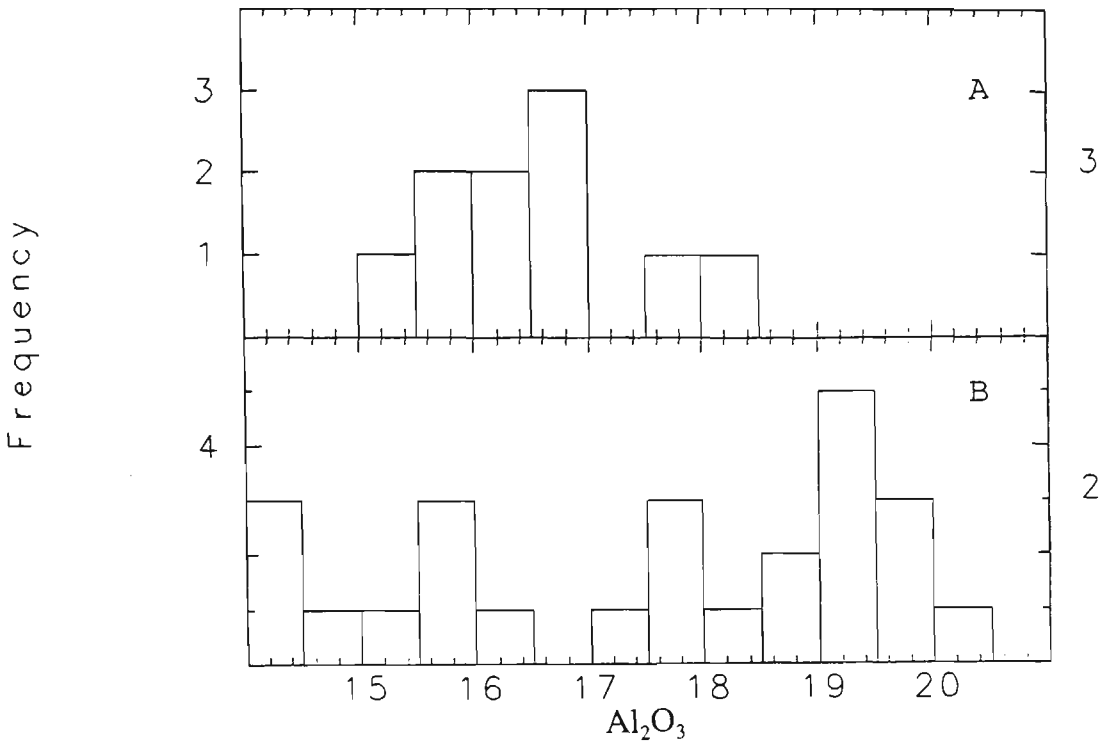

Fig. 7-10. Histogram of Al_2O_3 contents of shoshonite and high-K calcalkaline rocks from the U-DVB **(oxides, wt%).**

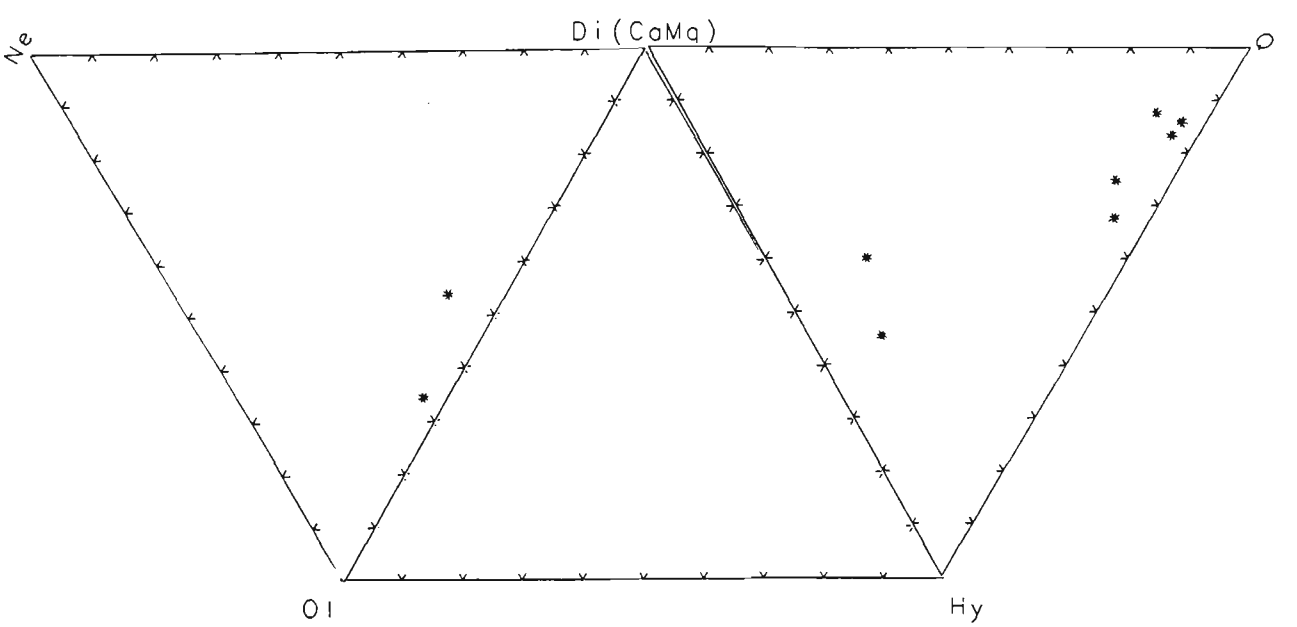

Fig. 7-11. CIPW normative mineralogy for high-K calcalkaline rocks from the U-DVB.

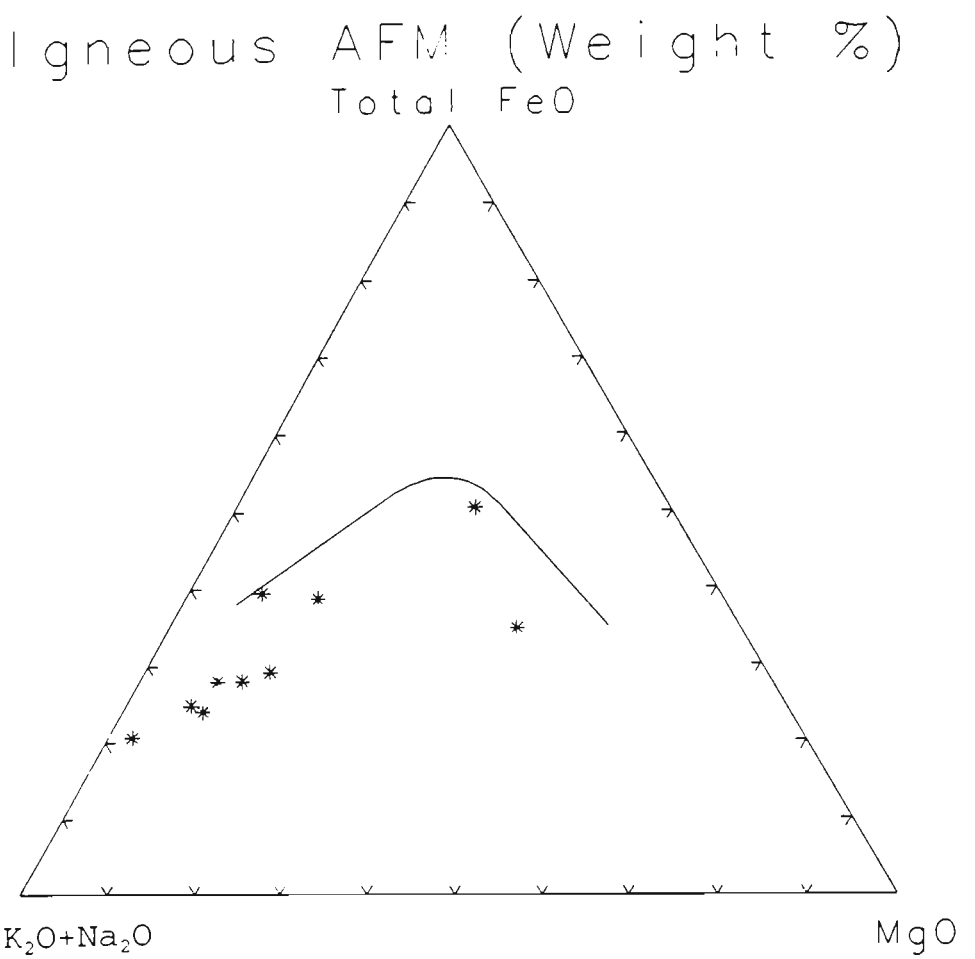

Fig. 7-12. AFM diagram for high-K calcalkaline rocks from the U-DVB.

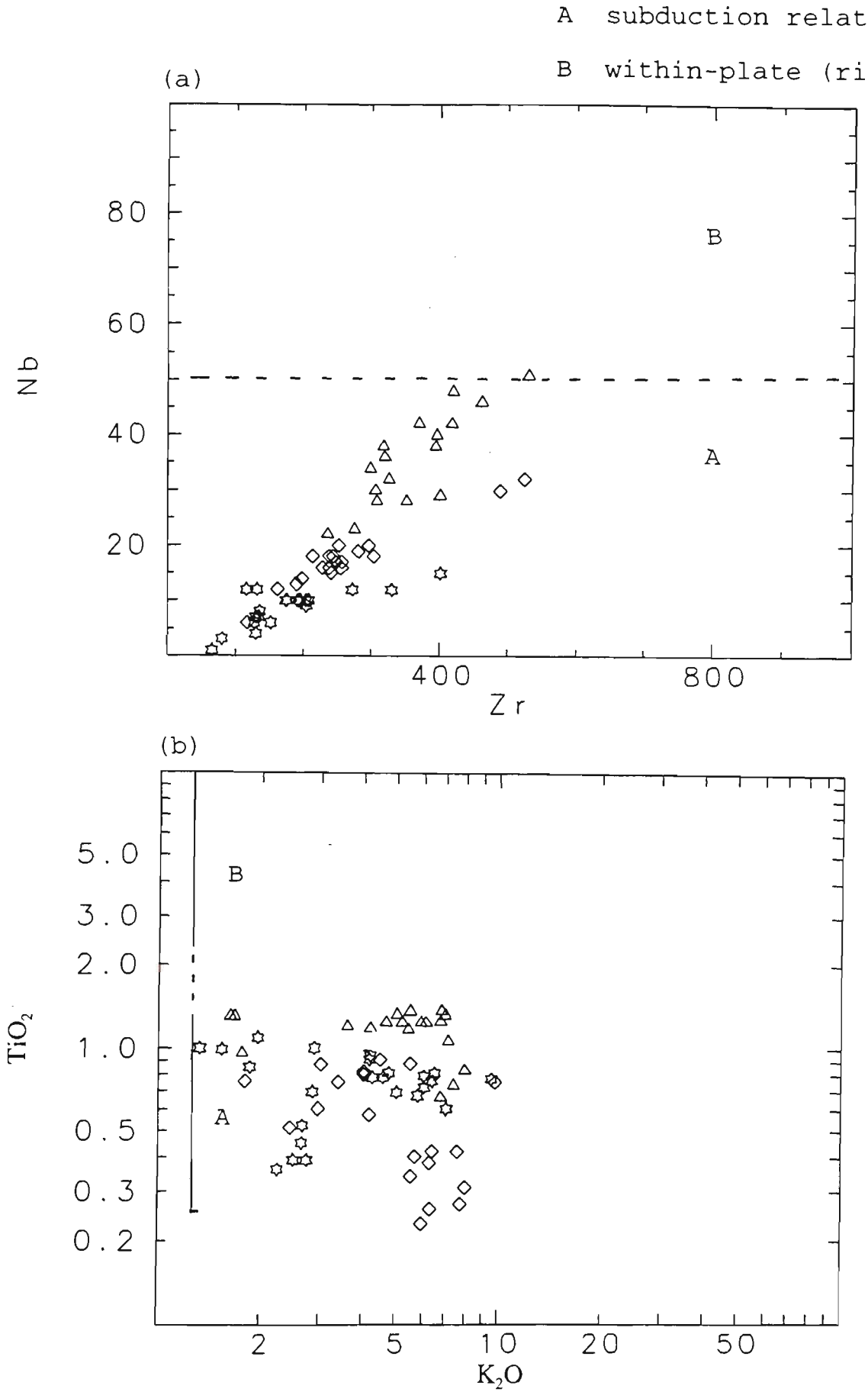

Fig 8-1. (a) Plot of Zr versus Nb (b) plot of TiO_2 versus K_2O for potassic volcanic rocks from the U-DVB (after Thorpe, 1987) (oxides, wt%).

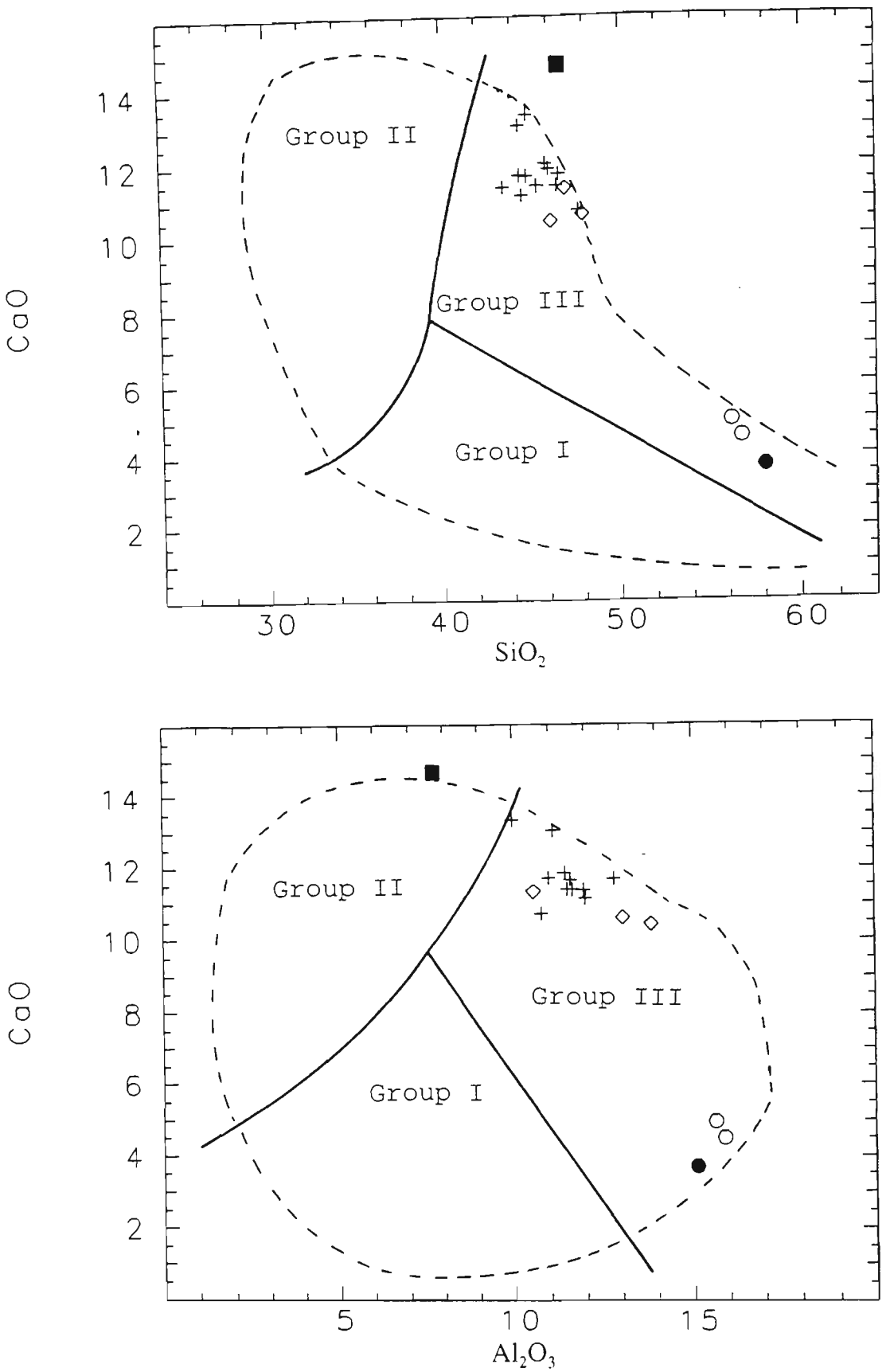

Fig 8-2. Classification of ultrapotassic igneous rocks from the Islamic Peninsula into group I, II, III, on the basis of wt% CaO versus Al_2O_3 and SiO_2 (after Foley et al., 1978) (oxides, wt%).

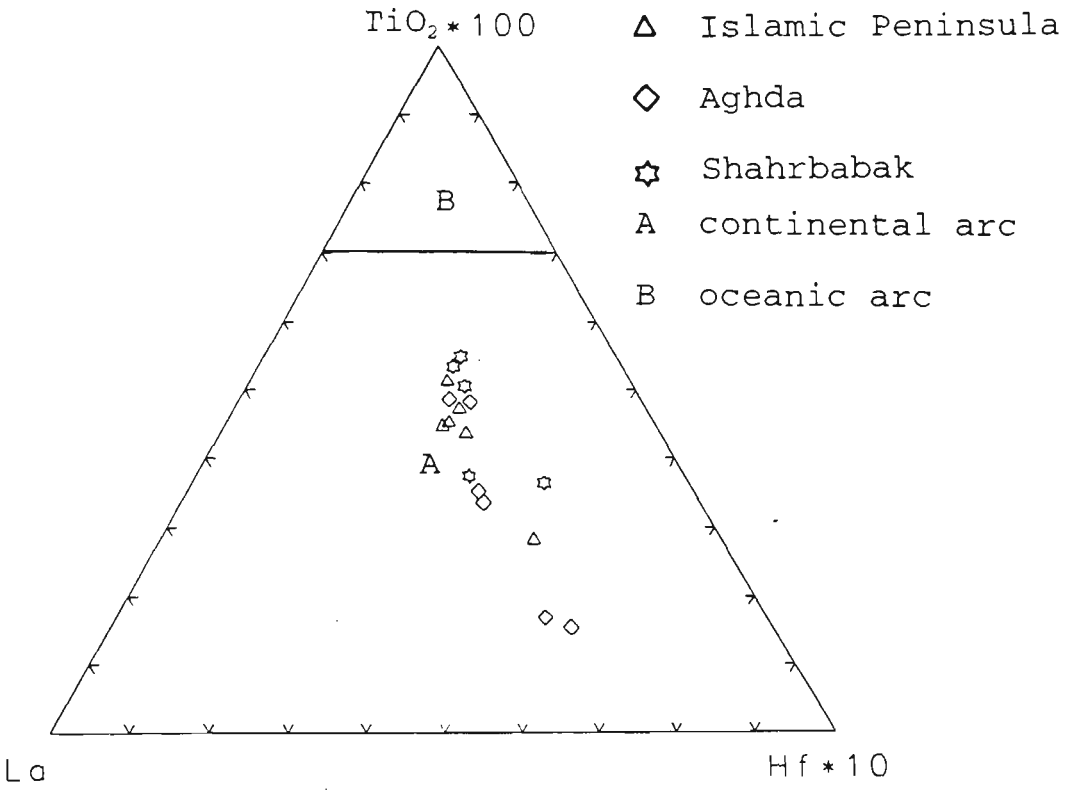

Fig 8-3. Discrimination diagrams for potassic volcanic rocks from the U-DVB, based on the immobile elements, used to separate oceanic arc from continental/postcollisional arcs (after Muller et al., 1992).

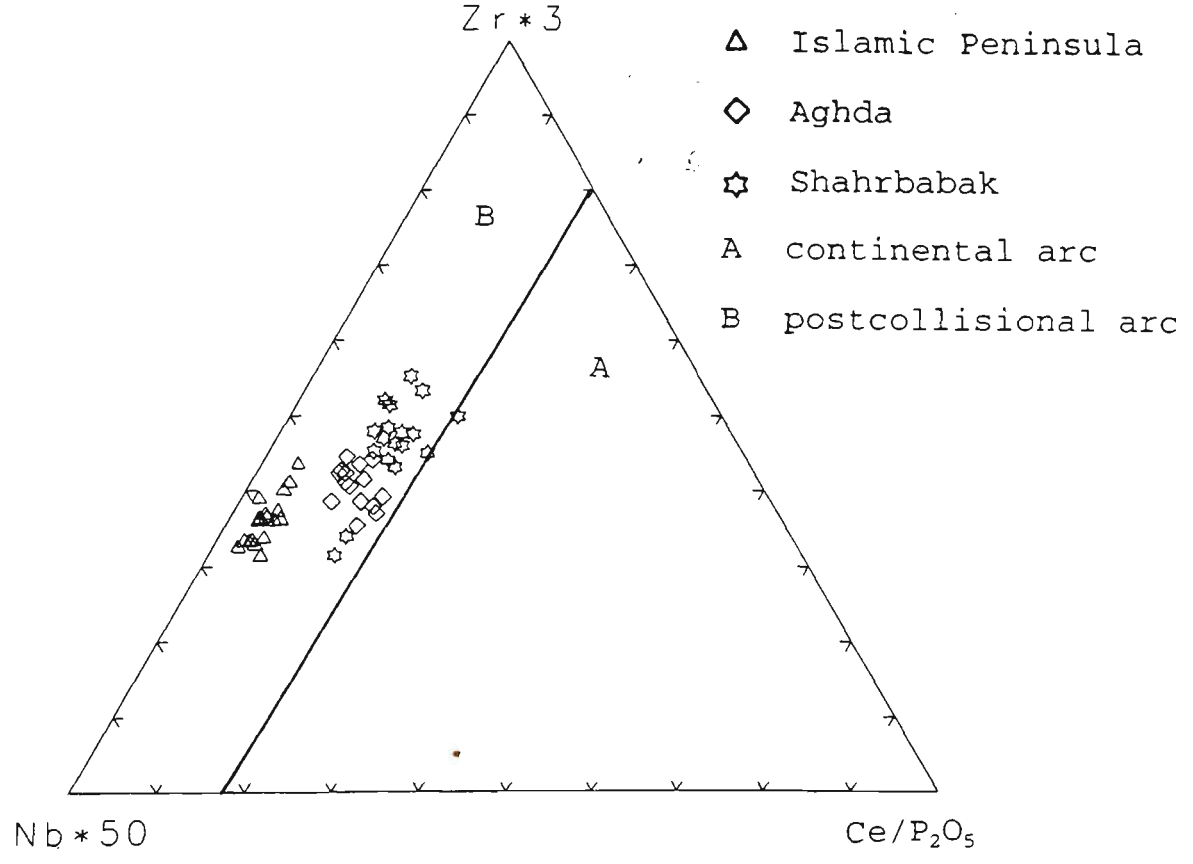

Fig 8-4. Discrimination diagram for potassic volcanic rocks from the U-DVB, based on simple ratios of immobile elements, used to separate continental from postcollisional arcs (after Muller et al., 1992).

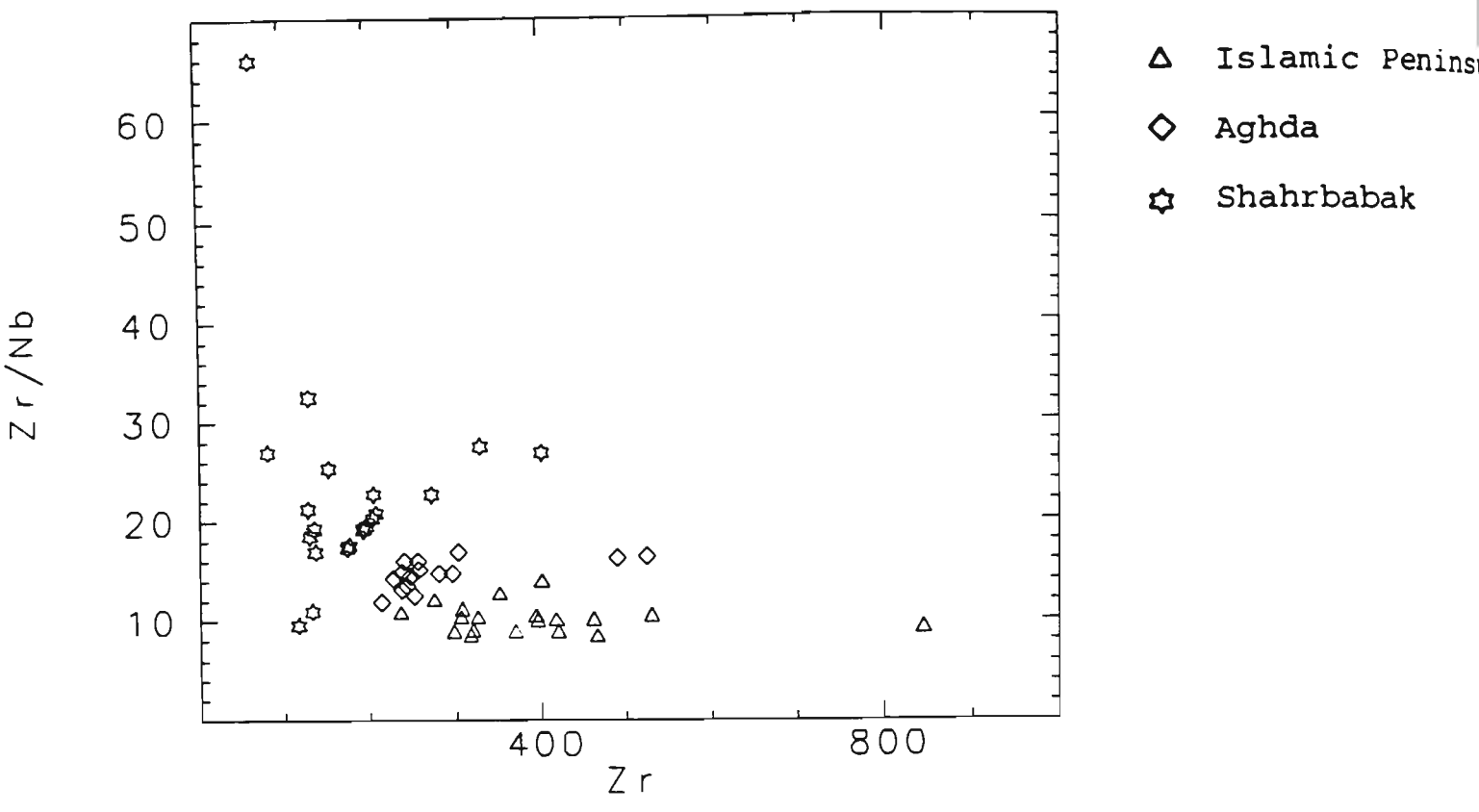

Fig. 8-5. Plot of Zr versus Zr/Nb for rocks from the U-DVB

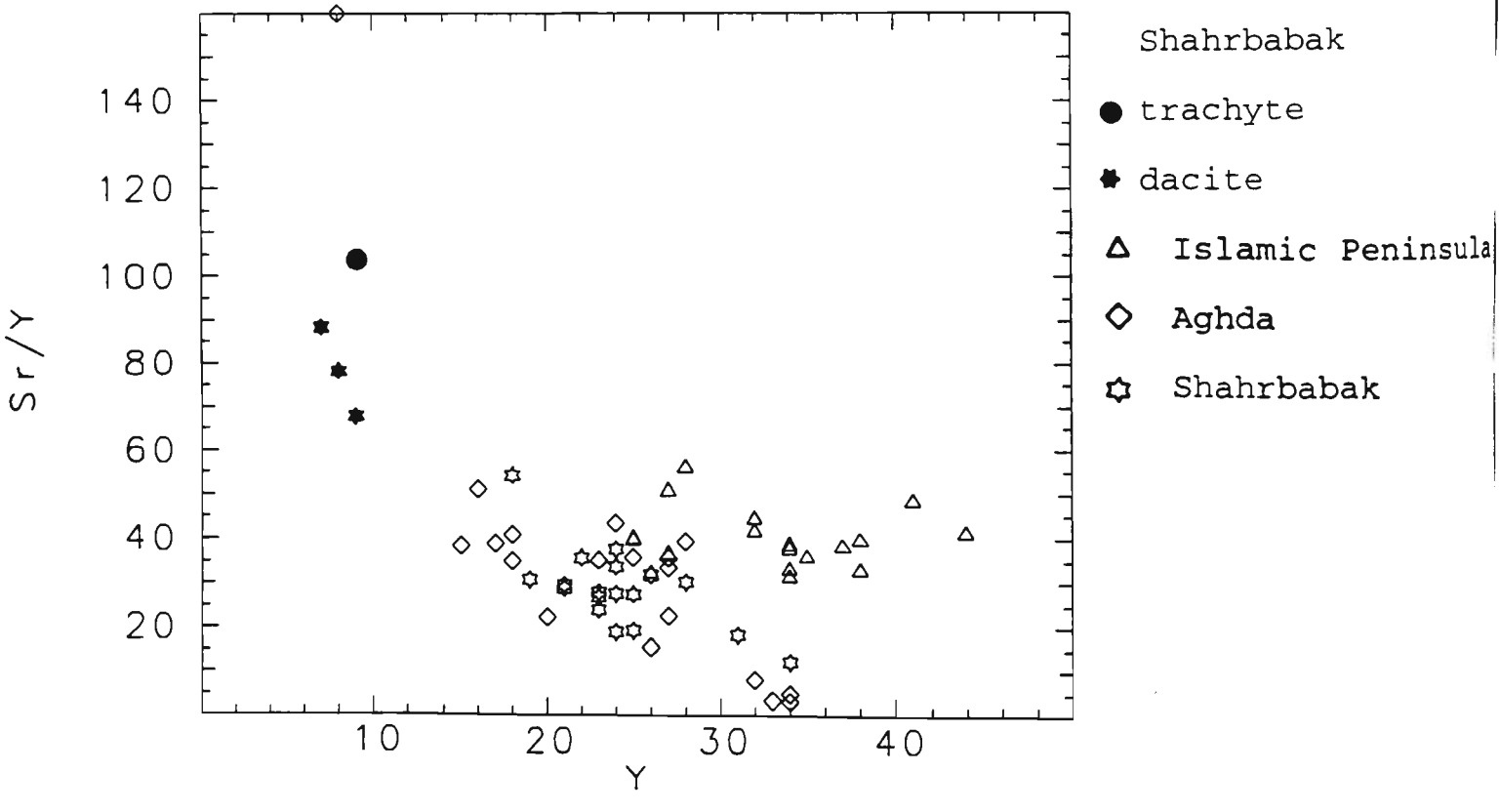

Fig 8-6. Plot of Y versus Sr/Y discrimination diagram of Defant and Drummond (1990) for rocks from the Islamic Peninsula, Aghda and Shahrbabak.

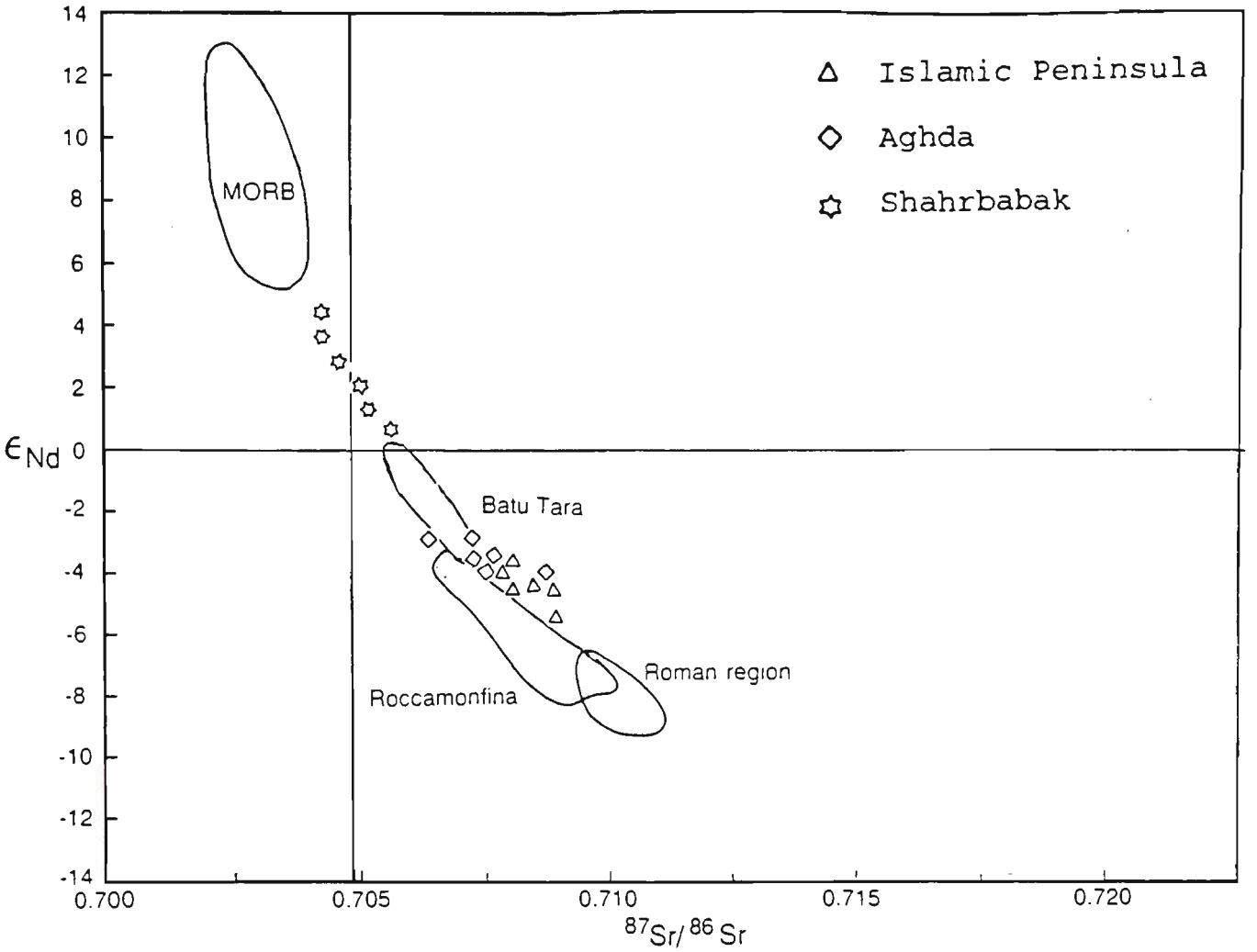

Fig. 8-7. Plot of ε_{Nd} versus $^{87}Sr/^{86}Sr$ for samples from the U-DVB, compared to the field for MORB and potassic suites: Batu Tara, Roccamonfina and Roman region (after Nelson, 1992).

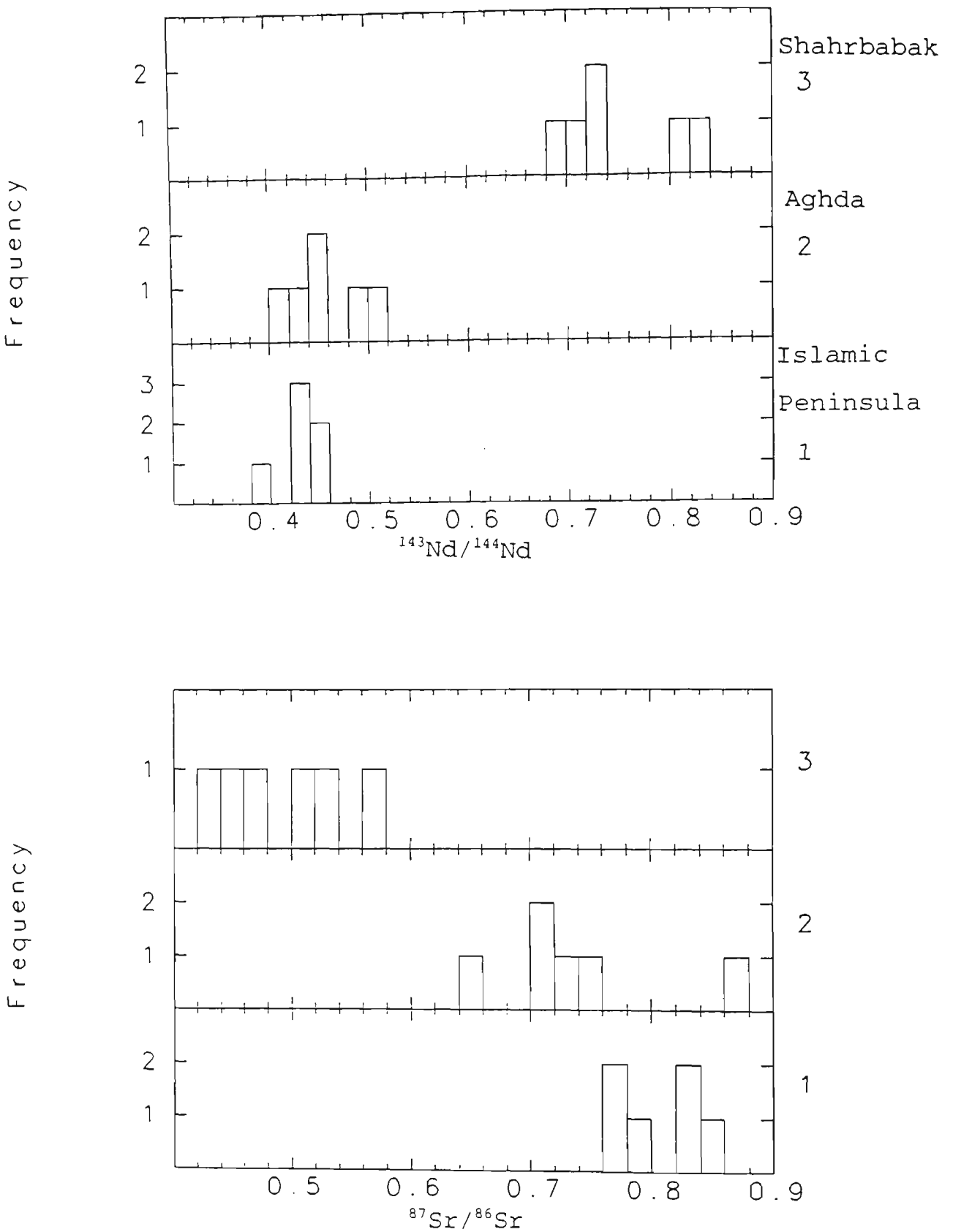

Fig 8-8. Histogram of $^{87}Sr/^{86}Sr$ and $^{143}Nd/^{144}Nd$ for Tertiary rocks from the Islamic Peninsula, Aghda and Shahrbabak.

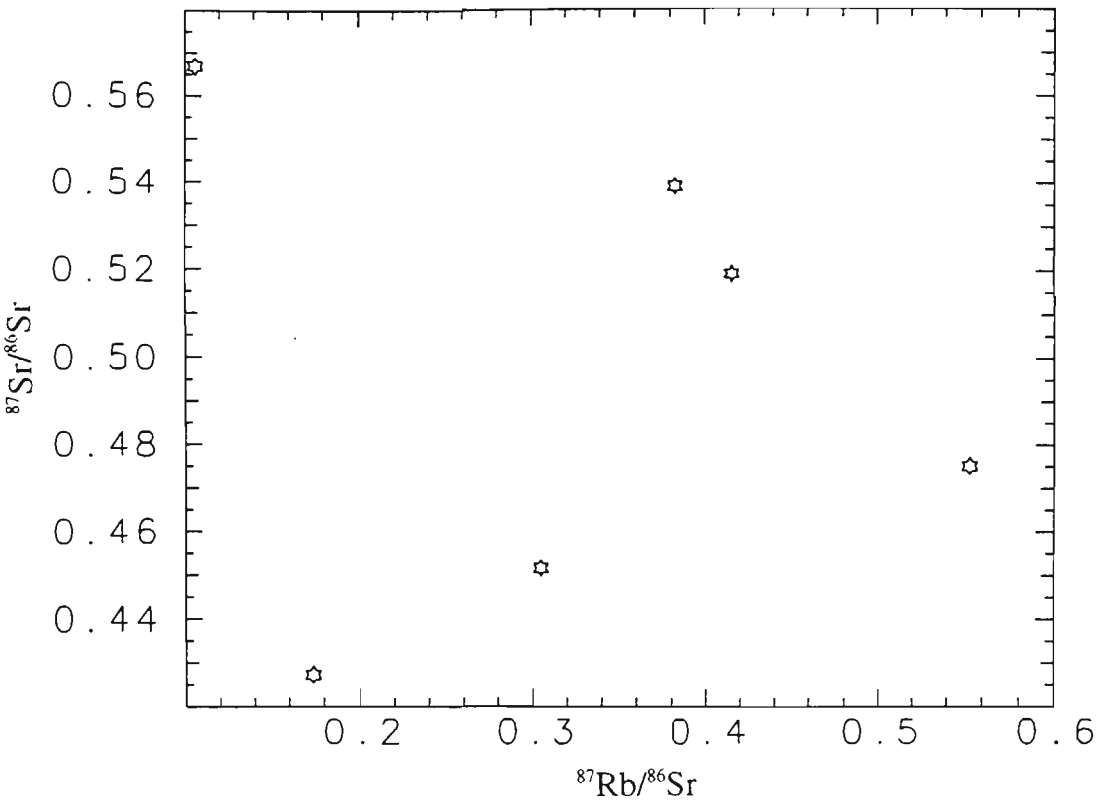

Fig 8-9. Plot of $^{87}Sr/^{86}Sr$ versus $^{87}Rb/^{86}Sr$ for samples from Shahrbabak.

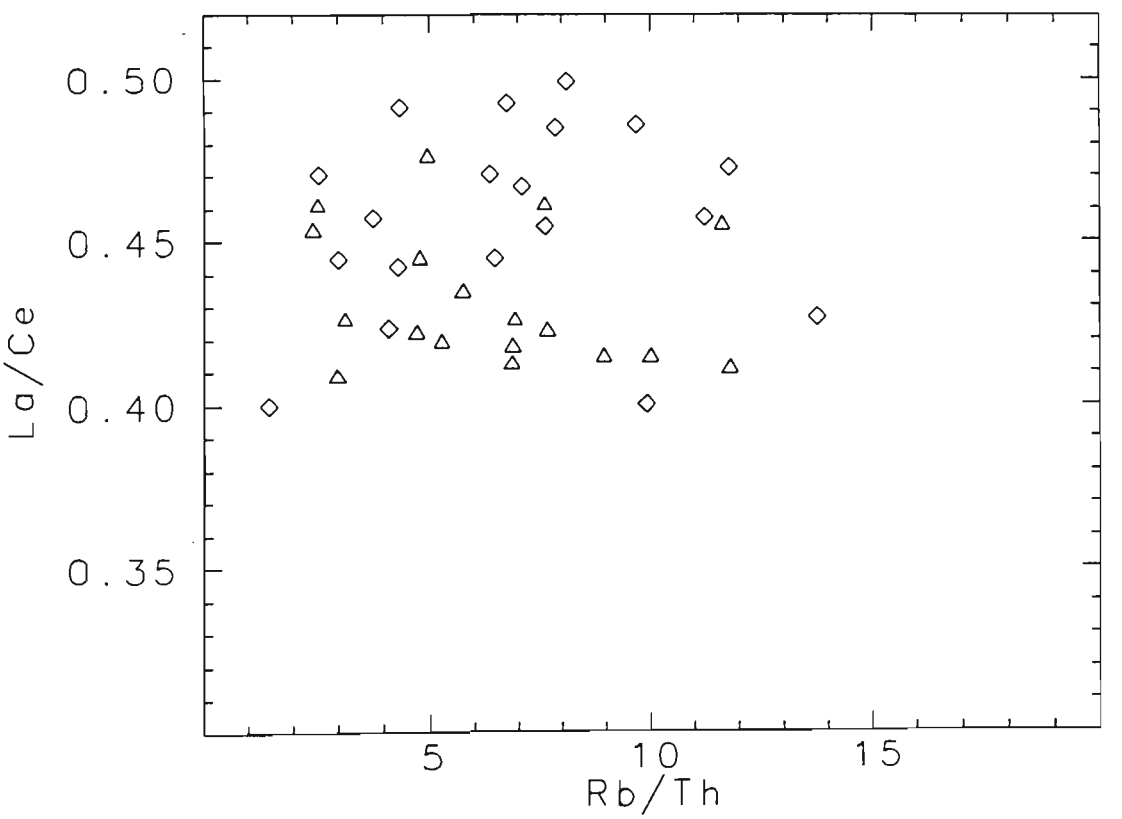

Fig. 8-10. Plot of Rb/Th versus La/Ce for samples from the Islamic Peninsula and Aghda.

Station	Location	Altitude (m)	Average Temperature (°C)			Maximum	Minimum	Average Rain fall (mm)
			January	June	Annual			
Islamic Peninsula	37° 50′ N 45° 30′ E	1349	-1.9	25.1	12.0	41.5	-25.4	328.7
Aghda	32° 14′ N 53° 13′ E	1230	6.1	31.7	18.8	45.0	-16.0	56.2
Shahrbabak	30° 28′ N 55° 5′ E	1740	3.8	26.6	15.6	40.4	-24.8	155.0

Table 1.1. Rain fall and temperature data for the three study areas (data from: Rahnemaie, 1991).

Table 3-1. Isotopic age data for igneous rocks from the U-DVB.

Sample No	Lithology	Material dated	Method	K2O	$^{40}Ar^{*}\times10^{-11}$ moles gm^{-1}	$^{40}Ar^{*}$%	Age (Ma)	Ref.
Islamic Peninsula								
R15806	trachyte	sanidine	K-Ar	9.16	8.608	24.14	6.5±1	a
-	tephrite	whole-rock	K-Ar	-	-	-	7.8±0.29	b
R15807	trachyandesite	biotite	K-Ar	8.36	9.621	12.42	8.0±2	a
R15807	trachyandesite	sanidine	K-Ar	9.72	6.966	39.72	12.1±1	a
Aghda								
R15809	trachyandesite	hornblende	K-Ar	0.91	2.058	23.62	15.7±1	a
R9061	tephriphonolite	whole-rock	K-Ar	-	-	-	23.5±1.2	c
Shahrbabak								
SH4a	rhyodacite	biotite	Ar-Ar	-	-	-	2.8±0.2	d
PQ23	andesite	hornblende	Ar-Ar	-	-	-	6.3±0.9	d
AB9	andesite	hornblende	Ar-Ar	-	-	-	6.4±0.8	d
R15813	trachyandesite	biotite	K-Ar	8.81	8.233	18.45	6.5±1	a
AB9	andesite	biotite	Ar-Ar	-	-	-	6.8±0.4	d
R15811	dacite	biotite	K-Ar	8.22	20.36	49.87	16.4±1	a
PQ14	quartz monzonite	hornblende	Ar-Ar	-	-	-	16.9±0.2	d
PQ4	quartz monzonite	hornblende	Ar-Ar	-	-	-	17.9±0.2	d
PQ4	quartz monzonite	K-feldspar	Ar-Ar	-	-	-	18.3±0.2	d
SH9	andesite	hornblende	Ar-Ar	-	-	-	19.3±0.4	d
JZ3a	tephriphonolite	analcime	Ar-Ar	-	-	-	21.3±1.7	d
JZ3a	tephriphonolite	K-feldspar	Ar-Ar	-	-	-	22.8±3.2	d
FT3	phonolite	nepheline	Ar-Ar	-	-	-	28.4±0.6	d
FT3	phonolite	-	Rb-Sr	-	-	-	28.4±1	d
FT3	phonolite	sanidine	Ar-Ar	-	-	-	29.8±0.6	d
JZ1	tephriphonolite	analcime	Ar-Ar	-	-	-	32.7±6.3	d
MD30	trachyte	albite	Ar-Ar	-	-	-	37.5±1.4	d

$^{40}Ar^{*}$ = radiogenic argon; $\lambda_{e+e'}$ = 0.581 $10^{-10}a^{-1}$; λ_{β} = 4.962 $10^{-10}a^{-1}$. K content determined by flame photometry; $^{40}K/K$ = 1.167 10^{-4} mol/mol. Ar content determined by isotope dilution (cf McDougall and Schmincke, 1977). References: (a) this study; (b) Moin-Vaziri (1985); (c) Bina et al. (1986); (d) Hassanzadeh (1993).

Component	Modal data (vol%)		Grain Size
	Mean (26)	Range	
PHENOCRYSTS			
diopside	30.4	20.0-40.2	diopside to 6.6mm mostly 2.0-4.5 mm
sanidine	7.4	1.0-24.2	
leucite	**24.8**	**2.0-37.7**	other minerals 1.0 to 2.8 mm
Fe-Ti oxide	0.3	2.2-5.0	
GROUNDMASS			
olivine	0.2	0.5-3.0	
diopside	10.3	1.5-2.0	normally 0.3 to 0.5 mm
sanidine	11.3	0.5-44.0	
leucite	9.0	0.2-30.2	range 0.02-0.8 mm
biotite	2.0	0.2-10.0	
Fe-Ti oxide	1.9	0.2-4.2	
Others: (1.8) apatite, chlorite, iddingsite, serpentine, calcite, sericite, zeolite, analcime			

Table 4-1. Petrography of tephrite from the Islamic Peninsula.

Component	Modal data (vol%)		Grain Size
	Mean (7)	Range	
PHENOCRYSTS			
diopside	27.7	27.7-37.7	diopside 1.5 to 5.9 mm mostly 1.0-4.0 mm
sanidine	8.1	1.0-24.7	
leucite	20.9	6.7-40.2	other minerals 1.0 to 4.5 mm
GROUNDMASS			
diopside	8.8	1.0-12.0	
sanidine	18.2	2.7-48.5	
leucite	6.0	0.2-37.2	normally 0.2 to 0.5 mm
olivine	1.5	0.8-2.6	range 0.02-0.8 mm
biotite	0.3	1.0-3.7	
Fe-Ti oxide	4.1	1.2-7.7	
Others: (4.5) calcite, zeolite, apatite, chlorite			

Table 4-2. Petrography of phonotephrite from the Islamic Peninsula.

Component	Modal data (vol%)		Grain Size
	Mean (2)	Range	
PHENOCRYSTS			
diopside	48.0	46.5-49.5	1.8-20.0 mm
leucite	18.2	15.0-21.4	1.0-1.6 mm
GROUNDMASS			
diopside	14.5	11.7-17.3	
leucite	9.0	7.5-10.5	normally
biotite	3.7	2.4-5.0	0.04-0.34 mm
olivine	2.0	1.0-3.0	
Fe-Ti oxide	1.7	1.4-2.0	
Others: (3.2) chlorite, calcite, apatite			

Table 4-3. Petrography of basalt from the Islamic Peninsula.

Component	Modal data (vol%)		Grain Size
	Mean (2)	Range	
PHENOCRYSTS			
diopside	7.7	7.2-8.2	1.3-3.6 mm
sanidine	9.4	2.0-16.7	2.3-25. mm
biotite	4.9	4.7-5.2	1.2-4.4 mm
GROUNDMASS			
sanidine	73.4	68.0-81.4	
Fe-Ti oxide	0.6	0.2-1.0	normally 0.01-0.6 mm
Others: (4.0) sericite, calcite			

Table 4-4. Petrography of trachyandesite from the Islamic Peninsula.

Component	Modal data (vol%)		Grain Size
	Mean (6)	Range	
PHENOCRYSTS			
diopside	7.8	0.7-17.5	1.0-2.5 mm
sanidine	9.5	1.0-21.0	1.5-8.9 mm
biotite	0.7	1.7-2.5	1.0-5.3 mm
GROUNDMASS			
diopside	2.8	1.0-6.2	normally 0.01 to 0.9 mm
sanidine	75.2	55.7-91.4	
Fe-Ti oxide	1.5	0.2-2.0	
Others: (3.0) calcite, apatite, sericite, zircon, sphene			

Table 4-5. Petrography of trachyte from the Islamic Peninsula.

Component	Modal data (vol%)		Grain Size
	Mean (5)	Range	
PHENOCRYSTS			
diopside	4.3	0.5-8.0	1.6-5.4 mm
sanidine	6.0	0.5-15.7	1.0-5.9 mm
plagioclase	9.7	4.0-19.2	2.0-5.7 mm
analcime	7.2	5.0-10.0	3.0-8.9 mm
GROUNDMASS			
diopside	1.1	0.2-2.2	normally 0.1-0.8 mm range 0.02-1.0 mm
sanidine	50.3	19.7-70.0	
analcime	12.1	16.0-56.7	
olivine	0.8	0.1-1.7	
biotite	0.5	0.3-1.3	
Fe-Ti oxide	2.1	0.2-5.5	
Others: (6.1) calcite, sericite, epidote, chlorite, apatite, zeolite, iddingsite, serpentine			

Table 4-6. Petrography of phonotephrite from Aghda.

Component	Modal data (vol%)		Grain Size
	Mean (8)	Range	
PHENOCRYSTS			
diopside	3.1	1.0-8.0	1.0-2.7 mm
sanidine	5.5	2.0-7.5	1.5-3.9 mm
plagioclase	4.5	1.5-7.0	1.0-5.9 mm
analcime*	21.8	19.2-42.2	4.3-32.0 mm
pumpellyite*	9.5	5.8-20.7	4.0-32.0 mm
GROUNDMASS			
diopside	1.4	0.2-3.0	normally 0.2-0.7 mm range 0.02-0.9 mm
sanidine	34.5	24.5-45.2	
plagioclase	13.0	4.7-20.0	
nepheline	1.0	0.8-1.3	
biotite	0.3	0.2-0.9	
olivine	1.5	0.9-2.5	
Fe-Ti oxide	1.3	0.2-2.7	
Others: (2.8) calcite, sericite, apatite, chlorite, kaoline, prehnite, zeolite			

Table 4-7. Petrography of tephriphonolite from Aghda.
* Both analcime and pumpellyite are pseudomorphs after leucite (section 5.4)

Component	Modal data (vol%)		Grain Size
	Mean (8)	Range	
PHENOCRYSTS			
diopside	3.0	2.5-11.0	1.5-3.8 mm
sanidine	8.1	1.5-17.0	2.0-7.7 mm
plagioclase	8.0	5.6-15.0	1.0-6.0 mm
analcime	11.9	2.0-10.5	1.5-3.0 mm
GROUNDMASS			
sanidine	50.9	35.0-85.0	normally 0.2 to 0.6 mm range 0.01-0.8 mm
analcime	2.1	1.2-17.7	
biotite	0.1	0.5-0.7	
Fe-Ti oxide	3.2	1.0-10.5	
Others: (12.2) calcite, sericite, epidote, apatite, zeolite, chlorite, sericite			

Table 4-8. Petrography of phonolite from Aghda.

Component	Modal data (vol%)		Grain size
	Mean (4)	Range	
PHENOCRYSTS			
diopside	6.7	2.0-10.0	2.0-4.0 mm
sanidine	9.9	7.2-12.0	1.0-3.6 mm
plagioclase	9.8	2.5-14.0	2.0-5.0 mm
nepheline	3.6	4.0-10.2	1.0-3.2 mm
GROUNDMASS			
diopside	3.1	1.0-7.7	normally 0.1 to 0.5 mm range 0.01-0.8 mm 0.3-0.7 mm
sanidine	54.9	45.0-60.5	
plagioclase	2.5	1.0-6.0	
biotite	0.3	0.1-1.0	
olivine	1.4	0.3-2.5	
Fe-Ti oxide	2.3	0.5-3.5	
Others: (5.5) calcite, sericite, cholorite, zeolite, epidote.			

Table 4-9. Petrography of basaltic trachyandesite from Aghda.

Component	Modal data (vol%)		Grain Size
	Mean (5)	Range	
PHENOCRYSTS			
hornblende	4.2	8.2-8.7	1.0-3.4 mm
sanidine	10.9	6.0-20.0	2.0-4.8 mm
plagioclase	15.1	6.2-25.0	1.5-5.0 mm
GROUNDMASS			
diopside	0.8	1.8-2.0	normally 0.2 to 0.6 mm range 0.02-0.9 mm
plagioclase	55.5	50.0-61.0	
biotite	0.1	0.1-0.7	
Fe-Ti oxide	3.6	2.0-5.0	
Others: (9.9) calcite, sericite, apatite, zeolite, kaoline			

Table 4-10. Petrography of trachyandesite from Aghda.

Coponent	Modal data (vol%)		Grain Size
	Mean (10)	Range	
PHENOCRYSTS			
diopside	0.8	1.0-4.7	1.0-2.8 mm
sanidine	13.5	0.2-38.2	1.5-6.8 mm
plagioclase	3.5	1.0-12.2	2.0-5.0 mm
nepheline	4.5	4.2-15.5	1.0-5.3 mm
GROUNDMASS			
sanidine	64.8	30.7-82.7	normally 0.3 to 0.7 mm
biotite	0.3	0.2-1.0	range 0.01-1.0 mm
Fe-Ti oxide	3.1	0.5-6.2	
Others:(9.2) calcite, epidote, chlorite, zeolite			

Table 4-11. Petrography of trachyte from Aghda.

Component	Modal data (vol%)		Grain Size
	Mean (2)	Range	
PHENOCRYSTS			
sanidine	12.5	10.7-14.2	1.5-4.0 mm
plagioclase	4.0	1.5-6.5	2.0-6.3 mm
quartz	18.0	15.5-20.5	1.5-3.5 mm
GROUNDMASS			
quartz	10.1	8.0-12.2	normally 0.3 to 0.7 mm
sanidine	52.9	29.0-76.7	
biotite	0.8	0.4-1.2	range 0.02-1.0 mm
Fe-Ti oxide	0.6	0.2-1.0	
Others: (1.3) calcite, sericite, zeolite, zircon			

Table 4-12. Petrography of rhyolite from Aghda.

Component	Modal data (vol%)		Grain Size
	Mean (6)	Range	
PHENOCRYSTS			
diopside	1.2	0.6-2.3	1.0-2.5 mm
sanidine	10.1	5.3-22.3	2.0-5.0 mm
plagioclase	10.5	8.0-16.6	1.2-5.8 mm
analcime	30.0	22.0-38.0	5.0-30.0 mm
nepheline	3.0	2.0-4.0	1.5-2.5 mm
GROUNDMASS			
diopside	1.5	0.3-4.1	normally 0.3 to 0.6 mm
sanidine	41.1	7.3-60.0	range 0.01-1.0 mm
Fe-Ti oxide	3.1	1.0-5.2	
Others: (4.4) calcite, chlorite, apatite, sericite, kaoline, epidote, zeolite			

Table 4-13. Petrography of tephriphonolite from Shahrbabak.

Component	Modal data (vol%)		Grain Size
	Mean (2)	Range	
PHENOCRYSTS			
olivine	3.0	1.5-4.5	1.3-2.8 mm
diopside	6.3	4.4-8.2	1.0-5.4 mm
plagioclase	17.7	15.4-20.0	2.0-4.6 mm
sanidine	7.5	6.5-8.5	1.0-2.5 mm
GROUNDMASS			
diopside	15.0	14.0-16.0	normally 0.1 to 0.3 mm
plagioclase	41.3	35.2-47.4	range 0.01-0.6 mm
Fe-Ti oxide	5.6	5.2-6.0	
Others: (3.3) sericite, chlorite, iddingsite, serpentine			

Table 4-14. Petrography of basalt from Shahrbabak.

Component	Modal data (vol%)		Grain Size
	Mean (2)	Range	
PHENOCRYSTS			
diopside	2.0	1.3-2.7	1.5-3.7 mm
plagioclase	19.9	3.6-36.3	1.5-2.2 mm
sanidine	1.25	0.9-1.6	1.0-2.0 mm
olivine	2.5	1.5-3.5	1.0-2.5 mm
GROUNDMASS			
diopside	3.5	0.0-7.0	normally 0.3-0.5 mm range 0.01-0.8 mm
plagioclase	53.3	29.3-77.3	
Fe-Ti oxide	7.7	7.0-8.3	
Others: (6.0) calcite, chlorite, sericite, apatite, iddingsite, serpentine			

Table 4-15. Petrography of trachybasalt from Shahrbabak.

Component	Modal data (vol%)		Grain Size
	Mean (2)	Range	
PHENOCRYST			
diopside	2.7	2.0-3.3	1.6-4.5 mm
sanidine	22.0	10.6-33.3	1.0-2.2 mm
plagioclase	9.3	7.3-11.3	2.0-4.2 mm
GROUNDMASS			
olivine	3.3	2.6-4.0	normally 0.2 to 0.7mm
sanidine	1.8	0.0-3.6	
plagioclase	41.7	40.0-43.3	range 0.01-1.0 mm
Fe-Ti oxide	5.1	3.6-6.6	
Others: (14.0) calcite, zeolite, chlorite, sericite, apatite, kaolinite, iddingsite, serpentine			

Table 4-16. Petrography of basaltic trachyandesite from Shahrbabak.

Component	Modal data (vol%)		Grain Size
	Mean (3)	Range	
PHENOCRYSTS			
hornblende	1.7	0.0-5.0	1.3-2.5 mm
diopside	0.9	0.0-2.6	1.2-1.8 mm
sanidine	13.0	1.3-23.6	1.5-3.4 mm
plagioclase	18.2	7.6-30.6	1.0-1.7 mm
GROUNDMASS			
hornblende	2.1	1.2-3.3	normally 0.4-0.7 mm range 0.01-0.9 mm
diopside	0.2	0.0-0.6	
sanidine	28.0	21.3-35.6	
plagioclase	30.4	17.0-40.3	
Fe-Ti oxide	2.9	2.3-4.0	
Others: (2.6) calcite, epidote, sericite, zeolite, chlorite, zircon, apatite			

Table 4-17. Petrography of trachyandesite from Shahrbabak.

Component	Modal data (vol%)		Grain Size
	Mean (4)	Range	
PHENOCRYSTS			
hornblende	9.7	9.3-10.0	1.3-2.8 mm
sanidine	4.3	3.0-5.6	1.8-4.9 mm
plagioclase	26.0	25.0-27.0	1.4-4.0 mm
biotite	3.2	1.3-5.0	1.0-2.3 mm
GROUNDMASS			
sanidine	55.0	52.0-61.0	normally 0.2 to 0.9 mm
Fe-Ti oxide	0.5	0.3-0.6	
Others: (1.5) zircon, apatite, calcite, sericite			

Table 4-18. Petrography of trachyte from Shahrbabak.

Component	Modal data (vol%)		Grain Size
	Mean (3)	Range	
PHENOCRYSTS			
hornblende	3.8	3.0-4.5	1.2-3.2 mm
sanidine	4.9	2.6-6.0	1.0-3.2 mm
plagioclase	20.5	16.6-25.3	1.5-4.6 mm
quartz	4.5	3.5-5.0	1.0-1.5 mm
biotite	3.6	0.5-5.8	1.2-1.8 mm
GROUNDMASS			
hornblende	3.9	5.0-5.6	normally 0.1 to 0.8 mm range 0.02-1.0 mm
sanidine	7.9	1.8-11.3	
plagioclase	30.4	15.0-49.3	
quartz	16.0	15.0-18.0	
biotite	1.4	0.7-2.3	
Fe-Ti oxide	3.5	0.6-5.5	
Others: (4.7) calcite, sericite, kaolinite, apatite, zircon			

Table 4-19. Petrography of dacite from Shahrbabak.

	Cores		Rims	
	Mean (9)	Range	Mean (13)	Range
SiO_2	50.98	48.38-53.84	50.49	45.57-52.54
TiO_2	0.75	0.20-1.22	1.09	0.43-2.37
Al_2O_3	2.00	0.62-4.98	2.48	0.62-5.19
MgO	15.03	13.12-17.75	13.20	3.97-15.53
CaO	23.86	22.97-24.67	21.86	6.49-24.70
MnO	0.14	0.04-0.25	0.17	0.05-0.29
FeO	5.40	2.82-7.32	7.84	5.02-8.27
Na_2O	0.42	0.18-0.84	**0.49**	**0.32-1.00**
K_2O	0.01	0.00-0.03	0.01	0.00-0.03
Wo	48.80	46.88-50.00	**48.74**	**47.67-50.26**
En	42.96	37.50-48.48	39.89	35.48-43.75
Fs	8.23	3.03-12.5	14.59	9.09-12.90

Table 4-20. Chemical data for pyroxene in tephrite from the Islamic Peninsula (oxides, wt%).

	Cores		Rims	
	Mean (3)	Range	Mean (3)	Range
SiO_2	50.14	49.13-51.15	48.45	47.83-48.91
TiO_2	0.87	0.47-1.18	1.35	1.16-1.59
Al_2O_3	3.13	2.61-3.98	4.32	3.70-4.82
MgO	14.35	13.50-15.30	13.28	12.96-13.77
CaO	23.24	22.98-23.45	23.18	23.02-23.37
MnO	0.16	0.08-0.26	0.19	0.21-0.61
FeO	6.30	5.61-6.99	7.26	7.17-7.32
Na_2O	0.49	0.42-0.58	0.56	0.52-0.59
K_2O	0.02	0.01-0.04	0.15	0.02-0.40
Wo	48.79	48.48-49.40	49.49	48.48-50.00
En	41.17	39.39-42.42	38.13	37.50-39.39
Fs	10.53	9.09-12.12	12.37	12.12-12.50

Table 4-21. Chemical data for pyroxene in phonotephrite from the Islamic Peninsula (oxides, wt%).

	Cores		Rims	
	Mean (3)	Range	Mean (3)	Range
SiO_2	49.68	49.00-50.53	48.45	47.89-48.83
TiO_2	0.78	0.71-0.86	1.03	0.87-1.15
Al_2O_3	3.69	2.32-4.53	4.42	3.55-5.27
MgO	13.25	13.21-13.30	12.36	11.55-13.14
CaO	21.96	21.80-22.05	21.15	20.45-22.55
MnO	0.26	0.22-0.30	0.29	0.22-0.37
FeO	9.25	8.95-9.69	10.03	8.88-11.39
Na_2O	0.40	0.38-0.41	0.43	0.36-0.50
K_2O	0.00	0.00-0.01	0.02	0.01-0.03
Wo	45.93	45.42-46.34	46.73	46.41-47.05
En	38.54	38.34-38.67	36.27	34.10-38.13
Fs	15.05	15.05-16.25	17.00	14.82-19.49

Table 4-22. Chemical data for pyroxene in phonotephrite from Aghda (oxides, wt%).

	Cores		Rims	
	Mean (6)	Range	Mean (6)	Range
SiO_2	49.48	49.05-50.30	49.92	49.74-50.07
TiO_2	0.86	0.61-0.90	0.82	0.71-0.92
Al_2O_3	3.44	2.67-4.16	2.63	2.27-3.51
MgO	12.34	11.11-13.11	12.00	10.99-12.66
CaO	22.08	21.73-22.44	22.00	21.69-22.77
MnO	0.33	0.28-0.41	0.38	0.31-0.46
FeO	10.20	9.02-12.18	10.75	9.19-12.11
Na_2O	0.47	0.39-0.55	0.48	0.43-0.52
K_2O	0.01	0.00-0.02	0.06	0.00-0.11
Wo	46.52	46.00-47.17	46.43	45.95-47.64
En	36.16	32.83-38.08	35.23	32.55-36.84
Fs	17.32	15.21-20.85	18.34	15.52-20.85

Table 4-23. Chemical data for pyroxene in tephriphonolite from Aghda (oxides, wt%).

	Cores		Rims	
	Mean (10)	Range	Mean (9)	Range
SiO_2	49.34	44.81-50.45	49.82	48.75-51.21
TiO2	0.94	0.86-1.02	0.93	0.68-1.08
Al_2O_3	3.10	2.22-5.19	2.88	1.41-4.43
MgO	12.81	10.85-13.75	12.38	9.80-13.27
CaO	22.40	21.75-24.87	22.02	21.61-22.39
MnO	0.35	0.25-0.53	0.38	0.25-0.51
FeO	9.27	8.29-11.65	9.87	8.37-12.62
Na_2O	0.50	0.43-0.76	0.53	0.44-0.84
K_2O	0.01	0.00-0.06	0.02	0.00-0.05
Wo	46.93	45.88-51.43	46.61	44.18-51.49
En	38.02	33.33-39.69	37.20	34.72-38.86
Fs	14.54	13.40-15.98	16.94	16.04-19.39

Table 4-24. Chemical data for pyroxene in tephriphonolite from Shahrbabak (oxides, wt%).

	Cores		Rims	
	Mean (6)	Range	Mean (4)	Range
SiO_2	52.18	48.89-54.24	52.48	49.93-54.02
TiO_2	0.56	0.16-1.29	0.46	0.13-1.27
Al_2O_3	1.84	0.79-3.77	1.53	0.83-3.20
MgO	16.23	14.22-18.08	16.00	14.33-17.85
CaO	24.24	23.60-24.80	24.21	24.01-24.39
MnO	0.10	0.06-0.16	0.07	0.02-0.11
FeO	3.00	1.98-6.12	3.40	2.06-6.05
Na_2O	0.28	0.19-0.54	0.26	0.17-0.35
K_2O	0.01	0.00-0.02	0.00	0.00-0.01
Wo	49.24	48.48-50.00	47.53	47.15-48.48
En	45.60	40.63-48.48	45.96	40.63-48.48
Fs	5.16	3.03-9.38	4.99	3.03-9.38

Table 4-25. Chemical data for pyroxene in basalt from the Islamic Peninsula (oxides, wt%).

	Cores		Rims	
	Mean (3)	Range	Mean (3)	Range
SiO_2	51.69	50.64-53.06	50.75	50.22-51.72
TiO_2	0.35	0.27-0.48	0.68	0.57-0.89
Al_2O_3	1.57	0.84-2.44	2.38	1.96-2.65
MgO	13.57	12.74-15.20	13.61	12.04-16.09
CaO	23.71	23.00-24.12	23.42	23.21-23.69
MnO	0.25	0.17-0.31	0.20	0.13-0.27
FeO	7.26	5.03-8.60	7.45	4.45-9.16
Na_2O	0.62	0.53-0.75	0.57	0.32-0.70
K_2O	0.01	0.00-0.03	0.02	0.00-0.05
Wo	48.99	48.48-50.00	49.52	48.48-51.61
En	38.76	36.36-42.42	39.10	35.48-45.45
Fs	12.25	9.09-15.15	11.37	6.06-15.15

Table 4-26. Chemical data for pyroxene in trachyandesite from the Islamic Peninsula (oxides, wt%).

	Cores		Rims	
	Mean (4)	Range	Mean (4)	Range
SiO_2	48.77	47.61-50.05	48.87	47.71-49.62
TiO_2	0.97	0.68-1.44	0.95	0.81-1.11
Al_2O_3	3.47	2.79-4.42	3.86	2.80-4.96
MgO	12.18	11.29-13.21	12.00	11.24-12.91
CaO	21.66	21.49-21.78	21.78	21.40-22.00
MnO	0.34	0.31-0.37	0.38	0.22-0.47
FeO	10.00	9.18-11.39	10.50	9.47-10.45
Na_2O	0.47	0.41-0.53	0.58	0.38-0.94
K_2O	0.00	0.00-0.00	0.01	0.00-0.03
Wo	46.23	45.79-46.88	46.45	45.59-47.06
En	35.86	33.78-38.63	36.37	34.31-37.75
Fs	17.92	15.58-19.23	17.19	16.07-18.72

Table 4-27. Chemical data for pyroxene in basaltic trachy-andesite from Aghda (oxides, wt%).

	Cores		Rims	
	Mean (4)	Range	Mean (4)	Range
SiO_2	50.65	49.24-51.46	49.13	47.16-51.46
TiO_2	0.70	0.51-1.10	1.03	0.51-1.52
Al_2O_3	3.98	3.28-5.32	4.55	3.28-5.86
MgO	15.42	14.66-15.86	13.67	11.10-15.59
CaO	22.01	21.30-22.62	21.83	21.54-22.62
MnO	0.11	0.06-0.16	0.20	0.10-0.34
FeO	5.75	5.03-6.40	7.43	5.03-10.74
Na_2O	0.42	0.37-0.48	0.66	0.37-0.91
K_2O	0.00	0.00-0.02	0.01	0.00-0.02
Wo	45.82	45.42-46.65	46.65	43.50-52.56
En	44.64	44.30-45.65	40.63	37.67-41.70
Fs	9.53	8.70-10.29	12.73	9.77-14.80

Table 4-28. Chemical data for pyroxene in trachybasalt from Shahrbabak (oxides, wt%).

	Mean (4)	Minimum	Maximum
SiO_2	46.92	46.33	47.62
TiO_2	1.00	0.09	1.09
Al_2O_3	6.44	5.36	7.07
MgO	12.85	12.51	13.39
CaO	21.50	21.35	21.70
MnO	0.22	0.17	0.26
FeO	8.66	8.10	9.15
Na_2O	0.43	0.34	0.52
K_2O	0.01	0.00	0.03
Wo	46.37	45.52	47.23
En	38.78	38.49	39.07
Fs	14.85	14.28	15.41

Table 4-29. Chemical data for pyroxene in basalt from Sahrbabak (oxides, wt%).

	Phenocrysts		
	Mean (4)	Minimum	Maximum
SiO_2	64.50	64.14	64.71
TiO_2	0.11	0.09	0.14
Al_2O_3	18.97	18.80	19.29
MgO	0.00	0.00	0.02
CaO	0.50	0.22	0.85
MnO	0.02	0.00	0.05
FeO	0.47	0.37	0.60
Na_2O	4.75	4.16	5.25
K_2O	9.68	8.81	10.57
An	3.01	1.31	5.00
Ab	29.60	25.62	32.79
Or	67.40	62.77	72.91

Table 4-30. Chemical data for sanidine in trachyandesite from the Islamic Peninsula (oxides, wt%).

	Mean (2)	Core	Rim
SiO_2	64.47	63.97	64.97
TiO_2	0.06	0.04	0.07
Al_2O_3	19.17	18.69	19.65
MgO	0.01	0.00	0.02
CaO	0.63	0.52	0.73
MnO	0.00	0.00	0.00
FeO	0.48	0.41	0.54
Na_2O	0.02	0.00	0.03
K_2O	11.61	11.13	12.08
An	3.56	2.88	4.23
Ab	20.26	19.36	21.15
Or	76.21	74.65	77.76

Table 4-31. Chemical data for sanidine in phonotephrite from Aghda (oxides, wt%).

	Mean (14)	Minimum	Maximum
SiO_2	62.61	60.46	64.30
TiO_2	0.03	0.00	0.14
Al_2O_3	18.82	18.12	20.86
MgO	0.03	0.00	0.24
CaO	0.25	0.00	0.61
MnO	0.01	0.00	0.08
FeO	0.16	0.00	0.54
Na_2O	1.01	0.19	3.28
K_2O	14.88	11.33	16.17
An	1.35	0.00	6.19
Ab	5.74	0.99	19.29
Or	92.91	74.57	98.11

Table 4-32. Chemical data for sanidine in tephriphonolite from Aghda(oxides, wt%).

	Mean (3)	Minimum	Maximum
SiO_2	63.43	61.36	64.60
TiO_2	0.12	0.10	0.15
Al_2O_3	18.80	16.52	20.25
MgO	0.59	0.00	1.77
CaO	2.00	1.08	3.22
FeO	0.86	0.26	1.99
Na_2O	5.89	4.32	7.32
K_2O	6.60	5.27	7.40
An	9.79	8.03	16.20
Ab	51.46	39.40	62.43
Or	38.75	31.54	44.40

Table 4-33. Chemical data for sanidine in basalt from Shahrbabak (oxides, wt%).

	Mean (3)	Minimum	Maximum
SiO_2	62.78	62.05	63.54
TiO_2	0.05	0.01	0.10
Al_2O_3	19.15	18.74	19.54
MgO	0.01	0.00	0.02
CaO	0.66	0.41	0.83
MnO	0.02	0.00	0.05
FeO	0.20	0.13	0.31
Na_2O	2.67	1.84	3.19
K_2O	12.31	11.24	14.27
An	4.09	3.17	4.86
Ab	15.81	10.11	19.37
Or	80.42	76.35	87.74

Table 4-34. Chemical data for sanidine in basaltic trachy-andesite from Aghda (oxides, wt%).

	Mean (3)	Minimum	Maximum
SiO_2	65.44	64.97	66.26
TiO_2	0.03	0.00	0.09
Al_2O_3	18.28	18.16	18.35
MgO	0.02	0.00	0.03
CaO	0.12	0.01	0.28
FeO	0.17	0.06	0.31
Na_2O	2.40	0.79	4.82
K_2O	13.13	9.73	15.61
An	0.59	0.00	1.36
Ab	21.33	7.10	42.37
Or	78.08	56.27	92.90

Table 4-35. Chemical data for sanidine in trachyandesite from Shahrbabak(oxides, wt%).

	Mean (12)	Minimum	Maximum
SiO_2	64.34	61.75	65.17
TiO_2	0.04	0.00	0.10
Al_2O_3	18.80	18.21	19.60
MgO	0.05	0.00	0.48
CaO	0.48	0.09	1.76
MnO	0.02	0.00	0.10
FeO	0.20	0.05	0.27
Na_2O	2.44	0.50	4.01
K_2O	12.88	10.90	15.47
An	2.38	0.48	8.94
Ab	21.69	4.65	35.07
Or	75.93	62.72	93.80

Table 4-36. Chemical data for sanidine in tephriphonolite from Shahrbabak(oxides, wt%).

	Cores		rims	
	Mean (10)	Range	Mean (4)	Range
SiO_2	53.67	52.11-54.74	68.42	67.51-69.03
TiO_2	0.06	0.04-0.10	0.06	0.03-0.11
Al_2O_3	28.05	27.27-29.00	20.12	19.68-20.65
MgO	0.00	0.00-0.00	0.00	0.00-0.00
CaO	11.16	10.24-12.15	1.02	0.80-1.63
FeO	0.56	0.45-0.68	0.14	0.08-0.28
Na_2O	4.70	4.16-5.24	9.74	8.01-10.67
k_2O	0.73	0.41-1.25	1.45	0.11-5.05
An	54.41	49.53-59.19	5.06	3.90-8.44
Ab	41.37	37.15-46.15	86.87	67.94-95.40
Or	4.22	2.39-7.18	8.16	0.68-28.16

Table 4-37. Chemical data for plagioclase in tephriphonolite from Shahrbabak (oxides, wt%).

	Cores		Rims	
	Mean (2)	Range	Mean (3)	Range
SiO_2	46.29	46.17-46.41	53.11	49.59-55.42
TiO_2	0.03	0.02-0.04	0.05	0.02-0.06
Al_2O_3	32.92	32.63-33.21	25.94	22.26-30.54
MgO	0.00	0.00-0.00	0.17	0.00-0.52
CaO	17.03	16.75-17.31	9.87	6.85-14.24
FeO	0.79	0.71-0.87	0.94	0.32-1.41
Na_2O	1.84	1.67-2.01	3.90	2.65-5.85
K_2O	0.12	0.12-0.12	0.20	0.07-0.38
An	83.06	81.56-84.55	57.47	38.31-70.55
Ab	16.25	14.75-17.74	41.21	28.65-59.2
Or	0.70	0.70-0.71	1.32	0.67-2.49

Table 4-38. Chemical data for plagioclase in basalt from Shahrbabak (oxides, wt%).

	Mean (2)	Core	Rim
SiO_2	67.40	67.11	67.68
TiO_2	0.02	0.03	0.01
Al_2O_3	19.84	20.09	19.59
MgO	0.01	0.01	0.00
CaO	0.78	1.07	0.48
MnO	0.02	0.00	0.03
FeO	0.11	0.06	0.16
Na_2O	11.17	11.09	11.24
K_2O	0.12	0.07	0.17
An	6.19	8.45	3.92
Ab	92.73	90.98	94.74
Or	1.12	1.60	0.63

Table 4-39. Chemical data for plagioclase in tephriphonolite from Aghda(oxides, wt%).

	Mean (24)	Minimum	Maximum
SiO_2	60.98	54.99	64.07
TiO_2	0.08	0.08	0.08
Al_2O_3	25.00	23.38	26.94
MgO	0.08	0.08	0.08
CaO	5.59	4.25	7.77
FeO	0.17	0.09	0.26
Na_2O	8.56	6.93	8.73
K_2O	0.69	0.52	0.87
An	27.83	24.18	31.48
Ab	68.67	64.81	72.53
Or	3.50	3.30	3.70

Table 4-40. Chemical data for plagioclase in trachyte from Shahrbabak(oxides, wt%).

	Cores		Rims	
	Mean (3)	Range	Mean (3)	Range
SiO_2	51.78	51.15-52.67	56.75	51.28-66.70
TiO_2	0.03	0.01-0.06	0.03	0.03-0.04
Al_2O_3	29.18	28.44-29.67	26.01	19.96-29.37
MgO	0.00	0.00-0.00	0.00	0.00-0.00
CaO	12.52	11.88-12.96	8.73	0.81-13.09
MnO	0.00	0.00-0.00	0.01	0.00-0.03
FeO	0.58	0.55-0.61	0.55	0.31-0.77
Na_2O	3.68	3.43-4.03	6.33	3.60-11
K_2O	0.94	0.71-1.16	0.46	0.19-0.72
An	71.81	68.20-74.04	50.45	6.55-74.11
Ab	21.95	20.52-24.04	46.34	21.16-91.69
Or	6.26	4.73-7.75	3.21	1.75-4.73

Table 4-41. Chemical data for plagioclase in phonotephrite from Aghda (oxides, wt%).

	Cores		Rims	
	Mean (3)	Range	Mean (2)	Range
SiO_2	58.66	54.26-66.26	65.05	64.81-65.28
TiO_2	0.03	0.00-0.05	0.08	0.06-0.10
Al_2O_3	24.99	20.56-27.53	20.41	19.90-20.92
MgO	0.00	0.00-0.01	0.03	0.00-0.05
CaO	7.04	1.04-10.51	1.34	0.92-1.75
MnO	0.02	0.00-0.05	0.02	0.00-0.04
FeO	0.33	0.09-0.51	0.26	0.23-0.28
Na_2O	6.73	4.90-9.53	9.43	8.45-10.40
K_2O	1.23	0.63-1.98	2.21	0.38-4.03
An	43.03	7.88-62.37	9.96	6.42-13.50
Ab	47.19	30.18-74.71	72.10	61.04-83.17
Or	9.78	4.47-17.35	17.96	3.37-32.54

Table 4-42. Chemical data for feldspar in basaltic trachy-andesite from Aghda (oxides, wt%).

	Cores		Rims	
	Mean (3)	range	Mean (3)	Range
SiO_2	55.93	54.68-57.12	63.01	56.46-67.64
TiO_2	0.04	0.02-0.07	0.05	0.03-0.08
Al_2O_3	26.78	25.98-27.73	22.84	20.99-26.36
MgO	0.00	0.00-0.00	0.00	0.00-0.01
CaO	9.56	8.48-10.67	4.36	1.63-8.75
MnO	0.03	0.01-0.06	0.00	0.00-0.00
FeO	0.45	0.39-0.55	0.28	0.06-0.40
Na_2O	5.38	4.93-5.72	8.16	5.70-9.75
K_2O	1.14	0.94-1.42	1.11	0.51-1.51
An	46.27	41.31-51.51	21.2	8.21-42.48
Ab	47.12	43.11-50.44	72.38	50.04-88.67
Or	6.60	5.38-8.25	6.41	3.11-8.64

Table 4-43. Chemical data for plagioclase in trachyandesite from Shahrbabak (oxides, wt%).

	Cores		Rims	
	Mean (3)	Range	Mean (3)	Range
SiO_2	57.90	52.87-63.13	57.21	54.52-62.54
TiO_2	0.14	0.10-0.19	0.15	0.11-0.20
Al_2O_3	26.09	21.12-28.82	25.43	21.54-27.57
MgO	0.00	0.00-0.00	0.00	0.00-0.00
CaO	7.40	2.97-11.86	8.05	3.86-10.27
FeO	0.99	0.62-1.30	0.78	0.55-0.98
Na_2O	6.20	4.66-7.51	6.17	5.25-7.76
K_2O	1.47	0.25-3.31	1.02	0.35-2.33
An	36.27	14.50-57.55	39.56	18.71-50.20
Ab	55.17	40.95-66.32	54.55	47.60-67.87
Or	8.55	1.50-19.18	5.90	2.06-13.43

Table 4-44. Chemical data for plagioclase in trachybasalt from Shahrbabak (oxides, wt%).

	Cores		Rims	
	Mean (2)	Range	Mean (4)	Range
SiO_2	60.31	59.61-61.01	60.97	59.58-62.40
TiO_2	0.02	0.02-0.02	0.01	0.00-0.03
Al_2O_3	24.10	23.55-24.65	23.75	23.02-24.52
MgO	0.00	0.00-0.00	0.00	0.00-0.00
CaO	5.85	5.14-6.57	5.48	4.54-6.62
Feo	0.13	0.12-0.14	0.15	0.12-0.18
Na_2O	7.92	7.62-8.23	8.09	7.73-8.48
k_2O	0.6	0.43-0.77	0.63	0.47-0.79
An	27.98	24.48-31.48	26.25	21.81-29.91
Ab	68.61	66.06-71.16	70.14	66.20-73.78
Or	3.41	2.46-4.36	3.62	2.65-4.54

Table 4-45. Chemical data for plagioclase in dacite from Shahrbabak (oxides, wt%).

	Core		
	Mean (2)	Range	Rim
SiO_2	39.74	39.44-40.03	39.53
TiO_2	0.04	0.02-0.06	0.05
Al_2O_3	0.03	0.02-0.04	0.05
Cr_2O_3	0.03	0.01-0.05	0.04
MgO	45.13	45.05-45.21	44.64
CaO	0.61	0.60-0.61	0.61
MnO	0.43	0.42-0.43	0.42
FeO	14.39	14.30-14.48	14.62
NiO	0.09	0.09-0.09	0.10
Na_2O	0.02	0.01-0.03	0.00
K_2O	0.01	0.01-0.01	0.01
Fo	84.85	84.00-85.71	84.00
Fa	15.15	14.29-16.00	16.00

Table 4-46. Chemical data for olivine in tephrite from the Islamic Peninsula (oxides, wt%).

	Cores		Rims	
	Mean (3)	Range	Mean (5)	Range
SiO_2	39.67	39.54-39.85	39.46	39.28-39.65
TiO_2	0.04	0.03-0.07	0.01	0.00-0.03
Al_2O_3	0.01	0.00-0.02	0.02	0.00-0.03
Cr2O3	0.04	0.00-0.07	0.02	0.00-0.04
MgO	45.88	45.48-46.51	45.39	45.18-45.70
CaO	0.18	0.13-0.22	0.19	0.13-0.23
Mno	0.51	0.34-0.61	0.55	0.47-0.60
FeO	13.73	13.47-13.95	14.16	13.93-14.41
NiO	0.20	0.08-0.39	0.21	0.11-0.30
Na_2O	0.02	0.01-0.03	0.01	0.00-0.03
K_2O	0.01	0.00-0.02	0.00	0.00-0.00
Fo	85.62	85.31-86.02	85.10	84.83-85.25
Fa	14.42	13.98-14.83	14.90	14.75-15.17

Table 4-47. Chemical data for olivine in trachybasalt from Shahrbabak (oxides, wt%).

	Mean (2)	Core	Rim
SiO_2	37.26	37.01	37.51
TiO_2	0.00	0.00	0.00
Al_2O_3	0.03	0.03	0.03
Cr_2O_3	0.00	0.00	0.00
MgO	36.09	36.00	36.07
CaO	0.29	0.31	0.27
MnO	0.53	0.46	0.60
FeO	25.07	24.97	25.18
Ni	0.04	0.00	0.07
Na_2O	0.01	0.01	0.01
K_2O	0.01	0.02	0.02
Fo	71.96	72.06	71.85
Fa	28.05	27.94	28.15

Table 4-48. Chemical data for olivine in basalt from Shahrbabak (oxides, wt%).

$Mg/Mg+Fe^{2+}$							
				Calculated equilibrium liquid			
Sample	Grain	Spot	Olivine	Kd=0.3	Kd=0.4	whole Rock A	whole Rock B
Basalt							
R14527	1	core	0.72	0.43	0.51	0.52	0.49
R14527	1	rim	0.72	0.44	0.51		
Trachybasalt							
R15812	3	core	0.86	0.65	0.71		
R15812	3	core	0.85	0.64	0.70		
R15812	1	rim	0.85	0.64	0.70		
R15812	1	rim	0.85	0.63	0.69	0.69	0.67
R15812	1	rim	0.85	0.63	0.69		
R15812	1	rim	0.85	0.63	0.70		
R15812	1	rim	0.85	0.63	0.70		

Table 4-49. comparison of $Mg/Mg+Fe^{2+}$ for olivine, calculated equilibrium liquids and host basalt and trachybasalt for Shahrbabak. For whole rock A and B, FeO = 0.8 and 0.9 total Fe as FeO respectively.

$Mg/Mg+Fe^{2+}$							
				Calculated equilibrium liquid			
Sample	Grain	Spot	Olivine	Kd=0.3	Kd=0.4	whole rock A	whole rock B
R14466	1	core	0.85	0.63	0.69	0.69	0.67
R14466	1	rim	0.84	0.62	0.69		
R14466	1	core	0.85	0.63	0.69		

Table 4-50. comparison of $Mg/Mg+Fe^{2+}$ for olivines, calculated equilibrium liquids and host tephrite for the Islamic Peninsula. For whole rock A and B, FeO = 0.80 and 0.90 total Fe as FeO respectively.

	Mean (4)	Minimum	Maximum
SiO_2	36.13	35.92	36.33
TiO_2	4.58	4.48	4.73
Al_2O_3	13.95	13.84	14.12
MgO	15.17	14.52	16.09
CaO	0.07	0.07	0.07
MnO	0.14	0.10	0.22
FeO	15.03	13.50	16.18
Na_2O	0.37	0.29	0.43
K_2O	8.69	8.46	8.89

Table 4-51. Chemical data for biotite in trachyte from Shahrbabak (oxides, wt%).

	Mean (4)	Minimum	Maximum
SiO_2	36.63	36.05	37.23
TiO_2	3.82	3.58	3.95
Al_2O_3	13.85	13.81	13.93
MgO	13.80	13.06	14.35
CaO	0.16	0.06	0.23
MnO	0.15	0.07	0.24
FeO	14.55	13.34	16.63
Na_2O	0.51	0.39	0.56
K_2O	8.14	7.96	8.43

Table 4-52. Chemical data for biotite in dacite from Shahrbabak (oxides, wt%).

	Phenocrysts		
	Mean (5)	Minimum	Maximum
SiO_2	37.12	35.66	38.28
TiO_2	4.05	3.54	4.73
Al_2O_3	13.41	12.13	14.98
MgO	15.32	12.20	18.42
CaO	0.02	0.00	0.08
MnO	0.33	0.28	0.36
FeO	13.55	10.96	15.87
Na_2O	0.72	0.62	1.20
K_2O	9.18	8.69	9.46

Table 4-53. Chemical data for biotite in trachyandesite from the Islamic Peninsula(oxides, wt%).

	Mean (4)	Minimum	Maximum
SiO_2	0.11	0.09	0.15
TiO_2	2.46	1.84	3.07
Al_2O_3	1.36	0.76	2.76
MgO	1.09	1.03	1.20
CaO	0.07	0.06	0.09
MnO	0.34	0.22	0.61
FeO	84.08	81.44	85.58
Na_2O	0.20	0.20	0.21
K_2O	0.05	0.05	0.05

Table 4-54. Chemical data for magnetite in trachyte from Shahrbabak (oxides, wt%).

	Mean (3)	Minimum	Maximum
SiO_2	1.87	1.38	2.53
TiO_2	1.95	0.93	3.51
Al_2O_3	0.65	0.44	1.01
MgO	0.03	0.02	0.05
CaO	0.29	0.16	0.53
MnO	0.56	0.54	0.59
FeO	83.12	80.79	84.81
Na_2O	0.05	0.01	0.08
K_2O	0.03	0.00	0.04

Table 4-55. Chemical data for magnetite in trachyandesite from Shahrbabak (oxides, wt%).

	Mean (7)	Minimum	Maximum
SiO_2	0.12	0.04	0.26
TiO_2	9.88	8.54	11.86
Al_2O_3	1.58	0.33	4.61
MgO	1.01	0.02	1.86
CaO	0.13	0.00	0.52
MnO	1.14	0.60	1.94
FeO	77.09	71.65	79.80
Na_2O	0.12	0.00	0.74
K_2O	0.02	0.00	0.03

Table 4-56. Chemical data for titanomagnetite in tephrite from the Islamic Peninsula (oxides, wt%).

	Mean (3)	Minimum	Maximum
SiO_2	0.11	0.08	0.14
TiO_2	8.46	7.44	10.01
Al_2O_3	2.03	0.85	2.72
MgO	3.18	1.76	4.82
CaO	0.39	0.34	0.49
MnO	0.87	0.58	1.07
FeO	75.64	75.30	76.10
Na_2O	0.01	0.00	0.02
K_2O	0.02	0.01	0.04

Table 4-57. Chemical data for titanomagnetite in basalt from the Islamic Peninsula (oxides, wt%).

	Mean (2)	Minimum	Maximum
SiO_2	0.11	0.09	0.12
TiO_2	7.51	7.36	7.66
Al_2O_3	4.76	4.67	4.85
MgO	4.76	4.11	5.41
CaO	0.10	0.06	0.14
MnO	0.68	0.61	0.75
FeO	74.27	73.76	74.78
Na_2O	0.02	0.00	0.04
K_2O	0.02	0.00	0.04

Table 4-58. Chemical data for titanomagnetite in phonotephrite from the Islamic Peninsula (oxides, wt%).

	Mean (3)	Minimum	Maximum
SiO_2	0.36	0.06	0.69
TiO_2	6.94	5.97	7.63
Al_2O_3	0.69	0.65	0.74
MgO	0.76	0.73	0.81
CaO	0.06	0.04	0.08
MnO	1.45	1.35	1.56
FeO	79.10	78.16	79.99
Na_2O	0.04	0.03	0.05
K_2O	0.11	0.03	0.19

Table 4-59. Chemical data for titanomagnetite in trachyandesite from the Islamic Peninsula (oxides, wt%).

	Mean (2)	Minimum	Maximum
SiO_2	0.05	0.01	0.09
TiO_2	15.10	3.08	27.13
Al_2O_3	0.95	0.26	1.64
MgO	0.71	0.68	0.75
CaO	0.07	0.06	0.08
MnO	0.49	0.35	0.63
FeO	72.16	62.69	81.64
Na_2O	0.02	0.00	0.05
K_2O	0.02	0.02	0.02

Table 4-60. Chemical data for titanomagnetite in dacite from Shahrbabak (oxides, wt%).

	Cores		Rims	
	Mean (3)	Range	Mean (2)	Range
SiO_2	0.46	0.11-0.91	0.27	0.14-0.39
TiO_2	15.43	10.81-18.40	17.11	16.06-18.16
Al_2O_3	1.64	0.95-1.70	1.93	1.67-2.18
MgO	0.01	0.00-0.02	0.02	0.01-0.03
CaO	0.41	0.19-0.66	0.39	0.23-0.54
MnO	1.02	0.24-1.43	1.03	0.87-1.19
FeO	73.41	69.16-80.14	70.53	70.03-71.02
Na_2O	0.03	0.00-0.06	0.05	0.03-0.07
K_2O	0.04	0.03-0.05	0.07	0.06-0.08

Table 4-61. Chemical data for titanomagnetite in phonotephrite from Aghda (oxides, wt%).

	Mean (12)	Minimum	Maximum
SiO_2	1.80	0.08	2.12
TiO_2	15.41	4.44	20.88
Al_2O_3	2.31	0.60	5.25
MgO	0.19	0.00	0.67
CaO	1.47	0.00	16.12
MnO	0.89	0.00	2.33
FeO	69.16	38.01	80.89
Na_2O	0.03	0.00	0.06
K_2O	0.07	0.00	0.17

Table 4-62. Chemical data for titanomagnetite in tephriphonolite from Aghda (oxides, wt%).

	Cores		Rims	
	Mean (2)	Range	Mean (2)	Range
SiO_2	3.21	3.16-3.25	1.94	1.57-2.31
TiO_2	15.56	11.96-19.15	16.39	15.09-17.69
Al_2O_3	0.72	0.70-0.74	0.69	0.60-0.77
MgO	0.00	0.00-0.00	0.02	0.00-0.04
CaO	3.00	2.81-3.18	1.71	1.46-1.96
MnO	0.64	0.44-0.84	1.42	0.82-2.01
FeO	66.79	63.89-69.68	68.41	66.36-70.46
Na_2O	0.01	0.00-0.02	0.00	0.00-0.00
K_2O	0.00	0.00-0.00	0.01	0.00-0.01

Table 4-63. Chemical data for titanomagnetite in basaltic trachyandesite from Aghda (oxides, wt%).

	Mean (3)	Minimum	Maximum
SiO_2	0.04	0.02	0.06
TiO_2	8.67	7.96	9.43
AL_2O_3	2.55	2.44	2.71
MgO	5.06	4.61	5.40
CaO	0.04	0.00	0.11
MnO	0.74	0.58	1.00
FeO	75.15	73.96	75.77
Na_2O	0.01	0.00	0.04
K_2O	0.01	0.00	0.02

Table 4-64. Chemical data for titanomagnetite in trachybasalt from Shahrbabak (oxides, wt%).

	Mean (3)	Minimum	Maximum
SiO_2	0.31	0.11	0.69
TiO_2	9.73	8.02	11.14
Al_2O_3	6.81	4.96	9.41
MgO	1.86	0.39	2.94
CaO	0.04	0.00	0.09
MnO	1.00	0.48	1.94
FeO	71.12	70.52	71.96
Na_2O	0.01	0.00	0.02
K_2O	0.01	0.00	0.02

Table 4-65. Chemical data for titanomagnetite in basalt from Shahrbabak (oxides, wt%).

	Mean (9)	Minimum	Maximum
SiO_2	0.92	0.06	3.23
TiO_2	17.18	13.62	21.22
Al_2O_3	1.16	0.32	1.97
MgO	0.05	0.00	0.11
CaO	0.52	0.00	1.65
MnO	1.99	0.50	3.97
FeO	69.37	65.71	71.30
Na_2O	0.02	0.00	0.09
K_2O	0.04	0.00	0.09

Table 4-66. Chemical data for titanomagnetite in tephriphonolite from Shahrbabak (oxides, wt%).

	Mean (5)	Minimum	Maximum
SiO_2	45.25	44.31	46.23
TiO_2	1.37	1.19	1.73
Al_2O_3	7.90	7.38	8.61
MgO	14.28	13.89	14.67
CaO	11.21	11.09	11.28
MnO	0.30	0.25	0.34
FeO	13.30	12.86	13.64
Na_2O	1.61	1.39	1.86
K_2O	0.63	0.55	0.72
	Structural formulae (23 oxygens)		
Si	7.10	6.99	7.22
Ti	0.16	0.14	0.21
Al	2.19	2.05	2.39
Fe	1.74	1.67	1.78
Mn	0.04	0.03	0.05
Mg	3.36	3.29	3.44
Ca	1.71	1.01	1.89
Na	0.43	0.19	0.57
K	0.13	0.11	0.14

Table 4-67. Chemical data for amphibole phenocrysts in trachyte from Shahrbabak (oxides, wt%).

	Mean (4)	Minimum	Maximum
SiO_2	44.34	43.88	45.30
TiO_2	1.61	1.25	2.20
Al_2O_3	9.40	8.09	10.41
MgO	13.57	12.70	14.47
CaO	10.69	10.34	10.98
MnO	0.27	0.10	0.42
FeO	13.10	11.46	14.55
Na_2O	1.88	1.60	2.13
K_2O	0.56	0.48	0.66
	Structural formulae (23 oxygens)		
Si	6.68	6.57	6.83
Ti	0.18	0.14	0.25
Al	1.67	1.44	1.84
Fe	1.65	1.63	1.67
Mn	0.03	0.01	0.05
Mg	3.05	2.88	3.22
Ca	1.72	1.66	1.77
Na	0.55	0.47	0.62
K	0.11	0.09	0.13

Table 4-68. Chemical data for amphibole phenocrysts in dacite from Shahrbabak (oxides, wt%).

	Phenocrysts		
	Mean (3)	Minimum	Maximum
SiO_2	54.23	54.13	54.42
TiO_2	0.10	0.07	0.13
Al_2O_3	22.64	22.57	22.76
MgO	0.01	0.00	0.02
CaO	0.00	0.00	0.00
MnO	0.00	0.00	0.02
FeO	0.57	0.49	0.68
Na_2O	0.03	0.01	0.04
K_2O	21.65	21.59	21.74

Table 4-69. Chemical data for leucite in phonotephrite from the Islamic Peninsula (oxides, wt%).

	Cores		Rims	
	Mean (7)	Range	Mean (2)	Range
SiO_2	53.89	53.39-54.21	42.38	38.77-45.99
TiO_2	0.15	0.06-0.50	0.03	0.00-0.05
Al_2O_3	22.33	22.05-22.64	30.92	30.48-31.35
MgO	0.04	0.00-0.12	0.07	0.03-0.11
CaO	0.01	0.00-0.07	0.06	0.03-0.09
MnO	0.02	0.00-0.08	0.03	0.01-0.04
FeO	1.00	0.80-1.29	0.95	0.51-1.39
Na_2O	0.20	0.11-0.58	18.81	16.55-21.06
K_2O	21.41	21.14-21.49	2.54	0.24-4.83

Table 4-70. Chemical data for leucite with nepheline rims in tephrites from the Islamic Peninsula (oxides, wt%).

	Mean	Minimum	Maximum
SiO_2	54.58	53.88	55.39
TiO_2	<0.09	<0.09	<0.09
Al_2O_3	23.23	22.82	24.04
MgO	<0.09	<0.09	<0.09
CaO	0.18	0.07	0.31
MnO	<0.09	<0.09	<0.09
FeO	0.25	0.09	0.43
Na_2O	13.76	13.31	14.47
K_2O	0.13	0.04	0.22

Table 5-1. Chemical data for analcime in tephriphonolite from Aghda (oxides, wt%).

	pumpellyite			prehnite			albite
	Mean (8)	Min	Max	Mean (2)	Min	Max	
SiO_2	37.13	36.14	37.60	43.03	43.02	43.04	65.56
TiO_2	<0.08	<0.08	<0.09	<0.08	<0.08	<0.08	<0.07
Al_2O_3	25.84	23.32	27.67	24.32	23.74	24.91	21.97
MgO	0.93	<0.09	3.05	<0.08	<0.08	<0.08	<0.08
CaO	22.37	21.44	22.86	26.18	25.97	26.38	0.71
MnO	0.13	<0.09	0.26	<0.09	<0.09	<0.09	<0.08
FeO	7.58	2.19	12.08	1.28	0.53	2.03	0.13
Na_2O	0.13	<0.12	0.19	<0.12	<0.12	<0.12	11.18
K_2O	0.06	<0.04	0.11	0.05	<0.05	0.05	0.22

Table 5-2. Chemical data for minerals in pumpellyite-bearing tephriphonolite from Aghda (oxides, wt%).

	pyroxene			plagioclase			Fe-Ti ox
	Mean (3)	Min	Max	Mean (3)	Min	Max	
SiO_2	48.52	48.18	48.87	52.18	50.55	53.81	1.37
TiO_2	1.00	0.97	1.03	0.08	<0.08	0.10	11.96
Al_2O_3	5.02	4.89	5.09	30.73	29.65	31.65	5.51
MgO	12.96	12.86	13.02	<0.09	<0.08	<0.09	<0.11
CaO	22.09	21.78	22.42	12.63	11.39	13.79	0.52
MnO	0.12	<0.10	0.15	<0.09	<0.09	<0.09	0.29
FeO	9.34	9.24	9.41	0.55	0.53	0.56	68.73
Na_2O	0.26	0.15	0.32	3.50	2.91	4.06	1.04
K_2O	<0.05	<0.05	<0.05	1.00	0.71	1.33	0.05

Table 5-3. Chemical data for minerals in analcime-bearing tephriphonolite from Aghda (oxides, wt%).

	Number of values	Mean	Range Minimum	Maximum
SiO_2	12	45.40	43.54	47.71
TiO_2	12	1.26	1.06	1.37
Al_2O_3	12	11.62	9.98	13.49
Fe_2O_3	12	9.50	8.35	10.28
MnO	12	0.15	0.13	0.18
MgO	12	7.87	5.28	10.15
CaO	12	11.78	10.73	13.32
Na_2O	12	2.27	0.51	5.07
K_2O	12	4.90	1.63	7.11
P_2O_5	12	1.53	1.20	1.78
LOI	12	3.80	2.17	6.25
Total	12	100.07	97.87	100.98
Ba	12	3472	2380	4800
Rb	12	229	66	380
Sr	12	1314	835	1980
Pb	12	44	22	70
Th	12	29	11	44
U	12	5	2	11
Zr	12	362	275	462
Nb	12	36	23	48
Y	12	34	25	44
La	12	71	32	96
Ce	12	168	75	230
Nd	3	69.00	53.10	78.60
Sm	3	14.83	11.30	16.80
Eu	3	3.23	2.53	3.76
Tb	3	1.50	1.18	1.70
Ho	3	1.45	1.22	1.58
Yb	3	2.25	1.90	2.53
Lu	3	0.27	0.24	0.30
Sc	3	30.00	28.50	31.00
V	12	208	144	262
Cr	12	174	15	390
Ni	12	49	15	92
Cu	12	114	82	148
Zn	12	82	66	104
Ga	12	14	11	16
Hf	3	7.93	5.19	8.87
Ta	3	1.86	1.40	2.18
DI		38.9	29.8	44.7
Mg#		66.7	56.0	74.2
K_2O/Na_2O		2.2	1.4	3.2
K/Rb		178	155	205
Zr/Hf		45.7	52	53
Zr/Nb		10.0	9.6	11.6

Table 6-1. Whole-rock geochemical data for tephrite from the Islamic Peninsula (oxides, wt% and traces, ppm).

	Number of values	Mean	Range Minimum	Maximum
SiO_2	3	47.04	46.17	47.94
TiO_2	3	1.24	1.24	1.25
Al_2O_3	3	12.51	10.57	13.88
Fe_2O_3	3	9.10	8.82	9.51
MnO	3	0.15	0.14	0.16
MgO	3	6.80	5.95	8.36
CaO	3	10.79	10.43	11.33
Na_2O	3	2.47	1.95	2.80
K_2O	3	5.98	5.22	6.78
P_2O_5	3	1.35	1.34	1.37
LOI	3	2.35	2.10	2.58
Total	3	99.79	99.51	99.94
Ba	3	3780	3050	4160
Rb	3	197	132	233
Sr	3	1250	1060	1410
Pb	3	45	44	46
Th	3	30	28	34
U	3	6	2	9
Zr	3	340	306	394
Nb	3	34	30	38
Y	3	35	34	37
La	3	73	68	78
Ce	3	169	158	185
Nd	1	73.50		
Sm	1	15.00		
Eu	1	3.75		
Tb	1	1.70		
Ho	1	1.67		
Yb	1	2.76		
Lu	1	0.33		
Sc	1	25.80		
V	3	201	188	213
Cr	3	115	46	244
Ni	3	36	22	56
Cu	3	117	106	124
Zn	3	82	70	97
Ga	3	15	14	16
Hf	1	7.72		
Ta	1	2.61		
DI		45.4	44.2	46.4
Mg#		64.5	61.4	70.1
K_2O/Na_2O		2.5	2.4	2.7
K/Rb		252	242	328
Zr/Hf		44	-	-
Zr/Nb		10.3	10.2	10.4

Table 6-2. Whole-rock geochemical data for phonotephrite from the Islamic Peninsula (oxides, wt% and traces, ppm).

	Number of values	Mean
SiO_2	1	46.65
TiO_2	1	0.96
Al_2O_3	1	7.71
Fe_2O_3	1	8.34
MnO	1	0.14
MgO	1	14.33
CaO	1	14.68
Na_2O	1	2.36
K_2O	1	1.77
P_2O_5	1	1.14
LOI	1	2.74
Total	1	100.82
Ba	1	3070
Rb	1	44
Sr	1	989
Pb	1	32
Th	1	18
U	1	47
Zr	1	236
Nb	1	22
Y	1	25
La	1	49.40
Ce	1	109
Nd	1	54.40
Sm	1	11.40
Eu	1	2.74
Tb	1	1.24
Ho	1	1.28
Yb	1	2.30
Lu	1	0.32
Sc	1	38.50
V	1	167
Cr	1	650
Ni	1	153
Cu	1	87
Zn	1	68
Ga	1	9
Hf	1	5.81
Ta	1	1.39
DI		22.9
Mg#		80.9
K_2O/Na_2O		0.8
CaO/Al_2O_3		1.9
K/Rb		334.0
Zr/Hf		40.6
Zr/Nb		10.7
La/Nb		2.25
La/Th		2.74
Ba/La		62.15
Ba/Nb		139.50

Table 6-3. Whole rock geochemical data for basalt from the Islamic peninsula (oxides, wt% and traces, ppm).

	Number of values	Mean	Range Minimum	Maximum
SiO_2	2	56.43	56.15	56.70
TiO_2	2	0.70	0.66	0.73
Al_2O_3	2	15.76	15.88	15.64
Fe_2O_3	2	5.45	5.25	5.64
MnO	2	0.10	0.10	0.11
MgO	2	2.75	2.64	2.86
CaO	2	4.71	4.48	4.94
Na_2O	2	3.69	3.32	4.06
K_2O	2	7.10	6.78	7.42
P_2O_5	2	0.50	0.50	0.51
LOI	2	2.19	2.12	2.26
Total	2	99.38	99.17	99.58
Ba	2	2990	2490	3490
Rb	2	226	220	232
Sr	2	1470	1370	1570
Pb	2	66	64	68
Th	2	47	46	47
U	2	16	15	17
Zr	2	498	466	530
Nb	2	53	51	56
Y	2	28	27	28
La	2	61	60	62
Ce	2	134	132	135
Nd	1	63.60		
Sm	1	11.60		
Eu	1	2.45		
Tb	1	1.36		
Ho	1	1.47		
Yb	1	2.37		
Lu	1	0.33		
Sc	1	10.90		
V	2	103	94	111
Cr	2	40	22	57
Ni	2	16	12	19
Cu	2	79	74	84
Zn	2	57	50	64
Ga	2	19	19	19
Hf	1	12.30		
Ta	1	3.03		
DI		72.9	71.7	74.2
Mg#		55.6	55.5	55.7
K_2O/Na_2O		1.9	1.8	2.0
K/Rb		260.8	255.8	265.5
Zr/Hf		40.5	-	-
Zr/Nb		9.3	9.1	9.5

Table 6-4. Whole-rock geochemical data for trachyandesite from the Islamic Peninsula (oxides, wt% and traces, ppm).

	Number of Values	Mean
SiO_2	1	58.02
TiO_2	1	0.83
Al_2O_3	1	15.12
Fe_2O_3	1	6.18
MnO	1	0.12
MgO	1	2.30
CaO	1	3.69
Na_2O	1	3.50
K_2O	1	7.98
P_2O_5	1	0.39
LOI	1	1.03
Total	1	99.16
Ba	1	2840
Rb	1	269
Sr	1	1420
Pb	1	66
Th	1	86
U	1	11
Zr	1	845
Nb	1	92
Y	1	32
La	1	66
Ce	1	155
V	1	130
Cr	1	30
Ni	1	12
Cu	1	42
Zn	1	70
Ga	1	20
DI		77.3
Mg#		47.9
K_2O/Na_2O		2.3
K/Rb		246.2
Zr/Nb		9.2

Table 6-5. Whole-rock geochemical data for trachyte from the Islamic Peninsula (oxides, wt% and traces, ppm).

	Number of values	Mean	Range Minimum	Maximum
SiO_2	19	47.55	43.54	58.02
TiO_2	19	1.16	0.66	1.37
Al_2O_3	19	12.18	7.71	15.88
Fe_2O_3	19	8.78	5.25	10.27
MnO	19	0.15	0.10	0.18
MgO	19	7.21	2.30	14.33
CaO	19	10.61	3.69	14.68
Na_2O	19	2.52	0.51	5.07
K_2O	19	5.30	1.63	7.98
P_2O_5	19	1.31	0.39	1.78
LOI	19	3.20	1.03	6.25
Total	19	99.95	99.16	100.98
Ba	19	3416	2380	4800
Rb	19	216	44	380
Sr	19	1309	835	1980
Pb	19	47	22	70
Th	19	34	11	86
U	19	9	2	47
Zr	19	392	236	845
Nb	19	40	22	92
Y	19	33	25	44
La	19	69	32	96
Ce	19	161	75	230
Nd	6	66.50	53.10	78.60
Sm	6	13.75	11.30	16.80
Eu	6	3.11	2.45	3.76
Tb	6	1.47	1.18	1.70
Ho	6	1.46	1.22	1.67
Yb	6	2.37	1.90	2.76
Lu	6	0.30	0.24	0.33
Sc	6	27.62	10.90	38.50
V	19	190	94	262
Cr	19	168	15	650
Ni	19	47	12	153
Cu	19	106	42	148
Zn	19	78	50	104
Ga	19	15	8	20
Hf	6	8.00	5.19	12.30
Ta	6	2.10	1.39	3.03
DI		44.7	22.8	77.3
Mg#		64.9	47.9	80.9
K_2O/Na_2O		3.1	0.3	10.7
K/Rb		203.9	174.3	307.5
Th/Nb		0.9	0.5	0.9
Zr/Nb		9.8	9.2	10.7

Table 6-6. Whole-rock geochemical data for all rocks from the Islamic Peninsula (oxides, wt% and traces, ppm).

Sample No	Rock types	Rb ppm	Sr ppm	87Rb/86Sr	87Sr/86Sr	87Sr/86Sr initial	Sm ppm	Nd pmm	147Sm/144Nd	143Nd/144Nd	143Nd/144Nd initial	εNd	Age(Ma)
Islamic Peninsula													
R14447	Tephrite	214	1121	0.552	0.708548	0.708478	16.80	78.60	0.12921	0.512394	0.512386	-4.7	9
R14454	phonoteph.	225	1280	0.509	0.707804	0.707735	15.00	73.50	0.12338	0.512464	0.512456	-3.3	"
R14455	Tephrite	66	1410	0.135	0.708273	0.708253	16.40	75.80	0.13080	0.512432	0.512424	-3.9	"
R14457	Basalt	44	989	0.129	0.707798	0.707784	11.40	54.40	0.12669	0.512458	0.512450	-3.4	"
R14466	Tephrite	207	997	0.601	0.708277	0.708203	11.30	53.10	0.12865	0.512439	0.512431	-3.8	"
R14698	Trachyande.	232	1370	0.490	0.708064	0.707997	11.60	63.60	0.11026	0.512428	0.512421	-4.0	"
Aghda													
R14480	Trachyte	382	262	0.422	0.708826	0.708710	7.84	40.40	0.11732	0.512431	0.512415	-3.8	20
R14483	Tephripho.	353	818	0.125	0.707523	0.707485	5.25	27.50	0.11541	0.512457	0.512442	-3.3	"
R14488	B.trachyan.	111	890	0.361	0.706612	0.706508	7.15	33.70	0.12827	0.512497	0.512480	-2.6	"
R14493	Rhyolite	186	165	0.326	0.707274	0.707177	6.73	33.70	0.12073	0.512517	0.512501	-2.2	"
R14500	Phonoteph.	183	1340	0.395	0.707118	0.707008	7.40	37.60	0.11898	0.512466	0.512450	-3.2	"
R14508	Tephripho.	371	659	0.163	0.707430	0.707384	5.37	27.50	0.11805	0.512453	0.512437	-3.4	"
Shahrbabak													
R14512	Trachyte	56	930	0.174	0.704305	0.704273	3.75	17.10	0.13259	0.512828	0.512815	3.8	15
R14522	Tephripho.	176	482	0.106	0.705687	0.705668	6.43	31.50	0.12341	0.512697	0.512684	1.3	"
R14528	Trachyande.	109	570	0.553	0.704874	0.704752	6.76	33.30	0.12273	0.512785	0.512733	3.0	"
R14550	Trachybasa.	77	582	0.383	0.705473	0.705389	4.38	18.40	0.14392	0.512724	0.512709	1.8	"
R14557	Tephripho.	116	807	0.416	0.705275	0.705191	5.94	29.70	0.12092	0.512740	0.512728	2.6	"
R14699	Dacite	65	617	0.305	0.704575	0.704515	3.40	19.70	0.10435	0.512839	0.512828	4.1	"

Table 6.7. Sr and Nd isotopic data for the Islamic Peninsula, Aghda and Shahrbabak volcanic rocks. $^{87}Sr/^{86}Sr$ and $^{143}Nd/^{144}Nd$ were measured on a VG 54E mass spectrometer and were normalised to $^{86}Sr/^{88}Sr = 0.1194$ and $^{146}Nd/^{144}Nd = 0.7219$ respectively. Replicate analyses of NBSSRM 98 gave $^{87}Sr/^{86}Sr = 0.710251 \pm 28$ (external precision at 2σ, n = 17) and the JM-Nd standard gave $^{143}Nd/^{144}Nd = 0.51111 \pm 12$ (external precision at 2σ, n = 17).

	Number of values	Mean	Range Minimum	Maximum
SiO_2	6	54.15	53.08	55.35
TiO_2	6	0.42	0.34	0.57
Al_2O_3	6	20.13	19.06	20.83
Fe_2O_3	6	4.44	3.98	5.83
MnO	6	0.11	0.08	0.15
MgO	6	1.31	0.95	1.63
CaO	6	4.01	2.47	6.90
Na_2O	6	4.94	3.14	6.15
K_2O	6	5.97	4.20	7.61
P_2O_5	6	0.27	0.22	0.41
LOI	6	3.84	2.32	5.25
Total	6	99.57	98.33	100.11
Ba	6	1308	940	1680
Rb	6	306	178	382
Sr	6	703	575	818
Pb	6	57	24	134
Th	6	31	28	35
U	6	7	4	9
Zr	6	242	214	257
Nb	6	18	17	20
Y	6	18	15	23
La	6	34	28	40
Ce	6	70	60	85
Nd	2	27.50	27.50	27.50
Sm	2	5.31	5.25	5.37
Eu	2	1.15	1.05	1.25
Tb	2	0.66	0.57	0.75
Ho	2	0.81	0.64	0.97
Yb	2	1.62	1.42	1.82
Lu	2	0.22	0.20	0.23
Sc	2	3.70	3.67	3.72
V	6	48	36	76
Cr	6	2	1	2
Ni	6	2	2	3
Cu	6	40	16	82
Zn	6	157	40	466
Ga	6	17	16	19
Hf	2	4.60	4.40	4.80
Ta	2	1.17	0.91	1.42
DI		73.6	62.5	79.5
Mg#		41.4	35.2	50.3
K_2O/Na_2O		1.2	1.2	1.3
Zr/Nb		12.72	12.59	12.85

Table 6-8. Whole-rock geochemical data for tephriphonolite from Aghda (oxides, wt% and traces, ppm).

	Number of Values	Mean
SiO_2	1	49.81
TiO_2	1	0.75
Al_2O_3	1	19.02
Fe_2O_3	1	7.46
MnO	1	0.15
MgO	1	2.81
CaO	1	6.42
Na_2O	1	4.75
K_2O	1	3.40
P_2O_5	1	0.62
LOI	1	3.84
Total	1	99.03
Ba	1	2050
Rb	1	183
Sr	1	1340
Pb	1	55
Th	1	23
U	1	4
Zr	1	190
Nb	1	13
Y	1	22
La	1	38.30
Ce	1	79.00
Nd	1	37.60
Sm	1	7.40
Eu	1	1.74
Tb	1	0.88
Ho	1	1.02
Yb	1	1.94
Lu	1	0.25
Sc	1	11.60
V	1	124
Cr	1	11
Ni	1	10
Cu	1	215
Zn	1	116
Ga	1	18
Hf	1	4.11
Ta	1	0.97
DI		57.5
Mg#		48.3

Table 6-9. Whole-rock geochemical data for phonotephrite from Aghda (oxides, wt.% and traces, ppm).

	Number of values	Mean
SiO_2	1	56.06
TiO_2	1	0.75
Al_2O_3	1	16.68
Fe_2O_3	1	6.81
MnO	1	0.11
MgO	1	1.91
CaO	1	1.94
Na_2O	1	2.47
K_2O	1	9.82
P_2O_5	1	0.29
LOI	1	2.69
Total	1	99.53
Ba	1	1470
Rb	1	385
Sr	1	406
Pb	1	114
Th	1	28
U	1	8
Zr	1	304
Nb	1	18
Y	1	26
La	1	32
Ce	1	75
V	1	94
Cr	1	30
Ni	1	12
Cu	1	20
Zn	1	294
Ga	1	14
DI		79.9
Mg#		40.9

Table 6-10. Whole-rock geochemical data for phonolite from Aghda (oxides, wt% and traces, ppm).

	Number of values	Mean	Range Minimum	Maximum
SiO_2	6	51.16	50.17	53.22
TiO_2	6	0.84	0.76	0.91
Al_2O_3	6	17.67	15.29	19.14
Fe_2O_3	6	8.49	7.88	9.38
MnO	6	0.15	0.11	0.17
MgO	6	3.32	3.03	3.72
CaO	6	7.57	6.47	8.02
Na_2O	6	3.66	2.83	4.84
K_2O	6	3.82	1.80	5.53
P_2O_5	6	0.50	0.40	0.56
LOI	6	2.75	2.47	3.20
Total	6	99.93	98.76	100.54
Ba	6	1437	1270	1610
Rb	6	121	35	238
Sr	6	916	610	1100
Pb	6	28	24	32
Th	6	27	24	30
U	6	6	5	8
Zr	6	233	198	256
Nb	6	15	14	16
Y	6	26	24	28
La	6	37	32	42
Ce	6	86	75	95
Nd	1	33.70		
Sm	1	7.15		
Eu	1	1.75		
Tb	1	0.93		
Ho	1	1.11		
Yb	1	2.66		
Lu	1	0.37		
Sc	1	13.60		
V	6	161	132	184
Cr	6	27	8	96
Ni	6	14	8	28
Cu	6	73	18	222
Zn	6	88	82	94
Ga	6	18	18	19
Hf	1	4.89		
Ta	1	0.95		
DI		52.9	50.4	57.6
Mg#		49.2	48.2	50.1
K_2O/Na_2O		1.1	0.7	1.1
K/Rb		262.0	192.9	426.9
Zr/Nb		15.53	14.14	16.00
La/Nb		2.4	2.3	2.6
Ba/Nb		92.7	90.7	100.6
Ba/La		38.83	38.33	39.69

Table 6-11. Whole-rock geochemical data for basaltic trachyandesite from Aghda (oxides, wt% and traces, ppm).

	Number of values	Mean	Range	
			Minimum	Maximum
SiO_2	2	60.23	57.95	62.51
TiO_2	2	0.56	0.51	0.60
Al_2O_3	2	16.49	16.14	16.84
Fe_2O_3	2	5.62	4.01	7.23
MnO	2	0.12	0.06	0.17
MgO	2	1.61	1.41	1.80
CaO	2	4.82	4.62	5.02
Na_2O	2	5.08	4.54	5.62
K_2O	2	2.71	2.45	2.97
P_2O_5	2	0.33	0.26	0.40
LOI	2	2.51	2.20	2.81
Total	2	100.06	99.80	100.32
Ba	2	1118	685	1551
Rb	2	60	59	61
Sr	2	864	448	1280
Pb	2	51	48	54
Th	2	20	16	24
U	2	4	3	5
Zr	2	140	118	162
Nb	2	9	6	12
Y	2	14	8	20
La	2	36	32	40
Ce	2	78	71	85
V	2	94	70	118
Cr	2	14	4	24
Ni	2	13	4	22
Cu	2	31	20	42
Zn	2	91	86	96
Ga	2	18	14	22
DI		68.5	68.5	68.5
Mg#		42.6	32.6	52.6

Table 6-12. whole-rock geochemical data for trachyandesite from Aghda (oxides, wt% and traces, ppm).

	Number of values	Mean	Range Minimum	Maximum
SiO_2	2	64.42	63.85	64.99
TiO_2	2	0.29	0.27	0.31
Al_2O_3	2	16.09	15.94	16.24
Fe_2O_3	2	3.33	3.20	3.45
MnO	2	0.09	0.09	0.09
MgO	2	0.30	0.27	0.32
CaO	2	1.26	1.07	1.45
Na_2O	2	3.95	3.66	4.23
K_2O	2	7.90	7.75	8.04
P_2O_5	2	0.10	0.08	0.11
LOI	2	1.27	0.90	1.63
Total	2	98.97	98.80	99.14
Ba	2	288	181	395
Rb	2	382	381	383
Sr	2	186	111	262
Pb	2	27	26	28
Th	2	49	47	51
U	2	12	11	13
Zr	2	508	490	526
Nb	2	31	30	32
Y	2	33	32	34
La	2	51	50	52
Ce	2	107	104	110
Nd	1	40.40		
Sm	1	7.84		
Eu	1	0.93		
Tb	1	0.93		
Ho	1	1.41		
Yb	1	3.72		
Lu	1	0.55		
Sc	1	4.13		
V	2	13	12	14
Cr	2	2	2	2
Ni	2	2	1	3
Cu	2	11	8	14
Zn	2	49	46	52
Ga	2	18	17	19
Hf	1	11.80		
Ta	1	2.40		
DI		89.7	88.9	90.6
Mg#		18.1	16.2	19.8

Table 6-13. Whole-rock geochemical data for trachyte from Aghda (oxides, wt% and traces, ppm).

	Number of value	Mean	Range Minimum	Maximum
SiO_2	2	71.01	70.86	71.15
TiO_2	2	0.24	0.23	0.26
Al_2O_3	2	14.17	14.10	14.24
Fe_2O_3	2	1.98	1.92	2.04
MnO	2	0.03	0.03	0.04
MgO	2	0.25	0.16	0.34
CaO	2	0.85	0.54	1.16
Na_2O	2	3.78	3.40	4.15
K_2O	2	6.15	5.97	6.32
P_2O_5	2	0.04	0.04	0.04
LOI	2	0.33	1.02	1.63
Total	2	99.82	99.62	100.02
Ba	2	570	545	595
Rb	2	203	186	220
Sr	2	136	106	166
Pb	2	36	26	46
Th	2	31	28	34
U	2	5	3	7
Zr	2	289	282	296
Nb	2	20	19	21
Y	2	34	34	34
La	2	39	38	40
Ce	2	84	78	90
Nd	1	33.70		
Sm	1	6.73		
Eu	1	0.87		
Tb	1	1.07		
Ho	1	1.55		
Yb	1	4.29		
Lu	1	0.60		
Sc	1	4.82		
V	2	12	11	13
Cr	2	2	1	3
Ni	2	2	2	2
Cu	2	10	8	12
Zn	2	34	24	44
Ga	2	14	13	15
Hf	1	7.43		
Ta	1	1.91		
DI		92.4	91.3	93.6
Mg#		23.2	17.1	29.2

Table 6-14. Whole-rock geochemical data for rhyolite from Aghda (oxides, wt% and traces, ppm).

	Number of values	Mean	Range Minimum	Maximum
SiO_2	20	56.45	49.81	71.15
TiO_2	20	0.56	0.23	0.91
Al_2O_3	20	17.80	14.10	20.83
Fe_2O_3	20	5.69	1.92	9.38
MnO	20	0.11	0.03	0.17
MgO	20	1.84	0.16	3.72
CaO	20	4.58	0.54	8.02
Na_2O	20	4.22	2.47	6.15
K_2O	20	5.27	1.80	9.82
P_2O_5	20	0.32	0.04	0.62
LOI	20	2.82	0.90	5.25
Total	20	99.66	98.33	100.54
Ba	20	1197	180	2050
Rb	20	221	35	385
Sr	20	692	106	1340
Pb	20	46	24	134
Th	20	30	16	50
U	20	7	3	12
Zr	20	261	118	490
Nb	20	18	6	32
Y	20	24	8	34
La	20	37	28	52
Ce	20	81.45	60.00	110.00
Nd	6	33.40	27.50	40.00
Sm	6	6.62	5.25	7.84
Eu	6	1.27	0.93	1.74
Tb	6	0.86	0.57	1.07
Ho	6	1.12	0.64	1.55
Yb	6	2.64	1.94	4.29
Lu	6	0.37	0.20	0.60
Sc	6	6.92	3.67	13.60
V	20	85	11	184
Cr	20	13	1	96
Ni	20	8	1	28
Cu	20	52	8	222
Zn	20	112	24	466
Ga	20	17	13	21
Hf	6	6.24	4.11	11.80
Ta	6	1.43	0.91	1.91
DI		69.9	50.4	93.6
Mg#		40.0	16.2	52.6
Th/Nb		1.67	1.56	2.66

Table 6-15. Whole-rock geochemical data for all rocks from Aghda (oxides, wt% and traces, ppm).

	Number of value	Mean	Range Minimum	Maximum
SiO_2	10	54.44	53.06	56.14
TiO_2	10	0.75	0.60	0.81
Al_2O_3	10	19.10	18.04	19.98
Fe_2O_3	10	5.65	4.25	6.39
MnO	10	0.12	0.09	0.14
MgO	10	1.69	0.94	2.28
CaO	10	3.82	2.71	4.82
Na_2O	10	4.46	2.47	5.39
K_2O	10	6.31	4.68	9.58
P_2O_5	10	0.41	0.26	0.55
LOI	10	3.59	2.99	4.16
Total	10	100.34	100.17	100.61
Ba	10	1227	1060	1450
Rb	10	218	89	383
Sr	10	631	455	807
Pb	10	31	28	34
Th	10	18	15	19
U	10	4	2	6
Zr	10	191	174	205
Nb	10	10	9	10
Y	10	24	22	25
La	10	30.50	29.80	33.20
Ce	10	64.94	59.90	75.00
Nd	2	30.60	29.70	31.50
Sm	2	6.19	5.94	6.43
Eu	2	1.51	1.50	1.52
Tb	2	0.86	0.80	0.92
Ho	2	1.11	0.99	1.22
Yb	2	2.66	2.53	2.78
Lu	2	0.39	0.38	0.40
Sc	2	7.67	7.58	7.76
V	10	83	40	116
Cr	10	6	1	22
Ni	10	5	2	16
Cu	10	65	26	114
Zn	10	70	50	98
Ga	10	17	13	19
Hf	2	3.72	3.69	3.75
Ta	2	0.68	0.67	0.68
DI		72.8	68.1	80.2
Mg#		42.1	35.4	49.4

Table 6-16. Whole-rock geochemical data for tephriphonolite from Shahrbabak (oxides, wt% and traces, ppm).

	Number of value	Mean
SiO_2	1	50.67
TiO_2	1	0.69
Al_2O_3	1	20.33
Fe_2O_3	1	6.52
MnO	1	0.12
MgO	1	2.27
CaO	1	6.22
Na_2O	1	5.58
K_2O	1	2.86
P_2O_5	1	0.48
LOI	1	4.44
Total	1	100.18
Ba	1	1020
Rb	1	37
Sr	1	1320
Pb	1	22
Th	1	12
U	1	3
Zr	1	128
Nb	1	6
Y	1	21
La	1	26
Ce	1	60
V	1	104
Cr	1	4
Ni	1	6
Cu	1	178
Zn	1	64
Ga	1	20
DI		59.7
Mg#		46.9

Table 6-17. Whole-rock geochemical data for phonotephrite from Shahrbabak (oxides, wt% and traces, ppm).

	Number of values	Mean	Range Minimum	Maximum
SiO_2	2	47.63	47.23	48.02
TiO_2	2	1.05	1.00	1.09
Al_2O_3	2	18.02	17.93	18.11
Fe_2O_3	2	10.42	9.61	11.22
MnO	2	0.19	0.18	0.20
MgO	2	5.63	5.48	5.77
CaO	2	9.41	9.18	9.64
Na_2O	2	3.14	3.07	3.21
K_2O	2	1.65	1.33	1.96
P_2O_5	2	0.33	0.30	0.35
LOI	2	3.38	3.35	3.41
Total	2	100.82	100.73	100.91
Ba	2	537	280	794
Rb	2	48	19	77
Sr	2	601	582	620
Pb	2	10	6	14
Th	2	4	4	4
U	2	2	1	3
Zr	2	74	66	82
Nb	2	2	1	3
Y	2	20	19	21
La	2	15.35	14.70	16.00
Ce	2	34	33	35
Nd	1	18.40		
Sm	1	4.38		
Eu	1	1.40		
Tb	1	0.69		
Ho	1	0.79		
Yb	1	1.81		
Lu	1	0.27		
Sc	1	28.40		
V	2	263	242	284
Cr	2	59	46	72
Ni	2	47	44	50
Cu	2	128	85	171
Zn	2	73	66	80
Ga	2	17	15	18
Hf	1	1.66		
Ta	1	0.50		
DI		36.3	34.2	38.3
Mg#		57.3	54.7	59.8

Table 6-18. Whole-rock geochemical data for basalt from Shahrbabak (oxides, wt% and traces, ppm).

	Number of values	Mean	Range	
			Minimum	Maximum
SiO_2	3	53.36	52.46	54.53
TiO_2	3	0.93	0.85	1.00
Al_2O_3	3	16.51	14.81	17.99
Fe_2O_3	3	7.32	6.22	8.33
MnO	3	0.13	0.12	0.13
MgO	3	4.24	2.23	7.32
CaO	3	7.18	6.42	8.03
Na_2O	3	4.12	3.73	4.77
K_2O	3	2.99	1.86	4.23
P_2O_5	3	0.41	0.30	0.53
LOI	3	3.19	1.51	5.15
Total	3	100.39	99.86	100.73
Ba	3	865	605	1200
Rb	3	83	39	129
Sr	3	802	605	975
Pb	3	13	12	16
Th	3	11	8	16
U	3	3	2	4
Zr	3	204	132	272
Nb	3	11	10	12
Y	3	22	18	26
La	3	31	24	40
Ce	3	72	55	90
V	3	143	108	174
Cr	3	95	20	246
Ni	3	63	16	156
Cu	3	51	28	74
Zn	3	77	72	80
Ga	3	18	17	20
DI		54.5	49.7	57.0
Mg#		55.5	47.0	70.9
La/Nb		2.82	2.4	3.33
La/Th		2.82	2.5	3.0
Ba/La		27.90	25.21	30.0
Ba/Nb		78.64	60.5	100.0
Zr/Nb		18.55	13.20	22.67

Table 6-19. Whole-rock geochemical data for basaltic trachyandesite from Shahrbabak (oxides, wt% and traces, ppm).

	Number of values	Mean
SiO_2	1	50.40
TiO_2	1	0.99
Al_2O_3	1	15.28
Fe_2O_3	1	8.32
MnO	1	0.14
MgO	1	8.60
CaO	1	9.45
Na_2O	1	3.90
K_2O	1	1.54
P_2O_5	1	0.56
LOI	1	0.85
Total	1	100.03
Ba	1	800
Rb	1	29
Sr	1	1330
Pb	1	8
Th	1	9
U	1	2
Zr	1	116
Nb	1	12
Y	1	18
La	1	42
Ce	1	90
V	1	170
Cr	1	326
Ni	1	158
Cu	1	66
Zn	1	76
Ga	1	18
DI		40.1
Mg#		71.9

Table 6-20. Whole-rock geochemical data for trachybasalt from Shahrbabak (oxides, wt% and traces, ppm).

	Number of values	Mean	Range	
			Minimum	Maximum
SiO_2	2	59.10	58.58	59.62
TiO_2	2	0.80	0.69	0.91
Al_2O_3	2	18.07	17.70	18.43
Fe_2O_3	2	5.32	4.94	5.70
MnO	2	0.07	0.06	0.08
MgO	2	1.43	1.26	1.60
CaO	2	3.31	2.39	4.22
Na_2O	2	4.75	3.82	5.68
K_2O	2	4.62	4.20	5.04
P_2O_5	2	0.31	0.24	0.37
LOI	2	1.96	1.87	2.04
Total	2	99.88	99.84	99.92
Ba	2	415	305	525
Rb	2	135	109	161
Sr	2	490	410	570
Pb	2	17	14	20
Th	2	21	16	26
U	2	5	4	6
Zr	2	366	330	402
Nb	2	14	13	15
Y	2	32	31	33
La	2	34.75	34.00	35.50
Ce	2	74.45	73.90	75.00
Nd	1	33.30		
Sm	1	6.76		
Eu	1	1.33		
Tb	1	0.97		
Ho	1	1.41		
Yb	1	3.59		
Lu	1	0.56		
Sc	1	8.25		
V	2	113	64	162
Cr	2	5	4	6
Ni	2	4	3	5
Cu	2	155	27	283
Zn	2	68	59	77
Ga	2	15	11	19
Hf	1	8.51		
Ta	1	0.96		
DI		73.8	67.9	79.7
Mg#		39.9	35.4	44.5
Zr/Hf		43.0	-	-

Table 6-21. Whole-rock geochemical data for trachyandesite from Shahrbabak(oxides, wt% and traces, ppm).

	Number of values	Mean
SiO_2	1	63.84
TiO_2	1	0.52
Al_2O_3	1	16.54
Fe_2O_3	1	3.84
MnO	1	0.06
MgO	1	1.47
CaO	1	4.32
Na_2O	1	4.79
K_2O	1	2.67
P_2O_5	1	0.16
LOI	1	1.51
Total	1	99.72
Ba	1	605
Rb	1	56
Sr	1	930
Pb	1	14
Th	1	7
U	1	2
Zr	1	130
Nb	1	7
Y	1	9
La	1	22.60
Ce	1	40.90
Nd	1	17.10
Sm	1	3.75
Eu	1	0.99
Tb	1	0.38
Ho	1	0.39
Yb	1	0.72
Lu	1	0.10
Sc	1	5.91
V	1	73
Cr	1	17
Co	1	49
Ni	1	17
Cu	1	117
Zn	1	95
Ga	1	20
Hf	1	2.84
Ta	1	0.51
DI		71.9
Mg#		48.7
Na_2O/K_2O		1.79

Table 6-22. Whole-rock geochemical data for trachyte from Shahrbabak(oxides, wt% and traces, ppm).

	Number of values	Mean	Range	
			Minimum	Maximum
SiO_2	4	66.59	65.38	67.65
TiO_2	4	0.40	0.36	0.45
Al_2O_3	4	16.23	15.54	17.68
Fe_2O_3	4	2.67	1.99	3.24
MnO	4	0.03	0.02	0.05
MgO	4	0.75	0.24	1.01
CaO	4	3.60	2.16	4.37
Na_2O	4	4.39	4.00	4.66
K_2O	4	2.54	2.25	2.75
P_2O_5	4	0.17	0.14	0.19
LOI	4	2.58	1.50	3.52
Total	4	100.04	99.41	100.48
Ba	4	716	580	825
Rb	4	64	57	69
Sr	4	674	610	845
Pb	4	14	12	16
Th	4	8	7	11
U	4	3	2	3
Zr	4	138	130	152
Nb	4	6	4	8
Y	4	13	7	28
La	4	25.30	16.00	32.00
Ce	4	49.48	35.00	65.00
Nd	1	19.70		
Sm	1	3.40		
Eu	1	0.82		
Tb	1	0.37		
Ho	1	0.40		
Yb	1	0.60		
Lu	1	0.08		
Sc	1	4.18		
V	4	50	42	68
Cr	4	18	6	42
Ni	4	8	4	10
Cu	4	23	8	36
Zn	4	43	24	54
Ga	4	18	17	19
Hf	1	3.61		
Ta	1	0.91		
DI		76.7	72.7	81.0
Mg#		37.9	23.0	46.2
Zr/Hf		38.23	-	-
Na_2O/K_2O		1.73	1.69	1.78

Table 6-23. Whole-rock geochemical data for dacite from Shahrbabak (oxides, wt% and traces, ppm).

	Number of values	Mean	Range Minimum	Maximum
SiO_2	25	56.18	47.23	67.65
TiO_2	25	0.75	0.36	1.04
Al_2O_3	25	17.80	14.44	20.33
Fe_2O_3	25	5.80	1.99	11.22
MnO	25	0.11	0.02	0.20
MgO	25	2.49	0.24	8.60
CaO	25	5.06	2.16	9.64
Na_2O	25	4.43	2.47	5.68
K_2O	25	4.16	1.33	9.58
P_2O_5	25	0.36	0.14	0.56
LOI	25	2.98	0.85	**5.15**
Total	25	100.24	99.41	100.91
Ba	25	915	280	1450
Rb	25	125	19	383
Sr	25	750	411	1330
Pb	25	21	6	34
Th	25	14	4	27
U	25	3	1	6
Zr	25	180	66	402
Nb	25	9	2	15
Y	25	20	7	34
La	25	27.64	14.70	**42.00**
Ce	25	56.41	33.00	90.00
Nd	6	24.95	17.10	33.30
Sm	6	5.11	3.40	6.76
Eu	6	1.26	0.82	1.52
Tb	6	0.69	0.37	0.97
Ho	6	0.87	0.39	1.41
Yb	6	2.01	0.60	3.59
Lu	6	0.30	0.08	0.56
Sc	6	10.35	4.18	**1**8.40
V	25	110	40	284
Cr	25	36	1	326
Ni	25	23	2	158
Cu	25	78	8	283
Zn	25	66	23	98
Ga	25	17	12	20
Hf	6	4	2	9
Ta	6	0.71	0.50	0.96
DI		66.1	34.2	81.0
Mg#		45.8	23.0	71.9
Th/Nb		1.56	1.8	2.0

Table 6-24. Whole-rock geochemical data for all rocks from Shahrbabak (oxides, wt% and traces, ppm).

Leucitite Gupta and Yagi(1980)	Leucitite U-DBV
Potassium-rich mafic and ultramafic rocks	potassium-rich mafic and ultramafic rocks
SiO_2<52.50%	SiO_2<50%
SiO_2/K_2O<20	SiO_2/K_2O<9
K_2O/Na_2O>1	K_2O/Na_2O>1
Enrichment in Rb, Sr, Nb, Zr	Enrichment in Rb, Sr, Nb, Zr

Table 7-1. A comparison between geochemical characteristics of the leucite-bearing rocks (Gupta and Yagi, 1980) and the U-DVB rocks.

	Number of values	Mean	Range Minimum	Maximum
SiO_2	26	50.00	43.54	56.06
TiO_2	26	0.94	0.34	1.37
Al_2O_3	26	15.30	9.98	20.83
Fe_2O_3	26	7.52	3.98	10.12
MnO	26	0.14	0.08	0.18
MgO	26	5.11	0.94	10.15
CaO	26	7.91	1.94	13.32
Na_2O	26	2.99	0.51	5.78
K_2O	26	6.18	3.61	9.82
P_2O_5	26	0.93	0.22	1.78
LOI	26	3.28	2.10	5.53
Total	26	99.94	98.33	100.98
Ba	26	2405	1060	4800
Rb	26	256	122	385
Sr	26	1020	406	1980
Pb	26	46	22	70
Th	26	28	11	44
U	26	5	2	11
Zr	26	292	176	462
Nb	26	25	9	48
Y	26	28	15	44
La	26	51.59	30.00	94.00
Ce	26	118.72	60.00	230.00
Nd	6	48.62	27.50	78.60
Sm	6	10.03	5.25	16.80
Eu	6	2.25	1.05	3.75
Tb	6	1.14	0.57	1.70
Ho	6	1.21	0.64	1.67
Yb	6	2.17	1.42	2.78
Lu	6	0.28	0.20	0.40
Sc	6	17	4	31
V	26	141	34	246
Cr	26	93	1	390
Ni	26	27	1	92
Cu	26	91	18	148
Zn	26	104	40	466
Ga	26	15	11	18
Hf	6	5.79	3.75	8.87
Ta	6	1.53	0.68	2.61
DI	26	55.9	29.8	79.9
$^{87}Sr/^{86}Sr$	7	0.70779	0.70738	0.7085
εNd	7	-3.7	-4.7	-3.2
Mg-number	26	54.2	36.9	74.2
K_2O/Na_2O	26	2.9	1.0	10.7

Table 7-2. Whole-rock geochemical data for leucititic rocks from the U-DVB (oxides, wt% and traces, ppm).

Shoshonite (Morrison, 1980)	Shoshonite (U-DVB)
1- Basalts near saturated in silica (rarely have normative Ne or Q)	Rocks with average 56% SiO_2 are from undersaturated to saturated and range from Ne-normative to Q-normative (Fig. 7.5)
2- Low iron enrichment (Flat trend on AFM)	Low iron enrichment (linear trend on AFM plot; Fig. 7.6)
3- High total alkalies (Na_2O+K_2O)	High total alkalies, in general >5% but mostly between 6.5 and 11% (Fig. 7.7)
4- High K_2O/Na_2O (>0.6 at 50% SiO_2; >1.0 at 55% SiO_2)	High K_2O/Na_2O (0.5 at 50% SiO_2; between 0.7 and 0.12 at 55%) (Fig. 7.8)
5- Steep positive slope on K_2O vs SiO_2 at low SiO_2 (0.5 at 45-57% but zero or negative at >57% SiO_2	Steep positive slope on K_2O vs SiO_2 (Fig 7.1)
6- Enrichment in P, Rb, Sr, Ba, LREE (in accord with potassium enrichment)	Relatively enriched in LILE compared to other rocks of similar SiO_2 content
7- low TiO_2 (<1.3%)	low TiO_2 (less than 1.3% but mostly range between 0.65-1.1% (Fig. 7.9)
8- High but variable Al_2O_3 (14-19%)	High Al_2O_3 (14.10-20.33)

Table 7-3. A comparison between geochemical characteristics of the shoshonite suite (Morrison, 1980) and the U-DVB rocks.

	Number of values	Mean	Range Minimum	Maximum
SiO_2	25	56.07	48.02	71.15
TiO_2	25	0.72	0.23	1.09
Al_2O_3	25	17.53	14.10	20.33
Fe_2O_3	25	6.00	1.92	9.61
MnO	25	0.11	0.03	0.20
MgO	25	2.43	0.16	5.77
CaO	25	4.80	0.54	9.18
Na_2O	25	4.41	3.32	6.15
K_2O	25	4.86	1.80	8.04
P_2O_5	25	0.38	0.04	0.62
LOI	25	2.59	0.90	4.44
Total	25	99.92	98.78	100.73
Ba	25	1274	180	3490
Rb	25	161	35	382
Sr	25	822	111	1570
Pb	25	32	12	68
Th	25	28	4	86
U	25	6	2	17
Zr	25	289	81	845
Nb	25	21	3	92
Y	24	26	19	34
La	24	38.61	30.00	66.00
Ce	24	85.87	33.00	155.00
Nd	8	36.30	18.40	63.60
Sm	8	7.23	4.38	11.60
U	8	1.50	0.87	2.45
Tb	8	0.95	0.69	1.36
Ho	8	1.22	0.79	1.55
Yb	8	2.86	1.81	4.29
Lu	8	0.41	0.25	0.60
Sc	8	11	4	28
V	25	109	11	241
Cr	24	23	1	246
Ni	25	16	2	156
Cu	25	71	8	215
Zn	25	70	23	138
Ga	24	18	13	20
Hf	8	6.80	1.66	12.30
Ta	8	1.42	0.50	3.03
DI	25	65.4	38.3	93.6
$^{87}Sr/^{86}Sr$	9	0.70658	0.70475	0.7080
εNd	9	-0.8	-4.0	+3.0
Mg-number	25	44.3	16.2	70.9
K_2O/Na_2O	25	1.2	0.5	2.3

Table 7–4. Whole-rock geochemical data for shoshonitic rocks from the U-DVB (oxides, wt% and traces, ppm).

	Number of values	Mean	Range Minimum	Maximum
SiO_2	10	60.28	47.23	67.65
TiO_2	10	0.61	0.36	1.00
Al_2O_3	10	16.46	15.28	18.11
Fe_2O_3	10	5.19	1.99	11.22
MnO	10	0.09	n.d.	0.18
MgO	10	2.40	0.24	8.60
CaO	10	5.45	2.16	9.64
Na_2O	10	4.43	3.07	5.62
K_2O	10	2.30	1.33	2.97
P_2O_5	10	0.27	0.14	0.56
LOI	10	2.62	0.85	5.15
Total	10	100.08	99.41	100.91
Ba	10	739	280	1550
Rb	10	52	19	69
Sr	10	791	605	1330
Pb	10	20	6	54
Th	10	10	4	23
U	10	2	2	5
Zr	10	135	66	208
Nb	10	7	2	12
Y	10	15	7	28
La	10	27.78	16.00	42.00
Ce	10	57.38	35.00	90.00
Nd	2	18.40	17.10	19.70
Sm	2	3.58	3.40	3.75
Eu	2	0.91	0.82	0.99
Tb	2	0.38	0.37	0.38
Ho	2	0.40	0.39	0.40
Yb	2	0.66	0.60	0.72
Lu	2	0.09	0.08	0.10
Sc	2	5	4	6
V	10	102	42	284
Cr	10	51	4	326
Ni	10	29	4	158
Cu	10	56	8	172
Zn	10	68	24	96
Ga	10	18	14	21
Hf	2	3.23	2.84	3.61
Ta	2	0.71	0.51	0.91
DI	10	64.7	40.1	81.1
$^{87}Sr/^{86}Sr$	2	0.70440	0.70427	0.7045
εNd	2	+3.9	+3.8	+4.1
Mg-number	10	45.9	23.0	71.9
K_2O/Na_2O	10	0.5	0.4	0.7

Table 7-5. Whole-rock geochemical data for high-K calcalkaline rocks from the U-DVB (oxides, wt% and traces, ppm).

	A	B	C	D	E	F	G
SiO_2	45.40	48.07	48.64	43.63	45.90	47.73	44.40
TiO_2	1.26	0.81	0.78	1.66	5.26	0.73	2.10
Al_2O_3	11.62	17.29	17.34	11.93	8.25	17.13	15.60
Fe_2O_3	9.50	7.86	7.37	9.71	10.65	7.42	9.60
MnO	0.15	0.15	0.15	0.17	0.13	0.15	0.20
MgO	7.87	4.94	4.05	10.51	9.71	7.22	7.30
CaO	11.78	10.67	10.04	10.22	7.86	12.24	11.50
Na_2O	2.27	2.70	1.66	3.61	1.21	1.35	3.20
K_2O	4.90	6.30	7.46	5.23	7.24	5.54	4.10
P_2O_5	1.53	0.41	0.41	0.76	0.67	0.49	0.20
LOI	3.80	0.72	1.30	0.48		1.17	
Ba	3472	1093	1368	5864	1350	1090	
Rb	228	418	530	125	299	336	
Sr	1314	1572	1471	1449	830	1040	
Pb	44		69	10			
Th	29	38	58	9		35	
U	5	8	11	5			
Zr	362	287	308	131		192	
Nb	36	20	22			12	
Y	34	36	34	21		30	
La	71.34	87.60	108	51.40		73	
Ce	168.17	180.60	182	102.90		133	
Nd	69.17	71.00	90	43.70		67	
Sm	14.83	12.83		7.90		13	
Eu	3.23	2.73		2.18		2.46	
Tb	1.50	1.62		0.80			
Yb	2.25	2.32		1.45		2.38	
Lu	0.27	0.32		0.21		0.36	
Sc	30		24	24		19	
V	208	209	225			215	
Cr	174	55	96		266	68	
Co	65		29	50	41	33	
Ni	50	121	46			92	
Cu	115	63	52	219			
Zn	82	75	74	118			
Hf	7.93	6.24		3.50			
Ta	2	1.02		0.97			

Table 7-6. Compilation of mean whole-rock major and trace element data for leucititic rocks (<52% SiO_2). A = present study; B = Vulsini, Central Italy (Rogers et al., 1985); C = Roman province, Central Italy (Holm et al., 1982); D = Kuh-e-Geri, Iran (Hassanzadeh 1993); E = El Capitan, New South Wales, Australia (Cundari, 1973); F = Vulsini District, Central Italy (Coltorti et al., 1991) and East Eifel, West Germany (Duda and Schminke, 1978) (oxides, wt% and traces, ppm).

		A	B	C	D	E	F	G	H	I
1	$^{87}Sr/^{86}Sr$	0.70779	0.71010	0.70959	0.70615	0.71037	0.7058	0.71049	0.70462	0.70565
	$^{143}Nd/^{144}Nd$	0.51243		0.51220						
2	$^{87}Sr/^{86}Sr$	0.70658	0.70519	0.70494	0.70410	0.70608	0.70760	0.70740	0.70439	0.7081
	$^{143}Nd/^{144}Nd$	0.51256		0.51231	0.51310				0.51279	
3	$^{87}Sr/^{86}Sr$	0.70440	0.70522	0.70436	0.70537	0.70410	0.70614	0.70575	0.70457	0.70455
	$^{143}Nd/^{144}Nd$	0.51282	0.51296		0.51281					0.51275

Table 7-7. Compilation of mean whole-rock Sr and Nd isotope data for leucitite, shoshonite and high-K calcalkaline rocks.

1 = Leucitites
A = Present study; B = Vulsini, Italy (Rogers et al., 1985); C = Roccamonfina, Italy (Giannetti and Ellam, 1994); D = Batu Tara Volcano, Indonesia (Bergen et al., 1992); E = Vico Volcano, Italy (Barbieri et al., 1988); F = Birunga and Toro-Ankole region, Africa (Bell and Powell, 1969); G = Alban Hills, Italy (Conticelli and Peccerillo, 1992); H = Western and Central Europe (Wilson and Downes, 1991); I = North East China (Zhang et al., 1995).

2 = Shoshonites
A = Present study; B = Ungaran, Indonesia (Claproth, 1989); C = Walton Peak, Colorado (Thompson et al., 1993); D = Taru Volcano, Fiji (Rogers and Setterfield, 1994); E = Stromboli, Italy (Francalanic et al., 1988); F = Tibetan Plateau (Turner, 1996); G = Northwestern Alps, Italy (Venturelli et al., 1984); H = Eastern Anatolia, Turkey (Pearce et al., 1990); I = Birunga and Toro-Ankole region, Africa (Bell and Powell, 1969).

3 = High-K calcalkalines
A = Present study; B = Lundy Bristal Channel, UK (Thorpe and Tindle, 1992); C = Imuta, japan (Notsu et al., 1990); D = Eastern Anatolia, Turkey (Pearce et al., 1990); E = Sunda arc, Indonesia (Whitford and Jezek, 1982); F = Latir volcanic, New Mexico (Johnson et al., 1990); G = Southern San Joaquin, California (Sharma et al., 1991); H = North Luzon arc, Philippines (McDermott et al., 1993); I = Miduk, Iran (Hassanzadeh, 1993).

	A	B	C	D	E	F	G
SiO_2	54.36	54.50	55.14	53.21	53.10	52.46	53.69
TiO_2	0.61	0.49	0.55	0.60	0.70	3.03	0.49
Al_2O_3	19.00	19.15	19.60	18.61	17.90	14.52	20.57
Fe_2O_3	5.82	4.24	4.60	7.23	6.00	8.57	4.59
MnO	0.12	0.11	0.14	0.19	0.13	0.10	0.17
MgO	1.53	1.42	1.11	3.54	3.30	3.86	1.67
CaO	4.06	4.19	4.21	7.04	6.10	5.16	3.54
Na_2O	4.06	4.40	2.99	3.62	2.40	3.98	4.07
K_2O	6.88	6.97	9.25	5.29	6.60	6.96	6.93
P_2O_5	0.34	0.15	0.20	0.59	0.48	1.30	
LOI	3.55	4.50	1.27	0.67		0.01	
Ba	1262	548	1679		1165	2037	
Rb	299	533	481	180	584	132	
Sr	603	1172	1679	1050	1205	1666	
Pb	50	57		10		17	
Th	25	47	112	35		7	
U	5	10				2	
Zr	228	341	475	251	469	695	
Nb	14	26	40	18		84	
Y	21	46	44	35		25	
La	31.80	100		71			
Ce	68.90	209		139			
Nd	28.83	86					
Sm	5.68	12.40		10.20			
Eu	1.27	2.32		2.74			
Tb	0.75	1.24		1.04			
Yb	2.01	3.03		2.43			
Lu	0.28	0.45		0.41			
Sc	5	4		21		10	
V	72	100	106			106	
Cr	10	12	5	23		34	
Ni	4		6	28		43	
Cu	51	5	12			23	
Zn	129	73	76			124	
Hf	4.32			6		16	
Ta	1.00	1.58				4.10	

Table 7.8. Compilation of mean whole-rock major and trace element data for leucititic rocks (>52% SiO_2). A = present study; B = Roccamonfina Volcano, Italy (Luhr and Giannetti, 1987); C = Vulsini Volcano, Italy (Parker, 1989); D = Batu Tara Volcano, Indonesia (Van Bergen et al., 1992); E = Vico volcanic area, Italy (Cundari and Mattias, 1974); F = Northeast China (Zhang et al., 1995). G = Northern Azarbaijan, Iran (Riou, 1979) (oxides, wt% and traces, ppm).

	A	B	C	D	E	F	G	H	I	J	K
SiO_2	48.71	51.00	49.40	50.01	51.97	50.63	48.73	51.35	50.78	49.04	51.72
TiO_2	0.81	0.90	0.93	0.83	1.03	0.93	1.39	1.45	0.88	3.11	0.74
Al_2O_3	16.26	17.20	13.40	16.01	17.55	16.89	15.83	15.22	17.25	15.24	18.13
Fe_2O_3	8.53	7.93	7.47	8.66	8.86	9.27	10.78	10.04	6.66	11.99	6.94
MnO	0.15	0.15	0.16	0.17	0.17	0.14	0.17	0.14	0.11	0.20	0.12
MgO	5.11	6.33	10.91	6.24	3.50	5.76	6.81	6.33	4.90	4.98	6.65
CaO	9.11	10.70	8.32	9.26	6.92	8.40	8.24	7.92	6.54	8.78	8.65
Na_2O	4.05	2.31	1.92	2.93	3.34	2.97	2.53	4.35	2.50	3.65	2.43
K_2O	2.72	2.33	2.87	2.74	3.19	2.27	2.37	2.33	3.54	1.25	3.01
P_2O_5	0.78	0.46	0.71	0.44	0.61	0.41	0.52	0.76	0.41	0.90	0.38
LOI	3.83	0.70	3.51	1.78	2.86	0.91	2.53	0.46	1.67		1.19
Ba	1990.51	1111		683.01		586.01	1284.01	2104.01	296.01		760.01
Rb	110.81	70	140.01	59.01	100	72.01	47.01	30.01	85.01		238.01
Sr	1068.11	736	58.01	943.01	1132	772.01	954	1339	237		894
Pb	31.81				21	10					
Th	22.24	16.10		12.81	6	6.51	3.31	8.81	13.51		
U	8.11			0.57	4	1.51	0.91	2	1.41		
Zr	228.41	180	236	67	221	112	131	255	147		157
Nb	17.91	22	17			11		46.21			
La	43.45	51			27	37.61	35.61	72			64
Ce	98.23	103			58	86.21	66	149			130
Nd	43.98	49				42	32	67			28
Sm	9.35	9			6.15	7.02	6.66	12.71			12.61
Eu	2.28	2.20			1.68	1.59	2.43	3.07			2.13
Tb	1.17	1				0.65	0.91	1.13			
Yb	2.25	2.49			2.47	1.80	2.31	1.51			2.15
Lu	0.31	0.37			0.40	0.25	0.33	0.22			0.33
V	173		160		214	174	259	197	256		
Cr	94	222	596	156	22	170	91	204	228		177
Ni	32	69	331	50	17	50	37		14.51		20
Hf	4.92	4			3.81	2.58	3.11	6.51	3.41		5.71
Ta	1.16	1.39				0.53	1.01	2.57			

Table 7.9. Compilation of mean whole-rock major and trace element data for shoshonitic rocks (<52% SiO_2). A = present study; B = Roman province, Italy (Peccerillo, 1992); C = Northwestern Alps, Italy (Venturelli et al., 1984); D = Island Arc compilation (Morrison, 1980); E = Sydney Basin (Carr, 1984); F = Abitibi Greenstone Belt (Dostal and Muller, 1992); G = Guffey Volcanic, Centeral Colorado (Wobus et al., 1990); H = Walton peak, Colorado (Thompson et al., 1993); I = Greece (Pe-piper, 1983); J = Ascension Island, Atlantic Ocean (Sorensen, 1974); K = Mt Vulsini, Italy (Civetta et al., 1981). 1979) (oxides, wt% and traces, ppm).

	A	B	C	D	E	F	G	H	I	J	K
SiO_2	54.48	55.46	52.03	54.83	54.94	57.00	52.99	53.11	54.74	59.50	57.43
TiO_2	0.77	0.93	0.56	1.03	0.91	0.81	0.71	1.11	1.09	0.69	1.32
Al_2O_3	18.11	16.75	17.56	16.54	17.24	15.71	18.38	17.21	16.61	17.50	19.46
Fe_2O_3	6.00	6.56	7.53	7.55	7.91	6.95	8.54	8.00	8.77	5.83	4.37
MnO	0.12	0.11	0.18	0.16	0.22	0.11	0.19	0.16	0.12	0.09	0.19
MgO	2.73	4.81	3.46	3.15	2.16	3.87	3.55	4.96	3.61	2.30	0.94
CaO	4.81	6.71	9.25	5.41	5.23	5.04	6.82	6.83	4.91	5.49	2.85
Na_2O	4.69	2.94	4.11	3.67	4.19	2.12	3.31	2.46	3.32	3.34	7.65
K_2O	5.11	3.66	4.12	4.48	3.45	4.91	4.19	2.65	3.18	3.77	4.43
P_2O_5	0.43	0.61	0.45	0.75	0.41	0.77	0.59	0.27	0.51	0.41	0.10
LOI	2.98			2.31		2.51	0.71	3.11	1.71	1	
Ba	1558	567	698		983	1935	830		745	1412	
Rb	158	63	73	112	88	176	72	90	97	118	
Sr	931.21	956	1600	794	547	1154	1446	521	611	600	
Pb	36		11	26			23		11		
Th	23.21	4.33	2.21	6		24	2.53	6.19	7.92	26	
U	7.02	1.34	1.31	4			1	2.51	1.92		
Zr	258.51	121	59	170	132	276	99	120	187	2790	
Nb	20.11		1			22	5	11	15.21	25	
Y	23.91	18	23	31	40	33.94	27	31	22	44	
La	38.26		12	29		59.38	16.21	22.71	52	63	
Ce	83.19		26	59		115.71	32	44.11	116	118	
Nd	46.65					49	20	24.31	54.21	43	
Sm	8.77			6.75		9.75	4.78	5.21	8.51	10.10	
Eu	1.96		1.21	1.67		2.35	1.51	1.43	1.95	2.40	
Tb	1.08		0.56				0.63	0.81	0.78	1.10	
Yb	2.45			2.62		2.44	2.11	2.51	2.22	3.33	
Lu	0.36			0.46		0.45	0.35	0.36	0.33	0.70	
Sc	9.33	26	15	18.31	19		16.21		18	15	
V	105.91	218	340	258	116	158	229	205	137		
Cr	38.61	141	3	8	8	37	17	77	100	20	
Ni	24.21	53	6	12	3	8		25	31		
Hf	8		1.41	4.51			2.35	3.18	4.37		
TA	1.03		0.04				0.22	0.53	0.68		

Table 7.10. Compilation of Mean whole-rock major and trace element data for shoshonitic rocks (>52% SiO_2). A = present study; B = Island Arc compilation (Morrison, 1980); C = Oceanic Island Arc, Fiji (Gill and Whelan, 1989); D = Sydney Basin (Carr, 1984); E = Shoshonitic volcanism in the Northern Mariana Arc (Bloomer et al., 1989); F = Northern Karakorum, Sinkiang, China (Pognante, 1990); G = Taru volcano, Fiji (Rogers and Setterfield, 1994); H = Northwest Alps, Italy (Venturelli et al., 1984); I = Abitibi Greenstone Belt, Quebec, Canada (Dostal and Muller, 1992); J = Roman province, Italy (Peccerillo, 1992); K = Canary Island, Atlantic Ocean (Borley, 1974) (oxides, wt% and traces, ppm).

	A	B	C	D	E	F	G	H	I	J	k
SiO_2	48.82	50.81	49.70	45.53	48.73	50.66	50.65	49.51	51.38	50.21	51.05
TiO_2	1.00	0.96	1.05	3.39	1.39	0.69	0.81	0.77	1.69	0.77	1.14
Al_2O_3	16.71	20.14		13.67	15.83	12.94	18.22	17.68	14.84	20.09	18.57
Fe_2O_3	9.77	9.23		9.09	10.78	9.99	8.63	10.16	11.07	8.41	8.91
MnO	0.16	0.18		0.13	0.17	0.19	0.12	0.18	0.13	0.13	0.16
MgO	7.04	4.21	7.40	8.81	6.81	8.15	5.08	5.84	7.93	3.81	5.54
CaO	9.55	8.65		14.83	8.24	9.07	10.17	11.27	8.87	9.05	8.87
Na_2O	3.49	2.81		4.15	2.53	3.22	2.53	2.57	3.31	1.97	3.98
K_2O	1.44	1.62	1.20	1.34	2.37	1.52	1.11	1.79	1.47	1.76	1.42
P_2O_5	0.43	0.34	0.25	0.48	0.52	0.24	0.16	0.24	0.62	0.13	0.38
LOI	2.11	1.15			2.53	1.71	4.08		0.06	3.61	
Ba	540	508.61			1284	728	295	477	914	410	
Rb	24	41	20		47	34	16	30	16	39	49.91
Sr	975	473.51	605		954	594	446	649	852	192.00	608
Pb	7	20.41				5					
Th	6.51	7.41	2.10		3	1.91	2.71		3.91	1.51	
U	0.51				0.91	0.55			1		
Zr	91	140	75		131	64	94	35	143	52	162
Nb	5	12.31				4.11	6	2	20.11	2	
Y	19.51	24			27	14		17	23		31
La	29	30.71	16.70		35.61	16.31	8.31		38	5.99	16.31
Ce	62.51	55.31	34		66	36.81	17	15	77	13.84	41.61
Nd					32	19.11		9	43		
Sm		5.61	3.5		6.66	4.15	2.64		8.11	2.24	
Eu		1.66			2.43	1.11	0.79		2.35	0.75	
Tb			0.57		0.91	0.48	0.35		0.89		
Yb		2.25	1.33		2.31	1.52	1.45		1.47	1.37	2.29
Lu		0.38			0.33	0.22	0.24		0.23	0.22	
Sc		22.96			29	27	25.61		20.11		
V	227	228.71			259	213	240	354	188		187
Cr	186	12.11	118		91	476	8	70	195	244	67.91
Ni	101		62		37	76	25	24	209	24	57.91
Hf		3.13	1.20		3.11	1.74	2.41		3.61	1.58	2.91
Ta		0.56	0.20		1	0.24			1.04	0.12	

Table 7.11. Compilation of Mean whole-rock major and trace element data for high-K calcalkaline rocks (<52% SiO_2). A = present study; B = Ungaran Indonesia (Claproth, 1989); C = Roman province, Italy (Peccerillo, 1985); D = East Africa Rift System, Africa (Gurenko, Sobolev and Kononkova, 1991); E = Guffey Volcanic, Central Colorado (Wobus et al., 1990); F = Abitibi Greenstone Belt, Canada (Dostal and Muller, 1992); G = Northern Azarbaijan, Iran (Riou et al., 1981); H = Oceanic Island Arc, Fiji (Gill and Whelan, 1989); I = Walton Peak, Northwest Colorado (Thompson et al., 1993); J = North wales (Kokelear, 1986); K = South America (Ewart, 1982)
(oxides, wt% and traces, ppm).

	A	B	C	D	E	F	G	H	I	J	K
SiO_2	60.23	57.39	55.17	58.76	61.08	59.57	59.21	62.03	59.31	58.12	59.91
TiO_2	0.56	0.67	0.92	0.66	0.62	0.71	0.69	0.71	0.66	0.76	0.91
Al_2O_3	16.49	18.77	15.91	18.62	17.79	14.48	16.51	15.35	17.55	16.11	16.51
Fe_2O_3	5.62	6.86	7.29	6.51	5.49	4.37	6.71	5.75	6.37	6.46	7.97
MnO	0.12	0.17		0.12	0.09	0.11	0.09	0.08	0.15	0.09	0.11
MgO	1.61	2.54	5.49	2.90	1.56	2.21	4.04	2.41	2.81	4.16	2.41
CaO	4.82	6.54	9.63	7.44	5.41	7.09	5.22	4.99	5.69	5.66	4.94
Na_2O	5.08	3.13	2.90	3.55	4.21	3.67	3.23	2.58	3.84	2.13	3.17
K_2O	2.71	2.81	2.69	1.28	3.93	2.67	2.85	3.04	2.45	2.78	2.61
P_2O_5	0.33	0.29		0.16	0.23	0.16	0.19	0.24		0.16	0.21
LOI	2.51	1.27			1.16		2.31	2.49	0.97	3.58	
Ba	1117.51	588.51	670		1052			852	708	418	1010
Rb	59.51	86.11	68		91		83	87	56	105	52
Sr	864	453	583		696		112	389	367	327	382
Pb	51	19.31	12.50								
Th	19.51	14.05	5.30		7.31		20.11	17	7	7	
U	4		1.31				12				
Zr	140	165	111		184		198	226	155	150	163
Nb	9	12.91	7		11			15		16	19
Y	14	27.81					25	29.57	39	26	44
La	36	35.41	15.30		20.81		51.31	41.54	50	38.71	
Nd			18.08				42.51	33.09		26.94	
Sm		5.03	3.49		3.48		7.21	6.68		6.54	
Eu		1.43	1.14		1.02		1.58	1.48		1.61	
Tb			0.52		0.41		0.73				
Yb		2.74	1.63		1.51		1.92	2.34		2.14	
Lu		0.42	0.29		0.24		0.19	0.41		0.71	
Sc		11.11	31		10.31			19.29	15	23	
V	94	131	190		142		148	107	138	136	
Cr	14	8.39	210		9		40	56		146	37
Ni	13		45.99		9		10	9		24	
Zn	91	111.11			68		81	57			182
Hf		4.03	2.30		3.51		3.41		4.41		91
Ta		0.73			1.22						

Table 7.12. Compilation of mean whole-rock major and trace element data for high-K calcalkaline rocks (>52% SiO_2). A = present study; B = Ungaran, Indonesia (Claproth, 1989); C = Kastamonu Area, Northern Turkey (Peccerillo and Taylor, 1976); D = Oceanic Island Arc, Figi (Gill and Whelan, 1989); E = Northern Azarbaijan, Iran (Riou et al., 1981); F = Lakmon mountains, Greece (Pe-Piper, 1983); G = Northwestern Alps, Italy (Venturelli et al., 1984); H = Northern Karakorum, Sinkiang, China (Pognante, 1990); I = Northeastern Kanaga island, Aleutians (Brophy, 1990); J = Atesina-Cimad, Italy (Barth et al., 1993); K = Costarica (Cigolini et al., 1991) (oxides, wt% and traces, ppm).

	A	B	C	D	E	F	G	H	I	J	K
SiO_2	66.04	66.11	65.54	63.66	64.01	66.14	64.83	65.36	62.70	63.51	63.93
TiO_2	0.42	0.51	0.67	0.43	1.12	0.65	0.54	0.63	0.58	0.91	0.58
Al_2O_3	16.29	16.51	15.48	16.44	14.51	16.19	15.81	16.22	19.83	16.32	15.75
Fe_2O_3	2.98	2.06	4.31	4.16	5.65	4.53	4.63	4.64	4.70	5.32	4.12
MnO	0.04	0.07	0.09	0.05	0.05	0.07	0.05	0.09		0.09	0.07
MgO	0.89	1.71	1.87	2.65	2.66	1.52	2.99	1.64	0.95	2.38	2.84
CaO	3.74	3.85	3.65	4.76	3.39	2.06	1.91	4.25	5.89	5.21	4.61
Na_2O	4.47	3.71	4.81	3.81	4.04	3.86	2.95	3.81	4.02	4.24	5.42
K_2O	2.57	1.94	3.51	2.43	3.78	3.46	3.02	3.15	1.41	2.22	2.69
P_2O_5	0.17	0.11	0.28	0.14	0.38	0.19	0.15	0.21		0.25	0.18
LOI	2.37		0.49	1.33	0.48		3.12			0.74	
Ba	694	690	1948	965	749	801	649	831		526	1313
Rb	62.61	36.51	50	69	131	126	109	109	31	63	85
Sr	725.41	240	59	751	376	194	125	330	383	389	536
Pb	14	20.51		27	14			7		9	
Th	8	3.21	10.51	9.51	14	8	14			8	
U	1	1.81	3.21	2.91							
Zr	136.61	130	161	132	179	167	185	170		243	139
Nb	6.41	3.41	21.51	9	28	12	18	21	15	13	6
Y	12.21	17.71	11	17	24	29	39	28	15	24	12
La	24.76	10.11	50	36.71		28	38.87	23			18
Ce	47.76	19.11	99	60.31		60	82.71	55			48
Nd	18.41	10	39	23		24	33.66				
Sm	3.58	2.31	5.71	4.11		5.71	7.53				
Eu	0.91	0.87	1.51	1.31		1.06	1.38				
Tb	0.38	0.52	0.54	0.41							
Yb	0.66	2.21	0.92	1.61		2.34	2.81	1.51			
Lu	0.09	0.35	0.14	0.25		0.49	0.47				
Sc	5.05	17.41	7.21	14.41	9		19			15	
V	54.61	90	77	87	74	61	68	72		120	
Cr	18	16	56	91	92	25	28	13		50	
Ni	9.61	13.31	124	19	34	15	9	11		18	26
Hf	3.23	4.02	4.81	3.91				3.41			
Ta	0.71	0.32	1.18	0.73							

Table 13. Compilation of mean whole-rock major and trace element data for calcalkaline rocks. A = present study; B = Valley of ten thousand smokes, Alaska (Papike et al., 1991); C = Northwest Colorado (Thompson et al., 1993); D = Andesite and dacite, Greece (Pe-Piper and Piper, 1994), E = Sardinia, Italy (Montanini et al., 1994); F = Souther Alpine Crust, Northern Italy (Boriani et al., 1995); G = Atesina-Cimad, Italy (Barth et al., 1993); H = Dacite from the Mediterranean (Ewart, 1979); I = Kastamonu Area, Northern Turkey (Peccerillo and Taylor, 1976); J = Eastern Anatolia, Turkey (Pearce et al., 1990); K = Nevada del Ruzi volcano, Colombia (Sigurdsson et al., 1990) (oxides, wt% and traces, ppm).

	R14447	R14455	R14466	R14454	R14483	R14508	R14500	R14522	R14557	R14550
SiO_2	46.06	44.42	46.65	46.17	54.16	55.35	49.81	54.67	53.36	48.02
TiO_2	1.24	1.31	1.06	1.24	0.42	0.42	0.75	0.81	0.81	1.09
Al_2O_3	11.45	12.83	11.00	13.88	19.98	20.36	19.02	18.44	19.62	17.93
Fe_2O_3	9.57	10.27	9.30	9.51	4.31	4.33	7.46	6.39	6.03	9.61
MnO	0.16	0.17	0.16	0.16	0.14	0.08	0.15	0.14	0.12	0.20
MgO	8.67	5.28	9.44	6.10	1.26	0.95	2.81	1.63	2.00	5.77
CaO	11.85	11.69	11.71	10.43	2.47	5.09	6.42	4.19	4.61	9.18
Na_2O	1.22	5.07	1.04	2.65	5.37	3.14	4.75	4.14	5.06	3.21
K_2O	6.15	1.68	7.11	5.93	6.40	7.61	3.40	6.50	4.77	1.96
P_2O_5	1.44	1.57	1.20	1.34	0.23	0.28	0.62	0.55	0.46	0.35
Mg-number	69.16	56.00	71.53	61.36	41.98	35.20	48.25	38.71	45.09	59.78

Table 8-1. Major element compositions of the most mafic rocks from the U-DVB (oxides, wt%).

	R14447		R14455		R14466		R14454		R14483	
	a	b	a	b	a	b	a	b	a	b
SiO_2	46.82	46.44	46.02	45.34	47.09	46.84	46.75	46.05	54.99	53.93
TiO_2	1.22	1.15	1.20	1.06	1.03	1.01	1.17	1.04	0.39	0.36
Al_2O_3	11.25	10.59	11.72	10.34	10.71	10.45	13.09	11.67	18.62	17.28
Fe_2O_3	9.96	10.11	11.94	12.10	9.57	9.63	10.37	10.67	6.57	7.06
MnO	0.16	0.15	0.16	0.14	0.16	0.15	0.15	0.13	0.13	0.12
MgO	10.31	12.44	10.70	14.90	11.02	11.92	9.28	13.32	5.82	8.75
CaO	11.64	10.97	10.67	9.42	11.40	11.12	9.84	8.77	2.30	2.14
Na_2O	1.20	1.13	4.63	4.09	1.01	0.99	2.50	2.33	5.00	4.64
K_2O	6.04	5.69	1.53	1.35	6.92	6.75	5.59	4.99	5.96	5.53
P_2O_5	1.41	1.33	1.43	1.27	1.17	1.14	1.26	1.13	0.21	0.20
A	3.90	9.50	13.90	24.00	3.90	6.30	8.10	18.10	11.70	18.10

Table 8-2. Ranges of possible primary magma compositions for lavas of U-DVB, calculated assuming equilibrium with mantle olivine of $Mg/Mg+Fe^{+2}$ = 0.84-0.88 and KD = 0.3.

A = amount of olivine removed (wt%) (oxides, wt%).

	R14508		R14500		R14522		R14557		R14550	
	a	b	a	b	a	b	a	b	a	b
SiO_2	54.08	53.08	50.34	49.29	52.99	51.77	52.83	51.75	48.40	47.55
TiO_2	0.37	0.34	0.67	0.60	0.68	0.62	0.72	0.66	1.01	0.91
Al_2O_3	17.87	16.58	17.03	15.26	15.58	14.10	17.44	15.95	16.67	14.94
Fe_2O_3	7.11	7.56	9.69	10.06	9.34	9.72	8.28	8.71	10.61	10.89
MnO	0.07	0.07	0.13	0.12	0.12	0.11	0.11	0.10	0.19	0.17
MgO	6.36	9.25	8.53	12.47	8.30	11.12	7.37	10.73	9.45	13.29
CaO	4.47	4.15	5.75	5.15	3.54	3.20	4.10	3.75	8.54	7.65
Na_2O	2.76	2.56	4.25	3.81	3.50	3.17	4.50	4.11	2.99	2.68
K_2O	6.68	6.20	3.04	2.73	5.49	4.97	4.24	3.88	1.82	1.63
P_2O_5	0.25	0.23	0.56	0.50	0.46	0.42	0.41	0.37	0.33	0.29
A	14.30	20.50	14.80	23.60	17.70	25.50	13.90	21.30	9.50	18.90

Table 8-2. (continued) Ranges of possible primary magma compositions for lavas of U-DVB, calculated assuming equilibrium with mantle olivine of Mg-number = 0.84-0.88 and KD = 0.3.
A = amount of olivine removed (wt%)

	A	B	C	D	E
SiO_2	47.30	47.27	46.88	50.67	50.30-51.20
TiO_2	1.00	2.59	2.03	1.28	2.80-3.10
Al_2O_3	15.00	13.65	13.69	15.45	12.80-14.40
FeO	10.90	11.59	11.79	9.67	10.50-12.40
MnO	0.20	0.17	0.17	0.15	-
MgO	11.60	9.15	9.78	9.05	6.70-9.50
CaO	10.10	11.05	10.81	11.72	10.00-10.90
Na_2O	2.50	2.01	2.47	2.51	2.20-2.50
K_2O	1.40	2.15	0.68	0.15	0.55-0.67
P_2O_5	-	0.42	0.24	0.20	-
Mg-number	0.69	0.65	0.61	0.63	0.56-0.66

Table 8-3. Primary magma compositions from several data sources (oxides, wt%).

A = Primary magma composition for Ungaran lavas as proposed by Nicholls and Whitford (1976)

B = Primitive K-basanite lavas from Karisimbi (Rogers et al., 1992)

C = Primary basalt from Hawaii (BVSP, 1981)

D = Average MORB from Atlantic (Best, 1982)

E = Range of liquid compositions from experimental work of Roeder and Emslie (1970).

APPENDIX A

METHODS OF INVESTIGATION

A.1 SAMPLING

Samples are listed in the tables below, according to their order of presentation in the text. Sample numbers refer to the rock collection of the School of Geosciences, University of Wollongong.

TE = tephrite; PT = phonotephrite; BA = basalt; TR = trachyte; TA = trachyandesite; TP = tephriphonolite; RH = rhyolite; BTA = basaltic trachyandesite; PH = phonolite; DA = dacite and TB = trachybasalt; T = Thin section; X = X-ray fluorescence (XRF); R = Rare earth elements (REE); I = Isotope determination

Cat.NO	Field NO	Locality	Sheet	Description	T	X	R	I
R14444	A-1	Islamic.P	Urumiyeh	TE	x	x		
R14445	A-5	"	"	TR	x			
R14446	A-7	"	"	TE	x	x		
R14447	A-8	"	"	"	x	x	x	x
R14448	A-10	"	"	"	x			
R14449	A-11	"	"	"	x	x		
R14450	A-13	"	"	"	x			
R14451	A-14	"	"	"	x			
R14452	A-15	"	"	"	x			
R14453	A-16	"	"	PT	x			
R14454	A-17	"	"	"	x	x	x	x
R14455	A-19	"	"	TE	x	x	x	x
R14456	A-21	"	"	"	x			
R14457	A-22	"	"	BA	x	x	x	x
R14458	A-23	"	"	TE	x			
R14459	A-24	"	"	"	x			
R14460	A-26	"	"	PT	x			
R14461	A-28	"	"	"	x			
R14462	A-29	"	"	TE	x	x		
R14463	A-33	"	"	"	x			
R14464	A-34	"	"	"	x			
R14465	A-37	"	"	TR	x			
R14466	A-39	"	"	TE	x	x	x	x
R14467	A-40	"	"	PT	x	x		
R14468	A-41	"	"	TE	x			
R14469	A-41b	"	"	"	x			
R14470	A-43	"	"	"	x			
R14471	A-44	"	"	"	x			
R14472	A-46	"	"	PT	x			
R14473	A-47	"	"	TE	x			
R14474	A-48	"	"	"	x	x		
R14475	A-51	"	"	"	x			
R14476	A-55	"	"	"	x			
R14477	A-60	"	"	"	x	x		
R14478	A-63	"	"	"	x	x		
R14479	A-64	"	"	"	x			
R14558	A-54	"	"	TA	x	x		
R14559	A-56	"	"	TR	x			
R14560	A-36	"	"	"	x	x		
R14561	A-35	"	"	"	x			
R14698	A-52	"	"	TA	x	x	x	x
R15806	A-30	"	"	TR	x	x		
R15807	A-53	"	"	TA	x	x		

Cat.NO	Feild.NO	Locality	Sheet	Description	T	X	R	I
R14480	1-k-2	Aghda	Nain	TR	x	x	x	x
R14481	1-k-6	"	"	"	x			
R14482	1-k-8	"	"	TP	x	x		
R14483	1-k-9	"	"	"	x	x	x	x
R14484	1-k-12	"	"	"	x			
R14485	1-k-14	"	"	PT	x			
R14486	1-k-15	"	"	TR	x	x		
R14487	1-k-19	"	"	BTA	x	x		
R14488	1-k-20	"	"	"	x	x	x	x
R14489	1-k-21	"	"	TR	x			
R14490	2-k-1	"	"	"	x			
R14491	2-K-2	"	"	"	x			
R14492	2-k-6	"	"	"	x			
R14493	2-k-9	"	"	BTA	x	x	x	x
R14494	3-k-2	"	"	TR	x			
R14495	3-k-5	"	"	BTA	x	x		
R14496	3-k-6	"	"	"	x	x		
R14497	3-k-8	"	"	TP	x	x		
R14498	3-k-9	"	"	PH	x			
R14499	3-k-10	"	"	"	x	x		
R14500	3-k-11	"	"	"	x	x	x	x
R14501	4-k-2	"	"	TP	x	x		
R14502	4-k-3	"	"	"	x			
R14503	4-k-9	"	"	BTA	x	x		
R14504	4-k-10	"	"	"	x			
R14505	4-k-12	"	"	PT	x			
R14506	4-k-13	"	"	PT	x			
R14507	5-k-1	"	"	"	x	x		
R14508	5-k-5	"	"	TP	x	x	x	x
R14510	5-k-8	"	"	PT	x			
R14562	3-k-8	"	"	"	x			
R14563	1-k-10	"	"	PH	x			
R14564	2-k-3	"	"	"	x			
R14565	3-k-3	"	"	"	x			
R14566	3-k-7	"	"	"	x			
R14569	1-k-13	"	"	"	x			
R14570	2-k-10	"	"	TR	x			
R14571	2-k-4	"	"	TA	x			
R14572	4-k-6	"	"	TA	x			
R14573	5-k-2	"	"	TA	x			
R15808	1-k-18	"	"	TR	x	x		
R15809	7-k-3	"	"	TA	x	x		
R14509	5-k-2	"	"	BTA	x	x		

Cat.NO	Field.NO	Locality	Sheet	Description	T	X	R	I
R14511	G-6	Shahrbabak	Shahrbabak	-	x			
R14512	G-9	"	"	TR	x	x		
R14513	1-G-2	"	"	-	x			
R14514	1-G-5	"	"	-	x			
R14515	1-G-10	"	"	DA	x	x		
R14516	1-G-11	"	"	TR	x			
R14517	2-G-1	"	"	TA	x			
R14518	2-G-2	"	"	-	x			
R14519	2-G-3	"	"	-	x			
R14520	2-G-5	"	"	-	x			
R14521	2-G-6	"	"	TP	x	x		
R14522	2-G-7	"	"	"	x	x	x	x
R14523	2-G-9	"	"	-	x			
R14524	2-G-10	"	"	-	x			
R14525	2-G-11	"	"	TA	x	x		
R14526	3-G-1	"	"	DA	x	x		
R14527	3-G-2	"	"	BA	x	x		
R14528	3-G-3	"	"	TA	x	x	x	x
R14529	3-G-4	"	"	-	x			
R14530	3-G-6	"	"	-	x			
R14531	3-G-8	"	"	PT	x	x		
R14533	3-G-9	"	"	TP	x	x		
R14534	3-G-10	"	"	"	x	x		
R14535	3-G-11	"	"	"	x			
R14536	4-G-4	"	"	TR	x			
R14537	4-G-5	"	"	BTA	x	x		
R14538	4-G-6	"	"	"	x	x		
R14539	4-G-8	"	"	TP	x	x		
R14540	4-G-9	"	"	-	x			
R14541	4-G-10	"	"	TP	x	x		
R14542	4-G-11	"	"	-	x			
R14543	4-G-12	"	"	-	x			
R14544	4-G-13	"	"	TP	x	x		
R14545	4-G-14	"	"	-	x			
R14546	5-G-8	"	"	-	x			
R14550	6-G-4	"	"	TB	x	x	x	x
R14551	6-G-5	"	"	TP	x	x		
R14552	6-G-6	"	"	BA	x			
R14553	7-G-2	"	"	BTA	x	x		
R14554	7-G-4	"	"	"	x	x		
R14557	7-G-8	"	"	TP	x	x	x	x
R14575	G-10	"	"	TR	x			
R14576	5-G-6	"	"	DA	x			
R14699	5-G-4	"	"	"	x	x	x	x
R15811	5-G-3	"	"	"	x	x		
R15812	5-G-10	"	"	TB	x	x	x	x
R15813	1-G-2	"	"	TA	x			

A.2 FIELD STUDIES

All of the samples were collected on two field trips to Iran in 1992 (A. Moradian) and 1994 (Dr. P. F. Carr and A. Moradian). Maps published by the Geological Survey of Iran and air photos were used to locale samples. Outcrop sampling was carried out using air photos and geological sheets of Urumiyeh, Nain and Shahrbabak. Field work in these areas consisted of examining the igneous rock units and careful collecting of the freshest representative samples of various rock types. Sample locations and detailed geological information are shown on geological maps of the Islamic Peninsula, Aghda and Shahrbabak (Figs. 3.1, 3.3, 3.6).

A.3 SAMPLING AND ANALYTICAL PROCEDURES

Sample collection was designed to cover, where possible, the main magmatic phases. Samples for chemical analysis were selected after careful thin section study to eliminate material with significant alteration. Biotite and amphibole separates were made using standard magnetic hand-piking techniques. Large sanidine phenocrysts were separated by hand-picking.

A.4 SAMPLE PREPARATION

Thin sections were prepared from the least altered specimens.

and representative samples suitable for geochemical analysis were selected. After removal of weathered and contaminated surfaces with a diamond saw hagments were crushed into small chips between tungsten carbide plates in a 30 tonne hydraulic crusher. These chips were finally crushed to powder in a tungsten carbide "Siebtechnik" mill.

A.5 WHOLE ROCK MAJOR AND TRACE ELEMENT ANALYSES

Major and most trace element abundances were determined by X-ray fluorescence

(XRF) spectrometry using automated phillips PW1450 spectrometer at the Australian National University by professor Bruce Chappell following the methods of Norrish and Hutton (1969), Norrish and Chappell (1977). Other trace elements (REE, Hf, Sc, Ta, Th and U) were determined on 18 representative samples by instrumental neutron activation analysis (INAA) at Bequerel Laboratories by Dr David Garnett. CIPW norms were calculated using GDA program written by Sheraton and Simons (1988). Loss on ignition (LOI) was measured as the weight percent loss of 1g of powdered sample heated to 1000°C for 12 hours at the School of Geosciences, University of Wollongong

A.6 ISOTOPE DETERMINATIONS

A representative subset of 18 whole rock powders was analysed for strontium and neodymium isotopic ratios at School of Geosciences, University of Wollongong, and CSIRO by Dr P. F. Carr. Powder samples weighting 0.1 mg were dissolved in teflon capsules using a mixture of HNO_3 and HF. $^{87}Sr/^{86}Sr$ and $^{143}Nd/^{144}Nd$ were measured on a VG 54E mass spectrometer and were normalised to $^{86}Sr/^{88}Sr = 0.1194$ and $^{146}Nd/^{144}Nd = 0.7219$ respectively. Replicate analyses of NBSSRM98 gave $^{87}Sr/^{86}Sr = 0.710251\pm28$ (external precision at 2σ, n = 17) and the JM-Nd standard gave $^{143}Nd/^{144}Nd = 0.51111\pm12$ (external precision at 2σ, n = 17). The K-Ar dating was carried out by Dr Sue Golding, University of Queensland. The K and Ar content were determined by flame photometry and isotope dilution respectively (cf. McDougall and Schmincke, 1977) and the ^{40}K content was calculated using $^{40}K/K = 1.167\times10^{-4}$ mol/mol.

A.7 MICROPROBE MINERAL ANALYSIS

Mineral analyses were carried out on polished thin section. The analyses were performed using a fully automated, Cameca SX50 electron microprobe (Maquarie

University and the Australian National University) calibrated with natural mineral standards. Analytical operating conditions were set at an accelerating voltage of 15 KV and beam current of 20 nA.

APPENDIX B

MODAL MINERALOGY (VOLUME %)

Appendix B-1. Islamic Peninsula

Appendix B-2. Aghda

Appendix B-3. Shahrbabak

Appendix B-1. Modal mineralogy (volume %) of tephrite from the Islamic Peninsula.

Sample	R14447	R14450	R14456	R14458	R14459	R14473	R14463
PHENOCRYSTS							
diopside	29.0	39.0	39.0	34.2	40.2	24.5	29.6
K-feldspar	8.0	4.5	20.0	1.2	14.5	5.5	8.2
leucite	47.7	25.9	6.0	23.9	24.0	37.2	26.7
GROUNDMASS							
olivine	0.5	-	-	3.0	-	-	-
diopside	6.2	8.5	6.3	19.0	2.0	6.5	3.0
K-feldspar	2.0	8.5	14.5	7.5	8.0	28.0	30.0
leucite	0.2	7.2	3.2	7.7	5.0	12.0	-
biotite	4.9	2.7	9.0	-	2.2	1.0	1.5
Fe-Ti Oxide	1.2	3.2	2.0	3.0	4.2	3.5	1.2
apatite	0.6	0.5	-	0.5	-	0.5	0.6

Appendix B-1 (continued). Modal mineralogy (volume %) of tephrite from the Islamic Peninsula.

Sample	R14446	R14449	R14471	R14476	R14477	R14478	R14469
PHENOCRYSTS							
diopside	31.0	26.0	30.8	33.0	28.0	28.0	28.0
K-feldspar	4.0	5.7	5.4	2.2	6.0	24.2	10.0
leucite	22.4	6.2	17.7	30.0	37.5	9.0	29.5
Fe-Ti Oxide	2.2	-	0.6	-	-	-	-
GROUNDMASS							
diopside	18.0	15.0	1.5	0.7	8.0	5.7	23.0
K-feldspar	9.2	6.2	31.5	11.6	7.5	11.2	0.5
leucite	10.5	30.2	8.5	8.0	10.0	17.2	7.0
biotite	-	10.0	-	2.2	-	-	0.2
Fe-Ti Oxide	1.5	0.2	2.2	3.0	0.6	3.5	0.7
apatite	0.5	0.3	0.5	-	1.2	1.0	0.6
iddingsite	0.4	-	0.5	0.8	-	0.7	-
serpentine	0.3	0.2	0.6	1.5	1.2	-	0.5
chlorite	-	-	-	1.0	-	-	-

Appendix B-1 (continued). Modal mineralogy (volum %) of tephrite from the Islamic Peninsula.

Sample	R14448	R14451	R14462	R14466	R14470	R14444
PENOCRYSTS						
diopside	31.0	37.3	38.7	30.0	21.4	22.0
K-feldspar	8.7	1.7	1.0	2.5	3.2	17.2
leucite	31.0	12.0	36.2	29.5	22.6	19.7
Fe-Ti Oxide	-	-	-	-	-	5.0
GROUNDMASS						
olivine	0.7	-	-	-	-	-
diopside	15.0	21.0	7.4	8.1	19.7	1.2
K-feldspar	5.2	4.2	10.7	2.7	6.0	22.2
leucite	2.0	21.1	5.5	16.9	18.0	8.0
biotite	1.1	0.7	-	5.3	1.6	2.0
Fe-Ti Oxide	3.0	0.4	0.2	0.7	4.2	-
apatite	1.0	-	-	1.6	-	1.0
sericite	0.6	-	-	1.5	-	-
zeolite	0.7	0.5	-	-	-	1.2
serpentine	-	1.2	0.2	-	0.7	-
calcite	-	-	-	-	-	-
chlorite	-	-	-	1.2	-	0.5

Appendix B-1 (continued). Modal mineralogy (volume %) of tephrite from the Islamic Peninsula.

Sample	R14452	R14455	R14464	R14468	R14474	R14479
PHENOCRYSTS						
diopside	26.9	21.2	32.5	30.2	31.2	27.7
K-feldspar	12.5	7.0	2.7	7.5	5.5	3.5
leucite	24.7	43.3	30.0	12.0	37.2	42.0
GROUNDMASS						
olivine	-	-	0.4	-	-	-
diopside	3.0	4.7	21.2	18.3	4.2	14.2
K-feldspar	14.7	12.2	3.5	19.3	10.0	5.0
leucite	9.7	7.2	4.0	9.2	3.0	2.7
biotite	2.7	-	-	-	4.5	-
Fe-Ti Oxide	1.5	2.4	2.3	2.2	-	2.0
apatite	0.3	1.5	0.7	0.6	1.0	0.5
sericite	0.6	-	-	-	-	-
zeolite	1.6	-	1.0	-	0.6	-
serpentine	1.0	-	0.7	-	1.2	-
chlorite	0.8	-	-	-	0.8	-
calcite	-	0.5	0.6	-	1.4	1.2
iddingsite	-	-	0.5	0.7	-	1.2

Appendix B-1. Modal mineralogy (volume %) of phonotephrite from the Islamic Peninsula.

Sample	R14453	R14460	R14461	R14467	R14475	R14472	R14454
PHENOCRYSTS							
diopside	18.0	25.0	37.7	28.0	25.2	31.2	28.7
K-feldspar	6.0	6.2	8.2	24.7	1.0	10.5	-
leucite	28.7	40.2	28.5	11.0	6.7	10.5	20.7
GROUNDMASS							
diopside	1.0	9.5	8.7	11.2	11.0	11.0	8.7
K-feldspar	30.0	8.2	2.7	10.4	48.5	27.5	-
leucite	5.5	2.7	5.6	7.0	-	0.2	37.2
olivine	2.5	1.9	2.2	0.8	0.5	-	2.6
biotite	2.3	3.7	2.1	1.0	-	-	-
Fe-Ti Oxide	2.2	1.2	2.9	5.0	6.0	7.7	3.2
apatite	1.5	0.4	-	0.5	-	1.0	0.9
calcite	0.5	-	0.4	-	0.7	-	-
chlorite	-	0.5	-	-	-	0.4	-
sericite	-	-	-	-	0.6	-	-
serpentine	0.8	0.3	-	-	-	-	-
iddingsite	1.0	-	0.3	0.4	-	-	0.6

Appendix B-1. Modal mineralogy (volume %) of basalt and trachyandesite from the Islamic Peninsula.

Sample	R14457	R14558	R15807	R14698
PHENOCRYSTS				
diopside	49.5	46.5	8.2	7.2
leucite	15.0	21.4	-	-
sandine	-	-	2.0	16.7
biotite	-	-	5.2	4.7
GROUNDMASS				
diopside	17.3	11.7	-	-
sanidine	-	-	81.4	68.0
leucite	7.5	10.5	-	-
biotite	5.0	2.4	-	-
olivine	1.0	3.0	-	-
Fe-Ti Oxide	2.0	1.4	0.2	1.0
apatite	1.4	1.7	-	-
calcite	0.8	0.6	2.0	1.8
chlorite	0.5	0.9	-	-
sericite	-	-	1.0	0.6

Appendix B-1. Modal mineralogy (volume %) of trachyte from the Islamic Peninsula.

Sample	R14445	R14559	R14560	R14561	R15806	R14465
PHENOCRYSTS						
diopside	0.7	10.5	17.5	7.4	5.7	5.0
sanidine	1.0	4.4	21.0	13.2	9.0	8.4
biotite	-	-	-	2.5	1.7	0.5
GROUNDMASS						
diopside	6.2	3.0	3.6	-	3.0	1.0
sanidine	91.4	80.5	55.7	75.0	78.6	70.0
Fe-Ti Oxide	0.2	1.6	2.0	1.7	1.5	2.0
apatite	-	-	0.2	-	-	2.0
calcite	0.3	-	-	-	0.5	5.0
sericite	-	-	-	-	-	3.0
sphene	0.2	-	-	0.5	-	3.0

Appendix B-2. Modal mineralogy (volume %) Of tephriphonolite from Aghda.

Sample	R14482	R14483	R14497	R14501	R14508	R14484	R14502	R14507
PHENOCRYSTS								
diopside	2.2	1.7	1.2	2.0	1.0	3.2	5.5	8.0
sanidine	5.5	6.5	2.0	7.5	4.0	5.0	6.0	7.5
plagioclase	70.0	5.0	4.0	6.5	1.5	0.5	2.5	7.0
analcime	23.5	29.0	42.2	10.3	19.2	33.0	3.2	2.0
pumpellyite	14.0	20.7	12.0	15.5	-	5.5	5.8	2.5
GROUNDMASS								
diopside	1.2	1.2	1.7	1.4	-	0.2	3.0	2.2
sanidine	24.5	25.8	23.2	31.0	44.2	31.7	43.4	45.5
plagioclase	18.5	4.7	5.0	18.0	20.0	3.6	19.2	15.0
nepheline	0.8	0.8	1.0	0.9	1.0	1.3	1.0	1.2
biotite	0.5	0.2	-	-	0.9	-	0.8	-
olivine	1.0	1.8	1.0	0.2	2.3	2.3	2.5	0.9
Fe-Ti oxide	1.2	1.2	0.2	2.7	0.2	0.2	2.1	2.6
calcite	5.7	0.1	2.0	2.0	2.7	-	-	2.0
sericite	3.0	0.5	0.9	2.0	2.0	-	-	2.0
chlorite	-	-	1.6	-	1.0	7.0	-	0.8
zeolite	2.0	0.5	2.0	-	-	4.0	-	-
epidote	2.0	-	-	-	-	2.5	-	0.8

Appendix B-2. Modal mineralogy (volume %) of phonolite from Aghda.

Sample	R14563	R14564	R14565	R14566	R14498	R14499	R14567	R14568
PHENOCRYSTS								
diopside	3.0	-	11.0	-	-	-	7.5	2.5
K-feldspar	12.0	17.0	11.7	2.0	1.5	-	10.5	10.0
plagioclase	15.0	11.2	14.3	5.6	-	1.2	6.7	10.0
analcime	17.0	2.0	13.9	19.5	18.3	3.3	-	20.0
GROUNDMASS								
K-feldspar	35.0	46.2	35.0	58.3	62.0	85.0	40.7	45.0
analcime	-	-	1.2	-	-	-	17.7	-
biotite	-	0.5	-	-	-	-	0.7	-
Fe-Ti oxide	2.0	1.2	5.5	1.0	1.2	10.5	4.2	-
calcite	10.0	14.0	7.4	8.2	8.2	-	5.0	9.0
sericite	-	-	-	3.0	4.0	-	-	-
epidote	5.0	8.0	-	-	-	-	1.0	3.0
apatite	-	-	-	-	1.0	-	1.3	-
zeolite	1.0	-	-	2.4	-	-	-	-
chlorite	-	-	-	-	3.0	-	2.0	-
serpentine	-	-	-	-	1.0	-	3.7	-

Appendix B-2. Modal mineralogy (volume %) of phonotphrite from Aghda.

Sample	R14485	R14562	R14500	R14506	R14510
PHENOCRYSTS					
diopside	5.9	7.0	8.0	-	0.5
sanidine	0.5	6.5	4.0	3.3	15.7
plagioclase	19.2	11.2	8.0	6.2	4.0
analcime	10.0	9.7	5.0	10.0	1.3
GROUNDMASS					
diopside	2.2	2.0	1.1	-	0.2
sanidine	48.2	19.7	54.4	70.0	59.2
analcime	8.0	26.7	16.0	7.8	2.0
olivine	0.2	1.7	1.5	0.5	0.2
biotite	-	1.3	0.4	0.5	0.3
Fe-Ti oxide	1.5	1.5	1.6	0.2	5.5
apatite	1.0	2.0	-	-	-
calcite	1.8	5.9	2.0	-	6.0
epidote	1.5	2.0	-	-	2.0
zeolite	-	3.0	-	1.5	-
sericite	-	-	-	-	3.1

Appendix B-2. Modal mineralogy (volume %) of trachyte from Aghda.

Sample	R14480	R14486	R14494	R14490	R14489	R14491	R14569	R14570
PHENOCRYSTS								
diopside	-	-	1.0	-	1.5	-	-	-
K-feldspar	8.0	11.2	16.0	8.7	0.2	6.2	20.5	38.2
plagioclase	1.0	6.0	5.0	2.3	-	12.2	-	5.0
nephline	-	4.2	12.0	4.4	-	4.4	-	15.5
GROUNDMASS								
K-feldspar	81.0	72.3	63.0	82.7	79.0	71.3	36.5	30.7
biotite	1.0	0.5	-	0.2	-	0.5	0.5	-
Fe-Ti oxide	1.2	5.0	0.5	1.0	6.2	4.5	2.0	3.8
sericite	3.0	0.2	-	-	-	-	-	-
calcite	0.8	0.6	2.5	0.3	2.0	0.4	35.0	5.7
epidote	-	-	-	-	10.8	-	-	-
chlorite	1.0	-	-	-	-	-	3.5	-
kaoline	3.0	-	-	0.4	0.3	0.5	2.0	1.1

Appendix B-2. Modal mineralogy (volume %) of trachyandesite from Aghda.

Sample	R14487	R14571	R14572	R14573	R15809
PHENOCRYSTS					
hornblende	8.2	-	-	4.1	8.7
K-feldspar	10.0	6.0	20.0	18.5	-
plagioclase	6.5	10.0	25.0	11.0	23.0
GROUNDMASS					
diopside	1.8	2.0	-	-	-
plagioclase	61.0	65.0	50.0	38.5	63.0
biotite	-	0.7	-	0.1	-
Fe-Ti oxide	4.0	5.0	2.0	6.8	2.0
zeolite	3.5	2.0	-	6.0	-
calcite	3.0	5.3	2.0	8.0	2.0
apatite	-	-	-	2.0	-
sericite	2.0	4.0	1.0	5.0	1.3

Appendix B-2. Modal mineralogy (volume %) of basaltic trachyandesite and ryholite from Aghda.

Sample	R14493	R14504	R14488	R14495	R14496	R14503
PHENOCRYSTS						
diopside	-	-	2.0	5.6	9.2	10.0
sanidine	10.7	14.2	7.2	12.0	10.4	10.0
plagioclas	1.5	6.5	2.5	13.1	14.0	10.0
nepheline	-	-	10.2	4.0	-	-
quartz	1.5	20.5	-	-	-	-
GROUNDMASS						
diopside	-	-	7.7	1.0	3.0	0.7
sanidine	76.0	29.0	51.3	50.0	54.2	63.7
plagioclase	-	-	-	-	-	1.2
biotite	0.4	1.2	0.1	0.1	1.0	-
olivine	-	-	2.5	2.8	0.3	-
Fe-Ti oxide	1.0	0.2	3.5	0.5	3.5	1.7
quartz	8.0	12.2	-	-	-	-
calcite	0.6	8.0	7.5	4.5	3.5	1.7
sericite	-	3.0	0.5	1.4	-	1.0
zeolite	-	5.0	3.5	3.0	-	-
zircon	0.3	0.2	-	-	-	-
chlorite	-	-	1.5	2.0	0.9	-

Appendix B-3. Modal mineralogy (volum %) of basalt, trachybasalt and basaltic trachyandesite from Shahrbabak.

Sample	R14527	R14552	R14550	R15812	R14538	R14553
PHENOCRYSTS						
olivine	1.5	4.5	3.5	1.5	-	-
diopside						
plagioclase	8.2	4.4	1.3	2.7	2.0	3.3
sanidine	15.5	20.0	3.6	36.3	10.6	33.3
GROUNDMASS	8.5	6.5	0.9	1.6	11.3	7.3
olivine						
diopside	-	-	-	-	4.0	2.6
plagioclase	14.0	16.0	-	7.0	-	-
Fe-Ti oxide	47.4	35.2	77.3	29.3	43.3	40.0
sanidine	5.2	6.0	7.0	8.3	6.6	3.6
calcite	-	-	-	-	3.6	-
sericite	-	2.9	2.4	5.3	6.0	3.9
apatite	-	1.0	1.5	2.0	3.5	2.0
zzeolite	-	1.0	0.5	0.5	1.0	0.5
chlorite	-	-	0.5	1.5	3.0	1.5
iddingsite	-	-	0.5	1.0	1.0	-
serpentine	-	1.5	1.0	2.0	2.1	1.5
	-	1.0	-	1.0	2.0	0.5

Appendix B-3. Modal mineralogy (volume %) of tephriphonolite from Shahrbabak.

Sample	R14534	R14535	R14541	R14544	R14551	R14557
PHENOCRYSTS						
diopside	1.5	0.6	1.0	-	2.3	1.8
sanidine	11.5	5.2	22.3	6.0	10.8	5.3
plagioclase	-	15.2	8.0	5.4	14.6	16.6
analcime	38.0	31.7	30.4	23.0	22.0	25.6
nepheline	4.0	3.0	2.0	-	4.0	3.0
GROUNDMASS						
diopside	-	0.3	2.3	4.1	0.7	1.6
sanidine	37.3	40.4	23.8	60.0	39.3	42.0
Fe-Ti oxide	1.5	1.3	5.2	1.0	2.3	1.0
calcite	3.0	1.3	2.0	-	1.0	1.2
chlorite	1.0	0.5	1.5	-	-	-
iddingsite	1.5	0.5	1.0	-	1.0	0.5
serpentine	0.6	-	-	-	2.0	-
zeolite	-	-	0.5	-	-	0.4
sericite	0.6	-	-	0.5	-	1.0

Appendix B-3. Modal mineralogy (volume %) of trachyte from Shahrbabak.

Sample	R14512	R14575	R14536	R14516
PHENOCRYSTS				
hornblende	9.3	10.0	9.5	10.0
K-feldspar	5.6	3.0	4.6	4.0
plagioclase	25.0	24.4	27.0	27.0
biotite	5.0	1.3	4.0	2.5
GROUNDMASS				
K-feldspar	52.0	61.0	53.0	54.0
Fe-Ti Oxide	0.6	0.3	0.5	0.6
calcite	1.5	-	1.0	1.3
sericite	1.0	-	0.4	0.6

Appendix B-3. Modal mineralogy (volum %) of trachyandesite and dacite from Shahrbabak.

Sample	R14517	R15813	R14554	R15811	R14699	R14576
PHENOCRYSTS						
hornblende	-	5.0	0.1	4.5	3.0	3.9
diopside	2.6	-	0.1	-	-	-
sanidine	1.3	23.6	14.1	2.6	6.0	6.1
plagioclase	30.6	7.6	16.4	19.6	16.6	25.3
quartz	-	-	-	3.5	5.0	5.0
biotite	-	-	-	5.8	0.5	4.5
GROUNDMASS						
hornblende	1.2	3.3	1.8	5.0	1.1	5.6
sanidine	21.3	35.6	27.1	11.3	1.8	10.6
quartz	-	-	-	18.0	11.0	15.0
plagioclase	40.3	17.0	33.9	15.0	49.3	18.0
biotite	-	-	-	0.7	2.3	1.2
Fe-Ti oxide	2.3	4.0	2.4	5.5	0.6	2.0
calcite	0.5	1.5	2.1	4.0	1.3	1.5
sericite	0.3	0.6	1.0	2.0	1.5	1.3
zeolite	0.8	1.2	0.5	1.0	-	-
chlorite	-	0.5	0.5	1.5	-	-

APPENDIX C

MINERAL CHEMISTRY

first order subdivision (e.g. C-1) is for mineral types where,

1 = clinopyroxene
2 = olivine
3 = titanomagnetite
4 = biotite
5 = hornblende
6 = K-feldspar
7 = plagioclase
8 = leucite
9 = analcime

Second order subdivision (e.g. C-1.1) is for rock types where,

1 = basalt
2 = trachybasalt
3 = basaltic trachyandesite
4 = tephrite
5 = phonotephrite
6 = tephriphonolite
7 = trachyandesite
8 = trachyte
9 = dacite
10 = rhyolite

ABBREVIATION USED

Spot

C = core
R = rim

Appendix C-1.4. Mineral chemistry of pyroxene in tephrite from the Islamic Peninsula (oxides, wt%).

Sample	R14466	R14466	R14466	R14466	R14466	R14466	R14466
Spot	C	R	C	C	R	R	R
SiO_2	53.84	50.64	53.78	53.57	51.31	51.12	51.89
TiO_2	0.22	0.69	0.25	0.20	0.62	0.58	0.43
Al_2O_3	0.62	2.28	0.86	0.93	2.04	2.29	2.23
MgO	17.75	15.07	17.45	17.41	15.53	15.35	15.51
CaO	24.09	24.07	24.67	24.27	24.70	24.36	23.97
MnO	0.09	0.16	0.05	0.04	0.14	0.05	0.13
FeO	2.82	5.86	2.87	2.86	5.03	5.34	4.99
Na_2O	0.21	0.35	0.18	0.19	0.33	0.32	0.35
K_2O	0.02	0.00	0.01	0.00	0.00	0.01	0.01
Total	99.79	99.12	100.38	99.78	99.78	99.56	99.74
Wo	47.00	48.50	48.00	47.73	49.00	48.74	48.47
En	48.50	42.00	47.50	47.73	43.00	42.71	43.87
Fs	4.50	9.00	4.50	4.52	8.00	8.50	7.65

Appendix C-1.4 (continued). Mineral chemistry of pyroxene in tephrite from the Islamic Peninsula (oxides, wt%).

Sample	R14447	R14447	R14447	R14447	R14455	R14455	R14455
Spot	R	C	R	R	C	R	C
SiO_2	52.52	50.15	50.41	49.89	49.23	45.57	49.67
TiO_2	0.72	0.76	1.08	0.81	1.13	2.37	1.04
Al_2O_3	1.39	3.20	2.54	2.99	3.63	6.11	3.12
MgO	14.32	14.73	14.19	14.71	13.12	11.47	13.63
CaO	23.15	23.81	23.69	23.70	23.59	22.81	24.00
MnO	0.23	0.06	0.19	0.14	0.23	0.22	0.17
FeO	6.52	5.79	6.01	6.09	7.32	8.27	6.59
Na_2O	0.85	0.31	0.65	0.38	0.69	0.77	0.84
Total	99.75	98.89	98.84	98.86	98.95	97.70	98.74
Wo	47.67	48.79	48.97	48.48	49.48	50.26	49.49
En	41.45	41.84	40.81	41.92	38.14	34.92	39.29
Fs	10.36	9.18	9.69	9.60	11.85	14.28	10.72

Appendix C-1.4 (continued). Mineral chemistry of pyroxene in tephrite from the Islamic Peninsula (oxides, wt%).

Sample	R14466	R14466	R14466	R14447	R14447	R14447	R14447
Spot	R	R	R	C	R	C	R
SiO_2	51.01	52.54	46.07	50.55	49.84	48.38	50.57
TiO_2	0.60	0.64	2.10	0.90	1.27	1.22	1.05
Al_2O_3	2.33	0.92	5.19	2.93	3.05	4.98	2.36
MgO	15.39	14.34	12.48	13.79	14.35	13.48	13.74
CaO	24.25	23.11	23.60	22.97	23.61	23.54	23.38
MnO	0.10	0.24	0.14	0.25	0.18	0.17	0.16
FeO	5.02	6.41	9.20	6.84	6.25	6.72	6.68
Na_2O	0.55	1.00	0.73	0.61	0.63	0.57	0.81
Total	99.48	99.28	99.57	98.86	99.19	99.10	98.83
Wo	48.98	47.94	49.23	48.18	48.47	49.22	48.97
En	42.93	41.24	36.04	39.90	40.82	39.38	39.69
Fs	8.08	10.30	14.72	11.40	10.20	10.88	10.82

Appendix C-1.1.4 (continued). Mineral chemistry of pyroxene in tephrite and basalt from the Islamic Peninsula (oxides, wt%).

Sample	R14455	R14457	R14457	R14457	R14457	R14457	R14457
Spot	C	C	R	C	R	C	R
SiO_2	49.69	48.89	53.28	50.52	52.67	51.66	54.02
TiO_2	1.07	1.29	0.20	0.90	0.24	0.57	0.13
Al_2O_3	3.13	3.77	1.07	2.53	1.02	2.20	0.83
MgO	13.94	14.22	17.33	14.84	17.07	15.22	17.85
CaO	23.78	23.60	24.01	24.46	24.22	24.80	24.21
MnO	0.22	0.08	0.05	0.16	0.09	0.12	0.02
FeO	6.77	6.12	2.53	5.54	2.97	4.87	2.06
Na_2O	0.50	0.54	0.27	0.35	0.17	0.22	0.23
Total	99.10	98.56	99.29	99.41	98.66	99.72	100.06
Wo	48.98	49.23	47.98	49.49	48.24	50.00	47.72
En	39.80	41.03	47.98	41.92	47.24	42.42	49.24
Fs	10.71	9.74	4.04	8.58	4.52	7.58	3.05

Appendix C-1.1.5. Mineral chemistry of pyroxene in basalt and phonotephrite from the Islamic Peninsula (oxides, wt%).

Sample	R14457	R14457	R14457	R14457	R14454	R14454	R14454
Spot	C	R	C	R	C	R	C
SiO_2	54.23	49.93	54.24	53.52	51.15	48.91	50.13
TiO_2	0.16	1.27	0.16	0.26	0.47	1.16	0.95
Al_2O_3	0.84	3.20	0.79	0.93	2.61	3.70	2.81
MgO	18.08	14.33	17.71	17.31	15.30	13.77	14.24
CaO	24.12	24.39	24.29	24.18	23.29	23.37	23.45
MnO	0.07	0.11	0.06	0.08	0.08	0.21	0.26
FeO	1.98	6.05	2.21	2.23	5.61	7.17	6.31
Na_2O	0.20	0.35	0.19	0.19	0.47	0.52	0.42
Total	100.34	99.67	100.33	99.39	99.07	98.87	98.66
Wo	47.47	49.75	47.72	48.22	47.45	48.22	48.47
En	49.49	40.61	48.73	48.22	43.37	39.59	40.82
Fs	3.03	9.65	3.55	3.55	9.18	11.68	10.20

Appendix C-1.5 (continued). Mineral chemistry of pyroxene in phonotephrite from the Islamic Peninsula (oxides, wt%).

Sample	R14454	R14454
Spot	R	C
SiO_2	48.61	49.13
TiO_2	1.29	1.18
Al_2O_3	4.44	3.98
MgO	13.11	13.50
CaO	23.02	22.98
MnO	0.21	0.14
FeO	7.29	6.99
Na_2O	0.57	0.58
Total	99.01	98.49
Wo	48.69	48.69
En	38.74	39.79
Fs	12.04	11.52

Appendix C-1.7. Mineral chemistry of pyroxene in trachyandesite from the Islamic Peninsula (oxides, wt%).

Sample	R14698	R14698	R14698	R14698	R14698	R14698	R14698
Spot	R	C	R	C	R	C	R
SiO_2	47.83	51.38	50.30	50.64	50.22	53.06	51.72
TiO_2	1.59	0.27	0.58	0.48	0.57	0.30	0.89
Al_2O_3	4.82	1.43	2.65	2.44	2.54	0.84	1.96
MgO	12.96	12.78	12.04	12.74	12.71	15.20	16.09
CaO	23.15	24.02	23.21	23.00	23.36	24.12	23.69
MnO	0.16	0.31	0.25	0.27	0.27	0.17	0.13
FeO	7.32	8.15	9.16	8.60	8.73	5.03	4.45
Na_2O	0.59	0.75	0.70	0.59	0.69	0.53	0.32
Total	98.44	99.09	98.93	98.81	99.28	99.49	99.30
Wo	48.96	49.75	49.22	48.45	48.47	48.73	47.72
En	38.54	36.55	35.23	37.11	36.73	42.64	45.18
Fs	11.98	13.20	15.02	13.92	14.29	8.12	7.10

Appendix C-1.6. Mineral chemistry of pyroxene in tephriphonolite from Aghda (oxides, wt%).

Sample	R14497	R14497	R14497	R14497	R14497	R14497
Spot	C	R	C	R	C	R
SiO_2	49.13	49.74	49.38	49.91	49.05	49.99
TiO_2	0.89	0.82	0.97	0.82	0.98	0.79
Al_2O_3	4.16	3.51	2.76	2.27	4.16	2.51
MgO	12.51	12.66	11.11	10.99	12.39	12.10
CaO	22.24	22.77	21.80	21.89	21.73	21.89
MnO	0.29	0.31	0.39	0.43	0.28	0.35
FeO	9.86	9.19	12.18	12.11	10.07	10.80
Na_2O	0.44	0.43	0.54	0.52	0.55	0.45
Total	99.58	99.42	99.14	99.00	99.21	98.99
Wo	46.63	47.67	46.39	46.63	46.35	46.15
En	36.79	36.79	32.99	32.64	36.46	35.38
Fs	16.06	15.03	20.10	20.21	16.67	17.95

Appendix C-1.6 (continued). Mineral chemistry of pyroxene in tephriphonolite from Aghda (oxides, wt%).

Sample	R14483	R14483	R14483	R14483	R14483	R14483	R14488
Spot	C	R	C	R	C	R	C
SiO_2	49.69	49.93	49.28	50.07	50.30	49.86	50.05
TiO_2	0.90	0.83	0.81	0.71	0.61	0.92	0.68
Al_2O_3	2.80	2.49	3.72	2.35	3.01	2.65	2.79
MgO	12.17	12.31	12.74	12.33	13.11	11.58	13.21
CaO	21.92	22.03	22.44	21.72	22.37	21.69	21.78
MnO	0.41	0.36	0.31	0.34	0.31	0.46	0.31
FeO	10.86	10.49	9.18	10.42	9.02	11.48	9.18
Na_2O	0.46	0.49	0.41	0.44	0.39	0.51	0.41
Total	99.24	99.06	98.94	98.52	99.11	99.32	98.48
Wo	46.15	46.39	47.15	46.11	46.67	45.88	45.88
En	35.38	35.08	37.31	36.27	37.95	34.02	38.66
Fs	17.95	17.01	15.03	17.10	14.87	19.07	14.95

Appendix C-1.5. Mineral chemistry of pyroxene in phonotephrite from Aghda (oxides, wt%).

Sample	R14500	R14500	R14500	R14500	R14500	R14500
Spot	C	R	C	R	C	R
SiO_2	50.53	48.83	49.51	47.89	49.00	48.62
TiO_2	0.71	1.15	0.76	1.08	0.86	0.87
Al_2O_3	2.32	3.55	4.22	5.27	4.53	4.44
MgO	13.23	11.55	13.30	12.39	13.21	13.14
CaO	21.80	21.86	22.02	22.03	22.05	22.55
MnO	0.30	0.37	0.25	0.27	0.22	0.22
FeO	9.69	11.39	9.12	9.81	8.95	8.88
Na_2O	0.38	0.42	0.41	0.50	0.40	0.36
Total	99.03	99.13	99.59	99.27	99.27	99.16
Wo	45.41	46.63	45.88	46.88	46.60	47.18
En	38.27	34.20	38.66	36.46	38.74	37.95
Fs	15.82	18.65	14.95	16.15	14.66	14.36

Appendix C-1.3. Mineral chemistry of pyroxene in basaltic trachyandesite from Aghda (oxides, wt%).

Sample	R14488	R14488	R14488	R14488	R14488	R14488	R14488
Spot	R	C	R	C	R	C	R
SiO_2	47.71	49.26	49.39	48.16	48.75	47.61	49.62
TiO_2	1.11	0.87	0.81	0.88	0.88	1.44	1.01
Al_2O_3	4.96	3.81	2.80	2.85	3.88	4.42	3.79
MgO	12.17	12.49	12.91	11.29	12.72	11.31	11.24
CaO	22.00	21.49	21.97	21.60	21.73	21.76	21.40
MnO	0.28	0.31	0.32	0.37	0.22	0.36	0.47
FeO	9.74	9.98	9.47	11.39	10.34	11.07	10.45
Na_2O	0.53	0.47	0.38	0.53	0.45	0.46	0.94
Total	98.63	98.68	98.05	97.10	99.01	98.43	99.01
Wo	46.88	45.83	46.15	46.67	45.64	46.88	46.77
En	36.46	36.98	37.95	33.85	36.92	33.85	34.40
Fs	16.15	16.67	15.38	18.97	16.92	19.75	17.74

Appendix C-1.1. Mineral chemistry of pyroxene in basalt from Shahrbabak (oxides, wt%).

Sample	R14527	R14527	R15812	R15812	R15812	R15812	R15812
Spot	C	C	C	C	R	R	C
SiO_2	47.62	47.14	51.46	49.24	47.87	51.01	50.71
TiO_2	0.90	1.02	0.51	1.10	1.52	0.53	0.64
Al_2O_3	5.36	6.31	3.28	5.32	5.46	3.61	3.77
Cr_2O_3	0.04	0.00	0.46	0.33	0.05	0.85	0.72
MgO	13.39	12.90	15.59	14.66	13.38	15.01	15.57
CaO	21.70	21.38	22.62	21.30	21.54	21.69	22.25
MnO	0.17	0.21	0.10	0.12	0.26	0.12	0.06
FeO	8.10	8.83	5.03	6.36	7.81	5.29	5.21
Na_2O	0.34	0.52	0.37	0.48	0.85	0.91	0.42
Total	97.64	98.38	99.51	98.91	98.76	99.12	99.35
Wo	46.11	46.03	46.88	45.45	46.03	46.49	46.32
En	39.90	38.62	44.79	43.85	40.21	44.86	45.26
Fs	13.47	14.81	8.33	10.70	13.22	8.65	8.42

Appendix C-1.1 (continued). Mineral chemistry of pyroxene in basalt from Shahrbabak (oxides, wt%).

Sample	R15812	R15812	R15812
Spot	C	R	R
SiO_2	51.21	47.16	48.13
TiO_2	0.56	1.20	1.38
Al_2O_3	3.54	5.86	4.56
Cr_2O_3	0.51	0.00	0.00
MgO	15.86	13.28	11.10
CaO	21.88	21.70	21.60
MnO	0.16	0.17	0.34
FeO	6.40	8.28	10.74
Na_2O	0.42	0.69	0.47
K_2O	0.02	0.01	0.01
Total	99.60	98.44	98.33
Wo	45.55	47.40	47.28
En	45.55	32.29	33.79
Fs	8.90	19.7	18.94

Appendix C-1.6. Mineral chemistry of pyroxene in tephriphonolite from Shahrbabak(oxides, wt%).

Sample	R14544	R14544	R14544	R14544	R14544	R14544	R14544
Spot	C	R	C	R	C	R	R
SiO_2	49.75	50.27	50.28	50.17	50.45	48.75	50.43
TiO_2	1.04	0.91	0.90	1.03	0.86	1.08	0.82
Al_2O_3	3.26	2.76	2.76	2.52	2.66	3.83	1.61
MgO	13.07	13.03	13.15	11.78	13.22	12.52	12.91
CaO	22.29	22.06	22.28	21.61	22.39	21.97	21.94
MnO	0.32	0.38	0.35	0.46	0.36	0.38	0.47
FeO	9.02	9.66	9.25	11.16	9.17	9.26	10.45
Na_2O	0.51	0.49	0.45	0.58	0.48	0.52	0.48
Total	99.31	99.56	99.45	99.43	99.50	98.37	99.19
Wo	46.39	45.88	46.39	45.50	46.67	46.88	45.45
En	38.14	37.63	38.14	34.72	37.95	36.98	36.87
Fs	14.95	15.98	14.95	18.65	14.87	15.63	16.67

Appendix C-1.6 (continued). Mineral chemistry of pyroxene in tephriphonolite from Shahrbabak (oxides, wt%).

Sample	R14557	R14557	R14557	R14557	R14557	R14557	R14557
Spot	C	C	R	C	C	R	C
SiO_2	44.81	49.52	49.04	48.48	49.96	49.51	50.08
TiO_2	0.97	0.95	1.03	0.98	0.94	1.06	1.02
Al_2O_3	2.48	3.48	4.43	5.19	3.25	3.23	2.59
MgO	11.64	13.37	12.96	13.03	13.75	13.27	12.83
CaO	24.87	21.86	22.00	21.75	22.02	21.78	21.94
MnO	0.33	0.37	0.28	0.25	0.33	0.31	0.36
FeO	9.06	8.65	8.37	8.66	8.70	8.81	9.65
Na_2O	0.43	0.49	0.48	0.44	0.50	0.44	0.47
Total	94.66	98.73	98.69	98.82	99.50	98.44	99.03
Wo	51.43	46.11	46.84	46.32	45.88	46.11	45.88
En	33.33	39.38	38.42	38.95	39.69	38.86	37.63
Fs	14.76	13.99	14.20	14.21	13.91	14.51	15.98

Appendix C-1.6 (continued). Mineral chemistry of pyroxene in tephriphonolite from Shahrbabak (oxides, wt%).

Sample	R14557	R14522	R14522	R14527	R14527
Spot	R	C	R	C	R
SiO_2	51.21	49.88	49.72	46.59	46.33
TiO_2	0.68	1.02	0.77	1.00	1.09
Al_2O_3	1.41	2.22	2.14	7.02	7.07
MgO	11.91	10.85	9.80	12.63	12.51
CaO	21.97	22.19	22.23	21.57	21.35
MnO	0.51	0.53	0.48	0.25	0.26
FeO	10.71	11.65	12.62	8.57	9.15
Na_2O	0.50	0.76	0.84	0.42	0.44
K_2O	0.10	0.01	0.00	0.03	0.00
Total	99.01	99.15	98.60	98.11	98.30
Wo	46.39	47.42	46.91	46.81	46.56
En	35.05	38.66	38.66	38.30	37.57
Fs	17.53	13.40	13.92	14.36	15.34

Appendix C-2.4. Mineral chemistry of olivine in tephrite from the Islamic Peninsula (oxides, wt%).

Sample	R14466	R14466	R14466
Spot	C	C	C
SiO_2	39.44	39.53	40.03
TiO_2	0.02	0.05	0.06
Al_2O_3	0.05	0.04	0.00
MgO	45.21	44.64	45.05
MnO	0.42	0.42	0.43
FeO	14.48	14.62	14.30
Na_2O	0.01	0.00	0.03
Total	100.38	100.08	100.60
Fo	84.00	84.00	85.71
Fa	16.00	16.00	14.29

Appendix C-2.1. Mineral chemistry of olivine in basalt from Shahrbabak (oxides, wt%).

Sample	R15812	R15812	R15812	R14527	R14527
Spot	R	C	R	C	R
SiO_2	39.28	39.85	39.39	37.51	37.01
TiO_2	0.02	0.07	0.03	0.00	0.00
Al_2O_3	0.02	0.02	0.00	0.03	0.03
MgO	45.18	45.64	45.20	36.07	36.11
CaO	0.20	0.22	0.23	0.27	0.31
MnO	0.60	0.61	0.54	0.60	0.46
FeO	13.93	13.76	14.41	25.18	24.97
NiO	0.19	0.08	0.20	0.07	0.00
Na_2O	0.00	0.02	0.00	0.01	0.01
K_2O	0.00	0.00	0.00	0.00	0.02
Total	99.42	100.28	100.01	99.74	98.92
Fo	85.25	85.54	84.83	71.85	72.06
Fa	14.75	14.46	15.17	28.15	27.94

Appendix C-2.2. Mineral chemistry of olivine in trachybasalt from Shahrbabak(oxides, wt%).

Sampl	R15812	R15812	R15812	R15812	R15812
Spot	C	R	R	R	C
SiO_2	39.62	39.63	39.65	39.37	39.54
TiO_2	0.03	0.00	0.00	0.00	0.03
Al_2O_3	0.02	0.03	0.03	0.03	0.00
MgO	46.51	45.70	45.55	45.33	45.48
CaO	0.13	0.13	0.19	0.21	0.20
MnO	0.34	0.47	0.56	0.60	0.59
FeO	13.47	14.18	14.28	14.02	13.95
NiO	0.38	0.30	0.11	0.25	0.14
Na_2O	0.03	0.03	0.00	0.00	0.01
K_2O	0.01	0.00	0.00	0.00	0.02
Total	100.61	100.51	100.44	99.85	100.00
Fo	86.02	85.18	85.03	85.22	85.31
Fa	13.98	14.82	14.97	14.78	14.83

Appendix C-3.4. Mineral chemistry of titanomagnetite in tephrite from the Islamic Peninsula (oxides, wt%).

Sample	R14455	R14455	R14447	R14447	R14447	R14466	R14466
Spot	C	C	C	C	C	C	C
SiO_2	0.26	0.23	0.06	0.10	0.07	0.08	0.04
TiO_2	11.12	8.40	11.86	10.13	9.93	8.54	9.18
Al_2O_3	0.86	4.61	1.07	1.52	2.15	0.33	0.50
Cr_2O_3	0.01	0.05	0.29	0.42	0.48	2.72	2.17
MgO	0.02	0.04	1.42	0.74	1.81	1.17	1.86
CaO	0.27	0.10	0.03	0.52	0.01	0.00	0.00
MnO	1.94	1.41	0.98	1.19	0.60	0.95	0.92
FeO	71.65	72.94	78.85	78.32	78.72	79.80	79.34
Na_2O	0.74	0.02	0.04	0.03	0.00	0.00	0.00
Totl	86.90	87.85	94.65	93.11	93.92	93.64	94.03

Appendix C-3.6. Mineral chemistry of titanomagnetite in tephriphonolite from Aghda (oxides, wt%).

Sample	R14497	R14497	R14497	R14497	R14497	R14508	R14508
Spot	C	C	C	C	C	C	C
SiO_2	2.12	0.11	0.12	0.43	0.10	0.12	17.19
TiO_2	4.44	12.55	12.53	16.00	12.71	18.57	20.88
Al_2O_3	0.60	5.25	5.08	1.83	4.99	1.95	1.66
Cr_2O_3	0.00	0.10	0.11	0.00	0.07	0.00	0.02
MgO	0.01	0.67	0.64	0.06	0.65	0.00	0.00
CaO	0.22	0.00	0.09	0.32	0.04	0.08	16.12
MnO	0.07	1.12	0.73	2.23	1.93	0.41	0.00
FeO	80.89	72.96	73.08	70.49	73.08	70.62	38.01
Na_2O	0.06	0.02	0.00	0.03	0.01	0.00	0.04
Total	88.55	92.82	92.41	91.45	93.66	91.81	93.93

Appendix C-3.1.5.7. Mineral chemistry of titanomagnetite in basalt, phonotephrite and trachyandesite from the Islamic Peninsula (oxides, wt%).

Sample	R14457	R14457	R14457	R14454	R14454	R14698	R14698
Spot	C	C	C	C	C	C	C
SiO_2	0.14	0.12	0.08	0.12	0.09	0.69	0.33
TiO_2	10.01	7.44	7.93	7.66	7.36	5.97	7.21
Al_2O_3	0.85	2.51	2.73	4.67	4.85	0.67	0.65
Cr_2O_3	0.71	0.06	0.47	0.07	0.08	0.00	0.10
MgO	1.76	4.82	2.95	4.11	5.41	0.81	0.75
CaO	0.34	0.49	0.35	0.14	0.06	0.08	0.04
MnO	1.07	0.58	0.96	0.75	0.61	1.43	1.56
FeO	75.53	75.30	76.10	73.76	74.78	78.16	79.99
Total	90.50	91.48	91.64	91.40	93.22	88.13	90.74

Appendix C-3.5.6. Mineral chemistry of titanomagnetite in phonotephrite and tephriphonolite from Aghda (oxides, wt%).

Sample	R14508	R14508	R14483	R14483	R14483	R14500	R14500
Spot	C	C	C	C	C	C	R
SiO_2	0.28	0.08	0.58	0.36	0.10	0.35	0.39
TiO_2	11.25	18.19	17.72	19.50	20.53	18.40	16.06
Al_2O_3	0.99	1.59	1.25	1.02	1.50	1.70	1.67
MgO	0.00	0.02	0.16	0.00	0.03	0.00	0.01
CaO	0.08	0.13	0.14	0.15	0.26	0.38	0.54
MnO	0.24	0.45	0.73	2.33	0.43	1.40	1.19
FeO	0.76	70.03	70.67	66.15	67.92	69.16	71.02
NiO	0.00	0.02	0.00	0.03	0.13	0.00	0.02
Na_2O	0.05	0.02	0.05	0.02	0.00	0.04	0.07
K_2O	0.12	0.10	0.07	0.17	0.05	0.05	0.08
Total	89.01	90.62	91.38	89.74	90.97	91.50	91.10

Appendix C-3.3.5. Mineral chemistry of titanomagnetite in basaltic trachyandesite and phonotephrite from Aghda (oxides, wt%).

Sample	R14500	R14500	R14500	R14488	R14488	R14488	R14488
Spot	C	C	R	C	R	C	R
SiO_2	0.91	0.11	0.14	3.16	2.31	3.25	1.57
TiO_2	10.81	17.09	18.16	19.15	15.09	11.96	17.69
Al_2O_3	0.95	2.28	2.18	0.70	0.60	0.74	0.77
Cr_2O_3	0.17	0.08	0.17	0.04	0.03	0.06	0.08
CaO	0.66	0.19	0.23	2.81	1.96	3.18	1.46
MnO	0.24	1.43	0.87	0.84	0.82	0.44	2.01
FeO	80.14	70.94	70.03	63.89	70.46	69.68	66.36
NiO	0.17	0.00	0.08	0.00	0.05	0.04	0.13
Na_2O	0.06	0.00	0.03	0.00	0.00	0.02	0.00
K_2O	0.04	0.03	0.06	0.00	0.00	0.00	0.01
Total	94.14	92.16	91.97	90.59	91.33	89.37	90.12

Appendix C-3.1.7. Mineral chemistry of titanomagnetite in basalt and trachyandesite from Shahrbabak (oxides, wt%).

Sample	R14527	R15812	R15812	R15812	R14699	R14699
SiO_2	0.11	0.02	0.06	0.04	0.01	0.09
TiO_2	10.02	8.61	9.43	7.96	27.13	3.08
Al_2O_3	6.05	2.49	2.44	2.71	0.26	1.64
Cr_2O_3	0.25	1.15	0.17	2.50	0.02	0.02
MgO	2.24	5.18	4.61	5.40	0.68	0.75
CaO	0.00	0.01	0.11	0.00	0.06	0.08
MnO	0.59	0.58	1.00	0.64	0.35	0.63
FeO	71.96	75.71	75.77	73.96	62.69	81.64
NiO	0.05	0.15	0.14	0.15	0.00	0.03
Total	91.28	93.90	93.74	93.39	91.23	88.03

Appendix C-3.6.7. Mineral chemistry of titanomagnetite in trachyandesite and tephriphonolite from Shahrbabak (oxides, wt%).

Sample	R14528	R14528	R14528	R14544	R14544	R14544	R14557
SiO_2	1.69	1.38	2.53	3.23	0.44	1.69	0.10
TiO_2	0.93	1.40	3.51	15.35	21.22	17.83	21.05
Al_2O_3	0.51	0.44	1.01	1.02	0.52	0.61	1.78
MgO	0.03	0.02	0.05	0.11	0.09	0.06	0.00
CaO	0.17	0.16	0.53	1.65	0.06	0.87	0.29
MnO	0.54	0.56	0.59	1.07	0.60	0.50	1.64
FeO	84.81	83.57	80.97	67.89	68.66	69.83	65.71
Na_2O	0.07	0.01	0.08	0.00	0.00	0.02	0.02
K_2O	0.04	0.00	0.04	0.09	0.03	0.05	0.04
Total	88.79	87.54	89.32	90.44	91.73	91.49	90.64

Appendix C-3.6 (continued). Mineral chemistry of titanomagnetite in tephriphonolite from Shahrbabak (oxides, wt%).

Sample	R14557	R14557	R14522	R14522	R14522	R14527	R14527
SiO_2	0.70	1.86	0.06	0.08	0.10	0.69	0.14
TiO_2	13.62	14.50	17.34	17.30	16.39	11.14	8.02
Al_2O_3	0.32	1.03	1.97	1.37	1.82	4.96	9.41
Cr_2O_3	0.03	0.09	0.00	0.00	0.05	0.28	0.32
MgO	0.00	0.00	0.09	0.03	0.09	0.39	2.94
CaO	0.25	1.45	0.00	0.05	0.04	0.09	0.02
MnO	3.97	3.60	2.50	2.80	1.26	1.94	0.48
FeO	71.21	68.69	71.09	69.96	71.30	70.52	70.89
Na_2O	0.03	0.09	0.00	0.04	0.00	0.02	0.00
K_2O	0.04	0.07	0.00	0.04	0.00	0.02	0.00
Total	90.24	91.40	93.06	91.67	91.06	90.15	92.24

Appendix C-3.8. Mineral chemistry of titanomagnetite in trachyte from Shahrbabak (oxides, wt%).

Sample	R14512	R14512	R14512	R14512
SiO_2	0.10	0.15	0.09	0.09
TiO_2	1.84	3.07	3.03	1.88
Al_2O_3	0.87	0.89	2.76	0.92
Cr_2O_3	0.18	0.14	0.16	0.17
MgO	1.03	1.03	1.20	1.10
CaO	0.06	0.06	0.09	0.06
MnO	0.22	0.32	0.61	0.22
FeO	85.58	84.75	81.44	84.53
Na_2O	0.21	0.20	0.20	0.20
K_2O	0.05	0.05	0.05	0.05
Total	89.81	90.35	89.37	88.82

Appendix C-4.7. Mineral chemistry of biotite in trachyandesite from the Islamic Peninsula (oxides, wt%).

Sample	R14698	R14698	R14698	R14698	R14698
Spot	C	C	R	R	C
SiO_2	37.55	38.28	35.66	36.34	37.78
TiO_2	4.73	3.91	4.31	3.54	3.78
Al_2O_3	12.52	12.13	13.90	13.51	14.98
Cr_2O_3	0.06	0.01	0.05	0.06	0.11
MgO	16.94	18.42	14.03	15.01	12.20
MnO	0.33	0.36	0.35	0.32	0.28
FeO	12.61	10.96	15.87	14.79	13.50
Na_2O	0.63	0.62	0.59	0.56	1.20
K_2O	9.30	9.46	8.95	9.51	8.69
Total	94.57	94.17	93.73	93.69	92.66

Appendix C-4.8. Mineral chemistry of biotite in trachyte from Shahrbabak (oxides, wt%).

Sample	R14512	R14512	R14512	R14512
SiO_2	36.23	36.33	35.92	36.05
TiO_2	4.48	4.57	4.73	4.55
Al_2O_3	13.84	14.12	13.95	13.88
MgO	15.48	16.09	14.52	14.60
MnO	0.14	0.10	0.22	0.10
FeO	14.42	13.50	16.18	16.03
Na_2O	0.34	0.29	0.43	0.42
K_2O	8.46	8.70	8.89	8.71
Total	93.38	93.59	94.84	94.22

Appendix C-4.9. Mineral chemistry of biotite in dacite from Shahrbabak (oxides, wt%).

Sample	R14699	R14699	R14699	R14699
Spot	C	R	C	R
SiO_2	36.05	36.55	37.23	36.71
TiO_2	3.84	3.58	3.95	3.91
Al_2O_3	13.81	13.93	13.81	13.84
MgO	13.06	14.35	13.80	14.00
CaO	0.06	0.12	0.23	0.22
MnO	0.24	0.12	0.07	0.16
FeO	16.63	14.61	13.34	13.64
Na_2O	0.39	0.55	0.56	0.55
K_2O	8.43	8.21	7.97	7.96
Total	92.52	92.07	90.97	90.98

Appendix C-5.8. Mineral chemistry of hornblende in trachyte from Shahrbabak (oxides, wt%).

Sample	R14512	R14512	R14512	R14512	R14512
SiO_2	44.83	44.31	46.23	45.38	45.49
TiO_2	1.22	1.73	1.19	1.52	1.20
Al_2O_3	8.16	8.61	7.67	7.70	7.38
MgO	13.99	13.89	14.51	14.67	14.34
CaO	11.23	11.09	11.24	11.21	11.28
MnO	0.34	0.25	0.34	0.26	0.32
FeO	13.64	13.09	13.50	12.86	13.40
Na_2O	1.63	1.86	1.62	1.55	1.39
K_2O	0.72	0.58	0.68	0.55	0.60
Total	95.77	95.42	96.98	95.71	95.40

Appendix C-5.9. Mineral chemistry of hornblende in dacite from Shahrbabak (oxides, wt%).

Sample	R14699	R14699	R14699	R14699
Spot	R	R	C	C
SiO_2	45.30	44.20	43.88	43.99
TiO_2	1.25	1.25	1.76	2.20
Al_2O_3	8.09	9.14	10.41	9.98
MgO	13.06	12.70	14.07	14.47
CaO	10.98	10.88	10.34	10.57
MnO	0.42	0.36	0.10	0.21
FeO	14.55	14.33	12.08	11.46
Na_2O	1.60	1.69	2.12	2.13
K_2O	0.59	0.66	0.52	0.48
Total	95.90	95.20	95.31	95.56

Appendix C-6.7. Mineral chemistry of K-feldspar in trachyandesite from the Islamic Peninsula (oxides, wt%).

Sample	R14698	R14698	R14698	R14698
Spot	C	C	C	C
SiO_2	64.71	64.51	64.65	64.14
TiO_2	0.14	0.09	0.10	0.10
Al_2O_3	19.29	18.82	18.80	18.98
CaO	0.85	0.25	0.22	0.69
MnO	0.01	0.05	0.00	0.02
FeO	0.51	0.40	0.37	0.60
NiO	0.01	0.01	0.00	0.00
Na_2O	5.25	4.16	4.46	5.13
K_2O	9.13	10.57	10.20	8.81
Total	99.90	98.87	98.86	98.47
An	5.00	1.49	1.31	4.25
Ab	32.25	25.62	27.72	32.79
Or	62.77	72.91	70.94	62.97

Appendix C-6.6. Mineral chemistry of K-feldspar in tephriphonolite from Aghda(oxides, wt%).

Sample	R14497	R14497	R14508	R14508	R14508	R14508	R14508
Spot	C	C	C	R	C	C	R
SiO_2	60.46	61.20	62.78	63.03	63.45	61.89	62.14
TiO_2	0.06	0.02	0.00	0.01	0.00	0.05	0.02
Al_2O_3	20.86	19.43	18.20	18.52	18.12	18.79	18.32
CaO	0.24	0.61	0.02	0.06	0.03	0.18	0.08
FeO	0.26	0.17	0.03	0.11	0.09	0.15	0.02
Na_2O	0.82	0.19	0.38	0.40	0.56	0.97	0.43
K_2O	14.87	16.17	15.34	16.04	16.20	14.84	15.27
Total	97.57	97.79	96.79	98.17	98.50	96.93	96.35
An	1.29	3.11	0.12	0.29	0.13	0.97	0.44
Ab	4.62	0.99	2.14	2.15	2.99	5.46	2.42
Or	94.09	95.86	97.75	97.56	96.83	93.53	97.07

Appendix C-6.6 (continued). Mineral chemistry of K-feldspar in tephriphonolite from Aghda (oxides, wt%).

Sample	R14508	R14508	R14508	R14483	R14483	R14483	R14483
Spot	C	R	R	R	C	R	C
SiO_2	64.30	62.67	63.44	63.12	62.81	61.96	63.24
TiO_2	0.00	0.00	0.05	0.14	0.01	0.06	0.04
Al_2O_3	18.42	18.39	18.28	19.44	18.46	19.71	18.54
Cr_2O_3	0.02	0.00	0.05	0.01	0.01	0.01	0.02
CaO	0.12	0.03	0.06	1.09	0.00	0.58	0.35
FeO	0.06	0.00	0.40	0.25	0.06	0.54	0.12
Na_2O	1.09	0.49	0.81	3.28	0.34	3.00	1.32
K_2O	15.16	15.56	15.28	11.33	15.82	11.76	14.73
Total	99.19	97.13	98.46	98.68	97.53	97.97	98.41
An	0.64	0.14	0.33	6.19	0.00	3.33	1.87
Ab	5.98	2.73	4.52	19.29	1.88	17.94	7.27
Or	93.31	97.17	95.19	74.57	98.11	78.75	90.89

Appendix C-6.3.5. Mineral chemistry of K-feldspar in basaltic trachyandesite and phonotephrite, nepheline in basaltic trachyandesite from Aghda(oxides, wt%).

Sample	R14500	R14500	R14488	R14488	R14488	R14488	R14488
Spot	C	R	R	R	C		
SiO_2	63.97	64.97	62.05	62.75	63.54	52.69	53.71
TiO_2	0.07	0.04	0.03	0.10	0.01	0.11	0.06
Al_2O_3	19.65	18.69	19.54	19.16	18.74	28.60	27.95
CaO	0.73	0.52	0.83	0.73	0.41	11.67	10.95
FeO	0.41	0.54	0.13	0.31	0.15	0.52	0.59
Na_2O	3.53	3.37	2.97	3.19	1.84	3.94	4.47
K_2O	11.13	12.08	11.41	11.24	14.27	1.23	1.32
Total	99.56	100.26	97.06	97.57	99.01	98.80	99.06
An	4.23	2.88	4.86	4.25	3.17		
Ab	21.15	19.36	17.95	19.37	10.11		
Or	74.65	77.76	77.17	76.35	87.74		

Appendix C-6.1. Mineral chemistry of K-feldspar in basalt from Shahrbabak(oxides, wt%).

Sample	R14527	R14527	R14527	R14557
Spot	C	R	R	C
SiO_2	61.36	64.34	64.60	61.00
TiO_2	0.15	0.10	0.10	0.14
Al_2O_3	16.52	20.25	19.63	15.27
Cr_2O_3	0.06	0.03	0.04	0.05
MgO	1.77	0.00	0.01	1.20
CaO	3.22	1.71	1.08	2.89
MnO	0.07	0.08	0.02	0.07
FeO	1.99	0.26	0.34	1.57
Na_2O	4.32	7.32	6.02	3.85
K_2O	7.40	5.27	7.38	7.80
Total	96.92	99.37	99.21	93.87
An	16.20	8.03	5.15	15.80
Ab	39.40	62.43	52.54	38.98
Or	44.40	31.54	42.31	45.10

Appendix C-6.7. Mineral chemistry of K-feldspar in trachyandesite from Shahrbabak(oxides, wt%).

Sample	R14528	R14528	R14528
Spot	C	C	C
SiO_2	65.09	64.97	66.26
TiO_2	0.09	0.00	0.00
Al_2O_3	18.35	18.16	18.32
MgO	0.03	0.02	0.00
CaO	0.08	0.01	0.28
MnO	0.00	0.00	0.02
FeO	0.31	0.06	0.15
Na_2O	1.58	0.79	4.82
K_2O	14.05	15.61	9.73
Total	99.58	99.66	99.58
An	0.41	0.00	1.36
Ab	14.51	7.10	42.37
Or	85.08	92.90	56.27

Appendix C-7.1. Mineral chemistry of plagioclase in basalt from Shahrbabak(oxides, wt%).

Sample	R14527	R14527	R14527	R14527	R14527	R15812	R15812
Spot	C	R	R	C	R	C	R
SiO_2	46.17	49.59	54.32	46.41	55.42	52.87	54.58
TiO_2	0.02	0.06	0.02	0.07	0.06	0.10	0.15
Al_2O_3	33.21	30.54	22.26	32.63	25.01	28.33	27.57
CaO	17.31	14.24	8.52	16.75	6.85	11.86	10.27
MnO	0.00	0.00	0.03	0.00	0.02	0.05	0.00
FeO	0.71	1.08	0.32	0.87	1.41	1.30	0.81
Na_2O	1.67	3.20	2.65	2.01	5.85	4.66	5.50
K_2O	0.12	0.14	0.07	0.12	0.38	0.25	0.35
Total	99.25	98.85	88.22	98.87	95.55	99.45	99.23
An	84.55	70.55	63.55	81.56	38.31	57.55	49.76
Ab	14.75	28.65	35.79	17.74	59.20	40.95	48.18
Or	0.71	0.80	0.67	0.70	2.49	1.50	2.06

Appendix C-6.6. Mineral chemistry of K-feldspar in tephriphonolite from Shahrbabak (oxides, wt%).

Sample	R14544	R14544	R14544	R14544	R14522	R14522
Spot	C	R	R	C	C	C
SiO_2	64.85	64.23	64.35	65.11	64.97	65.15
TiO_2	0.03	0.06	0.10	0.04	0.04	0.01
Al_2O_3	18.83	18.84	19.14	18.45	19.07	18.76
CaO	0.44	0.62	0.65	0.10	0.46	0.20
MnO	0.04	0.00	0.05	0.07	0.03	0.00
FeO	0.20	0.10	0.27	0.18	0.09	0.05
Na_2O	2.97	2.66	3.65	2.04	4.01	2.34
K_2O	12.19	12.30	11.53	13.98	10.90	13.72
Total	99.56	98.83	99.76	100.03	99.61	100.26
An	2.16	3.06	3.11	0.48	2.21	0.94
Ab	26.42	23.97	31.47	18.06	35.07	20.36
Or	71.42	72.97	65.42	81.46	62.72	78.69

Appendix C-6.6 (continued). Mineral chemistry of K-feldspar in tephriphonolite from Shahrbabak (oxides, wt%).

Sample	R14557	R14557	R14557	R14557	R14557
Spot	C	R	C	R	C
SiO_2	63.58	63.98	64.60	65.17	61.75
TiO_2	0.02	0.06	0.06	0.02	0.03
Al_2O_3	19.15	19.60	18.43	18.21	18.56
CaO	0.30	0.49	0.30	0.09	1.76
FeO	0.05	0.11	0.25	0.27	0.71
NiO	0.04	0.01	0.04	0.00	0.10
Na_2O	0.50	3.18	2.12	1.24	1.67
K_2O	15.47	11.25	13.15	14.68	12.52
Total	99.14	98.75	98.97	99.68	98.67
An	1.55	2.48	1.55	0.49	8.94
Ab	4.65	29.31	19.40	11.36	15.39
Or	93.80	68.21	79.05	88.15	75.66

Appendix C-7.6. Mineral chemistry of plagioclase in tephriphonolite from Shahrbabak (oxides, wt%).

Sample	R14557	R14557	R14557	R14557	R14557	R14557	R14557
Spot	C	R	C	C	C	R	C
SiO_2	54.17	54.19	52.91	52.11	52.79	52.97	54.74
TiO_2	0.04	0.10	0.08	0.06	0.05	0.05	0.05
Al_2O_3	27.93	27.83	28.13	29.00	28.59	28.68	27.27
Cr_2O_3	0.00	0.00	0.05	0.01	0.00	0.05	0.02
CaO	10.80	10.99	11.55	12.05	11.90	12.15	10.24
MnO	0.00	0.00	0.02	0.00	0.00	0.03	0.00
FeO	0.50	0.66	0.45	0.64	0.53	0.54	0.56
Na_2O	4.57	5.11	4.41	4.18	4.16	4.36	4.95
K_2O	1.09	0.48	0.94	0.63	0.70	0.67	1.25
Total	99.10	99.35	98.54	98.67	98.74	99.52	99.07
An	53.09	52.83	55.96	59.19	58.69	58.31	49.53
Ab	40.58	44.42	38.64	37.15	37.15	37.85	43.30
Or	6.34	2.75	5.41	3.66	4.16	3.84	7.18

Appendix C-7.6 (continued). Mineral chemistry of plagioclase in tephriphonolite from Shahrbabak (oxides, wt%).

Sample	R14557	R14557	R14557	R14557	R14557	R14557	R14557
Spot	R	C	R	R	R	C	C
SiO_2	54.55	54.36	53.92	68.79	69.03	67.51	68.35
TiO_2	0.06	0.05	0.05	0.04	0.11	0.03	0.08
Al_2O_3	27.39	27.57	28.12	20.12	20.03	19.68	20.65
CaO	10.46	10.49	10.99	0.80	0.82	0.83	1.63
FeO	0.49	0.51	0.68	0.08	0.28	0.12	0.10
NiO	0.00	0.02	0.04	0.06	0.04	0.03	0.00
Na_2O	5.24	4.96	4.99	10.67	10.67	8.01	9.60
K_2O	0.52	0.58	0.41	0.11	0.30	5.05	0.34
Total	98.79	98.57	99.20	100.70	101.32	101.28	100.80
An	50.83	52.06	53.59	3.91	3.97	3.90	8.44
Ab	46.15	44.47	44.02	95.40	94.26	67.94	89.52
Or	3.01	3.47	2.39	0.68	1.77	28.16	2.04

Appendix C-7.5.6. Mineral chemistry of plagioclase in phonotephrite and tephriphonolite from Aghda (oxides, wt%).

Sample	R14508	R14508	R14500	R14500	R14500	R14500	R14500
Spot	R	C	C	R	C	R	C
SiO_2	67.68	67.11	51.15	51.28	52.67	66.70	51.53
TiO_2	0.01	0.03	0.02	0.03	0.06	0.03	0.01
Al_2O_3	19.59	20.09	29.67	29.37	28.44	19.96	29.44
CaO	0.48	1.07	12.96	13.09	11.88	0.81	12.71
FeO	0.16	0.06	0.55	0.57	0.61	0.31	0.58
Na_2O	11.24	11.09	3.59	3.60	4.03	11.00	3.43
K_2O	0.17	0.07	0.71	0.72	1.16	0.19	0.94
Total	99.38	99.54	98.65	98.72	98.85	99.04	98.65
An	3.92	8.45	74.04	47.11	68.20	6.55	73.20
Ab	94.47	90.98	21.29	21.16	24.04	91.69	20.52
Or	1.60	0.63	4.73	4.73	7.75	1.75	6.29

Appendix C-7.3.5. Mineral chemistry of plagioclase in basaltic trachyandesite and phonotephrite from Aghda (oxides, wt%).

Sample	R14500	R14488	R14488	R14488	R14488	R14488
Spot	R	C	R	C	C	R
SiO_2	52.28	54.26	65.28	55.45	66.26	64.81
TiO_2	0.04	0.05	0.10	0.03	0.00	0.06
Al_2O_3	28.71	27.53	19.90	26.88	20.56	20.92
CaO	12.30	10.51	0.92	9.58	1.04	1.75
MnO	0.00	0.05	0.00	0.00	0.00	0.04
FeO	0.77	0.39	0.23	0.51	0.09	0.28
Na_2O	4.39	4.90	8.45	5.76	9.53	10.40
K_2O	0.47	1.09	4.03	0.63	1.98	0.38
Total	98.94	98.78	98.95	98.87	99.46	98.70
An	70.69	62.37	6.42	60.83	7.88	13.50
Ab	26.17	30.18	61.04	36.68	74.71	83.17
Or	3.16	7.51	32.54	4.47	17.35	3.37

Appendix C-7.2. Mineral chemistry of plagioclase in trachybasalt from Shahrbabak(oxides, wt%).

Sample	R15812	R15812	R15812	R15812
pot	R	C	R	C
SiO_2	54.52	63.13	62.54	57.71
TiO_2	0.11	0.19	0.20	0.14
Al_2O_3	27.18	21.12	21.54	28.82
CaO	10.02	2.97	3.86	7.36
MnO	0.00	0.01	0.00	0.03
FeO	0.98	0.62	0.55	1.04
Na_2O	5.25	7.51	7.76	6.44
K_2O	0.38	3.31	2.33	0.84
Total	98.49	98.95	98.81	98.40
An	50.20	14.50	18.71	36.76
Ab	47.60	66.32	67.87	58.25
Or	2.20	19.18	13.43	4.98

Appendix C-7.7. Mineral chemistry of plagioclase in trachyandesite from Shahrbabak(oxides, wt%).

Sample	R14528	R14528	R14528	R14528	R14528	R14528
Spot	R	C	R	R	C	C
SiO_2	56.46	54.68	67.64	64.92	57.12	55.99
TiO_2	0.03	0.02	0.04	0.08	0.03	0.07
Al_2O_3	26.36	27.73	21.16	20.99	25.98	26.64
CaO	8.75	10.67	1.63	2.69	8.48	9.54
FeO	0.38	0.55	0.06	0.40	0.40	0.39
Na_2O	5.70	4.93	9.75	9.02	5.72	5.48
K_2O	1.30	0.94	0.51	1.51	1.42	1.07
Total	99.00	99.62	100.79	99.62	99.18	99.23
An	42.48	51.51	8.21	12.91	41.31	46.00
Ab	50.04	43.11	88.67	78.45	50.44	47.82
Or	7.48	5.38	3.11	8.64	8.25	6.18

Appendix C-7.8 (continued). Mineral chemistry 0f plagioclase in trachyte from Shahrbabak (oxides, wt%).

Sample	R14512	R14512	R14512	R14512	R14512	R14512
SiO_2	61.44	60.38	59.23	60.57	61.03	62.40
TiO_2	0.08	0.08	0.08	0.08	0.08	0.08
Al_2O_3	25.16	25.00	26.20	25.30	24.88	24.14
CaO	5.64	5.65	6.90	6.05	5.52	4.67
MnO	0.09	0.09	0.09	0.09	0.09	0.09
FeO	0.18	0.19	0.14	0.16	0.11	0.22
Na_2O	8.07	7.82	7.32	7.81	8.13	8.56
K_2O	0.68	0.65	0.53	0.67	0.70	0.84
Total	101.17	99.69	100.53	100.55	100.37	100.82

Appendix C-7.8 (continued). Mineral chemistry of plagioclase in trachyte from Shahrbabak (oxides, wt%).

Sample	R14512	R14512	R14512	R14512	R14512	R14512
SiO_2	60.71	60.93	61.16	58.30	60.84	62.12
TiO_2	0.08	0.08	0.08	0.08	0.08	0.08
Al_2O_3	25.33	25.34	24.92	26.94	25.10	25.57
CaO	6.04	5.79	5.69	7.77	5.69	5.10
FeO	0.09	0.22	0.16	0.26	0.15	0.21
Na_2O	7.84	8.06	8.17	6.93	7.90	8.29
K_2O	0.60	0.70	0.67	0.46	0.66	0.74
Total	100.53	101.04	100.78	100.66	100.33	101.09

Appendix C-7.9. Mineral chemistry of plagioclase in dacite from Shahrbabak (oxides, wt%).

Sample	R14699	R14699	R14699	R14699	R14699	R14699
Spot	C	R	R	C	R	R
SiO_2	61.01	62.14	62.40	59.61	59.76	59.58
TiO_2	0.02	0.00	0.02	0.02	0.03	0.00
Al_2O_3	23.55	23.02	23.02	24.65	24.46	24.52
CaO	5.14	4.54	4.56	6.57	6.22	6.62
FeO	0.12	0.12	0.13	0.14	0.18	0.17
Na_2O	8.23	8.48	8.37	7.62	7.73	7.77
K_2O	0.77	0.77	0.79	0.43	0.50	0.47
Total	98.89	99.13	99.30	99.11	98.98	99.19
An	24.48	21.81	22.12	31.48	29.91	31.15
Ab	71.16	73.78	73.34	66.06	67.22	66.20
Or	4.36	4.41	4.54	2.46	2.86	2.65

Appendix C-8.4.5 (continued). Mineral chemistry of leucite in tephrite and phonotephrite from the Islamic Peninsula (oxides, wt%).

Sample	R14466	R14466	R14454	R14454	R14454	R14454
Spot	C	C	C	C	C	R
SiO_2	53.79	53.76	54.13	54.42	54.13	53.96
TiO_2	0.16	0.08	0.11	0.07	0.13	0.04
Al_2O_3	22.43	22.23	22.57	22.76	22.59	22.59
MnO	0.04	0.05	0.02	0.00	0.01	0.01
FeO	1.02	0.92	0.68	0.55	0.49	0.77
NiO	0.10	0.09	0.00	0.06	0.00	0.01
Na_2O	0.12	0.11	0.04	0.01	0.03	0.29
K_2O	21.51	21.48	21.74	21.62	21.59	20.82
Total	99.18	98.72	99.28	99.56	99.06	98.54
Si	0.33	0.33	0.33	0.33	0.33	0.33
Al	0.16	0.16	0.16	0.16	0.16	0.16
Na	0.00	0.00	0.00	0.00	0.00	0.00
K	0.17	0.17	0.17	0.17	0.17	0.16
Total	0.66	0.66	0.66	0.66	0.66	0.65

Appendix C-8.4. Mineral chemistry of leucite in tephrite from the Islamic Peninsula(oxides, wt%).

Sample	R14447	R14447	R14447	R14447	R14447	R14466	R14466
Spot	C	C	R	R	C	C	C
SiO_2	54.21	54.05	45.99	38.77	53.39	54.14	53.90
TiO_2	0.10	0.10	0.05	0.00	0.50	0.08	0.06
Al_2O_3	22.64	22.51	30.48	31.35	22.05	22.21	22.24
MgO	0.01	0.00	0.11	0.03	0.12	0.05	0.04
CaO	0.00	0.00	0.03	0.09	0.07	0.00	0.00
MnO	0.00	0.02	0.04	0.01	0.08	0.04	0.00
FeO	0.80	0.72	1.39	0.51	1.29	1.19	1.11
Na_2O	0.13	0.12	16.55	21.06	0.58	0.16	0.15
K_2O	21.49	21.21	4.83	0.24	21.14	21.63	21.40
Total	99.43	98.72	99.48	92.10	99.31	99.50	99.01
Si	0.33	0.33	0.28	0.25	0.33	0.33	0.33
Al	0.16	0.16	0.22	0.23	0.16	0.16	0.16
Na	0.00	0.00	0.19	0.26	0.01	0.00	0.00
K	0.17	0.17	0.04	0.02	0.17	0.17	0.17
Total	0.66	0.66	0.73	0.76	0.66	0.66	0.66

Appendix C-9.1.4. Mineral chemistry of analcime in basalt and tephrite from the Islamic Peninsula(oxides, wt%).

Sample	R14457	R14457	R14457	R14455	R14455
Spot	C	C	R	C	R
SiO_2	57.04	41.44	56.37	57.27	55.90
TiO_2	0.12	0.03	0.01	0.07	0.05
Al_2O_3	23.44	29.88	23.75	23.43	23.75
MgO	0.25	0.00	0.02	0.02	0.00
CaO	0.34	8.22	0.02	0.14	0.24
FeO	1.05	0.30	0.44	0.55	0.30
Na_2O	6.05	5.52	8.94	7.20	8.02
K_2O	0.35	0.04	0.16	0.13	0.12
Total	88.66	85.43	89.71	88.90	88.44

Appendix C-9.6. Mineral chemistry of analcime in tephriphonolite from Aghda (oxides, wt%).

Sample	R14497	R14497	R14497	R14483	R14483	R14483
Spot	C	C	C	C	C	C
SiO_2	57.31	58.50	57.47	56.83	55.56	55.78
TiO_2	0.03	0.08	0.04	0.02	0.19	0.05
Al_2O_3	22.89	22.94	22.33	22.97	22.93	22.82
CaO	0.65	0.44	0.66	0.50	1.45	0.62
FeO	0.16	0.24	0.29	0.11	0.93	0.35
NiO	0.05	0.04	0.05	0.04	0.02	0.00
Na_2O	7.82	6.60	7.61	8.80	8.27	9.56
K_2O	0.10	0.01	0.04	0.01	0.02	0.02
Total	89.04	88.85	88.49	89.28	89.39	89.25

Appendix C-9.6. Mineral chemistry of analcime in tephriphonolite from Shahrbabak (oxides, wt%).

Sample	R14544	R14557	R14557	R14557
SiO_2	61.69	61.20	61.88	62.14
TiO_2	0.07	0.01	0.08	0.07
Al_2O_3	22.94	22.23	22.80	22.28
CaO	0.11	0.08	0.13	0.15
FeO	0.30	0.26	0.32	0.38
NiO	0.05	0.01	0.04	0.03
Na_2O	6.10	9.31	6.23	6.20
K_2O	0.02	0.30	0.02	0.03
Total	91.32	93.49	91.52	91.33

Appendix C-9.5. Mineral chemistry of analcime in phonotephrite from Aghda (oxides, wt%).

Sample	R14500	R14500	R14500	R14500	R14500	R14500	R14500
Spot	C	R	C	R	C	C	R
SiO_2	55.27	57.08	54.99	55.63	58.22	58.63	57.85
TiO_2	0.05	0.05	0.00	0.00	0.05	0.08	0.05
Al_2O_3	22.52	22.62	24.09	25.02	23.01	23.08	22.61
CaO	1.12	0.36	1.52	6.53	0.60	0.55	0.57
FeO	0.35	0.32	0.09	0.50	0.34	0.33	0.33
Na_2O	8.43	8.63	8.92	5.00	6.40	6.43	7.22
K_2O	0.07	0.13	0.68	2.66	0.05	0.06	0.05
Total	87.87	89.26	90.40	95.39	88.69	89.18	88.69

Appendix C-9.6. Mineral chemistry of analcime in tephriphonolite from Shahrbabak (oxides, wt%).

Sample	R14544	R14544	R14544	R14544	R14544	R14544	R14544
SiO_2	52.83	51.91	52.25	52.44	60.68	59.35	61.65
TiO_2	0.02	0.02	0.00	0.00	0.05	0.11	0.08
Al_2O_3	27.60	27.75	27.37	27.02	22.43	23.22	23.19
CaO	0.80	0.59	1.21	1.70	0.10	0.38	0.24
MnO	0.00	0.02	0.01	0.08	0.04	0.05	0.00
FeO	0.09	0.07	0.02	0.29	0.30	0.78	0.33
NiO	0.04	0.00	0.02	0.00	0.00	0.03	0.00
Na_2O	9.10	9.15	8.60	7.67	7.24	6.84	6.09
K_2O	0.01	0.01	0.02	0.02	0.05	0.03	0.04
Total	90.50	89.53	89.51	89.25	90.98	90.78	91.62

APPENDIX D

TOTAL-ROCK GEOCHEMISTRY

Appendix D-1. Islamic Peninsula

Appendix D-2. Aghda

Appendix D-3. Shahrbabak

Appendix D-1. Major and trace elment data for samples from the Islamic Peninsula (oxides, wt% and traces, ppm).

Sample	R14444	R14446	R14447	R14455	R14458	R14462
SiO_2	47.71	44.82	46.06	44.42	44.81	43.54
TiO_2	1.20	1.36	1.24	1.31	1.17	1.37
Al_2O_3	10.80	11.61	11.45	12.83	9.98	11.96
Fe_2O_3	8.35	10.12	9.57	10.27	8.74	9.68
MnO	0.13	0.16	0.16	0.17	0.13	0.16
MgO	8.96	7.50	8.67	5.28	10.15	8.83
CaO	10.73	11.66	11.85	11.69	13.32	11.37
Na_2O	3.10	2.34	1.22	5.07	0.51	0.94
K_2O	3.61	5.51	6.15	1.68	5.45	6.82
P_2O_5	1.55	1.71	1.44	1.57	1.23	1.78
LOI	4.00	2.96	2.73	6.25	4.70	3.73
Total	100.14	99.75	100.54	100.54	100.19	100.18
Ba	2380	3820	3080	3910	2500	3580
Rb	380	232	214	66	197	275
Sr	835	1240	1121	1410	985	1980
Pb	22	48	37	42	28	66
Th	11	44	30.90	26.10	22	40
U	3	6	<2	<2	4	6
Zr	308	420	401	326	352	370
Nb	28	48	29	32	28	42
Y	26	38	34	37	27	41
La	32	88	71.90	81.10	58	96
Ce	75	210	169	176	140	230
Nd	-	-	78.60	75.80	-	-
Sm	-	-	16.80	16.40	-	-
Eu	-	-	3.41	3.76	-	-
Tb	-	-	1.70	1.62	-	-
Ho	-	-	1.55	1.58	-	-
Yb	-	-	2.33	2.53	-	-
Lu	-	-	0.28	0.30	-	-
Sc	-	-	31	28.50	-	-
V	200	232	196	227	152	226
Cr	304	120	191	15	390	230
Ni	76	40	58	15	92	70
Cu	88	106	118	118	82	124
Zn	78	82	78	82	66	88
Sn	5	5	-	4	5	5
Ga	12	15	14	14	11	15
As	1	2	-	11	3	3
Hf	-	-	8.87	8.11	-	-
Ta	-	-	2.18	1.99	-	-
$\sum$REE	-	-	345.57	358.29	-	-
La_N/Yb_N	-	-	20.63	21.43	-	-
Eu/Eu^*	-	-	0.66	0.75	-	-
$^{87}Sr/^{86}Sr$	-	-	0.70848	0.70825	-	-
$^{143}Nd/^{144}Nd$	-	-	0.51239	0.51242	-	-

Appendix D-1 (continued). Major and trace elemenet data for samples from the Islamic Peninsula (oxides, wt% and traces, ppm).

Sample	R14464	R14466	R14471	R14474	R14477	R14478
SiO_2	44.36	46.65	45.89	44.54	46.55	45.42
TiO_2	1.31	1.06	1.33	1.18	1.32	1.24
Al_2O_3	11.13	11.00	13.49	12.03	11.53	11.66
Fe_2O_3	9.57	9.30	9.84	10.05	9.19	9.38
MnO	0.16	0.16	0.15	0.18	0.15	0.16
MgO	7.46	9.44	6.41	6.68	7.91	7.20
CaO	13.05	11.71	12.01	11.15	11.41	11.39
Na_2O	3.36	1.04	2.23	4.15	1.42	1.87
K_2O	1.63	7.11	5.04	4.21	6.98	4.70
P_2O_5	1.58	1.20	1.38	1.70	1.63	1.61
LOI	6.19	2.31	2.17	2.30	2.68	5.53
Total	99.80	100.98	99.94	97.87	100.77	100.16
Ba	3320	3370	4030	4800	3130	3750
Rb	342	207	178	122	270	261
Sr	1250	997	1310	1810	1330	1500
Pb	44	32	44	70	36	56
Th	29	17.80	31	41	27	34
U	2	<2	5	11	8	7
Zr	418	275	298	462	318	396
Nb	42	23	34	46	38	40
Y	35	25	34	44	32	38
La	76	49.10	76	94	58	76
Ce	185	108	175	230	140	180
Nd	-	53.10	-	-	-	-
Sm	-	11.30	-	-	-	-
Eu	-	2.53	-	-	-	-
Tb	-	1.18	-	-	-	-
Ho	-	1.22	-	-	-	-
Yb	-	1.90	-	-	-	-
Lu	-	0.24	-	-	-	-
Sc	-	31	-	-	-	-
V	262	178	214	246	220	144
Cr	140	289	52	54	218	82
Ni	44	75	20	32	44	32
Cu	146	93	142	148	118	96
Zn	88	71	74	104	84	88
Sn	5	-	<5	5	5	5
Ga	14	11.50	15	16	13	13
As	4	-	4	13	1	10
Hf	-	5.19	-	-	-	-
Ta	-	1.40	-	-	-	-
ΣREE	-	228.57	-	-	-	-
La_N/Yb_N	-	17.27	-	-	-	-
Eu/Eu*	-	0.73	-	-	-	-
$^{87}Sr/^{86}Sr$	-	0.70820	-	-	-	-
$^{143}Nd/^{144}Nd$	-	0.51243	-	-	-	-

Appendix D-1 (continued). Major and trace element data for samples from the Islamic Peninsula (oxides, wt% and traces, ppm).

Sample	R14454	R14467	R14449	R14457	R14698	R15807	R15806
SiO_2	46.17	47.94	47.00	46.65	56.15	56.70	58.02
TiO_2	1.24	1.24	1.25	0.96	0.73	0.66	0.83
Al_2O_3	13.88	13.09	10.57	7.71	15.64	15.88	15.12
Fe_2O_3	9.51	8.98	8.82	8.34	5.64	5.25	6.18
MnO	0.16	0.14	0.14	0.14	0.11	0.10	0.12
MgO	6.10	5.95	8.36	14.33	2.86	2.64	2.30
CaO	10.43	10.61	11.33	14.68	4.94	4.48	3.69
Na_2O	2.65	2.80	1.95	2.36	3.32	4.06	3.50
K_2O	5.93	5.22	6.78	1.77	7.42	6.78	7.98
P_2O_5	1.34	1.37	1.35	1.14	0.51	0.50	0.39
LOI	2.10	2.58	2.38	2.74	2.26	2.12	1.03
Total	99.51	99.92	99.94	100.82	99.58	99.17	99.16
Ba	3050	4160	4130	3070	2490	3490	2840
Rb	225	132	233	44	232	220	269
Sr	1280	1410	1060	989	1370	1570	1420
Pb	46	46	44	32	64	68	66
Th	29.60	28	34	18.10	46.80	46	86
U	2	6	9	47.14	17.10	15	11
Zr	320	306	394	236	530	466	845
Nb	36	30	38	22	51	56	92
Y	34	37	34	25	27	28	32
La	72.80	78	68	49.40	62.80	60	66
Ce	158	185	165	109	132	135	155
Nd	73.50	-	-	54.40	63.60	-	-
Sm	15	-	-	11.40	11.60	-	-
Eu	3.75	-	-	2.74	2.45	-	-
Tb	1.70	-	-	1.24	1.36	-	-
Ho	1.67	-	-	1.28	1.47	-	-
Yb	2.76	-	-	2.30	2.37	-	-
Lu	0.33	-	-	0.32	0.33	-	-
Sc	25.80	-	-	38.50	10.90	-	-
V	213	188	204	167	111	94	130
Cr	55	46	244	650	57	22	30
Ni	29	22	56	153	19	12	12
Cu	122	124	106	87	84	74	42
Zn	97	70	78	68	64	50	70
Sn	4	<5	10	-	-	-5	15
Ga	16	16	14	8.50	19	19	20
As	4	4	7	-	-	6	5
Hf	7.72	-	-	5.81	12.30	-	-
Ta	2.61	-	-	1.39	3.03	-	-
ΣREE	329.53	-	-	232.08	277.98	-	-
La_N/Yb_N	17.63	-	-	14.37	17.72	-	-
Eu/Eu^*	0.80	-	-	0.78	0.67	-	-
$^{87}Sr/^{86}Sr$	0.70774		-	0.70778	0.70799		-
$^{143}Nd/^{144}Nd$	0.512456		-	0.51245	0.51242		-

Appendix D-2. Major and trace element data for samples from Aghda (oxides, wt% and traces, ppm).

Sample	R14484	R14488	R14495	R14496	R14503	R14507	R14499
SiO_2	50.17	51.13	51.11	50.68	53.22	50.66	56.06
TiO_2	0.76	0.80	0.82	0.87	0.88	0.91	0.75
Al_2O_3	19.14	18.78	18.50	17.28	15.29	17.00	16.68
Fe_2O_3	7.88	8.31	8.54	8.79	8.05	9.38	6.81
MnO	0.14	0.15	0.15	0.16	0.11	0.17	0.11
MgO	3.10	3.13	3.37	3.57	3.03	3.72	1.91
CaO	7.93	7.37	6.47	8.02	7.71	7.91	1.94
Na_2O	4.84	3.43	3.88	4.01	2.95	2.83	2.47
K_2O	1.80	4.02	4.03	3.02	5.53	4.52	9.82
P_2O_5	0.53	0.50	0.47	0.56	0.40	0.55	0.29
LOI	2.47	2.85	3.20	2.91	2.53	2.56	2.69
Total	98.76	100.47	100.54	99.87	99.70	100.21	99.53
Ba	1540	1430	1330	1440	1270	1610	1470
Rb	35	111	123	90	238	129	385
Sr	1040	890	960	900	610	1100	406
Pb	32	24	26	28	30	30	114
Th	24	25.50	30	30	24	30	28
U	5	4.73	7	7	6	8	8
Zr	198	241	228	238	256	238	304
Nb	14	15	16	16	16	16	18
Y	24	25	27	27	27	28	26
La	36	37	36	40	32	42	32
Ce	90	75.30	85	90	80	95	75
Nd	-	33.70	-	-	-	-	-
Sm	-	7.15	-	-	-	-	-
Eu	-	1.75	-	-	-	-	-
Tb	-	0.93	-	-	-	-	-
Ho	-	1.11	-	-	-	-	-
Yb	-	2.66	-	-	-	-	-
Lu	-	0.37	-	-	-	-	-
Sc	-	13.60	-	-	-	-	-
V	148	132	142	182	180	184	94
Cr	16	8	8	16	96	20	30
Ni	10	9	8	14	28	14	12
Cu	80	41	42	36	18	222	20
Zn	88	94	82	88	90	90	294
Sn	<5	-	<5	<5	<5	5	<5
Ga	19	18.50	18	18	18	18	14
As	2	-	5	2	3	4	13
Hf	-	4.89	-	-	-	-	-
Ta	-	0.95	-	-	-	-	-
∑REE	-	159.97	-	-	-	-	-
La_N/Yb_N	-	9.30	-	-	-	-	-
Eu/Eu*	-	0.76	-	-	-	-	-
$^{87}Sr/^{86}Sr$	-	0.70651		-	-	-	-
$^{143}Nd/^{144}Nd$	-	0.51248		-	-	-	-

Appendix D-2 (continued). Major and trace element data for samples from Aghda (oxides, wt% and traces, ppm).

Sample	R14482	R14483	R14497	R14501	R14508	R14509	R14500
SiO_2	54.00	54.16	54.06	54.22	55.35	53.08	49.81
TiO_2	0.38	0.42	0.40	0.57	0.42	0.34	0.75
Al_2O_3	20.34	19.98	20.23	19.06	20.36	20.83	19.02
Fe_2O_3	4.04	4.31	4.15	5.83	4.33	3.98	7.46
MnO	0.09	0.14	0.08	0.12	0.08	0.15	0.15
MgO	0.97	1.26	0.98	2.07	0.95	1.63	2.81
CaO	2.53	2.47	3.45	3.59	5.09	6.90	6.42
Na_2O	5.07	5.37	5.78	6.15	3.14	4.10	4.75
K_2O	6.31	6.40	5.71	4.20	7.61	5.56	3.40
P_2O_5	0.22	0.23	0.23	0.41	0.28	0.22	0.62
LOI	4.38	5.25	4.86	3.89	2.36	2.32	3.84
Total	98.33	99.99	99.93	100.11	99.97	99.11	99.03
Ba	1280	1480	1310	1680	1160	940	2050
Rb	382	353	339	178	371	213	183
Sr	735	818	625	805	659	575	1340
Pb	36	69	30	52	24	134	55
Th	34	30	35	28	30	30	23.30
U	7	3.94	7	9	4.93	8	4.26
Zr	238	248	244	252	257	214	190
Nb	18	17	18	20	17	18	13
Y	18	16	18	23	17	15	22
La	32	33.30	34	40	35.10	28	38.30
Ce	70	70.50	70	85	66.60	60	79
Nd	-	27.50	-	-	27.50	-	37.60
Sm	-	5.25	-	-	5.37	-	7.40
Eu	-	1.05	-	-	1.25	-	1.74
Tb	-	0.57	-	-	0.75	-	0.88
Ho	-	0.64	-	-	0.97	-	1.02
Yb	-	1.42	-	-	1.82	-	1.94
Lu	-	0.20	-	-	0.23	-	0.25
Sc	-	3.67	-	-	3.72	-	11.60
V	34	41	36	76	45	54	124
Cr	<2	<1	<2	<2	<1	<2	11
Ni	<2	3	<2	<2	3	<2	10
Cu	82	33	46	16	45	28	215
Zn	48	193	40	138	56	466	116
Sn	<5	-	<5	<5	-	<5	<2
Ga	17	16	17	19	16	16	17.50
As	5	-	4	5	-	22	3.50
Hf	-	4.40	-	-	4.80	-	4.11
Ta	-	0.91	-	-	1.42	-	0.97
ΣREE	-	140.43	-	-	139.59	-	168.13
La_N/Yb_N	-	15.69	-	-	12.90	-	13.20
Eu/Eu^*	-	0.65	-	-	0.72	-	0.75
$^{87}Sr/^{86}Sr$	-	0.70748		-	0.70738		0.70701
$^{143}Nd/^{144}Nd$	-	0.51244		-	0.51244		0.51245

Appendix D-2 (continued). Major and trace element data for samples from Aghda (oxides, wt% and traces, ppm).

Sample	R14487	R15809	R14480	R14486	R14493	R15808
SiO_2	57.95	62.51	63.85	64.99	71.15	70.86
TiO_2	0.60	0.51	0.31	0.27	0.23	0.26
Al_2O_3	16.14	16.84	15.94	16.24	14.10	14.24
Fe_2O_3	7.23	4.01	3.45	3.20	2.04	1.92
MnO	0.17	0.06	0.09	0.09	0.04	0.03
MgO	1.41	1.80	0.27	0.32	0.34	0.16
CaO	5.02	4.62	1.45	1.07	0.54	1.16
Na_2O	5.62	4.54	3.66	4.23	4.15	3.40
K_2O	2.97	2.45	8.04	7.75	5.97	6.32
P_2O_5	0.40	0.26	0.11	0.08	0.04	0.04
LOI	2.81	2.20	1.63	0.90	1.02	1.63
Total	100.32	99.80	98.80	99.14	99.62	100.02
Ba	685	1550	395	180	545	595
Rb	60	59	382	381	186	220
Sr	448	1280	262	111	165	106
Pb	48	54	26	28	26	46
Th	16	23	47	50	27.60	34
U	3	5	11.40	12	3.68	7
Zr	162	118	525	490	281	296
Nb	12	6	32	30	19	20
Y	20	8	32	33	34	34
La	32	40	51.90	50	38.70	40
Ce	70	85	104	110	78.60	90
Nd	-	-	40.40	-	33.70	-
Sm	-	-	7.84	-	6.73	-
Eu	-	-	0.93	-	0.87	-
Tb	-	-	0.93	-	1.07	-
Ho	-	-	1.41	-	1.55	-
Yb	-	-	3.72	-	4.29	-
Lu	-	-	0.55	-	0.60	-
Sc	-	-	4.13	-	4.82	-
V	118	70	12	14	11	12
Cr	24	4	2	<2	<1	<2
Ni	22	4	1	<2	2	<2
Cu	42	20	13	8	11	8
Zn	86	96	52	46	24	44
Sn	<5	<5	6	5	2	<5
Ga	14	21	17	18	14.50	13
As	13	8	7.50	10	16	10
Hf	-	-	11.80	-	7.43	-
Ta	-	-	2.40	-	1.91	-
ΣREE	-	-	211.68	-	216.11	-
La_N/Yb_N	-	-	9.33	-	6.03	-
Eu/Eu*	-	-	0.37	-	0.39	-
$^{87}Sr/^{86}Sr$	-	-	0.70871	-	0.70718	
$^{143}Nd/^{144}Nd$	-	-	0.51242	-	0.51250	

Appendix D-3. Major and trace element data for samples from Shahrbabak (oxides, wt% and traces, ppm).

Sample	R14521	R14522	R14533	R14534	R14539	R14541
SiO_2	55.43	54.67	54.79	53.08	54.32	56.14
TiO_2	0.77	0.81	0.72	0.79	0.78	0.60
Al_2O_3	18.04	18.44	19.30	19.12	19.12	19.35
Fe_2O3	5.93	6.39	5.34	6.19	5.78	4.25
MnO	0.13	0.14	0.12	0.13	0.10	0.09
MgO	1.58	1.63	1.41	1.92	2.28	0.94
CaO	2.71	4.19	3.63	4.73	4.11	2.78
Na_2O	2.47	4.14	4.99	4.15	5.28	4.85
K_2O	9.58	6.50	6.07	6.05	4.60	7.05
P_2O_5	0.49	0.55	0.34	0.43	0.38	0.26
LOI	3.46	3.01	3.51	3.58	3.60	3.96
Total	100.59	100.47	100.22	100.17	100.35	100.27
Ba	1450	1330	1260	1200	1110	1060
Rb	362	176	229	204	149	383
Sr	455	482	660	685	615	550
Pb	32	34	30	32	28	32
Th	21	17	18	19	17	19
U	4	<2	6	6	4	5
Zr	204	205	196	192	176	204
Nb	10	9	10	10	10	10
Y	24	25	24	25	23	23
La	32	33.20	30	30	30	30
Ce	75	64.60	65	65	65	65
Nd	-	31.50	-	-	-	-
Sm	-	6.43	-	-	-	-
Eu	-	1.50	-	-	-	-
Tb	-	0.92	-	-	-	-
Ho	-	1.22	-	-	-	-
Yb	-	2.78	-	-	-	-
Lu	-	0.40	-	-	-	-
Sc	-	7.58	-	-	-	-
V	88	86	82	80	102	40
Cr	<2	<1	4	6	22	<2
Ni	<2	2	4	6	16	<2
Cu	48	52	42	96	58	26
Zn	98	71	68	66	78	50
Sn	<5	-	<5	<5	<5	<5
Ga	13	16.50	19	18	18	18
As	7	-	3	7	5	6
Hf	-	3.75	-	-	-	-
Ta	-	0.68	-	-	-	-
ΣREE	-	142.55	-	-	-	-
La_N/Yb_N	-	7.98	-	-	-	-
Eu/Eu^*	-	0.71	-	-	-	-
$^{87}Sr/^{86}Sr$	-	0.70567	-	-	-	-
$^{143}Nd/^{144}Nd$	-	0.51268	-	-	-	-

Appendix D-3 (continued). Major and trace element data for samples from Shahrbabak (oxides, wt% and traces, ppm).

Sample	R14544	R14551	R14557	R14531	R14550	R15812
SiO_2	53.06	55.09	53.36	50.67	48.02	50.40
TiO_2	0.76	0.67	0.81	0.69	1.09	0.99
Al_2O_3	19.21	19.71	19.62	20.33	17.93	15.28
Fe_2O_3	6.02	4.90	6.03	6.52	9.61	8.32
MnO	0.13	0.13	0.12	0.12	0.20	0.14
MgO	1.57	1.88	2.00	2.27	5.77	8.60
CaO	4.24	3.42	4.61	6.22	9.18	9.45
Na_2O	4.18	5.02	5.06	5.58	3.21	3.90
K_2O	6.40	5.80	4.77	2.86	1.96	1.54
P_2O_5	0.46	0.32	0.46	0.48	0.35	0.56
LOI	4.16	3.67	3.34	4.44	3.41	0.85
Total	100.19	100.61	100.18	100.18	100.73	100.03
Ba	1200	1300	1130	1020	795	800
Rb	185	157	116	37	77	29
Sr	640	785	807	1320	582	1330
Pb	32	30	30	22	13	8
Th	19	17	15.20	12	4.36	9
U	4	4	4.06	3	2.79	2
Zr	176	174	193	128	81	116
Nb	10	10	10	6	3	12
Y	23	22	24	21	19	18
La	30	30	29.80	26	14.70	42
Ce	65	60	59.90	60	33	90
Nd	-	-	29.70	-	18.40	-
Sm	-	-	5.94	-	4.38	-
Eu	-	-	1.52	-	1.40	-
Tb	-	-	0.80	-	0.69	-
Ho	-	-	0.99	-	0.79	-
Yb	-	-	2.53	-	1.81	-
Lu	-	-	0.38	-	0.27	-
Sc	-	-	7.76	-	18.40	-
V	82	70	116	104	241	170
Cr	4	4	5	4	72	326
NI	4	4	9	6	50	158
Cu	114	42	108	178	85	66
Zn	78	54	69	64	65	76
Sn	<5	<5	-	<5	-	<5
Ga	18	17	18	20	15.50	18
As	4	5	-	5	-	1
Hf	-	-	3.69	-	1.66	-
Ta	-	-	0.67	-	0.50	-
$\sum$REE	-	-	131.56	-	75.44	-
La_N/Yb_N	-	7.88	-	-	5.43	-
Eu/Eu*	-	0.79	-	-	0.96	
$^{87}Sr/^{86}Sr$	-	-	0.70519	-	0.70539	
$^{143}Nd/^{144}Nd$	-	-	0.51273	-	0.51271	

Appendix D-3 (continued). Major and trace elements data for samples from Shahrbabak (oxides, wt% and traces, ppm).

Sample	R14527	R14512	R14515	R14526	R14699	R15811
SiO_2	47.23	63.84	66.91	67.65	66.41	65.38
TiO_2	1.00	0.52	0.39	0.45	0.39	0.36
Al_2O_3	18.11	16.54	15.70	17.68	15.54	16.00
Fe_2O_3	11.22	3.84	2.91	1.99	2.91	3.24
MnO	0.18	0.06	0.04	0.00	0.04	0.05
MgO	5.48	1.47	0.80	0.24	1.01	0.94
CaO	9.64	4.32	3.74	2.16	4.12	4.37
Na_2O	3.07	4.79	4.66	4.00	4.56	4.34
K_2O	1.33	2.67	2.51	2.65	2.75	2.25
P_2O_5	0.30	0.16	0.19	0.14	0.18	0.16
LOI	3.35	1.51	2.30	3.52	1.50	3.02
Total	100.91	99.72	100.15	100.48	99.41	100.11
Ba	280	605	690	825	770	580
Rb	19	56	66	69	65	57
Sr	620	930	625	845	617	610
Pb	6	14	14	16	14	12
Th	4	6.72	8	11	7.25	7
U	<1	<2	3	3	<2	3
Zr	66	130	152	136	135	130
Nb	<2	7	6	8	7	4
Y	21	9	8	28	7	9
La	16	22.60	24	32	29.20	16
Ce	35	40.90	50	65	47.90	35
Nd	-	17.10	-	-	19.70	-
Sm	-	3.75	-	-	3.40	-
Eu	-	0.99	-	-	0.82	-
Tb	-	0.38	-	-	0.37	-
Ho	-	0.39	-	-	0.40	-
Yb	-	0.72	-	-	0.60	-
Lu	-	0.10	-	-	0.08	-
Sc	-	5.91	-	-	4.18	-
V	284	73	44	68	46	42
Cr	46	17	16	42	9	6
Ni	44	17	10	10	7	4
Cu	172	117	36	8	35	14
Zn	80	95	50	24	45	54
Sn	<5	<2	<5	<5	-	<5
Ga	18	19.50	19	19	17.50	19
As	<1	2.50	2	4	-	2
Hf	-	2.84	-	-	3.61	-
Ta	-	0.51	-	-	0.91	-
$\sum$REE	-	86.93	-	-	102.93	-
La_N/Yb_N	-	21.00	-	-	32.51	-
Eu/Eu^*	-	0.86	-	-	0.78	-
$^{87}Sr/^{86}Sr$	-	0.70427	-	-	0.70452	-
$^{143}Nd/^{144}Nd$	-	0.51282	-	-	0.51283	-

Appendix D-3 (continued). Major and trace element data for samples from Shahrbabak (oxides, wt% and traces, ppm).

Sample	R14537	R14538	R14553	R14525	R14528	R14554	R15813
SiO_2	54.53	53.09	52.46	59.62	58.58	54.61	58.19
TiO_2	0.85	1.00	0.94	0.91	0.69	0.78	1.04
Al_2O_3	16.74	14.81	17.99	17.70	18.43	19.98	14.44
Fe_2O_3	6.22	7.42	8.33	5.70	4.94	5.57	5.41
MnO	0.13	0.12	0.13	0.08	0.06	0.10	0.10
MgO	2.23	7.32	3.18	1.26	1.60	1.63	3.24
CaO	7.08	8.03	6.42	4.22	2.39	4.82	5.85
Na_2O	4.77	3.87	3.73	3.82	5.68	5.39	5.13
K_2O	1.86	2.89	4.23	4.20	5.04	4.28	4.16
P_2O_5	0.30	0.53	0.41	0.37	0.24	0.40	0.51
LOI	5.15	1.51	2.91	2.04	1.87	2.99	1.76
Total	99.86	100.59	100.73	99.92	99.84	100.55	99.83
Ba	605	1200	790	305	525	1130	-
Rb	39	81	129	161	109	89	89
Sr	605	975	825	411	570	900	1168
Pb	12	12	16	14	20	30	15
Th	8	8	16	16	26.50	20	-
U	2	2	4	4	6.36	5	2
Zr	208	132	272	330	402	194	159
Nb	10	12	12	12	15	10	15
Y	21	18	26	34	31	24	-
La	24	40	30	34	35.50	30	-
Ce	55	90	70	75	73.90	70	-
Nd	-	-	-	-	33.30	-	-
Sm	-	-	-	-	6.76	-	-
Eu	-	-	-	-	1.33	-	-
Tb	-	-	-	-	0.97	-	-
Ho	-	-	-	-	1.41	-	-
Yb	-	-	-	-	3.59	-	-
Lu	-	-	-	-	0.56	-	-
Sc	-	-	-	-	8.25	-	-
V	108	148	174	64	162	86	190
Cr	20	246	20	4	5	8	-
Co	-	-	-	-	-	31	-
Ni	16	156	16	4	5	8	19
Cu	52	74	28	26	283	34	158
Zn	72	80	78	76	59	74	23
Sn	<5	<5	5	<5	-	<5	-
Ga	17	18	20	19	11.50	19	-
As	2	3	7	6	-	8	-
Hf	-	-	-	-	8.51	-	-
Ta	-	-	-	-	0.96	-	-
$\sum$REE	-	-	-	-	157.32	-	-
La_N/Yb_N	-	-	-	-	6.61	-	-
Eu/Eu^*	-	-	-	-	0.60	-	-
$^{87}Sr/^{86}Sr$	-	-	-	-	0.70475		-
$^{143}Nd/^{144}Nd$	-	-	-	-	0.51273		-

APPENDIX E

CIPW NORMATIVE MINERALOGY

Appendix E-1. Islamic Peninsula

Appendix E-2. Aghda

Appendix E-3. Shahrbabak

Appendix E-1. CIPW normative mineralogy (in wt.%) from the Islamic Peninsula.

Sample	R14444	R14446	R14447	R14455	R14458
Name	TE	TE	TE	TE	TE
Q	-	-	-	-	-
Or	22.33	13.36	12.45	10.62	3.36
Ab	11.24	-	-	13.28	-
An	5.12	5.11	7.83	7.80	9.33
Lc	-	16.12	19.60	-	23.99
Ne	8.79	11.17	5.76	17.67	2.46
Di	32.10	35.27	34.70	35.49	41.56
Di (CaMg)	24.55	24.25	25.23	21.31	32.25
Hd	7.56	11.02	10.47	14.17	9.31
Ol	11.66	9.07	9.90	5.40	11.19
Fo	8.40	5.76	7.39	2.93	8.20
Fa	3.27	3.31	2.51	2.47	2.99
Mt	2.53	3.06	2.86	3.16	2.67
Cm	0.07	0.03	0.04	-	0.09
Il	2.39	2.69	2.43	2.66	2.34
Ap	3.84	4.22	3.51	3.98	3.07

Appendix E-1 (continued). CIPW normative mineralogy (in wt.%) from the Islamic Peninsula.

Sample	R14462	R14464	R14466	R14471	R14474
Name	TE	TE	TE	TE	TE
Q	-	-	-	-	-
Or	1.17	10.37	2.83	19.63	19.42
Ab	-	12.21	-	-	-
An	8.64	11.28	4.44	12.28	1.85
Lc	32.10	-	31.41	8.69	5.29
Ne	4.50	9.97	4.87	10.54	20.01
Di	30.73	38.30	37.70	32.42	36.34
Di(CaMg)	22.52	26.77	28.06	21.38	23.84
Hd	8.21	11.54	11.64	11.04	12.50
Ol	12.84	8.23	9.05	7.58	7.51
Fo	8.79	5.32	6.70	4.59	4.52
Fa	4.05	2.90	2.35	3.00	2.99
Mt	2.93	2.99	2.75	2.94	3.07
Il	2.72	2.68	2.05	2.60	2.36
Ap	4.41	4.03	2.90	3.37	4.24

Appendix E-1 (continued). CIPW normative mineralogy (In wt.%) from the Islamic Peninsula.

Sample	R14477	R14478	R14449	R14454	R14467
Name	TE	TE	PT	PT	PT
Q	-	-	-	-	-
Or	13.04	29.58	11.61	21.14	31.92
Ab	-	1.03	-	-	2.61
An	4.59	10.16	0.07	8.76	8.00
Lc	22.98	-	23.33	11.85	-
Ne	6.68	8.57	9.23	12.57	11.87
Di	34.37	31.44	39.32	29.08	30.25
Di(CaMg)	24.82	21.81	29.12	19.01	20.10
Hd	9.55	9.63	10.20	10.08	10.16
Ol	9.09	9.82	8.08	8.08	6.92
Fo	6.11	6.30	5.60	4.84	4.22
Fa	2.98	3.52	2.48	3.24	2.70
Mt	2.74	2.90	2.64	2.85	2.69
Cm	0.05	0.02	0.05	0.01	0.01
Il	2.57	2.51	2.45	2.44	2.44
Ap	3.96	4.06	3.30	3.28	3.36

Appendix E-1 (continued). CIPW normative mineralogy (in wt.%) from the Islamic Peninsula.

Sample	R14457	R14698	R15807	R15806
Name	BA	TA	TA	TR
Q	-	-	-	-
Or	10.73	45.26	41.46	48.30
Ab	2.24	23.51	29.46	27.48
An	5.35	6.05	5.26	2.03
Lc	-	-	-	-
Ne	9.88	2.97	3.30	1.54
Di	49.07	12.97	11.79	11.69
Di(CaMg)	40.85	7.74	7.00	6.11
Hd	8.22	5.23	4.79	5.58
Ol	15.53	4.89	4.66	4.58
Fo	12.38	2.64	2.50	2.12
Fa	3.15	2.25	2.16	2.45
Mt	2.48	1.69	1.58	1.84
Cm	0.14	0.01	-	0.01
Il	1.87	1.43	1.30	1.61
Ap	2.77	1.25	1.23	0.95

Appendix E-2. CIPW normative mineralogy (in wt.%) from Aghda

Sample	R14482	R14483	R14497	R14501	R14508	R14509
Name	TP	TP	TP	TP	TP	TP
Q	-	-	-	-	-	-
Or	39.83	40.07	35.62	25.92	46.24	34.06
Ab	31.56	29.21	29.71	38.99	19.69	19.57
An	11.87	11.39	13.08	12.53	19.52	22.82
Ne	7.73	10.25	11.87	8.32	4.13	8.88
Di	-	-	2.87	2.72	3.86	9.27
DiCaMg)	-	-	1.13	1.35	1.46	4.81
Hd	-	-	1.73	1.37	2.40	4.46
Ol	5.28	6.05	4.22	7.63	3.79	3.01
Fo	1.81	2.33	1.44	3.33	1.23	1.39
Fa	3.74	3.72	2.78	4.29	2.56	1.63
Mt	1.25	1.32	1.27	1.77	1.29	1.20
Il	0.77	0.84	0.80	1.13	0.82	0.67
Ap	0.56	0.58	0.58	1.01	0.68	0.54

Appendix E-2 (continued). CIPW normative mineralogy (in wt.%) from Aghda.

Sample	R14500	R14499
Name	PT	PH
Q	-	-
Or	21.24	60.26
Ab	28.89	17.27
An	21.71	5.63
Ne	7.37	2.40
Di	6.37	2.01
Di (CaMg)	3.26	0.89
Hd	3.11	1.12
Ol	9.11	8.20
Fo	4.13	3.17
Fa	4.98	5.03
Mt	2.29	2.05
Il	1.51	1.48
Ap	1.55	0.71

Appendix E-2 (continued). CIPW normative mineralogy (in wt.%) from Aghda.

Sample	R14484	R14488	R14495	R14496	R14503	R14507
Name	BTA	BTA	BTA	BTA	BTA	BTA
Q	-	-	-	-	-	-
Or	11.12	24.50	24.64	18.54	33.85	27.56
Ab	35.12	25.74	27.00	28.89	21.23	20.63
An	26.33	24.73	21.89	21.02	12.58	20.98
Ne	4.17	2.27	3.77	3.45	2.51	2.21
Di	9.27	7.98	6.74	13.67	20.17	13.09
Di(CaMg)	4.83	4.08	3.52	7.25	10.45	6.86
Hd	4.44	3.90	3.22	6.42	9.72	6.23
Ol	8.82	9.53	10.65	8.72	4.53	9.61
Fo	4.09	4.31	4.94	4.12	2.08	4.47
Fa	4.73	5.22	5.71	4.60	2.45	5.14
Mt	2.39	2.49	2.56	2.65	2.42	2.81
Il	1.51	1.57	1.61	1.72	1.73	1.78
Ap	1.31	1.22	1.15	1.38	0.98	1.34

Appendix E-2 (continued). CIPW normative mineralogy (in wt.%) from Aghda.

Sample	R14487	R15809	R14480	R14486	R14493	R15808
Name	TA	TA	TR	TR	RH	RH
Q	1.35	14.11	7.86	7.28	22.07	23.99
Or	18.11	14.88	49.03	46.74	35.84	38.02
Ab	49.06	39.49	31.96	36.53	35.67	29.29
An	10.36	18.85	3.43	2.49	2.25	5.02
Di	10.73	2.44	2.83	2.07	0.18	0.50
Di(CaMg)	3.69	1.39	0.49	0.44	0.06	0.10
Hd	7.04	1.05	2.34	1.64	0.12	0.40
Hy	6.09	7.42	2.98	3.23	2.86	2.03
En	1.91	3.96	0.46	0.61	0.83	0.36
Fs	4.18	3.45	2.52	2.62	2.02	1.67
Mt	2.16	1.20	1.03	0.95	0.60	0.57
Il	1.18	1.00	0.61	0.52	0.44	0.50
Ap	0.98	0.63	0.27	0.19	0.10	0.10

Appendix E-3. CIPW normative mineralogy (in wt.%) from Shahrbabak.

Sample	R14521	R14522	R14533	R14534	R14539
Name	TP	TP	TP	TP	TP
Q	-	-	-	-	-
Or	58.57	39.62	37.25	37.20	28.23
Ab	16.01	27.44	29.92	24.25	36.49
An	10.18	12.93	12.81	16.31	15.46
Ne	3.04	4.71	7.55	6.66	5.37
Di	0.35	4.03	3.01	4.32	2.60
Di(CaMg)	0.15	1.71	1.31	2.05	1.40
Hd	0.20	2.32	1.69	2.28	1.20
Ol	7.38	6.45	5.61	6.79	7.66
Fo	2.80	2.38	2.13	2.82	3.68
Fa	4.58	4.08	3.48	3.96	3.98
Mt	1.78	1.91	1.61	1.87	1.74
Il	1.51	1.59	1.42	1.56	1.54
Ap	1.20	1.34	0.84	1.06	0.93

Appendix E-3 (continued). CIPW normative mineralogy (in wt.%) from Shahrbabak.

Sample	R14541	R14544	R14551	R14557	R14531
Name	TP	TP	TP	TP	PT
Q	-	-	-	-	-
Or	43.41	39.58	35.50	29.25	17.75
Ab	29.80	23.99	32.37	32.22	32.89
An	10.64	15.44	14.62	17.37	23.08
Ne	7.02	7.06	6.30	6.62	9.05
Di	1.66	2.88	0.65	2.70	5.02
Di(CaMg)	0.66	1.24	0.34	1.33	2.48
Hd	1.00	1.64	0.31	1.37	2.54
Ol	4.38	6.60	7.00	7.32	7.69
Fo	1.50	2.47	3.29	3.19	3.35
Fa	2.88	4.13	3.71	4.13	4.33
Mt	1.28	1.83	1.47	1.81	1.99
Il	1.19	1.51	1.32	1.60	1.38
Ap	0.64	1.14	0.79	1.13	1.19

Appendix E-3 (continued). CIPW normative mineralogy (in wt.%) from Shahrbabak.

Sample	R14527	R14550	R15812	R14553	R14538	R14537
Name	BA	TB	TB	BTA	BTA	BTA
Q	-	-	-	-	-	2.53
Or	8.13	11.99	9.23	25.73	17.33	11.67
Ab	25.21	24.13	27.77	29.61	31.23	42.84
An	32.80	29.75	19.93	20.43	14.72	19.92
Ne	0.90	2.17	3.09	1.56	1.09	-
Di	12.05	12.29	19.24	7.95	17.86	12.67
Di(CaMg)	6.91	7.74	14.42	4.15	13.32	6.51
Hd	5.14	4.55	4.82	3.80	4.54	6.16
Hy	-	-	-	-	-	6.00
En	-	-	-	-	-	2.88
Fs	-	-	-	-	-	3.12
Ol	14.85	13.79	15.00	9.42	12.36	-
Fo	7.65	7.91	10.54	4.36	8.64	-
Fa	7.20	5.87	4.45	5.05	3.72	-
Mt	3.37	2.89	2.45	2.49	2.18	1.91
Il	1.96	2.14	1.91	1.84	1.93	1.71
Ap	0.74	0.86	1.35	1.00	1.27	0.75

Appendix E-3 (continued). CIPW normative mineralogy (in wt.%) from Shahrbabak.

Sample	R14525	R14528	R14554
Name	TA	TA	TA
Q	9.30	-	-
Or	25.48	30.52	26.04
Ab	33.18	49.09	37.17
An	19.01	10.15	18.21
Ne	-	0.08	5.31
Di	-	0.33	3.11
Di(CaMg)	-	0.16	1.45
Hd	-	0.16	1.66
Hy	8.60	-	-
En	3.22	-	-
Fs	5.38	-	-
Ol	-	6.45	6.02
Fo	-	2.81	2.46
Fa	-	3.64	3.56
Mt	1.70	1.47	1.66
Il	1.77	1.34	1.53
Ap	0.90	0.58	0.98

Appendix E-3 (continued). CIPW normative mineralogy (in wt.%) from Shahrbabak.

Sample	R14512	R14515	R14526	R14699	R15811
Name	TR	DA	DA	DA	DA
Q	14.39	21.37	29.90	19.90	21.07
Or	16.12	15.19	16.18	16.64	13.73
Ab	41.40	40.39	34.96	39.50	37.93
An	16.08	14.86	10.12	14.14	18.10
Di	3.92	2.40	-	4.63	2.68
Di (CaMg)	2.09	1.08	-	2.35	1.21
Hd	1.84	1.32	-	2.28	1.47
Hy	5.57	3.70	2.22	3.13	4.43
En	2.77	1.54	0.62	1.48	1.85
Fs	2.79	2.16	1.60	1.65	2.57
Mt	1.14	0.86	0.60	0.86	0.97
Il	1.01	0.76	0.88	0.76	0.71
Ap	0.39	0.46	0.34	0.44	0.39